

MASTER

Design of an outrigger structure for tall timber buildings

Boellaard, B.J.H.

Award date:
2012

[Link to publication](#)

Disclaimer

This document contains a student thesis (bachelor's or master's), as authored by a student at Eindhoven University of Technology. Student theses are made available in the TU/e repository upon obtaining the required degree. The grade received is not published on the document as presented in the repository. The required complexity or quality of research of student theses may vary by program, and the required minimum study period may vary in duration.

General rights

Copyright and moral rights for the publications made accessible in the public portal are retained by the authors and/or other copyright owners and it is a condition of accessing publications that users recognise and abide by the legal requirements associated with these rights.

- Users may download and print one copy of any publication from the public portal for the purpose of private study or research.
- You may not further distribute the material or use it for any profit-making activity or commercial gain

MASTER'S THESIS

DESIGN OF AN OUTRIGGER STRUCTURE FOR TALL TIMBER BUILDINGS

B.J.H. BOELLAARD

ID.0647377
APRIL, 2012

PROF. A.J.M. JORISSEN
DR.IR. S.P.G. MOONEN

EINDHOVEN UNIVERSITY OF TECHNOLOGY
MASTER STRUCTURAL DESIGN
DEPARTMENT OF ARCHITECTURE, BUILDING AND PLANNING

DESIGN OF AN OUTRIGGER STRUCTURE FOR TALL TIMBER BUILDINGS

MASTER'S THESIS
B.J.H. BOELLAARD

THE NETHERLANDS, APRIL 2012

EINDHOVEN UNIVERSITY OF TECHNOLOGY
MASTER STRUCTURAL DESIGN
DEPARTMENT OF ARCHITECTURE, BUILDING AND PLANNING

PARTNERS:
CENTRE FOR TIMBER ENGINEERING, NAPIER UNIVERSITY EDINBURGH
SP TRÄ, SKELLEFTEÅ SWEDEN
MARTINSONS BYGGSYSTEM KB, BYGDSILJUM SWEDEN

Design of an Outrigger Structure for Tall Timber Buildings
Master's Thesis presented at:
Unit of Structural Design
Department of Architecture, Building and Planning
Eindhoven University of Technology, Eindhoven, the Netherlands

Copyright: Bas Boellaard 2012. All rights reserved.

It was printed at Eindhoven University of Technology.
The printing was funded by Eindhoven University of Technology.
This thesis was set in Segoe UI, pt. 10

I | PREFACE

Timber has been a main theme during my studies in structural engineering over the last years, where it fascinates me due to its traditional characteristics but also because the material's potential for sustainable construction in the future. Being a natural and renewable material – and when it is manufactured from well-managed forests – it is one of the best resources available for architects, engineers and building industry to reduce greenhouse gas emissions in construction. *Sustainability* will be the keyword for future buildings and the opportunity for timber to play a significant role is self-evident.

However, merely promo-talks will not lead to increased use of timber in construction; it should be shown by innovative building systems and ingenious solutions for structures, and proven in practice if timber is the answer for sustainable buildings.

Research is usually the starting point to explore opportunities for new ideas, as this Thesis work. It is attempted to investigate the structural behaviour of a twenty-storey timber building, which may give a good impression of the feasibility of constructing tall timber buildings. Hopefully it leads to new ideas for sustainable constructions and insight of timber's potential for challenging structures.

Undoubtedly this research is supported and guided in the last few months by inspirational people and colleagues working in timber research and industry, resulting in my sincere gratitude to

- Prof. André Jorissen of Eindhoven University of Technology; for his thorough judgement on my work and teaching me a different perspective on research.
- Prof. Abdy Kermani of Napier University in Edinburgh; for giving me the opportunity to spend some valuable time at the Centre of Timber Engineering and make me feel welcome at his department.
- Dr. Ben Zhang of Napier University; for supervising me on structural dynamics, answering my questions at any time and awakening my interest in this field of structural engineering.
- M.Sc. Anders Gustafsson of SP Trä in Skellefteå; for providing the research topic and his hospitality in the inspiring environment of wood in Northern Sweden.
- Greger Lindgren of Martinsons Byggsystem KB in Bygdsiljum; for the direct link to the industry and sharing interesting thoughts on timber engineering.

The Netherlands, April 2012

Bas Boellaard

II | ABSTRACT

New innovative timber materials, such as Cross Laminated Timber, brought up new challenges for architects and engineers for timber construction in recent years. All over Europe many multi-storey housing projects were developed in CLT, which set new boundaries on structural limitations. Due to diaphragm action in CLT panels larger stiffness in structures can be attained resulting in better opportunities for more challenging structures and taller buildings. Today the tallest timber residential building in the world is located in London and has ten floors, all floors scattered with CLT shear walls to resist lateral wind loading. Taller buildings usually have multiple functions such as a commercial- and residential function, which require flexibility in plan design.

Multi-storey buildings erected in concrete and/or steel are frequently designed with a central core and attached frame structure to implement flexibility in design of rooms and open spaces. CLT has similar structural properties as concrete shear walls; hence a natural replacement for sustainable construction. However, a frame structure reduces the lateral stiffness in comparison to a structure with shear walls all over the building's footprint. Considering building designs in concrete and steel, the application of storey height horizontal trusses, so-called outriggers, connected to a central core improves the stiffness of a structure significantly.

However, tall timber buildings have certain properties which are disadvantageous for horizontal sway and dynamic behaviour of the structure, which are the low mass density and relatively low stiffness in comparison to concrete and steel buildings. Serviceability is commonly a decisive aspect in structural timber design, thus in particular for tall timber buildings.

Within this research the objective is to investigate the structural behaviour of a timber outrigger structure for tall buildings through a fictive twenty-storey building design, where serviceability is accentuated. Eurocodes are adopted for design of structural elements as well as connections in the Ultimate Limit State. Design in the Serviceability Limit State has been underpinned by Dutch building regulations set in NEN 6702.

A design process is followed starting with architectural sketches of a fictive twenty-storey building and preliminary structural analysis of multiple stability systems. The outrigger structure has been analysed on dynamic properties, such as the fundamental frequency, and dynamic response due to fluctuating wind loading obtained from a wind spectrum in EC1. Structural elements have been verified on strength in accordance with EC5, where structural forces are obtained from Finite Element analysis in the computer program STAAD Pro. Structural connections are designed according to EC5 likewise, for which aspects like prefabrication, assembly processes, fire safety and noise control are incorporated. Slip of fasteners in connections are analysed by various STAAD Pro models, resulting in a sense of the effects on the structural behaviour regarding to horizontal sway and horizontal accelerations.

In an early stage of the design process it became apparent that serviceability governs the structural design in buildings elements. The proposed outrigger structure with a CLT core and glulam frame structure including outriggers is capable to resist both lateral wind actions and vertical loading. Although the fundamental frequency was computed on rather low values, i.e. 0.58 Hz., the dynamic response to the time varying wind loading was well below permissible values in accordance with NEN 6702. Taking into account slip behaviour in connections both static deformations and horizontal accelerations increased to critical values. It appeared that connections should be considered in an early design phase, since they are as relevant for the stability of the structure as the system itself. Anyhow, with incorporation of thorough design of connections between timber members it can be concluded that timber has high potential for tall buildings up to twenty storeys and perhaps even more.

Keywords: tall timber buildings, Cross Laminated Timber, outrigger structure, dynamical behaviour, serviceability, lateral sway

III | SAMENVATTING

Nieuwe innovatieve houtproducten, zoals Cross Laminated Timber, hebben in de afgelopen jaren voor nieuwe uitdagingen gezorgd in de houtbouw, zowel voor architecten and ingenieurs. In heel Europa zijn vele meerlaagse woningbouw projecten gerealiseerd in CLT, wat grenzen heeft verlegd voor constructief ontwerpen met hout. Door de schijfwerking van CLT elementen kan een grotere stijfheid bereikt worden wat meer mogelijkheden geeft voor uitdagendere constructies en hogere gebouwen. Momenteel staat het hoogste houten woninggebouw in Londen en heeft tien verdiepingen, waarbij de constructie bestaat uit alleen CLT wanden om de benodigde stijfheid te behalen. Hogere gebouwen hebben veelal meerdere functies, zoals kantoren en appartementen, zodat een vrije plattegrond zeer gewenst is.

Meerlaagse gebouwen in beton en/of staal worden vaak ontworpen met een centrale kern en een skeletstructuur daaromheen om enige flexibiliteit in het ontwerp van ruimten te creëren. CLT heeft gelijksoortige eigenschappen als betonwanden en daardoor zijn deze elementen een natuurlijke vervanging ten behoeve van duurzaam bouwen. Een skeletstructuur zal echter de horizontale stijfheid verminderen in vergelijking met een constructie van alleen CLT wanden. Gebouwen in beton en staal compenseren dit veelal door de toepassing van verdiepingshoge vakwerkconstructies, zogenaamde 'outriggers', wat de stijfheid sterk verbetert.

Hoge houten gebouwen hebben echter eigenschappen welke nadelig zijn voor horizontale verplaatsingen en het dynamische gedrag van de constructie. Dit zijn het lage soortelijk gewicht van het materiaal en de relatief lage stijfheidseigenschappen in vergelijking met betonnen en stalen constructies. De bruikbaarheidsgrenstoestand is veelal een doorslaggevend aspect in het ontwerp bij constructieve houtbouw, dus zeker voor hoge houten gebouwen.

Het doel bij dit onderzoek is het bestuderen van het constructieve gedrag van een houten 'outrigger' constructie voor hoge gebouwen door middel van een fictief ontwerp van een twintig verdiepingen gebouw waarbij de nadruk ligt op de bruikbaarheidsgrenstoestand. De Eurocodes worden gebruikt voor het ontwerp van constructieve elementen en verbindingen in de uiterste grenstoestand. Ontwerp in de bruikbaarheidsgrenstoestand wordt uitgevoerd aan de hand van Nederlandse bouwregelgevingen vastgelegd in NEN 6702.

Het ontwerpproces begint met bouwkundige schetsen van een fictief twintig verdiepingen gebouw en voorlopige constructieve berekeningen van enkele stabiliteitssystemen. De 'outrigger' constructie is geanalyseerd op dynamische eigenschappen, zoals de eigenfrequentie en dynamisch gedrag door fluctuerende windbelastingen vanuit het windspectrum van EC1. Constructieve elementen zijn gecontroleerd op sterkte volgens EC5, waarbij statische krachten zijn verkregen uit een Eindige Elementen analyse met het programma STAAD Pro. Constructieve verbindingen zijn vervolgens ontworpen, eveneens aan de hand van EC5. Daarnaast zijn aspecten als prefabricatie, uitvoeringsprocessen, brandveiligheid en geluidswering meegenomen in het ontwerp van verbindingen. Verschuivingen in verbindingen zijn geanalyseerd door middel van verschillende STAAD Pro modellen, wat geresulteerd heeft in inzicht van de effecten op het constructieve gedrag met het oog op horizontale vervormingen en –versnellingen.

Al in een vroeg stadium van het ontwerpproces werd het duidelijk dat de bruikbaarheidsgrenstoestand het ontwerp van constructieve elementen zou gaan bepalen. De ontworpen 'outrigger' constructie met een CLT kern en gelamineerde skeletstructuur met 'outriggers' kan zowel de horizontale windbelasting als de verticale belastingen opnemen. Ondanks dat de eigenfrequentie een relatief lage waarde heeft van 0.58 Hz. voldoet het dynamische gedrag door de tijdsafhankelijke windbelasting aan ontwerpcriteria in NEN 6702. Door het in rekening brengen van afschuiving in verbindingen nemen zowel de statische vervormingen als horizontale versnellingen toe tot kritische waarden. Het blijkt dat

verbindingen al in een vroeg stadium van het ontwerpproces meegenomen dienen te worden, omdat ze net zo belangrijk blijken te zijn voor het stabiliteitsysteem van een twintig verdiepingen houten gebouw als de constructie zelf.

Desondanks kan, met inachtneming van een gedegen ontwerp van verbindingen tussen de houten constructieve elementen, worden geconcludeerd dat hout veel potentie heeft voor hoge gebouwen tot twintig verdiepingen, en wellicht zelfs meer.

Sleutelwoorden: hoge houten gebouwen, Cross Laminated Timber, outrigger constructie, dynamisch gedrag, bruikbaarheidsgrenstoestand, horizontale vervormingen

IV | TABLE OF CONTENTS

I PREFACE	III
II ABSTRACT	V
III SAMENVATTING	VII
IV TABLE OF CONTENTS	IX
1 INTRODUCTION	1
1 Background	1
2 Research motivation	2
3 Aim and research question	3
4 Research methodology	3
5 Importance on society aspects	4
6 Importance on scientific aspects	4
7 Research team	4
2 ARCHITECTURAL DESIGN	5
1 Starting points	5
2 Program of requirements	5
3 Plans and sections	6
3 PRELIMINARY STATIC DESIGN	9
1 Structural analysis on architectural plan	9
2 Static loading	10
3 Theories for preliminary design	11
4 Static analyses	14
5 Reflection on results	19
6 Design of outrigger structure	20
7 Preliminary static design	21
8 Conclusions on static design	23
Appendix: 30 storey building	
4 PRELIMINARY DYNAMIC DESIGN	25
1 Estimation of the fundamental frequency	26
2 Single Degree of Freedom system	29
3 Dynamic wind loading	34
4 Dynamic response of a SDOF system	43
5 Dynamic response of a MDOF system	47
6 3D computer model	58
7 Concluding remarks on dynamic analysis results	64
5 FINAL STATIC DESIGN	67
1 Loading actions according to Eurocode	67
2 Structural modelling	72
3 Quasi-static wind loading	73
4 Floor design	74
5 Beam design	80
6 Column design	84
7 Diagonal design	87

8 Core wall design	89
6 FINAL DYNAMIC DESIGN	93
1 Damping performances	93
2 Effects of outriggers on dynamic behaviour	94
3 Concluding remarks on dynamic analysis	96
7 STRUCTURAL CONNECTION DESIGN	97
1 Design considerations	97
2 Connection types	100
3 CLT wall connection design	101
4 Glulam column and beam connections	121
5 Glulam outrigger connections	139
6 Concluding remarks on connection design in ULS	151
7 Effects of joint rigidity on structural behaviour	152
8 Concluding remarks on connection design in SLS	164
8 DISCUSSION	165
1 Research reflections	165
2 Research question	166
3 Conclusions	167
4 Future research	167
9 REFERENCES	169
APPENDICES	
A.1 Wind actions – Eurocode 1	
A.2 Preliminary static calculations	
A.3 Preliminary dynamic calculations	
B.1 Derivation storey displacement rigid floors	
C.1 Final static calculations	
C.2 Final dynamic calculations	
D.1 Structural connections calculations	
D.2 Slip in connections – static results	
D.3 Slip in connections – dynamic results	

1 | INTRODUCTION

1.1 BACKGROUND

Tall buildings designed in timber are nowadays more close to reality than ever been in the past due to new innovative inventions of both materials and structural design methods. The introduction of Cross Laminated Timber (CLT) a decade ago has caused new opportunities for designers as well as for the building industry. The great benefit of constructing with this material involves higher permissible forces and thus results in both taller buildings and more challenging structures. Applications of CLT include walls, floors and roofs (Figure 1.1) providing a diaphragm structure for a structure in which both walls and floors are subjected to structural actions (Figure 1.2). Therefore building plans are scattered with structural walls reducing the architect's design freedom as well as occupant's flexibility.



Figure 1.1; CLT structural elements

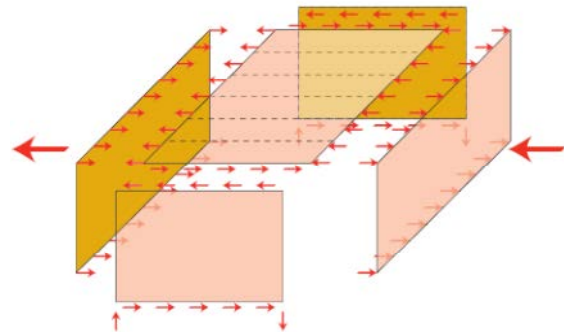


Figure 1.2; Diaphragm action due to lateral forces

A touch of flexibility to the plan can be marked by replacing a part of the diaphragm structure with a glulam column-beam structure, so that advantages of both structural systems come to light in a building. A system of stabilising cores and attached column-beam structures are widely applied in buildings with other structural materials such as concrete and steel.

Today, the tallest timber residential building is called 'Stadthaus' and is located in London. This building reaches nine storeys and is completely constructed out of CLT plates. Engineers, however, are in agreement with one another that structural limitations allow taller timber buildings up to twenty- or even thirty storeys. These limitations are not expected to comprise design in the Ultimate Limit State, but are assumed to be mainly dominated by design in the Serviceability Limit State. Both lateral

stiffness- and dynamical properties become decisive when designing tall timber buildings. Of course, other limiting aspects as fire and comfort shall always be addressed as well.

Obviously, a column-beam structure, which is not stabilised by itself, reduces the lateral stiffness in comparison with a complete diaphragm structure consisting out of CLT panels. A familiar measure in the steel industry for this shortcoming is integrating an outrigger to the column-beam structure connected to stabilising cores. This kind of structural system for tall timber buildings is a new application and could be an answer to twenty-storey buildings in timber with required flexibility as well as an open facade structure.

1.2 RESEARCH MOTIVATION

In general, the majority of politicians, scientist and participants in the industry are convinced that the future of construction will be fully dominated by sustainable buildings which will have a zero carbon footprint. Wood as a building material is nowadays more and more appreciated by architects and building users, thus causing a revival of this ancient building material. Many clients of all kinds of buildings acknowledge the natural expression of wood and in some way are attempting to identify to the sustainable revolution. Due to these appearances in the society as well as in the building industry, the future of wood in sustainable buildings may be bright and by some participants even labelled as the material of the twenty-first century.

As many cities in the world become denser the demand of tall buildings increases. On the other hand the trend of sustainable and healthy living may be in contradiction to growth in densely populated areas. Many trend watchers refer to so-called 'green living' in city environments by creating a sort of isolated living environment for inhabitants in residential complexes where sustainability plays an important role.

This mindset of sustainability – as well as the increasing relevancy of renewable raw materials for the construction industry – may result in an increasing demand of timber buildings in the future.

Designing tall timber buildings – from ten storeys and above – requires a different approach on constructing and structural design. As mentioned in the previous section, serviceability aspects such as deformations and dynamic behaviour of the structure become more important in the design. Due to the low mass density of wood the behaviour of tall timber buildings due to lateral actions, such as wind, may be negatively influenced.

The type of structural system affects the architectural design largely because tall buildings usually have multiple functions, which requires flexibility in spaces. The role of assembly processes in multi-storey construction also may influence design of structural elements and connections on some extent, where the ability of repetition in construction activities is highly beneficial for the competitiveness of a structural material and/or system.

Building projects of a similar building height have been widely constructed with either steel or concrete or a combination of these industrialised structural materials. Commonly, the layout of such buildings consists of a concrete core with a steel (or concrete) frame structure attached. This type of system has been shown to be effective in both providing the required lateral stiffness to the structure and flexibility in the design.

The application of CLT in many mid-rise buildings, i.e. 5-8 storeys, in Europe have proven the capability of the material to resist both lateral- and vertical loading, where previously for these projects concrete was an obvious choice as a structural material. The large in-plane stiffness of the CLT panels covers the beneficial structural properties of concrete in constructing. Therefore, it may be apparent that replacing a concrete core with CLT and steel frame structure with glulam columns and –beams is a natural consequence when it is desired to decrease the carbon footprints of building projects.

Research to the structural behaviour of a tall timber structure should clarify the potential – as well as the limitations – of the material for twenty-storey buildings. In addition, a timber outrigger structure for such buildings is a new application requiring unique solutions in structural elements as well as connections.

1.3 AIM AND RESEARCH QUESTION

The aim of this research is to investigate the structural performances of an outrigger structure – consisting of a CLT core and glulam frame structure – through a fictive twenty-storey building design. The focus of this analysis is on the Serviceability Limit State, where the structural behaviour such as deflections, structural vibrations and horizontal accelerations will be analysed.

Further, the design of structural elements and connection details are aimed to investigate – as well as their effects on the structural behaviour – to be able to identify the potential of timber as a structural material for tall buildings.

The research question can be defined as follows:

“How does a timber outrigger structure perform as a stability system for a twenty-storey building, with the focus on serviceability aspects?”

1.4 RESEARCH METHODOLOGY

Pre-research

Prior to the main research a comprehensive literature study has been carried out [1], which consists of analyses on: the material CLT, reference projects of tall timber buildings, glulam structures and properties of outrigger systems, as well as structural dynamics.

Research

The main research consists of a design of a fictive twenty-storey building which operates as a guideline for the design of the load-bearing structure. The design process can be subdivided in a *preliminary design* and a *final design*. A preliminary design process will be conducted alongside structural (hand) calculations with regard to both static and dynamic behaviour to propose a load-bearing structure. Subsequently, the preliminary design is the basis for extensive structural analyses on both the ULS and SLS resulting in a final design. At last, structural connection details will be designed to both comply with strength criteria and analyse the effects on serviceability aspects, e.g. deformations and horizontal accelerations.

Discussion

Results of the analyses carried out in the main research will be reflected. The efficiency and applicability of the proposed structure will be criticised with the help of advantages and disadvantages defined after the research.

Demarcations

For building design it is needed to set certain design criteria, by building regulations and/or -codes. For this project Eurocodes with Dutch National annexes are adopted for the design of structural elements and connections. Further, architectural design is conducted in accordance with Dutch Official Regulations and Standards for the Building Industry [2].

1.5 IMPORTANCE ON SOCIETY ASPECTS

The role of sustainability in the future of the construction industry will rather increase than it will reduce. The use of wood in construction has a positive influence on the emission of carbon dioxide due to the storage of this substance in growing trees. During the growing process of trees absorption of carbon dioxide is the most effective and therefore the process of deforestation and replanting is contributing to the storage of carbon dioxide.

The sustainable revolution in the society is highly benefitted by new sustainable solutions for living and working environments, in which the application of wood as a renewable building material could possess a dominant role. However, it is essential that the product becomes competitive with other conventional materials like concrete and steel where research can be a starting point.

1.6 IMPORTANCE ON SCIENTIFIC ASPECTS

In order to achieve the competitiveness of timber as a core building material for tall buildings, a thoroughly engineered product is essential. But first of all, the question; *“Can we build with this material these structures”* is the single most important issue before attempting to sophisticate a building system in order to make it an obvious choice for multi-storey construction. Therefore, a comprehensive research to the behaviour of a structure for tall timber buildings is desired to conduct in order to create innovative and sustainable solutions for the construction industry.

Research into a combined structural system of a CLT core and attached glulam column-beam structure with outriggers will enhance the knowledge of both the structural behaviour of such a system and the overall design with respect to connection details and construction aspects. In particular the design of an outrigger connected to a CLT core will require special attention and ingenious design solutions. Analyses on the dynamic behaviour of tall timber buildings has not yet been widely conducted since so far projects have been realised up to ten storeys only. More structural opportunities for taller timber buildings – due to engineered timber products like CLT – will increase the demand for insight in the behaviour of such buildings during serviceability.

1.7 RESEARCH TEAM

This research involves several members from both Universities and the industry. Figure 1.1 shows the project related parties and members.

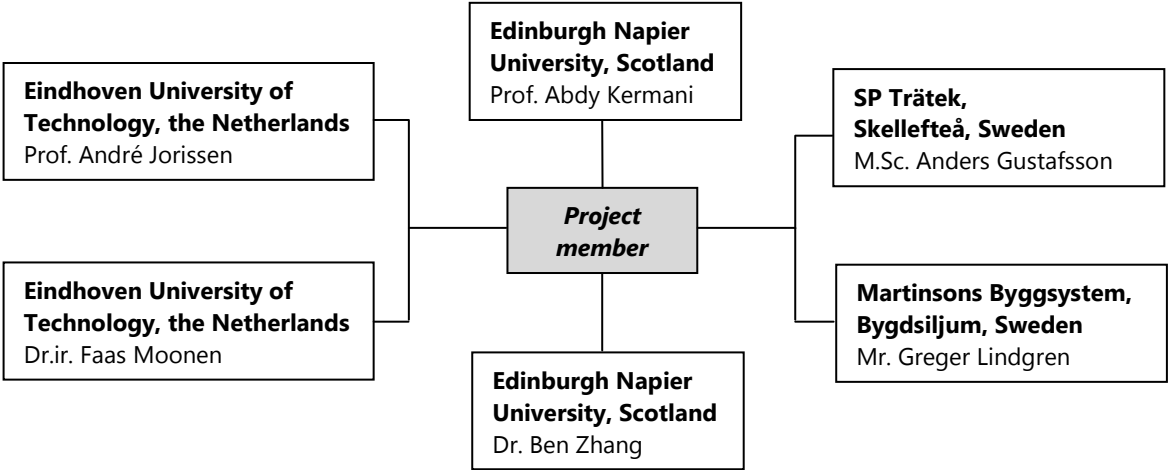


Figure 1.1; Overview of members in the research team

2 | ARCHITECTURAL DESIGN

Starting points and building regulations

In practice, the preliminary architectural design forwarded to the structural engineer usually consists of some sketchy plans and sections with approximate dimensions. Subsequently, the engineer scans the drawings on the importance of; rooms, transportation routes and free spaces, and attempts to integrate structural elements with esthetical thoughts of the architect at the back of his mind. In the following sections such a preliminary design is proposed, underpinned by a Program of Requirements, wherein the objective is more to prepare a basic design which is rather realistic regarding to building regulations and what can actually be build in practice, than going through a comprehensive architectural design process.

2.1 STARTING POINTS

Relevant for the first architectural sketches is the definition of some keywords which translate the architects (and/or clients) intentions for the building. In the case of the twenty-storey building the following main keywords can be defined:

Twenty storeys, offices and dwellings, square building, main construction material is timber, flexible plan- and façade design.

2.2 PROGRAM OF REQUIREMENTS

Further requirements on the building design are classified into; spatial-, functional- and technical requirements. The spatial requirements determine the types of rooms and their dimensions, whilst functional requirements translate the serviceability of the building and technical requirements are mainly based on building regulations.

Spatial requirements

Table 2.1 represents the spatial requirements pertaining to the twenty-storey building.

Table 1.1; Spatial requirements

Type of room	Number	Surface area / unit [m ²]
Dwelling	4 – 6 / residential floor	60 – 160
Office	4 – 6 / office floor	30 – 160
Staircase	min. 2	10 – 12
Elevator	4 – 6	2.5 – 4
Utility shaft	min. 2	2
Utility room	1	40 – 50

Regarding to the height of rooms in habitable areas (i.e. habitable rooms in dwellings and offices) the minimum dimension is 2.6 meters, whilst this also holds for escape routes in the building. The height of doors in an escape route should be at least 2.3 meters. The width of escape routes should in any case reach 1.2 meters including door openings. Furthermore, the Dutch building regulations [2] state that in a case of fire occupants should be able to escape from a habitable area (i.e. a single dwelling/office) in two directions. Therefore a minimum of two staircases in the building is required.

Functional requirements

Activities of occupants as well as their movements in a building are influenced by the functional properties of the building. Since two functions are part of the building (i.e. residential and commercial) it is important to determine their interrelations. It is desired to design commercial activities on the lower floors and locate the dwellings on the upper floors, wherein a combination of activities on a single floor is precluded. Separate use of vertical transportation is also desired, although shared egress routes such as staircases and elevators may be utilised in the case of emergency to meet building regulations.

Technical requirements

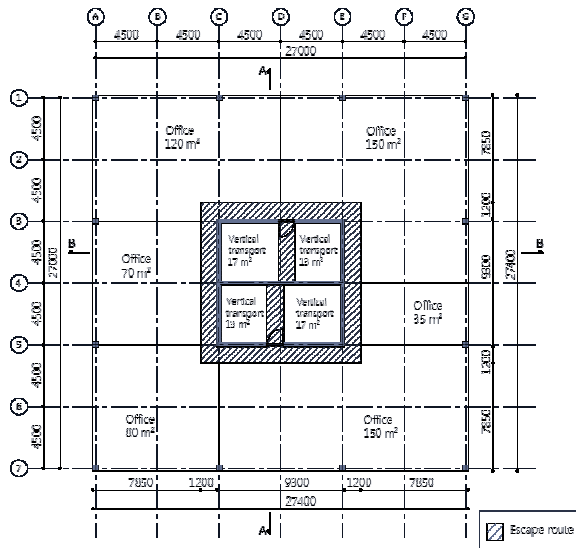
Regulations in the building code with technical contents are mainly based on constructional element design, such as thermal insulation, fire resistance and noise control. With respect to fire safety the Dutch building regulations state a minimum of 120 minutes fire resistance of structural elements for a habitable area floor located 13 meters above ground level.

Amount of penetrated daylight into the building is defined according to the functions. For both dwellings and offices there is a minimum of 0.5 square meter daylight surface area for each habitable room, for residential habitable areas applies a minimum of 10 percent whilst for commercial habitable areas the minimum daylight is 2.5 percent.

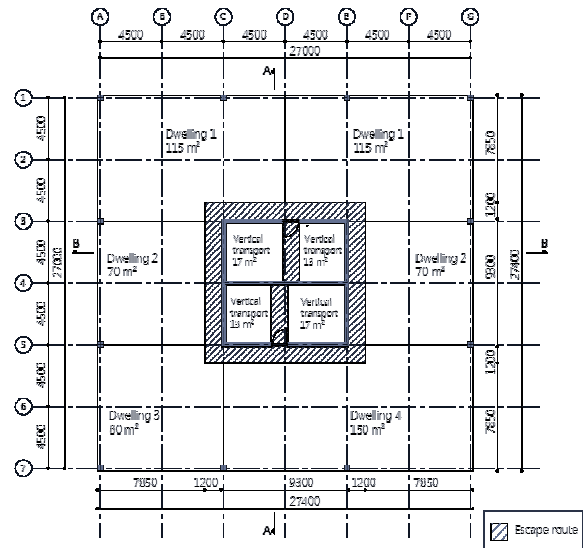
Building services are relevant for the location of utility shafts as well as for the design of floor constructions. It is desired to position utility shafts at a central location and to design them continuous over the building's height. The maximum mechanical piping dimensions which will be taken into account for the design of floor constructions is a height of 125 millimetres.

1.3 PLANS AND SECTIONS

Plans and sections for the preliminary architectural design comprise a design of habitable areas, escape routes and vertical transportation provisions. Figure 2.1 and 2.2 illustrate typical floor plans of the commercial function and residential function respectively. In order to meet the requirements on daylight penetration all habitable areas are located at the building's peripheral, so that vertical transportation occurs at the inner area. This results in a rather classic building design with a central core. To house the required rooms and their surface areas the building's envelope consists of an area of 27 x 27 meters.



Floor plan - offices
Architectural - 3200+

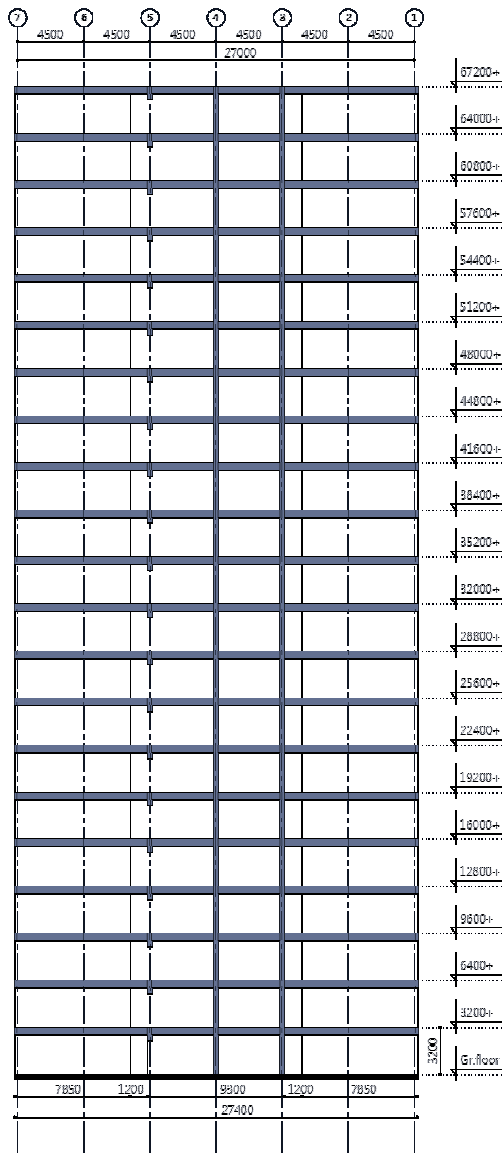


Floor plan - dwellings
Architectural - 41600+

Figure 2.1; Typical plan design of a commercial floor

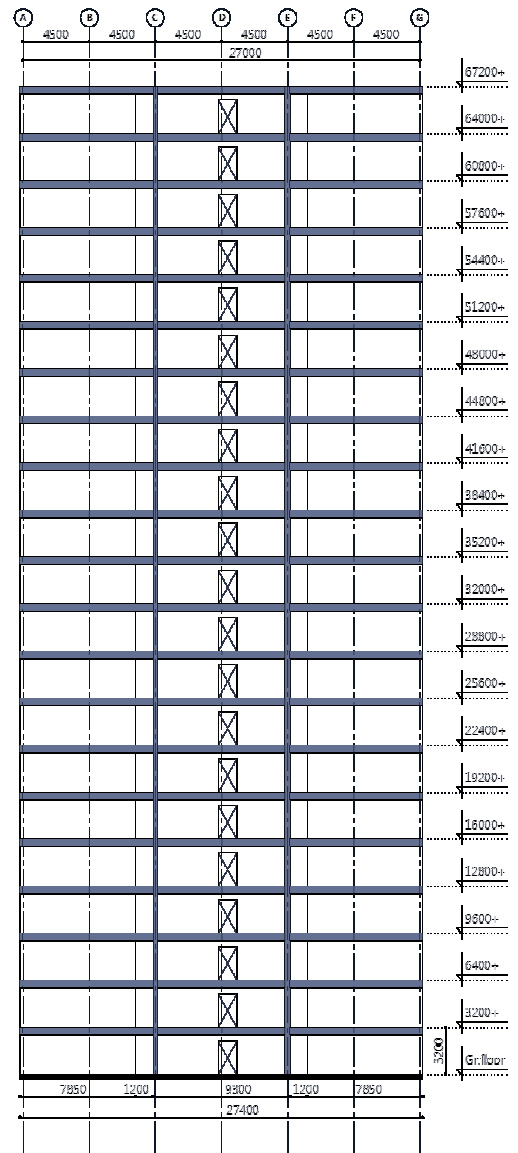
Figure 2.2; Typical plan design of a residential floor

The height of rooms in a habitable area as well as rooms located in an escape route should be at least 2.6 meters. At this stage the height of floor constructions is assumed to be 600 millimetres, so that floor to floor dimensions results in 3.2 meters. Designing for twenty storeys, the total building's height reaches approximately 67 meters. Figure 2.3 and 2.4 present Section A – A and Section B – B respectively as depicted on the plans.



Section A - A
Architectural

Figure 2.3; Architectural sketch design of Section A - A



Section B - B
Architectural

Figure 2.4; Architectural sketch design of Section B - B

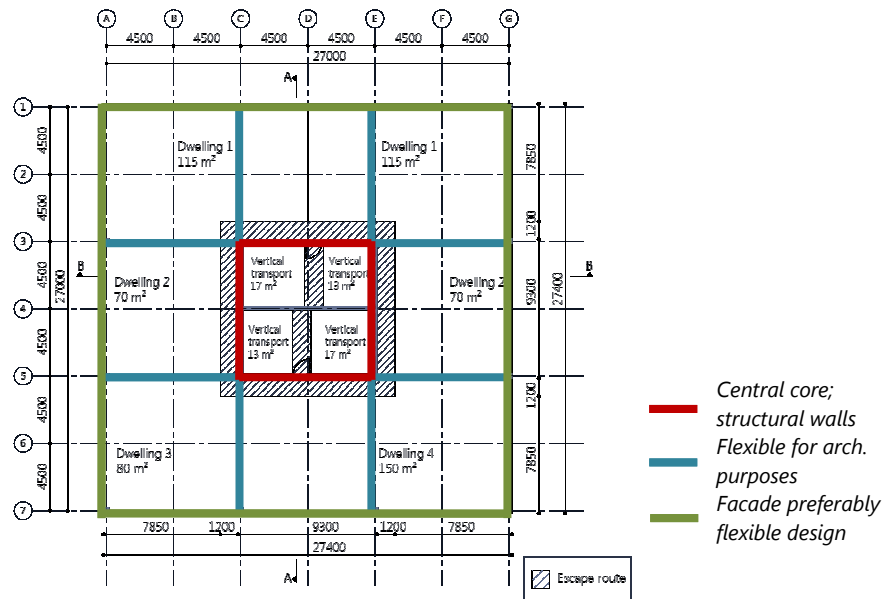
3 | PRELIMINARY STATIC DESIGN

First impressions on structural performance

In order to attain insight in the behaviour of timber load-bearing structures for a twenty-storey building, the structural design process consist of various design proposals which will be analysed through preliminary static design methods. These methods mainly consist of evaluation of the maximum horizontal deflection at the top of the building, allowing simple hand calculations. Furthermore, critical forces in the building are evaluated, which may be a prerequisite for the feasibility of a structural system. The aim in this chapter is to obtain a static preliminary design, suitable to proceed with dynamic analyses.

3.1 STRUCTURAL ANALYSIS ON ARCHITECTURAL PLAN

On a first glance of the architectural plans, several structural systems are possible to implement to comply with architectural objectives. However, the plans contain some constructional design elements which are obvious to exploit for structural purposes. For instance the central core, where vertical transport is positioned, is perfectly suitable to function as the main structural system to ensure lateral stability. Space outside the central core should be flexible for room design due to multiple functions, i.e. commercial and residential. Likewise, flexibility in façade design is desired. Figure 3.1 depicts obvious structural lines across the building, which can be incorporated for the design of a structural system.



Floor plan - dwellings

Architectural - 41600+

Figure 3.1; Structural provisions in the architectural plan

Besides the central core, it becomes apparent that opportunities for structural purposes may be sought in the façade and extended lines outside the central core. From the first point of view, a column-beam frame structure around the core is an obvious solution providing a degree of flexibility to the plan. Nevertheless, some shear wall structures might be possible to fit both commercial- and residential functions in the building, decreasing the flexibility but increasing structural stiffness. Table 3.1 presents three structural systems and their properties applicable for the twenty-storey building.

Table 3.1; Properties of structural systems

System	Stability elements	Remaining load-bearing structure
Tube structure	Fenestrated CLT wall in façade Central CLT core	Glulam columns and -beams
Shear wall structure	CLT shear walls in two directions Central core	Glulam columns and -beams
Outrigger structure	Single horizontal (two) storey high trusses outside core Central CLT core	Glulam columns and -beams

3.2 STATIC LOADING

Vertical actions

In the preliminary design stage certain assumptions are made regarding to static loading subject to the building's structure. For instance, the summation of vertical loading (i.e. self-weight, permanent loading and imposed loading) on a floor in a building is usually estimated on 10 kN/m^2 . Although, this assumption is based on heavier buildings, e.g. concrete or steel structures, and thus seems to be a rather conservative approach for timber structures, this value is deployed in the preliminary design calculations, which includes partial loading factors according to EC0 [3]. With respect to unfavourable actions, however, the loading may be non-conservative. For instance, overturning of CLT shear walls

should be resisted by unfavourable actions. Although loading combinations are not incorporated in the preliminary design, the effects of unfavourable actions are taken into account in Section 3.5.

Horizontal actions

On the other hand, lateral loading (i.e. wind loading) subjected to the structure is the main design load for preliminary calculations. Therefore, the design value is evaluated in Appendix A.1 according to EC1 [4]. The calculation method in EC1 incorporates dynamic effects, e.g. fluctuating wind around the building, for which in this stage certain assumptions have to be adopted such as the fundamental frequency of the structure. The result, however, is a quasi-static wind load.

In the Serviceability Limit State (SLS) the characteristic (q_k) value is implemented for building deformations, which yields 1.54 kN/m^2 . In the Ultimate Limit State (ULS) a partial loading factor γ_Q , of 1.5 applies so that the load increases to 2.31 kN/m^2 .

The maximum permissible horizontal deflection for buildings conform EC0, where reference is made to the Dutch code NEN 6702 [5], is confined to; $H/500$, where H is the total building height. However, it is recommended [6] to decrease this value in the preliminary design stage to $H/800$, to allow for rotations of foundation structures.

3.3 THEORIES FOR PRELIMINARY DESIGN

In the preliminary design stage it is desired to implement simple design techniques suitable for hand calculations. The purpose is to give an approximation of the structural behaviour under lateral loading of various structural systems in order to analyse their performances for the proposed building design.

Composite Theory for structural properties of CLT panels

Effective strength and stiffness properties of CLT panels can be obtained through the Composite Theory [7] [], by taking the influence of cross layers into account. Multiplication of the gross section properties by the composition factor, k_i , results in reduced panel strength and – stiffness values. For in-plane bending due to lateral loading of CLT wall elements, k_3 applies, which is expressed as

$$k_3 = 1 - \left(1 - \frac{E_{90}}{E_0} \right) \frac{a_2}{d} \quad (3.1)$$

where E_{90} and E_0 are the Young's Modulus of the boards perpendicular to the grain and parallel to the grain respectively, a_2 is the thickness of layers in cross direction (i.e. in the direction of loading) and d is the thickness of the panel.

Equivalent stiffness properties of fenestrated walls

In a preliminary design stage stiffness of tall shear walls with regular opening patterns can be estimated by a simplified method of analysis proposed by Khan & Stafford Smith [8]. The evaluation procedure is based on equivalent modulus of elasticity and shear modulus obtained by ratios of opening parameters. With the help of simple-to-determine graphs, which are compiled by the authors using Finite Element analysis, the bending stiffness and racking shear stiffness of a shear wall can be evaluated. An example of such a graph is shown in Figure 3.2a, which is related to a ratio of H/B (i.e. dimensions of a wall segment shown in the figure) of 1.5. Other design parameters are h , which equals half the height of a wall beam, and b , equating half the width of a wall column.

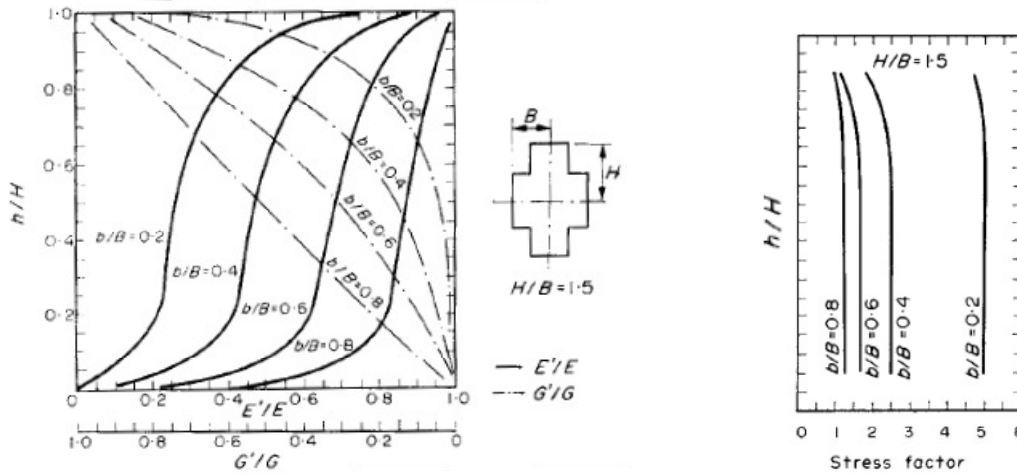


Figure 3.2; a) Design graph for equivalent stiffness properties, E' and G' , for fenestrated walls with $H/B = 1.5$

b) Design graph for normal stress factors for $H/B = 1.5$

Subsequently, maximum horizontal displacements of a fenestrated tube (or wall) structure can be approximated by cantilever beam theory, through the assumption of a cantilever representing the tube structure subjected to an equally distributed wind load. Obviously, both bending- and shear deformations should be taken into account when calculating lateral displacements.

Evaluation of stresses in wall columns and -beams requires a stress factor, which for instance transfers wall stresses at the bottom of a wall to governing stresses on half height in wall columns on the ground floor. Once again, the authors utilised Finite Element computations to derive design graphs, shown in Figure 3.2b for H/B equal to 1.5. It can be seen that for very small wall openings where half the width of wall column b is nearly equal to B , the stress factor almost becomes unity. In a similar fashion graphs are compiled to determine shear stress factors.

Compatibility equation for rotation of outrigger structures

The deflection effects of outriggers on the main structure can be determined by a compatibility equation at the intersection of neutral axes of the central main structure and outrigger [6] [9]. The compatibility equation is based on equalising the rotation of the main structure and rotation of the outriggers. As a consequence, the outriggers are assumed to be rigidly connected to the main structure and pin connected to peripheral columns. A comprehensive elaboration of calculations of horizontal displacements and the optimum outrigger height is discussed in [9]. The maximum horizontal displacement at the top of the structure is given by

$$U_{\max} = \frac{wH^4}{8EI} + \frac{wH^2}{2GA} - \frac{M_r(H^2 - x_0^2)}{2EI} - \frac{M_r}{\alpha GA} \quad (3.2)$$

where w is a uniformly distributed lateral load, H is the height of the building, EI bending stiffness of the main structure, GA racking shear stiffness of the main structure, M_r the restraining moment induced by axial restraining forces in peripheral columns, x_0 equals the outrigger distance from the top of the structure and α is the ratio between distances ℓ and b as displayed in Figure 3.3.

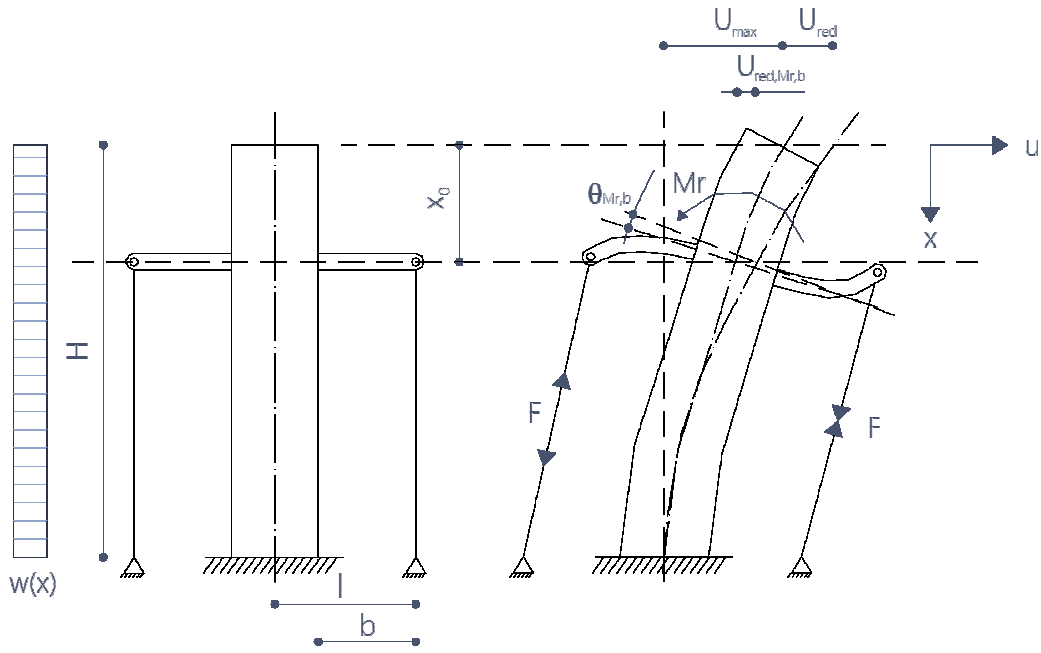


Figure 3.3; Structural effects of outriggers on deformations of a core structure

Equation 3.2 consists of two components for deflections due to lateral loading and two components for reverse bending by a restraining moment, M_r . The former two components represent displacements of the main structure, i.e. CLT core, by cantilever beam theory without outrigger effects. Reduced horizontal displacement at the top of the structure, U_{red} as depicted in Figure 3.3, is determined by the latter two components of equation 3.2, which consist of a bending- and racking shear part.

The third term is a combination of reversed displacement due to restraining moment M_r and the additional displacement above outrigger due to rotation of the main structure on outrigger level. A reversed displacement on outrigger level due to restraining moment M_r can be calculated as follows

$$U_{red,M_r,b} = \frac{M_r (H - x_0)^2}{2EI} \quad (3.3)$$

The reversed rotation of the main structure on outrigger level due to M_r is given by

$$\theta_{M_r} = -\frac{M_r (H - x_0)}{EI} \quad (3.4)$$

Multiplication by outrigger distance x_0 results in a reduced displacement at the top of the building due to reversed rotation of the main structure, as follows

$$U_{red,\theta,b} = \theta_{M_r} x_0 = \frac{M_r (H - x_0) x_0}{EI} \quad (3.5)$$

The total reduced displacement due to bending, i.e. third component of equation 3.2, becomes

$$U_{red,b} = U_{red,M_r,b} + U_{red,\theta,b} = \frac{M_r (H^2 - 2Hx_0 + x_0^2)}{2EI} + \frac{2M_r (Hx_0 - x_0^2)}{2EI} = \frac{M_r (H^2 - x_0^2)}{2EI} \quad (3.6)$$

The fourth term (eq. 3.2) represents a reduced racking shear displacement of the main structure due to the restraining moment, M_r , on outrigger level. Racking shear deformations are a function of lateral shear forces induced in the main structure by the outriggers and the racking shear stiffness, GA . In order to obtain lateral shear forces due to the restraining moment it is required to calculate the restraining moment at a distance b from the peripheral columns, as shown in Figure 3.3. As mentioned before the restraining moment at the intersection of neutral lines of the main structure and outriggers is caused by axial restraining forces in the columns and can be written as

$$M_r = 2F_r \ell \quad (3.7)$$

where F_r is the restraining axial force in a peripheral column and ℓ is the distance from the column to the centre of the main structure, as shown in Figure 3.3. The restraining moment on distance b becomes

$$M_{r,o} = \frac{M_r}{\alpha} \quad (3.8)$$

where α is a dimensionless parameter equal to

$$\alpha = \frac{\ell}{b} \quad (3.9)$$

Subsequently the reversed racking shear rotation induced by the restraining moment, $M_{r,o}$, can be calculated as follows

$$\theta_{rsh} = -\frac{M_r}{h\alpha GA} \quad (3.10)$$

where h is the height of the outrigger. The reversed displacement over the outrigger height becomes

$$U_{red,rsh} = \frac{M_r}{\alpha GA} \quad (3.11)$$

3.4 STATIC ANALYSES

The calculations for the static analyses are shown in Calculations Sheets (C.S.)2.1 to 2.3 in Appendix A.2, whilst the most relevant outcomes are summarised in Table 3.2 to 3.4 for the; tube structure, shear wall structure and outrigger structure respectively. The tables clarify the proposed structural system through; 3D illustrations, structural model and overview of the structural performances.

Tube structure

The tube structure's stiffness properties have been analysed by the equivalent stiffness method for fenestrated walls [8]. The tube dimensions are 27 x 27 meters. The layout of the wall openings consist of a regular pattern along the façade with openings of 1.4 x 1.6 meters (bxh). Wall columns are 0.8 meters wide and wall beams consist of a height of 1.6 meters. Due to the relatively slender central core compared to the tube structure, the contribution of the core to the lateral stabilisation has not been taken into account, since this is assumed to be marginal. Deformations due to lateral wind loading can be simply calculated by cantilever beam theory, as mentioned before and shown in the figure of Table 3.2.

As a starting point a wall thickness of 300 millimetres is assumed. An example of a CLT panel, which is manufactured by the Austrian company KLH, is shown in Figure 3.4. Longitudinal layers comprise three times two layers of 40 millimetres thickness and two cross layers of 30 millimetres.

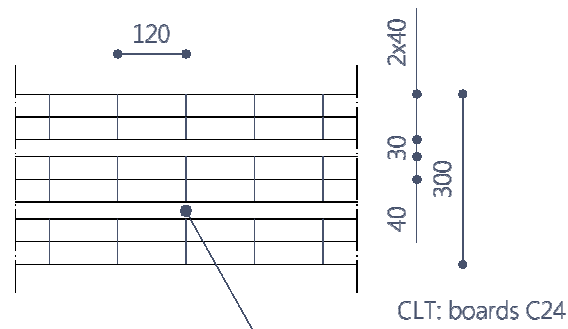


Figure 3.4; CLT panel with a thickness of 300 millimetres produced by KLH

The total thickness of cross layers (a_2), i.e. in the direction of wind loading, equals 60 millimetres. Stiffness properties of strength class C24 are as follows

$$E_{0,\text{mean}} = 12\,000 \text{ MPa.}$$

$$E_{90,\text{mean}} = 3\,700 \text{ MPa.}$$

so that the composite factor for reduced strength- and stiffness properties yields

$$k_3 = 1 - \left(1 - \frac{370}{12\,000} \right) \frac{60}{300} = 0.806$$

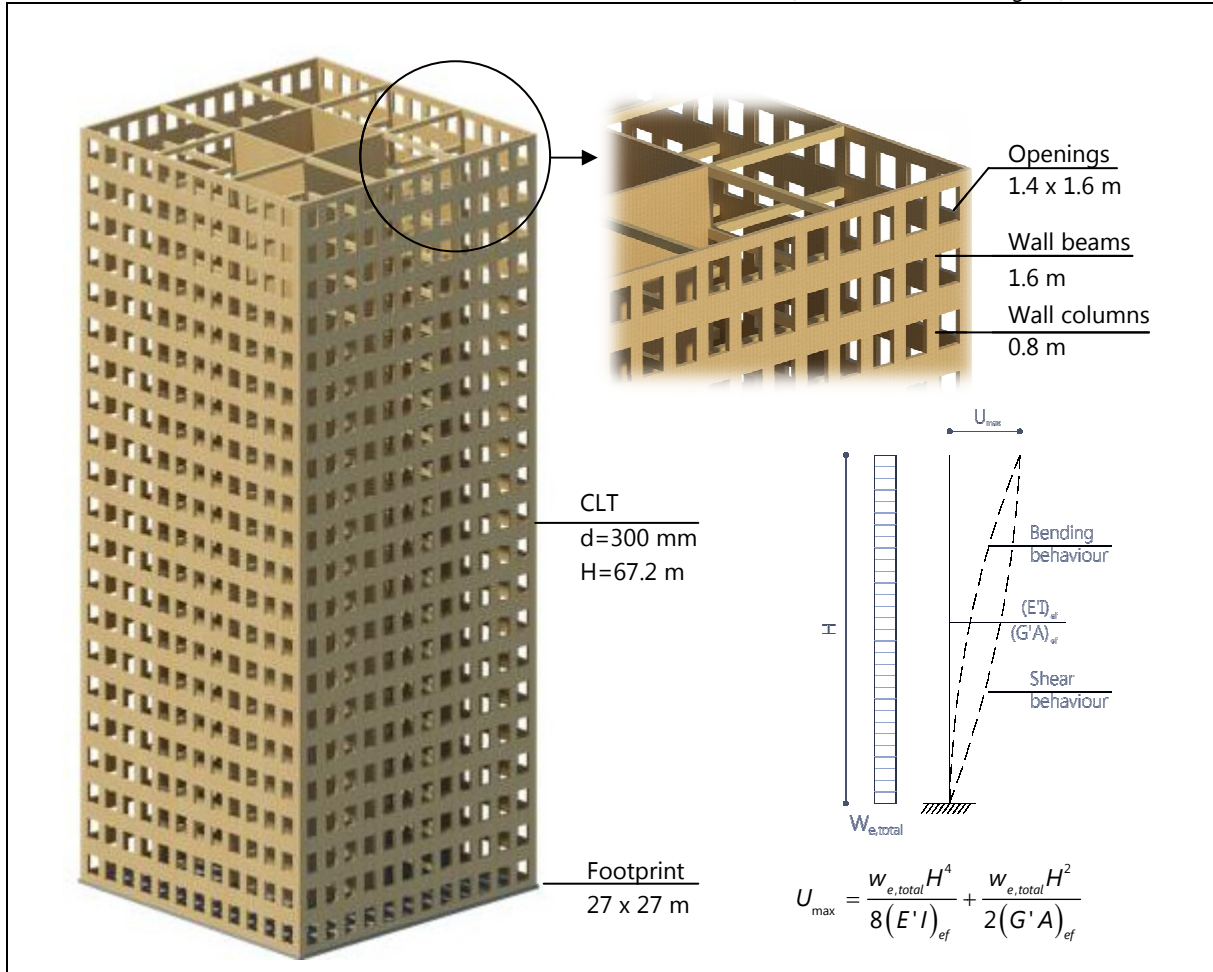
Shear wall structure

In each wind direction of the building, two shear walls are designed to enhance the lateral stiffness on top of the central CLT core. As has been shown in the previous chapter, due to architectural reasons, the core's perimeter is designed as an escape route of 1.4 meters width. Therefore, the length of shear walls is designed as 7.6 meters. The walls will be connected by spandrels to the CLT core inside the floor structure, thus within structural calculations they are assumed to be uncoupled. Hence hinge connected by a rigid link to the CLT core. The distribution of lateral loading over structural elements is conform stiffness ratios of a single element to the total stiffness in the pertaining direction [6]. Torsion of the structure around its longitudinal axes is not present due to the structure's double symmetry. Once again horizontal displacements can be determined by adopting the cantilever beam theory.

Outrigger structure

The connection between outrigger and peripheral columns is assumed to be hinged, so that columns are only subjected to axial forces and do not reduce the shear forces in the central core. The optimum height for the outrigger is determined in the SLS, since horizontal deflection is the main design criteria in this stage. The optimum outrigger location is determined by the structural parameters, ω and βH and a design graph in [6], as elaborated in C.S.2.3. This height is a dependant on the flexural stiffness of the central core and outriggers and on the axial stiffness of the columns.

Table 3.2; Overview of structural static design of tube structure



Facts:
 Stability system CLT tube structure (CLT core is neglected); 27 x 27 m
 Structural materials CLT; d=300 mm, ±C24 (KLH GmbH), Glulam; GL 28h
 Calculation method CLT properties; Composite Theory
 Fenestrated wall; "A Simple Method of Analysis for Deflection and Stresses in Wall – Frame Structures" after Khan & Stafford Smith

Loading (C.S.2.1):

Lateral design load	$W_{e,total} / W_{e,total,d}$	41.6 / 62.4 kN/m (SLS / ULS)
Vertical design load	Q_d	10 kN/m ²

Requirements:

Max. horizontal deflection	U_{max}	$H/800 = 67\ 200/800 = 84$ mm
----------------------------	-----------	-------------------------------

Results SLS & ULS (C.S.2.1):

Composition factor	k_3	0.81	-
Max. horizontal deflection	$U_{top,max}$	77.4	mm
Bending moment in tube due to wind	$M_{b,t,d}$	140 826.5	kNm
Normal stress in column due to bending	$\sigma_{n,b,d}$	2.01	MPa.
Normal stress in column due to vertical loading	$\sigma_{n,q,d}$	3.14	MPa.
Max. normal stress in column	$\sigma_{n,max,d}$	5.15	MPa.
Min. normal stress in column	$\sigma_{n,min,d}$	1.12	MPa.
Shear stress in column due to wind	τ_d	1.10	MPa.

Table 3.3; Overview of structural static design of shear wall structure

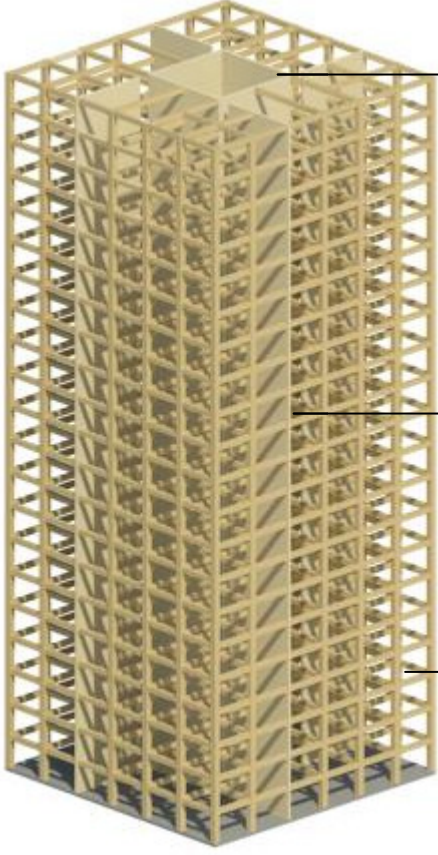
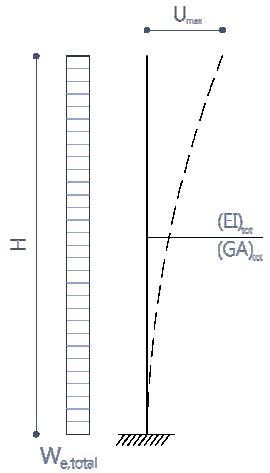
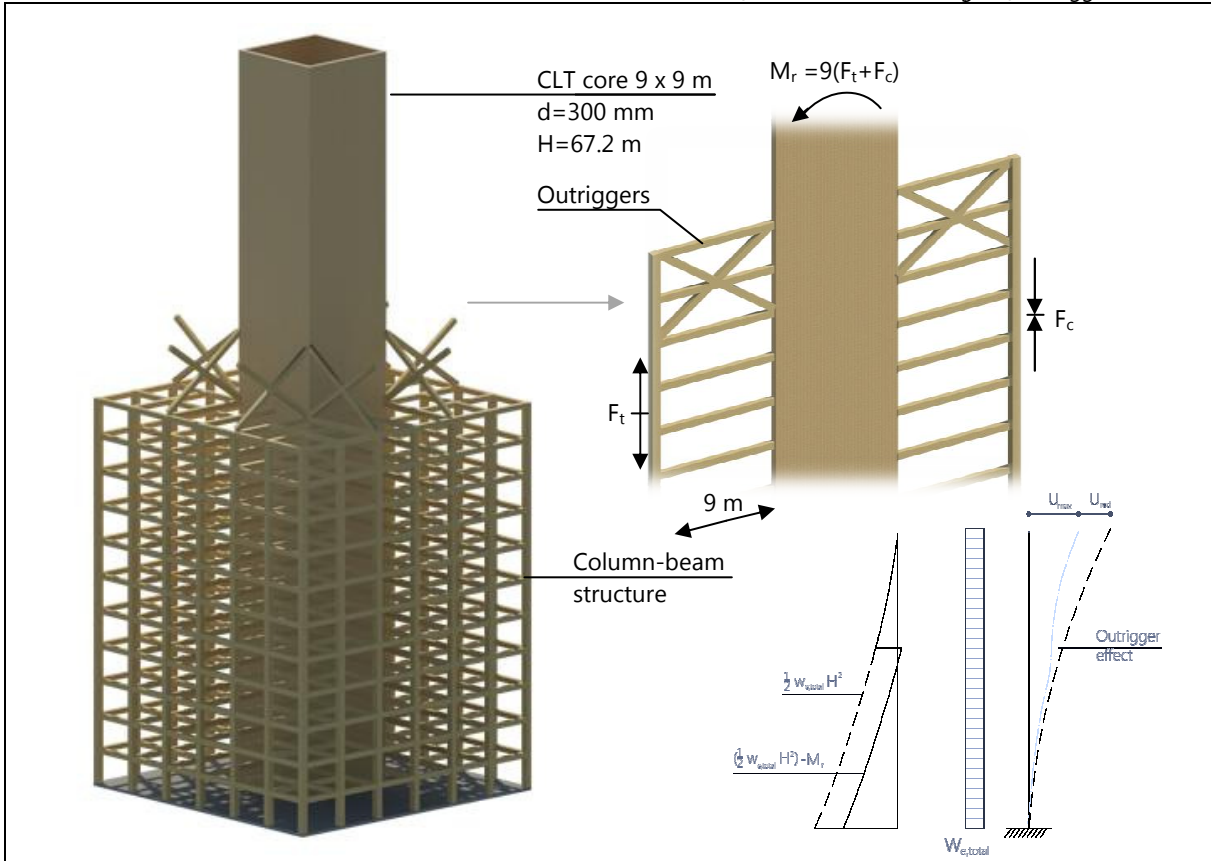
			
			
$(EI)_{tot} = (EI)_{core} + 2(EI)_{shwall}$ $(GA)_{tot} = (GA)_{core} + 2(GA)_{shwall}$			
$U_{max} = \frac{w_{e,tot} H^4}{8(EI)_{tot}} + \frac{w_{e,tot} H^2}{2(GA)_{tot}}$			
Facts:			
Stability system	CLT core; 9 x 9 m, 4 x CLT shear walls; L = 7.6 m		
Structural materials	CLT; d=300 mm, ±C24 (KLH GmbH), Glulam; GL 28h		
Calculation method	CLT properties; Composite Theory		
Loading: (C.S.2.2):			
Lateral design load	$w_{e,tot} / w_{e,tot,d}$	41.6 / 62.4 kN/m (SLS / ULS)	
Vertical design load	q_d	10 kN/m ²	
Requirements:			
Max. horizontal deflection	U_{max}	$H/800 = 67\,200/800 = 84$ mm	
Results SLS & ULS: (C.S.2.2):			
Composition factor	k_3	0.81	-
Max. horizontal deflection	$U_{top,max}$	88.4	mm
Bending moment in core due to wind	$M_{b,c,d}$	120 729.9	kNm
Bending moment in shear wall due to wind	$M_{b,sw,d}$	10 048.3	kNm
Normal stress in core due to bending	$\sigma_{n,b,c,d}$	5.11	MPa.
Normal stress in shear wall due to bending	$\sigma_{n,b,sw,d}$	4.32	MPa.
Max. normal stress in core, incl. vertical load	$\sigma_{n,max,c,d}$	10.89	MPa.
Min. normal stress in core, incl. vertical load	$\sigma_{n,min,c,d}$	0.66	MPa.
Max. normal stress in shear wall, incl. vertical load	$\sigma_{n,max,sw,d}$	6.16	MPa.
Min. normal stress in shear wall, incl. vertical load	$\sigma_{n,min,sw,d}$	-2.47	MPa.
Shear stress in core due to wind	$\tau_{c,d}$	0.42	MPa.
Shear stress in shear wall due to wind	$\tau_{sw,d}$	0.42	MPa.

Table 3.4; Overview of structural static design of outrigger structure



Facts:

Stability system	CLT core; 9 x 9 m, glulam outriggers; X-bracing two storey high
Structural materials	CLT; d=300 mm, ±C24 (KLH GmbH), Glulam; GL 28h
Calculation method	CLT properties; Composite Theory Outriggers; compatibility equation around neutral axes of outrigger and CLT core

Loading: (C.S.2.3):

Lateral design load	$W_{e,total} / W_{e,total,d}$	41.6 / 62.4 kN/m (SLS / ULS)
Vertical design load	Q_d	10 kN/m ²

Requirements:

Max. horizontal deflection	U_{max}	$H/800 = 67\ 200/800 = 84$ mm
----------------------------	-----------	-------------------------------

Results SLS & ULS: (C.S.2.3):

Composition factor	k_3	0.81	-
Max. horizontal deflection	$U_{top,max}$	75.3	mm
Total reduction in hor. deflection due to outrigger	$U_{top,red,total}$	39.4	mm
Optimum outrigger height SLS	x_0	28.2	m
Restraining moment due to outriggers ULS	M_r	35 546.7	kNm
Bending moment in core due to wind ULS	$M_{b,c,d}$	140 826.5	kNm
Normal stress in core due to bending	$\sigma_{n,b,d}$	4.46	MPa.
Normal stress in core due to vertical loading	$\sigma_{n,q,d}$	7.70	MPa.
Max. normal stress in core	$\sigma_{n,max,d}$	12.16	MPa.
Min. normal stress in core	$\sigma_{n,min,d}$	3.24	MPa.
Shear stress in core due to wind	$\tau_{c,d}$	0.78	MPa.
Compressive stress in column due to wind	$\sigma_{c,F,d}$	3.66	MPa.
Compressive stress in column due to vertical loading	$\sigma_{c,q,d}$	11.25	MPa.
Max. compressive stress in column	$\sigma_{c,max,d}$	14.91	MPa.
Min. compressive stress in column	$\sigma_{c,min,d}$	7.59	MPa.

3.5 REFLECTION ON RESULTS

Tube structure

Utilisation of the whole building depth appears to be beneficial to resist lateral wind loading. Regarding to horizontal displacements, the racking shear stiffness is that low it carries for the most amount of deformations (70 mm due to shear and 7 mm due to bending, as shown in C.S.2.1). Usually for shear walls bending deformations are superior, but the layout of the tube seems to result more or less as the behaviour of a shear frame structure. Nevertheless, the maximum horizontal displacement complies with the design value of 84 millimetres. In order to increase the tube's stiffness dimensions of wall openings should be reduced, hence increasing racking shear stiffness most effectively. Stresses in the CLT panels are negligible due to both the large depth of the structure and the total cross sectional area of the tube, with exception of shear stresses in wall columns on the ground floor. These shear stresses are likely to exceed the design value for shear strength and can be decreased by increasing the wall thickness and/or decreasing the width of wall openings.

Shear wall structure

The design of this structure is limited to available space for shear walls in the building. One of the significant consequences is the increased stress in both the central core and shear walls. For the shear walls, this results in uplifting forces, which may be even further increased due to unfavourable vertical loading. Due to uncoupling of the central core structure and adjacent shear walls structural stiffness is relatively low resulting in exceedance of the design value for horizontal displacement by 4 millimetres.

Outrigger structure

The outriggers, located on the 12th storey, effectively reduce the horizontal displacement of the whole building to a permissible value of 75.3 millimetres. Besides, the restraining moment due to axial forces in the peripheral columns results in reduced uplifting forces in the main structure. However, it should be noted that the central core is subjected to a larger floor area, and thus vertical load, due to absence of adjacent load-bearing shear walls. Therefore, the maximum compressive stresses in the core are slightly higher. Unfavourable actions of vertical loading, however, could result in uplifting forces in the core.

Comparison of the results

In the preliminary design phase, the performance of stability systems for tall buildings is usually classified according to their lateral stiffness. Therefore, the single most important design criterion is the horizontal displacement at the top of the building. The graph in Figure 3.5 shows the horizontal displacements over the height of the building of each structural system. The effect of the outriggers on the deformation mode is shown on a height between 30 and 40 meters (i.e. 12th floor), where the trusses reduce horizontal deflections both below and above their position.

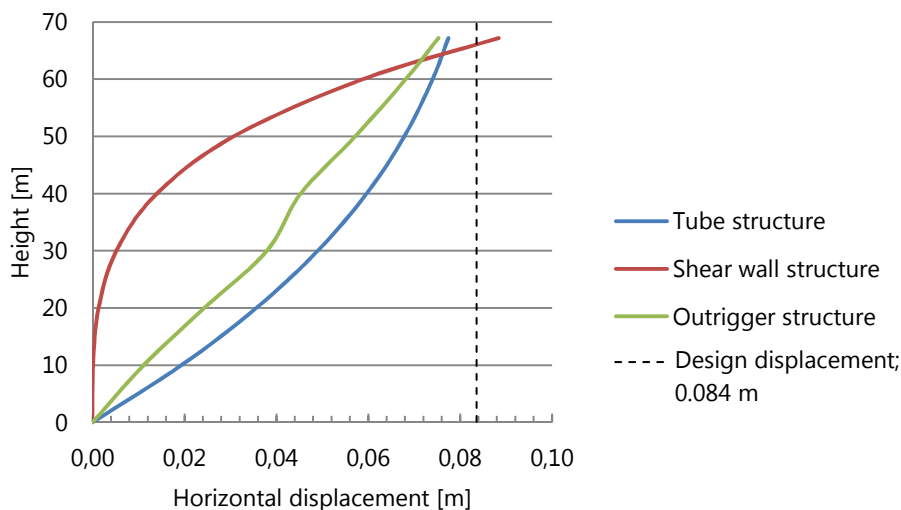


Figure 3.5; Horizontal deformation modes of structural systems

3.6 DESIGN OF OUTRIGGER STRUCTURE

Design on strength

Preliminary structural calculations include evaluations of some specific loading actions in structural elements. For instance, compressive stresses in CLT walls or stresses in the peripheral columns of the outrigger structure are relevant structural actions which are desired to be known by the engineer in an early design phase. Table 3.5 presents the values of governing loading actions and the corresponding checks on strength according to EC5 [10]. It should once more be emphasised that only critical structural elements are checked on their design stresses, where for instance instability effects are excluded. The performance of beams will be analysed in the final design phase.

Table 3.5; Check on strength of critical structural elements in outrigger structure

Loading action	Loading value	Design value	Check
Compressive stress CLT core	$\sigma_{n,max,d} = 12.16$ MPa.	$(f_{c,0,k}k_3k_{mod}) / \gamma_M$ $(24 \cdot 0.81 \cdot 0.9)/1.25 = 13.93$ MPa.	$\sigma_{n,max,d} \leq f_{c,0,d}$ $12.16 < 13.93$
Compressive stress perimeter column	$\sigma_{c,max,d} = 14.91$ MPa.	$(f_{c,0,g,k}k_{mod}) / \gamma_M$ $(26.5 \cdot 0.9)/1.25 = 19.08$ MPa.	$\sigma_{c,max,d} \leq f_{c,0,g,d}$ $14.91 < 19.08$

The validity of the loading values is in any case questionable, since the assumption of 10 kN/m² for vertical loading is quite conservative, i.e. upper bound value. In addition, the summation of stresses due to bending and vertical loading is also unlikely to result in governing stresses, since for design of vertical structural elements in multi-storey buildings the imposed loading should be multiplied by a reduction factor, α_n , in accordance with EC1 [11]. The presented simple verifications on strength properties in the table above shows that it can be expected that deformations will turn out to be governing in the design above strength, which is common in structural timber design.

Design alternatives

Various adjustments to the structural system are possible to enhance the structural performances in either the SLS or ULS. For the initial outrigger structural design the elements in the structural system, in accordance with C.S.2.3, are summarised in Table 3.6.

Table 3.6; Basic design of the outrigger structure

Structural element	Function	Dimensions	Properties
CLT central core	Lateral stability/load-bearing	Thickness; d=300 mm	C24, $k_3 = 0.81$
Outriggers	Lateral stability	Beams; 500 x 400 mm Columns; 600 x 600 mm Diagonals; 500 x 400 mm	Glulam GL 28h
Columns	Vertical load-bearing	600 x 600 mm	Glulam GL 28h
Beams	Vertical load-bearing	500 x 400 mm	Glulam GL 28h

In order to increase the stiffness in the structure, either the core or the outriggers can be redesigned, for which the latter both beams and diagonals can be modified. On the other hand, a more flexible design of trusses with respect to architectural purposes is desired to decrease the number of diagonals or to adopt a different plan design. For comparison, several modifications are recalculated in C.S.2.3a-d, shown in Appendix A.2. The results are summarised in Table 3.7.

Table 3.7; Modifications for structural stiffness of the outrigger structure

Modification	Horizontal displacement	Maximum stress [MPa.]
CLT core wall thickness to 410 mm	59.5 mm (-15.8 mm)	CLT wall: $\sigma_{n,b,c,d} = 3.55$ (-0.91) CLT wall: $\sigma_{n,max,c,d} = 9.39$ (-2.77)
Outrigger beams/diagonals to 600x600 mm + GL 32h	72.4 mm (-2.9 mm)	No difference $\rightarrow \leq 0.3$
Peripheral columns to 700x700 mm + GL 32h	73.2 mm (-2.1 mm)	Column: $\sigma_{c,F,d} = 2.83$ (-0.83) Column: $\sigma_{c,max,d} = 11.09$ (-3.82)
Outrigger diagonals to 2 x N-bracing	80.8 mm (+5.5 mm)	No difference $\rightarrow \leq 0.6$

Some remarkable occurrences can be noted in the results of modifications to the outrigger structure. Modifications to glulam beams, diagonals and/or columns show little gains in enhancing the stiffness of the stability system. It becomes apparent that increasing the core stiffness by increasing the wall thickness to 410 millimetres is the most effective modification for enhancing overall stiffness of the structure. With regard to two N-bracings for the outriggers instead of one X-bracing, hand calculations in C.S.2.3d show that the racking shear stiffness is highly reduced, affecting the restraining moment negatively and therefore reducing the overall stiffness of the structure.

3.7 PRELIMINARY STATIC DESIGN

Alterations to the basic outrigger structural design gained more insight in the behaviour of such a system subjected to lateral wind loading. Besides, it proved that the basic design performed quite effectively. Nevertheless, the benefits from fewer diagonals in the trusses on the 11th to the 13th floor are obvious regarding to architectural flexibility. X-bracing diagonals over two floors hinder the escape route adjacent to the central core and will create humungous difficulties in fitting architectural plans on these floors. N-bracing instead, provides more flexibility for the design of rooms as well as routes to vertical transport facilities. Therefore, this modification will be adopted in the preliminary static design, in spite of the reduced structural stiffness.

Plan

A typical structural plan of the preliminary design is shown in Figure 3.6. In the original architectural plan columns were designed with a distance of 9 meters, i.e. two grids. An additional column in-between not only reduces the compressive stresses in the columns but also makes a more efficient floor span design possible in order to reduce vertical loads on beams. Moreover, the span between central core and building's perimeter of 9 meters may be critical with regard to beam design. However, it is highly desired from the architect's point of view to maintain the free space between the core and façade. Therefore, floor spans are designed to circumvent large loads on the beams. On the other hand, a free span of 9 meters for a timber floor may be critical with respect to deflections and vibrations. CLT cassette floors, however, should be capable to carry the subjecting loads and perform well in serviceability conditions.

Openings in the central core will in any case reduce the lateral stiffness of the structure, which is not taken into account in the preliminary structural calculations. For compensation, also the partition wall between the two staircases is designed in CLT.

Sections

Cross sections over the building are shown in Figure 3.8 and 3.9, where the optimum height of the outriggers is located on the 12th floor, i.e. 38.4 meters. Prior to structural analyses, it was expected that the optimum height for outriggers will be found at approximately; $2/3H$, which is 44.8 meters. Apparently, the stiffness ratios of the; central core, outriggers and peripheral columns carry for a lower

value of ω (see C.S.2.3d), which results in a larger distance x_0 . By increasing the stiffness of the central core, ω increases, resulting in a smaller distance x_0 accordingly. Besides, it was concluded after the alterations to the initial design that by increasing the wall thickness of the core a higher stiffness of the overall stability system is gained most effectively. Therefore it might be necessary to implement an increased wall thickness for the core in later design analyses to increase the structural stiffness.

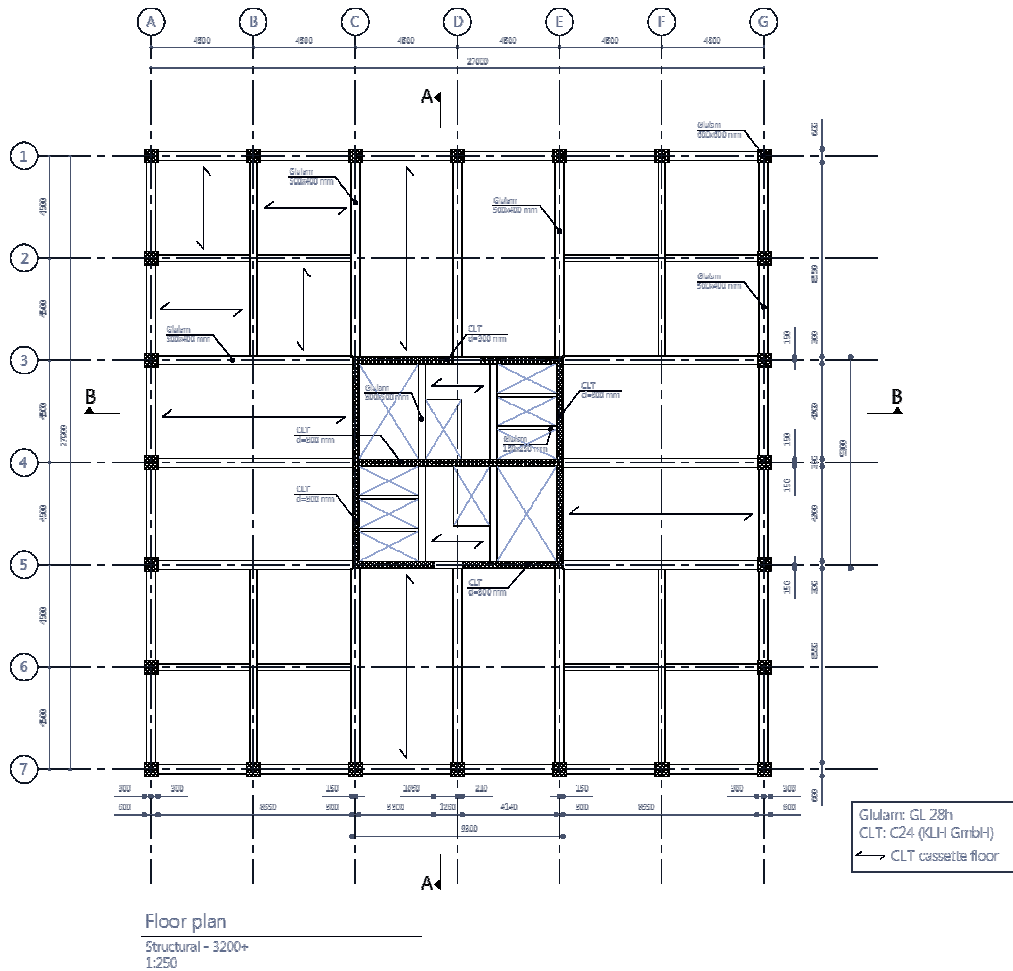


Figure 3.6; Preliminary structural typical plan

3D Impressions

In order to clarify the proposed structural design a 3D impression is shown in Figure 3.7.

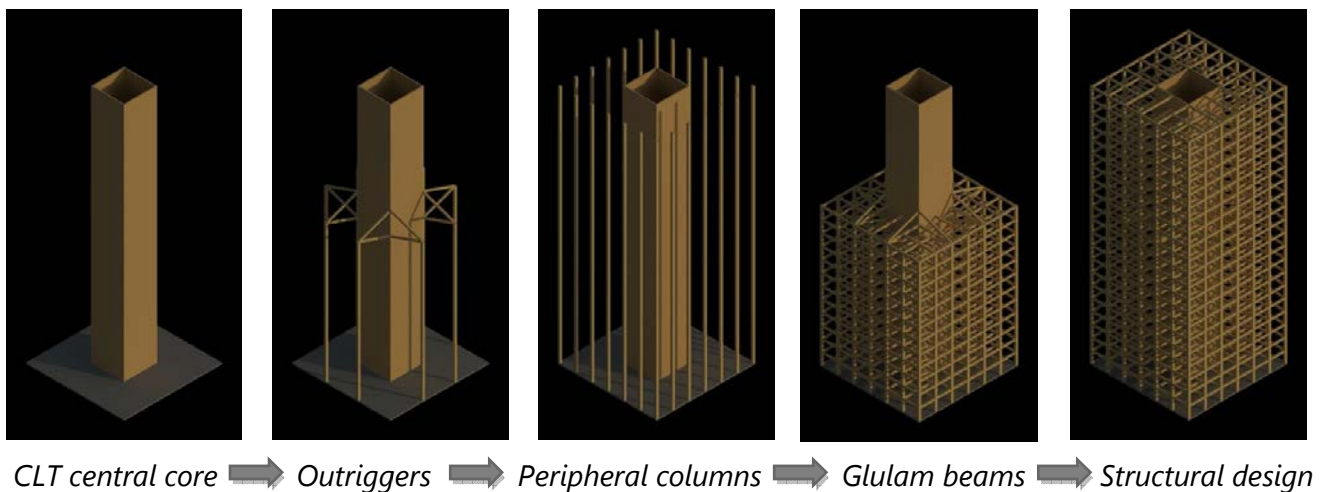


Figure 3.7; Build-up of the structural design

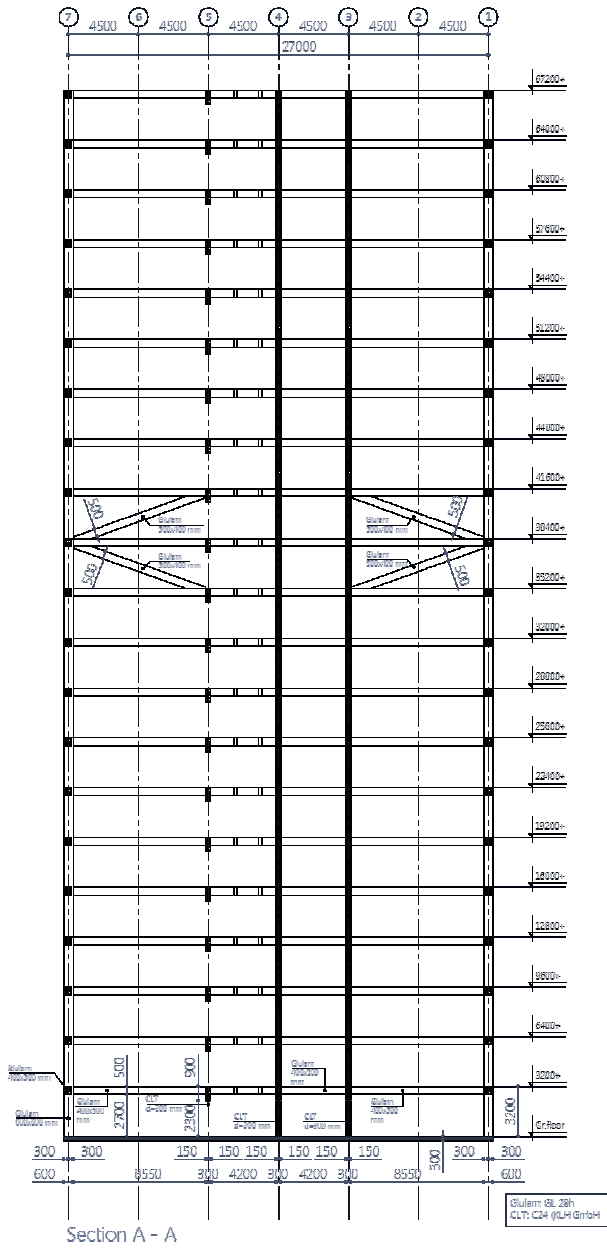


Figure 3.8; Structural design – Section A – A

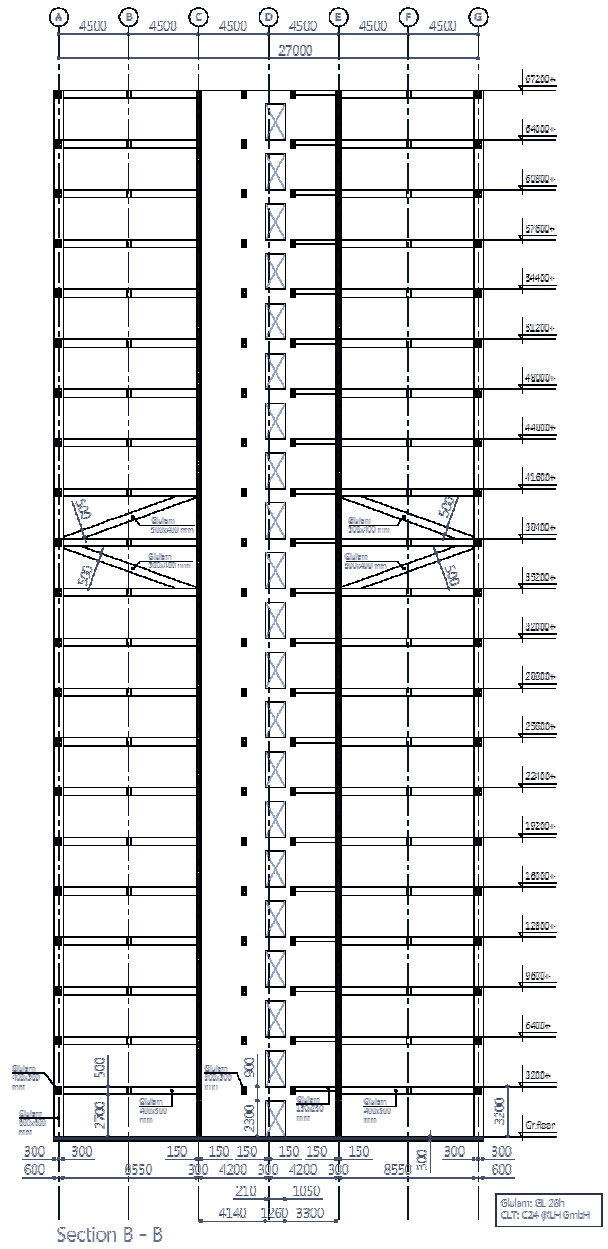


Figure 3.9; Structural design – Section B - B

3.8 CONCLUSIONS ON STATIC DESIGN

The structural analyses carried out in this chapter have shown the behaviour under static loading of several structural timber systems for a twenty-storey building. The final design proposal has proven to be capable to resist both lateral and vertical loading. Conclusions relevant for analyses in the upcoming chapter are as follows

- Horizontal displacements comply with $H/800$, which is adopted for preliminary design;
- Uplifting forces in the central core may occur at loading combinations according to EC0, but is not expected to cause significant design problems;
- In order to increase the structural stiffness, most effectively the central core should be modified through increasing the wall thickness.

APPENDIX: 30 STOREY BUILDING

An increment of 10 storeys to the proposed structural design would obviously result in larger horizontal deflections, but adding a second outrigger to the structure may compensate for the higher displacements due to lateral wind loading. As a starting point, two outriggers will be deployed at $1/3$ and $2/3$ of the building's height respectively, as shown in Figure 3.10. The characteristic wind load, $w_{e,total}$, is approximated on 2 kN/m^2 .

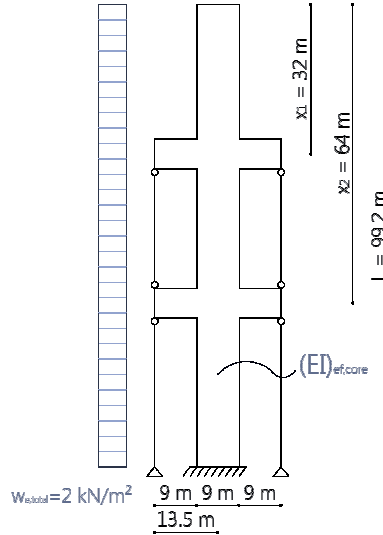


Figure 3.10; Illustration of structural model of 30 storey building

The calculation method is slightly different for two outriggers, although it is still based on the compatibility of rotations at the intersection of neutral axes of the central core and outriggers. In addition, racking shear influences are omitted from the equation. The full derivation of the compatibility equation is presented in [12].

The horizontal displacement at the top of the structure is calculated in a similar fashion as presented by equation 3.2 and is written as

$$U_{top,max} = \frac{w_{e,total}H^4}{8(EI)_{ef,core}} - \frac{1}{2(EI)_{ef,core}} \left[M_{r,1}(H^2 - x_1^2) + M_{r,2}(H^2 - x_2^2) \right] \quad (3.12)$$

where $M_{r,1}$ and $M_{r,2}$ are the restraining moments induced by the outriggers to the core at height x_1 and x_2 respectively. Further modifications to the structure are conducted at the central core ($d = 500 \text{ mm}$) and the peripheral columns ($A_b = 700 \times 700 \text{ mm}$). The calculations are presented in C.S.2.4 (Appendix A.2). The displacement at the top is evaluated on

$$U_{top,max} = 0.176 \text{ meters}$$

which is within a permissible deflection of $H/500$ ($= 0.198$ meters), but exceeds the design value for preliminary design, i.e. $H/800$ ($= 0.124$ meters).

Evaluation of stresses in the ULS is not conducted, since the accuracy in the preliminary design stage has already been defined as questionable due to the absence of loading combinations for design values compiled with EC0. However, it can already be stated that dimensions of structural elements may become that large, that reality of such buildings in practice might be doubtful.

4 | PRELIMINARY DYNAMIC DESIGN

Wind effects on a low-weight tall timber building

A structural dynamic design is largely benefitted by a thorough assessment of the behaviour under dynamic loading, starting with simplified models and estimations of the fundamental natural frequency up till an accurate simulation of the structure by a FEM computer model. During this process the static structural design will be modified when needed. However, the accuracy of design methods will be taken into account to determine whether modifications on the structural design are desired.

For the sake of clarity, a dynamic design process should be narrowed down to essential analyses of the structural behaviour characteristic for the design. In this case it means that

- The type of excitation to the structure is limited to alongside wind loading consisting of non-periodic loading as will be defined by spectral analysis;
- Any type of nonlinearity will be excluded in the analysis. The structure is assumed to behave linear under dynamic wind loading;
- Earthquake analysis and excitations are excluded, for which a nonlinear analysis is more appropriate.

During the design process a strategy as presented in Figure 4.1 will be adopted, which should; enhance the process as well as maintain overview during the different steps.

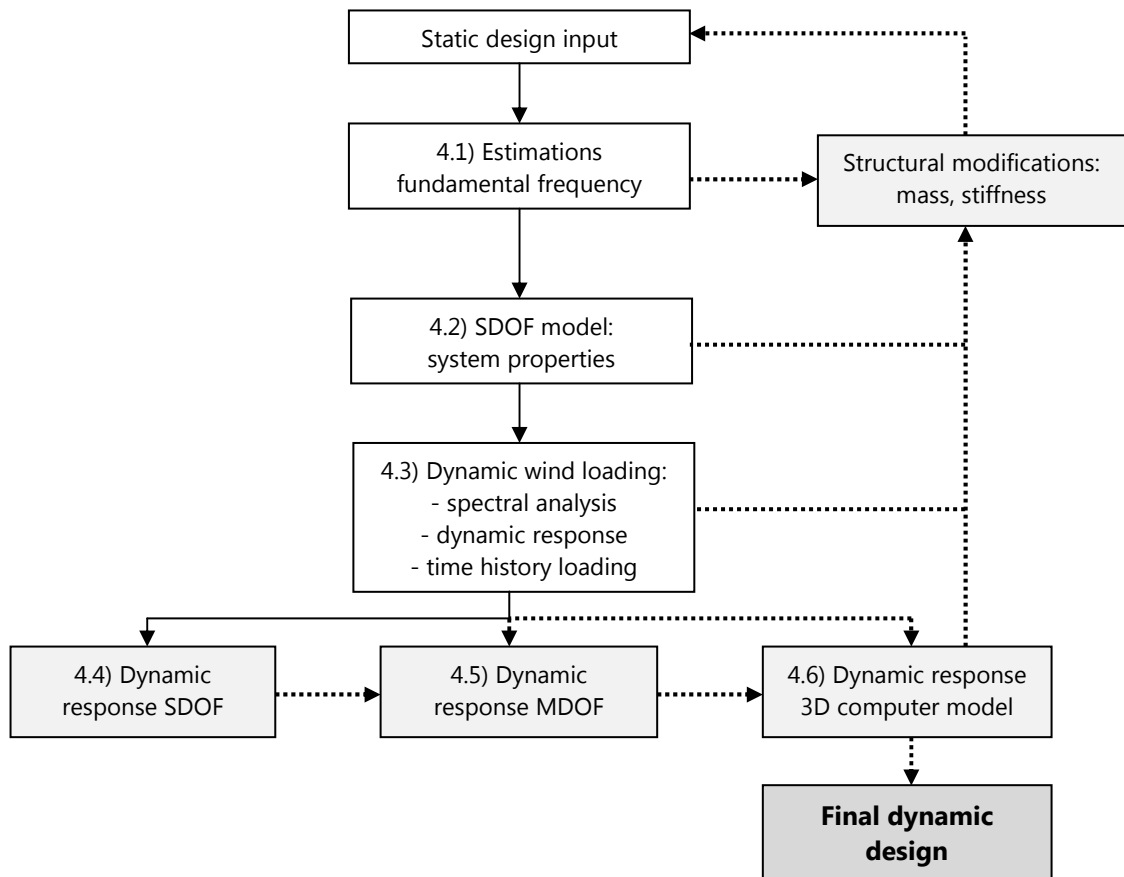


Figure 4.1: Strategy diagram for dynamic analysis

4.1 ESTIMATION OF THE FUNDAMENTAL FREQUENCY

An impression of the structural behaviour under dynamic loading in the first stages of the design process is predominantly obtained by estimations of the fundamental frequency, i.e. first natural frequency. In the literature many simplified methods are proposed in order to improve the accuracy of the estimation by taking into account both structural behaviour and mode shape.

Here, three methods are adopted consisting of a very simple approximation and more comprehensive methods, for which the accuracy is expected to improve accordingly.

Estimated fundamental frequency by Ellis, B.R.

A common approximation of the fundamental frequency for buildings [4] [6], which enables the structural designer to indicate the structural performance in a very early design stage, is proposed by Ellis, B.R. as follows

$$n_1 = \frac{46}{H} \quad (4.1)$$

where n_1 is the fundamental frequency in Hertz and H is the building height in meters.

It must be noted that this formula is based on fundamental frequencies of tall buildings designed with concrete or steel structures, which clearly differs from timber with respect to structural mass.

Fixed strut approximation

In the case of tall and/or slender buildings many structural engineers start their design process to simulate the structure as a single fixed strut in order to estimate horizontal displacements under static loading (see cantilever beam theory in the previous chapter). This method can also be adopted in the dynamic design process to incorporate structural properties such as the structural stiffness and mass. A continuous column, as depicted in Figure 4.2, with uniformly distributed properties is assumed resulting in a homogenous solution of the equation of motion. Therefore the influence of outriggers on the lateral stiffness is neglected, so that the result is expected to be rather on the conservative side. On the other hand, rotations of foundation structures is neglected which may cause a unconservative approximation.

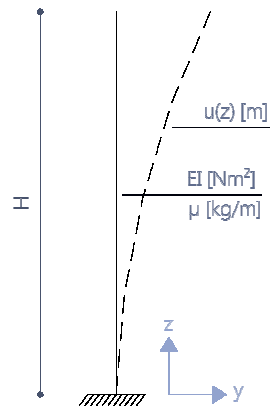


Figure 4.2; Fixed strut approach for estimation of fundamental frequency

An fundamental frequency of the fixed strut above can be obtained by the Rayleigh method [13]. This method is based on the Rayleigh's quotient, ω^2 , which expresses the equality of the maximum strain- and kinetic energy for undamped free vibrations. The maximum strain energy can be deduced from the fact that the stored energy must be equal to the work done by the applied load, thus

$$V_{\max} = \frac{1}{2} \int_0^H q(z) u(z) dz = \frac{1}{2} g \int_0^H m(z) u(z) dz \quad (4.2)$$

where the applied loading $q(z)$ is merely the weight of the structure¹, which can be expressed as

$$q(z) = g m(z) \quad (4.3)$$

in which g is the acceleration of gravity and $m(z)$ is the mass distribution². The displacement function is represented by $u(z)$, as depicted in Figure 4.2. Maximum kinetic energy of the system is given by

$$T_{\max} = \frac{1}{2} \omega^2 \int_0^H m(z) u(z)^2 dz \quad (4.4)$$

The squared circular frequency ω^2 , i.e. Rayleigh's quotient, can now be determined by equating the maximum strain- and kinetic energy as follows

¹ Note that for this purpose the gravity acts horizontally, as shown in the mode shape of Figure 4.2

² Some national codes allow for incorporation of imposed loading, e.g. the national code of Australia [14], which allow an addition of $0.4 \times Q_k$. EC0, however, does not refer to this opportunity so that mass evaluations solely consist of the self weight of structural elements.

$$\omega^2 = g \frac{\int_0^H m(z) u(z) dz}{\int_0^H m(z) u(z)^2 dz} \quad (4.5)$$

where a displacement function $u(z)$ for a distributed load, $q(z)$, can be approximated as

$$u(z) = \frac{mgH^4}{8EI} \left(1 - \frac{4z}{3H} + \frac{z^4}{3H^4} \right) \quad (4.6)$$

Substitution of the displacement function in equation 4.5 results in a Rayleigh's quotient equal to

$$\omega^2 = g \frac{\int_0^H m(z) u(z) dz}{\int_0^H m(z) u(z)^2 dz} = \frac{162EI}{13\mu H^4}$$

where μ is mass per meter height in [kg/m]. The fundamental frequency of the fixed strut becomes

$$n_1 = \frac{3.52}{2\pi} \sqrt{\frac{EI}{\mu H^4}} \quad (4.7)$$

where frequency n_1 can be deduced from the circular frequency, ω_1 , as follows

$$n_1 = \frac{\omega_1}{2\pi} \quad (4.8)$$

Method by 'van Oosterhout'

In order to take into account the racking shear influence of the structure, and thus outrigger effects, the presented method by 'van Oosterhout' [15] is expected to give the most accurate results. The fundamental natural frequency is given by

$$n_1 = f(\alpha H) \sqrt{\frac{w_{e,total}}{m} \cdot \frac{H}{U_{max}}} \quad (4.9)$$

where $w_{e,total}$ is the uniformly distributed characteristic quasi-static wind load, m is the total mass of the structure and U_{max} the maximum horizontal displacement due to static loading. It can be seen in equation 4.9 that a concentrated force, $w_{e,total}H$, assumed at the top of the structure is divided by the maximum displacement on the same position. As a result, a structural stiffness k is obtained so that the second term can be seen as the circular frequency, because

$$\omega = \sqrt{\frac{k}{m}} \quad (4.10)$$

The factor $f(\alpha h)$ accounts for the shape mode of the structure, where

$$\alpha^2 = \frac{(GA)_{total}}{(EI)_{total}} \quad (4.11)$$

The total racking shear- and total bending stiffness of the structure is represented by the sum of the central core and the outrigger structure. A comprehensive derivation of function, $f(\alpha H)$, is presented by van Oosterhout [15], which is written as

$$f(\alpha H) = \sqrt{\left[\frac{0.2365}{(\alpha H - 0.3)^{1.22}} + \frac{1}{16} \right] \left[\frac{-1 - \alpha H \cdot \sinh \alpha H + \cosh \alpha H}{(\alpha H)^2 \cosh \alpha H} + \frac{1}{2} \right]} \quad (4.12)$$

Overview of results

Table 4.1 summarises the estimated fundamental frequency of the structure evaluated by aforementioned calculation methods. Elaboration of the values is shown in C.S.3.1.

Table 4.1; Overview of estimated fundamental frequencies

Method	Relevant values	Result [Hz.]
Ellis	H = 67.2 meter	0.68
Fixed strut (without outriggers)	(EI) _{ef,core} = 1.276 · 10 ⁹ kNm ² ρ _{mean} = 90 kg/m ³ μ = 65 610 kg/m	0.55
van Oosterhout (with outriggers)	f(αH) = 0.188 m = 4 408 992 kg U _{max} = 0.0808 m	0.53

The over-estimated natural frequency of the former method was already predicted due to volumetric mass differences between steel/concrete and timber.

The latter two are based on the same principle, but the method by 'van Oosterhout' should give a more accurate estimation since both mode shape and outriggers are taken into account. In the case of pure bending, i.e. $GA = \infty$, $f(\alpha H)$ equals 0.198, whilst for pure shear $f(\alpha H)$ yields 0.176. The result in Table 4.1 shows that the system behaves in combined bending and shear, which also can be seen in the static mode shape of Figure 3.5.

For pure bending the frequency according to 'van Oosterhout' is 0.55 Hz., which is equal to the fixed strut result. This is remarkable because the introduction of ratio H/U_{max} takes into account the overall structural stiffness and thus contribution of the outriggers. Hence, when omitting contribution of the outriggers in equation 4.9 and assuming full bending, i.e. $f(\alpha H)$ equal to 0.198, the fundamental frequency will yield a lower value than 0.55 Hz. which is the result of equation 4.7. Therefore, the accuracy of 'van Oosterhout's' derivation of the fundamental frequency for structures acting in combined bending and shear seems to be doubtful.

Anyhow a fundamental frequency of 0.53 Hz., being a lower bound of estimations above, will be adopted as a starting point for subsequent analyses. The more frequently used frequency for structures is the circular frequency and can be calculated as follows

$$\omega_1 = 2\pi\eta_1 \quad (4.13)$$

This results in a circular natural frequency of ω_1 equal to 3.33 rad/s.

4.2 SINGLE DEGREE OF FREEDOM SYSTEM

Modal analysis of a dynamic problem is the most frequent adopted technique in a preliminary design phase for structures. Modal analysis can be either conducted by a single degree of freedom (SDOF) -

or a multi degree of freedom (MDOF) system. A SDOF system is characterised by a single rotation or displacement of a single node. As a consequence, there is only one single mode shape, i.e. a specific shape of a structure during vibration at a specific natural frequency. Since multiple mode shapes are usually possible, a structure has an equal amount of natural frequencies. Anyhow, a SDOF system only allows analysis of the first natural frequency, or fundamental frequency.

Structural properties of a SDOF system

A SDOF system is the simplest simulation to approximate the dynamic response of a structure. A degree of freedom in modal analysis is a single translation or rotation of a lumped mass in a system. Although this approach allows a quick analysis of the dynamic problem it contains certain restrictions to the system, which are

- Nonlinearities in the structural system are not allowed;
- The mass is simulated as a concentrated mass to obtain a one degree-of-freedom system;
- One degree of freedom means that only the fundamental mode can be analysed;
- Linear dynamic behaviour is assumed, which means that structural properties are independent on the response of the modal analysis;
- The SDOF system is energy equivalent to the structure in the response mode [16].

Translation of a structure to a SDOF system is conducted in several steps, which are as follows

1. Representation of the structure as a continuous structural model;
2. Simulation of a SDOF system on the basis of the continuous structural model in a *non-equivalent SDOF model*;
3. Translation of structural properties and loading to an *equivalent SDOF model*.

In the previous section it has been explained that outriggers carry for a discontinue stiffness of the structure, so that in order to comply with the first step the stiffness has to be approximated uniform over the height of the building. As a starting point the fixed strut shown in Figure 4.3 is adopted. The maximum horizontal displacement, U_{max} , is caused by an equally distributed quasi-static wind load as illustrated in the figure below.

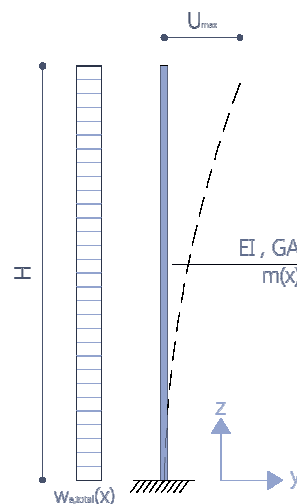


Figure 4.3; *Approximated structural model with continuous properties*

The second step is to simulate a non-equivalent SDOF model by adjusting structural properties of the continuous model [16]. The equally distributed load is assumed as a concentrated load at the top of the structure as follows

$$F = \int_0^H w_{e,total}(z) dz = w_{e,total} H \quad (4.14)$$

In order to comply with the second restriction stated above, the lumped mass at the top becomes

$$m = m(H) = \mu H \quad (4.15)$$

where μ is the mass per meter height of the structure.

Stiffness property, k , of the continuous model can be calculated by the assumption of a concentrated load, i.e. equation 4.14, as follows

$$k = \frac{F}{U_{max}} \quad (4.16)$$

By implementation of horizontal displacement, U_{max} , evaluated by equation 3.2 the contribution of the outriggers is taken into account. However, it must be noted that the deformation mode shown in Figure 3.5 is not resembled exactly due to the assumption of continuous properties; hence the adopted model is an approximation. The non-equivalent SDOF model is shown in Figure 4.4.

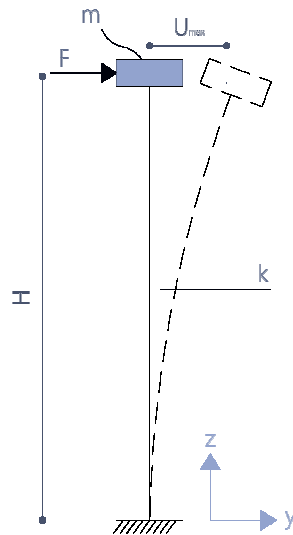


Figure 4.4; Non-equivalent SDOF model

The third step is related to the last restriction defined above, where equivalent properties of the structural system, i.e. m_{eq} , k_{eq} and F_{eq} , should be obtained from calculated properties in Figure 4.4. The equivalent mass at the top of the structure, m_{eq} , can be calculated from the distributed mass, shown in Figure 4.3, by assuming that both have the same *kinetic energy*.

The stiffness of the column can be made equivalent to the bending- and shear stiffness of the structure by assuming that both have the same *strain energy*.

An equivalent load, F_{eq} , can be determined from the uniformly distributed wind load by the assumption that the *work* done by both forces are equal.

The non-equivalent SDOF model modifies to a SDOF model with equivalent properties to the continuous model as shown in Figure 4.5.

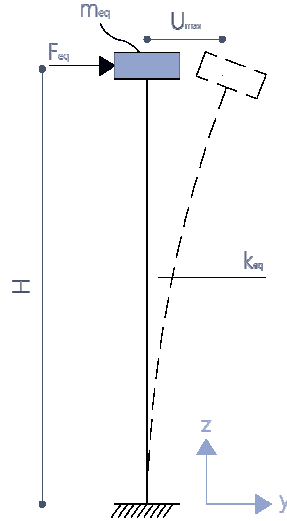


Figure 4.5; Equivalent SDOF model

The equivalences of energy between the continuous model and SDOF model gives rise to conversion factors [16], k_M , k_R , k_L , for the mass, stiffness (resistance) and loading respectively. Since both, non-equivalent and equivalent, systems should have the same static displacement

$$U_{\max} = \frac{F_{eq}}{k_{eq}} = \frac{k_L F}{k_R k} = \frac{F}{k} \rightarrow k_L = k_R \quad (4.17)$$

This means that the evaluation of the loading and the mass (k_M) conversion factor is sufficient in order to obtain an equivalent SDOF system. Thus with respect to the circular natural frequency of the first mode it can be concluded that

$$\omega_1 = \sqrt{\frac{k_{eq}}{m_{eq}}} = \sqrt{\frac{k_L k}{k_M m}} = \sqrt{\frac{k}{k_{LM} m}} \quad (4.18)$$

where k_{LM} is a load-mass conversion factor, expressed as

$$k_{LM} = \frac{k_M}{k_L} \quad (4.19)$$

The evaluation of the load-mass factor is depending on the slenderness of the structure, and thus whether shear deformation should be taken into account. In the case of an outrigger structure, shear deformation cannot be neglected³. Hence a Timoshenko, non-slender, beam is considered, wherein both geometrical- and material properties influence the load-mass conversion factor. The slenderness ratio and material property of a Timoshenko beam are as follows [16] [17]

$$s^2 = \frac{H^2 A_{core}}{I_{core}} \quad \gamma^2 = \frac{E}{G} = \frac{2(1+\nu)}{k'} \quad (4.20)$$

where ν is Poisson's ratio (≈ 0.3) and k' is the shear shape factor (≈ 1).

³ Racking shear deformation of the proposed outrigger structure yields approximately 30 percent of the total deformation, as shown in C.S.2.3d

The load-mass conversion factor, k_{LM} , can be written as a function of a single parameter, α , which is the ratio between the beam's slenderness and ratio between bending- and shear stiffness [16]

$$\alpha = \frac{s^2}{\gamma^2} \quad (4.21)$$

Without much explanation formulas for load-mass conversions are presented [16], which can be simply calculated by α for several load configurations (uniform, linear or triangular). However, it can be concluded that by taking into account the slenderness and ratio between bending- and shear stiffness as well as the loading configuration the load-mass conversion factor is influenced by the mode shape. For a uniformly distributed load the load-mass conversion factor is written as

$$k_{LM} = \frac{4(3024 + 999\alpha + 91\alpha^2)}{189(80 + 32\alpha + 3\alpha^2)} \quad (4.22)$$

Subsequently, equation 4.18 can be deployed to evaluate the fundamental frequency of the SDOF model.

Damping properties of the system

The logarithmic decrement of damping in a building can be calculated according to EC1 as

$$\delta = \delta_s + \delta_a \quad (4.23)$$

where δ_s is the structural logarithmic decrement of damping presented in table F.2 of EC1. The latter is represented by aerodynamic damping and has been determined for the quasi-static wind loading before in Appendix A.1 as follows

$$\delta_a = \frac{c_f \rho v_m(z_s)}{2n_1 \mu_e} \quad (4.24)$$

The logarithmic decrement of damping can be converted to the more frequently used damping ratio, ζ , by the following formula

$$\zeta = \frac{\delta}{\sqrt{(2\pi)^2 + \delta^2}} \quad (4.25)$$

Table 4.2 shows the damping ratio for the structure according to EC1 and evaluated in C.S.3.2 of Appendix A.3.

Table 4.2; Damping ratio of the structure according to EC1

<i>Value</i>	<i>Result</i>
Logarithmic decrement of structural damping; δ_s (table F.2 EC1)	0.10
Logarithmic decrement of aerodynamic damping; δ_a (eq. 4.24)	0.0166
Logarithmic decrement of damping; δ (eq. 4.23)	0.1166
Damping ratio; ζ (eq. 4.25)	0.019 (=1.9%)

The reliability of damping values of buildings is widely known as questionable [15], mainly due to the large influences of constructional elements in the building such as interior elements and finishes. The

Dutch Building code, NEN 6702, prescribes a damping ratio, ζ , for timber structures of 0.05 (i.e. 5%), which is higher than calculated conform EC1. In this stage, however, it seems to be more appropriate to adopt the more conservative value of 1.9 percent.

The influence of damping on the natural circular frequency can now be incorporated by the damped frequency as follows

$$\omega_d = \omega_1 \sqrt{1 - \zeta^2} \quad (4.26)$$

Overview of the results

The presented formulae can be used to evaluate the natural circular frequency of the SDOF system, for which calculations are shown in C.S.3.2 of Appendix A.3. Table 4.3 presents a summary of the most relevant evaluated properties of the SDOF system.

Table 4.3; Determination of the natural circular frequency of the SDOF system

Value	Result	
Concentrated load; F	2 794	kN
Max. static horizontal displacement; U(H)	0.0808	m
Uniform structural stiffness; k	34 576	kN/rad
$(EI)_{\text{struc}} = kH^3 / 3$	$3.497 \cdot 10^9$	kNm ²
Load-mass factor; k_{lm}	0.64	-
Structural mass; m	4 408 992	kg
Natural circular frequency; ω_1	3.495	rad/sec.
Damping ratio; ζ	0.019 (=1.9%)	-
Damped natural circular frequency; ω_d	3.494	rad/sec.

The natural circular frequency of the SDOF system appears to be slightly higher than the estimated frequency of 3.33 rad/s. Although this result seems to enhance the reliability of the estimated natural frequencies, it should be noted that the SDOF system only give accurate results for continuous systems. In particular, the approximated uniform structural stiffness, k , for the discontinuous structural system might introduce some errors, which means that the evaluated fundamental circular frequency can be quite misleading. The fundamental period is given by

$$T_1 = \frac{2\pi}{\omega_1} \rightarrow \frac{2\pi}{3.495} = 1.80 \text{ s} \quad (4.27)$$

The fundamental frequency becomes

$$n_1 = \frac{3.495}{2\pi} = 0.56 \text{ Hz.}$$

4.3 DYNAMIC WIND LOADING

Wind pressure on a building consists of a 'mean part' and a 'fluctuating part', where the latter represents the dynamic property of the loading. In Chapter 3, the design wind loading has been determined in accordance with EC1 as follows

$$q_p(z) = (1 + 2gI_v(z)) \frac{\rho}{2} v_m(z)^2 \quad (4.28)$$

where g is a peak factor, $I_v(z)$ is the turbulence intensity on height z , ρ is the density of air and $v_m(z)$ is the mean wind velocity on height z . The 'mean part' of the wind load is expressed as

$$q_{p,mean}(z) = \frac{\rho}{2} v_m(z)^2 \quad (4.29)$$

so that the 'fluctuating part' of the wind load is given by

$$q_{p,fluc}(z) = 2gI_v(z) \frac{\rho}{2} v_m(z)^2 \quad (4.30)$$

The calculation procedure in EC1 takes the turbulence intensity, $I_v(z)$, into account to obtain a peak wind pressure. The turbulence intensity is calculated as

$$I_v(z) = \frac{\sigma_v}{v_m(z)} \quad (4.31)$$

where σ_v is the standard deviation of the wind velocity. However, the result is a quasi-static wind loading, which does not represent the real dynamic behaviour of the wind and is thus unsuitable for dynamic analyses of structures subjected to wind.

Spectral analyses

A spectral analysis is a useful tool to determine the structural response on fluctuating wind loading. Besides it is possible to obtain a value for wind loading as a function of time, $q(t)$, which is required to perform dynamic response analyses. Davenport [18] proposed a procedure for determination of the structural response, a so-called *spectral analysis*, as depicted in Figure 4.6.

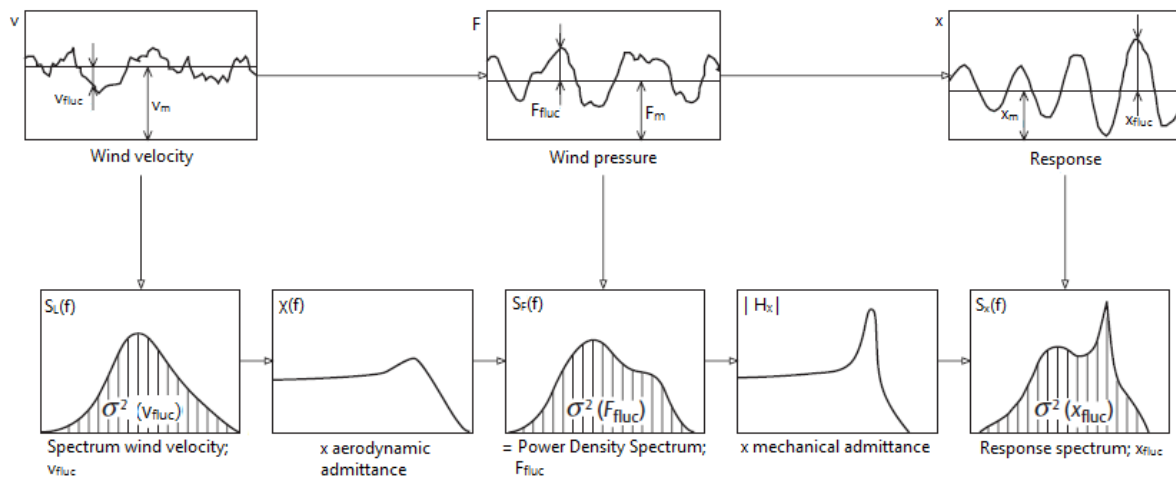


Figure 4.6; Design process of spectral analyses for dynamic wind loading, after Davenport [18]

A spectrum of the *fluctuating wind velocity* (lower left corner Figure 4.6), $S_L(f_L)$, can be modelled by real data of wind (upper left corner Figure 4.6). A spectrum portrays a variable from the time domain (wind statistics) into a frequency domain (spectrum). The function $S_L(f_L)$ is determined by the dimensionless frequency f_L . This frequency is introduced by EC1 and is non-dimensional because it is a function of both the fundamental frequency of the structure, n_1 , and height z . As a consequence, the magnitude of the fluctuating wind is determined by the fundamental vibration mode of the structure and the location on the building's facade, where fluctuations decrease upwards on the building.

The spectral density function is in accordance with EC1 written as

$$S_L(f_L) = \frac{6.8f_L(z_s, n)}{(1 + 10.2f_L(z_s, n))^{5/3}} \quad (4.32)$$

where $f_L(z_s, n)$ is a non-dimensional frequency on reference height z_s ($=0.6H$) given by

$$f_L(z_s, n) = \frac{nL(z_s)}{v_m(z_s)} \quad (4.33)$$

$L(z_s)$ is the size of gusts on reference height z_s as previously defined in Appendix A.1 and $v_m(z_s)$ is the mean wind velocity on reference height z_s .

The *aerodynamic admittance*, (f_L) , represents the size of wind fluctuating effects on the structure determined by the non-dimensional frequency and thus the height on the building as well as structure's fundamental frequency. The admittance function for the fundamental mode shape can be calculated in accordance with EC1 as follows

$$\chi^2(f_L) = R_h R_b \quad (4.34)$$

$$R_h = \frac{1}{\eta_h} - \frac{(1 - e^{-2\eta_h})}{2\eta_h^2} \quad (4.35)$$

where

$$\eta_h = \frac{4.6H}{L(z_s)} f_L(z_s, n) \quad (4.36)$$

The aerodynamic admittance function, R_b , can be written by replacing H into B , which is the width of the building. For low values of f_L , which refer to either low building heights or low fundamental frequencies, or a combination of these, the aerodynamic admittance approaches a unit value whilst higher values of f_L decreases the size of wind fluctuating effects to the structure. This is underpinned by definition of the Power Density Spectrum, $S_F(f_L)$.

The *Power Density Spectrum* (shown in lower centre of Figure 4.6) is a representation of the fluctuating wind forces in a frequency domain. When the fluctuating wind forces are known in the time domain (shown in top centre of Figure 4.6) it is possible to obtain the Power Density Spectrum through an inverse Fourier Transformation. However, since EC1 provides an approach to model the spectrum of the wind velocity it is more convenient to obtain a Power Density Spectrum with help of the following formula [19]

$$S_F(f_L) = (c_d A \rho v_m(z_s))^2 S_V(f_L) \chi^2(f_L) \quad (4.37)$$

where the dynamic building factor c_d was previously defined in Appendix A.1 in accordance with EC1 as

$$c_d = \frac{1 + 2k_p I_v(z_s) \sqrt{B^2 + R^2}}{1 + 7I_v(z_s) \sqrt{B^2}} \quad (4.38)$$

A is the surface area of the façade on the windward side of the building, ρ is the air density. The spectrum, $S_v(f_L)$, represents the spectrum of the variance of the fluctuating wind velocity and can be determined as [15]

$$S_v(f_L) = \frac{S_L(f_L) \sigma_v^2}{n_1} \quad (4.39)$$

where the variance of the fluctuating wind on the reference height is

$$\sigma_v^2 = [I_v(z_s) v_m(z_s)]^2 \quad (4.40)$$

In order to obtain a dynamic response (shown in lower right corner of Figure 4.6), first the *mechanical admittance* should be determined. The mechanical admittance is a function of the fundamental frequency, damping and stiffness of the structure and resembles the response of the structure to a certain frequency of the loading. Since resonance of a structure occurs when the frequency of the loading is at or near one of the natural frequencies of the structure, a peak in of the mechanical admittance is located near the fundamental frequency of the structure. The mechanical admittance function can be calculated as [20]

$$H_x(n) = \frac{1}{4\pi^2 n_1^2 m \sqrt{\left(1 - \left(\frac{n}{n_1}\right)^2\right)^2 + 4\zeta^2 \left(\frac{n}{n_1}\right)^2}} \quad (4.41)$$

where n is a certain frequency [Hz.], m is the mass of the structure [kg] and ζ is the damping ratio. It can be seen in the equation above that for n equal to n_1 the values between brackets result in a unit value, increasing the denominator significantly and decreasing the mechanical admittance function accordingly, resulting in a peak at the fundamental frequency. Moreover, the amount of damping in the structure, represented by ζ , determines the size of oscillations.

The last step in the diagram of Figure 4.6 is to evaluate a *response spectrum*, $S_x(f_L)$. The graph shows a profile which corresponds with both the Power Density Spectrum and the mechanical admittance spectrum. This is expressed in the formula of the response spectrum [19]

$$S_x(f_L) = |H_x(n)|^2 S_f(f_L) \quad (4.42)$$

It may be apparent that this formulation is valid for linear systems only. As shown in the diagram of Figure 4.6 it is possible to obtain a response of fluctuating displacements in the time domain. This can be done by performing a fourier transformation of the response spectrum.

Nonetheless, it is also possible to obtain a response of the structure directly from the Power Density Spectrum, $S_f(f_L)$, without the necessity of determining a mechanical admittance- and response spectrum.

The total response of the structure due to fluctuating wind actions consists of a quasi-static part and a resonance part as follows [19]

$$\sigma_{x,stat} = \frac{c_d A v_m \sigma_v}{k} \quad (4.43)$$

$$\sigma_{x,res} = \frac{1}{k} \sqrt{\frac{\pi n_1 S_F(f_L)}{4\zeta}} \quad (4.44)$$

where characteristics are as defined previously and k is the stiffness of the structure. The dynamic response can be written as the resultant of a quasi-static- and a resonance component

$$\sigma_{x,dyn} = \sqrt{\sigma_{x,stat}^2 + \sigma_{x,res}^2} \quad (4.45)$$

For determination of the expected horizontal accelerations, the theory of 'White noise approach' can be adopted. This theory implies that the spectral density of the loading at frequency n_1 is assumed constant with the frequency and has the value, $S_x(f_L)$. For a single degree-of-freedom system the structural response can be expressed as

$$\sigma_a = \sqrt{\frac{S_F(f_L) \pi n_1}{4\zeta m^2}} \quad (4.46)$$

where m is the mass of the structure [kg]. In the contrary to implementation of equivalent structural properties, k_{eq} and m_{eq} , for determination of the fundamental frequency (see previous section), in spectral analysis non-equivalent properties are used, m and k . It may be apparent that spectrums of fluctuating wind actions, as described above, are determined without the load conversion factor, k_L .

It is shown that through a known spectrum of fluctuating wind actions, $S_L(f_L)$, a spectral analysis can be performed which results in a dynamic response (horizontal displacements and –accelerations) of a SDOF model. However, the result of presented formulae is determined by the frequency of wind gusts, f_L , which is determined by the height of the building. Moreover, for the lower region of a building the frequency of gusts is higher in comparison to a region further upwards the building. It can be seen in equation 4.46 that the magnitude of horizontal accelerations is directly affected by f_L , and thus the height of the building. For evaluation of the dynamic response reference height of the building, i.e. 40.3 meters, which is defined by EC1 for calculation of quasi-static wind loads, is adopted to determine the frequency of fluctuating wind loads.

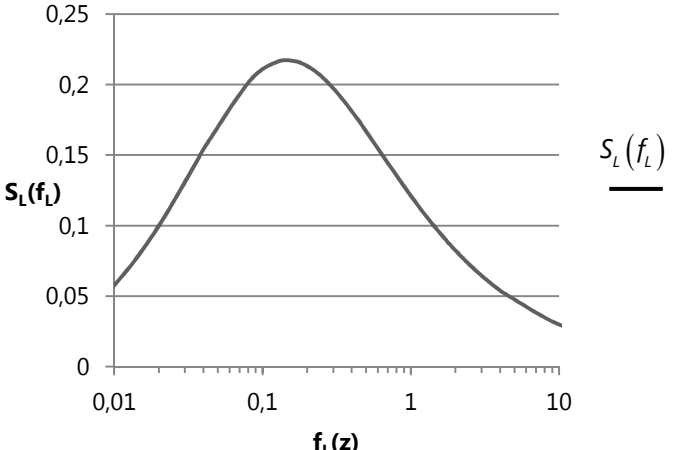
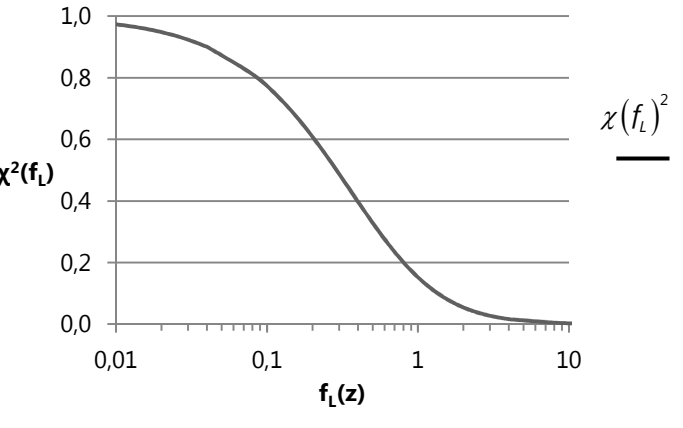
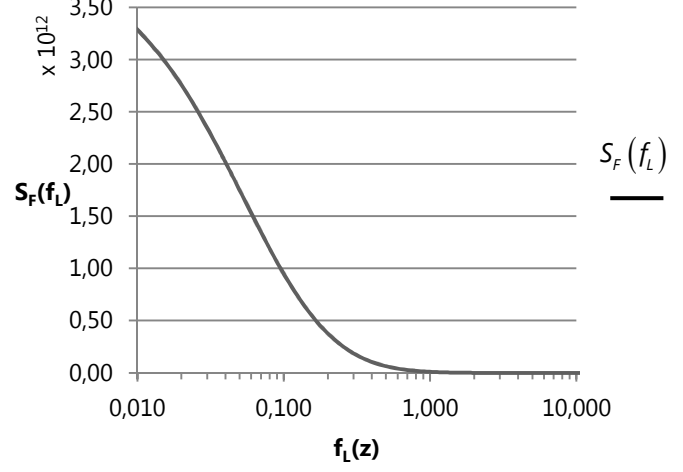
Spectral analysis results

The method of Davenport can be applied to the structural design along with the following starting points

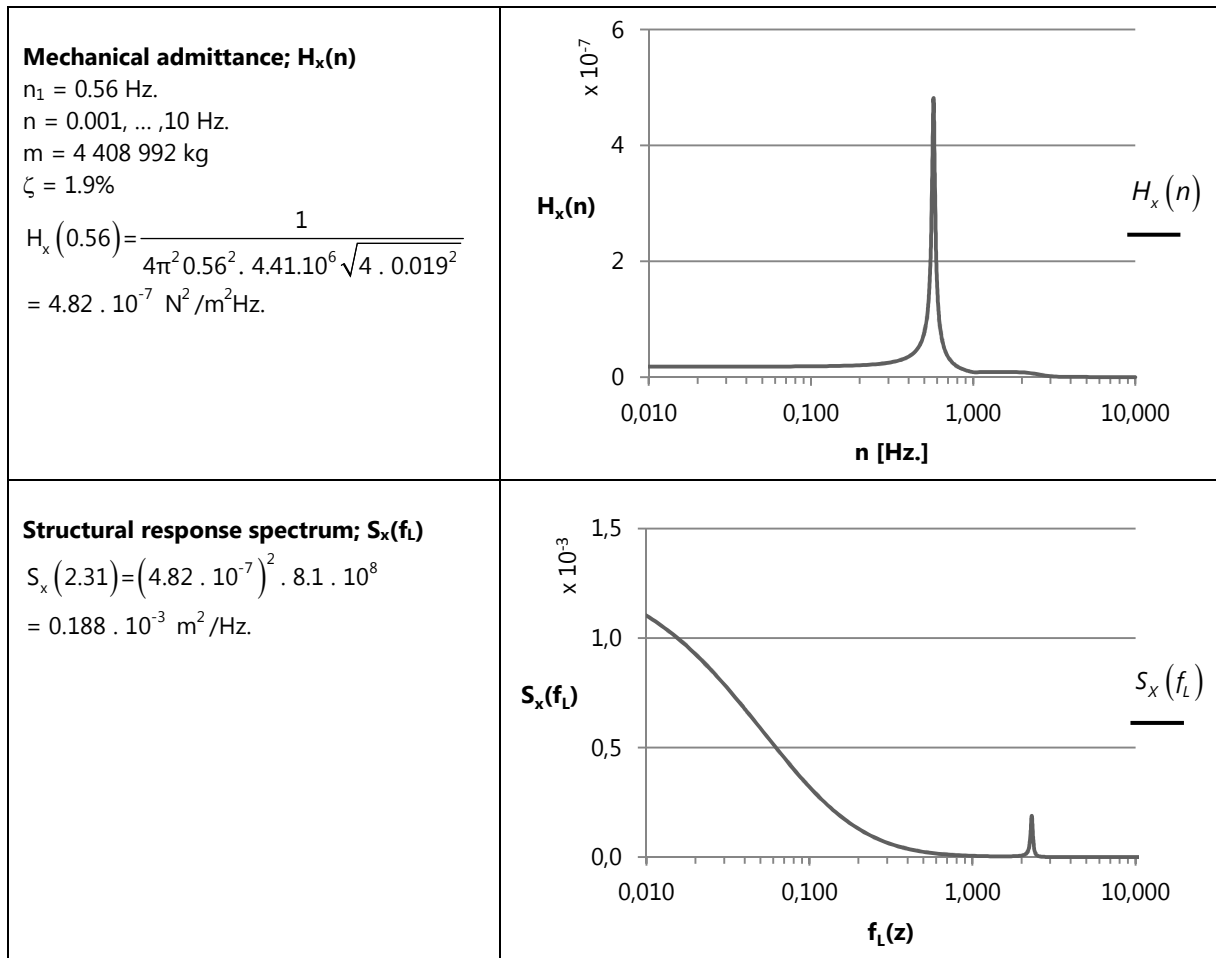
- Frequency, f_L , is made dimensionless by the turbulence length scale, $L(z_s)$ and mean wind velocity $v_m(z_s)$, both calculated on the reference height of the building. It seems obvious that this location may not be subjected to the largest wind gusts (lower in the building), but with respect to the dynamic response of the structure this location might be representative, since horizontal accelerations are usually the largest at the top floor of a building;
- Linear behaviour is assumed during the dynamic response of the structure;
- Results of the spectral analysis refer to a non-equivalent SDOF model. This is required because the fluctuating wind spectrum is determined without taking into account a load conversion factor, hence mass- and stiffness conversion factors are not applicable.

The results of the spectral analysis, i.e. equation 4.32 to 4.42, are shown in Table 4.6.

Table 4.6; Spectral analysis results

<p>Spectrum of fluctuating wind; $S_L(f_L)$ $n_1 = 0.56$ Hz.</p> <p>$L(z_s) = 107.61$ m</p> $f_L(z_s, n_1) = \frac{0.56 \cdot 107.61}{26.07} = 2.31$ $S_L(2.31) = \frac{6.8 \cdot 2.31}{(1 + 10.2 \cdot 2.31)^{5/3}} = 0.076 \frac{\text{s}}{\text{mHz}}$	 <p style="text-align: right;">$S_L(f_L)$</p>
<p>Aerodynamic admittance;</p> $\chi^2(f_L) = R_h R_b$ $\eta_h = \frac{4.6 \cdot 67.2}{107.61} \cdot 2.31 = 6.64 \quad \eta_b = 2.67$ $R_h = \frac{1}{5.1} \cdot \frac{(1 - e^{-2.51})}{2 \cdot 5.1^2} = 0.139 \quad R_b = 0.305$ $\chi^2(2.31) = 0.139 \cdot 0.305 = 0.042$	 <p style="text-align: right;">$\chi^2(f_L)^2$</p>
<p>Wind force spectrum; $S_F(f_L)$ Properties⁴ on reference height, z_s</p> $c_d = \frac{1 + 2 \cdot 3.437 \cdot 0.228 \sqrt{0.49 + 0.154}}{1 + 7 \cdot 0.228 \cdot \sqrt{0.49}} = 1.07$ <p>$A = 27 \cdot 67.2 = 1814.4$ m² $v_m(z_s) = 26.07$ m/s $\rho = 1.25$ kg/m³ $I_v(z_s) = 0.228$ $\sigma_v^2 = [0.228 \cdot 26.07]^2 = 35.28$</p> $S_v(f_L) = \frac{S_L(f_L) \cdot 35.28}{0.56} = 63 \cdot S_L(f_L)$ $S_F(2.31) = (2.567 \cdot 10^{11}) \cdot 4.77 \cdot 0.042$ $= 8.1 \cdot 10^8 \text{ N}^2/\text{Hz}$	 <p style="text-align: right;">$S_F(f_L)$</p>

⁴ The dynamic factor, c_d , is calculated with a natural frequency of 0.68 Hz. as shown in Appendix A.1



The mechanical admittance function shows a large peak near the natural frequency of the structure, the so-called resonance peak. The area underneath the response spectrum portrays the displacements of the structure, i.e. equation 4.45. Figure 4.7 shows a scaled area of the response spectrum where the background part is related to the quasi-static response and the resonance peak represents the dynamic part of the response.

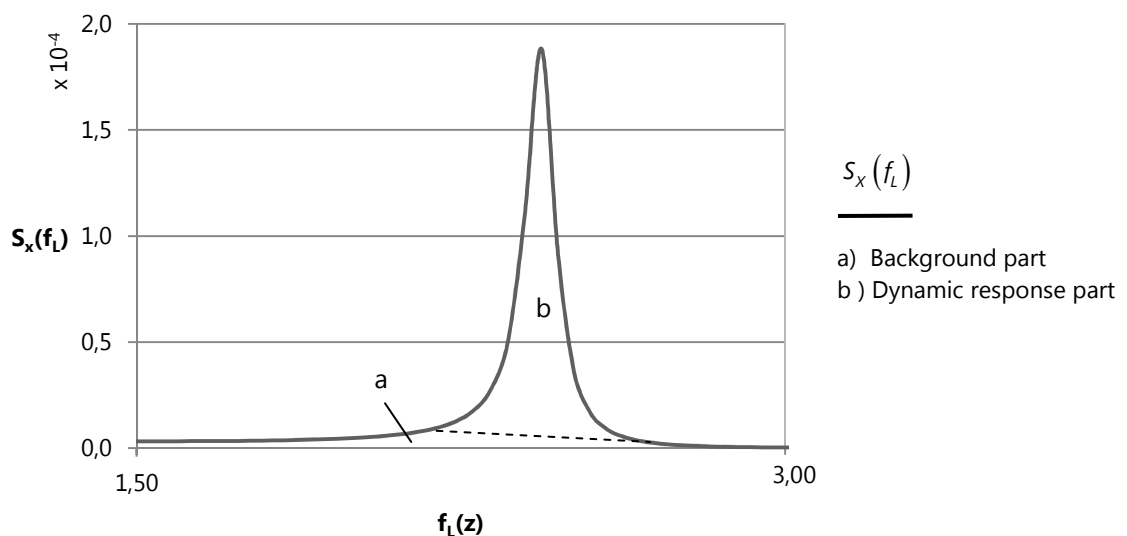


Figure 4.7; Dynamic response of the structure to fluctuating wind loads

Subsequently, the displacements and expected horizontal accelerations can be evaluated. Table 4.7 shows the results of C.S.3.3 in Appendix A.3.

Table 4.7; Dynamic response results

Structural property / result	Value	
Natural frequency; ω_1	0.56	Hz.
Power Density Spectrum; $S_f(2.31)$	$8.1 \cdot 10^8$	$N^2/Hz.$
Damping ratio; ζ	0.019	-
Mass; m	4 408 992	kg
Stiffness; k	34 576	kN/rad
Quasi-static displacement; $\sigma_{x,stat}$	0.0087	m
Resonance displacement: $\sigma_{x,res}$	0.0040	m
Dynamic displacement: $\sigma_{x,dyn}$	0.0096	m
Horizontal acceleration: σ_a	0.0314	m/s^2

It must be noted that the dynamic displacements, i.e. $\sigma_{x,dyn}$, are only a consequence of the fluctuating wind loads, which means that displacements due to the mean wind force should be added to obtain an indication of total displacements. These appearances will be discussed in the following sections. Horizontal accelerations, however, are representative for the behaviour of the structure under fluctuating wind loads as defined by the spectrum, $S_L(f_L)$. In order to clarify the accuracy of these values it is desired to excite the structure directly by a time-varying wind load, so that the dynamic response over a certain time period can be analysed in the following sections. This would clarify whether the evaluated values in Table 4.7 are representative as upper bound, lower bound or average responses.

Time history of wind loading

The introduction of this section has shown the inapplicability of EC1 to determine a realistic wind load as a function of time, which incorporates fluctuations in wind velocity. The spectral analysis, however, enables one to obtain a time signal of the wind velocity by carrying out an approximated technique. Wind forces are a continuous process of fluctuating behaviour excluding any repeating patterns, which is typical for stationary stochastic loading. Stochastic processes can be modelled as a sum of (infinite) sinusoidal waves, with each a unique; amplitude, a_i , phase angle, ψ_i , and frequency, f_i . The magnitude of the amplitudes is originated in the spectrum of fluctuating wind velocity and can be expressed as [19]

$$a_i = \sqrt{2S_i\Delta f} \quad (4.47)$$

where S_i equals the spectral density function $S_L(f_L)$ for a certain frequency. Values of S_i are determined by dividing the spectrum in a number of N -frequencies of band width Δf , so that the signal can be written as a sum of the sinusoidal waves as follows [19]

$$v(t) = \sum_{i=1}^N \left[a_i \sin \left[(f_i t) + \psi_i \right] \right] \quad (4.48)$$

where the phase angle, ψ_i , contains a random value. The magnitude of N is difficult to predict [19], but a distribution of 10 usually results in reliable outcomes.

Elaboration of the time history is given in Appendix A.3, where Figure 4.8 depicts the results of the analysis in a graph.

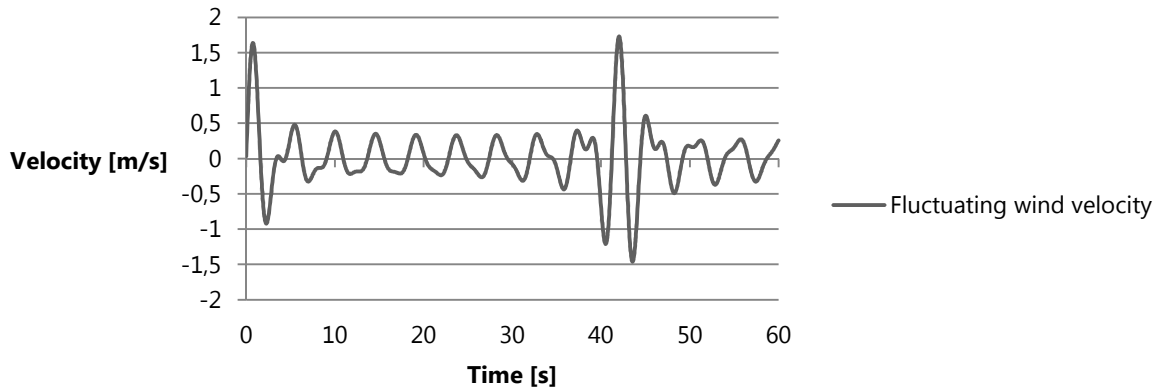


Figure 4.8; Time history of the fluctuating wind velocity determined by fluctuating wind spectrum in accordance with EC1

The wind fluctuations show significant gusts at zero and forty seconds of approximately 1.75 m/s. As mentioned in the introduction of this section the total wind loading comprises a 'mean part' and a 'fluctuating part'. The wind velocity can be simply transferred to wind forces. Assuming that the wind fluctuations are equal in magnitude on each location of the façade⁵ the fluctuated wind force on an area, A , can be approximated as

$$F(t) = \rho_{air} c_d A v_m v(t) \quad (4.49)$$

where the mean wind velocity, v_m , dynamic building factor, c_d , and fluctuating wind velocity, $v(t)$, shall be determined on reference height, z_s .

Wind forces caused by the 'mean part' are expressed as

$$F_m = \frac{\rho_{air}}{2} c_d A v_m^2 \quad (4.50)$$

where characteristics are as defined above.

Aero-elastic effects

Wind flow around a building may cause unfavourable motions in the transverse direction. The size of these phenomena is a dependant of the building shape and its susceptibility to fluctuating wind loading, determined by its fundamental frequency. Significant vortex shedding and galloping occur when the frequency of the wind approaches one of the natural frequencies of the building. Therefore, the design criteria as presented in EC1 are based on keeping the critical wind velocity, characteristic for the structure, above a factorised mean wind velocity. The presented formulae in this subsection can be found in Annex E of EC1.

The critical wind velocity for vortex shedding is given as

$$v_{crit,i} = \frac{b n_{i,y}}{St} \quad (4.51)$$

where b is the width of building's cross section, $n_{i,y}$ is the natural frequency of corresponding vibration mode i in cross-wind direction, St is the Strouhal number, which takes the cross section effects into account. The design criterion is defined as

⁵ The wind spectrum and mean wind velocity is determined by a reference height of the building, i.e. $0.6H$, see Section 3.2

$$v_{crit,i} \leq 1.25v_m \quad (4.52)$$

Galloping is characterised by oscillations of large amplitude in the cross-wind direction due to self-induced vibrations and may occur at non-circular cross sectional building shapes. Galloping vibrations starts at a wind velocity, v_{CG} , and usually the amplitude increases rapidly at increasing wind velocity. The starting wind velocity for galloping is written as follows

$$v_{CG} = \frac{2S_c}{a_G} n_{1,y} b \quad (4.53)$$

where S_c is the Scruton number, which defines the degree of vibrations depending on the structural damping and ratio of air- and structural mass densities and may be calculated as follows

$$S_c = \frac{2\delta_s m_{i,e}}{\rho b^2} \quad (4.54)$$

where δ_s is the logarithmic decrement of structural damping, $m_{i,e}$ may be approximated by the mass of the structure per meter height. Factor a_G is the galloping instability factor.

The starting wind velocity of the structure should comply with

$$v_{CG} > 1.25v_m \quad (4.55)$$

The results for the preliminary structural design is shown in Table 4.8, and elaborated in Appendix A.3.

Table 4.8; Check on aero-elastic effects to the structure

Value	Result	EC reference	
Mean wind velocity; $v_m(67.2)$	29.11	-	m/s
Strouhal number; St	0.12	Figure E.1	-
Log. decrement of structural damping; δ_s	0.10	Table F.2	-
Mass per meter height; $m_{i,e}$	65 610	-	kg/m
Scruton number; S_c	14.4	-	-
Galloping instability factor; a_G	1.2	Table E.7	-
Design wind velocity; $1.25 v_m(67.2)$	36.39	-	m/s
Critical wind velocity; $v_{crit,i}$	104.31	-	m/s
Starting wind velocity; v_{CG}	300.42	-	m/s

Presented values in the table above show that the wind velocities to comply with are well above the design wind velocity; hence no aero-elastic effects should be expected for the proposed building design. It is apparent that a square building shape and height of the building as well as the fundamental frequency results in insusceptible behaviour to wind flow effects.

4.4 DYNAMIC RESPONSE OF A SDOF SYSTEM

The dynamic response of a SDOF system can be numerically analysed in order to assess the motions of the building when subjected to dynamic loading. The type of analysis is very much depending on the excitation behaviour, which is in this case a non-periodic loading. A convenient tool to analyse the dynamic response for such a system is the *Step-by-Step Procedure*, involving numerically differentiation of the equation of motion for each time step [21].

The procedure consists of calculating the response during each time step from the initial conditions at the beginning of the step and the loading history during the step. A simple and applicable method for non-periodic excitations is the *Central Difference Method*. Figure 4.9 shows the basic concept of calculating the response (displacement) for each time step, where the response is approximated by finite-difference expressions.

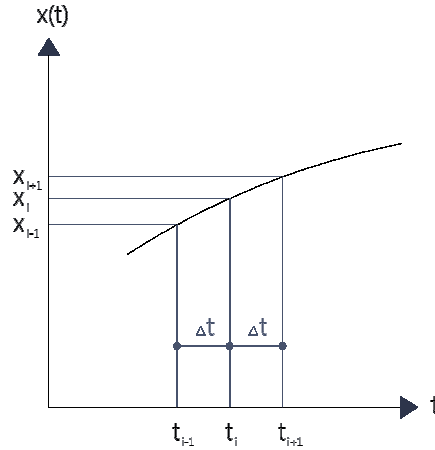


Figure 4.9; Displacement – time relationship for Central Difference Method

Therefore it is required to adopt an appropriate time step to ensure conditionally stable solutions, for which the objective is to obtain convergence to the actual response path. When the time step is too large the load-deformation curve cannot be followed during iterations resulting instability in computations. In general it is common practice to determine a time step according to

$$\Delta t \leq \frac{T_1}{10} \quad (4.56)$$

where T_1 is the fundamental period of the structure.

The velocity at time t_i can be determined by the first derivative of the displacement as follows

$$\dot{x}_i = \left(\frac{dx}{dt} \right)_{t_i} = \frac{\Delta x}{\Delta t} = \frac{x_{i+1} - x_{i-1}}{t_{i+1} - t_{i-1}} = \frac{x_{i+1} - x_{i-1}}{2\Delta t} \quad (4.57)$$

In a similar manner, the acceleration at time t_i is equal to the second derivative of the curve

$$\ddot{x}_i = \left(\frac{d^2x}{dt^2} \right)_{t_i} = \frac{\left(\frac{dx}{dt} \right)_{t_i + (\Delta t/2)} - \left(\frac{dx}{dt} \right)_{t_i - (\Delta t/2)}}{\Delta t} = \frac{\frac{x_{i+1} - x_i}{\Delta t} - \frac{x_i - x_{i-1}}{\Delta t}}{\Delta t} = \frac{x_{i+1} - 2x_i + x_{i-1}}{(\Delta t)^2} \quad (4.58)$$

The equation of motion at time t_i can be written as

$$m\ddot{x}_i + c\dot{x}_i + kx_i = F_i \quad (4.59)$$

Substituting equation 4.57 and 4.58 into 4.59 gives

$$m \left(\frac{x_{i+1} - 2x_i + x_{i-1}}{(\Delta t)^2} \right) + c \left(\frac{x_{i+1} - x_{i-1}}{2\Delta t} \right) + kx_i = \left(\frac{m}{(\Delta t)^2} + \frac{c}{2\Delta t} \right) x_{i+1} - \left(\frac{2m}{(\Delta t)^2} - k \right) x_i - \left(\frac{c}{2\Delta t} - \frac{m}{(\Delta t)^2} \right) x_{i-1} = F_i \quad (4.60)$$

which can be rewritten as

$$x_{i+1} = \frac{\left(\frac{2m}{(\Delta t)^2} - k \right) x_i + \left(\frac{c}{2\Delta t} - \frac{m}{(\Delta t)^2} \right) x_{i-1} + F_i}{\frac{m}{(\Delta t)^2} + \frac{c}{2\Delta t}} \quad (4.61)$$

where one can note that the numerator represents the effective load at time t_i and the denominator represents the effective stiffness at time t_i , leading to the pertaining displacement at the end of a time step. Equation 4.57 and 4.58 can be rearranged as

$$2\dot{x}_i \Delta t = x_{i+1} - x_{i-1} \quad \ddot{x}_i (\Delta t)^2 = x_{i+1} - 2x_i + x_{i-1} \quad (4.62)$$

These new equations can be combined to

$$x_{i-1} = x_i - \dot{x}_i \Delta t + \frac{\ddot{x}_i (\Delta t)^2}{2} \quad (4.63)$$

which is the displacement at the beginning of a time step. This process can be repeated for a given time so that on each time i the displacement, velocity and acceleration can be determined resulting in response graphs of the structure's motions.

Results of response analysis

The calculation starts with the initial conditions at $t = 0$ and subsequently for each time step the response (i.e. displacement, velocity and acceleration) is calculated. Table 4.9 presents an overview of the response calculations as shown in C.S.3.4 of Appendix A.3.

Table 4.9; Dynamic response to non-periodic excitation of the equivalent SDOF system

<p>Equivalent SDOF system</p> <p>Structural mass: $m_{eq} = m_{KM} = 4\,408\,992 \cdot 0.26 = 1\,146$ ton</p> <p>Structural stiffness: $k_{eq} = k_{KR} = k_{KL} = 34\,579 \cdot 0.40 = 13\,831$ k N/rad</p> <p>Damping properties: $\zeta = 0.019$, $c_{cr} = 2\sqrt{k_{eq} m_{eq}} = 1.966 \cdot 10^4$ kN-s/m, $c = \zeta \cdot c_{cr} = 373.53$ kN-s/m</p> <p>Fundamental circular frequency: $\omega_1 = \sqrt{k_{eq} / m_{eq}} = 3.495$ rad/s, $T_1 = 2\pi / \omega = 1.80$ s, $n_1 = 3.5 / 2\pi = 0.56$ Hz.</p> <p>Time step: $T / 10 = 0.18 \rightarrow 0.15$ s</p>
<p>Initial conditions</p> <p>$x_0 = F_{eq}(0) / k_{eq} \rightarrow F_{eq}(0) = 1.1$ kN $\rightarrow x_0 \approx 0$ m</p> <p>$\dot{x}_0 = 0$ m/s</p> <p>$\ddot{x}_0 = \frac{1}{m_{eq}} (F_{eq,0} - c\dot{x}_0 - k_{eq}x_0) = 0$ m/s²</p>

Excitation to the system

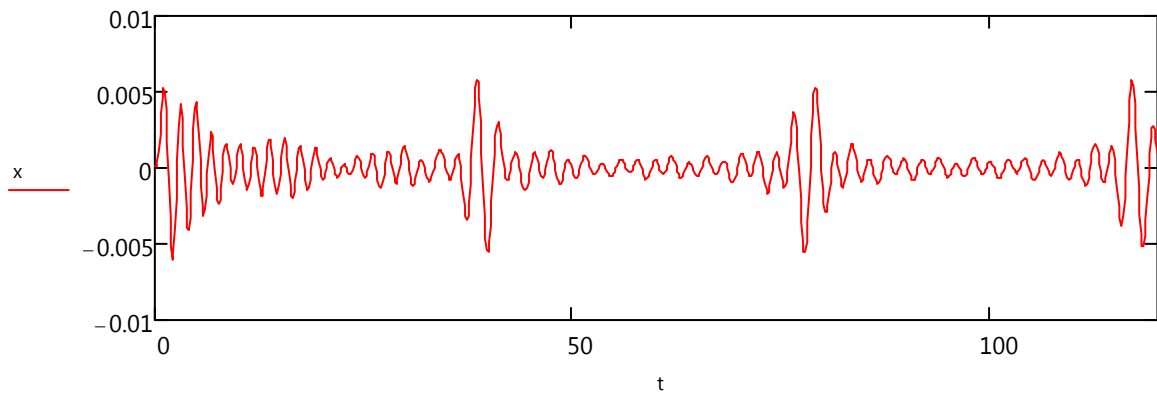
Loading for dynamic analysis comprises fluctuating wind:

$$q_{eq}(t) = \rho_{air} c_d A v_m v(t) k_L$$

$$F_{eq}(t) = q_{eq}(t) A_{façade} = q_{eq}(t) 1814.4 \text{ [kN]}$$

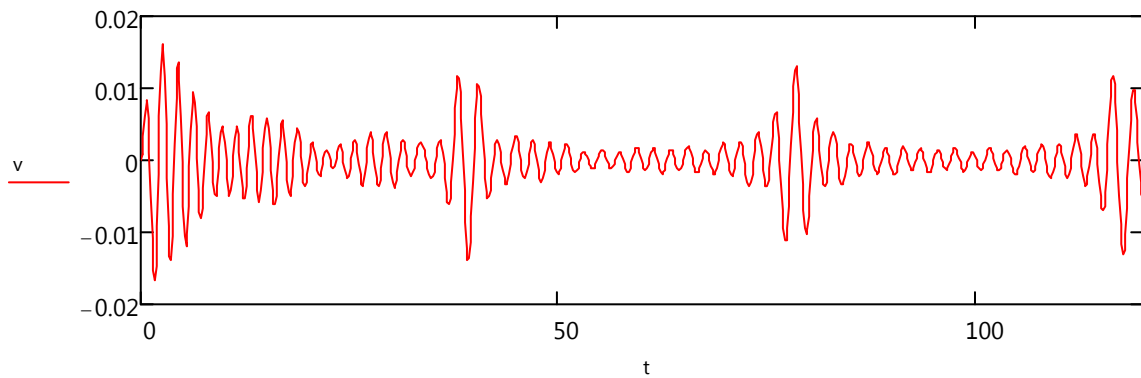
Dynamic response: displacements

$$x_{min} = -0.01 \text{ m} \quad x_{max} = 0.01 \text{ m}$$



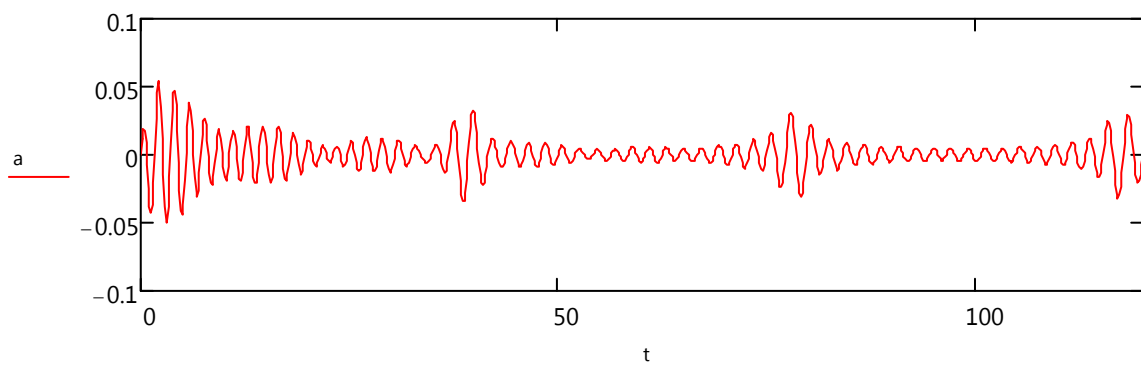
Dynamic response: velocity

$$a_{min} = -0.02 \text{ m/s} \quad a_{max} = 0.02 \text{ m/s}$$



Dynamic response: accelerations

$$a_{min} = -0.05 \text{ m/s}^2 \quad a_{max} = 0.05 \text{ m/s}^2$$



Discussion of the results

Initial conditions of the system include a negligible excitation where the structure is motionless. As depicted in the fluctuating wind profile of Figure 4.8 the wind spectrum consists of an initial gust at the very first seconds, which returns every forty seconds. Therefore the model is subjected from a situation of rest by a sudden wind gust, which resembles a clear response in the first seconds of excitation as shown in the response graphs of Table 4.9.

The maximum horizontal accelerations occur in this time period and reach a value of 0.05 m/s^2 , which is a higher value in comparison to the result of spectral analyses, i.e. 0.03 m/s^2 . However, the response later in the excitation period shows a horizontal acceleration of approximately 0.03 m/s^2 during wind gusts, which corresponds with spectral analysis results. Hence, horizontal accelerations of the structure due to fluctuating wind, as determined by a wind spectrum from EC1, can be expected to reach this value.

Accelerations of 0.03 m/s^2 are well below allowable values for both commercial- and residential building functions. The design graph of Figure 4.10, which is part of the Dutch building code NEN 6702 [5], shows maximum permissible horizontal accelerations as a function of the fundamental frequency of the building.

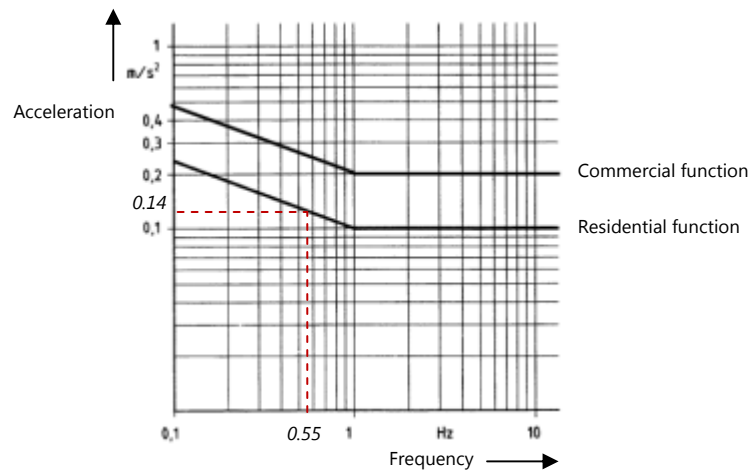


Figure 4.10; Design graph for permissible horizontal accelerations (NEN 6702)

It becomes apparent that the structure shows relatively good behaviour under dynamic wind loading, hence no modifications to the structural design is required at this stage.

Generally spoken, the accuracy of an approximated SDOF system to the actual MDOF structure depends on spatial distribution and time variation of the loading as well as stiffness and mass properties of the structure. Therefore it is desired to clarify the reliability of analyses so far by performing a dynamic analysis with a MDOF system.

4.5 DYNAMIC RESPONSE OF A MDOF SYSTEM

The approximation of the mode shape for a SDOF system, and hence the equivalent structural properties, may carry for deviated results of the dynamic response in case when the actual structure is a multi-degree-of-freedom system. Only if the actual system has one degree of freedom, the SDOF system is the exact solution to the equation of motion. In the previous section it has been attempted to approximate the mode shape by taking shear deformation into account, nonetheless, this only involved the slenderness and material properties of the structural system (Section 4.2). It has already been stated that the discontinuous stiffness over the height of the building, due to outriggers, affect

mode shapes of the structure's natural frequencies largely and thus the accuracy of dynamic properties such as the fundamental frequency.

For comparison, Figure 4.11 shows two models; a SDOF- and MDOF system. In general, a MDOF model approximates a *continuous* structural system more accurately since a higher amount of nodes can describe the mode shape. Modelling of structural properties becomes rather simple, since each beam element has the same stiffness and each lumped mass is the sum of mass per meter height over a shorter distance than one lumped mass at the top of the structure for a SDOF model. Therefore, there is no need for equivalent structural properties, i.e. k_{eq} and m_{eq} , as well as equivalent loading, F_{eq} . On the other hand, for a *discontinuous* structural system stiffness' of beam elements should differ along the height of the structure in order to approximate the actual mode shape. Although it is possible to simulate stiffness effects of outriggers by a rotary spring (since outriggers induce a restraining moment, M_r , to the central structural system) computations for the dynamic response becomes rather complicated and even impossible for most calculation methods.

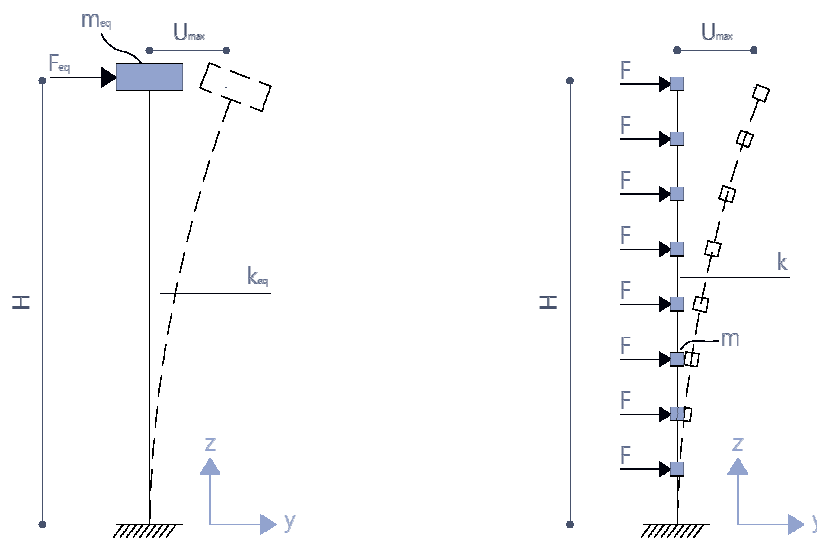


Figure 4.11; a) Equivalent SDOF model b) MDOF model

The objective is to simulate the static mode shape, as shown in Figure 3.5, by defining a unique stiffness property for each storey, i . This can be done through evaluation of the static horizontal displacement at each floor in the building and subsequently obtaining a stiffness, k_i , by taking into account the horizontal force, F_i . The result is a discontinuous stiffness over the height of the building and an accurate approach of the fundamental mode shape. With the assumption that each floor has a single DOF, which is horizontal deformation, the structure turns into a *twenty-one DOF* model. As a consequence, the same number of mode shapes is possible to occur, which at this stage seem to be appropriate for the analysis.

Nonetheless, the number of modes which is realistic to occur at a multi-storey building may be difficult to predict. If only displacements are of interest it may be enough to consider the first three to five modes [22]. However, higher modes resemble smaller oscillations and therefore higher accelerations. Moreover, modelling each storey as an independent coordinate is a frequently adopted method for MDOF analyses.

Modelling of a MDOF system

Taking into account above mentioned starting points for the MDOF model, it is aimed to model a *twenty-one DOF* system which can resemble the static deformation mode. When each floor has one

degree of freedom, i.e. horizontal displacement, the floors have to be modelled rigidly and the vertical structure should allow for deformations by designing them as flexural members.

Although the structural model does not correspond with the proposed structure, where the stabilising system consists of a central core and outriggers, the only purpose is to define a *twenty-one DOF* model which is able to simulate the static mode shape. In practice, floors are not rigidly connected to the vertical structural elements so that in reality each floor joint has multiple degree's-of-freedom. But as long as the equivalent MDOF model is able to simulate the static mode shape, where the stiffness of the MDOF model is made equivalent⁶ to the true structure, a useful model arises suitable for MDOF dynamic analysis. Transfer of the structural model to an equivalent MDOF model is conducted in steps as shown in Figure 4.12.

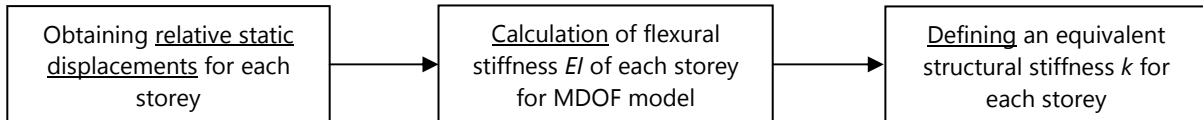


Figure 4.12; Steps for transferring a structural model to an equivalent MDOF model

Static displacements of the outrigger structure have been analysed in Chapter 3, where the mode shape has been shown in Figure 3.5. Relative displacements for each storey can be simply obtained by subtracting a specific floor displacement below from the displacement above, shown in C.S.3.5.

In order to calculate the lateral flexural stiffness EI for each storey, it is required to define the structural model suitable for MDOF dynamic analysis. Figure 4.13 shows a section of the real structure with the exact static deformations (4.13a) as well as an equivalent MDOF model where the same horizontal displacements on each floor are gained by flexure of the columns only (4.13b). Floors are modelled infinite stiff, in which columns are rigidly connected to constrain the joints from vertical displacements and rotations. Further, the figure highlights the mechanical model of a single storey including relative static displacement, u_i corresponding to a single floor.

Lumped masses, m_i are modelled on each floor pertaining to each degree-of-freedom as well as damping coefficients, c_i accordingly.

Forces on each floor can be evaluated as follows⁷

$$F_i = w_{e,total} (H - z_i) \quad (4.64)$$

where $w_{e,total}$ is the quasi-static wind load (=41.58 kN/m, as determined in Chapter 3), H is the total height of the building (=67.2 meters) and z_i is the vertical ordinate of floor i .

Considering the mechanical model of a single floor the following equation, for which a full derivation is shown in Appendix B.1, can be deployed to obtain an equivalent stiffness, $(EI)_i$

$$u_i \approx \frac{F_i h^3}{6.088 (EI)_i} \rightarrow (EI)_i \approx \frac{F_i h^3}{6.088 u_i} \quad (4.65)$$

where h is the storey height equal to 3.2 meters.

⁶ Equivalent stiffness in this case does not correspond to k_{eq} of a SDOF model

⁷ It must be noted that forces, $F(t)$, shown in Figure 4.13 refer to the dynamic wind loads for MDOF analysis, which are not used to determine the equivalent stiffness

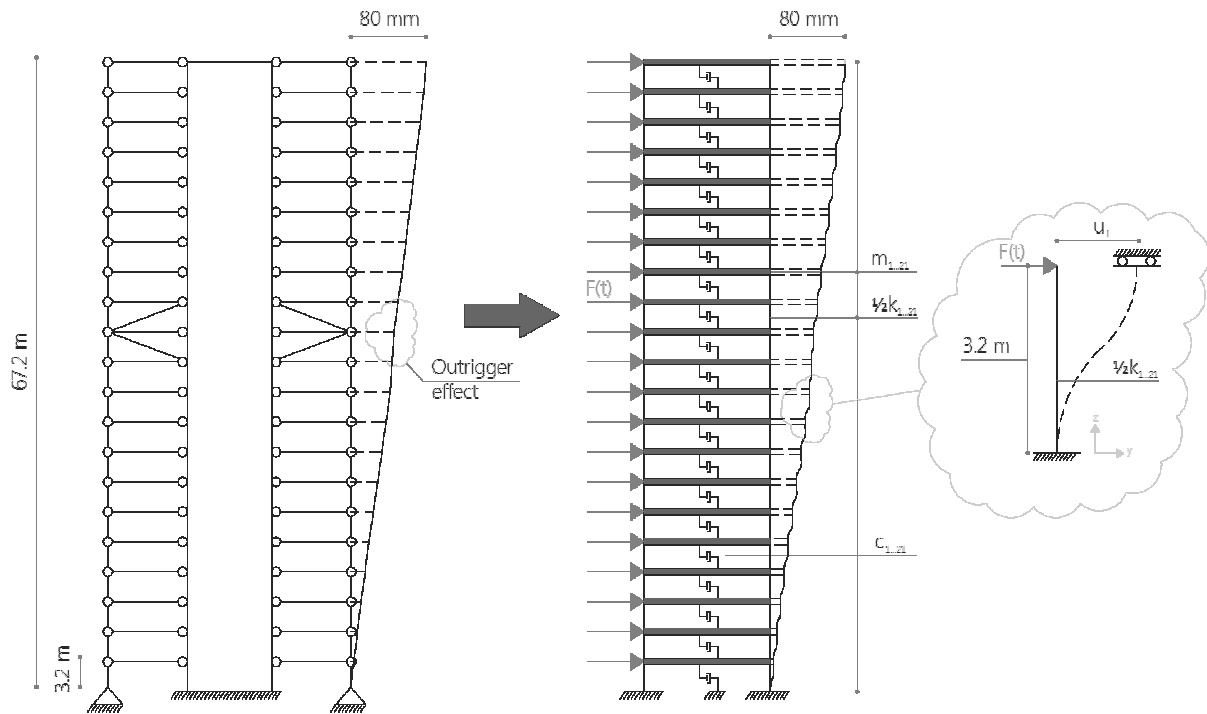


Figure 4.13; a) Real structural model with static mode shape b) Equivalent MDOF model

Subsequently structural stiffness k_i is determined by the boundary conditions, where in case of fixed supports as shown in Figure 4.13 the following formula applies

$$k_i = \frac{12(EI)_i}{h^3} \quad (4.66)$$

Evaluation of structural properties for each floor i are presented in C.S.3.5.

The damping coefficient can be written by the damping ratio, ζ , as follows

$$c_i = 2m_i\omega_i\zeta \quad (4.67)$$

where ω_i is the circular natural frequency for mode shape i , in which the number of mode shapes are equal to the number of degree's-of-freedom. The damping ratio equals 0.019 (=1.9 percent) as defined previously in Table 4.2.

Dynamic equilibrium of a MDOF system

The equation of motion of the total system can be formulated by the expression of equilibrium for each degree of freedom

$$\begin{aligned} (m\ddot{x})_1 + (c\dot{x})_1 + (kx)_1 &= F_1(t) \\ (m\ddot{x})_2 + (c\dot{x})_2 + (kx)_2 &= F_2(t) \\ (m\ddot{x})_3 + (c\dot{x})_3 + (kx)_3 &= F_3(t) \\ \dots \\ (m\ddot{x})_i + (c\dot{x})_i + (kx)_i &= F_i(t) \end{aligned} \quad (4.68)$$

where i is the number of mode shapes and other components are as defined in the previous subsection and shown in Figure 4.13.

Equation 4.68 can also be written in matrix form as

$$[m]\{\ddot{x}\} + [c]\{\dot{x}\} + [k]\{x\} = \{F(t)\} \quad (4.69)$$

For determination of dynamic properties of the system, i.e. the natural frequencies and mode shapes, the structure can be analysed on *free vibration* and hence damping shall be precluded in the equation of motion. Equation 4.69 reduces to

$$[m]\{\ddot{x}\} + [k]\{x\} = \{0\} \quad (4.70)$$

Free vibration assumes simple harmonic motions of the structure, thus the displacement vector for a MDOF system can be defined as

$$\{x(t)\} = \{A\} \sin(\omega t + \phi) \quad (4.71)$$

where $\{A\}$ represents the shape of the system, which does not change with time, and ϕ is a phase angle. The acceleration vector can be obtained by differentiating twice

$$\{\ddot{x}(t)\} = -\omega^2 \{A\} \sin(\omega t + \phi) = -\omega^2 \{x(t)\} \quad (4.72)$$

Substitution of equation 4.71 and 4.72 in 4.70 results in the following equation of motion

$$\begin{aligned} & -\omega^2 [m]\{A\} \sin(\omega t + \phi) + [k]\{A\} \sin(\omega t + \phi) \\ & = [[k] - \omega^2 [m]]\{A\} \sin(\omega t + \phi) = \{0\} \end{aligned} \quad (4.73)$$

The sine term is arbitrary and may therefore be omitted, so that equation 4.73 reduces to

$$[[k] - \omega^2 [m]]\{A\} = \{0\} \quad (4.74)$$

It can be seen that the equation of motion results in an eigenvalue problem, where the eigenvalues, ω^2 , represent the squared natural circular frequencies of free vibration. Since a nontrivial solution for the first part of the equation should be found in order to satisfy the equation, setting the determinant equal to zero will give the solutions for the eigenvalues as follows

$$|[[k] - \omega^2 [m]]| = 0 \quad (4.75)$$

Expanding the determinant will give an algebraic equation of the n^{th} order for n degrees of freedom. The n roots of this equation will lead to an n number of frequencies of the system possible to occur. The frequency vector is thus given by

$$\omega = \begin{Bmatrix} \omega_1 \\ \omega_2 \\ \vdots \\ \omega_n \end{Bmatrix} \quad (4.76)$$

where ω_1 is the first mode being the lowest frequency and the next highest frequency is the second mode, etc.

When the natural circular frequency of each mode is known, equation 4.74 can be used to obtain the corresponding mode shapes. The first part can be written as

$$[H]_i = [[k] - \omega^2 [m]] \quad (4.77)$$

so that

$$[H]_i \{A\}_i = \{0\} \quad (4.78)$$

For convenience during mode superposition (see pertaining subsection), $\{A\}$ will be generalised by the modal vector $\{\phi\}$ resulting in the modal matrix $[\Phi]$ as follows

$$[\Phi] = [\{\Phi\}_1, \{\Phi\}_2, \dots, \{\Phi\}_n] = \begin{pmatrix} \phi_{11} & \phi_{12} & \dots & \phi_{1n} \\ \phi_{21} & \phi_{22} & \dots & \phi_{2n} \\ \dots & \dots & \dots & \dots \\ \phi_{n1} & \phi_{n2} & \dots & \phi_{nn} \end{pmatrix} \quad (4.79)$$

Equation 4.78 can be rearranged to

$$\begin{pmatrix} [H]_{11} & [H]_{12} \\ [H]_{21} & [H]_{22} \end{pmatrix}_i \begin{Bmatrix} 1.0 \\ \{\Phi\}_{ci} \end{Bmatrix} = \begin{Bmatrix} 0 \\ \{0\} \end{Bmatrix} \quad (4.80)$$

where $\{\Phi\}_i$ has been normalised by setting ϕ_{1i} equal to 1.0 and $\{\Phi\}_{ci}$ is a complementary subvector with $n-1$ unknown terms of $\{\Phi\}_i$ and can be determined by the second sub-matrix of equation 4.80 as follows

$$[H]_{21} + [H]_{22} \{\Phi\}_{ci} = \{0\} \rightarrow \{\Phi\}_{ci} = -[H]_{22}^{-1} [H]_{21} \quad (4.81)$$

This procedure allows the determination of each mode shape i containing n generalised displacements.

Orthogonality conditions

Free vibration mode shapes have properties which are very useful for dynamic analyses, so called orthogonality relationships. The relationships can be expressed by Betti's law and considering two free vibration mode shapes, r and s as follows

$$[k] \{\Phi\}_r - \omega_r^2 [m] \{\Phi\}_r = \{0\} \quad (4.82)$$

$$[k] \{\Phi\}_s - \omega_s^2 [m] \{\Phi\}_s = \{0\} \quad (4.83)$$

Multiplying both sides of equation 4.82 by $\{\Phi\}_s^T$

$$\{\Phi\}_s^T [k] \{\Phi\}_r - \omega_r^2 \{\Phi\}_s^T [m] \{\Phi\}_r = \{0\} \quad (4.84)$$

and both sides of equation 4.53 by $\{\Phi\}_r^T$

$$\{\Phi\}_r^T [k] \{\Phi\}_s - \omega_s^2 \{\Phi\}_r^T [m] \{\Phi\}_s = \{0\} \quad (4.85)$$

Betti's law implies the following relationship for a symmetric matrix [A]

$$\{x\}^T [A] \{y\} = \{y\}^T [A] \{x\} \quad (4.86)$$

Since [k] and [m] are symmetric matrices, which means that $[k] = [k]^T$ and $[m] = [m]^T$, equation 4.82 and 4.83 can be rearranged to

$$\omega_r^2 \{\Phi\}_r^T [m] \{\Phi\}_s = \omega_s^2 \{\Phi\}_s^T [m] \{\Phi\}_r \quad (4.87)$$

The transposed matrices are arbitrary hence the equation may be rewritten as

$$(\omega_r^2 - \omega_s^2) \{\Phi\}_s^T [m] \{\Phi\}_r = 0 \quad (4.88)$$

The first orthogonality condition can be defined due to the fact that the first mode shape \neq second mode shape, and therefore equation 4.88 reduces to

$$\{\Phi\}_s^T [m] \{\Phi\}_r = 0 \quad (4.89)$$

Similarly the equation can be described by the stiffness matrix, and using equation 4.84

$$\{\Phi\}_s^T [k] \{\Phi\}_r = 0 \quad (4.90)$$

This result implies that the vibration mode shapes are orthogonal with respect to both the mass- and stiffness matrix. The orthogonality relationships will be proven to be very useful for mode superposition at MDOF systems. The orthogonality conditions apply to any two different modes, as long as they do not have the same frequency.

Mode superposition

MDOF systems are highly benefitted by uncoupling equations of motion, which is enabled by the generalised coordinates. Uncoupling gives the opportunity to solve these equations independently as SDOF systems. Subsequently, the uncoupled equations can be super-positioned to obtain a solution for MDOF systems. For uncoupling, normal coordinates are introduced as follows

$$\{q\} = \{q(x_1, x_2, \dots, x_n)\} \quad (4.91)$$

so that equation 4.69 can be transformed into a set of n independent equations, whose solutions can be solved independently. The normal coordinates $\{q\}$ can be determined as

$$\{x\} = [\Phi] \{q\} \quad (4.92)$$

where $[\Phi]$ is the $n \times n$ mode-shape matrix and $\{x\}$ is the displacement vector. Similarly the velocity- and acceleration vector can be written as

$$\{\dot{x}\} = [\Phi] \{\dot{q}\} \quad (4.93)$$

$$\{\ddot{x}\} = [\Phi]\{\ddot{q}\} \quad (4.94)$$

Substitution of the latter three equations in equation 4.69 and multiplying by $[\Phi]^T$ yields

$$[\Phi]^T [[m][\Phi]\{\ddot{q}\} + [c][\Phi]\{\dot{q}\} + [k][\Phi]\{q\}] = [\Phi]^T \{F(t)\} \quad (4.95)$$

which can also be written as

$$[M]\{\ddot{q}(t)\} + [C]\{\dot{q}(t)\} + [K]\{q(t)\} = \{P(t)\} \quad (4.96)$$

Equation 4.96 gives rise to the definition of the modal mass matrix [M], modal damping matrix [C], the modal stiffness matrix [K] and modal force vector as follows

$$[M] = [\Phi]^T [m][\Phi] \quad n \times n \quad (4.97)$$

$$[C] = [\Phi]^T [c][\Phi] \quad n \times n \quad (4.98)$$

$$[K] = [\Phi]^T [k][\Phi] \quad n \times n \quad (4.99)$$

$$\{P(t)\} = [\Phi]^T \{F(t)\} \quad n \times 1 \quad (4.100)$$

The former three matrices are all diagonal; hence equation 4.96 can be described as n uncoupled equations

$$M_r \ddot{q}_r + C_r \dot{q}_r + K_r q_r = P_r(t) \quad r = 1, 2, \dots, n \quad (4.101)$$

Average acceleration method

Although superposition is involved, MDOF systems can still be numerically analysed by the *Step-by-step procedure*, since the *twenty-one degree-of-freedom* model is assumed to behave linear under the time varying wind loading. The *Average Acceleration Method* shows improved convergence of the structural response [21] for MDOF systems and equals the *Central Difference Method* (see Section 4.4) of calculating the response during each time step from the initial conditions at the beginning of the step and the loading history during the step. The method consists of calculating the average acceleration during a time step on a linear basis, as depicted in the graph of Figure 4.14.

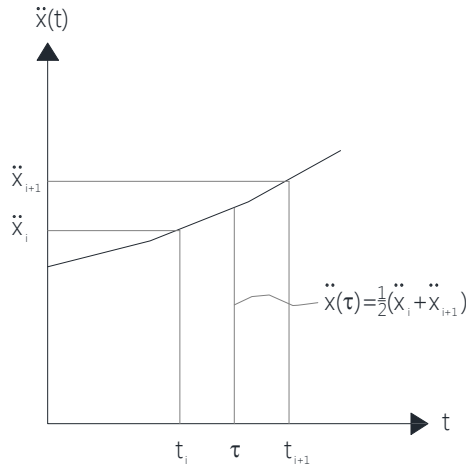


Figure 4.14; Average acceleration method by numerical integration

Calculations are starting with the determination of initial conditions. The magnitude of the displacement, velocity and acceleration at $t = 0$ are calculated by the equation of motion in complete analogy to the *Central Difference Method*. The effective stiffness is defined as

$$\hat{k} = k + \frac{4m}{(\Delta t)^2} + \frac{2c}{\Delta t} \quad (4.102)$$

where k , m and c are a dependant of the mode shape as defined in the pertaining modal matrix. The required time step, Δt , can be determined by dividing the natural period of the highest mode by π^2 . The *Average Acceleration method* has the important advantage that it provides an unconditionally stable integration procedure, which means that very small time steps, in order to gain an accurate solution at higher modes, is not necessary. The appropriate time step is determined by the natural period of the highest mode as follows

$$\Delta t \leq \frac{T_n}{\pi^2} \quad (4.103)$$

where T_n is the natural period of the n -th mode.

The calculation is followed by obtaining the dynamic response of each time step, starting with evaluating the effective incremental force as

$$\Delta \hat{F}_i = \Delta F_i + \left[\frac{4m}{\Delta t} + 2c \right] \dot{x}_i + 2m\ddot{x}_i \quad (4.104)$$

The incremental displacement within each time step is given by

$$\Delta x_i = \frac{\Delta \hat{F}_i}{\hat{k}} \quad (4.105)$$

The incremental velocity and acceleration results from the assumed linear relationship of magnitudes within each time step as follows

$$\Delta \dot{x}_i = \left(\frac{2}{\Delta t} \right) \Delta x_i - 2\dot{x}_i \quad (4.106)$$

$$\Delta\ddot{x}_i = \frac{4}{(\Delta t)^2} (\Delta x_i - \Delta t \dot{x}_i) - 2\ddot{x}_i \quad (4.107)$$

The dynamic response, i.e. displacements, velocities and accelerations, at time t_{i+1} , can now be calculated as follows

$$\begin{aligned} x_{i+1} &= x_i + \Delta x_i \\ \dot{x}_{i+1} &= \dot{x}_i + \Delta \dot{x}_i \\ \ddot{x}_{i+1} &= \ddot{x}_i + \Delta \ddot{x}_i \end{aligned} \quad (4.108)$$

Results of response analysis

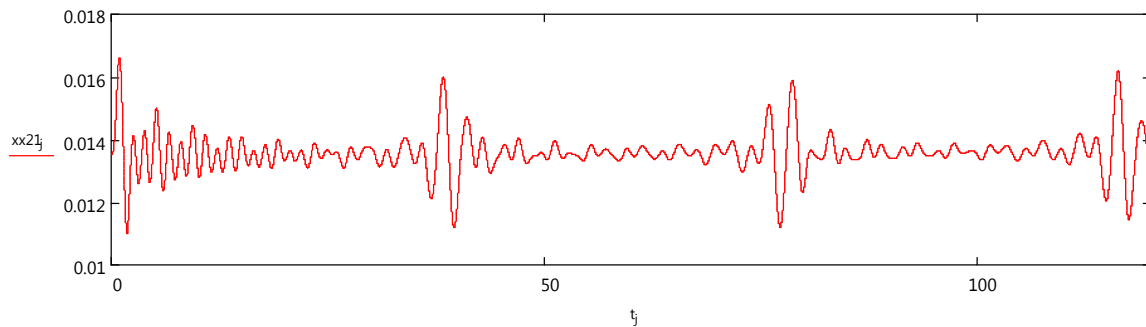
The presented *Average Acceleration Method* is used to perform a dynamic analysis of the proposed MDOF model, for which calculations are shown in C.S.3.6. Table 4.10 presents an overview of the response calculations, in which mode shapes 1 to 5 are displayed.

Table 4.10; Dynamic response of a MDOF system

<p>Structural properties</p> <p>Structural mass: $m_i = \rho_{\text{mean}} A_{\text{floor}} h = 90 \cdot 729 \cdot 3.2 = 209.952 \text{ ton}$</p> <p>Structural stiffness; k, according to C.S.3.5</p> <p>Damping properties: $\zeta = 0.019 \rightarrow c_i = 2m_i\omega_i\zeta$</p> <p>Adopted fundamental frequency for wind loading: 0.56 Hz.</p> <p>Fundamental circular frequency: 4.49 rad/s, $T_1 = 2\pi / \omega_1 = 1.40 \text{ s}$, $n_1 = 4.49 / 2\pi = 0.71 \text{ Hz}$.</p> <p>Natural circular frequencies of mode 2 - 21: [rad/s]</p> <table style="width: 100%; border: none;"> <tr> <td style="width: 50%;">$\omega_2 = 9.78$</td> <td style="width: 50%;">$\omega_5 = 26.54$</td> </tr> <tr> <td>$\omega_3 = 15.07$</td> <td>$\vdots \quad \vdots$</td> </tr> <tr> <td>$\omega_4 = 21.17$</td> <td>$\omega_{21} = 150.1$</td> </tr> </table>					$\omega_2 = 9.78$	$\omega_5 = 26.54$	$\omega_3 = 15.07$	$\vdots \quad \vdots$	$\omega_4 = 21.17$	$\omega_{21} = 150.1$
$\omega_2 = 9.78$	$\omega_5 = 26.54$									
$\omega_3 = 15.07$	$\vdots \quad \vdots$									
$\omega_4 = 21.17$	$\omega_{21} = 150.1$									
<p>Mode shape 1 - 5</p>										
<p>Initial conditions</p> <p>Time step: $T_{21} / 10 = 0.042 / \pi^2 = 0.005 \text{ s}$</p> <p><u>Example 1st mode:</u></p> <p>Initial generalised displacement: $q(x_1) = \frac{P(0)_1}{K_{1,1}}$</p> <p>Initial generalised velocity: $q(\dot{x}_1) = 0 \text{ m/s}$</p> <p>Initial generalised acceleration: $q(\ddot{x}_1) = \frac{1}{M_{1,1}} (P(0)_1 - C_{1,1}q(\dot{x}_1) - K_{1,1}q(x_1)) = 0 \text{ m/s}^2$</p>										

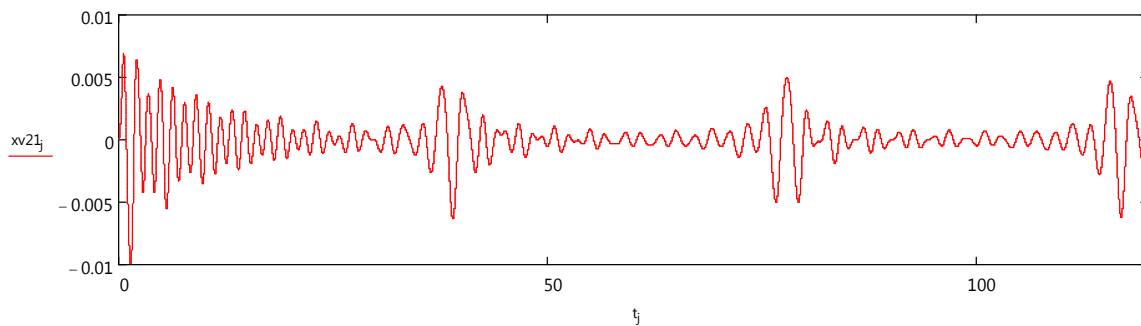
Dynamic response on top floor: displacements

$$x_{\min} = -0.01 \text{ m} \quad x_{\max} = 0.02 \text{ m}$$



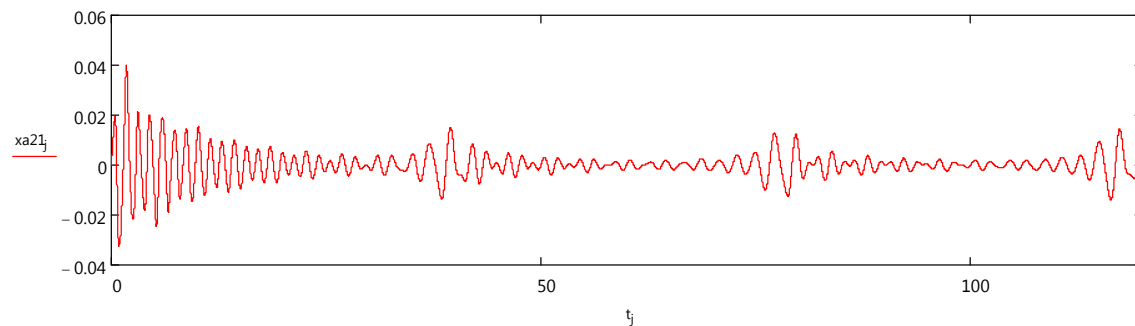
Dynamic response on top floor: velocity

$$v_{\min} = -0.01 \text{ m/s} \quad v_{\max} = 0.01 \text{ m/s}$$



Dynamic response on top floor: accelerations

$$a_{\min} = -0.03 \text{ m/s}^2 \quad a_{\max} = 0.04 \text{ m/s}^2$$



Discussion of the results

Most remarkable from the MDOF dynamic analysis is the relatively high fundamental frequency of n_1 equal to 0.71 Hz , in comparison to the SDOF analysis, which was 0.56 Hz . Estimates of the fundamental frequency, as presented in Section 4.1, has shown good agreement with the SDOF model, which means that it can be expected that the MDOF model either has a too high stiffness or too large deviations in mass modelling.

Dynamic responses correspond with results of the SDOF analysis, although the values are relatively low due to the over-estimated stiffness or deviated mass. It can be seen after the initial wind gusts that horizontal accelerations are very low in comparison to outcomes of spectral analyses and the SDOF model.

Although it has been aimed to approach the static mode shape by assigning an equivalent stiffness to each degree-of-freedom, it might be the modelling of infinite stiff floors and rigidly connected columns which causes *over-stiffness* of the MDOF system. The first mode shape, however, shows behaviour which corresponds with the static deformation mode as depicted in Figure 3.5 and 4.13, where outrigger effects are distinctive in the shape. These effects are also noticeable in higher modes, in which the increased stiffness affects the shape below and above the outriggers.

An inaccurate modelling of lumped masses at each degree-of-freedom is not expected to cause the relatively high fundamental frequency and low horizontal accelerations, since it is common practice [16] for MDOF models to directly transfer the mass density of the building to lumped masses on each storey.

On the basis of the performed dynamic analysis it can be concluded that modelling of a shear frame building by infinite stiff floors, in order to obtain *one* degree-of-freedom per storey, over-estimates the structural stiffness when the actual structural model is not influenced by stiffness of floors. In practice, however, floors may contribute to the structural stiffness of an outrigger structure increasing the fundamental frequency and reducing horizontal accelerations accordingly.

4.6 3D COMPUTER MODEL

Analysing a structure in a 3D computer model is always highly beneficial for improving the validity of results obtained by hand calculations, whether the model is statically or dynamically analysed. As stated before, the accuracy of both SDOF and MDOF models is affected by the mass- and stiffness properties of the system. Furthermore, SDOF systems are also influenced by the spatial distribution and time variation of the loading.

Nevertheless, for a symmetric structure 2D analysis should result in reliable values for the dynamic response, thus large differences with regard to prior calculations are not expected.

Modelling input

The Finite Element based program STAAD Pro enables the designer to model both beam elements and 2D elements, such as orthotropic plates. Materials and dimensions of elements are adopted from the static design, once more shown in Table 4.11.

In order to take into account the effective properties of CLT panels the stiffness, $E_{0,mean}$, is multiplied by the composite factor, k_3 , as determined in Chapter 3 on 0.806 so that

$$E_{0,mean} = 0.806 \cdot 12\,000 = 9\,672 \text{ MPa.}$$

In cross direction composite factor k_4 applies, which equates to 0.225, hence

$$E_{90,mean} = 0.225 \cdot 12\,000 = 2\,696 \text{ MPa.}$$

Table 4.11; Input properties of structural elements in STAAD Pro

<i>Element</i>	<i>Material</i>	<i>Dimensions</i>
CLT core	2D Orthotropic, $E_{0,mean} = 9\,672 \text{ MPa.}$, $E_{90,mean} = 2\,696 \text{ MPa.}$, $G = 550 \text{ MPa.}$, $\rho_{mean} = 380 \text{ kg/m}^3$, $\zeta = 1.9\%$	d = 300 mm
Glulam columns	GL28h, $E_{0,mean} = 12\,600 \text{ MPa.}$, $G = 600 \text{ MPa.}$, $\rho_{mean} = 410 \text{ kg/m}^3$, $\zeta = 1.9\%$	600 x 600 mm

Glulam beams and diagonals	GL28h, $E_{0,\text{mean}} = 12\,600\text{ MPa}$., $G = 600\text{ MPa}$., $\rho_{\text{mean}} = 410\text{ kg/m}^3$, $\zeta = 1.9\%$	500 x 400 mm
CLT floors	2D Orthotropic, $E_{0,\text{mean}} = 500\text{ MPa}$., $E_{90,\text{mean}} = 500\text{ MPa}$., $G = 100\text{ MPa}$., $\rho_{\text{mean}} = 380\text{ kg/m}^3$, $\zeta = 1.9\%$	d = 270.9 mm

The CLT core is provided with door openings, which are not taken into account at calculations for static design. On the other hand, the center wall in the core is modeled, which was neglected in the static design. All connections of glulam beams and diagonals are designed as pinned. Columns, however, are modeled as pinned at every four storeys so that their length consists of 12.8 meters. Floor connections are rigidly modeled in order to ensure structural stability⁸, but comprise relatively low stiffness properties. As a consequence, the contribution of floor slabs to the overall stability system will be negligible. Supports include fixed connections for the central core and hinge connections for the peripheral columns. The 3D model of the structure is shown in Figure 4.15.

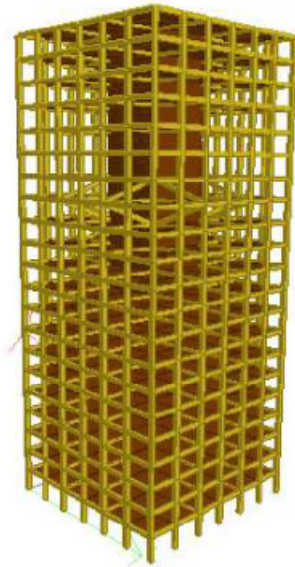


Figure 4.15; STAAD Pro 3D render of structural model

Excitations to the structure

A modal calculation can be performed to obtain natural frequencies and mode shapes of the structure. STAAD Pro equally transfers mass properties of elements to each node, simply by taking the assigned densities of materials, resulting in lumped masses. In complete analogy with previous analyses only the structure's self weight is incorporated in dynamic calculations.

Wind loading is modeled as a 'mean part' and a 'fluctuating part'. The mean wind velocity carries for a static lateral loading at each node on the windward side, whilst the fluctuating wind forces are defined as a 'time history load' previously defined in Section 4.3.

The mean wind force on any node of the windward side of the building is defined as follows

$$F_{\text{mean}} = \left(\frac{1}{2} \rho_{\text{air}} C_d V_m^2 \right) A \quad (4.109)$$

⁸ The program shows instability errors when floor connections are only constrained in displacements and are free to rotate at the floor edges

where ρ_{air} is 1.25 kg/m^3 , c_d is 1.07 (see Section 4.3), A is the façade area pertaining to a column-beam node. This area is equal to (h x centre-to-centre distance columns) $3.2 \times 4.5 = 14.4 \text{ m}^2$, whilst for nodes on the perimeter of the façade half of this area applies, i.e. $3.2 \times 2.25 = 7.2 \text{ m}^2$. The mean wind velocity, $v_{m,r}$ is determined on the reference height (i.e. $0.6H = 40.3$ meters) of the building and given in Appendix A.1 as 26.07 m/s . The mean wind force on a typical node is

$$F_{\text{mean}} = \left(\frac{1}{2} \cdot 1.25 \cdot 1.07 \cdot 26.07^2 \right) 14.4 \cdot 10^{-3} = 6.54 \text{ kN}$$

whilst for perimeter nodes

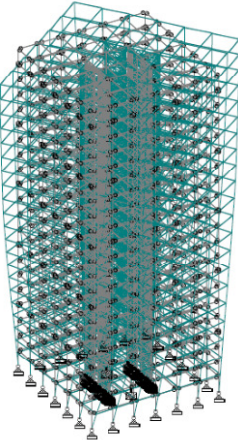
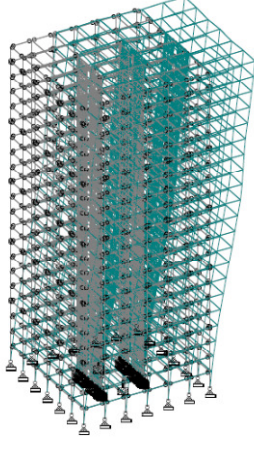
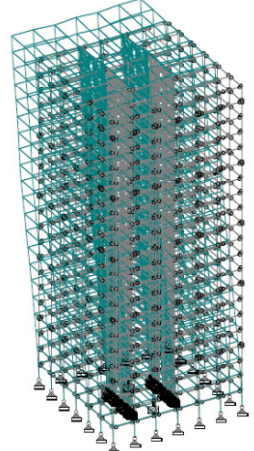
$$F_{\text{mean}} = \left(\frac{1}{2} \cdot 1.25 \cdot 1.07 \cdot 26.07^2 \right) 7.2 \cdot 10^{-3} = 3.27 \text{ kN}$$

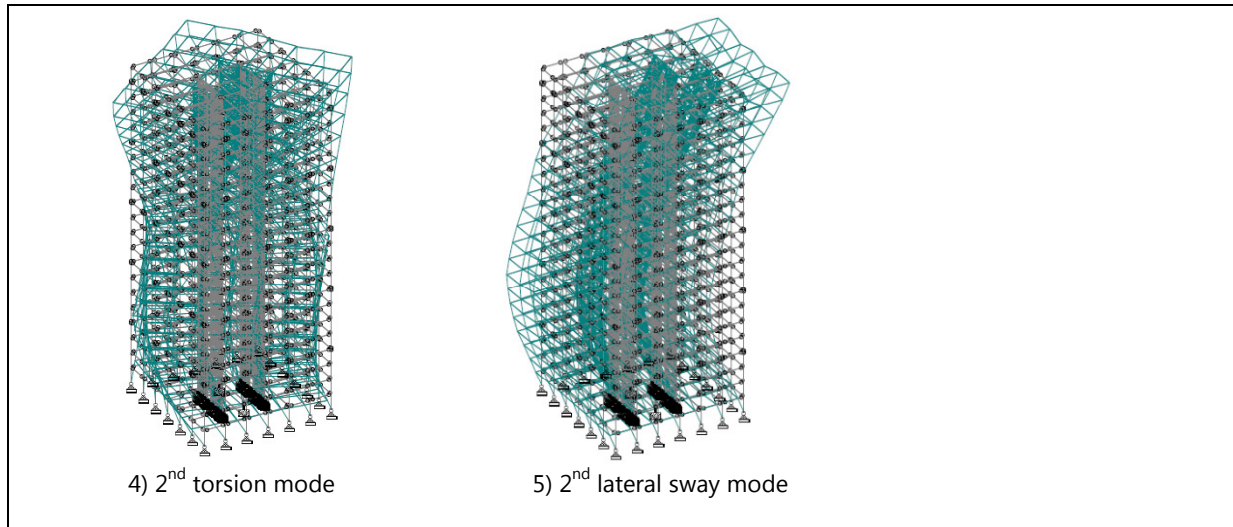
Natural frequency and mode shape results

The modal calculation is restricted to twenty mode shapes in order to confine the computation time. Moreover, analysis of higher modes is regarded as irrelevant for the dynamic response in practice. It must be emphasised that the most important mode shape is the fundamental mode shape, which is most likely to occur in practice under fluctuating wind loading. However, for analysis on structural vibrations higher modes are more usual to adopt.

Input properties and STAAD Pro outcomes are presented in C.S.3.7 of Appendix A.3, for which Table 4.12 shows the computed natural frequencies and pertaining shapes of the mode 1 to 5.

Table 4.12; STAAD Pro modal calculation results

<p>Natural frequencies Fundamental circular frequency: 2.64 rad/s, $n_1 = 2.64 / 2\pi = 0.42 \text{ Hz}$. Natural circular frequencies of mode 2 - 20: [rad/s]</p> <table style="width: 100%; border: none;"> <tr> <td style="width: 50%;">$\omega_2 = 3.64$</td> <td style="width: 50%;">$\omega_5 = 12.04$</td> </tr> <tr> <td>$\omega_3 = 3.82$</td> <td style="text-align: center;">\vdots</td> </tr> <tr> <td>$\omega_4 = 7.97$</td> <td style="text-align: center;">\vdots</td> </tr> <tr> <td>$\omega_5 = 12.04$</td> <td>$\omega_{20} = 25.15$</td> </tr> </table>			$\omega_2 = 3.64$	$\omega_5 = 12.04$	$\omega_3 = 3.82$	\vdots	$\omega_4 = 7.97$	\vdots	$\omega_5 = 12.04$	$\omega_{20} = 25.15$
$\omega_2 = 3.64$	$\omega_5 = 12.04$									
$\omega_3 = 3.82$	\vdots									
$\omega_4 = 7.97$	\vdots									
$\omega_5 = 12.04$	$\omega_{20} = 25.15$									
<p>Mode shape 1 - 5</p> <div style="display: flex; justify-content: space-around; align-items: flex-end;"> <div style="text-align: center;">  <p>1) torsion mode</p> </div> <div style="text-align: center;">  <p>2) lateral sway mode</p> </div> <div style="text-align: center;">  <p>3) lateral sway mode</p> </div> </div>										



The fundamental mode shows torsional behaviour and yields a natural frequency of 0.42 Hz., whilst the second mode resembles lateral sway. All previously analysed models, i.e. estimated fundamental frequencies, SDOF model and MDOF model, correspond to lateral oscillations only.

Torsional mode shapes and natural frequencies have not been studied in previous analysis and are very unlikely to occur as a fundamental frequency of a building structure⁹.

As shown in the table above, the second mode comprises lateral sway and has a natural frequency of 0.58 Hz., which is slightly higher than the estimated fundamental frequency (0.55 / 0.53 Hz.) and fundamental frequency obtained with equivalent properties (0.56 Hz.).

Further, it can be seen that lateral sway in cross direction, i.e. mode shape 3, has an almost similar natural frequency. Mode shape 12 and higher show longitudinal vibration modes of floor structures and is in any case not representing vibrating appearances in practice.

Torsional mode

Torsional vibrations occur due to local twisting of a beam or shaft about its longitudinal axis. Natural frequencies of torsion are a function of the torsional constant, J . This geometrical property is defined as the moment required to produce a torsional rotation of 1 radian over a unit length of the beam or shaft. J depends on the cross section, where in case of a square hollow section

$$J = \frac{2th^2b^2}{h+b} \quad (4.110)$$

where t is the thickness, h the height and b the width of the cross section.

The resistance of the cross section to torsion is expressed by the polar area moment of inertia as follows

$$I_p = I_x + I_y \quad (4.111)$$

where I_x and I_y represent the moment of inertia in the x-direction and y-direction respectively. The natural frequency of torsion for uniform shafts can be evaluated by [23]

$$n_i = \frac{\lambda_i}{2\pi H} \sqrt{\frac{JG}{\rho I_p}} \quad (4.112)$$

⁹ Cited by Dr. Johnson Zhang and Dr. Ben Zhang, Napier University Edinburgh

where λ_i is a dependant on the boundary conditions of the shaft and representing mode i as follows

$$\lambda_i = \frac{(2i-1)\pi}{2}, \quad i = 1, 2, 3, \dots, n \quad (4.113)$$

Material properties of the shaft are represented by the shear modulus, G . Mass properties in equation 4.112 includes the density of the material, ρ . It must be noted that the result of equation 4.112 is only exact for uniform, isotropic, homogeneous shafts with a circular cross section.

The outrigger structure, consisting of a CLT core and pinned frame structure with outriggers, does not comply with restrictions above. The structure is non-uniform, orthotropic and has a non-circular cross section. However, considering the torsional stiffness of the CLT core only and assuming isotropic material, which can be justified since the shear modulus of CLT panels is non-dependant of two in-plane directions, a torsional natural frequency can be estimated.

Further, the exact solution is found for circular cross sections only because the equation neglects warping of the shaft. However, the effect of warping on the deformation is very small for simple closed cross sections, which are small in comparison to the length of the shaft [23]. Although the slenderness of the CLT core might be too low for this statement, warping is not considered for this case.

Table 4.13 gives an overview of calculations according to presented equations 4.110 to 4.113, which results in an estimated natural frequency for the torsion mode.

Table 4.13; Determination of the fundamental frequency of torsion mode

<i>Structural property</i>	<i>Value</i>	
CLT core dimensions; $h \times b, t$	9.3 x 9.3, 0.3	m
Torsional constant; J	218.7	m ⁴
Shear modulus; G	550 000	kN/m ²
Material density; ρ	90	kg/m ³
Moment of inertia; $I_x (=I_y)$	$(9.3^4/12) - (8.7^4/12) = 145.962$	m ⁴
Polar area moment of inertia; I_p	$2 \cdot 145.962 = 291.924$	m ⁴
Factor λ_1	$\pi / 2$	-
Natural frequency; n_1	0.25	Hz.

The estimated natural frequency for torsional behaviour in the first mode appears to be lower than computed by STAAD Pro. As mentioned above, certain assumptions are taken into account, such as resistance to torsion by the central core only and neglecting warping effects during torsion. Contribution of the frame structure, together with the outriggers, is obviously of great importance for the difference in both outcomes. Although the floors are modelled with very low in-plane stiffness in STAAD Pro, the effects on the geometry are massively since outer dimensions of the structure are 27 x 27 meters.

As stated before, torsional modes for building structures are very unlikely to occur in practice, hence these are not taken into account for dynamic analysis.

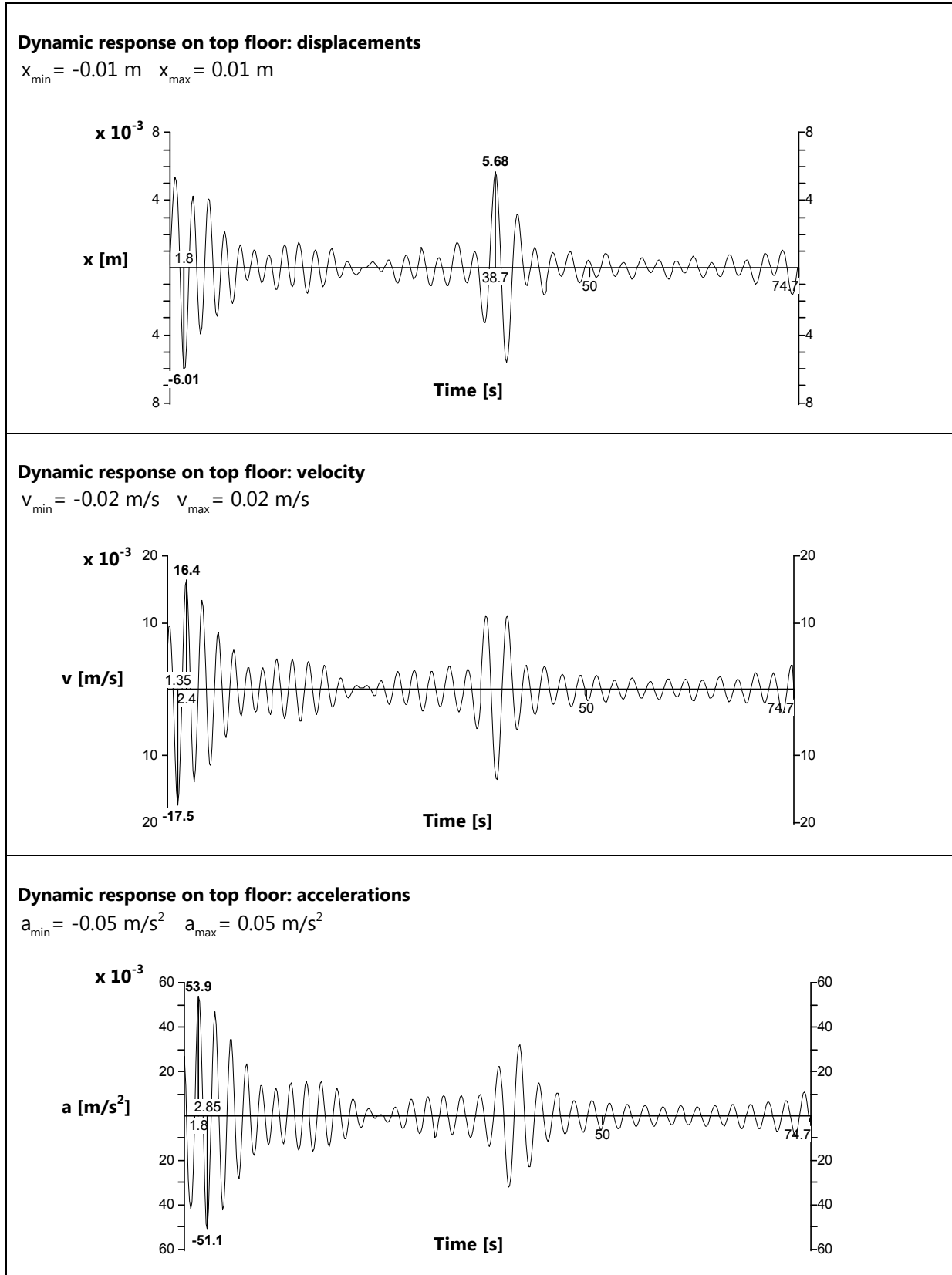
Effects which may induce torsional vibration modes are; asymmetric building plans and shapes of facades affecting wind loads to the structure. Obviously, local wind effects such as influences from terrain orography and surrounding structures may increase the probability of torsional vibration modes for structures.

Results of response analysis

STAAD Pro is able to compute the dynamic response at each time step and present this behaviour in a graph in a similar manner as conducted by previous analysis techniques. Table 4.14 shows the dynamic

response under fluctuating wind loading. The results are obtained from a single joint (grid 7-A Figure 3.6) on the top floor of the building, where differences between other joints on the top floor are negligible.

Table 4.14; STAAD Pro results of dynamic response



Discussion of the results

The dynamic responses show similar patterns as the SDOF model and MDOF model, which means that the former gust has the largest impact on the structure. Displacements are lower, however, in comparison to previous dynamic analysis. As a consequence, the maximum velocity as well as maximum horizontal acceleration on the top floor is higher. Nevertheless, horizontal accelerations remain within permissible values as defined by the Dutch building code NEN 6702 (Figure 4.10).

4.7 CONCLUDING REMARKS ON DYNAMIC ANALYSIS RESULTS

In this chapter five types of analysis have been performed in order to define the structural dynamic behaviour under fluctuating wind loads of the preliminary design for an outrigger structure of a twenty-storey timber building. Obtained results in dynamic properties and dynamic responses are given in Table 4.15.

Table 4.15; Overview of dynamic analysis results for the twenty-storey outrigger structure

Fundamental frequency	ω_1 [rad/s]	n_1 [Hz.]
Estimation by fixed strut	3.46	0.55
Estimation method by 'van Oosterhout'	3.33	0.53
SDOF model	3.50	0.56
MDOF model	4.49	0.71
STAAD Pro (torsion)	2.64	0.42
STAAD Pro (lateral sway)	3.64	0.58
Dynamic response; horizontal accelerations	\ddot{x}_{\max} [m/s ²]	
Spectral analysis	0.03	
SDOF model	0.05	
MDOF model	0.04	
STAAD Pro	0.05	

The fundamental frequencies of performed analyses may differ, the lowest (0.42 Hz.) and highest (0.71 Hz.) can be clarified by modelling issues. A torsional vibration mode obtained with STAAD Pro resembles a relatively low natural frequency, which was underpinned by a 'hand calculation', but it has been stated that this mode is not representative for the structure in practice.

MDOF analysis has shown a rather high value for the fundamental frequency, due to *over-stiffness* in the mechanical model. Despite it was questioned if the SDOF model would resemble accurate results for an outrigger structure, due to non-uniform stiffness over the height of the building, analysis has shown a fundamental frequency in between estimations (0.55 / 0.53 Hz.) and the result of STAAD Pro computations (0.58 Hz.)

With regard to dynamic responses, horizontal accelerations of the SDOF model and STAAD Pro model are nearly of the same magnitude, which can also be seen for dynamic displacements and –velocities (Table 4.9 and Table 4.14). Spectral analysis has resulted in a relatively low horizontal acceleration. It can be concluded that the first part of the excitation to the structure, i.e. wind gust at zero seconds, induces the largest accelerations, which not effects results of spectral analysis and therefore shows a lower magnitude. This can also be noted in the response graph of Table 4.9 and 4.14, where the second wind gust at approximately 40 seconds shows a similar acceleration of 0.03 m/s².

The effects of the immediate gust to the structure may be questionable. This sudden excitation, i.e. within 0 -5 seconds will normally not appear in practice, since there will always be a certain amount of initial wind excitation to the structure. Therefore, the response at 40 seconds may reflect the real behaviour more accurately.

The presented dynamic analyses in this chapter have shown that the structural response under dynamic wind loading complies with the design criteria as defined in the Dutch Building code NEN 6702 and thereby proves the successive dynamic behaviour of the proposed preliminary design of a timber outrigger structure for a twenty-storey building. Therefore, modifications to the structural design are not required before starting with a final structural design.

5 | FINAL STATIC DESIGN

Element design with Finite Element Analysis

The dynamic analyses have shown that modifications to the initial structural design, as defined in the preliminary static design phase, are not required. Hence the preliminary design will be adopted as starting point to perform a final static 3D analysis. Modelling the structure in a FE program enables the engineer to obtain an accurate stress distribution in structural elements as well as the deformation behaviour during serviceability. Due to full symmetry of the structural plan 2D analysis was a useful tool to indicate the performances of the structure under lateral loading in the preliminary design phase. Despite effects of vertical loading have been taken into account, their accuracy was already stated as doubtful due to; approximations on their magnitude as well as the lack of loading combinations in the Ultimate Limit State and the Serviceability Limit State.

The final static design phase starts with definitions of the static loading on the structure according to EC0 and EC1 along the Dutch National Annex. Subsequently a 3D analysis will be performed in the FE program 'STAAD Pro' in order to obtain structural actions in ULS and SLS. Elements in the structure will be verified on their strength according to the European code for timber structures, EC5. Possible required modifications to the design will be conducted in order to comply with unity checks on various structural actions. Nevertheless, deformations in the SLS are expected to dominate the design once again as is usually the case for timber structures generally spoken. This applies to both the structural system as a whole, as well as for single structural elements.

5.1 LOADING ACTIONS ACCORDING TO EUROCODE

Combinations of loading actions are defined in EC0 where distinctions are made between excitations according to the building's function as well as the ULS and SLS.

Magnitudes of imposed loading are defined in EC1 and are also a dependant on the function of the building.

Loadings on the structure

Loadings can be divided into three categories as follows

- Self weight of the structure;
- Permanent loading: partition walls, interior walls, floor- and ceiling constructions;
- Variable loading: imposed floor- and roof loading, lateral wind loading, snow loading.

Values of several excitations are defined in Table 5.1.

Table 5.1; Categorised loadings on the structure

Category	Type	Characteristic load; q_k
Self weight structure, G	Structural elements	Generated by STAAD Pro
Permanent loading, G	Partition walls	0.8 kN/m ² x 2.6 (height) = 2.08 kN/m
	Interior walls	0.5 kN/m ²
	Floor- and ceiling constructions	0.3 kN/m ²
	Total	2.08 kN/m and 0.8 kN/m ²
Variable loading, Q	Imposed floor loading offices	2.5 kN/m ²
	Imposed floor loading communal areas offices	3.0 kN/m ²
	Imposed floor loading apartments	1.75 kN/m ²
	Imposed floor loading communal areas apartments	2.0 kN/m ²
	Imposed roof loading	1.0 kN/m ²
	Lateral wind loading	see Section 3.2
	Snow loading	0.56 kN/m ²

Design criteria in the ULS

Criteria of the ULS in EC0 comprise a distinction between verifications on limit states in static equilibrium (EQU) and limit states of failures (STR). The former limit states are deployed for instance; to check 'toppling-over' of the structure or to compute vertical tensile forces in shear walls for connections. It should be noted that stresses caused by these tensile forces are related to the limit states for failure (STR). These states are used for verifications on strength for structural elements. For static equilibrium the structure should comply with

$$Ef_{d,dst} \leq Ef_{d,stb} \quad (5.1)$$

where $Ef_{d,dst}$ is the design value of the destabilising loading action and $Ef_{d,stb}$ is the design value of the stabilising action of the structure.

Checks on failures of structural elements should comply with the following requirement

$$Ef_d \leq R_d \quad (5.2)$$

where Ef_d is the design value of the loading action and R_d is the design value of the resistance of the pertaining structural element calculated as

$$R_d = k_{mod} \frac{R_k}{\gamma_M} \quad (5.3)$$

where k_{mod} is a modification factor which takes into account the duration of loading effects and Service Class shown in Table 5.2, R_k is the characteristic value of the resistance and γ_M is the partial factor for the material property. The partial factor for applied materials in the structure, i.e. CLT and glulam, is 1.25. The Service Class of the building, and thus all structural elements, is 1, which refers to an indoor climate.

Table 5.2; Modification factors for several loading durations

Loading action	Load duration	k_{mod} (glue laminated timber, Service Class 1)
Self weight	Permanent	0.6
Permanent loading	Permanent	0.6
Imposed floor loading	Medium – term	0.8
Snow loading	Short – term	0.9
Wind loading	Short - term	0.9

Design values of stiffness properties are determined by the partial factor for the material as follows

$$E_d = \frac{E_{mean}}{\gamma_M} \quad G_d = \frac{G_{mean}}{\gamma_M} \quad (5.4)$$

Design criteria in the SLS

Serviceability requirements of a building are predominantly based on deformations of both the whole structure and single structural elements. Furthermore, vibrations of floors should be limited to permissible frequencies by designing these elements above a certain minimum fundamental frequency. The Dutch National Annex refers to the Dutch National Code NEN 6702 for allowable deformations of the whole structure and individual structural elements. Permissible horizontal accelerations are previously defined (Figure 4.10) according to the occupant's function in the building. Table 5.3 sums up the requirements for the SLS as defined in NEN 6702.

Table 5.3; Design criteria in the SLS

Appearance during serviceability	Structural element	Requirement
Lateral displacement building	Structure	$U_{max} \leq H / 500$
Lateral displacement single storey	Structure	$U_{max} \leq h / 300$
Total vertical displacement	Floor / beam	$U_{max} \leq 0.004 \times L_{rep}$
Time dependent vertical displacement	Floor / beam	$U_{max} \leq 0.003 \times L_{rep}$
Time dependent vertical displacement	Roof /beam	$U_{max} \leq 0.004 \times L_{rep}$
Vibrations	Floor	$n_1 \geq 3 \text{ Hz}^{10}$
Horizontal accelerations (residential function)	Structure	$a \leq 0.14 \text{ m/s}^2$

It must be noted that requirements in the SLS on structural elements may also depend on requirements as agreed with the client. For instance the allowable magnitudes of deflected beams may depend on adjacent constructional elements, connections and so on. Considerations of these types will be taken into account during the element design.

Loading combinations in the ULS

Loading combinations for persistent or transient design situations in the ULS are as follows

- For static equilibrium, i.e. EQU (equation 6.10 EC0):

$$E_f = \sum_{j \geq 1} \gamma_{Gj} G_{k,j} + \gamma_{Q,1} Q_{k,1} + \sum_{i > 1} \gamma_{Q,i} \psi_{0,i} Q_{k,i} \quad (5.5)$$

¹⁰ Structural engineer Mr. Greger Lindgren of Martinsons Byggsystem KB designs timber floors on a minimum fundamental frequency between 10 and 12 Hz. in order to ensure a high level of comfort for occupants

- For limit state failures, i.e. STR (equation 6.10a and 6.10b EC0):

$$E f_d = \sum_{j \geq 1} \gamma_{Gj} G_{k,j} + \gamma_{Q1} \psi_{0,1} Q_{k,1} + \sum_{i > 1} \gamma_{Q,i} \psi_{0,i} Q_{k,i} \quad (5.6)$$

$$E f_d = \sum_{j \geq 1} \xi_j \gamma_{Gj} G_{k,j} + \gamma_{Q,1} Q_{k,1} + \sum_{i > 1} \gamma_{Q,i} \psi_{0,i} Q_{k,i} \quad (5.7)$$

where

- γ_G is a partial factor for permanent loading, i.e. 0.9 (equation 5.5), 1.35 (equation 5.6 and 5.7). For favourable effects of permanent loading the factor should be 0.9 in equation 5.6 and 5.7
- γ_Q is a partial factor for variable loading, i.e. 1.5 in all cases
- ψ_0 is a combination value depending on the building's function, defined in Table 5.4
- ξ is a reduction value for unfavourable permanent actions, i.e. 0.89
- G_k is the permanent action
- $Q_{k,1}$ is the leading variable action
- Q_k is an accompanying variable action

Combination values, ψ_i , as written in loading combinations of equation 5.5 to 5.7 are given in Table 5.4.

Table 5.4; Combination values, ψ_i

Loading action	ψ_0	ψ_1	ψ_2
Category A: residential	0.4	0.5	0.3
Category B: commercial	0.5	0.5	0.3
Category H: roofs	0	0	0
Snow loads	0	0.2	0
Wind loads	0	0.2	0

In the case of multiple loads on a structure it must be noted that all possible combinations should be considered. For timber structures, however, the k_{mod} factor is related to the load duration which introduces another dependant for governing loading combinations. For instance, when a simply supported beam is loaded by its self weight (k_{mod} is 0.6) and a variable action (k_{mod} is 0.8) the loading effect solely by its self weight may be governing due to the lower design strength.

Furthermore, EC0 (Clause 6.3.1.2(10)) refers to a reduction value for imposed floor loading in multi-storey constructions. This reduction value, α_n , is only allowed for the design of vertical structural elements, such as columns and shear walls. Background of this reduction for buildings with multiple floors is that it can be assumed that full imposed loading on each floor is very unlikely to occur. The reduction factor can be determined as

$$\alpha_n = \frac{2 + (n - 2)\psi_0}{n} \quad (5.8)$$

where n is the number of storeys above the calculated structural element. Due to multiple functions in the building two reduction values should be determined. For structural calculations of vertical elements on the ground floor, the reduction value for imposed floor loading of the commercial function and residential function respectively results in

$$\alpha_{n,1} = \frac{2 + (10 - 2)0.5}{10} = 0.6 \quad \alpha_{n,2} = \frac{2 + (10 - 2)0.4}{10} = 0.52$$

In order to minimise the number of loading combinations only relevant combinations for each structural element are summarised in Table 5.5.

Table 5.5; Loading combinations in the ULS

<i>Static equilibrium (EQU)</i>				
<i>Design</i>	<i>Loading combination</i>	<i>k_{mod}</i>	<i>Reference</i>	
Toppling over of	0.9G '+' 1.5Q _{k,wind}	0.6	ULS-EQU-1	
structure; tensile forces in columns and core	0.9G '+' 1.5Q _{k,wind} '+' 1.5(α _{n,1} Q _{k,v,off} '+' α _{n,2} Q _{k,v,ap})	0.9	ULS-EQU-2	
<i>Limit state failures (STR)</i>				
<i>Design</i>	<i>Loading combination</i>	<i>k_{mod}</i>	<i>Reference</i>	
Floor structures	1.35G	0.6	ULS-STR-1	
	1.35G '+' 1.5 ψ _{0,i} Q _{k,v,off}	0.8	ULS-STR-2	
	1.2G '+' 1.5Q _{k,v,off}	0.8	ULS-STR-3	
Beams / diagonals	1.35G	0.6	ULS-STR-1	
	1.35G '+' 1.5(ψ _{0,i} Q _{k,v,off} '+' ψ _{0,i} Q _{k,v,ap})	0.8	ULS-STR-4	
	1.2G '+' 1.5(Q _{k,v,off} '+' Q _{k,v,ap})	0.8	ULS-STR-5	
	1.2G '+' 1.5Q _{k,snow} '+' 1.5(ψ _{0,i} Q _{k,v,off} '+' ψ _{0,i} Q _{k,v,ap})	0.9	ULS-STR-6	
	1.2G '+' 1.5Q _{k,wind} '+' 1.5(ψ _{0,i} Q _{k,v,off} '+' ψ _{0,i} Q _{k,v,ap})	0.9	ULS-STR-7	
	Columns / walls	1.35G	0.6	ULS-STR-1V
	1.35G '+' 1.5(ψ _{0,i} α _{n,1} Q _{k,v,off} '+' ψ _{0,i} α _{n,2} Q _{k,v,ap})	0.8	ULS-STR-4V	
1.2G '+' 1.5(α _{n,1} Q _{k,v,off} '+' α _{n,2} Q _{k,v,ap})	0.8	ULS-STR-5V		
1.2G '+' 1.5Q _{k,snow} '+' 1.5(ψ _{0,i} α _{n,1} Q _{k,v,off} '+' ψ _{0,i} α _{n,2} Q _{k,v,ap})	0.9	ULS-STR-6V		
1.2G '+' 1.5Q _{k,wind} '+' 1.5(ψ _{0,i} α _{n,1} Q _{k,v,off} '+' ψ _{0,i} α _{n,2} Q _{k,v,ap})	0.9	ULS-STR-7V		
0.9G	0.6	ULS-STR-8V		
0.9G '+' 1.5(ψ _{0,i} α _{n,1} Q _{k,v,off} '+' ψ _{0,i} α _{n,2} Q _{k,v,ap})	0.8	ULS-STR-9V		
0.9G '+' 1.5(α _{n,1} Q _{k,v,off} '+' α _{n,2} Q _{k,v,ap})	0.8	ULS-STR-10V		
0.9G '+' 1.5Q _{k,snow} '+' 1.5(ψ _{0,i} α _{n,1} Q _{k,v,off} '+' ψ _{0,i} α _{n,2} Q _{k,v,ap})	0.9	ULS-STR-11V		
0.9G '+' 1.5Q _{k,wind} '+' 1.5(ψ _{0,i} α _{n,1} Q _{k,v,off} '+' ψ _{0,i} α _{n,2} Q _{k,v,ap})	0.9	ULS-STR-12V		

Loading combinations in the SLS

In the SLS partials factors, γ_G and γ_Q, are set equal to 1. Combinations of loadings are defined as reversible or irreversible, where reversible means that when actions causing an infringement and are subsequently removed the exceedance is also removed. Irreversible limit states are defined by the *characteristic combination* as follows (equation 6.14b EC0)

$$E f_d = \sum_{j \geq 1} G_{k,j} + Q_{k,1} + \sum_{i > 1} \psi_{0,i} Q_{k,i} \quad (5.9)$$

Reversible limit states are described by the *frequent combination* (equation 6.15b EC0) as follows

$$E f_d = \sum_{j \geq 1} G_{k,j} + \psi_{1,1} Q_{k,1} + \sum_{i > 1} \psi_{2,i} Q_{k,i} \quad (5.10)$$

For assessments of long term effects, such as creep, a *quasi-permanent combination* (equation 6.16b) is used which can be written as

$$E f_d = \sum_{j \geq 1} G_{k,j} + \sum_{i > 1} \psi_{2,i} Q_{k,i} \quad (5.11)$$

Relevant loading combinations for the structure as well as structural elements are presented in Table 5.6. It must be noted that the influence of the modification factor, k_{mod} , on the governing loading combinations does not apply for the SLS.

Table 5.6; Loading combinations in the SLS

<i>Frequent loading combination (FRE)</i>		
<i>Design</i>	<i>Loading combination</i>	<i>Reference</i>
Floor and beam deflections	$G \text{ ' + ' } \Psi_{1,i} Q_{k,v,off} \text{ ' + ' } \Psi_{1,i} Q_{k,v,ap}$	SLS-FRE-1
	$G \text{ ' + ' } \Psi_{1,i} Q_{k,snow} \text{ ' + ' } \Psi_{2,i} Q_{k,v,off} \text{ ' + ' } \Psi_{2,i} Q_{k,v,ap}$	SLS-FRE-2
	$G \text{ ' + ' } \Psi_{1,i} Q_{k,wind} \text{ ' + ' } \Psi_{2,i} Q_{k,v,off} \text{ ' + ' } \Psi_{2,i} Q_{k,v,ap}$	SLS-FRE-3
Lateral displacements	$G \text{ ' + ' } \Psi_{1,i} Q_{k,wind}$	SLS-FRE-4
	$G \text{ ' + ' } \Psi_{1,i} Q_{k,snow} \text{ ' + ' } \Psi_{2,i} Q_{k,v,off} \text{ ' + ' } \Psi_{2,i} Q_{k,v,ap}$	SLS-FRE-2
	$G \text{ ' + ' } \Psi_{1,i} Q_{k,wind} \text{ ' + ' } \Psi_{2,i} Q_{k,v,off} \text{ ' + ' } \Psi_{2,i} Q_{k,v,ap}$	SLS-FRE-3
<i>Characteristic loading combination (CHA)</i>		
<i>Design</i>	<i>Loading combination</i>	<i>Reference</i>
Floor and beam deflections	$G \text{ ' + ' } Q_{k,v,off} \text{ ' + ' } Q_{k,v,ap}$	SLS-CHA-1
	$G \text{ ' + ' } Q_{k,snow} \text{ ' + ' } \Psi_{0,i} Q_{k,v,off} \text{ ' + ' } \Psi_{0,i} Q_{k,v,ap}$	SLS-CHA-2
	$G \text{ ' + ' } Q_{k,wind} \text{ ' + ' } \Psi_{0,i} Q_{k,v,off} \text{ ' + ' } \Psi_{0,i} Q_{k,v,ap}$	SLS-CHA-3
Lateral displacements	$G \text{ ' + ' } Q_{k,snow} \text{ ' + ' } \Psi_{0,i} Q_{k,v,off} \text{ ' + ' } \Psi_{0,i} Q_{k,v,ap}$	SLS-CHA-2
	$G \text{ ' + ' } Q_{k,wind} \text{ ' + ' } \Psi_{0,i} Q_{k,v,off} \text{ ' + ' } \Psi_{0,i} Q_{k,v,ap}$	SLS-CHA-3
<i>Quasi-permanent loading combination (QUA)</i>		
<i>Design</i>	<i>Loading combination</i>	<i>Reference</i>
Floor and beam deflections	$G \text{ ' + ' } \Psi_{2,i} Q_{k,v,off} \text{ ' + ' } \Psi_{2,i} Q_{k,v,ap}$	SLS-QUA-1

5.2 STRUCTURAL MODELLING

The whole structure as defined in the preliminary static design is modelled in the FE program STAAD Pro. Properties of 3D orthotropic and 2D beam elements are also previously defined (Table 4.12) during the dynamic design stage.

Joints between elements

Modelling of nodes in a FE program is of great importance in order to obtain accurate force- and stress distributions in elements.

First of all, to circumvent large stress concentrations at joints, beam- and plate elements should always be connected together by nodes. This applies to; beam to beam, plate to plate and beam to plate joints.

Secondly, force transfer of floor slabs to beams and CLT wall elements should occur according to one-way spans. However, the program allows force transfer merely by corner nodes of plate elements and since these nodes are connected to the beam ends, forces in beam sections do not coincide with modelling in real practice.

Thirdly, to ensure overall structural stability during computations floor slabs are rigidly jointed to the beams and walls. This is required since all beams are pin jointed to columns and the CLT core; hence floor slabs should provide in-plane stiffness in order to transfer horizontal loads to the central core. In order to minimise the contribution of floor slabs to the lateral stability, orthotropic floor elements are provided with a very low in-plane flexural stiffness of $1\ 000\ \text{MPa}$, as well as a very low racking shear stiffness of $100\ \text{MPa}$.

As mentioned before, columns consist of 2D beam elements over four storeys connected by hinges. Interconnections between CLT wall elements are rigidly modelled, which means that no slip between wall joints is assumed. Analysis on the behaviour of these joints is covered in a later stage.

Supports of ground floor columns consist of simple hinged supports, which will coincide with connection details in practice. CLT wall elements on the ground floor, however, are modelled by fixed supports since it is expected that connections over the whole wall length will be designed.

5.3 QUASI-STATIC WIND LOADING

In the preliminary design phase the magnitude of wind loading on the building’s façade was assumed to be uniformly distributed over the whole height of the building. The evaluated value for wind loads on the structure, $w_{e,total,d}$ was taken on the reference height of the building, i.e. 0.6H is 40.3 meters. However, for relatively tall buildings it is more realistic to take into account different wind loadings over the height of the building, where the wind velocity increases higher up the façade. EC1 refers to a wind profile as depicted in Figure 5.1.

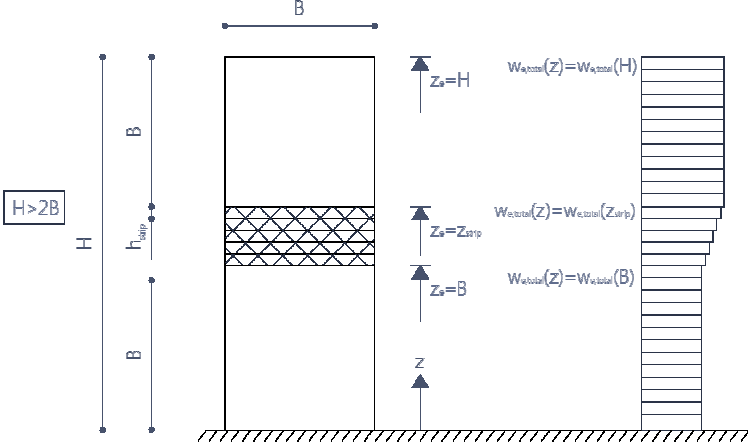


Figure 5.1; Increasing wind load distribution over the height of the building, according to Eurocode 1

The middle part of the façade comprises an area between the heights; $z = 27$ meters and $z = 67.2 - 27 = 40.2$ meters where z is the vertical ordinate as indicated in Figure 5.1. Wind loads on this part can be determined by linear interpolation between wind loads on $z = 27$ meters and $z = 67.2 (=40.2)$ meters. Therefore it is sufficient to calculate the wind loads on $z = 27$ meters and $z = 67.2$ meters.

The procedure as defined in EC1 is elaborated before in Appendix A.1, where the characteristic wind load, $w_{e,total}$ was evaluated on 1.54 kN/m^2 . Different at this stage is the fundamental frequency of the structure, n_1 , which in the preliminary design was estimated on 0.68 Hz . by equation 4.1. Dynamic analysis in STAAD Pro has resulted in a fundamental frequency of 0.58 Hz . Due to the decreased fundamental frequency gusts have a greater impact on the structure, hence the quasi-static wind loading will turn out slightly higher in comparison to the same reference height as calculated before. The implementation of the modified fundamental frequency and following the same procedure as shown in Appendix A.1 gives a wind loading profile on the building’s façade as illustrated in Figure 5.2.

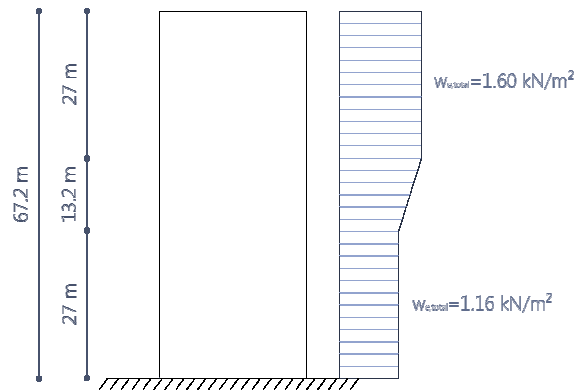


Figure 5.2; Characteristic wind load distribution over the building's façade, according to Eurocode 1

Wind loads are modelled as line loads on the columns in the façade on grid 7 of the floor plan as shown in Figure 5.3¹¹. With regard to the middle part, i.e. height between 27 meters – 40.2 meters, the loads are linearly interpolated and for each floor round off upwards.

5.4 FLOOR DESIGN

The structural analysis of floors is confined by an inaccurate transfer of forces by STAAD Pro, as mentioned in the previous section. Therefore a typical floor element is separately analysed in a similar structural engineering FE program; Scia Engineer. First the floor type and dimensions should be designed. Figure 5.3 shows the typical structural floor plan.

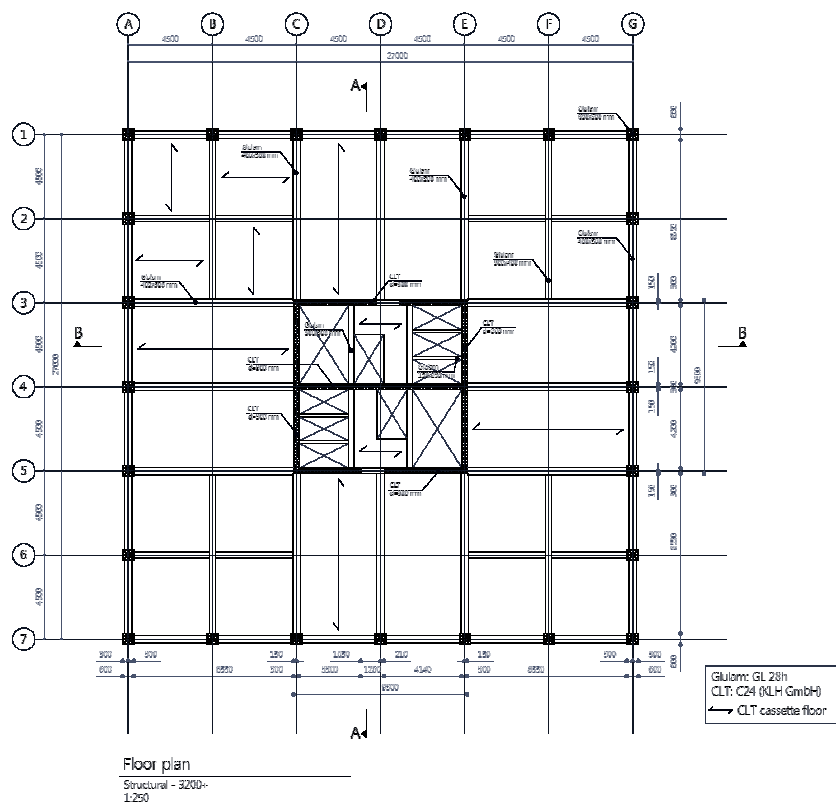


Figure 5.3; Typical structural floor plan

¹¹ Applying wind loads on the floors, as will occur in practice, will not result in different results on either force distributions or deformations. These loads will be transferred to the nodes of the beams in any case

In order to minimise large tensile forces in the central core due to lateral wind loading, it was desired to maximise the vertical loading on the core. Therefore floors span directly from façade to the central core, as depicted for instance from grid 1 to 3, between grid C and E. Another advantage is that the adjacent glulam beam – spanning in the same direction – is merely loaded by the floor construction between grid B and C. The floor spans 9 meters.

Calculations by hand conducted in the *pre-research* [1] of a simply supported CLT floor slab of 146 millimetres and a span of 6 meters have shown that the deflection due to a typical vertical floor loading is 39 millimetres. Table 5.3 shows that the maximum allowable deflection for the floor in this design is

$$U_{\max} = 0.004 \cdot 9\,000 = 36 \text{ mm}$$

which means that a larger stiffness is required. This can be achieved by designing glulam ribs underneath the CLT slab, such as the *MBK-07-02* floor of the Swedish company Martinsons Byggsystem KB. The glulam ribs – centre to centre 600 millimetres – effectively increase the stiffness without adding too much mass and volume to the floor construction. A product design sheet (C.S.4.1) of Martinsons Byggsystem KB, shown in Appendix C.1, evaluates the flexural stiffness of the floor cassette element according to full composite action. An *effective* flexural stiffness, $(EI)_{\text{eff}}$, is evaluated by first calculating the flexural stiffness, EI , and subsequently determining the bending- and shear deformations due to an arbitrary floor load. An effective flexural stiffness is deduced from the total deformation, hence shear influences are taken into account.

Further, the fundamental frequency of the floor is calculated as follows

$$n_1 = \frac{\pi}{2l^2} \sqrt{\frac{(EI)_{\text{eff}}}{m}} \quad (5.12)$$

where l is the floor span [m], $(EI)_{\text{eff}}$ in $[\text{Nm}^2/\text{m}]$ and m is the mass per unit area of the floor [kg].

Floor actions

Loading on the floor cassettes consist of actions in two directions; lateral loading due to wind and vertical floor loading. The transfer of lateral loads to the central core will be discussed in a separate subsection at the end of this section. A floor element with a span of 9 meters will be loaded by both permanent actions and variable actions as shown in Figure 5.4, and consist of

- Permanent loads: self weight, permanent load of 0.8 kN/m^2 and distributed load due to a partition wall of 2.08 kN/m positioned 1.2 meters from the CLT core, as shown in Figure 2.1;
- Variable loads: imposed floor load for commercial functions of 2.5 kN/m^2 and 3 kN/m^2 over a length of 1.2 meters for communal areas of commercial functions.

It may be apparent that a roof slab is loaded by a smaller variable load (snow load and imposed roof load) as presented in Table 5.1; hence an office floor slab governs the design of floor elements.

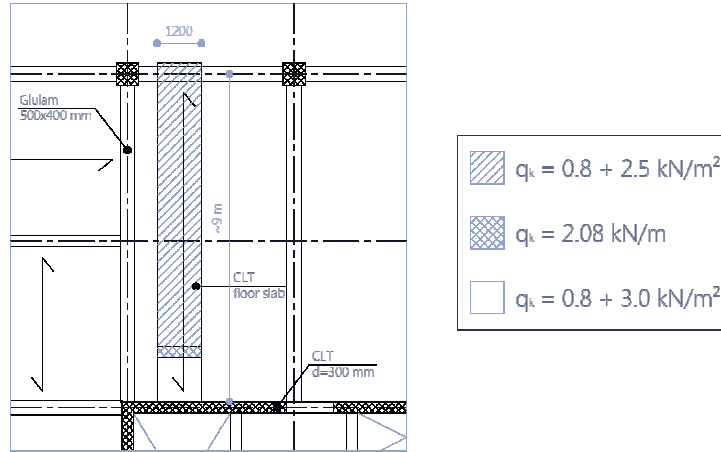


Figure 5.4; Typical floor cassette loaded by permanent- and variable actions on office floor

Design in the ULS

ULS equation *ULS-STR-1* and *ULS-STR-5* are governing for the calculation of stresses in the floor cassettes, which can be evaluated by basic structural mechanic techniques. For instance the maximum bending stresses can be determined by adopting the effective flexural stiffness, $(EI)_{ef}$, so that

$$\sigma_{m,y,d} = \frac{E_i M_{y,d} z_i}{(EI)_{ef}} \quad (5.13)$$

where E_i is the Young's Modulus of either the CLT floor slab or glulam rib, $M_{y,d}$ is the design bending moment, z_i is the distance of the outer fibre of either the CLT panel or glulam beam to the neutral axis.

Shear stresses in the cross section can be evaluated by

$$\tau_{max,d} = \frac{E_i V_{y,d} S_y}{b(EI)_{ef}} \quad (5.14)$$

where S_y is the first moment of area and b is a unit width of 1 meter.

The effect of rolling shear stresses for CLT panels loaded perpendicular to the plane has been outlined in [24]. Design rolling stresses for three- and five layer panels are given by

$$\tau_{R,d} = \frac{V_{y,d}}{ba} \quad (5.15)$$

where a is equal to the distance between the centre of the outer layers: $82 - (19/2) - (19/2) = 63$ millimeters. For a higher number of layers equation 5.14 applies for determination of rolling shear.

The out of plane loading of the floor slab refers to the composite factor, k_1 , [1] for the CLT panel and results in an effective bending strength, $f_{m,k,ef}$, as follows

$$f_{m,k,ef} = f_{m,k} k_1 \quad (5.16)$$

where $f_{m,k}$ is the characteristic bending strength for strength class of the boards.

Design in the SLS

Calculation methods in EC5 for deflections takes into account creep effects. When a floor is loaded by both permanent actions and variable actions, the deflections should be separately determined according to equation *SLS-CHA-1*, which means that characteristic loading values should be implemented. The final deflections due to permanent actions and variable actions respectively are expressed as

$$U_{fin,G} = U_{inst,G} (1 + k_{def}) \quad (5.17)$$

$$U_{fin,Q,1} = U_{inst,Q,1} (1 + \psi_2 k_{def}) \quad (5.18)$$

where $U_{inst,G}$ and $U_{inst,Q,1}$ are the instantaneous deflections due to permanent actions and variable actions respectively, k_{def} is a deformation factor which takes into account the increased deflection and the effect of moisture content, and ψ_2 is a combination value as shown in Table 5.4.

The total final deflection can be determined by simply adding both final deflections as follows

$$U_{fin} = U_{inst,G} + U_{inst,Q,1} \quad (5.19)$$

Overview of the results

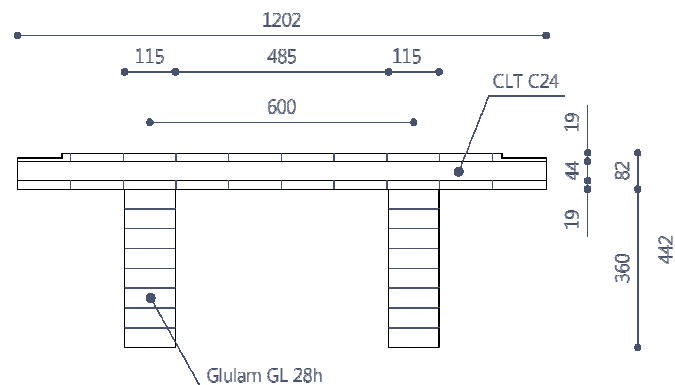
The design sheet of *MBK-07-02* presents an equivalent panel thickness of a solid rectangular slab and mass per unit area for a slab width of 1 meter for an arbitrary Young's Modulus, which simply can be implemented in the FE program Scia Engineer. An iterative process of floor dimension design and analysis in Scia Engineer has resulted in floor properties and related structural behaviour under given loading combinations as shown in Table 5.7, where calculations are presented in C.S.4.2. Strength and stiffness properties are provided by Martinsons Byggsystem KB.

Table 5.7; Floor slab design results

<i>MBK-07-02</i>	$E_{0,mean}$	$E_{90,mean}$	$G_{0,mean}$	$G_{90,mean}$	$f_{m,k,eff}$ [MPa.]
CLT panel	9 500	300	600	60	20.41
Glulam beam	13 000	-	700	-	28

Flexural stiffness; $(EI)_{ef}$ 21 532 kN/m²/m

Fundamental frequency; $(n_1)_{ef}$ 10.6 Hz.



<i>Scia Engineer results</i>	<i>ULS-STR-1</i>	<i>ULS-STR-5</i>	
$M_{y,d}$	30.07	84.10	kNm/m
$V_{y,d}$	15.77	49.67	kN/m

<i>Unity checks ULS</i>	<i>ULS-STR-1</i>	<i>ULS-STR-5</i>
Modification factor; k_{mod}	0.6	0.8
Bending stresses CLT; $\sigma_{m,y,d} / f_{m,d}$	0.24	0.51
Bending stresses glulam; $\sigma_{m,y,d} / f_{m,d}$	0.30	0.63
Rolling shear stresses CLT; $\tau_{R,d} / f_{R,v,d}$	0.32	0.75
Shear stresses glulam; $\tau_{max,d} / f_{v,d}$	0.07	0.17
<i>Deflection SLS</i>		
Permissible deflection; U_{max}	36 mm	
Final deflection; U_{fin}	22.76 mm	
Unity check	0.63 < 1	

As is most common for timber structures, deflections in the SLS are governing for the design. Although the final deflection is well below the permissible value of 36 millimeters, it is assumed that complaints by the occupants cannot be precluded by such a deflection. Therefore, a slightly stiffer floor is designed which most surely will preclude complaints by occupants on deflections and floor vibrations.

Lateral wind load transfer

Floor slabs are subjected to lateral wind loads by the façade, resulting in an equally distributed load on each floor edge on the windward side of the building. Subsequently the floor slabs transfer the shear forces to the stabilising elements, i.e. CLT core walls. An accurate stress distribution in the slabs due to wind loading is impossible to obtain from the STAAD Pro model since these elements are connected to beams, which means that they cooperate in transferring the shear forces. Therefore a simplified and conservative approach is proposed to indicate in-plane forces in floor elements.

The equally distributed load on the floor edge is as follows

$$w_{e,total} = 1.60 \text{ kN/m}^2 \rightarrow \text{wind load on façade at upper part of the building}$$

$$w_{e,total,d} = 1.60 \cdot 1.5 = 2.40 \text{ kN/m}^2 \rightarrow \text{design wind load for calculations in ULS}$$

$$w_{e,total,d} = 2.40 \cdot 3.2 = 7.68 \text{ kN/m} \rightarrow \text{design load on floor edge, where the storey height is 3.2 meters}$$

For floor element design it is only relevant to check the shear stresses in the floor slabs. Design of connections of floor elements between beams and walls is not considered in this report, since the floor structure is not part of the structural stability system.

A conservative approach to calculate the shear stresses in the floor slabs comprises the following assumptions

- Both the glulam ribs underneath the CLT decks and glulam beams do not participate in transferring the shear forces from the façade to the core;
- Supports, *A* and *B*, are located at shear walls in longitudinal direction, which results in the model shown in Figure 5.5.

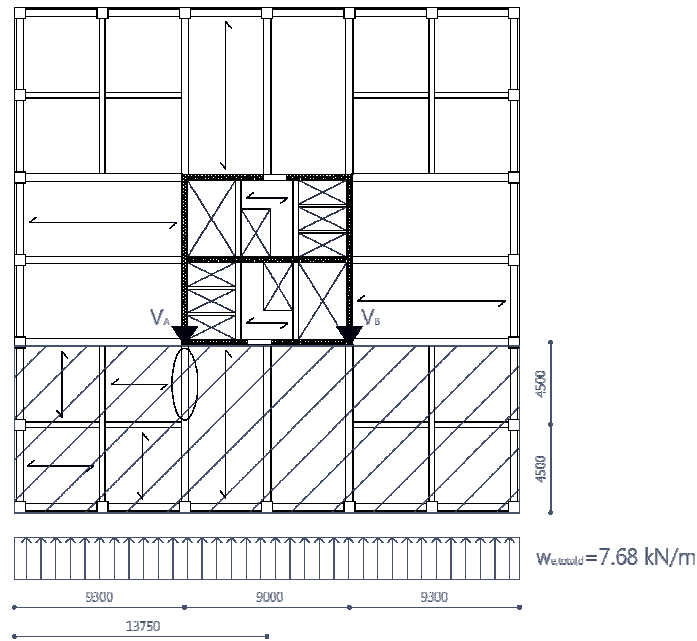


Figure 5.5; Floor structure of single storey subjected to lateral wind loading

The hatched area behaves as a thick beam, which might be a too conservative approach since a part of the forces are also distributed alongside the longitudinal shear walls. Even a small amount of tension forces could arise at the leeward side of the core.

Due to symmetry both supports resist half of the total wind loading, which is equal to

$$V_A = V_B = 7.68 \cdot 13.75 = 105.6 \text{ kN}$$

This reaction force should be able to transfer through the floor structure in the section as encircled in Figure 5.5. The length for distributing the shear force will be taken as 2 meters.

Shear stresses are resisted by the gross sectional area of the panels, thus no reduced shear strength properties applies. The design shear strength of a CLT panel can be evaluated as follows

$$f_{v,CLT,d} = \frac{k_{mod} f_{v,k}}{\gamma_M} \quad (5.20)$$

where k_{mod} yield 0.9 since loading is due to wind actions, the characteristic shear strength, $f_{v,k}$, of CLT boards is 2.7 MPa., and the material factor equals 1.25. The design shear strength becomes 1.94 MPa. The cross sectional area as mentioned above yields

$$A_{gross} = 82 \cdot 2000 = 164000 \text{ mm}^2$$

so that the shear stresses in the floor structure are

$$\tau_{CLT,d} = \frac{105.6 \cdot 10^3}{164000} = 0.64 \text{ MPa.} < 1.94 \text{ MPa.}$$

It appears that shear stresses in the CLT panels are well below the permissible stress value. Therefore it can be concluded that the designed floor cassette is capable to transfer horizontal shear forces to the core, only when adequate floor connections are designed between floor elements and other structural elements such as glulam beams and CLT walls.

5.5 BEAM DESIGN

The distribution of forces into 2D beam elements in the STAAD Pro model is adversely influenced by floor slab elements which transfers forces merely by its nodes, and since these nodes are always connected to beam ends only columns and walls are loaded correctly. As a consequence, it is necessary to model a typical beam structure separately in order to obtain an accurate force distribution from vertical loading.

On the other hand, lateral loading is modeled as member loads on the peripheral columns and transferred by the beam elements to the central core. Accordingly, floor slabs are loaded by the beam nodes and are therefore subjected to attendant membrane stresses¹².

Beam actions

Due to two types of loading, i.e. vertical loading¹³ and axial loading, combined stresses are present in beam elements and should therefore be exclusively verified. The design strategy for both the ULS and SLS starts by adoption of the largest bending moment due to vertical loading, and subsequently taking into account the pertaining axial forces. In analogy with the floor slabs also an analysis with merely permanent actions will be conducted to check the strength with a lower related k_{mod} value. Loading actions on a typical beam is depicted in Figure 5.6.

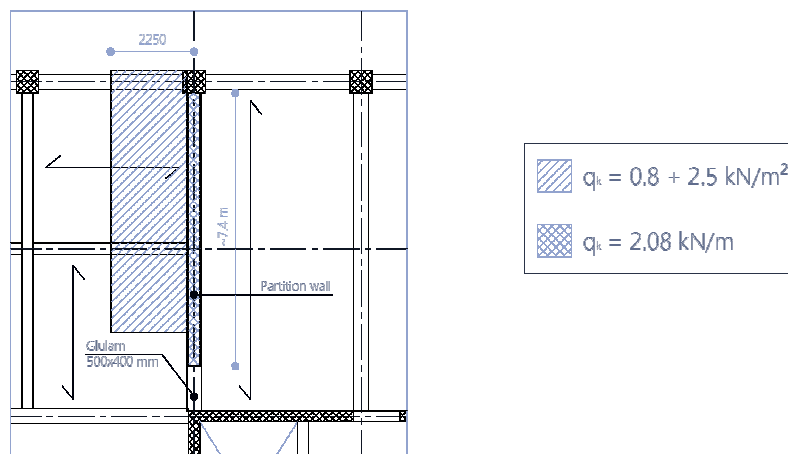


Figure 5.6; Typical beam loaded by permanent- and variable actions on office floor

Permanent- and variable actions can be categorised as follows

- Permanent loads: self weight beam, self weight floor slab, permanent load of 0.8 kN/m^2 and distributed load due to a partition wall of 2.08 kN/m ;
- Variable loads: imposed floor load for commercial functions of 2.5 kN/m^2 and 3 kN/m^2 over a length of 1.2 meters for communal areas of commercial functions.

As depicted in Figure 5.6 the beam is loaded by a cross beam resulting in a concentrated load in the centre of the span. The simply supported cross beam is loaded by a single floor span and analysed in Scia Engineer separately. The reaction load of this cross beam is divided in a concentrated load due to permanent actions and variable actions, and subsequently applied in the typical beam analysis.

¹² Modeling of lateral loading directly onto the floor edges at the facade resembles a similar loading distribution in both the floor beams and floor slabs.

¹³ Vertical loading is in this context equal to lateral beam loading

Design in the ULS

The governing loading combination in the ULS is *ULS-STR-5*, which includes permanent actions and imposed floor loading. Single checks of; bending, compressive, tensile and shear stresses can be performed according to simple structural mechanic techniques, as shown in C.S.4.3 of Appendix C.1 and Table 5.8.

EC5 presents two different methods to verify combined bending- and axial stresses. Clause 6.3.2(2) defines for the case when relative slenderness, λ_{rel} is lower or equal to 0.3 no stability effects are incorporated and the stresses should satisfy the following expressions

$$\left(\frac{\sigma_{c,0,d}}{f_{c,0,g,d}} \right)^2 + \frac{\sigma_{m,y,d}}{f_{m,g,d}} + k_m \frac{\sigma_{m,z,d}}{f_{m,g,d}} \leq 1 \quad (5.21)$$

$$\left(\frac{\sigma_{c,0,d}}{f_{c,0,g,d}} \right)^2 + k_m \frac{\sigma_{m,y,d}}{f_{m,g,d}} + \frac{\sigma_{m,z,d}}{f_{m,g,d}} \leq 1 \quad (5.22)$$

where $\sigma_{c,0,d}$ is the design compressive stress along the grain
 $f_{c,0,g,d}$ is the design compressive strength along the grain
 k_m is a modification factor which takes into account the effect of variation in material properties and also allows for re-distribution of stresses in the cross section
 $\sigma_{m,y,d}$ is the design bending stress about the y-axis
 $\sigma_{m,z,d}$ is the design bending stress about the z-axis
 $f_{m,g,d}$ is the design bending strength

On the other hand, when the relative slenderness exceeds a value of 0.3 the stresses should comply with the following expressions

$$\frac{\sigma_{c,0,d}}{k_{c,y} f_{c,0,g,d}} + \frac{\sigma_{m,y,d}}{f_{m,g,d}} + k_m \frac{\sigma_{m,z,d}}{f_{m,g,d}} \leq 1 \quad (5.23)$$

$$\frac{\sigma_{c,0,d}}{k_{c,z} f_{c,0,g,d}} + k_m \frac{\sigma_{m,y,d}}{f_{m,g,d}} + \frac{\sigma_{m,z,d}}{f_{m,g,d}} \leq 1 \quad (5.24)$$

where $k_{c,y}$ and $k_{c,z}$ are instability factors for the buckling strength about the y-ax and z-ax respectively.

Lateral torsional stability should be verified in the case of combined bending and compression stresses according to the following expression

$$\left(\frac{\sigma_{m,y,d}}{k_{crit} f_{m,g,d}} \right)^2 + \frac{\sigma_{c,0,d}}{k_{c,z} f_{c,0,g,d}} \leq 1 \quad (5.25)$$

where k_{crit} is a factor that takes into account the reduced bending strength due to lateral buckling and is determined by the relative slenderness for bending, which is equal to

$$\lambda_{rel,m} = \sqrt{\frac{f_{m,g,k}}{\sigma_{m,crit}}} \quad (5.26)$$

in which $\sigma_{m,crit}$ represents the critical bending stress written as

$$\sigma_{m,crit} = \frac{0,78b^2}{hl_{ef}} E_{0,9,05} \quad (5.27)$$

where l_{ef} is equal to $0.9l$, or 90 percent of the beam span, which applies for simply supported beams with uniformly distributed load.

When $\lambda_{rel,m} \leq 0.75$ the k_{crit} is taken as unity. In other cases the factor is evaluated by equation 6.34 of EC5.

Design in the SLS

The calculation method for vertical deflections of glulam beams equalises the procedure as presented for floor elements. Instantaneous deflections due to permanent- and variable actions should be determined separately followed by taking creep effects into account in order to obtain the final deflection of the beam during its design life. The permissible vertical deflection is set on 0.4 percent of the span (see Table 5.3), which results in 36 millimetres for the typical beam.

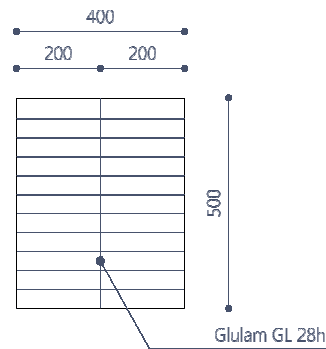
Overview of the results

The typical beam is modelled in Scia Engineer, due to aforementioned reasons, and subjected to loading combinations *ULS-STR-1* and *ULS-STR-5* in order to obtain a bending moment about the y-axis as well as vertical shear forces. Bending moments about the z-axis and compressive- and tensile forces are obtained from the STAAD Pro 3D model under equal loading combinations, which does not include wind loading. It may be apparent that the largest axial forces do not occur due to *ULS-STR-1* and *ULS-STR-5*, but *ULS-STR-7*.

Firstly, the results of the beam analysis, as elaborated in C.S.4.3 and C.S.4.3a, are shown in Table 5.8.

Table 5.8; Beam design results for loading combinations *ULS-STR-1* and *ULS-STR-5*

Material	$E_{0,mean}$	$E_{90,mean}$	$E_{0,9,05}$	$G_{0,mean}$	$f_{m,k}$	MPa.
Glulam GL 28h	12 600	420	10 200	780	28	



Scia Engineer / STAAD Pro results	<i>ULS-STR-1</i>	<i>ULS-STR-5</i>	
$M_{y,d}$	135.85	283.39	kNm
$M_{z,d}$	-2.25	-4.57	kNm
$N_{c,d}$	27.19	54.93	kN
$N_{t,d}$	-18.96	-40.43	kN
$V_{y,d}$	56.01	116.69	kN

<i>Unity checks ULS</i>	<i>ULS-STR-1</i>	<i>ULS-STR-5</i>
Modification factor; k_{mod}	0.6	0.8
Bending stresses; $\sigma_{m,y,d} / f_{m,d}$	0.54	0.85
Shear stresses; $\tau_{max,d} / f_{v,d}$	0.37	0.58
Relative slenderness; $\lambda_{rel,y/z}$	1.01 / 1.26	1.01 / 1.26
Combined stresses; equation 5.23 / 5.24	0.55 / 0.39	0.85 / 0.60
Lateral torsional stability; equation 5.25	0.31	0.74

<i>Deflection SLS</i>	
Time dependent deflection; U_{creep}	$9.04 \text{ mm} \leq 0.003 \times L_{rep} (=27 \text{ mm})$
Permissible deflection; U_{max}	36 mm
Final deflection; U_{fin}	32.44 mm
Unity check	$0.90 < 1$

The relatively low tensile force in the cross section makes verification on combined tensile stresses and bending stresses abundant and is therefore not taken into account.

Although the final deflection of the beam is within permissible values, the calculated sagging may cause problems for either constructional or visual matters. A frequently applied solution to decrease vertical deflections of beams is to do design a pre-camber. The instantaneous deflection due to permanent loading is 11.50 millimetres. Pre-cambering this dimension in the opposite direction of bending results in a final deflection of

$$U_{net,fin} = U_{fin} - U_c = 32.44 - 11.50 = 20.94 \text{ mm}$$

which is slightly lower than the deflection of a floor cassette element.

Furthermore, as aforementioned the largest axial forces in the beams can be found due to loading combination *ULS-STR-7*, both appearing in a typical beam with a span of 9 meters. A similar beam analysis is elaborated in C.S.4.3b and summarised in Table 5.9.

Table 5.9; Beam design results for loading combination *ULS-STR-7*

<i>Scia Engineer / STAAD Pro results</i>	<i>ULS-STR-7</i>	
$M_{y,d}$	202.13	kNm
$M_{z,d}$	-6.79	kNm
$N_{c,d}$	158.00	kN
$N_{t,d}$	-81.56	kN
$V_{y,d}$	83.26	kN

<i>Unity checks ULS</i>	<i>ULS-STR-7</i>
Modification factor; k_{mod}	0.9
Bending stresses; $\sigma_{m,y,d} / f_{m,d}$	0.54
Shear stresses; $\tau_{max,d} / f_{v,d}$	0.37
Combined stresses; equation 4.23 / 4.24	0.57 / 0.42
Lateral torsional stability; equation 4.25	0.36

It can be seen that combined stresses under a maximum compressive load does not result in governing unity checks, hence it can be concluded that the designed beam complies in the ULS as well as in the SLS.

5.6 COLUMN DESIGN

Forces in columns can be directly obtained from STAAD Pro 3D model, since vertical loads are correctly transferred by the beam nodes into the columns. Due to pin-connected beams all columns are predominantly loaded by axial loads, thus bending moments that occur are inferior. Nevertheless, columns are continuous over four storeys so that bending moments should not be ignored. The total length of a single column is 12.8 meters and each is vertically connected to another by hinges. Influences of rotational capacity of column connections with respect to additional bending moments will be discussed in Chapter 7. Secondary moments caused by eccentric introduction of axial forces due to beam supports are taken into account by STAAD Pro. Beams bear on a distance of 300 millimetres from the centre of columns, which is equal to column's edges.

Column actions

Axial loads in columns are obviously mainly caused by vertical permanent- and variable loads. Furthermore, due to lateral wind loading and the restraining effect initiated by the horizontal outriggers additional axial loads are significant, as can be seen in Table 3.4 and C.S.2.3. Therefore, the importance of a 3D model becomes apparent. The following actions apply for design checks in the ULS and SLS

- Permanent loads: self weight structure, permanent load of 0.8 kN/m^2 and partition wall loading of 2.08 kN/m ;
- Variable loads: imposed floor load of $1.75 / 2.5 \text{ kN/m}^2$ and $2.5 / 3 \text{ kN/m}^2$ over a length of 1.2 meters for communal areas, imposed roof loading of 1.0 kN/m^2 , snow loading of 0.56 kN/m^2 and static wind loading as given in Section 5.3.

Considering the significance of axial loading in the columns due to lateral wind actions, it is expected that due to outrigger position the largest compressive forces occur in columns on grid C and E (see Figure 5.3) on the leeward side and largest tensile forces on the same grids on the windward side.

The Dutch Annex of EC0 refer to the application of an unfavourable distribution of imposed floor loads in the case of multiple floor spans. Therefore, when maximum axial forces are analysed, on the locations as mentioned above, it is required to apply imposed floor loads merely on the leeward side of the building, as shown in Figure 5.7. This enhances the 'toppling-over' effect of the building due to lateral wind actions, resulting in largest axial compressive forces on the leeward side of the building. Obviously, tensile forces on the windward side become larger accordingly.

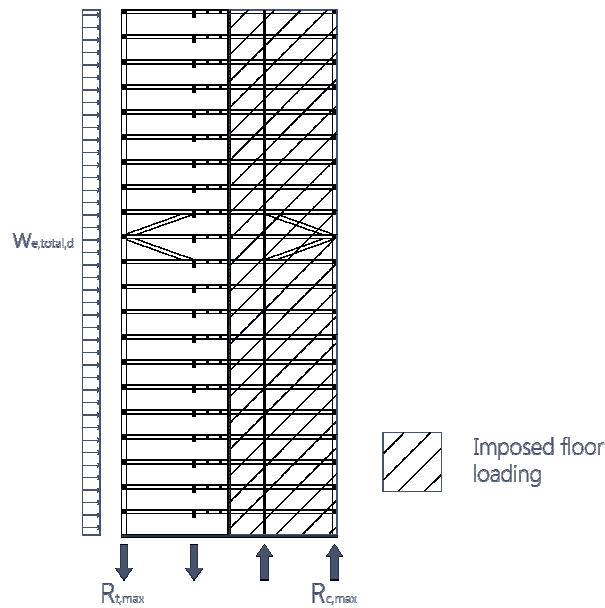


Figure 5.7; Maximum and minimum reaction forces in peripheral columns due to wind loading and unfavourable distribution of imposed floor loading

Design in the ULS

In the contrary to beam design, now it is the axial load leading for designing the columns on strength in the ULS. Thus the strategy is to analyse a governing column which is loaded by the largest axial load and subsequently check combined stresses due to additional stresses out of bending moments.

EC0 refer to reduced imposed floor loading, as defined in equation 5.8, for the analysis of vertical structural elements; hence loading combinations *ULS-STR-1V* up to *ULS-STR-12V* are governing in checks on strength. The reason for this that the code deems it is very unlikely that each floor in a multi-storey building is loaded by the full imposed floor loading.

For the design of combined stresses in the columns the similar procedure applies as for the design of beams, i.e. equation 5.21 to 5.24. Regarding the relative slenderness the following rules apply

$\lambda_{rel,y,z} \leq 0.3 \rightarrow$ buckling behaviour is not relevant and failure is based on the compressive strength,
 $\lambda_{rel,y,z} > 0.3 \rightarrow$ buckling can arise, thus the instability factor, $k_{c,y}$ or $k_{c,z}$ should be taken into account.

In the first condition the timber member is too stocky to cause buckling, which means that the maximum compressive strength will be attained before instability effects appear. The second condition implies that the slenderness ratio is too high to neglect instability effects and it is more likely that the failure mode of the axially compressed member shows buckling instead of wood crushing.

The effective length of a column is equal to a storey height, since buckling is constraint at the connections with floor beams.

Design in the SLS

Design criteria for the SLS, set in Table 5.3, contains lateral displacements of one single storey as well as the displacement of the whole structure. The permissible horizontal displacements are as follows

$$U_{max} \leq H / 500 = 67\,200 / 500 = 134.4 \text{ mm, for the whole building and}$$

$$U_{max} \leq h / 300 = 3\,200 / 300 = 10.7 \text{ mm, for a single storey.}$$

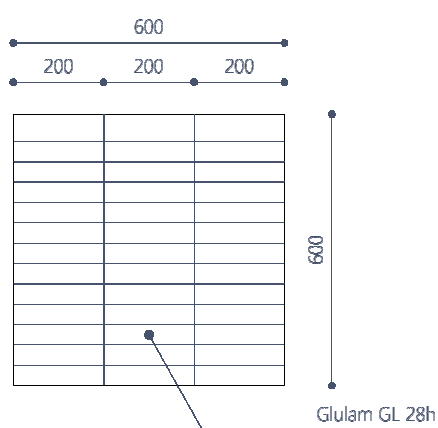
In the preliminary static design it was assumed to design for a maximum top displacement of $H/800$, i.e. 84 millimetres, due to additional displacements out of rotation of the foundation settlements. Since foundation design is excluded in the analysis, this value will be adopted also in the final static design. Loading combinations *SLS-FRE-1* up to *SLS-QUA-1*, as shown in Table 5.6, apply for design of columns.

Overview of the results

The results of the 3D static analysis in STAAD Pro are elaborated in C.S.4.4, whilst the most relevant values and unity checks are presented in Table 5.10.

Table 5.10; Column design results for loading combinations *ULS-STR-5V* and *ULS-STR-12V*

Material	$E_{0,mean}$	$E_{90,mean}$	$E_{0,g,05}$	$G_{0,mean}$	$f_{m,k}$
Glulam GL 28h	12 600	420	10 200	780	28 MPa.



STAAD Pro results	<i>ULS-STR-5V</i>	<i>ULS-STR-12V</i>	
$N_{c,d}$	2 316.56	-	kN
$N_{t,d}$	-	-220.58	kN
$M_{y,d}$	2.84	-	kNm
$M_{z,d}$	24.43	-	kNm
Unity checks ULS	<i>ULS-STR-5V</i>	<i>ULS-STR-12V</i>	
Modification factor; k_{mod}	0.8	0.9	
Compressive stresses; $\sigma_{c,0,d} / f_{c,0,g,d}$	0.38	-	
Tensile stresses; $\sigma_{t,0,d} / f_{t,0,g,d}$	-	0.04	
Relative slenderness; $\lambda_{rel,y/z}$	0.30 / 0.30	-	
Combined stresses; equation 5.21 / 5.22	0.17 / 0.18	-	
Combined stresses; equation 5.23 / 5.24	0.41 / 0.42	-	
Lateral displacements SLS	<i>SLS-CHA-3</i>		
Max. top displacement; $U_{top,max}$	92.14 mm > $H / 800$ (= 84 mm)		
Max. storey displacement; $U_{storey,max}$	5.38 mm \leq $h / 300$ (= 10.7 mm)		
Unity check; $U_{top,max} / U_{max}$	1.02 > 1		

Deformations are once more decisive in the structural design of the timber outrigger structure. Due to a relative slenderness of exactly 0.30, it is decided to perform both checks for combined stresses, but in none of the cases a critical situation arises. It becomes apparent that with respect to strength, a cross section of 600 x 600 millimetres is beyond the requirements, but for the sake of lateral sway they possess an important role in resisting loads during serviceability, since they highly affect the effectiveness of the outriggers.

Moreover, according to equation 6.11b of EC0 during a fire hazard only a maximum of 20 percent of wind loads should be taken into account in combination with the characteristic values of the permanent actions. This means that a significant part of the cross section can be used in order to obtain the required fire resistance. However, it must be emphasised that the columns are not designed for fire resistance.

Although the maximum horizontal displacement exceeds the design value of 84 millimetres ($=H/800$), the structure still complies with 134.4 millimetres ($H/500$) which is the actual maximum displacement.

5.7 DIAGONAL DESIGN

The diagonals are part of the outriggers and are essential in the structural design to obtain the required stiffness to the building. The members are hinge-connected to beams above and below a floor respectively. Similar as columns in the structure, the diagonals are mainly subjected to axial forces due to lateral wind actions, which can be obtained from the outcomes of the 3D STAAD Pro analysis. Cross sectional dimensions of the diagonals equalise the beams, i.e. 500 x 400 millimetres.

Diagonal actions

As the outriggers cause a reversed rotation of the central core due to wind actions, the axial forces are predominantly caused by the static wind loading, i.e. *ULS-STR-7*. Since the members span straight from the columns to the core bending moments are insignificant.

In order to initiate a larger horizontal displacement, and thus higher axial forces in the outriggers, imposed floor loading is applied at the leeward side of the building, in analogy with column design. However, the diagonals are not part of the vertical load-bearing structure and should therefore not be analysed by taking into account the reduction factor for imposed floor loading.

Structural actions in the diagonals under lateral loads as well as the deformed shape of the outriggers are shown in Figure 5.8

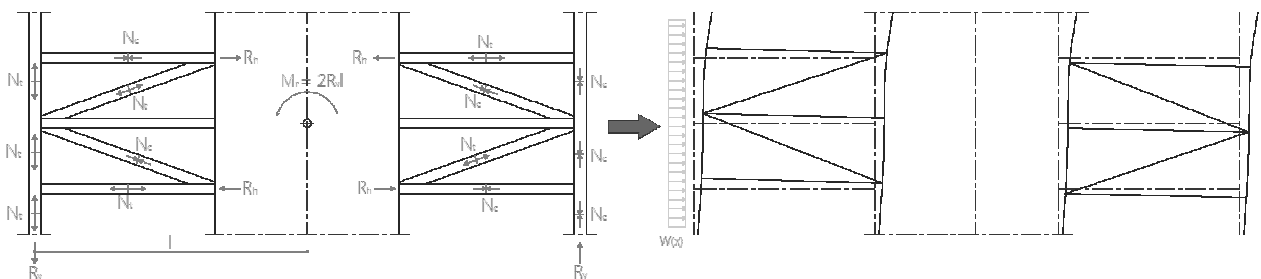


Figure 5.8; a) Structural actions in outrigger members due to lateral wind loading b) Deformed shape outriggers

Outrigger actions are strikingly illustrated in the deformed shape (Figure 5.8b) of the structure, where reversed rotation of the central core – due to restraining bending moment, M_r – leads to uplifting of the structure on the windward side and obviously to vertical tensile forces in the columns. As a result of the flexural bending stiffness of the outriggers columns are forced to deform like the core structure. It must be mentioned that deformations above and below the outriggers are exaggeratedly drawn in Figure 5.8 for the sake of clarity.

Design in the ULS

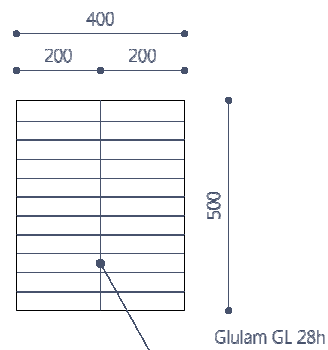
The design procedure for the ULS is due to the axial loading in analogy with column design. Combined stresses, as mentioned before, are not expected to cause any governing design criteria. Nevertheless, the relatively large length of a single diagonal, i.e. 9.5 meters, may cause instability effects to be relevant.

Overview of the results

Design in the ULS and SLS is performed in C.S.4.5 of Appendix C.1, where most relevant results are shown in Table 5.11.

Table 5.11; Diagonal design results for loading combinations ULS-STR-7

Material	$E_{0,mean}$	$E_{90,mean}$	$E_{0,g,05}$	$G_{0,mean}$	$f_{m,k}$
Glulam GL 28h	12 600	420	10 200	780	28 MPa.



STAAD Pro results

$N_{c,d}$	1 071.55	kN
$N_{t,d}$	-1035.59	kN
$M_{y,d}$	-10.37	kNm

Unity checks ULS

Modification factor; k_{mod}	0.9
Compressive stresses; $\sigma_{c,0,d} / f_{c,0,g,d}$	0.28
Tensile stresses; $\sigma_{t,0,d} / f_{t,0,g,d}$	0.37
Relative slenderness; $\lambda_{rel,y/z}$	1.07 / 1.34
Combined stresses; equation 5.23 / 5.24	0.43 / 0.59
Lateral torsional stability; equation 5.25	0.57

The outcomes of the unity checks show that the relatively slender diagonals, which are subjected to very low bending moments, causes a relatively high ratio for the 'combined stresses checks'. However, similar to columns the role in serviceability aspects, such as horizontal displacements, is more important when it comes to the design of these elements.

5.8 CORE WALL DESIGN

The CLT wall panels of the core have multiple structural purposes and possess a central role in the structure. They transfer a relatively large amount of vertical loads to the foundation and besides, lateral loading is transferred from the façade through the floor slabs into the wall panels.

Modelling of the core in STAAD Pro has been conducted by 2D orthotropic elements, which allows definitions of stiffness properties in two in-plane directions simulating the true structural properties of the panels. Accounting for effective properties, panel's thickness is set constant and their stiffness, E , is modified by composite factors, k_3 and k_4 . Performing a static analysis in STAAD Pro enables the engineer to obtain; membrane-, in-plane shear- and out of plane shear stresses as well as internal bending moments.

As mentioned before, joints between wall elements are rigidly modelled and thus do not allow for slip in interconnections. Possible consequences for this assumption will be discussed in the Chapter 7.

Core wall actions

Essential structural actions in the CLT panels involve diaphragm action in order to resist lateral loading. Therefore, vertical forces arise in opposite directions of the windward- and leeward side of the core, as depicted in Figure 5.9. In order to obtain maximum vertical forces, both appearing at the bottom side of the walls, i.e. ground floor, it is obvious that either minimum or maximum vertical loading should be added to the windward- and leeward side respectively. In other words, the maximum tensile force is found by the loading combination with maximum lateral wind forces and minimum vertical loading, i.e. *ULS-STR-12V*. Naturally, applying imposed floor loading on the leeward side of the building, as illustrated in Figure 5.7, enhances this 'toppling-over' effect¹⁴. On the other hand, maximum compressive forces in vertical direction appear with maximum vertical loading together with lateral loading, i.e. *ULS-STR-7V*.

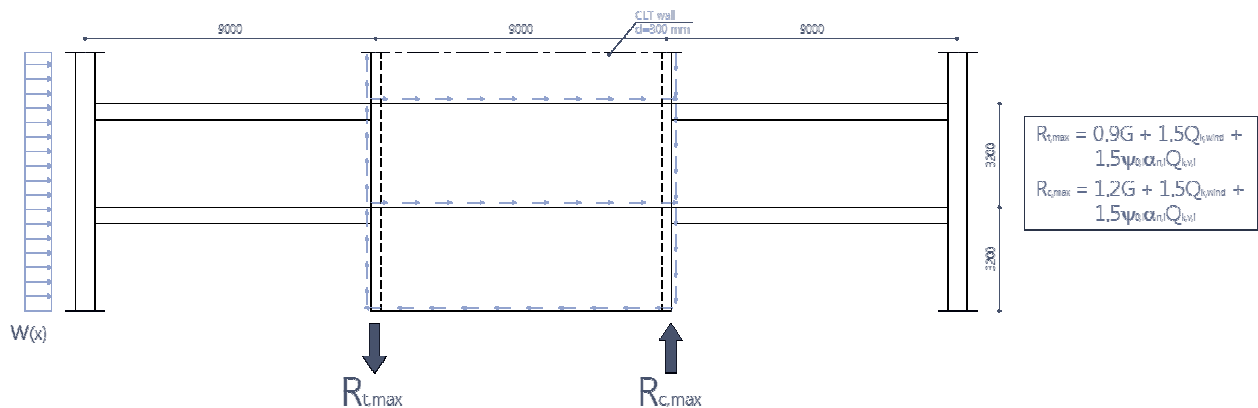


Figure 5.9; Force distribution CLT wall panel due to lateral wind loading and vertical loads

Design in the ULS

Effective strength properties of the panels are verified by the respective composite factors, either k_3 or k_4 , depending on the direction of the loading as well as the grain direction of the outer layers.

When evaluating *membrane stresses* in vertical direction the factor k_3 applies, which means that 81 percent (see C.S.2.3d Appendix A.2) of the cross section can be utilised to resist the loads.

Bending stresses arise from internal bending moments due to vertical loads, thus k_3 applies likewise for determining the effective out of plane flexural stiffness. Obviously, these stresses should be verified by unity checks, conform equation 5.23 and 5.24, for combined compressive- and bending stresses.

¹⁴ With regard to toppling-over of the whole structure; *ULS-STR-12V* equalises *ULS-EQU-2* and therefore the maximum tensile forces in the core are obtained with either combination

Shear stresses, however, are resisted by the gross cross section so that panel's shear strength should not be reduced due to cross layers.

Furthermore, the panels are loaded by forces due to lateral wind loading through the floor slabs, resulting in compressive forces in cross direction and therefore k_4 applies. Moreover, out of plane loading occur due to loading on walls in the cross direction. The magnitudes of these stresses are predominantly depending on connection details between floor and walls and are therefore analysed in the Chapter 7.

Design in the SLS

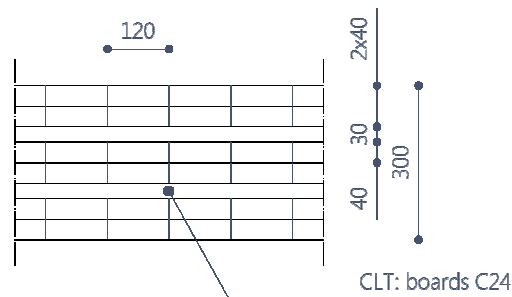
Horizontal displacements of the CLT core are the most important design criteria in the SLS. In order to compare the results of STAAD Pro with hand calculations conducted in the preliminary design stage, the model is computed with- and without outriggers.

Overview of the results

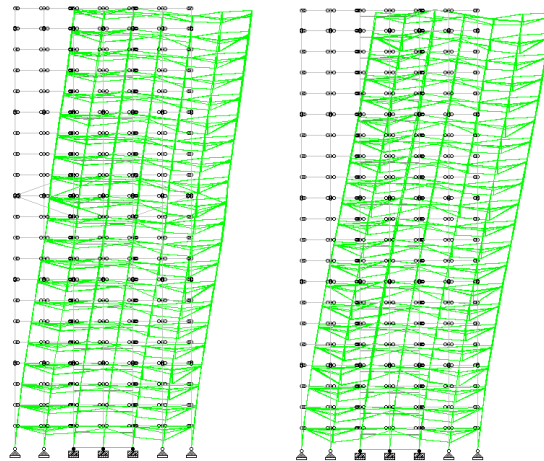
All results of structural actions are calculated by aforementioned 3D analysis in STAAD Pro. Calculations of strength properties as well as the verification of unity checks are elaborated in C.S.4.6 in Appendix C.1. Table 5.12 presents the most relevant results on ULS and SLS analysis.

Table 5.12; Core wall results of ULS and SLS analysis

Material	$E_{0,mean}$	$f_{m,k}$	$f_{c,0,k}$	$f_{t,0,k}$	$f_{v,k}$	
CLT – C24	12 000	23	24	16.5	5.2	MPa.



STAAD Pro results	ULS-STR-7V	ULS-STR-12V	
$\sigma_{c,0,d}$	-7.34	-	MPa.
$\sigma_{t,0,d}$	-	3.23	MPa.
$\tau_{max,d}$	-1.02	-	MPa.
$M_{y,d}$	-26.09	-	kNm/m
Unity checks ULS	ULS-STR-7V	ULS-STR-12V	
Modification factor; k_{mod}	0.9	0.9	
Compressive stresses; $\sigma_{c,0,d} / f_{c,0,CLT,d}$	0.53	-	
Tensile stresses; $\sigma_{t,0,d} / f_{t,0,CLT,d}$	-	0.34	
Shear stresses; $\tau_{max,d} / f_{v,d}$	0.27	-	
Bending stresses; $\sigma_{m,y,d} / f_{m,CLT,d}$	0.16	-	
Combined stresses; equation 5.24	0.67	-	



Max. top displacement; $U_{top,max}$	92.14	114.72	mm
Preliminary design results; $U_{top,max}$	80.80	114.70	mm

Unity checks on strength properties show that a certain amount of cross sectional capacity is unused, which appears to be required for managing the horizontal displacements. It may be obvious that performing unity checks on permanent loading only ($k_{mod} = 0.6$) is needless due to the large capacity on strength and since a large amount of stress is caused by wind loading, as can be seen at the results of compressive- and tensile stresses.

The difference on horizontal displacements between results of the STAAD Pro model and hand calculations of the actual model with outriggers seem to be caused by the modelling of imposed floor loading on the leeward side of the building. When imposed floor loading is applied at all floor spans the horizontal displacement yields 79.90 millimetres, which approaches the preliminary design result. The model without outriggers is modelled with imposed floor loading on all floor spans, which obviously resembles the model in preliminary design more accurately.

Comparison of the results of STAAD Pro with hand calculations proves the accuracy of the stability system modelled in STAAD Pro as aimed for structural analyses. It appears that contribution of the floor structure is negligible as well as the contribution of the column – beam structure in resisting lateral wind loading.

6 | FINAL DYNAMIC DESIGN

Effects of damping and the necessity of outriggers

Static design analysis in the FE-program STAAD Pro has not resulted in necessary modifications to structural elements in the building. Therefore, the prior dynamic analysis still applies with regard to; natural frequencies, mode shapes and dynamic response of the structure, i.e. displacements, velocities and accelerations due to fluctuating wind actions.

Although the structure of the building performs rather well on dynamic behaviour – which means that the dynamic response in relation with the natural frequencies is within acceptable limits regarding to Dutch regulations as stated in NEN 6702 (see Figure 4.10) – there remains one design criteria uncertain, which is the ability of the structure to dissipate energy to the foundation, i.e. *damping*.

The crucial effect of the outriggers on horizontal displacements due to static wind loading was already stated in the latter part of the previous chapter. In order to define the contribution of the outriggers to control the dynamic response due to the fluctuating wind loads, a similar comparison can be made by simply omitting the outriggers in the dynamic model of STAAD Pro.

6.1 DAMPING PERFORMANCES

The contribution of damping to control the dynamic response of the structure is previously assumed by adopting general design rules of EC1, which consist of a summation of structural damping (i.e. damping due to material properties) and aerodynamic damping. Clearly, other damping contributing elements, such as constructional elements, are ignored and therefore the adopted damping ratio, ζ , of 0.019 (i.e. 1.9%) may underestimate the real dissipation capabilities of a twenty-storey timber office / residential building. The Dutch Building code, NEN 6702, refers to a damping ratio, ζ , for timber structures of 0.05 (i.e. 5%), which could significantly influence the dynamic behaviour compared to the application of the damping ratio defined in EC1.

Due to the unreliability of damping values of buildings (also stated by van Oosterhout [15]) it is desired to perform multiple dynamic analyses in STAAD Pro with various damping ratios, in order to define the contribution of rather low or high damping values.

It must be noted that local damping in the building, such as connections, are not possible to simulate in STAAD Pro, so that only damping values can be attached to structural materials. However, the behaviour of structural connections affecting the overall deformation of the building as well as the dynamic behaviour will be discussed in the following chapter.

STAAD Pro analyses by various damping ratios

The greatest effects of damping to the dynamic behaviour of a building can be attached to horizontal accelerations, as stated in the *pre-research* [1]. Hence it can be expected that this dynamic response is directly affected by the STAAD Pro analyses with various damping ratios.

In order to define 'low' and 'high' damping ratios for a multi-storey timber building, a range between 0.01 and 0.08 is assumed. It must be emphasised that this range is based on the assumption that a damping ratio of 0.019 is already conservative due to ignoring constructional elements and higher damping ratios than 0.05, as defined by NEN 6702, might not be likely to occur¹⁵.

Anyhow, it is aimed to analyse the *differences* in dynamic response due to various damping ratios instead of defining accurate values of horizontal accelerations at the top of the building.

Table 6.1 presents the dynamic response results of analyses in STAAD Pro with multiple damping ratios. Input of both the structural model and time varying wind loads are according to Section 4.6, hence these properties are unmodified. Values in Table 6.1 are obtained in the same node of the structural model as defined in Section 4.6, i.e. top node on grid 7-A, and shown in Appendix D.1.

Table 6.1; STAAD Pro results of dynamic behaviour with various damping ratios

Damping ratio; ζ	Maximum dynamic displacement [mm]	Maximum horizontal acceleration [m/s^2]
0.01	-6.20	0.056
0.019	-6.01	0.054
0.05	-5.52	0.047
0.08	-5.42	0.042

Differences in horizontal displacements due to the fluctuating wind loads are negligible, but horizontal accelerations effectively decrease by increasing higher damping ratios. A very likely damping ratio of 0.05 for timber buildings results in a reduction of $0.007 m/s^2$ in comparison to damping defined by EC1, where a top acceleration of $0.047 m/s^2$ for a twenty-storey timber building with a fundamental frequency of 0.58 Hz. can be regarded as 'very acceptable' (conform Dutch criteria in NEN 6702, shown in Figure 4.10) for the residential function located in the upper part of the building.

However, it can be concluded that the differences of horizontal accelerations between damping ratios in the range defined in Table 6.1 are marginal and human perception on these various accelerations may be hard to predict. On the basis of analyses of possible damping ratios in the structure it can be concluded that the influence of connection design might turn out to be more significant with regard to dynamic response behaviour.

6.2 EFFECTS OF OUTRIGGERS ON DYNAMIC BEHAVIOUR

Stiffness of the structural system determines the natural frequencies of the structure and thus affects the dynamic response, where the outriggers may also be essential to the performance of the whole building.

In order to define the contribution of the outriggers in resisting the fluctuating wind loads the model is analysed with- and without outriggers. The results of STAAD Pro analyses are obtained from the top floor on the corner of grid 7-A (see Figure 5.3) and are presented in Table 6.2. It must be noted that the damping ratio remains unchanged and is set on 0.019, i.e. 1.9 percent.

¹⁵ According to Dr. Ben Zhang of Napier University Edinburgh, damping ratios for timber structures are normally between 0.01 and 0.05.

Table 6.2; STAAD Pro results of dynamic behaviour with- and without outriggers

Structural response	Including outriggers	No outriggers	
Max. horizontal displacement due to mean wind load according to equation 4.107; U_{mean}	29.17	41.70	mm
Max. horizontal displacement due to fluctuating wind load; U_{fluc} ¹⁶	5.68	15.20	mm
Max. horizontal displacement due to mean + fluctuating wind load; U_{total}	34.85	56.9	mm
Max. velocity due to fluctuating wind load; v_{max}	0.018	0.044	m/s
Max. acceleration due to fluctuating wind load; a_{max}	0.054	0.122	m/s^2

Once again, the effects of the outriggers are obvious and in particular with regard to the horizontal accelerations their contribution is essential. The lack of stiffness in the structure leads to a drop of the fundamental frequency to 0.49 Hz. As a matter of fact, the behaviour of the building becomes critical, since regulations from NEN 6702 (Figure 4.10) allow a horizontal acceleration for a fundamental frequency of 0.49 Hz. of 0.150 m/s^2 . Further, the dynamic response of the structure to the time varying wind load completely changes, as shown for the horizontal accelerations in Figure 6.1. It can be clearly seen that due to the lack of stiffness the structure is not able to anticipate on the loading frequency resulting in unfavourable large accelerations.

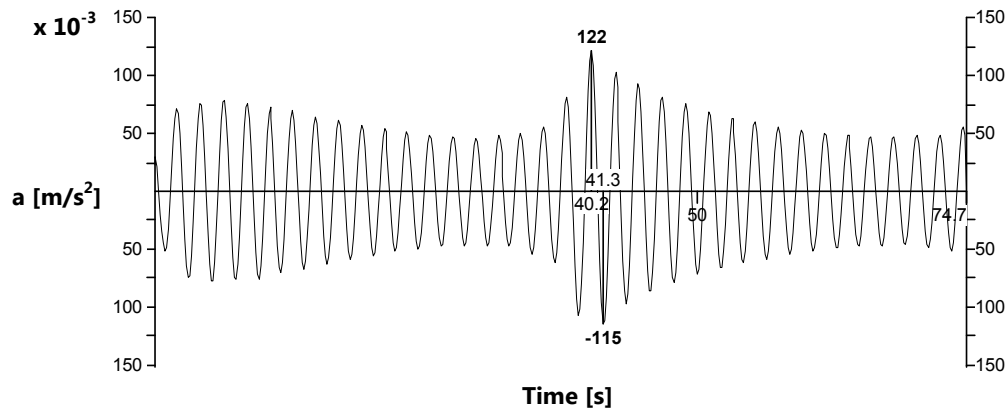


Figure 6.1; Horizontal accelerations – time graph for structure without outriggers

It should be noted that the total displacements are the sum of displacements due to the mean wind load and the maximum displacement due to the time varying wind load. It appears that the sway is less than half the displacement (i.e. 79.9 millimetres) due to quasi-static wind loads as determined by EC1 (see Section 5.3). Considering equations 4.28 to 4.31 it can be seen that the dynamic part of the quasi-static wind loading is determined by the turbulence intensity $I_v(z)$, which is equal to 0.23 on the reference height z_s (= 40.3 meters). Equation 4.31 shows that the standard deviation of the wind velocity on a certain height can be evaluated by the product of $I_v(z)$ and the mean wind velocity $v_m(z)$. On the reference height the standard deviation of the wind velocity is

$$\sigma_v = 0.23 \cdot 26.07 = 6.00 \text{ m/s}$$

¹⁶ The maximum displacement is equal to -6.01 millimetres. For the total displacement – due to mean and fluctuating loads – one should adopt the maximum displacement in positive x-direction

with a mean wind velocity on the reference height equal to 26.07 m/s. Considering the deduced wind profile, shown in Figure 4.8, where the maximum wind velocity is approximately 1.75 m/s (evaluated on the reference height by spectral analysis), it becomes apparent that the determination of the quasi-static wind load by EC1 is very conservative. As a consequence, the static horizontal displacements are significantly higher.

6.3 CONCLUDING REMARKS ON DYNAMIC ANALYSIS

The result of the maximum horizontal acceleration in the preliminary dynamic analysis, i.e. 0.054 m/s^2 , is affected by the amount of damping in the structure but will in any case not turn out to be unfavourable since the adopted damping ratio, ζ , of 0.019 is on the conservative side so that a more likely ratio of 0.05 will only result in a more favourable dynamic behaviour, i.e. lower horizontal accelerations. Nevertheless, the effects of slip in connections on the overall dynamic behaviour, which are expected to be more relevant, of the structure will be investigated in the following chapter.

The importance of the outriggers on the 12th floor of the building has been shown by comparing STAAD Pro analysis with- and without outriggers. In particular the effects on horizontal accelerations are significant, for which it appears that the increased stiffness as well as the more favourable mode shape due to the outriggers effectively reduce the accelerations at the top of the building.

Connection design, however, may influence the overall stiffness of the structure significantly so that above results may not resemble the real behaviour of the timber outrigger structure accurately.

7 | STRUCTURAL CONNECTION DESIGN

Timber connection design and structural behaviour

Connections between structural elements in a building can affect the overall behaviour of the structure significantly. Their rigidity determines the deformation modes of structural elements or the whole structural system. Likewise moment- and force distributions are affected. Moreover, excessive deformed connections could change the overall performance of the structure and even cause local collapse of either connections or connected elements. Before starting with the design of the connections it is needed to identify the role of the connections in a twenty-storey timber outrigger structure.

7.1 DESIGN CONSIDERATIONS

In timber buildings – where serviceability aspects such as horizontal displacements and horizontal accelerations are critical design issues – the performance of connections are affected by the connected material, wood. The cyclic nature of the loading, i.e. fluctuating wind actions, may carry for cavities in the timber around the connectors, due to crushing of the wood, so-called ‘pinching effect’. As a consequence, fasteners lose contact with the timber in which deformations of the joint may cause subjection of the wood in a direction of weak strength, e.g. tension perpendicular to the grain. This appearance may result in brittle failure modes, such as splitting of the timber, even at relatively low load levels [25]. Furthermore, the connectors determine the ductility of a joint, which is relevant for the energy dissipating capacity of the structure.

Outriggers

The importance of the outriggers on the behaviour of the structure has been shown both in the static analysis (Table 5.12) and the dynamic analysis (Table 6.2). It can be concluded from these results that their performance is crucial for the overall structural system in order to obtain the required stiffness in the building. Furthermore, the restraining moment induced by the outriggers effectively limits both the compressive- and tensile stresses in the central core.

Therefore it is of utmost importance to design appropriate connections between outrigger elements in order to ensure good structural performance under static loading as well as dynamic wind loading. For instance excessive slip of connections may result in a deformed structural system, affecting the performance of the outriggers. Lateral wind loads induces structural behaviour of the outriggers as shown in Figure 5.9, where on each side of the core one diagonal is subjected to tensile forces and the other to compressive forces. If for example the compression diagonal has too large tolerances due to slip of fasteners, the force distribution between the members may differ; possibly over-loading the tensile diagonal and/or connections.

Ductility versus strength and stiffness

With regard to tall timber buildings – where serviceability aspects such as horizontal displacements and horizontal accelerations are critical design issues – the requirements on connections are extended by a certain degree of *ductility*. This phenomenon describes the amount of energy which can be dissipated due to dynamic excitations. It has been stated [25] that slender mild steel connectors with a large deformation capacity are generally more suitable to dissipate energy. The dissipation of energy is resembled by the area inside the hysteretic loop (Figure 7.1). The load – deformation curves of a typical timber joint are affected by the ‘pinching effect’. It can be seen, in Figure 7.1, that this results in thinner loops near the middle, which is caused by loss of stiffness due to the formation of a cavity around the fastener which is a result of crushing of the wood. The stiffness gradually increases again as the fastener regains contact with the surrounding wood. Since the inner area reduces due to this effect the energy dissipating capacity of the connection decreases accordingly. Studies in New Zealand [25] have shown, however, the ability of timber structures to sustain large deformations without significant strength deterioration. This statement is supported by Deam and King [26] who diagnosed a low damage ratio at timber buildings suffered by earthquakes.

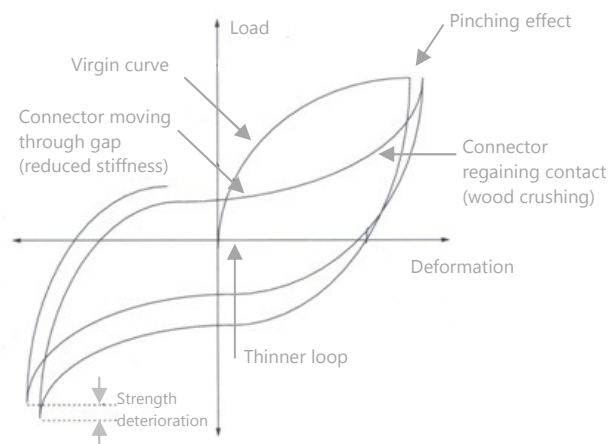


Figure 7.1; Typical hysteretic behaviour of a structural timber component, after Thelandersson [25]

Nevertheless, from the beginning of the dynamic analysis it has been assumed that only linear behaviour of the structure is assumed under lateral wind actions. Therefore, it is questionable that pinching, as shown in Figure 7.1, of connections will affect the structural behaviour at all since the possibility that a connection will reach its ultimate load will be doubtful.

On the other hand, strength criteria in EC5 are based on the Johansen strength equations, which are derived by the assumption of perfect plastic behaviour of the fasteners. With other words, connection design in the ULS by EC5 is based on attaining the ultimate strength of the fasteners. Therefore, it is required to design some additional strength capacity on top of the Johansen strength equations in order to circumvent pinching as described by Figure 7.1. Dutch design criteria for timber structures, NEN 6760 [29], refer to an over-capacity of 33 percent for dowel-type fasteners subjected to lateral shear forces.

Anyhow, ductility should be considered when designing timber connections for tall timber buildings in order to ensure adequate response to dynamic excitations and moreover to attain a certain degree of durability.

In the contrary to ductility, the structure needs to maintain its *stiffness* to resist excessive deformations and to avoid elimination of the intended structural action, such as the role of the outriggers. Therefore it is important to design structural connections on a balanced level between ductile-, strength- and rigid behaviour. Largely deformed connections may result in significantly deformed structural

components in the building, in particular for tall buildings where the number of connections may have a cumulative effect.

It should be emphasised that the dynamic response (Chapter 4 and Chapter 6) with a conservative damping ratio, ζ , of 0.019 (i.e. 1.9%) have shown acceptable results when subjected to cyclic excitations, i.e. fluctuating wind loads. Although higher ratios of damping have shown (Table 6.1) more favourable magnitudes of horizontal accelerations, it appears that increased damping might be desired but not essential to ensure acceptable levels of occupants comfort. Hence, maintaining *stiffness* in the stability system is the *primary objective* for the design of structural connections.

Analysis on structural effects

The influence of rigidity of structural connections can be analysed by modelling translation- or rotation springs at joints in the 3D model of the program STAAD Pro. Subsequently, results on both static loads and dynamic loads can be compared with the basic model as adopted in previous analyses. The proposed strategy as implemented for analysis on the effects of various damping ratios (Chapter 6), can also be used for analysis on rigidity of connections. This means that multiple magnitudes of rigidity can be compared to obtain both upper- and lower levels of effects on structural behaviour.

Behaviour of dowel type connections

The application of slender dowels and a relatively large space between them can give excellent energy dissipating characteristics under cyclic loading [26] [27]. Stocky dowels or dowels with small spacing, on the other hand, tend to fail in a brittle mode before large deformations are reached. Thus ductile connections can be attained by applying slender dowels and large distances between them. It is stated [27] that dowel type connectors with a slenderness ratio of 10 and more are preferable for ductile connections. Low slenderness ratios for dowel-type fasteners exhibit high stresses in the wood at performed shake table tests for braced timber frames, due to high flexural rigidity of fasteners, which caused abrupt wood splitting and sudden loss of bearing capacity. In addition, it was concluded from the tests that connections with high slenderness ratios had higher dissipation of energy than stocky dowel-type connectors.

Design to Eurocode 5

Structural connections should comply with design rules and requirements as given in EC5. The code contains a distinction, similar as timber elements, between the Ultimate Limit State and Serviceability Limit State, where strength conditions are verified in the former and displacement conditions in the latter. Regulations in EC5, however, do not refer to displacement limits, but the effect of connection displacements should be taken into account when determining instantaneous- and final deflections of the structure.

Design rules in EC5 have been developed in order to ensure that failure, due to lateral loading, in the ULS of connections occur in a *ductile* rather than a brittle manner [28]. Typical brittle failure of timber connections is splitting of the timber due to tension perpendicular to the grain. The minimum spacings, end- and edge distances have been derived to prevent splitting failure when the connection is subjected to lateral loading. The adopted ductile failure theory assumes perfect plastic behaviour of the fasteners. As mentioned before strength equations are based on Johansen's failure theory. These equations are dependent on; the geometry of the connection, embedment strength of the connected timber or wood-based material, the bending strength of the fastener and on the basis that the fastener will not withdraw from the connection.

Design strategy

The main objectives of connection design in the twenty-storey timber outrigger structure are

- Designing connections which comply with strength requirements in the ULS in accordance with EC5;
- Incorporation of assembly requirements and optimisation to erection time on-site;
- Analysing the effects of translational- and rotational rigidity of connections on structural behaviour in the 3D STAAD Pro model, with emphasis on the SLS.

Taking into account over-capacity in order to circumvent that fasteners will attain their ultimate strength, and pinching may affect lateral stiffness of the connection or the whole structure, depends on the type of connection and its role in resisting lateral wind loading. For instance, CLT wall connections and outrigger joints are essential in the stability system; hence overcapacity is desired. First connections will be designed according to Johansen’s strength equations, whilst for design in SLS the required over-capacity of 33 percent will be considered.

Prior to starting with actual design of the connection it is important to define *key words*, which represent the purpose of the connection, e.g. desired function, transfer of forces, assembly requirements and so on.

For each type of connection one typical design will be made, which takes into account governing structural forces in concerning joints. For instance core wall connections for lateral shear forces are designed for actions at ground floor level. Although it might be efficient for either economical and/or assembly reasons to modify this type of connection for floors further up the height of the building, it is not taken into account in this report.

EC5 contains calculation methods for slip behaviour of connections which enables the designer to incorporate translational- and rotational rigidity of joints in structural analysis. As mentioned before, the stiffness behaviour of joints is expected to have major effects on the structural behaviour of a tall timber building, especially on deformations in the SLS.

Building physical aspects, such as fire resistance, acoustics and thermal performances, are not part of connection design, although they will be mentioned when defining requirements on the connections. The design strategy for connection design is illustrated in Figure 7.2.

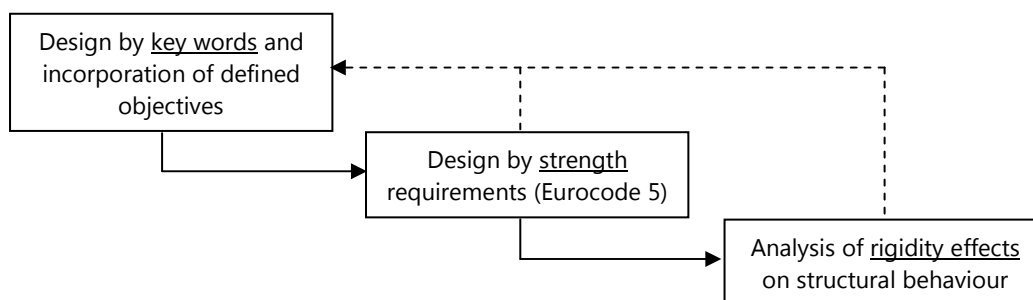


Figure 7.2; Design strategy for structural connections

7.2 CONNECTION TYPES

Due to various types of structural elements in the building several types of connections arise, for which it is most convenient to classify them according to their connected members.

Types of connections between elements in the structure are defined as presented in the overview of Figure 7.3. As mentioned before, connections of floor slabs, i.e. interconnections, floor – beam and floor CLT walls, are not considered in this report, since floors are not part of the stability system.

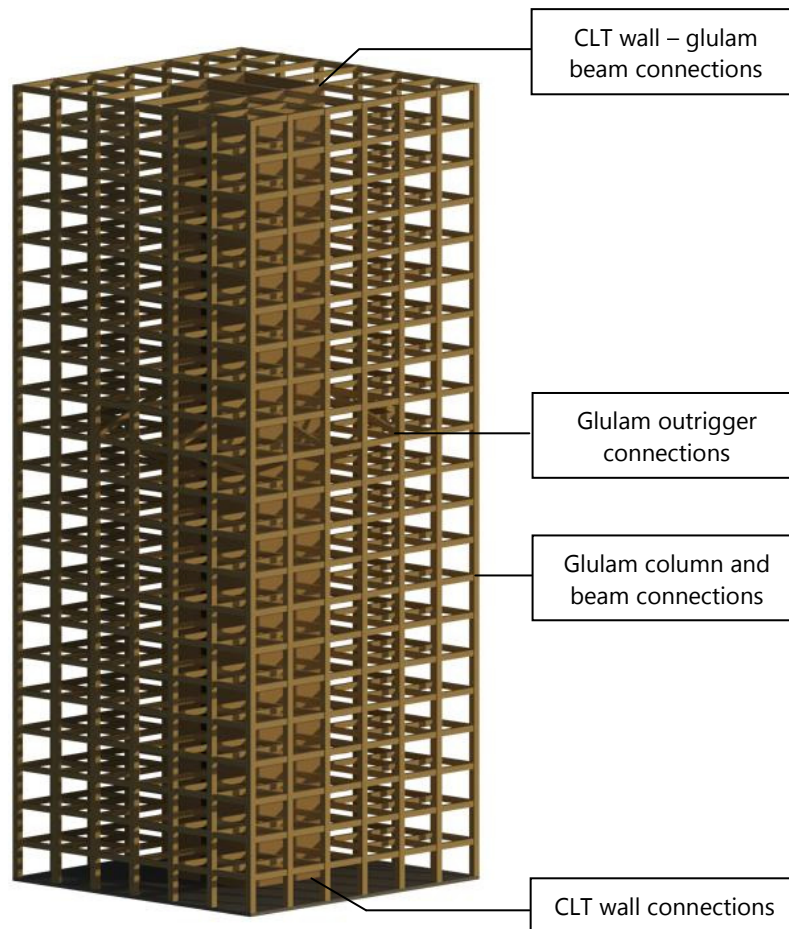


Figure 7.3; Connection types between structural elements

In the following sections it is aimed to design the structural connections on the basis of defined key words for each single type of connection and subsequently verify the performance on strength requirements as set in EC5. As shown in the design strategy (Figure 7.2) it might be needed to modify the design depending on the results of strength verifications.

7.3 CLT WALL CONNECTION DESIGN

CLT walls of the central core consist of 1 200 millimetres wide panel segments interconnected to wall elements. The layout of wall elements is such that fenestrated walls are fastened between non-fenestrated walls, so that the former have a length of 8 700 millimetres ($6 \times 1\,200 + 900 + 600$) and the latter have a length of 9 300 millimetres ($7 \times 1\,200 + 900$). Typical connections are depicted in Figure 7.4, which is a rendered view of the central core of the bottom storey only, thus adjacent structural elements are omitted for the sake of clarity.

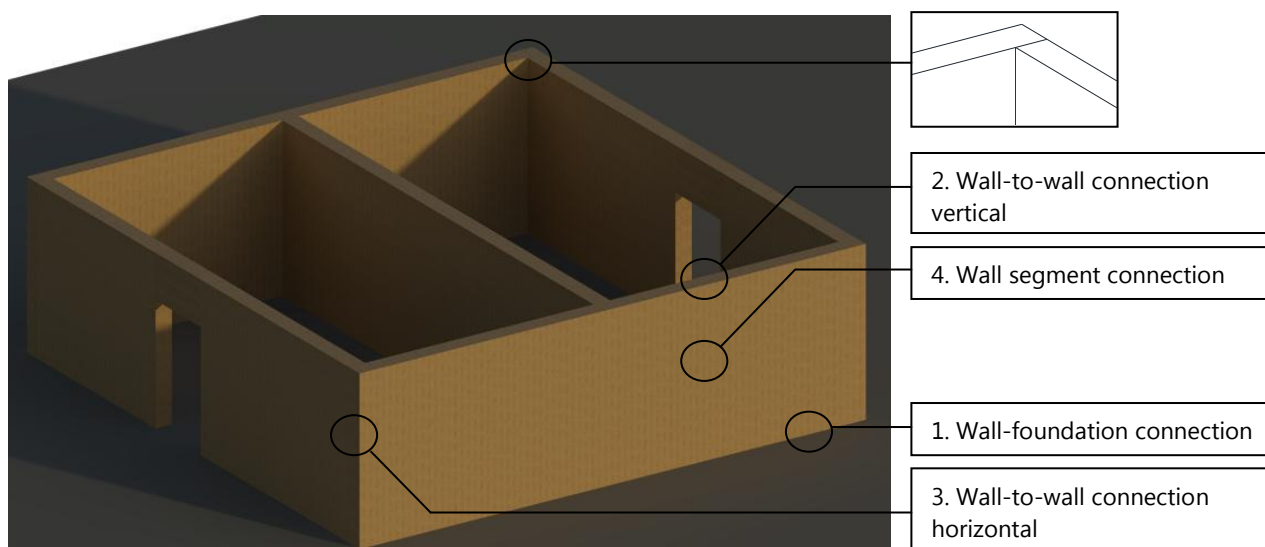


Figure 7.4; CLT wall connections

1. Wall-foundation connection

Connection type 1 should ensure a tight fit between the CLT wall elements and the foundation structure. Due to diaphragm action, the connections should be able to resist the arising tensile forces on the windward side of the wall. Furthermore lateral shear forces on the bottom side of the walls due to wind loading should be transferred to the foundation slab¹⁷ by shear fittings.

Repetition of this connection type is limited to the ground floor only, hence assembly requirements are low. *Functionality* is most relevant for this type of connection as well *fire safety* aspects. Acoustic performance of this connection is irrelevant since adjacent rooms of the wall construction consist of merely communal areas for which no requirements apply in accordance with Dutch regulations [2].

Structural forces in the connection are obtained from static analysis in STAAD Pro, where the governing loading combination is given in Table 7.1. The maximum stresses are related to membrane stresses in orthotropic elements of the model, whilst the lateral shear force is obtained from reaction forces of wall supports at a single shear wall (parallel to grid E, Figure 5.3) (see Appendix E.1).

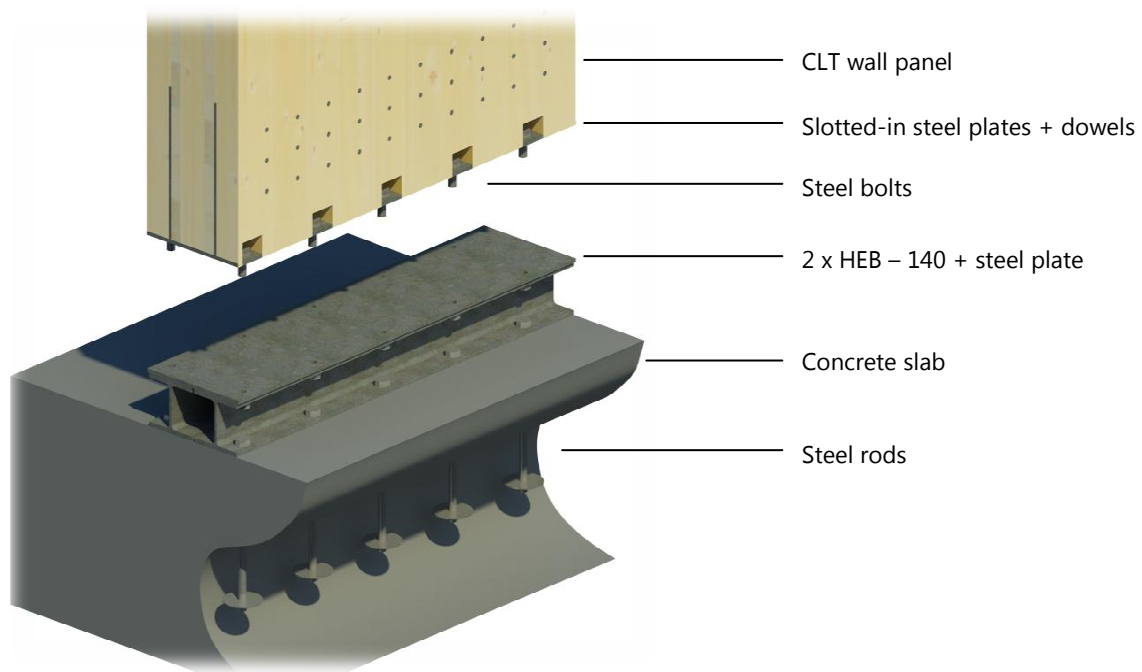
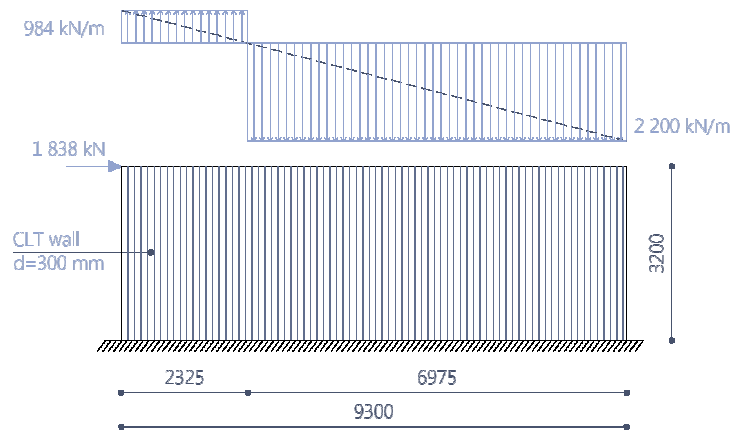
Subsequently, these stresses are conservatively transferred to line forces along the bottom of the pertaining wall element, where it is assumed that these maximum tensile- and compressive stress values are present all along the wall under tension or compression respectively. Further, the design for connection type 1 as well as a proposal for assembly sequence is presented in Table 7.1.

Table 7.1; Connection design type 1

Key words for design:	Functionality, fire safety aspects			
Load on connection	Loading combination ¹⁸	Stress [MPa.]	Width [mm]	Load
Vertical compressive force	ULS-STR-7V	7.34	300	2 200 kN/m
Vertical tensile force	ULS-EQU-2	3.28	300	984 kN/m
Lateral shear force	ULS-EQU-2	-	-	1 836 kN

¹⁷ The foundation structure is assumed to consist of a concrete slab of arbitrary depth, since foundation design is excluded in the report

¹⁸ For connections which ensure overall stability of the structure, e.g. toppling-over and sliding of walls, 'EQU loading combinations' should be used according to EC0



Assembly sequence

1. Steel rods poured-in with foundation slab erection
2. Fastening of steel beams on concrete slab
3. Assembly of wall element (with prefabricated slotted-in plates) by steel bolts

As mentioned before, the distribution of forces is assumed conservatively, as shown in the figure of Table 7.1. The dotted line presents the actual force distribution due to *ULS-EQU-2*, which shows that tension in the CLT wall elements is limited to a distance of 2 325 millimetres. Connection design for tensile forces is only required for this particular length on both sides of the wall due to opposite direction of wind loading.

Bolted connections of the steel beams with a welded plate not only ensure simple assembly on-site but also can adopt certain flexibility in dimensional deviations which might be required since the steel rods are poured-in during the concrete slab erection. This can be attained by designing elongating holes in the steel beams.

Slotted-in plates fastened by dowels enable the CLT wall elements to transfer a large amount of forces to the foundation, since a relatively large wall area is utilised. Moreover, fire resistance of the connection is increased by applying internal steel plates. Steel components underneath the wall obviously need to be protected to achieve fire resistance for structural elements.

Verification of the proposed connection to strength requirements in the ULS consists of the following calculations

- Slotted-in plates fastened by steel dowels subjected to tensile- and lateral shear forces;
- Steel bolts loaded by tensile- and shear forces;
- Steel beams (HEA-140) subjected to compressive forces;
- Poured-in steel rods under tensile- and shear forces.

As shown in Table 7.1 two *slotted-in plates* are designed in the CLT walls, which are welded to a steel head plate in order to connect the prefabricated wall element to the steel beams with bolts. The cross section of a prefabricated wall element is depicted in Figure 7.5, in which grain directions of longitudinal layers on one half of the cross section is shown.

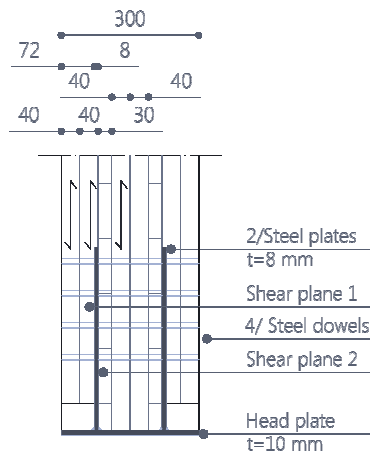


Figure 7.5; Build-up of prefabricated wall element

Due to symmetry of the cross section the load-carrying capacity of a single steel plate, comprising two shear planes, is sufficient to evaluate. The timber adjacent to the outer shear plane (1) is 72 millimetres wide, whilst layers adjacent to the inner shear plane (2) comprise one cross layer (30 millimetres) and one longitudinal layer (40 millimetres). The embedment strength of the timber depends on the angle of applied loading to grain direction.

For vertical tensile forces the embedment strength of longitudinal layers can be written as

$$f_{h,0,k} = 0.082(1 - 0.01d)\rho_k \quad (7.1)$$

where ρ_k is the characteristic mass density and d the diameter of the fastener.

For cross layers and vertical tensile forces fasteners are subjected perpendicular to the grain, where the embedment strength is reduced by the factor k_{90} as follows

$$f_{h,\alpha,k} = \frac{f_{h,0,k}}{k_{90} \sin^2 \alpha + \cos^2 \alpha} \quad (7.2)$$

where k_{90} takes into account the embedment strength in cross direction, which for softwoods can be written as

$$k_{90} = 1.35 + 0.015d \quad (7.3)$$

The angle of load direction to the grain is represented by α . Characteristic yield moment of steel dowels is expressed as

$$M_{y,Rk} = 0.3f_{u,k}d^{2.6} \quad (7.4)$$

where $f_{u,k}$ is the characteristic tensile strength of the fastener [MPa].

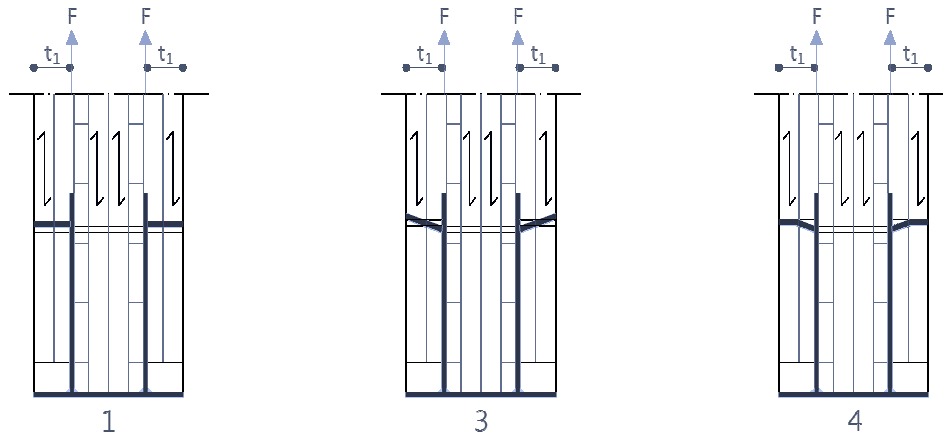
At this stage a diameter of $\varnothing 12$ mm is assumed, which results in a slenderness ratio of: $300 / 12 = 25$. In Section 7.1 it has been concluded that a slenderness ratio of at least 10 should be applied in order to attain a ductile connection.

The behaviour of the dowels during failure for shear plane 1 can be directly deduced from Johansen failure modes. But for layers adjacent to shear plane 2 different embedment strengths carry for another approach to determine the dowel's behaviour and thus load carrying capacity.

Table 7.2 presents Johansen failure modes for shear plane 1 only, where for the sake of clarity behaviour of the dowel in the middle layer, i.e. between steel plates, is omitted.

Table 7.2; Embedment strength and strength equations for connection type 1, vertically loaded

Material properties	$f_{u,k}$ [MPa.]	$M_{y,Rk}$ [Nmm]
Steel dowels, $\varnothing 12$ mm	800	153 491
Equation 7.1	Value	
Embedment strength longitudinal layer; $f_{h,0,k}$	27.42	MPa.
<i>Johansen failure modes</i>		



Strength equations	Value [kN]
$F_{v,Rk,1} = f_{h,0,k}t_1d$	23.69
$F_{v,Rk,3} = f_{h,0,k}t_1d \left[\sqrt{2 + \frac{4M_{y,Rk}}{f_{h,0,k}dt_1^2}} - 1 \right]$	12.70
$F_{v,Rk,4} = \sqrt{4M_{y,Rk}f_{h,0,k}}d$	14.21

It becomes apparent that the development of one plastic hinge on shear plane 1 results in the lowest strength capacity, i.e. failure mode 3.

Behaviour of the dowels between the steel plates is affected by different embedment strengths. Independent on this build-up of layers possible failure modes are 1 and 4, which are failure due to exceedance of the embedment strength of the timber and the development of two plastic hinges. Which failure mode occurs depends on the ratio t_2/d , or the slenderness of the dowel. The plastic yielding moment of the dowels, represented by equation 7.4, basically determines if the dowel is stiff enough to fail by wood crushing, i.e. failure mode 2. A relatively weak dowel, obviously, tends to fail by the development of two plastic hinges. Figure 7.6 shows two possible failure modes of the dowel between the steel plates.

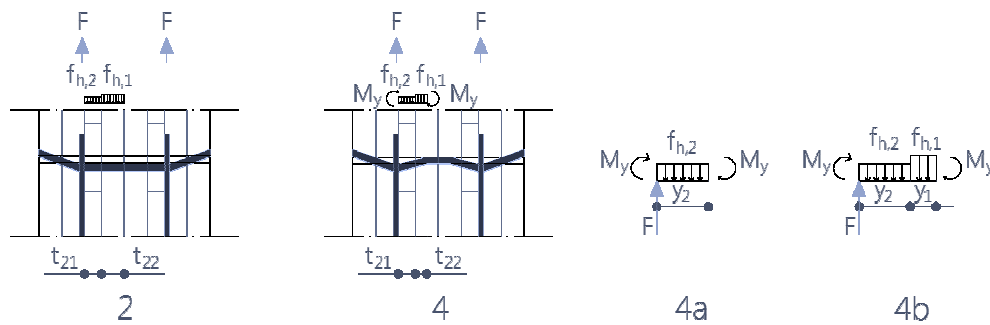


Figure 7.6; Possible failure modes for dowel between steel plates

Failure mode 2 consists of wood crushing determined by embedment strengths $f_{h,1}$ and $f_{h,2}$ of the longitudinal layer and cross layer respectively, for which $f_{h,1}$ equals $f_{h,0,k}$ and $f_{h,2}$ is $f_{h,90,k}$ accordingly. Thickness of layers is for t_{21} equal to 30 millimetres and for t_{22} 40 millimetres.

The load-carrying capacity of failure mode 4 depends on the location of the plastic hinge in the timber, which may be represented by either distance y_2 or the sum of y_1 and y_2 . With other words, the plastic hinge may occur in the cross layer or longitudinal layer. Assuming that the hinge develops in the cross layer the equilibrium state of forces on the dowel becomes (failure mode 4a, Figure 7.6)

$$2M_y - \frac{1}{2}y_2^2 f_{h,2} d = 0 \quad (7.5)$$

The distance y_2 can be expressed as

$$y_2 = \sqrt{\frac{4M_y}{f_{h,2} d}} \quad (7.6)$$

As a consequence, when distance y_2 is larger than thickness, t_{21} , the plastic hinge will not occur in the cross layer, i.e. failure mode 4a will not appear.

Equilibrium state of forces on the dowel in failure mode 4b becomes

$$2M_y - \frac{1}{2}y_2^2 f_{h,2} d - y_1 f_{h,1} d \left(y_2 + \frac{y_1}{2} \right) = 0 \quad (7.7)$$

where y_2 is equal to t_{21} or 30 millimetres, hence equation 7.7 results in a quadratic equation of variable y_1 .

Determination of the governing failure mode for the steel dowel in the middle part of the cross section and characteristic load carrying capacity is shown in Table 7.3.

Table 7.3; Strength equations of failure modes 2 and 4

Embedment strengths	Value [MPa.]		
Embedment strength longitudinal layer; $f_{h,2}$	27.42		
Embedment strength cross layer; $f_{h,1}$	17.92		
Failure mode 2	Value [kN]		
$F_{v,Rk,2} = (f_{h,1}t_{22}d) + (f_{h,2}t_{21}d)$	19.61		
Failure mode 4	Value		
Failure mode 4a, distance y_2 (equation 7.6)	53.4	> t_{21}	mm
Failure mode 4b, distance y_1 (equation 7.7)	16.7	< t_{22}	mm
$F_{v,Rk,4b} = (f_{h,2}t_{21}d) + (f_{h,1}y_1d)$	11.94		kN

The slenderness of the dowel reflects the behaviour during failure, for which it appears that two plastic hinges occur before the embedment strength of the timber is attained. Equation 7.7 shows that the plastic hinge in the timber is located in the longitudinal layer and results in a characteristic load carrying capacity for shear plane 2 of 11.94 kN.

The load-carrying capacity for a single steel plate by shear plane 1 and 2 yields

$$F_{v,Rk} = F_{v,Rk,3} + F_{v,Rk,4b} = 12.70 + 11.94 = 24.64 \text{ kN}$$

The design value of the load-carrying capacity is expressed as follows

$$F_{v,Rd} = k_{mod} \frac{F_{v,Rk}}{\gamma_M} \quad (7.8)$$

where k_{mod} is equal to 0.9 for short-term actions (wind loading) and γ_M is determined by the material property for connections as 1.3. The design value of the load-carrying capacity per fastener involving two steel plates becomes

$$F_{v,Rd} = 0.9 \frac{(2 \cdot 24.64)}{1.3} = 34.12 \text{ kN}$$

Distance y_1 can be up to 40 millimetres, than the plastic hinge is located in the exact centre of the panel. Moving the steel plate more to the centre means that the outer distance, t_1 , increases and therefore load-carrying capacity $F_{v,Rk,3}$ increases accordingly. To utilise the cross section and dowel's capacity most efficiently it is proposed to move the steel plate in the cross layer so that t_1 is equal to 80 millimetres. The characteristic load carrying capacity of shear plane 1 becomes

$$F_{v,Rk,3} = 27.42 \cdot 80 \cdot 12 \left[\sqrt{2 + \frac{4 \cdot 153 \, 491}{27.42 \cdot 12 \cdot 80^2}} - 1 \right] = 13.52 \text{ kN}$$

where it can be seen that $F_{v,Rk,3}$ is still the governing failure mode in comparison to $F_{v,Rk,1}$ and $F_{v,Rk,4}$ in Table 7.2.

Distance y_2 decreases to 22 millimetres, whilst distance y_1 can be recalculated by considering equilibrium of forces on the dowel through equation 7.7. The solution to the quadratic equation yields a value for y_1 of 23.1 millimetres. The characteristic load carrying capacity of shear plane 2 equates to

$$F_{v,Rk,4b} = (17.92 \cdot 22 \cdot 12) + (27.42 \cdot 23.1 \cdot 12) = 12.33 \text{ kN}$$

The design value of the load-carrying capacity per fastener with two steel plates is now

$$F_{v,Rd} = 0.9 \frac{2(13.52+12.33)}{1.3} = 35.79 \text{ kN}$$

It can be seen that the effects of moving the steel plate to the cross layer are marginal. Anyhow it yields a higher load carrying capacity of the connection, so that this modification will be adopted in the design.

In order to take into account the 'grouping effect', which refers to possible splitting of the timber due loading of a row of dowels along the grain direction, an effective number of dowels per row should be designed as follows

$$n_{ef} = n^{0.9} \sqrt[4]{\frac{a_1}{13d}} \quad (7.9)$$

where n is the number of dowels in the row, a_1 is the spacing between dowels in the grain direction. Although cross laminated sections may decrease the susceptibility of splitting of the timber, the panel predominantly comprises longitudinal layers (when loaded in vertical direction) and therefore this appearance is taken into account.

When it is assumed that each row of dowels comprises three dowels with a spacing of 80 millimetres ($>5d$, see Table 7.6), the effective number of dowels per row is 2.3.

The load-carrying capacity in lateral direction of the CLT wall is determined by different material properties. The outer layers are now subjected perpendicular to the grain by the lateral shear force, hence $f_{h,90,k}$ applies. Failure modes are similar in comparison to the case when dowels are loaded in longitudinal direction of outer layers. Table 7.4 summarises the results of the load-carrying capacity in lateral direction for shear plane 1.

Table 7.4; Embedment strength and strength equations for shear plane 1, laterally loaded

Equation 7.1 – 7.3		
Factor k_{90}	1.53	-
Embedment strength longitudinal layer; $f_{h,0,k}$	27.42	MPa.
Embedment strength cross layer; $f_{h,90,k}$	17.92	MPa.
Strength equations ¹⁹		Value [kN]
$F_{v,Rk,1} = f_{h,90,k} t_1 d$		17.20
$F_{v,Rk,3} = f_{h,90,k} t_1 d \left[\sqrt{2 + \frac{4M_{y,Rk}}{f_{h,90,k} dt_1^2}} - 1 \right]$		9.70
$F_{v,Rk,4} = \sqrt{4M_{y,Rk} f_{h,90,k}} d$		11.49

¹⁹ The 'rope effect' for dowels is neglected

Failure mode 3 is again the governing mode for the load-carrying capacity in lateral direction.

Determination of the load carrying capacity of shear plane 2 involves the same approach as carried out for vertical tensile forces in the connection. Forces in lateral direction, however, changes the embedment strengths of $f_{h,1}$ into $f_{h,90,k}$ and $f_{h,2}$ into $f_{h,0,k}$. Failure mode 4 remains similar as before, as well as equilibrium states as defined in equations 7.5 to 7.7.

Table 7.5 shows determination of the position of the plastic hinge in the timber of the middle part in the cross section and the pertaining strength equations. Distances t_{21} and t_{22} are 22 and 40 millimetres.

Table 7.5; Failure modes 2 and 4 for forces in lateral direction of connection type 1

Embedment strengths	Value [MPa.]		
Embedment strength longitudinal layer; $f_{h,2}$	27.42		
Embedment strength cross layer; $f_{h,1}$	17.92		
Failure mode 2	Value [kN]		
$F_{v,Rk,2} = (f_{h,1}t_{22}d) + (f_{h,2}t_{21}d)$	15.84		
Failure mode 4	Value		
Failure mode 4a, distance y_2 (equation 7.6)	43.20	> t_{21}	mm
Failure mode 4b, distance y_1 (equation 7.7)	28.98	< t_{22}	mm
$F_{v,Rk,4b} = (f_{h,2}t_{21}d) + (f_{h,1}y_1d)$	13.47		kN

The location of the plastic hinge in the timber for loading in lateral direction is more to the centre of the panel in comparison to loading in vertical direction (28.98 > 23.10 mm), resulting in a higher load carrying capacity for shear plane 2 despite the lower embedment strength for the thicker layer (t_{22}).

The characteristic load-carrying capacity for laterally loaded dowels per fastener and two steel plates becomes

$$F_{v,Rk} = 2 \cdot (F_{v,Rk,3} + F_{v,Rk,4b}) = 2 \cdot (9.70 + 13.47) = 46.34 \text{ kN}$$

The design value for each fastener, $F_{v,Rd}$, results in 32.08 kN.

Splitting of the timber will not affect the load carrying capacity for loading in lateral direction, since layers are predominantly oriented in cross direction.

Minimum end- and edge distances and spacings between fasteners are given in table 8.5 of EC5. Table 7.6 resembles the final design of connection type 1.

Table 7.6; Design of connection type 1

Load-carrying capacity per fastener	Value [kN]		
Vertical tensile forces; $F_{v,Rd}$	35.79		
Lateral shear forces; $F_{v,Rd}$	32.08		
Minimum end-, edge distances and spacings	Vertical loading	Lateral loading	
End distance, loaded; $a_{3,t}$	84 (7d)	84 (7d)	mm
Edge distance, loaded; $a_{4,t}$	36 (3d)	36 (4d)	mm
Spacing parallel to grain direction; a_1	60 (5d)	36 (3d)	mm
Spacing perpendicular to grain direction; a_2	36 (3d)	36 (3d)	mm

Fasteners		Value	
Vertical tensile loading; $q_{t,s,d}$		984	kN/m
Lateral shear force; $F_{v,s,d}$		1 836	kN
Number of fasteners for tensile loading; n		28	n/m
Number of rows with effective number of dowels		13	row/m
Number of fasteners for shear force; n		58	-

Distance	29 x 3 dowels	20 x 3 dowels	
$a_{3,t}$	100	-	mm
$a_{4,t}$	100	100	mm
a_1	80	200	mm
a_2	80	80	mm

Distances between fasteners as well as to ends/edges of the CLT wall element are taken on the conservative side, since it was stated in Section 7.1 that slender dowels with relatively large distances in between are beneficial when it comes to design of ductile connections.

A complete design of other components in the connection, as shown in the figure of Table 7.1, e.g. steel beam *HEA-140*, bolts and steel rods *M20* and washers with a diameter of $\varnothing 100$ millimetres are beyond the scope of this work. However, simple checks on these components, as shown in C.S.6.1 of Appendix E.1, have proven the applicability of these components for the proposed connection.

The final design of connection type 1 is depicted in Figure 7.7.

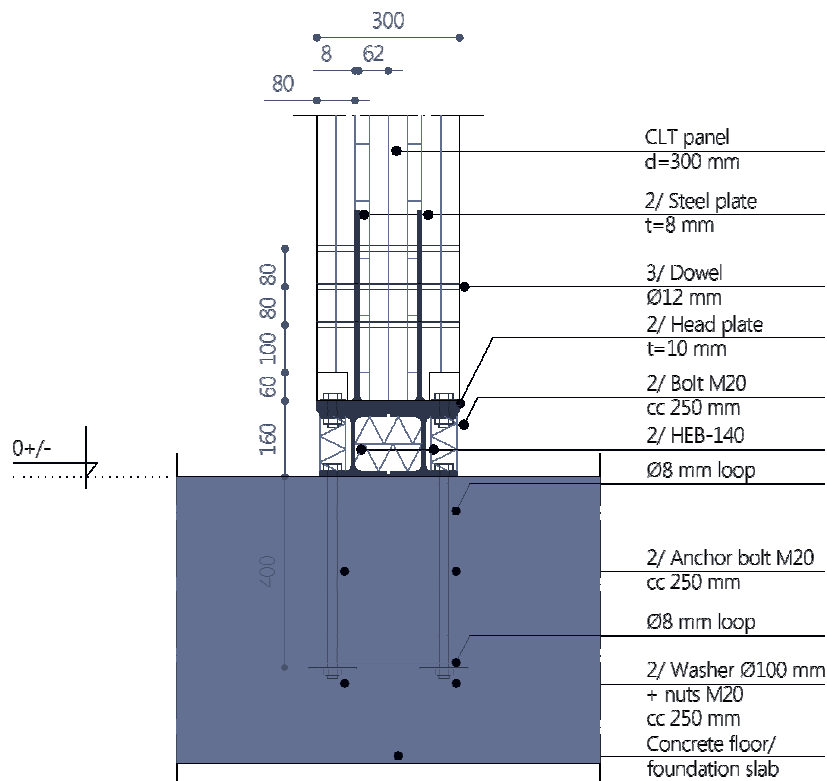


Figure 7.7; Connection type 1

2. Wall-to-wall connection vertical

The main purpose of connection type 2 is to transfer vertical tensile forces as well as lateral shear forces to the structure below, similar as connection type 1. Subjecting forces, both tensile and shear become lesser higher up the structure. Therefore, the designed connection (1) of the wall to the foundation will comply with strength requirements of connections (2) between upper floors. With other words dowels, slotted-in steel plates and bolts can be directly taken from connection type 1.

In addition, the connection should be amplified with the provision of floor bearing on one side of the wall structure, i.e. floor structure in egress route outside the core. It may be obvious that the 'platform method', i.e. floor bearing between the walls, is not applicable for a twenty-storey building due to compressive stresses in the wall structure. The design compressive stress of 7.34 MPa. (Table 5.12) will broadly exceed the design compressive strength perpendicular to the grain of the CLT floor slabs. Therefore floor elements should be designed outside the wall structure, by the so-called 'balloon method'.

In the contrary to connection type 1 this connection should be designed for advantageous assembly processes, which means that a *simple connection* suitable for *repetition* throughout the building is desirable. The *assembly process* is of great importance for a multi-storey building, wherein the use of timber creates great opportunities by implementing a high degree of *prefabrication*. As been shown in the previous subsection, the application of bolted fasteners between prefabricated timber elements can result in simplified erection processes on-site (Table 7.1). Devastating construction failures can be circumvented by simply bolting building elements together on-site, and moreover bolted connections can adopt a certain amount of flexibility in dimensional deviations.

Once again, requirements on acoustic performance are irrelevant since adjacent rooms of the connection consist of communal areas only. For these rooms, no requirements on noise control apply according to the Dutch Building code [2].

Naturally, fire resistance is important since the connection is part of the structural system. In analogy with connection type 1, internal connections in timber elements are beneficial. Connection components should be protected by fire resistant board materials, if necessary.

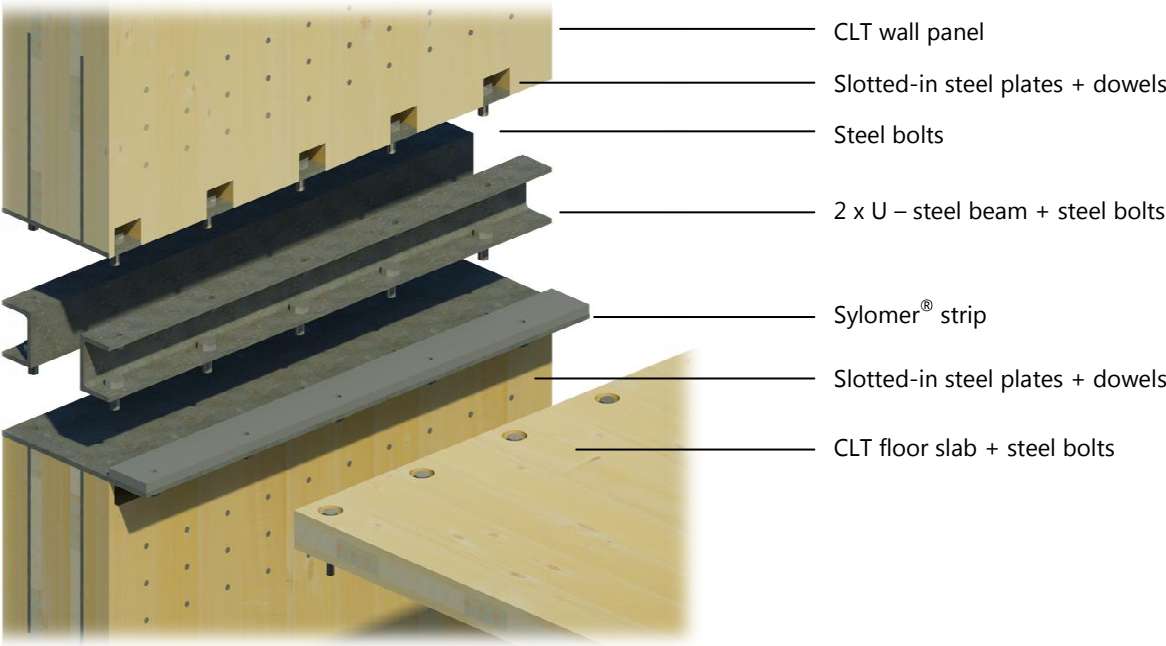
The proposed connection and assembly sequence on-site is presented in Table 7.7.

The application of steel U-beams creates space for insulation material in the contrary to *HEA-140* beams on the ground floor. The U-beams, however, should possibly be manufactured exclusively, since the dimensions do not correspond with standardised steel profiles available on the Dutch construction market. Of great importance is the position and thickness of the webs, here designed as 10 millimetres, since these should transfer the vertical forces from one slotted-in steel plate to the one below.

Designs of floor element connections, such as shown in the figure of Table 7.7, are not discussed in this report. However, lateral shear forces from the façade into the floor slabs to the core are transferred by this connection. The stresses are introduced in the steel head plate by the bolts fixed to the floor slabs. Subsequently, wall elements are subjected by the slotted-in steel plates resulting in compression perpendicular to the grain, as shown in Figure 7.8. Possibly splitting of the timber could occur, due to crushing of wood surrounding the internal steel plates, depending on the magnitude of the stresses. Floor design in Chapter 5 has shown that each floor structure is subjected to a design wind load, $w_{e,total,d}$ of 7.68 kN/m (Figure 5.6). With regard to maximum shear stresses in the floor slabs it has been conservatively assumed that all wind loads for each floor are transferred to supports, i.e. two shear walls. However, it can be expected that the cross shear wall on grid 5 (Figure 5.3) is directly subjected to a line load of 7.68 kN/m.

Table 7.7; Connection design type 2

Key words for design: Simple connection, repetition, prefabrication



Assembly sequence

1. Erection of prefabricated wall with slotted-in plates, head plate and steel beams
2. Floor slab element bolted to head plate, filling connection components with insulation material
3. Prefabricated wall element bolted to steel beams

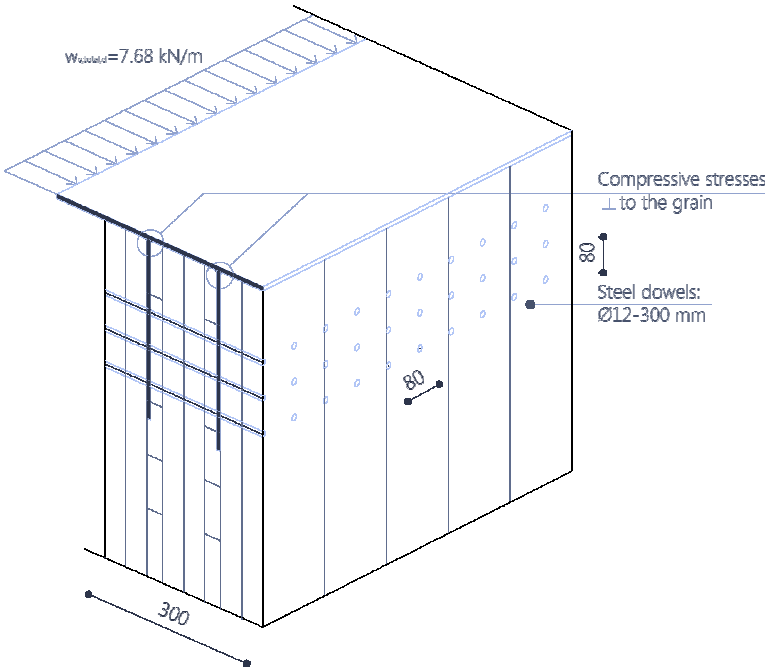


Figure 7.8; Slotted-in steel plates subjected to lateral shear forces

The force transfer leads to peak compressive stresses perpendicular to the grain, for which the design strength of the CLT wall elements is

$$f_{c,90,k} = 2.5 \text{ MPa} \rightarrow f_{c,90,d} = k_{\text{mod}} \frac{f_{c,90,k}}{\gamma_M} = 0.9 \frac{2.5}{1.25} = 1.8 \text{ MPa}.$$

For each steel plate a stress on the timber arises, by assuming a height of 20 millimetres, of

$$\sigma_{c,90,d} = \frac{7.68/2}{20} = 0.192 \text{ MPa} < 1.8 \text{ MPa}.$$

The connection complies with resistance to lateral shear forces from the floor structure. Moreover, slotted-in steel plates of the wall above will cooperate in transferring these forces. The final design of connection type 2 is resembled in Figure 7.9.

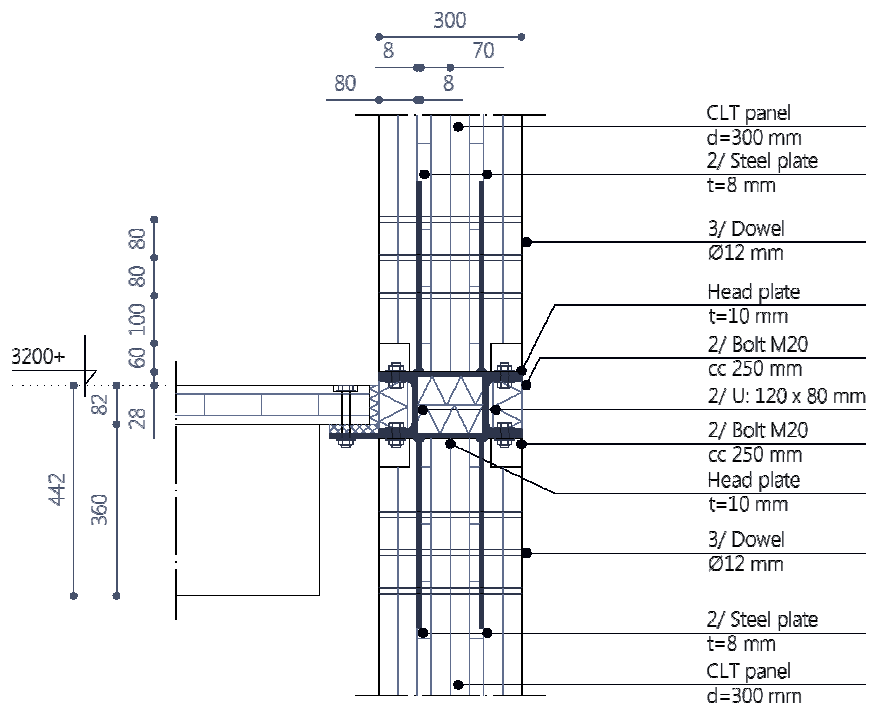


Figure 7.9; Connection type 2

3. Wall-to-wall connection horizontal

A typical connection between core wall elements consist of butt joints between CLT panels, as illustrated in Figure 7.4. The joint is subjected to forces from multiple directions.

Firstly, shear forces in the wall structures may be resisted by individual walls, in order to maintain the structural integrity of the core as a whole these forces should also be able to transfer between horizontal joints. It is of utmost importance to maintain the rigid connection between single walls, since the lateral stiffness of the core is largely influenced by this integrity. Hence connection type 3 is loaded by vertical shear forces.

Secondly, lateral forces are introduced in the connection due to shear forces from the floor slabs, as discussed in the previous subsection. Each floor structure is subjected to a line wind load, $w_{e,total,d}$ of 7.68 kN/m. In Section 5.4 it has been determined that the supports at the wall joints are subjected to a lateral design reaction force of, $V_A = V_B = 105.6 \text{ kN}$.

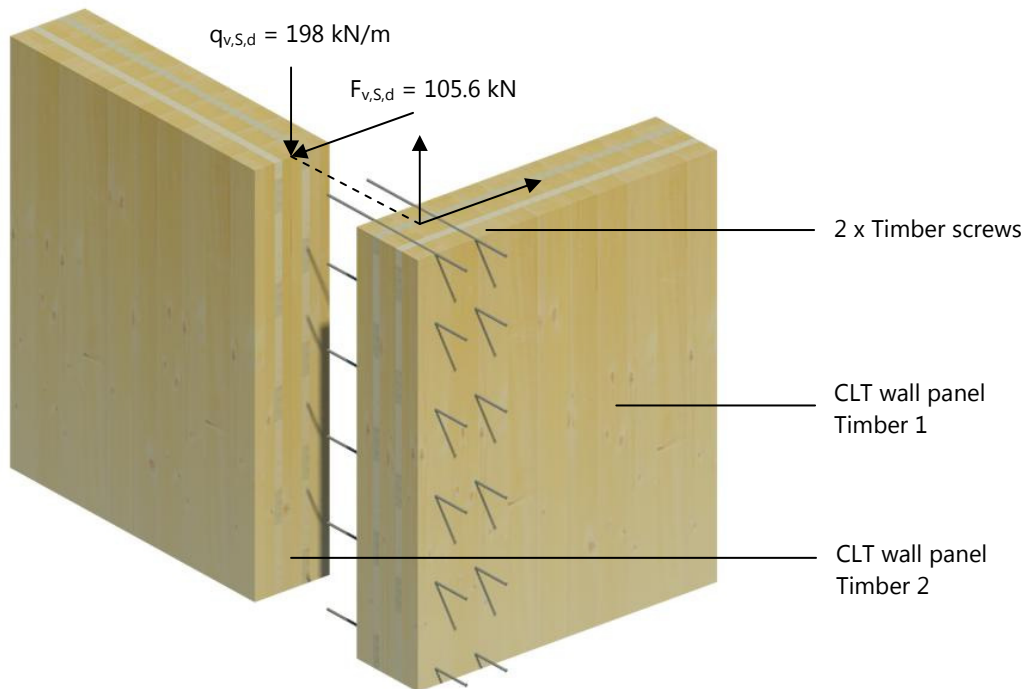
Requirements from an assembly process point of view comprise an emphasis on *simplicity* and a connection suitable for *repetition*. The connection appears over the whole height of the building and therefore a simple and cost-efficient design is desired.

In analogy with previous discussed connections no specific requirements on acoustics apply since the connected structural elements do not need to comply with regulations on noise control between adjacent rooms as defined by regulations [2].

A design for connection type 3 is proposed in Table 7.8, which also gives an overview of subjecting forces.

Table 7.8; Connection design type 3

Key words for design:		Simplicity, repetition		
Load on connection	Loading combination	Load [kN]	Length [mm]	Shear force
Vertical shear force; $q_{v,S,d}$	ULS-EQU-2	1 836	9 300	198 kN/m
Lateral shear force; $F_{v,S,d}$	ULS-EQU-2	105.6	-	105.6 kN



The application of a timber screw as a fastener both simplify the assembly process and create a tight connection between both wall elements. The embedment strength of a timber screw differs from steel dowels, but also the timber elements carry for another material capacity.

As fasteners penetrate the full cross section, and the panel consist of layers in two directions, a combination of $f_{h,0,k}$ (eq. 7.1) and $f_{h,90,k}$ (eq. 7.2) applies. German researchers Uibel and Blass [30] [31] have derived strength equations for the embedment strength of CLT panels with screw fasteners on the basis of test results.

For fasteners penetrated perpendicular to the panel's plane, i.e. timber 1, the embedment strength is

$$f_{h,pred} = 0.13d^{-0.53} \rho_k^{1.05} \quad (7.10)$$

where d is the *outer diameter* of the screw and ρ_k is the characteristic density of the panels (380 kg/m³). For timber 2, where fasteners are penetrated on the panel's edge surface the embedment strength equates to

$$f_{h,pred} = 0.8622d^{-0.46} \rho_{k,layer}^{0.56} \quad (7.11)$$

where $\rho_{k,layer}$ is the characteristic density of the layers (350 kg/m³ for strength class C24). Derivation of equation 7.10 and 7.11 has been conducted by performance of a range of tests where screws are penetrated on various positions in the panels. For instance screws are positioned in the centre of a board as well as in small gaps between individual boards.

For comparison, the embedment strength of timber 1 can be evaluated by assuming all layers of the CLT panel in cross direction of the load, $f_{h,90,k}$ as shown in Table 7.9.

Furthermore, the load-carrying capacity of timber screws are also affected by the characteristic withdrawal capacity, $F_{ax,k,Rk}$. Uibel and Blass present an equation of the withdrawal capacity on the basis of performed tests of screws both perpendicular to the plane and in-plane of CLT as follows

$$F_{ax,k,Rk} = \frac{0.35d^{0.8} \ell_{ef}^{0.9} \rho_k^{0.75}}{1.5\cos^2 \varepsilon + \sin^2 \varepsilon} \quad (7.12)$$

where ℓ_{ef} is the effective point side penetration length [mm], ε is equal to 90° for penetration in timber 1 and 0° for penetration in timber 2.

The proposed design of connection type 3 and the results of equation 7.10 to 7.12 are shown in Table 7.7.

Table 7.9; Embedment strengths and withdrawal capacity of timber in connection type 3

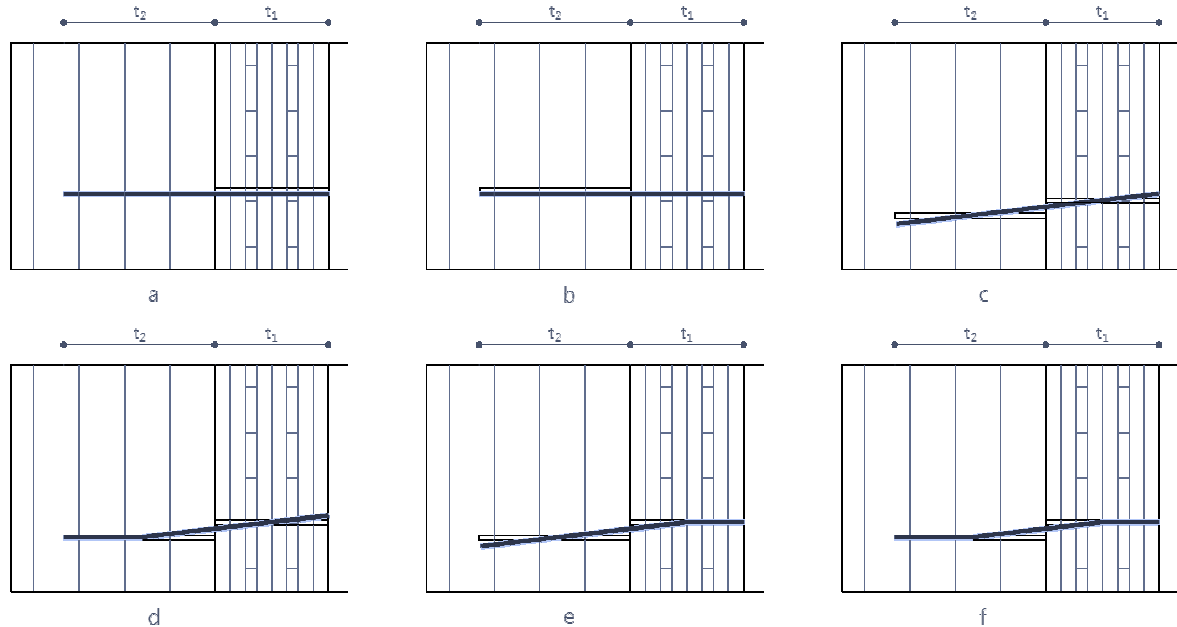
Material properties	$f_{u,k}$ [MPa.]	$M_{y,Rk}$ [Nmm]
Timber screws, $\varnothing 13 - 700$ mm	800	189 001
<i>Characteristic withdrawal capacity (eq. 7.12)</i>		
Effective point side penetration length timber 1; ℓ_{ef}	300	mm
Angle between screw axis and grain direction timber 1; ε	90	°
Characteristic withdrawal capacity timber 1; $F_{ax,k,Rk}$	39.76	kN
Effective point side penetration length timber 2; ℓ_{ef}	400	mm
Angle between screw axis and grain direction timber 2; ε	0	°
Characteristic withdrawal capacity timber 2; $F_{ax,k,Rk}$	34.34	kN
<i>Embedment strength</i>		
Embedment strength timber 1 (eq. 7.10); $f_{h,pred,1}$	17.07	MPa.
Factor k_{90}	1.55	-
Embedment strength timber 1, cross layers only (eq. 7.2); $f_{h,90,k}$	17.55	MPa.
Embedment strength timber 2 (eq. 7.11); $f_{h,pred,2}$	7.04	MPa.
Ratio embedment strengths; $\beta = f_{h,pred,1} / f_{h,pred,2}$	0.41	-

Embedment strength of an assumed build-up of cross sections only, which should be a conservative approach, results in a higher strength than proposed by Uibel and Blass [30] [31]. This could be due to the fact that equation 7.10 and 7.11 takes into account positions such as between two single boards. Nevertheless the lowest value, $f_{h,pred,1}$, will be implemented in calculations for load-carrying capacity of the connection.

Strength equations of the load-carrying capacity can be deduced from the Johansen failure theory for timber-to-timber joints as presented by equation 8.6 of EC5. Table 7.10 shows possible failure modes of the connections and the pertaining load-carrying capacity. The lowest value gives the governing capacity.

Table 7.10; Strength equations of connection type 3

Johansen failure modes



Strength equations (equation 8.6 EC5)²⁰

Strength equations (equation 8.6 EC5) ²⁰	Value [kN]
$F_{v,Rk,a} = f_{h,1,k} t_1 d$	66.57
$F_{v,Rk,b} = f_{h,2,k} t_2 d$	36.61
$F_{v,Rk,c} = \frac{f_{h,1,k} t_1 d}{1 + \beta} \left[\sqrt{\beta + 2\beta^2 \left[1 + \frac{t_2}{t_1} + \left(\frac{t_2}{t_1} \right)^2 \right] + \beta^3 \left(\frac{t_2}{t_1} \right)^2} - \beta \left(1 + \frac{t_2}{t_1} \right) \right] + \frac{F_{ax,Rk}}{4}$	28.75
$F_{v,Rk,d} = 1.05 \frac{f_{h,1,k} t_1 d}{2 + \beta} \left[\sqrt{2\beta(1 + \beta) + \frac{4\beta(2 + \beta) M_{y,Rk}}{f_{h,1,k} \cdot d \cdot t_2^2}} - \beta \right] + \frac{F_{ax,Rk}}{4}$	28.16
$F_{v,Rk,e} = 1.05 \frac{f_{h,1,k} t_2 d}{1 + 2\beta} \left[\sqrt{2\beta^2(1 + \beta) + \frac{4\beta(1 + 2\beta) M_{y,Rk}}{f_{h,1,k} \cdot d \cdot t_2^2}} - \beta \right] + \frac{F_{ax,Rk}}{4}$	23.43
$F_{v,Rk,f} = 1.15 \sqrt{\frac{2\beta}{1 + \beta}} \sqrt{2M_{y,Rk} \cdot f_{h,1,k} \cdot d} + \frac{F_{ax,Rk}}{4}$	16.62

It appears that the development of two plastic hinges is the weakest link in the connection, resulting in a characteristic load-carrying capacity of 16.62 kN per fastener.

The design value for the load-carrying capacity of the screw in connection type 3 can be evaluated by equation 7.8 as follows

²⁰ The minimum value of the withdrawal capacity, $F_{ax,Rk}$, applies, which yields 34.34 kN and is related to timber 2

$$F_{v,Rd} = 0.9 \frac{16.62}{1.3} = 11.51 \text{ kN}$$

The loading direction, e.g. vertical shear force or lateral shear forces as indicated in the figure of Table 7.8, has no effect on the load-carrying capacity of the connection. The embedment strengths has been determined by tests performed by Uibel and Blass [30] [31], in which different test setups includes multiple loading directions as well as various positions of the screws in the panel. Hence, the evaluated maximum load-carrying capacity of 11.51 kN on a single screw applies for loading in two directions.

As been shown in the figure of Table 7.8 the lateral shear force, $F_{v,S,d}$, from the floor structure acts as a concentrated load on the connection. However, this force is introduced in the connection by the slotted-in steel plates, as shown in Figure 7.8. Therefore it can be assumed that this concentrated force will be distributed over approximately 500 millimetres from the topside of a wall. The resultant of both shear forces subjecting over 500 millimetres on the topside of the wall than becomes

$$F_{v,S,d} = \sqrt{(198 \cdot 0.5)^2 + (105.6)^2} = 144.75 \text{ kN}$$

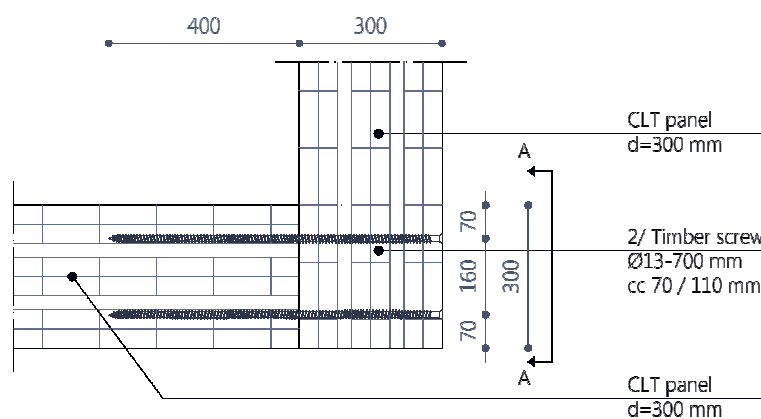
The number of required screws over 500 millimetres will be

$$n = \frac{144.75}{11.51} = 13 \text{ screws} \rightarrow 7 \times 2 \text{ screws with a spacing of 70 millimetres}$$

The remaining height of the wall is subjected to a shear load of, $q_{v,S,d}$ equal to 198 kN/m, so that

$$n = \frac{198}{11.51} = 18 \text{ screws} \rightarrow 9 \times 2 \text{ screws per meter with a spacing of 110 millimetres}$$

Final design of connection type 3 is presented in Figure 7.10, where the narrow spacing over half a meter of the topside of a wall is also applied at the bottom side, since possibly the lateral shear forces are partly transferred via the slotted-in steel plates of the upper wall as shown in connection type 2 of Figure 7.9.



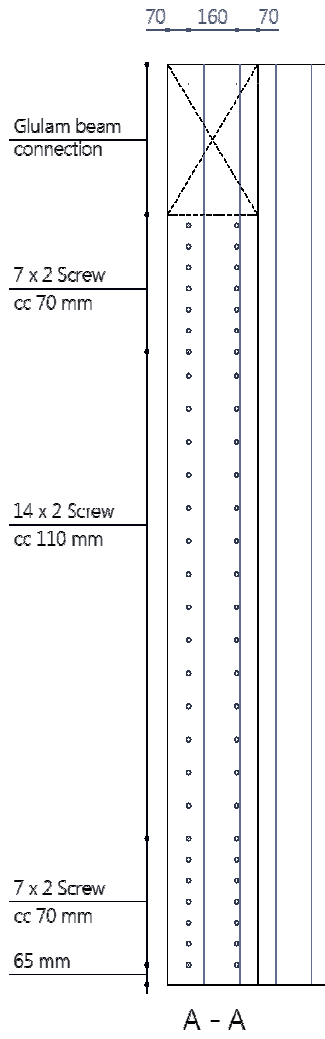


Figure 7.10; Connection type 3

4. Wall segment connection

Joints between single wall segments are subjected to vertical shear forces similar to a full wall element, which was determined before on, $q_{v,S,d} = 198 \text{ kN/m}$. As illustrated in Figure 7.11, the same amount of shear forces should be able to transfer between the wall segment connections. Keywords of the connection are *functionality* and *repetition*. A functional connection is desired because integrity of the joint is important for the stiffness in lateral direction. Further, the connection should be suitable for quick erection since a high number of connections appear in the structure.

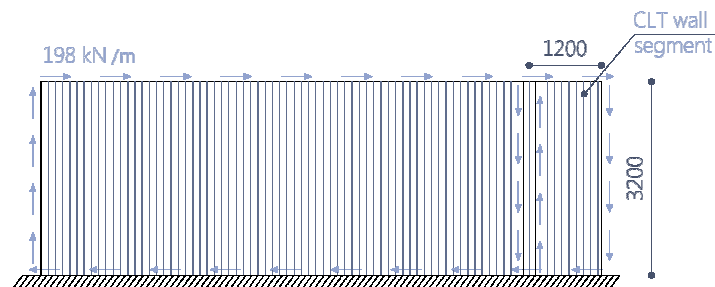
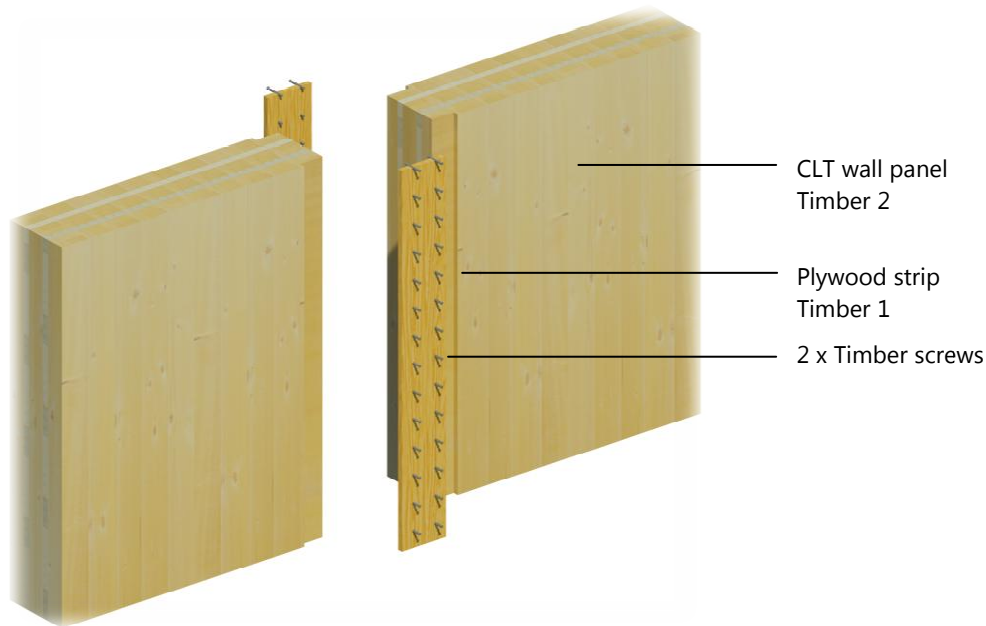


Figure 7.11; Shear force distribution in a CLT core wall

Table 7.11 presents a preliminary design of connection type 4.

Table 7.11; Connection design type 4

Key words for design:	Functionality, repetition			
Load on connection	Loading combination	Load [kN]	Length [mm]	Shear force
Vertical shear force; $q_{v,s,d}$	ULS-EQU-2	1 836	9 300	198 kN/m



Actions on the connections result in lateral loaded screws, for which the calculation procedure is in analogy with connection type 3. As a starting point, timber screws with a diameter of $\varnothing 6$ millimetres and a length of 80 millimetres are assumed.

The characteristic yield moment for screws with a diameter equal or smaller than 6 millimetres can be evaluated by (equation 8.14 EC5)

$$M_{y,Rk} = 0.45f_u d^{2.6} \quad (7.13)$$

where f_u is the tensile strength of the screws, equal to 800 MPa. and d is the effective diameter of the timber screw, equal to 5.5 millimetres²¹.

The thickness of plywood strips is 22 millimetres. The embedment strength of plywood can be calculated according to equation 8.20 of EC5, as follows

$$f_{h,k} = 0.11\rho_k d^{-0.3} \quad (7.14)$$

where and ρ_k is the characteristic density of plywood, which is 600 kg/m³ and d is the effective diameter.

²¹ In accordance with Clause 8.7.1(3) the effective diameter can be taken as $1.1d_{net}$, where d_{net} is the diameter of the shank equal to 5 millimetres

The rope effect of timber screws can be determined by incorporating the withdrawal capacity as follows

$$F_{ax,k,Rk} = \frac{n_{ef} f_{ax,k} d \ell_{ef} k_d}{1.2 \cos^2 \alpha + \sin^2 \alpha} \quad (7.15)$$

where $f_{ax,k}$ is the characteristic pointside withdrawal strength written as

$$f_{ax,k} = 0.52d^{-0.5} \ell_{ef}^{-0.1} \rho_k^{0.8} \quad (7.16)$$

in which d is the outer thread diameter and ℓ_{ef} is the penetration length of the threaded part. Other symbols of equation 7.15 are; k_d equal to the lower value of $d/8$ or 1 and α is the angle between screw axis and grain direction. The lowest value of the characteristic withdrawal capacity of timber 1 or 2 applies in the strength equations.

Strength calculations are similar as presented in the previous subsection, since the connection consist of a single shear timber-to-timber connection. Table 7.12 presents material properties and Johansen strength equations related to connection type 3.

Table 7.12; Strength equations for connection type 3

Material properties	$f_{u,k}$ [MPa.]	$M_{y,Rk}$ [Nmm]
Timber screws, $\varnothing 6 - 80$ mm, $d_{ef} = 5.5$ mm	800	30 286
<i>Characteristic withdrawal capacity</i>		
Effective point side penetration length timber 1; ℓ_{ef}	22	mm
Angle between screw axis and grain direction timber 1; α	90	°
Characteristic pointside withdrawal strength timber 1; $f_{ax,k,Rk}$	26.01	MPa.
Characteristic withdrawal capacity timber 1; $F_{ax,k,Rk}$	3.30	kN
Effective point side penetration length timber 2; ℓ_{ef}	58	mm
Angle between screw axis and grain direction timber 2; α	90	°
Characteristic pointside withdrawal strength timber 2; $f_{ax,k,Rk}$	16.38	MPa.
Characteristic withdrawal capacity timber 2; $F_{ax,k,Rk}$	2.08	kN
<i>Embedment strength</i>		
Embedment strength timber 1 (eq. 7.10); $f_{h,1,k}$	38.56	MPa.
Embedment strength timber 2 (eq. 7.11); $f_{h,pred,2,k}$	25.72	MPa.
Ratio embedment strengths; $\beta = f_{h,pred,2}/f_{h,k,1}$	0.67	-
<i>Strength equations (equation 8.6 EC5)²²</i>		<i>Value [kN]</i>
$F_{v,Rk,a} = f_{h,1,k} t_1 d$		4.30
$F_{v,Rk,b} = f_{h,pred,2,k} t_2 d$		8.20
$F_{v,Rk,c} = \frac{f_{h,1,k} t_1 d}{1 + \beta} \left[\sqrt{\beta + 2\beta^2 \left[1 + \frac{t_2}{t_1} + \left(\frac{t_2}{t_1} \right)^2 \right]} + \beta^3 \left(\frac{t_2}{t_1} \right)^2 - \beta \left(1 + \frac{t_2}{t_1} \right) \right] + \frac{F_{ax,Rk}}{4}$		3.50
$F_{v,Rk,d} = 1.05 \frac{f_{h,1,k} t_1 d}{2 + \beta} \left[\sqrt{2\beta(1 + \beta) + \frac{4\beta(2 + \beta)M_{y,Rk}}{f_{h,1,k} dt_2^2}} - \beta \right] + \frac{F_{ax,Rk}}{4}$		2.22

²² Diameter d in the strength equations equals d_{ef} , as defined above

$$F_{v,Rk,e} = 1.05 \frac{f_{h,1,k} t_2 d}{1 + 2\beta} \left[\sqrt{2\beta^2 (1 + \beta) + \frac{4\beta(1 + 2\beta) M_{y,Rk}}{f_{h,1,k} d t_2^2}} - \beta \right] + \frac{F_{ax,Rk}}{4} \quad 4.16$$

$$F_{v,Rk,f} = 1.15 \sqrt{\frac{2\beta}{1 + \beta}} \sqrt{2M_{y,Rk} f_{h,1,k} d} + \frac{F_{ax,Rk}}{4} \quad 4.21$$

The minimum value is found at failure mode d , for which the design value for the load-carrying capacity for a single fastener is as follows

$$F_{v,Rd} = 0.9 \frac{2.22}{1.3} = 1.54 \text{ kN}$$

With a subjecting shear force in the connection of 198 kN/m, there is a need of 129 screws per meter. A two-sided connection means that 65 screws are required per meter on each side of a CLT panel. This results in a spacing of 15 millimetres. The minimum spacing for screws ($d \leq 6 \text{ mm}$) (Table 8.2²³ EC5) with predrilled holes is $4.25d$ ($=25 \text{ mm}$), hence it can be concluded that the connection should be strengthened. Therefore, it is proposed to design an extra timber screw for each fastener horizontally, in a staggered pattern. Two rows of timber screws increase the required spacing to 30 millimetres. The final design of connection type 4 is shown in Figure 7.12.

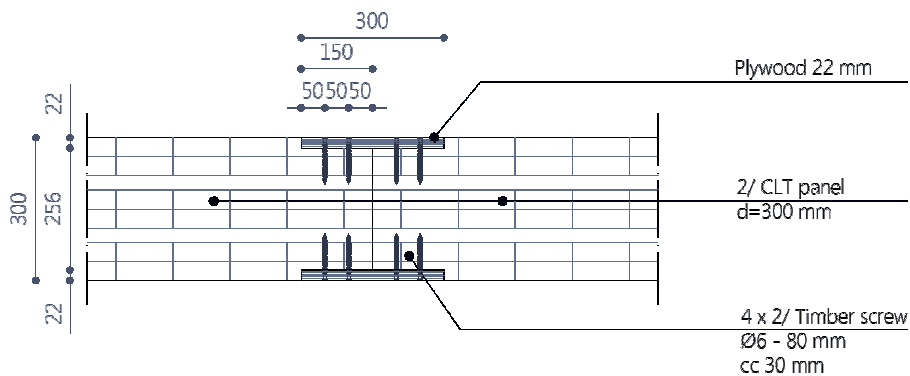


Figure 7.12; Final design of connection type 4

7.4 GLULAM COLUMN AND BEAM CONNECTIONS

Connections between glulam members are located at the perimeter of the building, as shown in Figure 7.13. In an early stage of the preliminary design phase it was already stated that connections of the frame structure should be designed as *pin jointed* connections. This would spare the frame structure of undesirable bending moments and shear forces. Moreover, the efficiency of the outriggers will be higher, since the central core will have a larger rotation due to wind with a pinned frame structure and thus will induce larger forces in the outriggers. Nevertheless, a purely hinged connection is difficult to achieve, for which usually strength capacities are lacking. STAAD Pro outcomes related to forces in connections are shown in Appendix E.1.

²³ In accordance with Clause 8.3.1.3(1) of EC5 minimum spacings can be multiplied with a factor 0.85 for screwed panel-to-timber connections

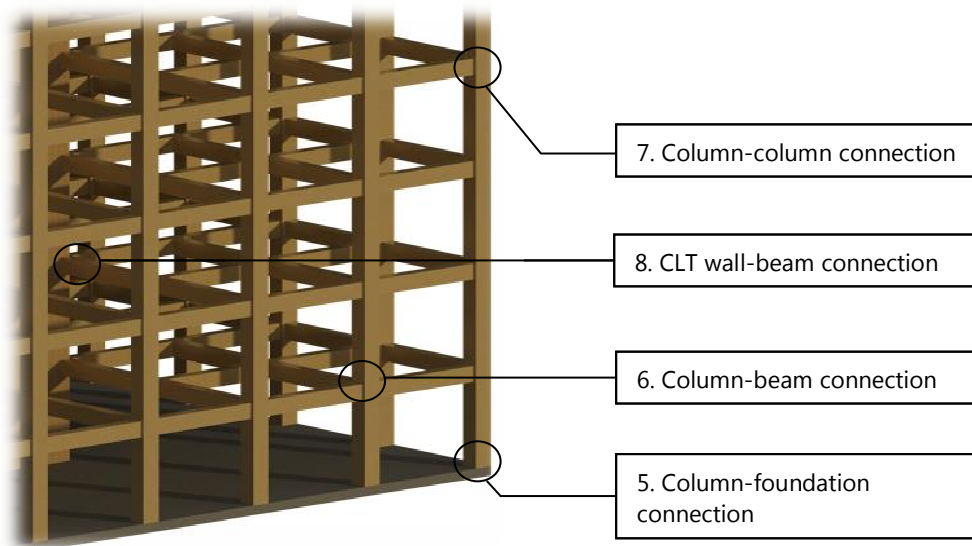


Figure 7.13; Glulam member connections

5. Column-foundation connection

Vertical tensile forces in columns due to the restraining moment, M_r , induced by the outriggers merely appear in columns directly underneath the outriggers. In columns on the ground floor these forces are counterbalanced by vertical loading, which appears to be dominant. The aimed distribution of large vertical loading (Section 3.7) to the columns by designing beams directly from the core to the columns appears to be efficient in controlling vertical tensile forces. As a consequence, forces in connection type 5 consist of compressive axial forces and lateral shear forces. As mentioned before, due to pin modelled connections between glulam members in the 3D STAAD Pro model, these lateral shear forces are very low in comparison with the axial compression.

In the contrary to CLT core walls, column connections around the building's façade should have certain *aesthetical requirements*, since rooms (offices / apartments) are designed on these locations. Likewise, noise control issues are now relevant, although it should be once more emphasised that connection design is predominantly focussed on structural aspects. Furthermore, continuous columns over four storeys introduce flanking sound transmissions between floors anyhow, so that optimisation for acoustic performances on structural connections is complicated to achieve.

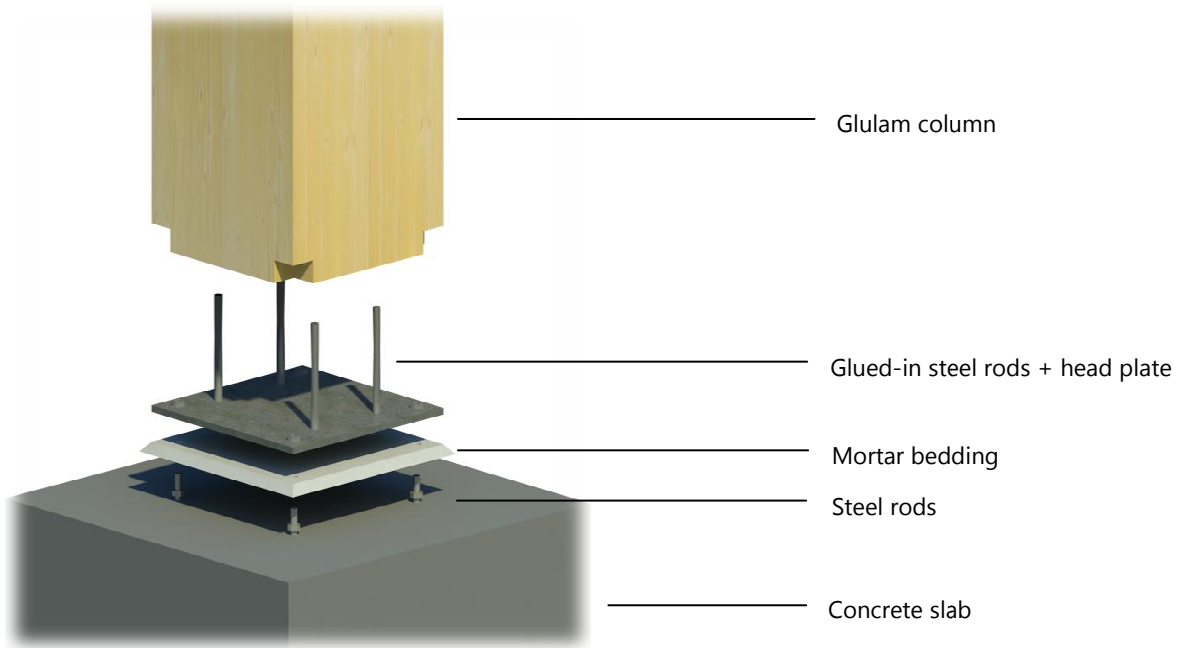
Although aesthetical requirements on structural elements usually affect *fire resistant performances* negatively, designing structural connections invisible to meet these requirements means enhanced fire resistant properties.

Connection type 5 only appears on the ground floor, and therefore assembly processes and optimisation for repetition are irrelevant in comparison to *functionality*. A functional connection means in this context a design optimised on; material- and cost efficiency and an efficient transfer of structural forces.

Table 7.13 presents an overview of actions on the structural connection, a proposal of the design for structural calculations and assembly sequence on-site. The presented forces are obtained from the reaction force of the column on grid 3-A (Figure 5.3). The governing loading combination is *ULS-STR-5V* and has a single variable load, which is imposed floor loading. Therefore, restraining forces due to outrigger effects do not induce the largest axial compressive forces in the columns.

Table 7.13; Connection design type 5

<i>Key words for design:</i>		<i>Functionality, fire safety aspects, aesthetics</i>
<i>Load on connection</i>	<i>Loading combination</i>	<i>Load [kN]</i>
Axial compressive force; $N_{c,d}$	ULS-STR-5V	2 317
Lateral shear force; $V_{y,d}$	ULS-STR-5V ²⁴	7.64



Assembly sequence

1. Steel rods poured-in with foundation slab erection
2. Assembly of column (with prefabricated glued-in rods and head plate) by steel bolts

Lateral shear forces on the connection seem to be negligible with regard to outcomes of the STAAD Pro analysis. Nonetheless, some extra shear forces may arise due to rotational stiffness of the connection. Eccentricities of glulam members may induce similar forces in the connection, although STAAD Pro has taken into account eccentricities from glulam beams (see Section 5.6). Anyhow, some load-carrying capacity in lateral direction is required.

At this stage it is desired to take into account structural actions in connection type 7, which may be designed similarly, in order to integrate some continuity between connections. For instance tensile forces in axial direction directly below the outriggers require pull-out capacity of the glued-in steel rods. Therefore, as a starting point, a rod diameter of $\varnothing 24$ millimetres is assumed.

Connection design in EC5 only consists of joints with mechanical fasteners, thus one should refer to former (national) regulations and/or literature available on glued-in rods. Simple equations for load-carrying capacity of such fasteners are presented in [32], which are originally proposed by Riberholt [33].

In lateral direction the strength of glued-in rods depends on both the embedment strength of the timber and strength capacity of the fastener. Further, the eccentricity of timber's end and acting of the

²⁴ The maximum lateral shear force in the connection is caused by loading combination *ULS-STR-12V* and consist of *8.02 kN*

force also affects the load-carrying capacity. The strength equation suggested by Riberholt is as follows

$$F_{v,Rk} = \left(\sqrt{e^2 + \frac{4M_{y,Rk}}{df_{h,k}}} - e \right) df_{h,k} \quad (7.17)$$

where e represents the eccentricity in [mm]. Considering equation 7.17 it can be seen that the pertaining failure mode consists of two plastic hinges in the steel rod. The embedment strength, $f_{h,k}$, for glued-in rods parallel to the grain direction is expressed by [32]

$$f_{h,k} = (0.0023 + 0.75d^{-1.5}) \rho_k \quad (7.18)$$

Acting of the force is assumed at the bottom side of the head plate, i.e. e equal to 20 millimetres. The results of load-carrying capacity of M24 steel rods in steel strength 8.8 are given in Table 7.14.

Table 7.14; Embedment strength and lateral load-carrying capacity of glued-in rods

Material properties	$f_{u,k}$ [MPa.]	$M_{y,Rk}$ [Nmm]
Steel rods, $\varnothing 24 - 320$ mm	800	930 594
<i>Embedment strength</i>		
Embedment strength; $f_{h,k}$	3.30	MPa.
<i>Load-carrying capacity in lateral direction</i>		
Eccentricity; e	20	mm
Load-carrying capacity; $F_{v,Rk}$	17.24	kN

The design value for the load-carrying capacity for resistance to lateral shear forces for a single rod becomes

$$F_{v,Rd} = 0.9 \frac{17.24}{1.3} = 11.94 \text{ kN}$$

In analogy with mechanical fasteners, Riberholt derived minimum end-, and edge distances, spacings and internal length of the rod. The minimum internal length of a rod should be 240 millimetres (=10d). A loaded end, when the rods are subjected to lateral shear forces, should be at least 96 millimetres (=4d). However, the required distances can be calculated by analysing the failure mode, represented by equation 7.17. Figure 7.14 shows the failure mode of two plastic hinges, one at the welded steel plate and one in the timber.

Equilibrium between the two plastic hinges, i.e. distance y_1 , is in accordance with equation 7.6, so that distance y_1 equals

$$y_1 = \sqrt{\frac{4M_y}{f_h d}}$$

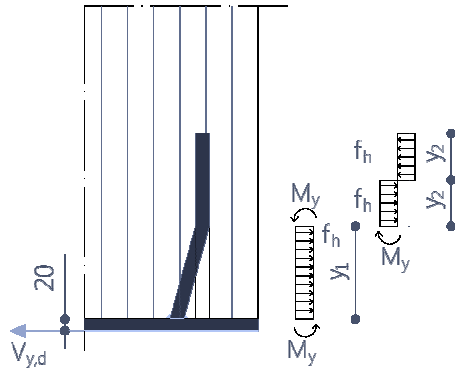


Figure 7.14; Failure mode for laterally loaded glued-in rod

For second part of the steel rod, distance y_2 can be determined as follows

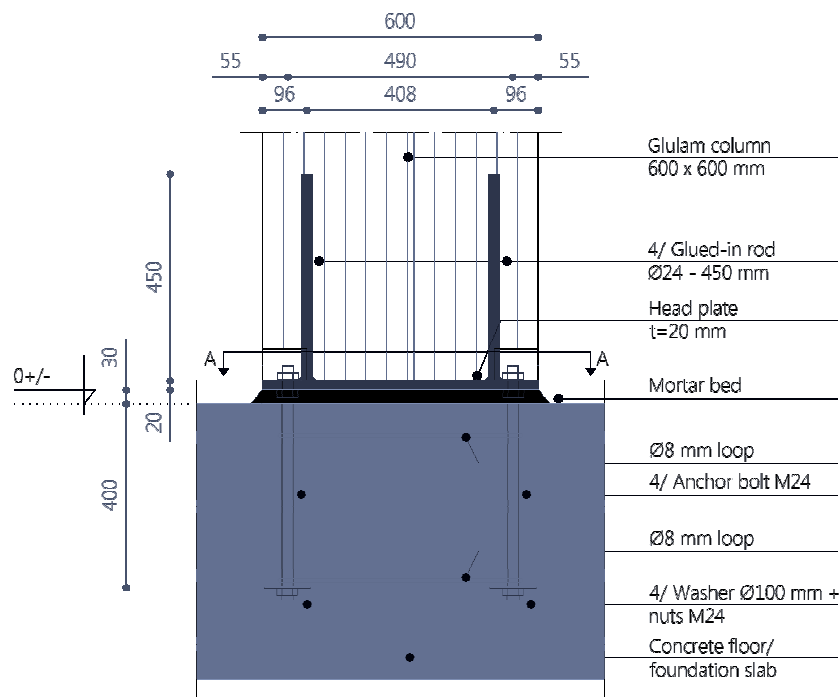
$$M_y - \frac{1}{2}y_2^2df_h - \frac{3}{2}y_2^2df_h = 0 \rightarrow M_y = y_2^2df_h \quad (7.19)$$

$$y_2 = \sqrt{\frac{M_y}{df_h}} \quad (7.20)$$

The required distance in order to attain equilibrium for development of two plastic hinges, i.e. equation 7.19. becomes

$$l \geq y_1 + 2y_2 = \sqrt{\frac{16M_y}{df_h}} = 435 \text{ mm } (\approx 18d) \quad (7.21)$$

The final design of the connection detail, with an internal length of steel rods of 450 millimetres, is shown in Figure 7.15.



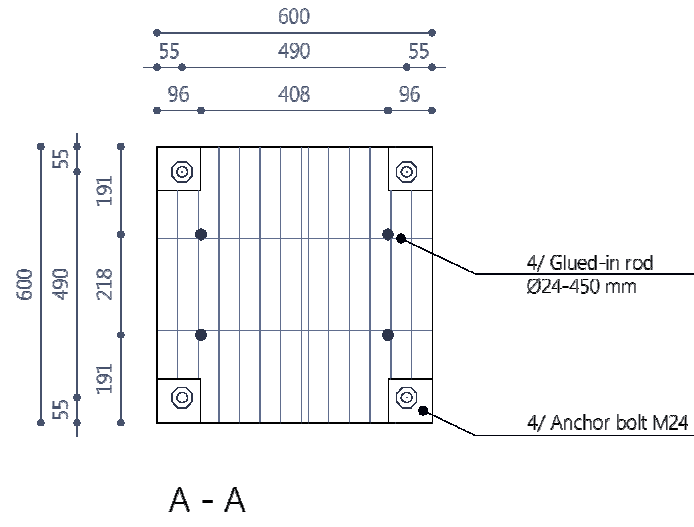


Figure 7.15; Connection type 5

6. Column-beam connection

Connection type 6 consists of a joint where three glulam beams meet a continuous column. Two of these span a relatively short distance from one peripheral column to another, as shown in the typical joint of Figure 7.13. The third beam spans from the central core over 9 meters and therefore introduces higher forces in the connection than the others. In order to avoid undesirable additional forces, like bending moments and shear forces, in both the beams and columns, it is required to design a connection of low rigidity.

Forces in the connection comprise vertical shear forces due to vertical floor loading and lateral forces as a consequence from wind actions. It must be noted that although wind loading is introduced in the floor slabs, beams are also subjected to lateral wind loading since they are connected to the floor structure. Further, the largest axial forces in the beams are found at outrigger level where the restraining moment, M_r , introduces additional axial forces in upper- and lower beam of the horizontal trusses; this is analysed in Section 7.5.

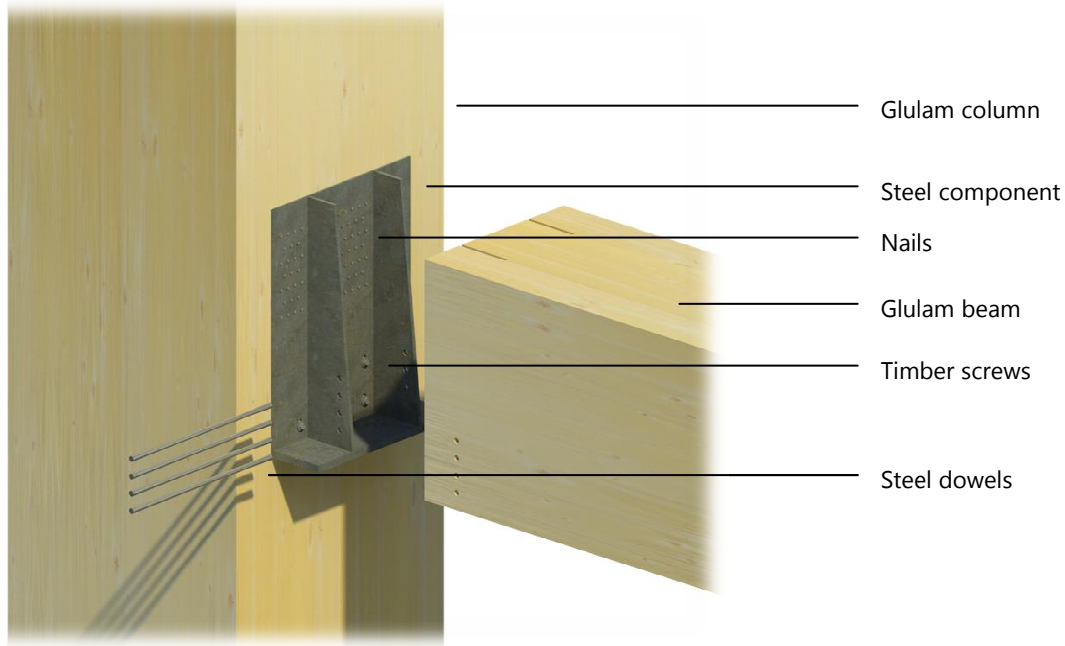
Column-beam joints appear frequently in the structure; hence a connection suitable for an *efficient assembly process* and *repetition* is required. A high degree of *prefabrication* and simple bolted fasteners for erection on-site are preferable. Acoustic requirements are limited to the floor structure itself, since continuous columns already transmit sound vibrations alongside the connections. *Fire safety*, however, is largely benefitted by internal fasteners and connection parts.

Governing loading actions to a typical connection, a proposal of the connection to start structural analysis in the ULS and possible assembly guidelines are presented in Table 7.15.

Table 7.15; Connection design type 6

Key words for design:		Assembly efficiency, repetition, prefabrication, fire safety	
Load on connection	Loading combination	Load [kN] ²⁵	Location
Vertical shear force; $V_{y,d}$	ULS-STR-5	117	Typical 9 meter beam
Axial compressive force; $N_{c,d}$	ULS-STR-7	160	Top outrigger beam
Axial tensile force; $N_{t,d}$	ULS-STR-7	75	Bottom outrigger beam

²⁵ Axial forces are obtained from the static STAAD Pro model with imposed floor loading on the leeward side of the building. These are slightly higher values in comparison to Table 5.9



Assembly sequence

1. Erection of glulam column with prefabricated connection steel component
 2. Fastening of glulam beams by steel dowels
-

As shown in the 3D image of the table above two types of connectors are designed for fastening to the column. Nails on the topside of the connection should transfer vertical shear forces from the beams to the column and the group of timber screws should resist axial tensile forces predominantly resulting from lateral wind loading on the façade. Moreover, steel dowels should also be able to transfer compressive forces from the glulam beam to the column. It can be seen that a fully hinged connection is approached by designing a minimum number of dowels, all positioned at the bottom side of the beam. Vertical shear is directly transferred by the steel component to the nails, since the designed connection provides a bearing plate at the bottom of the beam.

Strength equations for characteristic load-carrying capacity of steel-to-timber connections with nails depend on the thickness of steel plates. Thin plates are defined as less or equal to $0.5d$ and thick plates comprises a thickness of d or greater. A 5 millimetres thick steel plate is classified as a thick plate for which strength equations in equation 8.10 of EC5 applies. The embedment strength for nails is given by

$$f_{h,k} = 0.082 \rho_k d^{-0.3} \quad (7.22)$$

Characteristic yield moment of nails is expressed by equation 7.4. The withdrawal capacity of smooth nails is the minimum value of

$$F_{ax,Rk,a} = f_{ax,k} dt_{pen} \quad F_{ax,Rk,b} = f_{ax,k} dt + f_{head,k} d_h^2 \quad (7.23)$$

where the characteristic pointside withdrawal strength is as follows

$$f_{ax,k} = 20 \cdot 10^{-6} \rho_k^2 \quad (7.24)$$

and d is the diameter of the nail, which is taken as 4 millimetres. The penetration depth, t_{pen} , is assumed as 45 millimetres, whilst the thickness of the headside member, t , is 1 millimetre. The characteristic headside pull-through strength is given by

$$f_{head,k} = 70 \cdot 10^{-6} \rho_k^2 \quad (7.25)$$

and d_h represents the nail head diameter, which is equal to 6 millimetres.

Table 7.16 presents the embedment strength and characteristic strength equations for nail fasteners in the connection.

Table 7.16; Determination of embedment strength and characteristic strength equations

Material properties	$f_{u,k}$ [MPa.]	$M_{y,Rk}$ [Nmm]
Nails, Ø4 - 50 mm	800	8 822
<i>Equation 7.22 – 7.25</i>		
Embedment strength (parallel to grain); $f_{h,k}$	22.18	MPa.
Characteristic pointside withdrawal strength; $f_{ax,k}$	3.36	MPa.
Characteristic headside pull-through strength; $f_{head,k}$	11.77	MPa.
Characteristic withdrawal capacity; $F_{ax,Rk,a}$	0.61	kN
Characteristic withdrawal capacity; $F_{ax,Rk,b}$	0.44	kN
<i>Strength equations (equation 8.10 EC5)</i>		<i>Value [kN]</i>
$F_{v,Rk,c} = f_{h,k} t_1 d$		3.99
$F_{v,Rk,d} = f_{h,k} t_1 d \left[\sqrt{2 + \frac{4M_{y,Rk}}{f_{h,k} d t_1^2} - 1} \right] + \frac{F_{ax,Rk}}{4}$		2.03
$F_{v,Rk,e} = 2.3 \sqrt{M_{y,Rk} f_{h,k} d} + \frac{F_{ax,Rk}}{4}$		2.14

Strength equations show that the lowest value is found for failure mode d , which is related to development of one plastic hinge in the fastener.

The design value for the load-carrying capacity can be evaluated by a modification factor, k_{mod} , of 0.8 (Service Class 1), which refers to imposed loading as the shortest load duration for vertical shear actions on the connection, so that

$$F_{v,Rd} = 0.8 \frac{2.03}{1.3} = 1.41 \text{ kN}$$

is the load-carrying capacity for a single nail. The number of required nails results in

$$n = \frac{V_{y,d}}{F_{v,Rd}} = \frac{117}{1.41} = 83 \text{ nails} \rightarrow \text{Ø4 - 50 mm}$$

Edge- and end distances as well as spacings are given by Table 8.2 in EC5 and taken into account in the connection design as eventually shown in Figure 7.15. Nail spacings for steel-to-timber connections shall be multiplied by 0.7 in accordance with Clause 8.3.1.4(1) of EC5. The reason for this is that splitting of the thinnest component, which is the steel plate, is circumvented and therefore less spacing between fasteners can be applied.

The withdrawal capacity of timber screws is expressed by equation 7.15 and 7.16, where the effective number of screws, n_{ef} , is given by $n^{0.9}$ (Clause 8.7.2(8) EC5).

The result of the characteristic withdrawal capacity is shown in Table 7.17.

Table 7.17; Characteristic withdrawal capacity of timber screws

Material properties	$f_{u,k}$ [MPa.]	
Timber screws, $\varnothing 10 - 160$ mm	800	
<i>Characteristic withdrawal capacity</i>		
Penetration length; ℓ_{ef}	155	mm
Characteristic withdrawal strength; $f_{ax,k}$	12.22	MPa.
Characteristic withdrawal capacity; $F_{ax,90,Rk}$	18.22	kN

The presented withdrawal capacity applies to a single screw, for which the 'group effect' represented by $n^{0.9}$ is not yet taken into account. The design value is determined by a modification factor, k_{mod} , of 0.9, since the axial tensile force in a beam is caused by lateral wind loading. Hence for a single fastener

$$F_{ax,90,Rd} = 0.9 \frac{18.22}{1.3} = 12.61 \text{ kN}$$

The number of required screws, including incorporation of the 'group effect', becomes

$$n = \frac{N_{t,d}}{F_{ax,90,Rd}} = \frac{75}{12.61} = 8 \text{ screws} \quad (8^{0.9} = 6.5 \rightarrow F_{ax,90,Rd} = 81.94 \text{ kN})$$

Final part to design in the connection is the steel dowels, which are subjected to stresses in axial direction of the beam. The presence of two slotted-in steel plates results in a load-carrying capacity of the sum of two steel plates. Strength equations are previously adopted for connection type 1, which also comprises two slotted-in steel plates. The connection resembles three failure modes, which – as for any type of connection – consist of; wood crushing, development of one plastic hinge in the fastener and two plastic hinges. The governing failure mode is a dependant on the embedment strength of the timber, slenderness of the dowel and positions of the steel plates.

Thickness of steel plates is of 8 millimetres, whilst dowel's diameter is $\varnothing 12$ millimetres. As a starting point, steel plates are positioned 100 millimetres from the outer surface ($=t_1$), thus the distance between the plates is 184 millimetres ($400-200-16$) (t_2). In analogy with two internal plates designed in the CLT walls, the outer shear plane (1) has three possible failure modes while for the inner shear plane (2) two modes are possible to occur.

Table 7.18 shows the results of strength equations for shear plane 1 and 2 for one internal steel plate.

Table 7.18; Embedment strength and strength equations for steel dowels; shear plane 1

Material properties	$f_{u,k}$ [MPa.]	$M_{y,Rk}$ [Nmm]
Steel dowels, $\varnothing 12$ mm	800	153 491
<i>Equation 7.1</i>		
Embedment strength (parallel to grain); $f_{h,k}$	29.59	MPa.
<i>Strength equations</i>		
$F_{v,Rk,1} = f_{h,k} dt_1$		Value [kN]
		35.51

$$F_{v,Rk,2} = f_{h,k} d \frac{t_2}{2} \quad 32.67$$

$$F_{v,Rk,3} = f_{h,k} t_1 d \left[\sqrt{2 + \frac{4M_{y,Rk}}{f_{h,k} dt_1^2}} - 1 \right] \quad 16.83$$

$$F_{v,Rk,4} = \sqrt{4M_{y,Rk} f_{h,k} d} \quad 14.77$$

Failure mode 4, i.e. two plastic hinges in the fastener, represents the governing mode for shear plane 1. Shear plane 2 has also a load-carrying capacity determined by two plastic hinges. The distance to the second hinge in the timber can be evaluated by equation 7.6 as follows

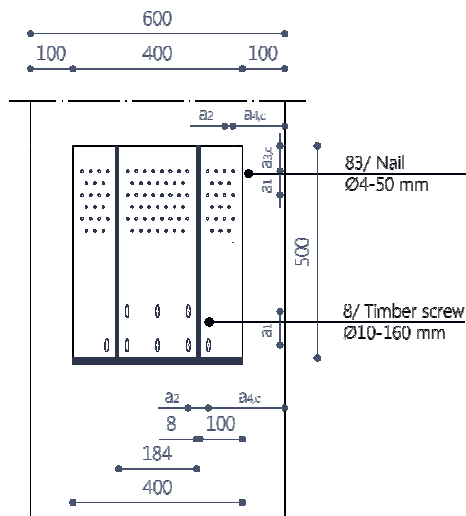
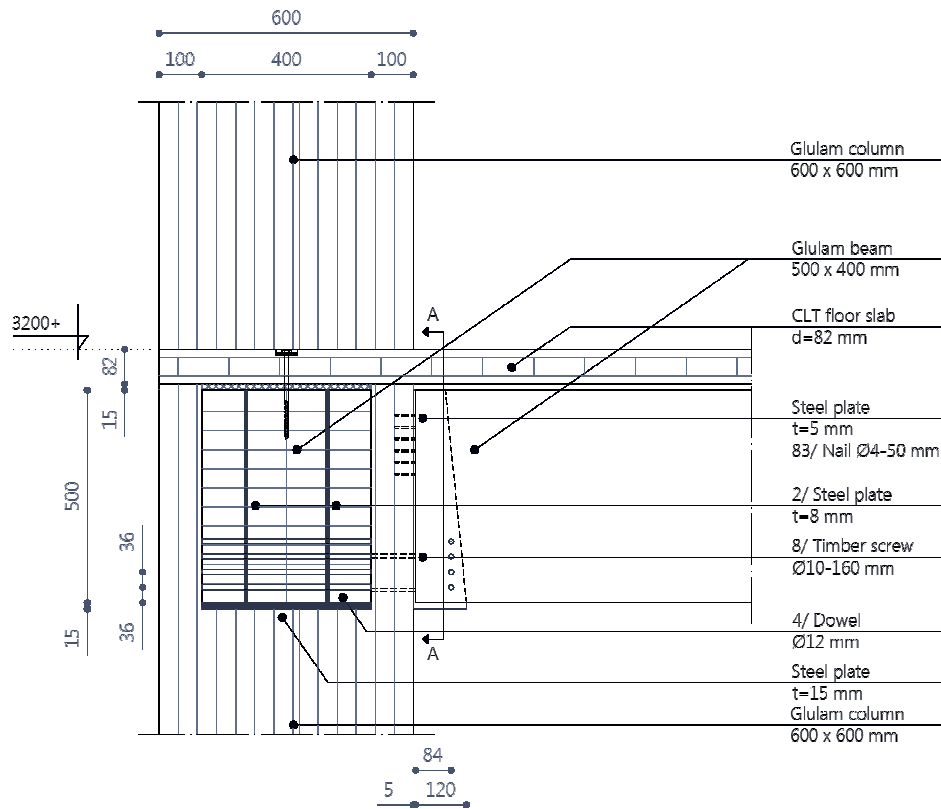
$$y = \sqrt{\frac{4M_y}{f_{h,k} d}} = \sqrt{\frac{4 \cdot 153\,491}{29.59 \cdot 12}} = 41.58 \text{ mm}$$

It may be apparent that there is no beneficial effect for the load carrying capacity of shear plane 1 to move the steel plates more to the centre of the cross section, since two plastic hinges already occur on the outer side of the steel plates. Therefore, the design load carrying capacity of one dowel and two steel plates yields

$$F_{v,Rd} = 0.9 \frac{2(14.77 \cdot 2)}{1.3} = 40.90 \text{ kN}$$

In order to resist a tensile force in the beam of 75 kN two dowels should be designed, whilst compression in the beam requires 4 dowels to transfer the forces to the column.

End- and edge distances as well as spacing between the two dowels are given in table 8.5 of EC5, subsequently adopted in the final design of the connection design shown in Figure 7.16.



A - A

Nails	Screws
a1 = 56 mm	a1 = 60 mm
a2 = 20 mm	a2 = 48 mm
a3,c = 60 mm	a4,c = 180 mm
a4,c = 122 mm	

Figure 7.16; Connection type 6

7. Column-column connection

Joints between two glulam columns should be able to transfer a certain amount of tensile forces as well as lateral shear forces. For this type of connection similar requirements applies as defined for connection type 5 with regard to *aesthetical-*, *fire safety-* and *functional* aspects. *Assembly on-site*

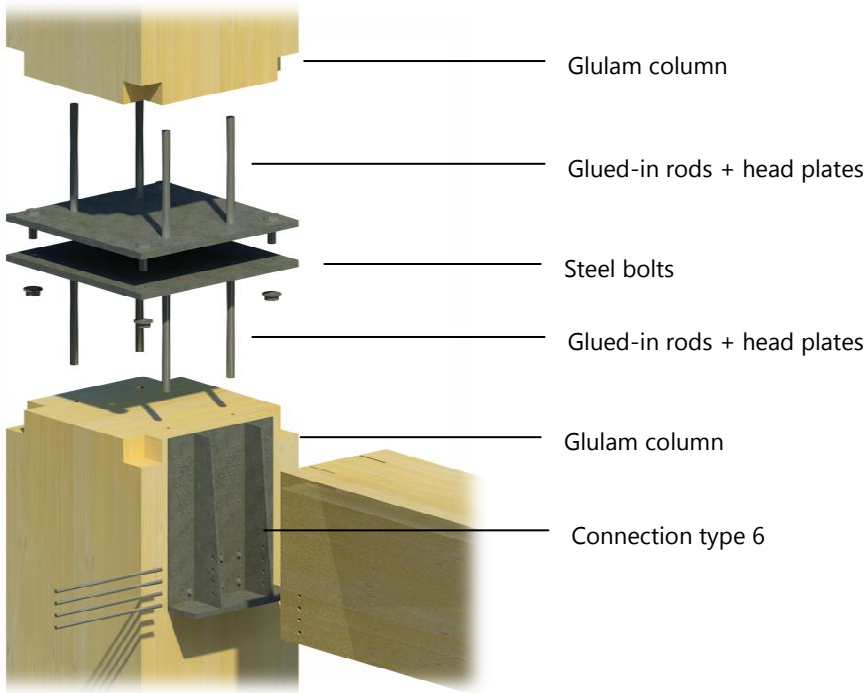
however, is more important to optimise since the connection appears over multiple floors in the building. At previous connection types, it has been stated that erection processes are improved with a high degree of prefabrication and simple fasteners such as steel bolts.

It may be obvious that dowel type connections, like slotted-in steel plates do not fulfil aesthetical requirements since dowel's ends will appear at the member's surface. Glued-in rods, on the other hand, do meet these demands and are also able to transfer tensile forces to a certain degree.

A proposal for connection type 7 is presented in Table 7.19, where also subjecting forces to the connection are given.

Table 7.19; Connection design type 7

<i>Key words for design:</i>	<i>Functionality, fire safety aspects, aesthetics, assembly processes</i>	
<i>Load on connection</i>	<i>Loading combination</i>	<i>Load [kN]</i>
Axial tensile force; $N_{t,d}$	ULS-EQU-2	276
Lateral shear force; $V_{y,d}$	ULS-STR-7V	40



Assembly sequence

1. Erection of column with prefabricated glued-in rods and head plate
2. Fastening of upper column by steel bolts

Static equilibrium loading combinations (EQU) are used to obtain maximum tensile forces in columns (276 kN), since this type of force is induced by the outriggers for which this connection carries for stabilisation of the whole structure. The governing force appears just below the outriggers on the windward side of the building.

The lateral load-carrying capacity of a single glued-in rod with a diameter of Ø24 millimetres was determined as 11.94 kN at connection type 5. With a design shear force of 40 kN it becomes apparent that four glued-in rods satisfies the maximum subjecting shear force in connection type 7.

The fastener's capacity to resist axial forces depends on a large extent on the strength and durability of the glue line [32]. The type of glue affects the behaviour of the joint, for which polyurethane adhesives show ductile behaviour under axial loading and epoxy and phenol-resorcinol adhesives resemble rather brittle joint behaviour.

Riberholt [32] proposes the following strength formula for the characteristic load-carrying capacity of glued-in rods loaded in axial direction

$$F_{ax,Rk} = f_{ws} \rho_k d \sqrt{\ell_g} \quad (7.26)$$

where f_{ws} is equal to 0.65 for polyurethane adhesives and 0.52 for epoxy or phenol-resorcinol adhesives and ℓ_g represents the internal length of the steel rod in [mm]. Equation 7.26 applies to internal rod lengths of at least ($\ell_g \geq$) 200 millimetres.

For connection type 7 a polyurethane adhesive is assumed since this will both give a higher load-carrying capacity and a more ductile connection. The characteristic load-carrying capacity for a single fastener with a diameter of $\varnothing 24$ millimetres yields

$$F_{ax,Rk} = 0.65 \cdot 410 \cdot 24 \cdot \sqrt{450} \cdot 10^{-3} = 135.68 \text{ kN}$$

Design value of the characteristic load-carrying capacity for a single fastener results in

$$F_{v,Rd} = 0.9 \frac{135.68}{1.3} = 93.93 \text{ kN}$$

The number of required steel rods becomes

$$n = \frac{N_{t,d}}{F_{ax,Rd}} = \frac{276}{93.93} = 2.94 \rightarrow 4 \text{ steel rods } \varnothing 24 \text{ mm}$$

Designed steel rods of connection type 5 fulfils tensile forces higher up in the structure, hence these fasteners remain unchanged.

Besides the load-carrying capacity of the steel rods, it should be verified that arising stresses in the effective area of material behind the fasteners do not exceed permissible tensile stresses. The effective area, A_{wr} , for each fastener can be determined [34] by taking a square with length equal to the shortest distance from the rod to the edge of the material, as illustrated in Figure 7.17.

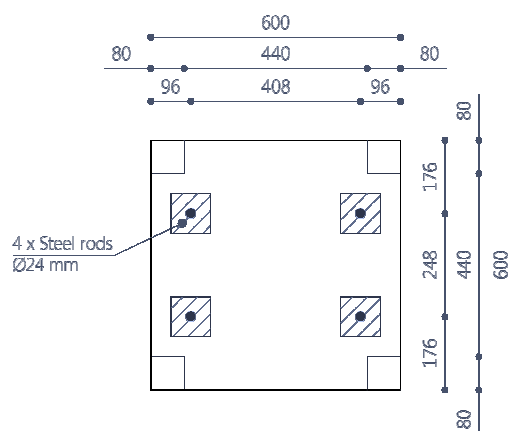


Figure 7.17; Effective area of wood for resisting tensile forces in the rod

The effective area, A_w for each fastener becomes

$$A_w = 96 \times 96 = 9\,216 \text{ mm}^2$$

Tensile stresses can be simply evaluated by dividing the maximum axial force per fastener to the effective area A_w as follows

$$\sigma_{t,0,d} = \frac{N_{t,d}/4}{A_w} \cdot 10^3 = 7.49 \text{ MPa} < f_{t,0,g,d} (=14.04 \text{ MPa.})$$

It can be concluded that the designed connection complies with strength requirements in the ULS. Detailed drawing of the connection is depicted in Figure 7.18.

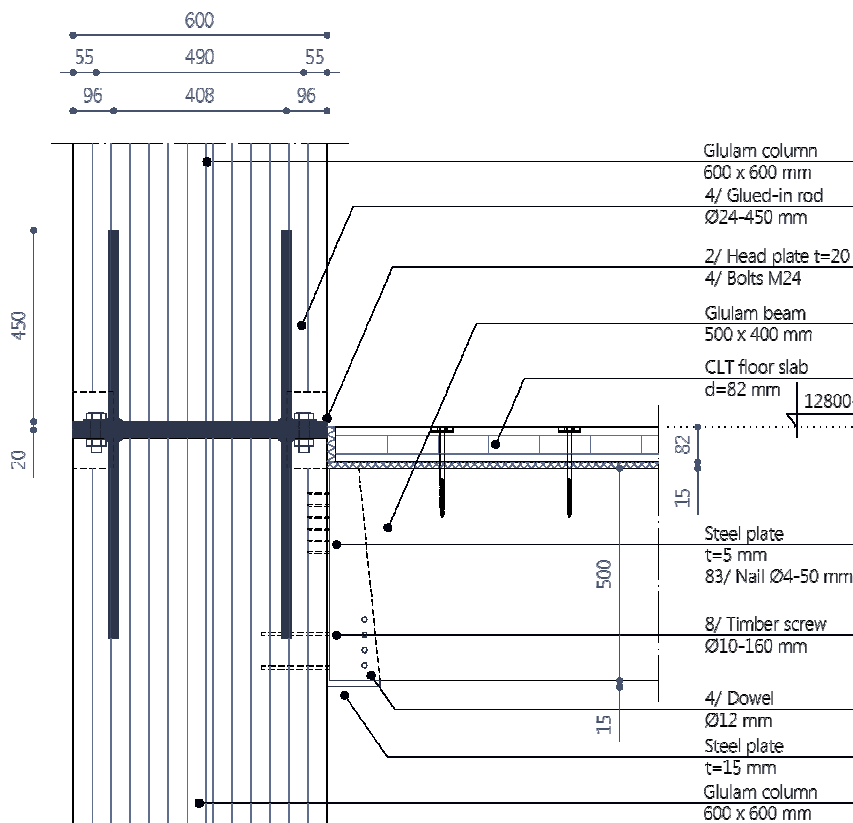


Figure 7.18; Connection type 7

8. CLT wall-beam connection

The designed connection for column-beam joints is also applicable for the other end of a 9 meter beam, which meets CLT core walls. The load-carrying capacity of the connection differs with regard to the fasteners; nails and timber screws. Further, it depends on the surface behind the connection, e.g. to the plane of the elements or edge side, as been shown at connection type 3 where the embedment strength of fasteners was a dependant on the penetration direction.

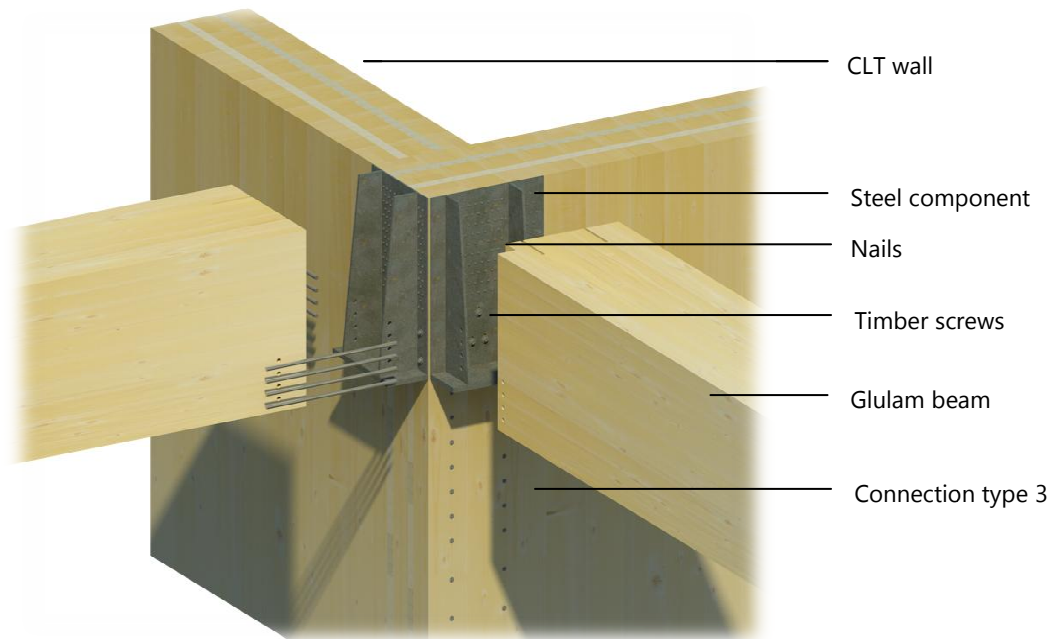
Governing forces in the joint are similar to connection type 6, hence a vertical shear force, $V_{y,d}$, of 117 kN and an axial tensile force, $N_{t,d}$, of 75 kN applies.

Requirements in the field of *assembly processes*, *prefabrication* and *fire safety* do not differ from the other beam's end joint.

A proposed design for connection type 8 is resembled in Table 7.20.

Table 7.20; Connection design type 8

<i>Key words for design:</i>	<i>Assembly efficiency, repetition, prefabrication, fire safety</i>	
<i>Load on connection</i>	<i>Loading combination</i>	<i>Load [kN]</i>
Vertical shear force; $V_{y,d}$	ULS-STR-5	117
Axial tensile force; $N_{t,d}$	ULS-STR-7	75



Assembly sequence

1. Erection of CLT core with prefabricated connection steel component
2. Fastening of glulam beams by steel dowels

Design 8a: connection to the plane of CLT wall

Due to a thickness of 80 millimetres of the CLT panel's outer layers nails in the connection do not penetrate cross layers, hence embedment strength parallel to the grain of the timber can be adopted. On the other hand the 160 millimetres long timber screws reach the middle layer of the panel and therefore equivalent withdrawal capacity, proposed by Uibel and Blass [30] should be taken into account. One might assume that nail design can remain unmodified with respect to connection type 6, i.e. nails penetrated in columns parallel to the grain. Nonetheless, butt joints between individual boards should be taken into for the load-carrying capacity. Figure 7.19 shows an elevation of the connection fastened to a panel's surface (without timber screws), where it can be seen that at least three rows of nails should be assumed not contributing to the load-carrying capacity of the connection. Therefore an additional 13 nails are designed.

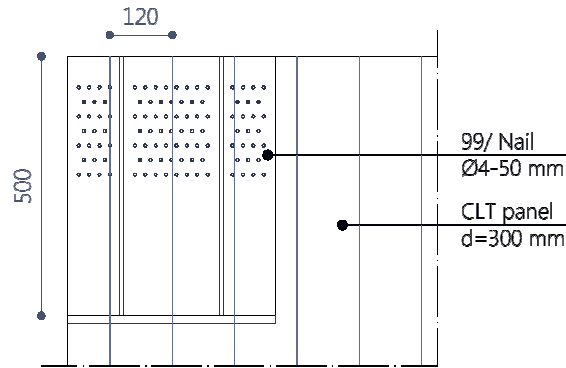


Figure 7.19; Elevation of connection type 8a

Withdrawal capacity of timber screws in CLT panels was determined before at connection type 3 in equation 7.12. For timber screws with a diameter of Ø10 millimetres and a penetration length of 155 millimetres the characteristic withdrawal capacity per fastener becomes

$$F_{ax,90,Rk} = \frac{0.35 \cdot 10^{0.8} \cdot 155^{0.9} \cdot 380^{0.75}}{1.5 \cos^2 90 + \sin^2 90} = 16.17 \text{ kN}$$

The design value of the withdrawal capacity, taking into account a k_{mod} factor of 0.9, results in

$$F_{ax,90,Rd} = 0.9 \frac{16.17}{1.3} = 11.19 \text{ kN}$$

The number of required screws, with incorporation of the 'group effect' which reduces the capacity of the connection in comparison with a single screw, will be

$$n = \frac{N_{t,d}}{F_{ax,90,Rd}} = \frac{75}{11.19} = 9 \text{ screws} \quad (9^{0.9} = 7.22 \rightarrow F_{ax,90,Rd} = 80.84 \text{ kN})$$

Design 8b: connection on CLT panel's edge

The load-carrying capacity of the nails is affected by the lower embedment strength when penetrating in the panel's edge. The embedment strength can be determined in accordance with equation 7.11, derived by Uibel and Blass [31].

Table 7.21 shows load-carrying capacity results for nails penetrated in the CLT panel's edge.

Table 7.21; Load-carrying capacity results of nails for connection design 8b

Material properties	$f_{u,k}$ [MPa.]	$M_{y,Rk}$ [Nmm]
Nails, Ø4 - 50 mm	800	8 822
<i>Characteristic withdrawal capacity, equation 7.12</i>		
Effective point side penetration length timber 2; ℓ_{ef}	45	mm
Angle between screw axis and grain direction timber 2; ε	0	°
Characteristic withdrawal capacity; $F_{ax,k,Rk}$	1.87	kN
<i>Equation 7.11</i>		
Embedment strength; $f_{h,pre}$	12.12	MPa.

Strength equations (equation 8.10 EC5)	Value [kN]
$F_{v,Rk,c} = f_{h,k} t_1 d$	2.18
$F_{v,Rk,d} = f_{h,k} t_1 d \left[\sqrt{2 + \frac{4M_{y,Rk}}{f_{h,k} d t_1^2}} - 1 \right] + \frac{F_{ax,Rk}}{4}$	1.64
$F_{v,Rk,e} = 2.3 \sqrt{M_{y,Rk} f_{h,k} d} + \frac{F_{ax,Rk}}{4}$	1.97

Failure mode *d*, i.e. one plastic hinge in the fastener, represents the governing load-carrying capacity, for which the design value for a nail in single shear is

$$F_{v,Rd} = 0.8 \frac{1.64}{1.3} = 1.00 \text{ kN}$$

where k_{mod} refers to imposed floor loading as the shortest loading duration (=0.8). The required number of nails becomes

$$n = \frac{V_{y,d}}{F_{v,Rd}} = \frac{117}{1.00} = 117 \text{ nails} \rightarrow \text{Ø4 - 50 mm}$$

The withdrawal capacity of timber screws penetrated in the panel's edge can be calculated according to equation 7.12 likewise. Characteristic value for a single timber screw will be

$$F_{ax,0,Rk} = \frac{0.35 \cdot 10^{0.8} \cdot 155^{0.9} \cdot 380^{0.75}}{1.5 \cos^2 0 + \sin^2 0} = 11.86 \text{ kN}$$

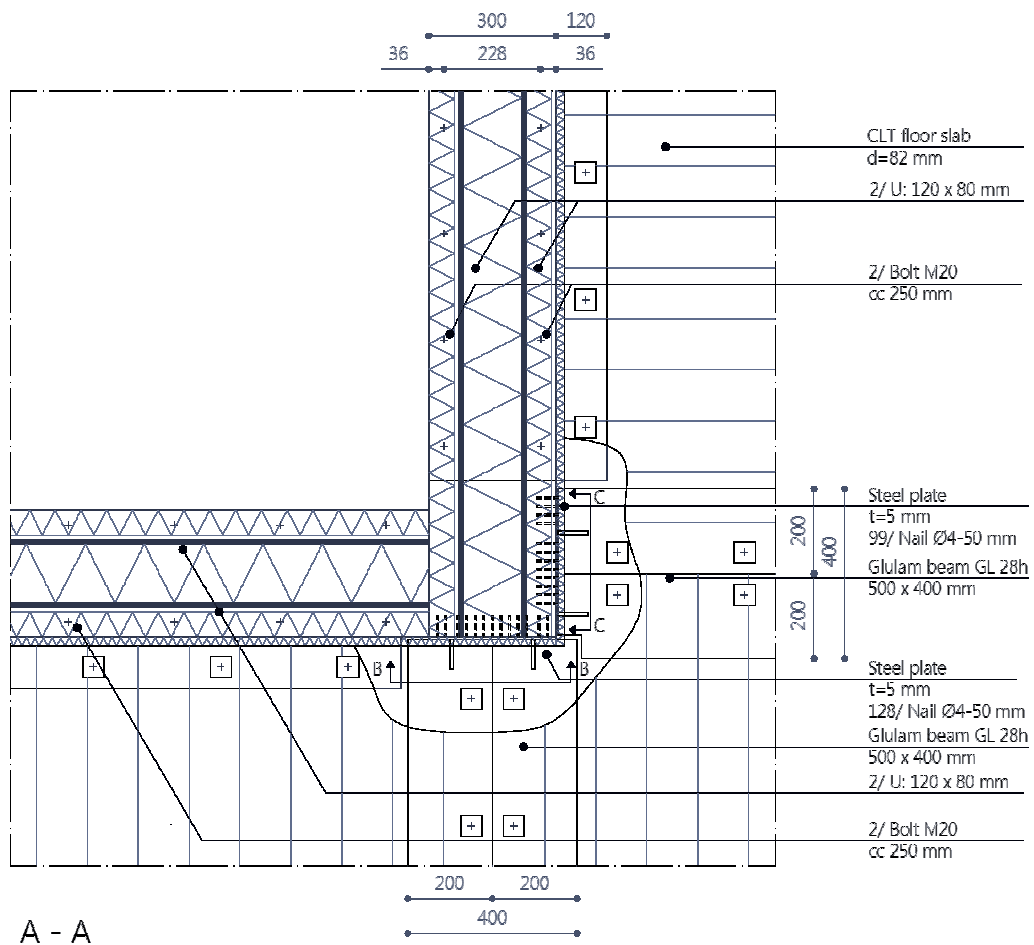
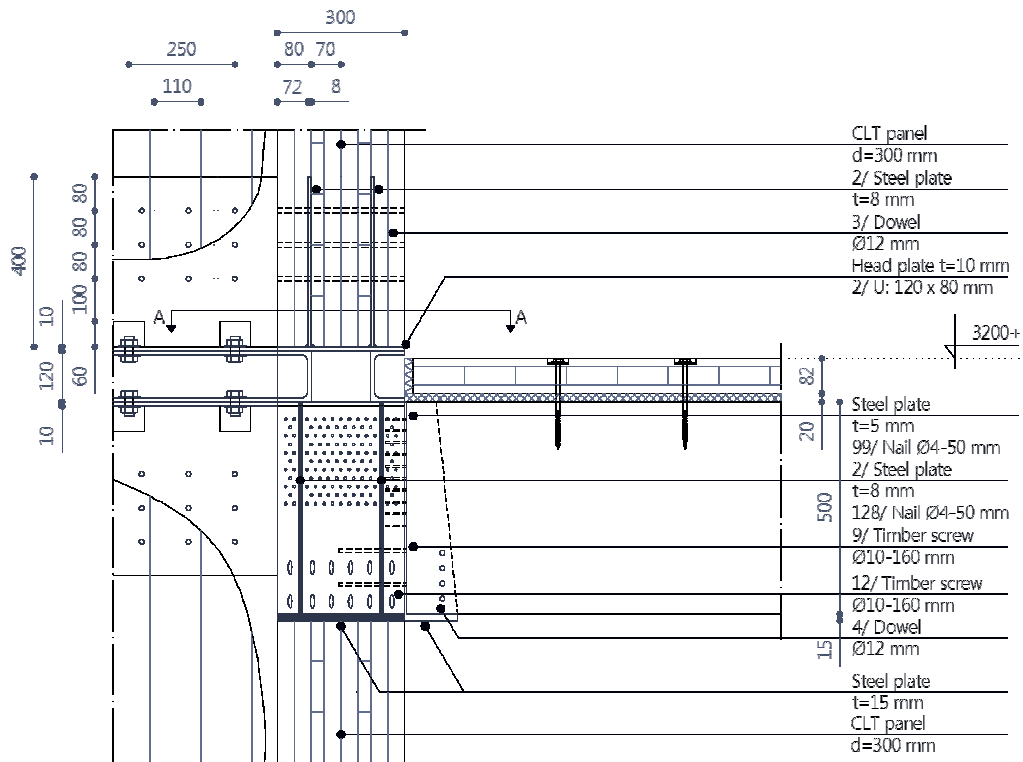
The design value for axial loading due to wind actions is equal to

$$F_{ax,90,Rd} = 0.9 \frac{11.86}{1.3} = 8.21 \text{ kN}$$

Further, the number of required screws for connection type *8b* in order to resist an axial tensile force of 75 kN is

$$n = \frac{N_{t,d}}{F_{ax,0,Rd}} = \frac{75}{8.21} = 12 \text{ screws} \left(12^{0.9} = 9.36 \rightarrow F_{ax,90,Rd} = 76.84 \text{ kN} \right)$$

For prefabrication purposes the surface area for nails and screws on the material behind is limited due to a panel's thickness of 300 millimetres. For the beam in cross direction, which is fastened to the panel's surface a limited area is suitable to position both fasteners in a single CLT wall element, as shown in the final connection design details of Figure 7.20.



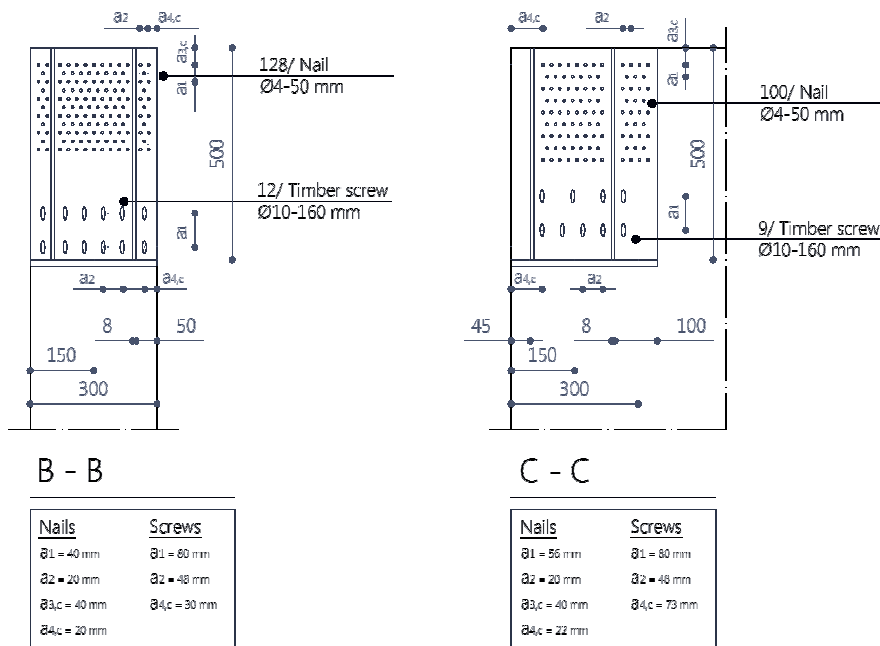


Figure 7.20; Connection detail 8

7.5 GLULAM OUTRIGGER CONNECTIONS

In the introduction of this chapter it has been stated that maintenance of the outrigger's integrity (relative deformations) under lateral wind actions is of utmost importance to ensure appropriate structural performance of the whole stability system. With regard to joint rigidity, pinned connections are preferable to circumvent undesirable additional moments and forces in structural elements. However, the outrigger's geometry shows (Figure 7.21) to be complicated to aim for pure hinged connections between structural elements. Both the angle and dimensions of structural elements carries for joints of large volume of timber and in order to design for strength relatively large connection components may be required.

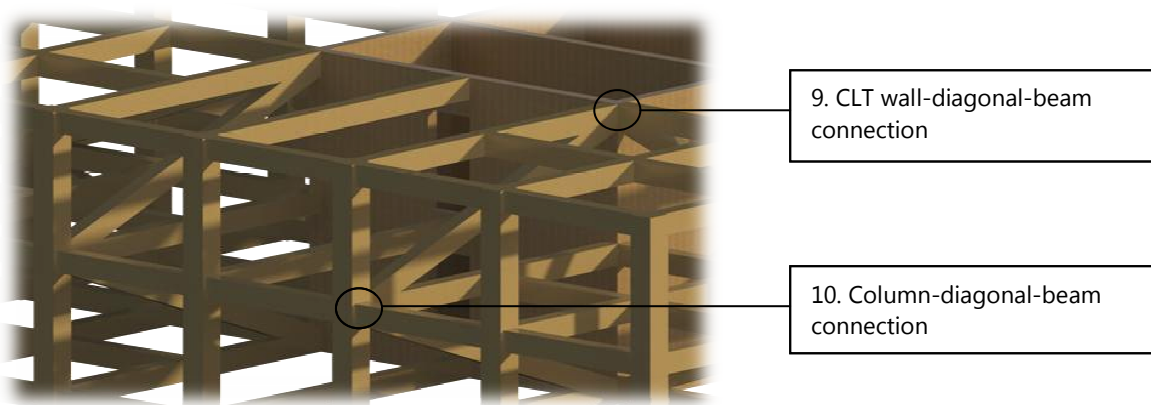


Figure 7.21; Glulam outrigger connections

Force distributions in outrigger members are influenced by the restraining moment, M_r , induced by the peripheral columns. The outriggers form a horizontal truss with a height over two storeys, as depicted in Figure 7.22 (see Appendix E.1 for outcomes of STAAD Pro). The lower column connected to diagonals on the windward side of the building is subjected to tensile forces and therefore compression arises in the lower diagonal and tension in the upper diagonal. Obviously, the leeward side of the building comprises compression in peripheral columns only, hence opposite types of forces

appear in diagonals. Forces indicated in Figure 7.22, due to loading combination *ULS-STR-7*, are values for the outrigger parallel to grid C, which is subjected to slightly higher forces in comparison to outrigger on grid E.

9. CLT wall-diagonal-beam connection

The greatest challenge in this type of connection is to transfer forces from the diagonal to the CLT core wall. As shown in Figure 7.22 the largest axial force is located in the lower diagonal. The axial force in the beam, however, is lower (53 kN) than the upper beam (160 kN).

The difference between these axial forces is due to the direction of axial forces in the diagonals. The *upper* diagonal initiates a compressive force in the *upper* beam in the direction of the facade, while on the other side of the beam compression is introduced due to wind loading.

In the contrary to these actions, the *lower* beam is subjected to a tensile force by the *lower* diagonal and a compressive force on the other side by wind loading, where the latter is compensating the tensile force. Therefore the axial force in the lower beam is lower than the compressive forces – which act in opposite directions – of the upper beam.

Due to the larger axial force in the beam, an upper joint, as indicated in Figure 7.22, will be implemented for connection design.

Functionality is the primary keyword for the connection, since structural performance on both strength- and stiffness criteria are defined before as most important objective. As stated for previous connection types, the efficiency of dowel-type connections in transferring forces between structural elements as well as the favourable *fire safety* when designing slotted-in steel plates is highly beneficial for this connection.

Requirements on *assembly processes* on the construction site are less important, since outriggers are only designed on a single floor, i.e. 12th floor. Nevertheless, large connections due to relatively high forces and the geometry of structural elements may affect erection on-site. As a consequence, *prefabrication* of structural members with (parts of) the connection is required.

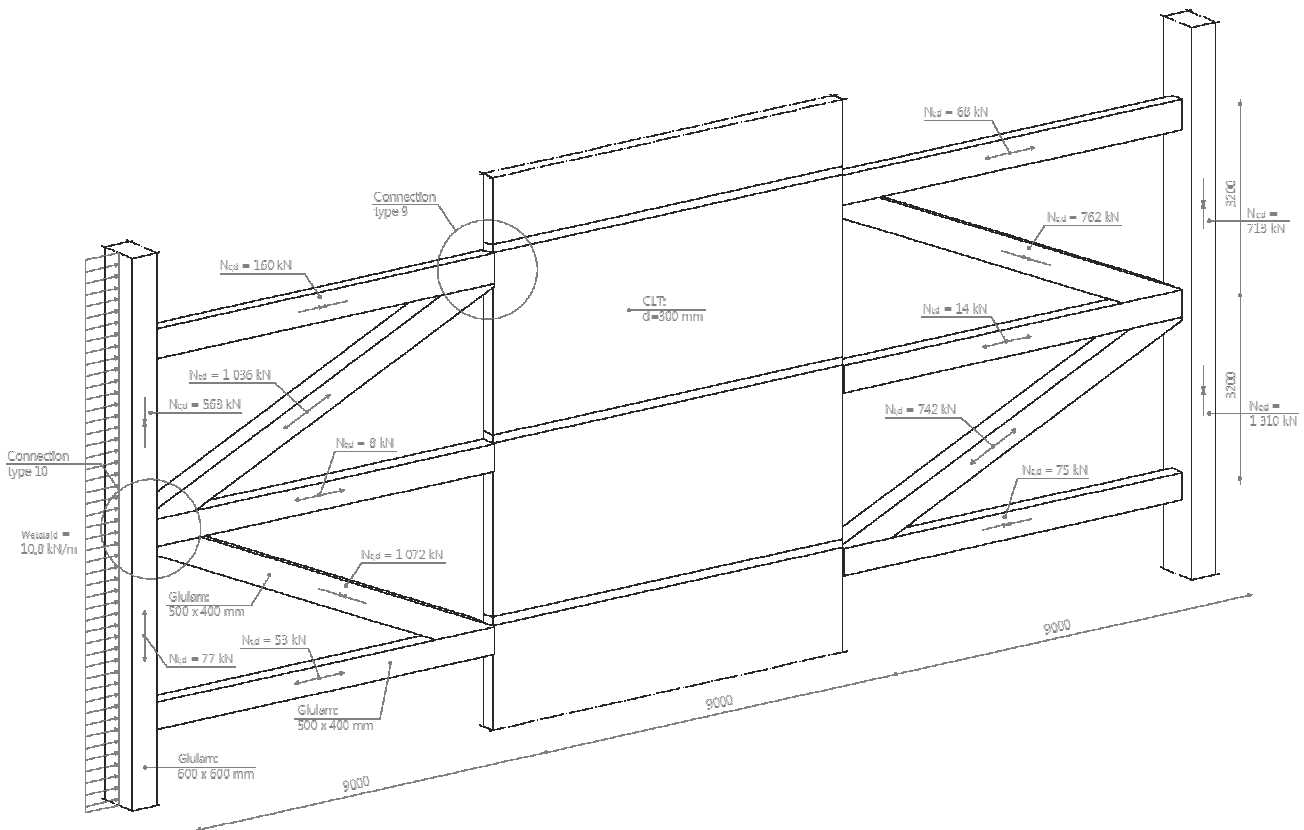
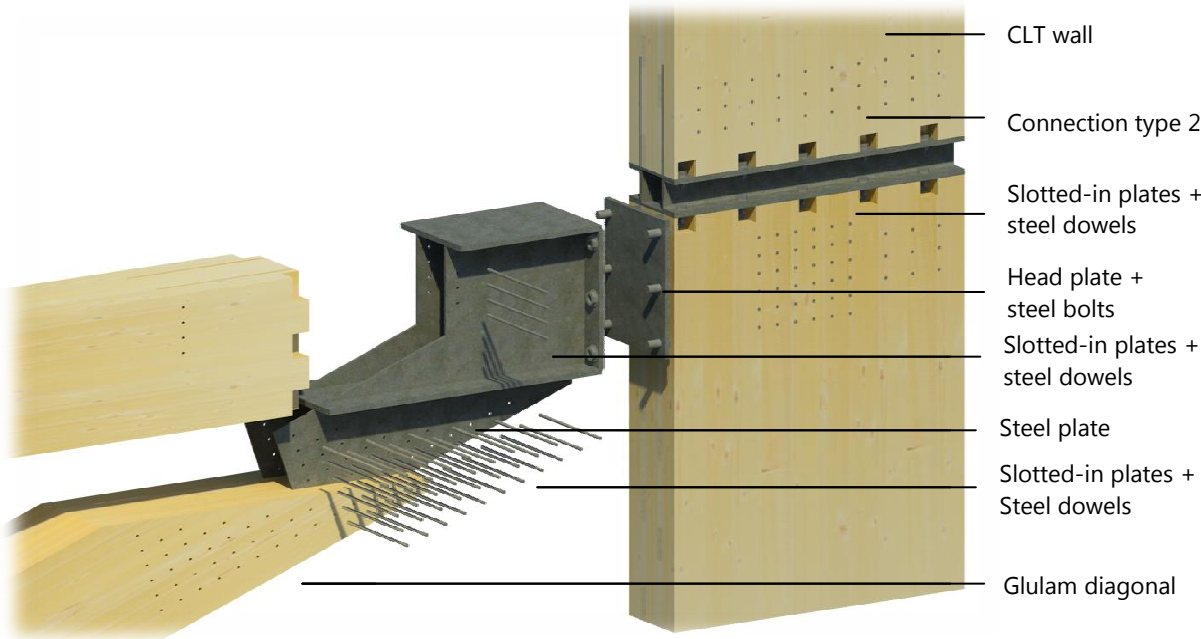


Figure 7.22; Forces in outrigger on grid C by loading combination *ULS-STR-7*

The adoption of above starting points resulted in a preliminary design of connection type 9, as depicted in Table 7.22.

Table 7.22; Connection design type 9

<i>Key words for design:</i>	<i>Functionality, fire safety, prefabrication</i>
<i>Load on connection by ULS-STR-7</i>	<i>Load [kN]</i>
Axial tensile force diagonal; $N_{t,d}$	1 036
Axial compressive force beam; $N_{c,d}$	160
Vertical shear force; $V_{y,d}$	77



Assembly sequence

1. Erection of CLT core wall with prefabricated connection steel component
2. Fastening of glulam beam and diagonal by steel bolts, where the diagonal is prefabricated with the beam as a single element off-site

Although head plates bolted together between the CLT wall and glulam members reduces the fire resistance of the connection, it simplifies the assembly process, since no steel dowels have to be fastened on-site. The dowels in the connection are loaded differently, depending on the connected structural element. Figure 7.23 resembles for each structural element how the dowels are loaded. Intersection of neutral lines of structural elements is located in the CLT wall on 150 millimetres from the wall's edge.

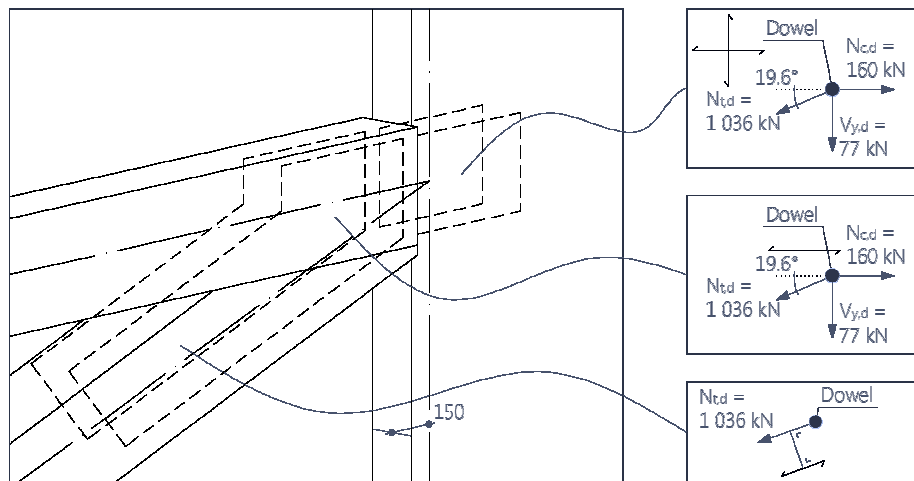


Figure 7.23; Loading on steel dowels in connection type 9

Dowels in the diagonal are loaded parallel to the grain by a tensile force of 1 036 kN. Since dimensions of the diagonal and beam are equal, and therefore both the build-up of slotted-in steel plates and embedment strength, results of connection type 6 can be used. The load-carrying capacity per steel dowel with a diameter of Ø12 millimetres was evaluated on

$$F_{v,Rd} = 40.90 \text{ kN}$$

Load-carrying capacity of multiple dowels in a row loaded parallel to the grain should be calculated by taking into account an effective number of fasteners, i.e. equation 7.9. An iterative procedure is needed to determine the number of dowels, since each row has a different number of dowels. A number of 42 dowels are designed; both in order to resist a tensile force of 1 036 kN and for a practical design with edge- and end distances as well as spacings.

Connections with a loaded end and a force component parallel to the grain may comprise a reduced load-carrying capacity due to failure along the perimeter of the fastener area, so-called *block shear failure* and *plug shear failure*. The former failure mode consists of exceedance of timber's tensile stresses along the most distant fasteners in crosswise direction, while the latter failure mode comprises exceedance of permissible shear stresses in the member's sectional area along outer fastener rows in parallel direction of the timber. Governing failure mode and pertaining load-carrying capacity can be determined according to Annex A in EC5. For a number of 42 dowels near the end of a diagonal member the design load-carrying capacity is 1 264 kN (see C.S.6.2 in Appendix E.1), which is above design actions in the outrigger diagonals as depicted in Figure 7.22.

Axial forces in the diagonal induce a vertical force resultant in the beam, which results in tension perpendicular to the grain around the dowels. To control this unfavourable occurrence steel plates on topside as well as underside of the beam are welded to both slotted-in plates and the head plate, so that a stiff steel component arises in vertical direction. In order to prevent local buckling of the slotted-in steel plates of the beam the thickness of these plates will be increased to 15 millimetres. Consequently vertical shear forces in the beam are directly transferred through the head plate to the bolts, circumventing splitting possibilities around dowels in the glulam beam. However, connectors in the beam are required to transfer an axial force, $N_{c,d}$, of 160 kN to the CLT core wall. Since this load acts parallel to the grain the load-carrying capacity, $F_{v,Rd}$, is 40.90 kN per dowel. Designing these in a single vertical row, 4 dowels are sufficient to resist the axial force. Thicker internal steel plates, as mentioned above, will not affect the load carrying capacity of the connection, since

failure mode 4 (see Table 7.18) comprises two plastic hinges and is not influenced by thickness of the timber.

Steel bolts connecting the head plates together are loaded by a resultant force from actions illustrated in Figure 7.23, which are; an axial force in the diagonal and an axial- and shear force in the beam. Consequently, this resultant force has a horizontal- and a vertical component subjecting the steel bolts in tension and shear respectively. Figure 7.24 shows the acting forces on the steel bolts.

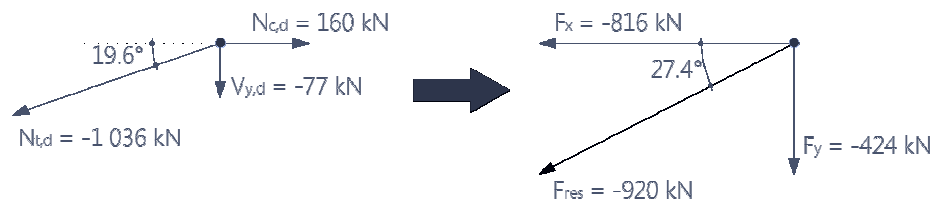


Figure 7.24; a) Force components in glulam members b) Resultant force and horizontal- and vertical component

In order to comply with a combination of tension- and shear forces in the head plate 6 bolts M30 are required (see elaboration C.S.6.3 in Appendix E.1).

Another head plate is welded to slotted-in plates inside the CLT core wall element, so that similar actions are present in the walls as illustrated in Figure 7.24. The resultant force causes stresses around dowels under an angle to grain directions of the different layers of the CLT panel. In analogy with calculations for load-carrying capacity in lateral direction of connection type 1 a distinction shall be made between shear plane 1 (outer shear plane) and shear plane 2 (inner shear plane) to account for the different build-up of board layers.

Failure modes in shear plane 1 possible to occur are; wood crushing (1), one plastic hinge in the dowel (3) and two plastic hinges (4). Due to acting of the resultant force under an angle with vertical layers, for which α equals 62.6 degrees, embedment strength of the timber should be evaluated by equation 7.2.

Positions of slotted-in steel plates remain in the cross layer, so that distance t_1 is 80 millimetres. Load-carrying capacity calculations for dowels in shear plane 1 of the CLT wall element are presented in Table 7.23.

Table 7.23; Load-carrying capacity results of dowels in CLT wall for shear plane 1

Material properties	$f_{u,k}$ [MPa.]	$M_{y,Rk}$ [Nmm]
Steel dowels, $\varnothing 12$ mm	800	153 491
<i>Equation 7.1 – 7.2</i>		
Embedment strength ($\alpha=0^\circ$) ; $f_{h,0,k}$	27.42	MPa.
Embedment strength ($\alpha=62.6^\circ$) ; $f_{h,62.6,k}$	19.34	MPa.
<i>Strength equations</i>		<i>Value [kN]</i>
$F_{v,Rk,1} = f_{h,62.6,k} dt_1$		18.57
$F_{v,Rk,3} = f_{h,62.6,k} t_1 d \left[\sqrt{2 + \frac{4M_{y,Rk}}{f_{h,62.6,k} dt_1^2}} - 1 \right]$		10.28
$F_{v,Rk,4} = \sqrt{4M_{y,Rk} f_{h,62.6,k} d}$		11.94

The strength equations show that a single plastic hinge on the outer side of a steel plate is the governing failure mode for shear plane 1.

The load carrying capacity of shear plane 2 is either determined by failure mode 2, 4a or 4b, as depicted in Figure 7.6. Failure mode 2 consists of exceedance of the timber embedment strength, resulting in wood crushing, whilst mode 4a and 4b is a dependant on the location of the plastic hinge in the timber.

Failure mode 2 consists of wood crushing determined by embedment strengths $f_{h,1}$ and $f_{h,2}$ of the longitudinal layer and cross layer respectively, for which $f_{h,1}$ equals $f_{h,62.6,k}$ and $f_{h,2}$ is $f_{h,27.4,k}$ accordingly. Thickness of layers is for t_{21} equal to 22 millimetres and for t_{22} 40 millimetres as shown in Figure 7.25.

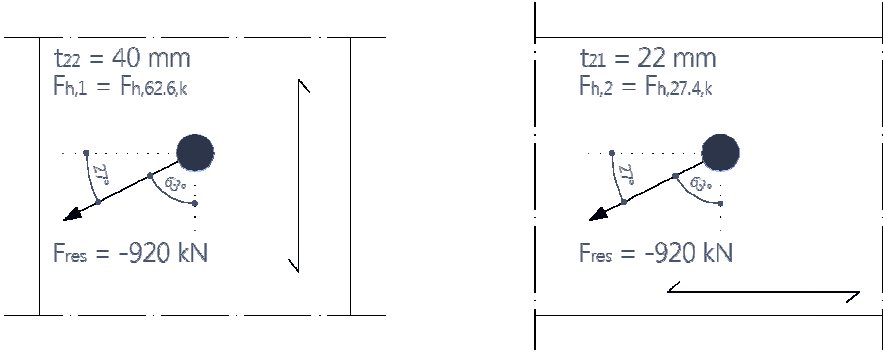


Figure 7.25; a) Resultant force on dowel in longitudinal layer b) Resultant force on dowel in cross layer

The plastic hinge of failure mode 4 may occur in the cross layer (4a) or longitudinal layer (4b). The location of the hinge can be determined by first assuming the hinge to develop in the cross layer (failure mode 4a, Figure 7.6), where equation 7.6 can be used to determine distance y_2 as follows

$$y_2 = \sqrt{\frac{4M_y}{f_{h,2}d}}$$

When $y_2 > t_{21}$, the plastic hinge will not occur in the cross layer, i.e. failure mode 4b will be governing, hence equation 7.7 leads to the distance of the plastic hinge.

Determination of the governing failure mode for the steel dowel in the middle part of the cross section and characteristic load carrying capacity is shown in Table 7.24.

Table 7.24; Strength equations of failure modes 2 and 4

Embedment strengths	Value [MPa.]	
Embedment strength longitudinal layer; $f_{h,1}$ ($=f_{h,62.6,k}$)	19.34	
Embedment strength cross layer; $f_{h,2}$ ($=f_{h,27.4,k}$)	24.65	
Failure mode 2	Value [kN]	
$F_{v,Rk,2} = (f_{h,1}t_{22}d) + (f_{h,2}t_{21}d)$	15.79	
Failure mode 4	Value	
Failure mode 4a, distance y_2 (equation 7.6)	45.56	$> t_{21}$ mm
Failure mode 4b, distance y_1 (equation 7.7)	28.13	$< t_{22}$ mm
$F_{v,Rk,4b} = (f_{h,2}t_{21}d) + (f_{h,1}y_1d)$	13.04	kN

In analogy with connection type 1 the plastic hinge is located in the longitudinal layer, where it can be seen that due to the slight difference between load carrying capacities of failure mode 2 and 4b, the design of steel plate locations as well as the dowels is relatively efficient.

One steel plate has a load carrying capacity determined by two plastic hinges on both shear planes, which results in a total connection capacity per fastener of

$$F_{v,Rk} = F_{v,Rk,3} + F_{v,Rk,4b} = 10.28 + 13.04 = 23.32 \text{ kN}$$

The design value per fastener and two steel plates, and incorporating wind actions as the shortest load duration, yields

$$F_{v,Rd} = 0.9 \frac{(2 \cdot 23.32)}{1.3} = 32.29 \text{ kN}$$

Since dowels are not loaded parallel to the grain the 'group effect' is not adopted, hence the required number of fasteners are

$$n = \frac{920}{32.29} = 29 \text{ dowels}$$

Although the centre of neutral lines of structural elements is located inside the wall element it may be assumed that acting of the vertical force component is located near the head plates, resulting in a moment at the centre of dowel group inside the wall. Designing additional dowels to resist the forces caused by this moment will be too conservative since the structure above will contribute to resist these actions. Moreover, the internal steel plates are welded to a head plate on top of the lower wall. As a result, this plate is directly connected to the upper structure by bolts.

On the other hand connection type 2 is forced to start on a distance of 775 millimetres from the wall's edge as shown in the figure of Table 7.22, so that slotted-in plates of connection type 9 should compensate the reduced load-carrying capacity in vertical direction. Therefore a number of 7 dowels are added to the connection, resulting in a practical number of dowels to fit in the connection of 36.

Furthermore, connection type 9 is located at a corner of the CLT core where in cross direction a similar connection is required to accommodate another outrigger in crosswise direction. As a consequence, the slotted-in steel plates inside the CLT walls are crossing each other resulting in a rather complicated steel component as depicted in Figure 7.26. Manufacturing such steel components might be cost-inefficient; however it has some functional benefits. The slotted-in plates are directly connected to connection type 2, i.e. steel bolts, U-beams and structure above, so that stresses in the connection are distributed over a larger area in the CLT walls resulting in a stronger and stiffer connection accordingly. Assembly, on the other hand, becomes more complicated since at least one group of dowels – penetrated in a single wall element – should be fastened on-site.

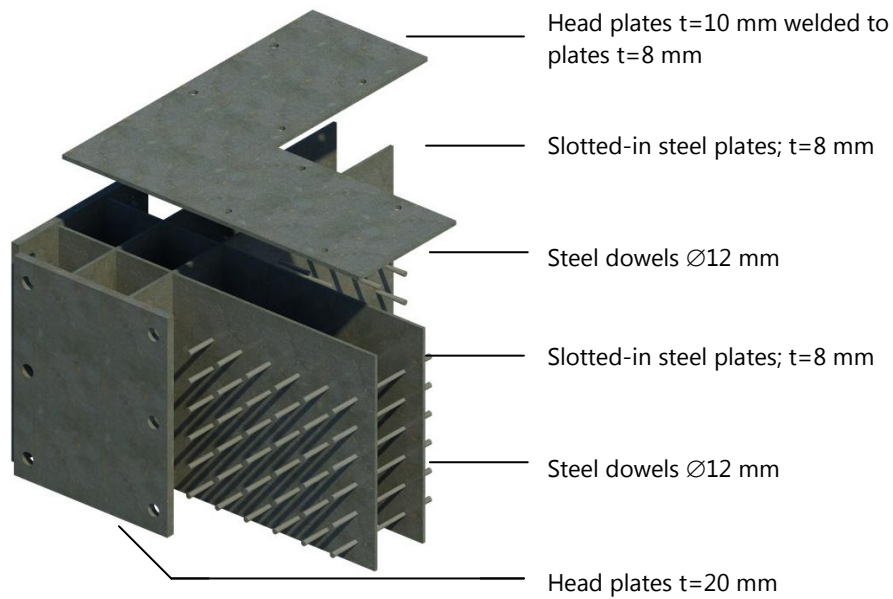


Figure 7.26; Slotted-in steel plates with head plates for two outriggers in two directions at a corner of CLT core

The lower connection detail between the diagonal, beam and CLT wall element is subjected to opposite forces in both the diagonal and the beam, as shown in Figure 7.22. Contact between glulam members, i.e. diagonal and beam, should be prevented in order to avoid unfavourable compressive stresses and possibly crushing of wood. Therefore a cavity between the diagonal and steel plate of 30 millimetres is designed, which forces the dowels and slotted-in steel plates to transfer the stresses to the CLT walls.

The final design of the connection with incorporation of end- and edge distances of dowels as well as spacings between them is presented in Figure 7.27.

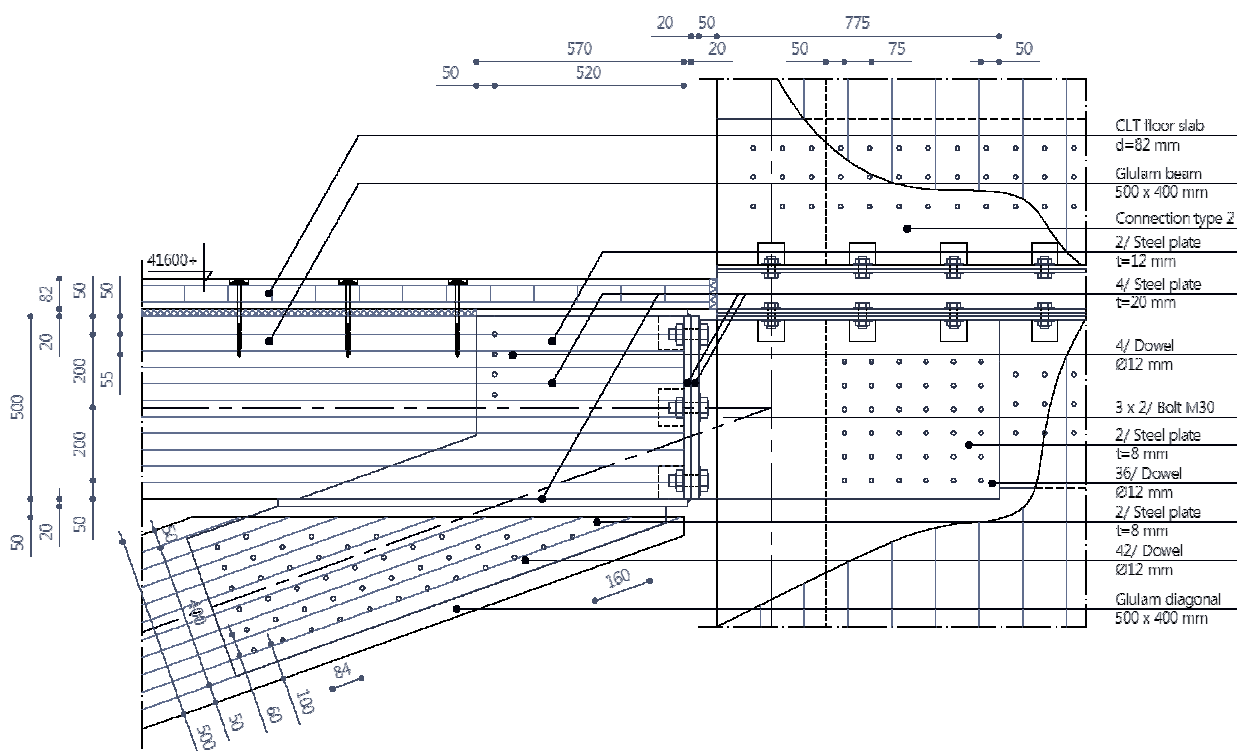


Figure 7.27; Connection detail 9

10. Column-diagonal-beam connection

The largest difference in comparison to connection type 9 is that a column-diagonal-beam joint comprises two diagonals (see Figure 7.22), which introduce a vertical force resultant on the joint in the same direction. Being a critical design issue at the prior connection detail, high compressive stresses on or near an angle perpendicular to the grain in the beam is for connection type 10 even more an issue. Furthermore, the axial force in the beam is relatively low since its location is in the middle of the outrigger truss.

Requirements on the connection contain the same keywords as defined for connection type 9, i.e. *functionality*, *fire safety* and *prefabrication*. Since it is impossible, or at least very complicated and cost inefficient when it comes to transportation and erection on-site, to prefabricate the outriggers as two storey high trusses, the structural elements should be divided into two parts. Inevitable, this separation is located in the column-diagonal-beam connection. Further, column to column connections are located every four storeys and since the pertaining joint is positioned at the twelfth storey also provisions for load-transfer between glulam columns should be taken into account. An overview of prefabricated structural elements is depicted in Figure 7.28.

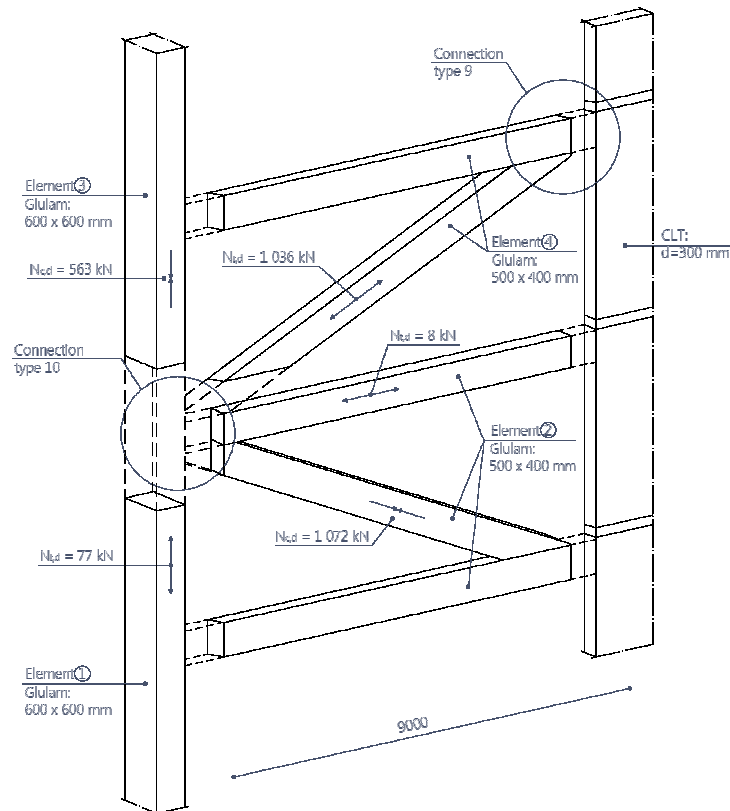


Figure 7.28; Prefabricated structural elements in an outrigger

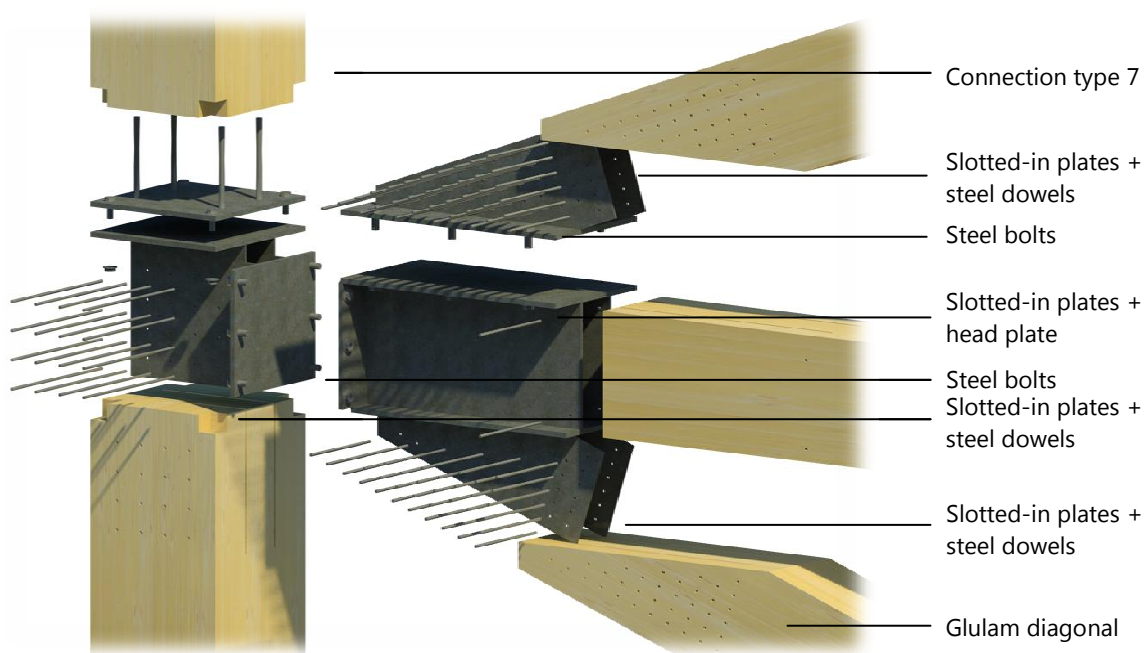
Connection type 10 is build-up out of four elements for which preferably the assembly sequence should be as follows

1. Lower column erected over four storeys below;
2. Beam-diagonal connection fastened to lower column;
3. Erection of upper column;
4. Diagonal fixed to connection type 10.

By taking the defined requirements, actions in the connection and the assembly sequence into account the joint can be build-up as shown in the proposed design of Table 7.25.

Table 7.25; Connection design type 10

Key words for design:	Functionality, fire safety, prefabrication
<hr/>	
Forces on connection by ULS-STR-7	Load [kN]
Axial tensile force diagonal; $N_{t,d}$	1 036
Axial compressive force diagonal; $N_{c,d}$	1 072
Axial compressive force beam; $N_{c,d}$	7.6
Axial compressive force upper column; $N_{c,d}$	563
Axial tensile force lower column; $N_{t,d}$	77
Vertical shear force beam; $V_{y,d}$	77



Assembly sequence

1. Erection of lower column with prefabricated steel connection component
2. Bolting structural element 2 to lower column
3. Fastening of upper column by steel bolts to lower column
4. Erection of structural element 4 to connection by bolting on topside of beam

The result of requirements and key words defined as starting points is a connection between four elements where each can be prefabricated to a high degree off-site and simply bolted together on-site. Alternatively, steel plates and bolts could be spared in the connection by dowelling the elements together during erection. However, construction failures are more likely to occur when connecting steel to timber than bolting steel parts of prefabricated elements together. For instance, when fastening the dowels dimensional deviations between structural elements are unfavourably solved by smashing of surrounding wood.

Most relevant in the connection is the transfer of the vertical force resultant to the column by circumvention of stresses perpendicular to the grain in the beam. In analogy with connection type 9, where a single diagonal induces a vertical resultant force to the beam, it should be the steel components to transfer the forces from the beam through the head plates to the column. Although the centre of neutral lines is located in the horizontal beam it is assumed for *beam analysis* that the

bolted connection between the beam and column causes redistribution of forces so that resultant forces are determined as illustrated in Figure 7.29.

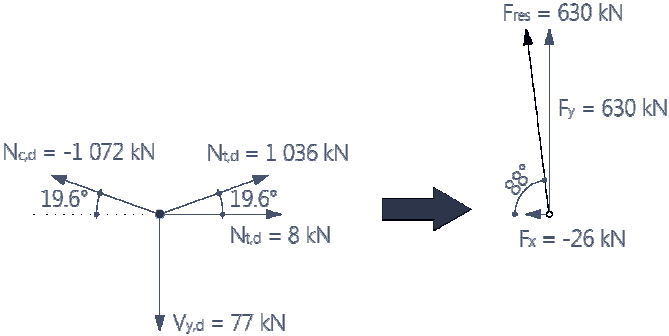


Figure 7.29; a) Actions in horizontal beam conform Figure 6.28 b) Resultant forces in beam

A vertical shear force of 630 kN is acting to the beam as a result of axial forces in the diagonals and should subsequently be transferred to the column. In horizontal direction a compressive force of 26 kN is negligible in the analysis.

Steel dowels in the diagonals are as determined in connection type 9 for an axial force of 1 036 kN. The load-carrying capacity, $F_{v,Rd}$, of 42 dowels in the connection is 1 180 kN, so that this design also complies for the lower diagonal which is subjected to an axial force of 1 072 kN. Calculations in C.S.6.3 of Appendix E.1 show that a number of 6 bolts M24 are required to transfer a vertical shear force of 630 kN to the steel component in the column, in which some additional capacity is included for the relatively low axial force in the beam. Bolts in steel plates between the upper diagonal and beam are subjected to a combination of tension and shear. Assuming the vertical force resultant of 630 kN and lateral shear force solely from the upper diagonal the following actions on the bolts apply

$$F_{t,S,d} = F_{res} = 630 \text{ kN}$$

$$F_{v,S,d} = 1\,036 \cos(\alpha) = 976 \text{ kN} \quad (\alpha = 19.6^\circ)$$

Verification to combined loading on the bolts, shown in C.S.6.3, results in 6 bolts M30.

As shown in the 3D impression of the connection in Table 7.25 the vertical resultant force should be transferred to the column-to-column joint through slotted-in steel plates. The force direction acts under an angle of 2 degrees to the grain direction, so timber's strength is only decreased to a negligible degree in comparison to parallel to the grain. Position of two slotted-in plates in the column are parallel to plates in the beam, so that $t_1 = 200$ millimetres and $t_2 = 600 - 2(200+8) = 184$ millimetres. Table 7.26 show the results of the load-carrying capacity of the dowelled connection in the column, where failure modes are equal to connection type 6, i.e. dowels with slotted-in steel plates in glulam beam.

Table 7.26; Embedment strength and strength equations for steel dowels in lower column

Material properties	$f_{u,k}$ [MPa.]	$M_{y,Rk}$ [Nmm]
Steel dowels, $\varnothing 12$ mm	800	153 491
Equation 7.1		
Embedment strength (parallel to grain); $f_{h,k}$	29.59	MPa.

Strength equations	Value [kN]
$F_{v,Rk,1} = f_{h,k} dt_1$	71.02
$F_{v,Rk,2} = f_{h,k} d \frac{t_2}{2}$	32.67
$F_{v,Rk,3} = f_{h,k} t_1 d \left[\sqrt{2 + \frac{4M_{y,Rk}}{f_{h,k} dt_1^2}} - 1 \right]$	30.50
$F_{v,Rk,4} = \sqrt{4M_{y,Rk} f_{h,k} d}$	16.98

Each steel plate has a load-carrying capacity per fastener of

$$F_{v,Rk} = F_{v,Rk,4} + F_{v,Rk,4} = 2 \cdot 16.98 = 33.96 \text{ kN}$$

which results in a design value per dowel and two steel plates under loading combination *ULS-STR-7* of

$$F_{v,Rd} = 0.9 \frac{(2 \cdot 33.96)}{1.3} = 47.02 \text{ kN}$$

Since the dowels will be loaded parallel to the grain the effective number of fasteners on each row should be taken into account by implementing equation 7.9. Designing 4 rows with 5 dowels and a spacing, a_1 , of 100 millimetres the effective number of fasteners for each row becomes

$$n_{ef} = 5^{0.9} \sqrt[4]{\frac{100}{13 \cdot 12}} = 3.81 \text{ dowels}$$

The total load-carrying capacity of the slotted-in plates with 20 dowels will be

$$F_{v,Rd} = 4 \cdot 3.12 \cdot 47.02 = 717 \text{ kN}$$

which is comfortably above the design action.

The connection between lower- and upper column is subjected to two forces in opposite direction (see Figure 7.22 and 7.28), which results in a vertical resultant of

$$N_{S,d} = 563 - 630 = -67 \text{ kN}$$

which is slightly lower than computed by STAAD Pro ($= -77 \text{ kN}$). The cause for this deviation may be due to the distribution of floor loading as modelled in the 3D model, where in Chapter 5 it has been decided to obtain force distributions in glulam beams by a separate model in Scia Engineer, since STAAD Pro transfers floor loading solely through nodes and not as line loads on beams.

Despite the difference in tensile forces, both of them can be easily transferred by a standard column-column connection (type 7) as shown in Figure 7.18.

Lastly, two steel dowels are applied in the glulam beam in order to transfer the relatively low axial force resultant of 26 kN. As can be seen in Figure 7.22 the force in the beam on the other side of the core is slightly higher (14 kN instead of 7 kN). Both axial force resultants can be easily transferred by two dowels. The final connection design is depicted in Figure 7.30.

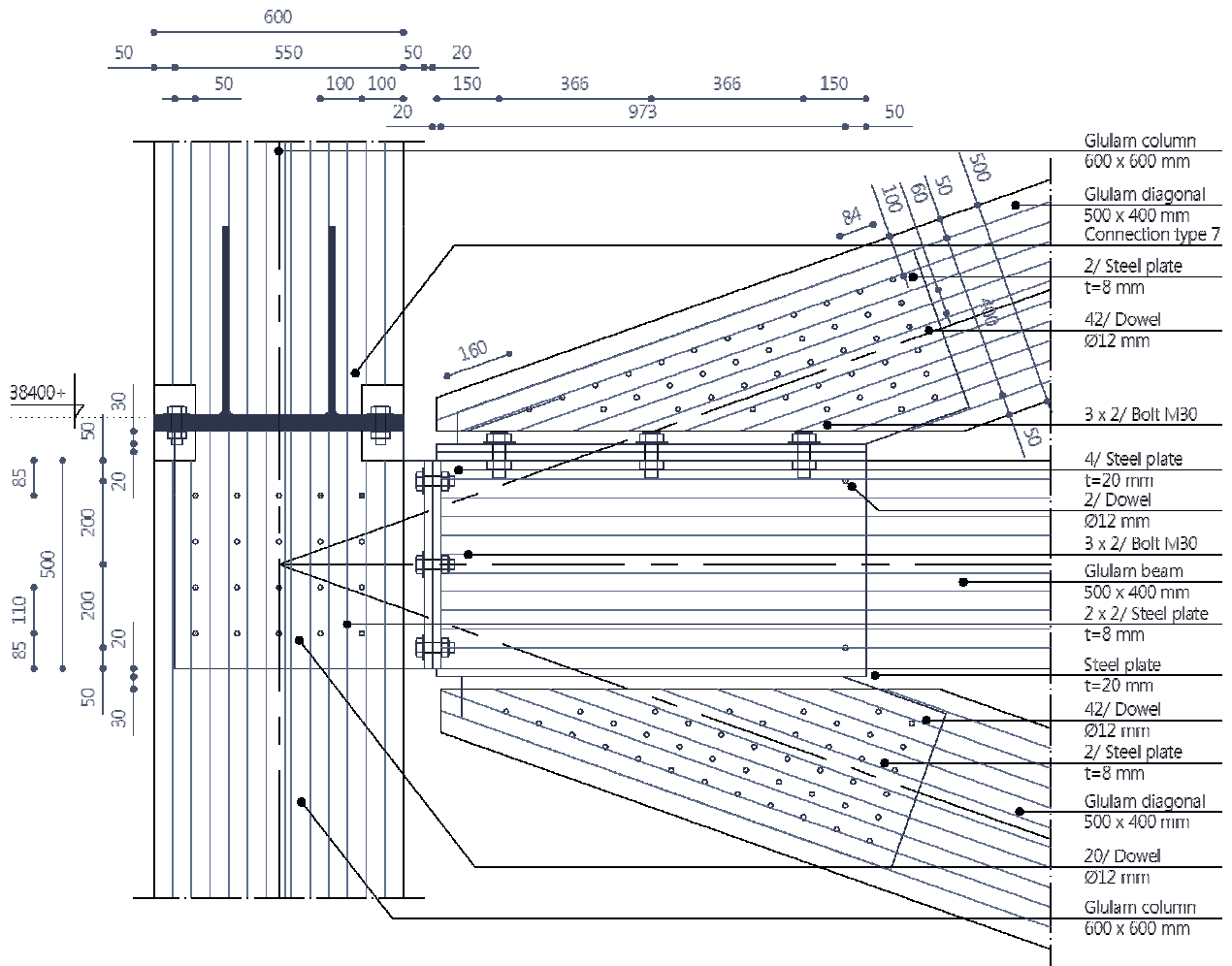


Figure 7.30; Connection detail 10

7.6 CONCLUDING REMARKS ON CONNECTION DESIGN IN ULS

In the previous sections structural connections are designed on strength criteria in the ULS. The designed connections comply with design actions as computed in the 3D Finite Element model of the program STAAD Pro. Although the program accounted for additional forces in members due to eccentricities in connections, the effects of extra forces on fasteners due to rotational capacities of joints has not been analysed.

Prior starting the design of each connection keywords were defined in order to incorporate assembly processes, prefabrication, building physical aspects such as fire safety and acoustics and cost efficiency. However, the latter aspect may not be utilised in the design of connections on a maximum level, since in particular outrigger joints comprise large steel component, which may be cost inefficient.

When designing the layout of fasteners in structural members, conservative edge-, and end distances as well as spacing between fasteners were adopted, which means that large distances are designed to ensure ductile behaviour under lateral wind actions and also prevent splitting of surrounding wood of structural members. Moreover, rotational rigidity of connections causes a force resultant of fasteners perpendicular to the grain of the member for which conservative edge- and end distances are beneficial.

It must be emphasised that proposed connection designs in previous sections comply with strength equations based on Johansen failure modes; hence plastic behaviour is assumed. It was stated in Section 7.1 that 33 percent over-capacity is desired in order to circumvent pinching (see Figure 7.1).

7.7 EFFECTS OF JOINT RIGIDITY ON STRUCTURAL BEHAVIOUR

The objective in this section is to analyse the effects of translational- and rotational rigidity of joints on the structural behaviour under lateral wind actions in the SLS. Already in an early stage of the design of the twenty-storey building it was mentioned that connections were expected to have a large effect on the deformations of the overall structure.

As for structural elements in a timber structure, due to a relatively low stiffness to strength ratio of the structural material in connections non-compliance of serviceability criteria is more likely to occur during the design life than exceedance of strength criteria [28]. However displacement limits of structural members in connections in the SLS are not incorporated in EC5, which means that it is left to the designer to determine acceptable deformations both in a connection and the effects on the structure as a whole.

Slip of fasteners is caused by tolerance allowances in the assembly process or yielding of the fasteners and/or the timber product in the connection, or through a combination of these factors. It is the type of fastener which determines the amount of slip and thus rigidity of the connection, where it may be obvious that self-drilled screws resemble a different behaviour in comparison to bolted connections which require a dimensional tolerance.

The stiffness of a fastener per shear plane in the SLS is represented by the slip modulus, K_{ser} , which is the secant modulus of the load-displacement curve at a 40 percent load level of the maximum load able to be taken by the fastener. EC5 presents (table 7.1) values of K_{ser} for various types of fasteners depending on the mean density of the material, ρ_m , and diameter of the fastener, which are determined by many tests on joints [28].

For steel-to-timber connections EC5 allows (Clause 7.1(3)) a doubled slip modulus, i.e. $2 \times K_{ser}$, to take into account instantaneous slip, however it is concluded [28] that this will overestimate the real stiffness since it ignores; the effect of clearance between fastener and steel and rotation of the fastener in the steel member. Therefore it is recommended to adopt a smaller value for structures which are sensitive to deflections, which is certainly the case for the twenty-storey building. Independent of slotted-in steel plates applied in a connection, slip modulus K_{ser} will not be increased in calculations for connection rigidity.

Effective number of fasteners was required to be taken into account at strength calculations for multiple fastener connections when loaded parallel to the grain. EC5 gives no guidance on an effective number of fasteners for determination of the connection's stiffness. This because an effective number of fasteners are meant to prevent occurrences such as splitting of the timber and block shear in the ULS, whilst in the SLS the loading will be lower, hence there is no need to account for an effective number of fasteners. It is recommended [28] that the actual number of fasteners is used irrespective of the angle of load relative to the grain.

Moment capacity of joints has effects on the overall structural behaviour and thus on deformations in the SLS. In timber design it is normal practice to classify joints as either *pinned* or *rigid*. Nonetheless, in reality most connections resemble *semi-rigid* behaviour, where the degree of rigidity is dependent on many factors, such as tolerance allowances of fasteners, embedment of the fasteners in timber connection members and stiffness of the fasteners itself. Further, the layout of fasteners around the centre of rotation as well as the variety of components applied in a connection also affects the moment capacity.

For certain joints in the structure of the twenty-storey building a very low rigidity may be obvious (type (5-8)), whilst other joints may resemble rather full rigid behaviour due to their large connection components (type 9-10). Since it is the objective to analyse the effects of joint rigidity, both *translational* and *rotational*, on the structural behaviour several assumptions on the moment capacity will be adopted in the STAAD Pro 3D model to compare their effects in the SLS. For instance semi-rigid

joints will be either assumed as pinned or rigid in the analysis so that their effects on the structural behaviour become distinctive.

Translational slip of structural members reduces the overall stiffness of the structure resulting in larger horizontal displacement at the top of the building. Further, the reduced stiffness may affect the *dynamic performance* of the building, i.e. natural frequency of the building, horizontal displacements under fluctuating wind loading and horizontal accelerations. Therefore it is required to analyse the joint rigidity effects of the structure in the dynamic model accordingly.

Strategy for analysis on joint rigidity effects

Firstly, connection types designed in Section 7.3 to 7.5 should be analysed on their behaviour under lateral loading and subjected forces, so that effects on the structural behaviour can be determined and subsequently modelled in the Finite Element STAAD Pro models. Either translational slip or moment capacity, or a combination of both, of a joint in the structure can have an influence on the behaviour. Secondly, translational rigidity of respective joints is calculated and combinations of rotational rigidity are compiled to alternative computer models in order to analyse each effect.

Thirdly, outcomes of STAAD Pro static- and dynamic computations in the SLS are analysed in order to define the importance of several connections in a timber structure for a twenty-storey timber building.

Lastly, it must be mentioned that checks in the ULS of structural elements as well as components in connections due to moment capacity of joints and translational slip is excluded in this research, since the focus is on serviceability aspects such as horizontal displacements and dynamic responses.

The strategy of the analysis is illustrated in Figure 7.31.

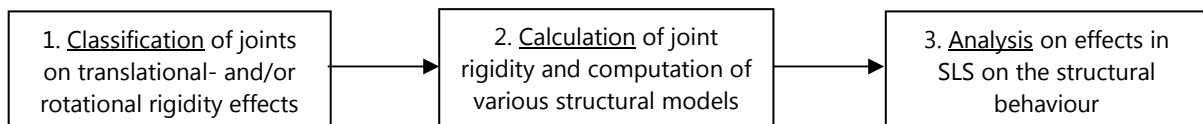


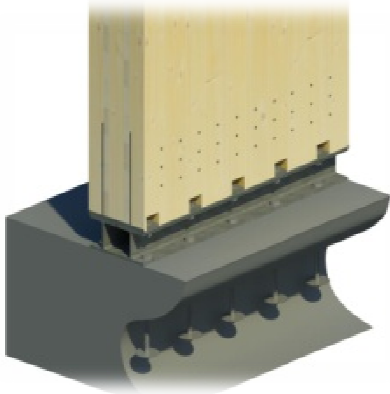



Figure 7.31; Steps for analysis on joint rigidity effects


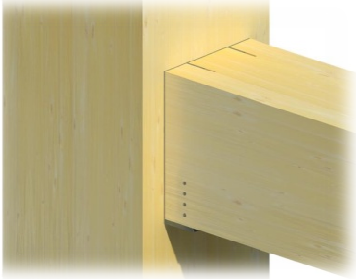


1. Joint classification by translational- and rotational rigidity effects


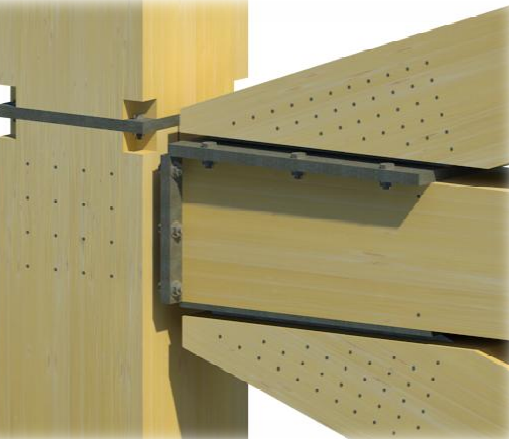
The effects of rigidity on the structural behaviour of each individual joint depend on the direction of subjected forces and the role of the joint in the structure as a whole. In the introduction of this chapter it has been stated that maintaining stiffness in the structure is superior to increasing ductility – and thus damping. Critical structural elements in the building with respect to lateral stabilisation are the CLT core in the centre of the building and the outriggers, hence related connections are relevant to analyse on their rigidity.

For each connection type, Table 7.27 presents an analysis on their translational- and rotational effects to the structural behaviour of the building under lateral wind actions.

Table 7.27; Joint classification on rigidity behaviour

<p><u>Connection 1:</u></p> 	<p><i>Joint rigidity effects</i> Slip of dowels due to vertical uplifting forces results in additional horizontal displacements at the top of the building</p> <p><i>Modelling in STAAD Pro</i> Translational springs at supports on windward side of the core representing slip modulus of the connection</p>
<p><u>Connection 2:</u></p> 	<p><i>Joint rigidity effects</i> In analogy with connection type 1, slip of dowels reduces the wall stiffness</p> <p><i>Modelling in STAAD Pro</i> Translational springs at supports on windward side of the core</p> <p>NB! Springs at each floor is not possible since this will constrain the whole structure to deform in vertical direction</p>
<p><u>Connection 3:</u></p> 	<p><i>Joint rigidity effects</i> Timber screws between wall elements affect the stiffness of the core due to slip under vertical uplifting forces</p> <p><i>Modelling in STAAD Pro</i> Translational springs at corner supports on windward side of the core</p>
<p><u>Connection 4:</u></p> 	<p><i>Joint rigidity effects</i> Negligible, since connection type 1 & 2 ensures the overall stiffness of a wall element significantly</p> <p><i>Modelling in STAAD Pro</i> None</p>

<p><u>Connection 5:</u></p> 	<p><i>Joint rigidity effects</i> Only when the connection is subjected to vertical uplifting forces translational rigidity will influence the overall stiffness, which is not the case in both the SLS and ULS. Rotational rigidity is relatively low, but effects will be analysed</p> <p><i>Modelling in STAAD Pro</i> Pinned- or rigid supports</p>
<p><u>Connection 6:</u></p> 	<p><i>Joint rigidity effects</i> Translational stiffness of the dowels may affect the overall behaviour, but is not expected to be significant. Rotational rigidity is negligible since four dowels are designed at the lower half of the beam</p> <p><i>Modelling in STAAD Pro</i> Translational springs at beam ends</p>
<p><u>Connection 7:</u></p> 	<p><i>Joint rigidity effects</i> Only vertically tensile loaded joints have an influence on the overall behaviour. Rotational rigidity effects will be analysed</p> <p><i>Modelling in STAAD Pro</i> Pinned- or rigid joints between columns</p>
<p><u>Connection 8:</u></p> 	<p><i>Joint rigidity effects</i> In analogy with connection type 6, i.e. other end of beams connecting peripheral columns and core</p> <p><i>Modelling in STAAD Pro</i> Translational springs at beam ends</p>

<p><u>Connection 9:</u></p> 	<p><i>Joint rigidity effects</i> Translational slip of the dowelled connection between diagonal and steel component as well as the beam and steel component. The steel plates in the core walls are assumed to rigid, both translational and rotational, since they are connected to head plates and steel components of connection type 2. Rotation capacity of the joint connecting beam and diagonal will be taken as either zero or infinite</p> <p><i>Modelling in STAAD Pro</i> Translational springs at beam- and diagonal ends. Pinned or rotational rigid joint between diagonal, beam and core</p>
<p><u>Connection 10:</u></p> 	<p><i>Joint rigidity effects</i> Diagonals and the beam comprise a translational stiffness like connection type 9. The vertical uplifting force in the connection causes translational slip of the dowels in the column. Rotational stiffness of diagonals, beam and lower column are taken as either pinned or rigid</p> <p><i>Modelling in STAAD Pro</i> Translational springs at beam- and diagonal ends. Rotational pinned- or rigid joint between diagonals, beam and lower column</p> <p>NB! The upper column contains a connection like type 7.</p>

2. Joint rigidity and modelling

As stated before, over-capacity in certain connections is desired in order to avoid pinching (as shown in Figure 7.1) in the ULS. This applies for joints which are susceptible to structural forces due to wind loading, i.e. connection type 1, 2, 3, 9 and 10. Additional capacity is referred to by NEN 6760 [29] as 33 percent of the design value in the ULS. Table 7.28 presents the required capacity in the respective connections.

Table 7.28; Additional capacity in connection types susceptible to wind actions

Connection type	Type of fastener	Design to EC5	Required capacity
1 / 2	Dowel, Ø12 mm	3 / row	4 / row
3	Timber screw, Ø13 mm	56 / storey	75 storey
9 / 10	Dowel, Ø12 mm (diagonal)	42	56

Fasteners in glulam beams and -columns of connection type 9 and 10 are neglected since it is expected that their contribution to the structural behaviour is very little.

Translational stiffness of a connection is determined by the slip modulus of a fastener, K_{ser} , which is dependent on the diameter, d , of the dowel and the density, ρ_m , of the connected material. Table 7.1 of

EC5 presents values for each fastener type per shear plane in a connection. For dowels the slip modulus is expressed by

$$K_{ser} = \rho_m^{1.5} \frac{d}{23} \tag{7.27}$$

The total translational stiffness of a connection is determined by the individual stiffness of fasteners in each connected member. Structural analysis program STAAD Pro allows for modelling stiffness properties for any member; hence it is required to obtain a slip modulus for fasteners in each structural member separately. Table 7.29 gives the values for K_{ser} (slip modulus per shear plane) and translational stiffness per fastener, $K_{ser,fas}$, relevant for each connection.

The outcomes in the table below show that the translational stiffness of glued-in rods is negligible for the relative low tensile forces in connection type 7. Therefore modelling in STAAD Pro of the translational stiffness of these glued-in rods is not taken into account.

Table 7.29; Values for K_{ser} for structural members in each connection type

Connection type	Structural member	Type of fastener	K_{ser} [N/mm]	$K_{ser,fas}$ [N/mm]
1 / 2	CLT wall panel	Dowel, Ø12 mm	3 865	15 459
3	CLT wall panel	Timber screw, Ø13 mm	4 187	4 187
6 / 8 / 9 / 10	Glulam beam / column	Dowel, Ø12 mm	4 331	17 326
7	Glulam column	Glued-in rod, Ø24 mm	-	632 00 ²⁶
9 / 10	Glulam diagonal	Dowel, Ø12 mm	4 331	17 326

Translational slip of dowels in CLT walls, i.e. connection type 1 and 2, can be modelled as a series of translational springs, where a single spring represents the stiffness of one connection. Subsequently, the total translational stiffness is modelled by a single spring at the wall supports on the ground floor. The system of springs for the two bottom storeys is resembled in Figure 7.32 in which the CLT wall elements are taken as infinite stiff members, since they are subjected to an in-plane tension force.

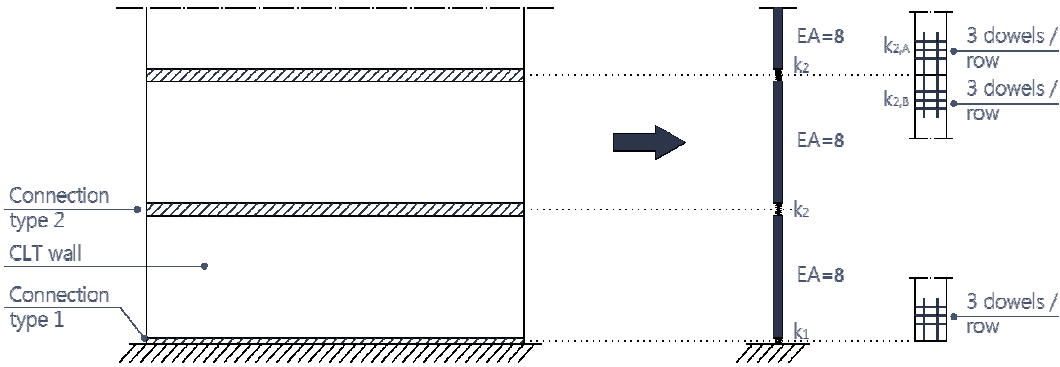


Figure 7.32; Simulation of translational stiffness by springs of CLT walls under tension forces

Spring stiffness, k_1 , refers to translational slip of dowels in connection type 1 (see Table 7.27) where equation 7.27 represents the translational stiffness of a single dowel in the connection. Therefore, the magnitude of k_1 is a function of the number of dowels in a certain wall region²⁷.

²⁶ The slip modulus for a glued-in rod is obtained from load-deformation curves [25] from tests performed by Aicher et al. (1999)

²⁷ Supports of CLT walls in STAAD Pro consists of point supports at nodes of wall elements so that the spring stiffness is determined by the number of dowels related to the wall region of a specific support

Connection type 2 on the other hand consists of two members jointed by two sets of dowels, in the lower wall and upper wall. Hence spring stiffness k_2 can be written as

$$\frac{1}{k_2} = \frac{1}{k_{2,A}} + \frac{1}{k_{2,B}} \quad (7.28)$$

where $k_{2,A}$ equals $k_{2,B}$ due to joint symmetry with respect to the upper- and lower wall. Since designed dowels in connection type 1 are similar to dowels in connection type 2, both dowel's diameter and spacing, spring stiffness k_1 equates to $k_{2,A}$ as well as to $k_{2,B}$.

For a single row, consisting of four dowels (Table 7.28), k_1 becomes

$$k_1 = 4 \cdot K_{\text{ser,fas}} = 61\,837 \text{ N/mm}$$

and k_2 results in

$$k_2 = \left(\frac{1}{61\,837} + \frac{1}{61\,837} \right)^{-1} = 30\,919 \text{ N/mm}$$

The total spring stiffness at the support representing joint stiffness of all storeys is given by

$$\frac{1}{k} = \frac{1}{k_1} + \frac{n}{k_2} \quad (7.29)$$

where n is the number of storeys in the building, equal to 20.

The total translational stiffness of CLT core fasteners in a single row over twenty storeys, which are subjected to vertical uplifting forces, becomes

$$k = \left(\frac{1}{61\,837} + \frac{20}{30\,919} \right)^{-1} = 1\,508 \text{ N/mm}$$

Subsequently, the spring stiffness can be multiplied by the number of rows related to each point support on the windward side of the core, i.e. supports under vertical uplifting forces, in the STAAD Pro model.

Translational stiffness between CLT wall elements is affected by slip of timber screws in connection type 3, see Figure 7.4 and 7.10. As a consequence stiffness between spring stiffness' k_2 as shown in Figure 7.32 becomes finite, represented by k_3 , so that the systems of springs modifies to a series of springs depicted in Figure 7.33.

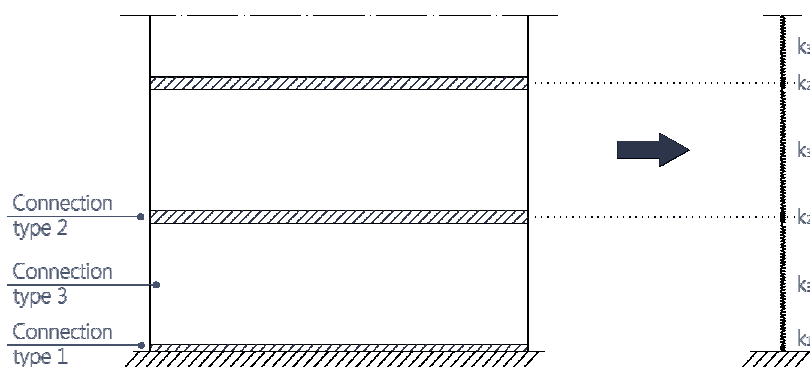


Figure 7.33; System of springs for corner wall supports representing joint stiffness type 1, 2 and 3

Due to the requirement of over-capacity the number of timber screws per storey is 75, so that spring stiffness k_3 results in

$$k_3 = 75 \cdot K_{ser,fas} = 314\,016 \text{ N/mm}$$

The corner supports of the STAAD Pro model can be modelled by a single spring for the number of dowels related to the corner wall region per connection and total number of timber screws between wall elements per storey as follows

$$\frac{1}{k} = \frac{1}{k_1} + \frac{n}{k_2} + \frac{n}{k_3} \quad (7.30)$$

where characteristics are as defined previously and according to Figure 7.33.

Joint rigidity in translational direction of glulam members, e.g. columns under tension below outriggers, beams and diagonals, are easily determined by multiplying the evaluated values of slip moduli in Table 7.29 with the number of dowels designed in the related connection. For connection type 6 and 8, i.e. dowels in glulam beams this results in

$$k = 4 \cdot 17\,326 = 69\,303 \text{ N/mm}$$

Translational stiffness of diagonals, which comprise 56 dowels gives a value of 970 236 N/mm and for 20 dowels in the column of connection type 10 the joint stiffness becomes 346 514 N/mm accordingly.

Computations in previous chapters are conducted by a 'standard model', which includes following modelling assumptions:

- CLT walls translational stiff between individual elements and fixed supports;
- Columns pin connected over four storeys as well as at supports;
- Beams pinned to columns and CLT walls;
- Diagonals pin jointed to beams/CLT walls or beams/columns.

Further, all 2D members in the 'standard model', i.e. columns, beams and diagonals, are precluded from any translational stiffness at their joints.

In order to analyse effects of each single type of slip individually it is desirable to compute results of multiple STAAD Pro models, with either a single type of slip or a combination of these. As a consequence, the significance of slip in each connection on both static deformations and the dynamic behaviour can be identified.

Firstly, there are three main types of translational slip in the model, i.e. slip of fasteners in CLT walls, slip of dowels in beams and slip of dowels in diagonals. Secondly, rotational stiffness of several joints as described in Table 7.27 may influence static deformations and dynamic behaviour of the structure. Figure 7.34 presents a strategy of analysis of joint stiffness effects in the SLS.

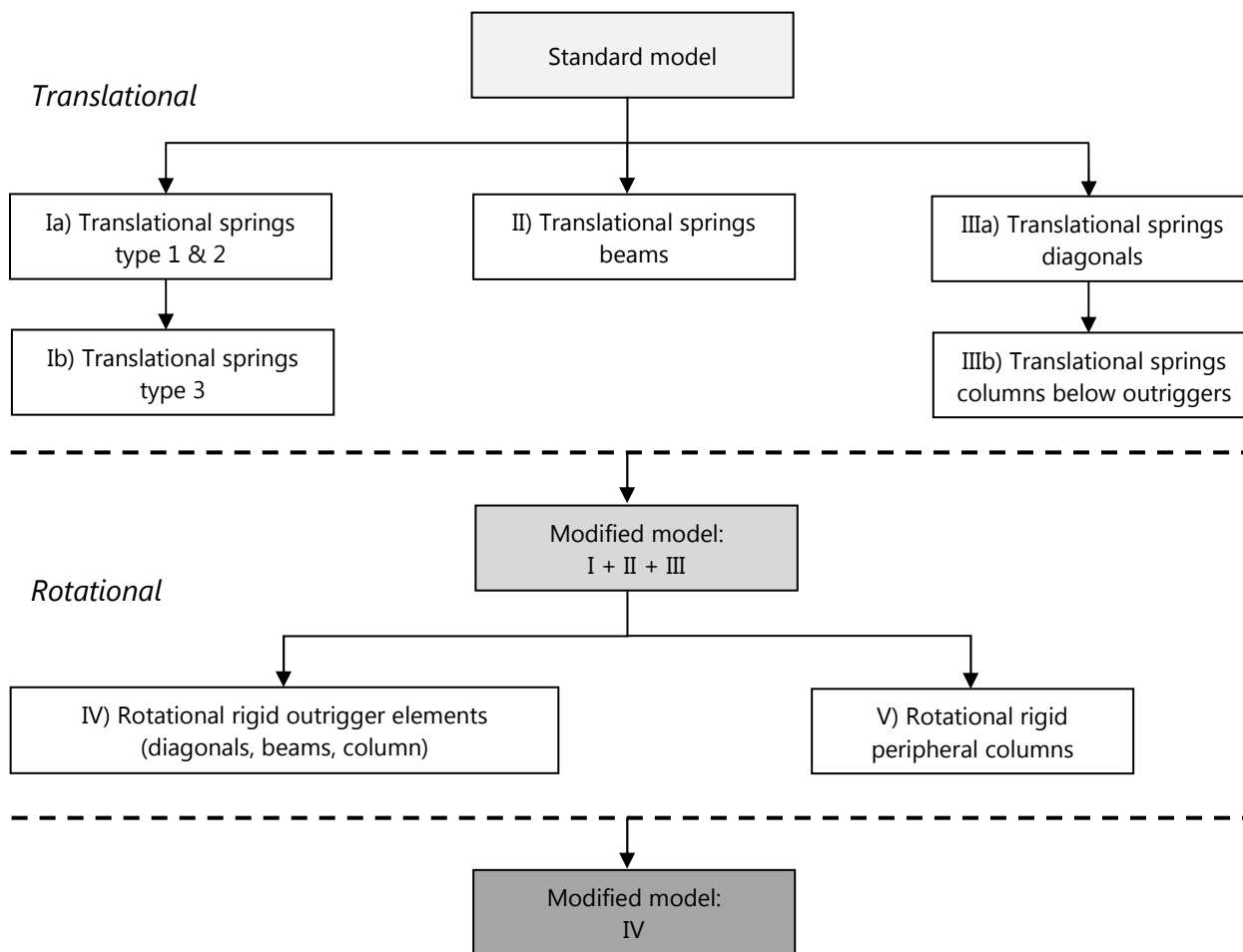


Figure 7.34; Strategy of analysis for slip in connections in SLS

3. Analysis on joint stiffness effects to structural behaviour

The diagram above implies that the final model includes rotational rigid outrigger connections, i.e. connection type 9 and 10, and excludes rotational stiffness in column-to-column joints, i.e. connection type 7. Outrigger connection details as presented in Figure 7.27 and 7.30 can be classified as rotational rigid, although a fully rigid joint is hard to achieve. Nevertheless, the large steel components in the connections will result in a rotational rigid joint, for which the magnitude is rather complicated to determine due to the geometry and multiple components in the connection.

On the other hand, four bolts in connection type 7 between two columns induce a relatively low rotational rigidity and therefore these joints can be classified as pinned. As a consequence *Model IV* will be adopted as a final model, which includes slip of fasteners in all connections such as classified in Table 7.27.

The effects of translational slip in joints on static deformations are presented in the graph depicted in Figure 7.35.

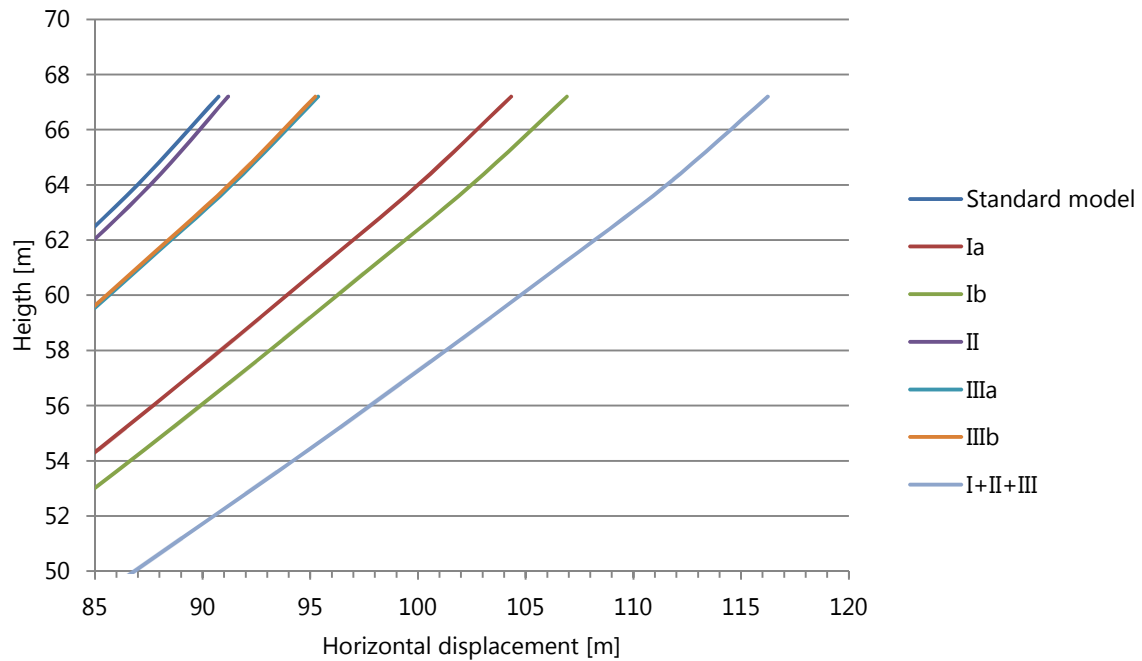


Figure 7.35; Deformation modes of STAAD Pro models with implementations of several translational joint slip

The deformation modes show that slip of dowels in connection type 1, 2 and 3 (Ia and Ib) have a major affect on horizontal displacements under quasi-static wind actions. Stiffness of the central core appears to be of great importance and thus integrity between CLT wall elements has a large affect on controlling horizontal displacements.

On the contrary, translational slip of dowels in beam elements (II) has a minor influence on the structure's horizontal displacements.

Further, slip of fasteners in diagonals (IIIa) result in higher horizontal displacements, which defines the importance of maintaining the overall stiffness of the outriggers and underpins the great role of these structural elements in the whole stability system. Slip of dowels in the column (IIIb) of connection type 10 results in nearly similar deformations when only slip of fasteners in diagonals are taken into account; hence this has a negligible effect on static deformations.

Rotational capacity effects on the structural behaviour under quasi-static wind actions of two models as presented in Figure 7.34, i.e. *Model IV* and *V*, are shown in the graph of Figure 7.36.

Modelling of rotational rigid joints of outriggers (IV) only reduces the horizontal displacements on a low extent. Rotational rigid column joints (V) over the total building height reduces the deformations more. Without the presence of the outriggers this reduction would be minor since beams are pin connected, which means that only the outriggers introduce some stiffness to the frame structure.

However, implementation of joint stiffness in the STAAD Pro model in accordance with designed connections on strength as presented in the previous section, which complies with *Model IV*, shows that the horizontal displacement at the top of the structure will be 115.6 millimetres. In comparison to the 'standard model' there is an increment of 25 millimetres (or 27 %), which clearly shows that slip in connections becomes rather a serious design consideration for tall timber buildings regarding to the SLS instead of a quick check at the final stage of the design process.

In addition, most relevant connections which are subjected to wind actions are already designed with *over-capacity* by 33 percent. Increasing this percentage may not be unnecessary when maintaining stiffness in a specific connection is essential for adequate structural behaviour.

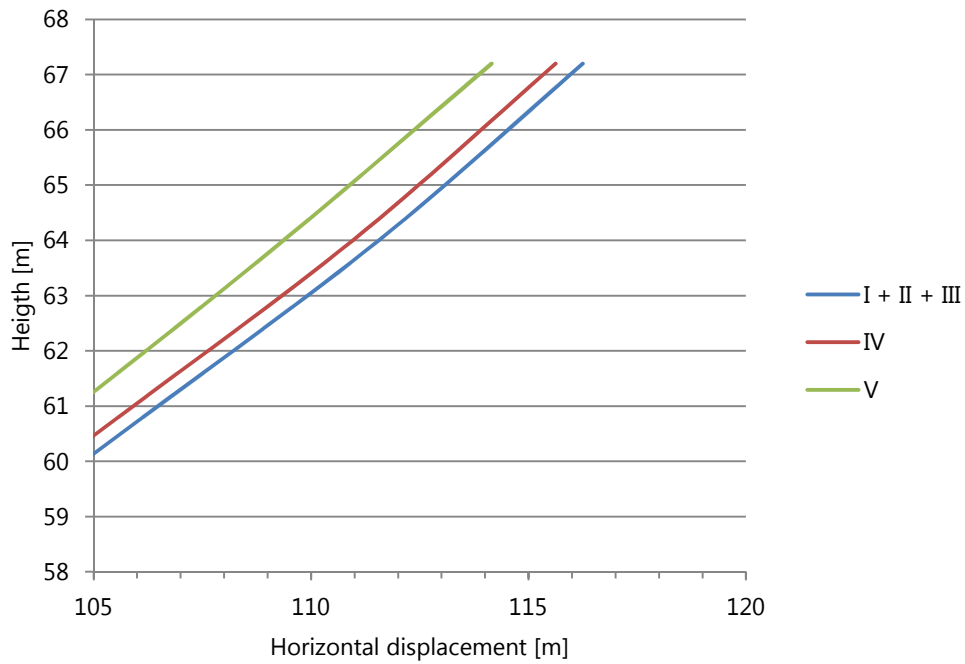


Figure 7.36; Deformation modes of STAAD Pro models with incorporation of rotational joint capacity and modified connections

Consequently, the large reduction in the structure's stiffness will have effects on dynamic properties of the building, e.g. fundamental mode, and horizontal accelerations at the top of the structure. Dynamical computations of the various STAAD Pro models results, in accordance with the diagram of Figure 7.34, in fundamental modes and maximum horizontal accelerations as shown in Table 7.30.

Table 7.30; Dynamic properties and horizontal accelerations with incorporation of joint stiffness

Model	Fundamental frequency [Hz.]	Maximum horizontal accelerations [m/s^2]
Standard model	0.58	0.054
<i>Translational slip</i>		
Ia	0.59	0.088
Ib	0.57	0.092
II	0.75	0.053
IIIa	0.73	0.057
IIIb	0.73	0.069
I+II+III	0.55	0.102
<i>Rotational capacity</i>		
IV	0.55	0.102
V	0.56	0.995

Although the fundamental frequency remains the same when modelling springs as supports at the windward side of the CLT core (Ia), the horizontal accelerations increases significantly. Since accelerations in the building are mainly affected by damping properties of the structure [1], it appears that by modelling translational springs for CLT wall supports dissipation of energy due to fluctuating wind loads is significantly decreased.

Another remarkable result is that by incorporation of translational stiffness of beams (II) and diagonals (IIIa) the fundamental frequency increases but horizontal accelerations remain nearly the same. It is no surprise that horizontal accelerations increase when the stability system loses stiffness due to joint slip, but a higher fundamental frequency is harder to interpret. One knows that the frequency of a structure is determined by the square root of stiffness, k , divided by mass, m , (see equation 4.18 for a SDOF system) so that it is about the relation between those factors which determines the resulting frequency. In this case it is the lower stiffness which may have resulted in a higher ratio between these two design values. So far, it seems that the magnitudes of horizontal accelerations are in better accordance with various structural models.

The final model (IV), which is a combination of joint stiffness' as designed for ULS in the previous section, shows that horizontal accelerations double to 0.102 m/s^2 . Considering the pattern of horizontal accelerations for *Model IV* as a function of time it can be noted (Figure 7.37) that the capability of dissipating energy in the structure is lacking. It can be seen that accelerations remain relatively high after wind gusts, in comparison to the figure in Table 4.14.

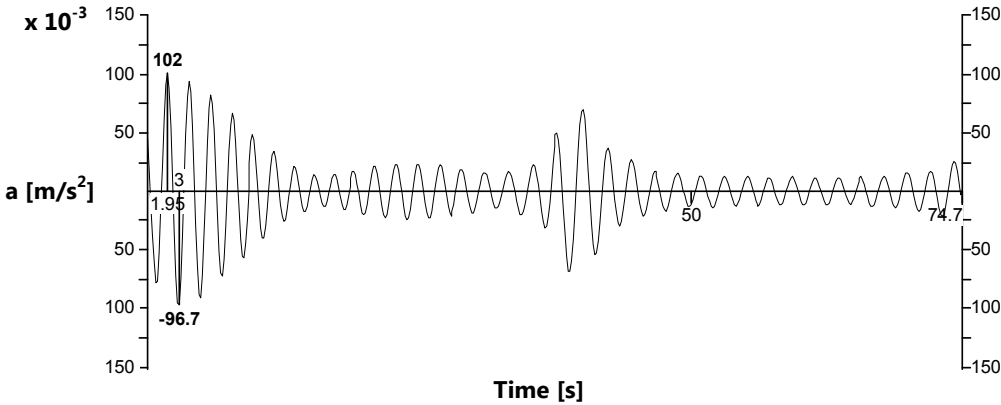


Figure 7.37; Horizontal accelerations as a function of time for Model IV

It is shown in Table 6.1 that increasing the damping ratio to 5 percent, which was stated as more likely for timber buildings, horizontal accelerations decrease effectively. Implementation of this number for *Model IV* results in the pattern of horizontal accelerations shown in Figure 7.38. As a consequence, the dynamic response resembles the wind pattern, shown in Figure 4.8, more accurately and horizontal accelerations decreases accordingly to a maximum value of 0.089 m/s^2 .

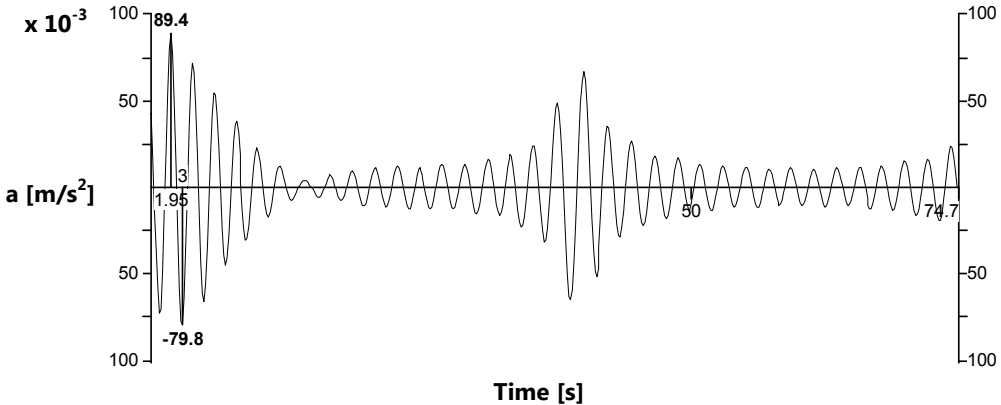


Figure 7.38; Dynamic response of Model IV for a damping ratio of 5 percent

7.8 CONCLUDING REMARKS ON CONNECTION DESIGN IN SLS

Prior to analysing the effects of joint stiffness on the structural behaviour it was repeatedly mentioned that this occurrence was expected to have major effects on static deformations and dynamic responses. Multiple STAAD Pro models with implementation of various joint slip has shown that the effects cannot be underestimated for timber structures, in particular for tall timber buildings where serviceability dominates the structural design. As a matter of fact, joint slip increases static displacements with an impressive 27 percent, so that it becomes apparent that serviceability aspects not only dominate the design of structural timber elements for a twenty-storey timber building but also connection design. Permissible static displacements for a building with a height of 67.2 meters are 134.4 millimetres so that an evaluated displacement of 115.6 millimetres will comply with regulations in EC0. Nonetheless, rotations of foundation elements are not taken into account, which may result in critical values for total horizontal displacements. Most certainly there is need for a relatively stiff foundation structure in order to minimise displacements at the top.

Design criteria for horizontal accelerations in case of residential functions in buildings refer to a magnitude of 0.125 m/s^2 (see Figure 4.10) for a fundamental frequency of 0.58 Hz. Although both models, with either a damping ratio of 1.9 percent or 5 percent, comply with this design criteria it is more likely that an acceleration of 0.089 m/s^2 approaches the real behaviour of such a structure in practice.

Overall it can be concluded that prior to taking into account joint slip in structural calculations the proposed design for a twenty-storey building complies relatively easily to design criteria in the ULS as well as SLS. Although incorporation of joint slip effects have resulted in a design which may comply with regulations and design criteria set by EC0 and EC5, tolerances in both static displacements and horizontal accelerations are rather low.

8 | DISCUSSION

Conclusions and prospect of tall timber buildings

The objective of this research has been defined in the introduction and consisted of an investigation to the structural performance of a timber outrigger structure for a twenty-storey building. The focus was set on serviceability aspects, such as static deformations and dynamic behaviour, since these are decisive in the structural design. A basic architectural design was the starting point for a preliminary structural design on statics and dynamics. Structural elements have been designed in accordance with EC5 as well as connections. Lastly, effects of slip in joints on the structural behaviour have been taken into account. This thorough design process has led to a proposal for a timber structure of a fictive twenty-storey building.

8.1 RESEARCH REFLECTION

Preliminary static design

Various structural systems for a basic design of a twenty-storey building have been analysed by preliminary structural calculations. Most important design criteria in this stage are the horizontal deflections, where the outrigger structure performed well below the design value of $H/800$. Quick checks on strength of structural elements have shown the applicability of an outrigger structure for tall timber buildings. Dimensions of structural elements included; CLT walls of 300 millimetres, glulam columns 600 x 600 millimetres, glulam beams and -diagonals of 500 x 400 millimetres.

Preliminary dynamic design

Dynamic analysis on the static design has been carried out by estimation formulas, spectral analysis, a SDOF- and a MDOF model, as well as FE analysis in STAAD Pro. The fundamental frequency of the outrigger structure has resulted in values between 0.53 and 0.71 Hz. The MDOF model resulted in a high frequency of 0.71 Hz. due to an *over-stiffened* model. The FE analysis lead to a fundamental frequency of 0.58 Hz., which appeared to be a reliable value considering estimated frequencies and the SDOF model.

Dynamic response of the structure to fluctuating wind loading appeared to be within permissible values for horizontal accelerations, as defined in NEN 6702. The FE analysis in STAAD Pro resulted in 0.05 m/s^2 , which is in good agreement with hand calculations of a SDOF- and MDOF model as well as spectral analysis. After preliminary design it can be concluded that the behaviour in SLS is very acceptable, which means that deformations and horizontal accelerations are well below maximum criteria.

Final static design

For structural design in ULS a static analysis is performed by a 3D FE model in STAAD Pro. Structural elements are checked on strength in the ULS in accordance with EC5, which included floor cassette elements, glulam beams, -columns, -diagonals and CLT core walls. Designed elements in the preliminary design phase complied quite easily with strength criteria, hence serviceability governs the design which was expected for a twenty-storey timber building.

Final dynamic design

In this phase the dynamic behaviour is investigated by various modifications on damping ratios. A damping ratio of 0.019 was determined by EC1, whilst it was stated that a ratio of 0.05 is more likely for timber buildings. The latter damping ratio resulted in lower horizontal accelerations in comparison to damping according to EC1, although the difference is very small (-0.007 m/s^2). The contribution of the outriggers to the lateral stiffness, and the dynamic behaviour, is significant. Without outriggers the performance of the structure drops to critical values in static deformations and horizontal accelerations. Therefore, it was stated that the outriggers are essential in the structure for adequate behaviour due to wind actions.

Structural connection design

Connections between structural members are designed in accordance with EC5 and incorporation of aspects like; prefabrication, assembly processes, fire safety and noise control. For certain connections, which are susceptible to wind actions, some *over-capacity* (33 percent) is taken into account on top of design according to EC5. Slip in connections in the SLS is modelled in STAAD Pro by translational springs in joints in order to analyse the effects on static deformations and dynamic behaviour. Rotational capacity of connections are analysed on their contribution to the stability system by modelling either pinned- or full rigid connections. It appeared that slip in connections is a rather serious design issue for a twenty-storey timber building, which should be incorporated in a very early design stage to account for additional deformations and reduction in lateral stiffness.

8.2 RESEARCH QUESTION

The research question has been defined in the introduction as follows

"How does a timber outrigger structure perform as a stability system for a twenty-storey building, with the focus on serviceability aspects?"

In order to answer this question it was decided to design a structural system for a fictive twenty-storey building, which may have resulted in scattered activities on several types of research area it did lead to an impression of the opportunities of constructing tall buildings in timber. However, the main question was to analyse the behaviour of the structural design due to wind actions in the SLS.

Overall, it can be stated that the structure performed rather well when static deformations and dynamic behaviour was investigated without taking into account the effects of connections. At the end, connection design appeared to be a significant design issue, what cannot be neglected in an early design stage for tall timber buildings. Final results of static deformations as well as horizontal accelerations reached a critical value for design criteria. Although the structural design still complied with these criteria tolerances are rather low. It can be concluded that their relevance is as great as the design of structural elements and the whole stability system. However, when adequate connection design is implemented in the process, timber as a structural material has high potential for buildings up to twenty storeys and even taller buildings may be possible.

Moreover, the sustainable aspects of constructing in timber are obvious, which may be decisive for architects, engineers and clients to embrace this material in their future projects. It is a great challenge

to make timber an important competitor for sustainable construction in the future. The prospect of timber for construction purposes all depends on how its potential is utilised in innovative building systems and ingenious solutions for structural designs. Undoubtedly the competitiveness is largely influenced by material costs, which today may have a negative influence for the use of timber in comparison to building materials as concrete, limestone and steel. Anyhow, the great advantage of timber above these materials is the opportunity of prefabrication on a large extent, which may have a large impact on construction in the future.

8.3 CONCLUSIONS

Designing a structural system for a fictive building

Static design

- Static deformations due to wind loading can relatively easily be handled by the proposed outrigger structure, where lateral sway did not exceed the design value of $H/800$;
- Strength criteria for structural elements does not govern the design, in which all elements designed in the preliminary phase comply with EC5;
- The outriggers are essential in the design. Without their presence lateral stiffness is lacking and the static deformations rise with an impressive 44 percent.

Dynamic design

- The fundamental frequency of the structure is computed by; estimation formulas, a SDOF model, MDOF model and FE analysis. Values are in the range of 0.53 – 0.58 Hz.;
- Dynamic response is analysed by the models mentioned above and through spectral analysis. The results are in good agreement between the methods, where maximum horizontal accelerations due to fluctuating wind loads are between 0.03 and 0.05 m/s^2 ;
- The dynamic response complies with comfort criteria for the residential function set by NEN 6702, where a maximum allowable acceleration for a fundamental frequency of 0.58 Hz. is approximately 0.125 m/s^2 .

Connection design

- Static forces in the structure can be taken by designed connections. Connections are predominantly designed with prefabricated slotted-in plates, steel dowels and head plates, which can simply be bolted together on-site;
- Slip in fasteners of connections carry for a significant reduction in lateral stiffness. Static deformations increase by 27 percent to 115 millimetres, whilst horizontal accelerations nearly double to 0.102 m/s^2 .

8.4 FUTURE RESEARCH

The dynamic analysis consisted of multiple computations of the fundamental frequency and dynamic response. However, the excitations only comprised a time varying wind load given by the wind spectrum of EC1. The deduced wind profile contained a wind fluctuation of approximately 1.75 m/s^2 . This may be accurate for certain geographic locations but for other it may underestimate the dynamic effects of the loading on a structure.

One of the most remarkable conclusions of the research is the large effects of the connections on the structural behaviour under lateral wind loading. It is of large interest on both the structural behaviour and cost efficiency to optimise the design of these connections between structural elements.

A research area not taken into account in the project is effects of load duration and appearances like shrinkage of different materials. The application of two materials, i.e. CLT and glulam, might lead to differential settlements of the structure. Although it is not expected to cause significant problems for low-rise construction cumulative effects for tall buildings may be worthwhile investigating.

The following topics on structural design for tall timber buildings are recommended to adopt for research:

- Structural behaviour of other stability systems, such as; a CLT tube structure or glulam frame with large diagonals – a so-called superstructure;
- Taller buildings, where is the limit? The appendix of Chapter 3 has given a glance of static displacements of a 30 storey building, where it was questioned if the required dimensions of structural elements to resist lateral wind loading were desired at all. Other stability systems may be more efficient and more beneficial for taller buildings;
- Analysis to asymmetrical design of structures. What are the effects of torsion to the lateral stiffness, natural frequencies and response to dynamic excitations?
- Dynamic response of tall timber buildings due to a true profile of wind loading obtained by meteorological measurements. These accurate fluctuations in wind loading may resemble another behaviour of the structure;
- Dynamic response due to earthquakes;
- Behaviour of dowel-type connections in CLT panels in ULS and SLS;
- Design of connections between glulam members and CLT walls, for instance connection type 9 and 10. In particular cost efficiency should be analysed as well as assembly processes;
- Optimised connections between CLT shear walls. Connection type 1 and 2 has the largest effect on reduced lateral stiffness of the structure, causing additional rotations at the ground floor and thus more horizontal displacements at the top of the building.

9 | REFERENCES

- [1] Boellaard, B. (2011). Design of an Outrigger Structure for Tall Timber Buildings – Literature Research – Master Project 3. Eindhoven University of Technology. The Netherlands.
- [2] Strct (2011). Bouwbesluit 2012.
- [3] Nederlands Normalisatie-instituut. (2002). Eurocode 0. Grondslagen van het constructief ontwerp. NEN-EN 1990.
- [4] Nederlands Normalisatie-instituut. (2002). Eurocode 1-4. Belastingen op constructies. Deel 1-4: Algemene belastingen – Windbelasting. NEN 1991-1-4.
- [5] Nederlands Normalisatie-instituut. (2007). NEN 6702, Technische grondslagen voor bouwconstructies. TGB 1990 – Belastingen en vervormingen.
- [6] Hoenderkamp, H. (2007). High-Rise Structures – Preliminary Design for Lateral Load – Second Edition. Department of Architecture, Building and Planning. Eindhoven University of Technology, the Netherlands.
- [7] Blaß, H. & Fellmoser, P. (2004). Design of Solid Wood Panels with Cross Layers. Proceedings of the 8th World Conference on Timber Engineering, Volume II, Lahti, Finland.
- [8] Khan, A. & Stafford Smith, B. (1976). A Simple Method of Analysis for Deflection and Stresses in Wall-frame Structures. Building and Environment, Vol.11, pp.69-78. Pergamon Press. UK.
- [9] Hoenderkamp, H. & Bakker, M. (2003). Analysis of High-rise Braced Frames with Outriggers. The Structural Design of Tall and Special Buildings, 12, 335-350. Wiley Interscience.
- [10] Nederlands Normalisatie-instituut. (2005). Eurocode 5. Ontwerp en berekeningen van houtconstructies. NEN 1995-1.
- [11] Nederlands Normalisatie-instituut. (2002). Eurocode 1-1. Belastingen op constructies. Deel 1-1: Algemene belastingen – Volumieke gewichten, eigen gewicht en opgelegde belastingen voor gebouwen. NEN 1991-1-1.

- [12] Stafford Smith, B. & Coull, A. (1991). Tall Building Structures: Analysis and Design. John Wiley & Sons Inc. US.
- [13] Karnovsky, I. & Lebed, O. (2001). Formulas for structural dynamics. The McGraw-Hill Companies, Inc. US. ISBN. 0-07-136712-8.
- [14] Ken Chung, Y. (2010). Optimization of Outrigger Locations for Tall Buildings Subjected to Wind Loads. Master Thesis. Department of Civil and Environmental Engineering. The University of Melbourne. Australia.
- [15] Oosterhout van, G. (1996). Wind-induced Dynamic Behaviour of Tall Buildings. Technische Universiteit Delft. ISBN. 90-9009703-1.
- [16] Meer, van der, L. (2008). Dynamic response of high-rise building structures to blast loading. Master Thesis. Department of Architecture, Building and Planning. Eindhoven University of Technology, the Netherlands.
- [17] Han, S. & Benaroya, H & Wei, T. (1999). Dynamics of Transversely Vibrating Beams Using Four Engineering Theories. Journal of Sound and Vibration 225(5), 935-988.
- [18] Davenport, A. (1976). Gust Loading Factors. Journal of the Structural Division (ASCE), 93 (1976) (ST3).
- [19] Vrouwenvelder, A. & Geurts, C. (2006). Dynamica, windbelasting en voorschriften. Cement 1, 2006, pp 20-24. The Netherlands.
- [20] Geurts, C. (1997). Wind-induced Pressure Fluctuations on Building Facades. PhD Thesis. Unit Structural Design, Eindhoven University of Technology, the Netherlands. ISBN 90-6814-545-2.
- [21] Clough, R. & Penzien, J. (1993). Dynamics of structures. 2nd edition. The McGraw-Hill Companies, Inc. US. ISBN. 0-07-011394-7.
- [22] Sircovich-Saar, O. (2006). Dynamics in the Practice of Structural Design. WIT Press. UK. ISBN. 1-84564-161-2.
- [23] Blevins, R. (1979). Formulas for natural frequency and mode shape. Van Nostrand Reinhold Company, Inc. US. ISBN. 0-89464-830-6.
- [24] Mestek, P. & Winter, S. (2010). Berechnung und Bemessung von Brettsper Holz - Ein Überblick. Fachtagung Holzbau, Leinfelden, Germany.
- [25] Thelandersson, S. & Larsen, H.J. (2003). Timber Engineering. John Wiley & Sons Ltd. England. ISBN. 0-470-84469-8.
- [26] Deam, B. & King, A. (1994). The Seismic Behaviour of Timber Structures, State-of-the-art. Proceedings of Pacific Timber Engineering Conference, Gold Coast, Australia, Vol. 1, p.215.
- [27] Popovski, M. *et al* (1998). Earthquake Resistance of Braced Timber Frames. Recent Advances in Understanding Full – Scale Behaviour of Wood Buildings. Forest Products Society, Madison, WI.
- [28] Porteous, J. & Kermani, A. (2007). Structural Timber Design to Eurocode 5. Blackwell Publishing Ltd. UK. ISBN. 978-14051-4638-8.

- [29] Nederlands Normalisatie-instituut. (2008). NEN 6760, Technische grondslagen voor bouwconstructies. TGB 1990 – Houtconstructies – Basiseisen en bepalingsmethoden.
- [30] Uibel, T. & Blass, H. (2006). Load Carrying Capacity of Joints with Dowel Type Fasteners in Solid Wood Panels. International Council for Research and Innovation in Building and Construction. Florence, Italy.
- [31] Uibel, T. & Blass, H. (2007). Edge Joints with Dowel Type Fasteners in Cross Laminated Timber. International Council for Research and Innovation in Building and Construction. Bled, Slovenia.
- [32] Madsen, B. (2000). Behaviour of Timber Connections. 1st edition. Timber Engineering Ltd. Canada. ISBN. 1-55056-738-1.
- [33] Riberholt, H. (1986). Glued Bolts in Glulam. Report No. 210, Technical University Denmark, Department of Structural Engineering, Lyngby, Denmark.
- [34] Gustafsson, P. & Serrano, E. (2000). A Strength Design Equation for Glued-in Rods. Rilem Proceedings Pro 22, Joints in Timber Structures. Rilem Publications s.a.r.l. France.

A.1 | WIND ACTIONS – EUROCODE 1

PEAK WIND PRESSURE

Peak wind pressure with a return period of 50 years is evaluated by

$$q_p(z) = (1 + 2gI_v(z)) \frac{\rho}{2} v_m^2 \quad (\text{A.1.1})$$

where v_m is the mean wind value on a height z above the terrain and can be evaluated by

$$v_m(z) = c_r(z) c_0(z) v_b \quad (\text{A.1.2})$$

The terrain roughness factor $c_r(z)$ is as follows

$$c_r(z) = k_r \ln\left(\frac{z}{z_0}\right) \quad (\text{A.1.3})$$

The terrain factor, k_r , can be obtained by

$$k_r = 0.19 \left(\frac{z_0}{0.05}\right)^{0.07} \quad (\text{A.1.4})$$

where z_0 is a measurement of the terrain roughness and equals 0.5 for an urban area. Resulting in

$$k_r = 0.19 \left(\frac{0.5}{0.05}\right)^{0.07} = 0.22$$

The factor $c_0(z)$ takes the terrain orography into account. In this case it is a unit value. The basic wind speed v_b can be calculated as

$$v_b = v_{b,0} c_{dir} c_{season} c_{prob} \quad (\text{A.1.5})$$

in which $v_{b,0}$ is the extreme 10 minutes mean wind speed with a return period of 50 years at 10 meters above ground level and is a dependant on the wind area. The city of Amsterdam has been chosen as location for the project, thus wind area II applies.

$$v_{b,0} = 27.0 \text{ m/s}$$

The factor c_{dir} and c_{season} takes the wind direction and wind season respectively into account and both has a unit value. The probability of exceeding the basic wind speed, calculated by c_{prob} , should only be taken into account when the return period differs from 50 years, thus for preliminary design

$$v_b = v_{b,0} = 27.0 \text{ m/s}$$

The turbulence intensity $I_v(z)$ expresses the ratio between the mean value and standard deviation of the wind speed and is given by

$$I_v(z) = \frac{k_1}{c_0(z) \ln(z/z_0)} \quad (\text{A.1.6})$$

where k_1 is the turbulence factor and equals 1. Remaining values are: air density, $\rho = 1.25 \text{ kg/m}^3$ and the peak factor g , which is equal to 3.5.

The distribution of peak wind pressure values over the height of the building depends on the building's shape. Since $h > 2b$ [i.e. $67.2 > (2 \cdot 27 = 54)$] a distribution according to Figure A.1.1 applies.

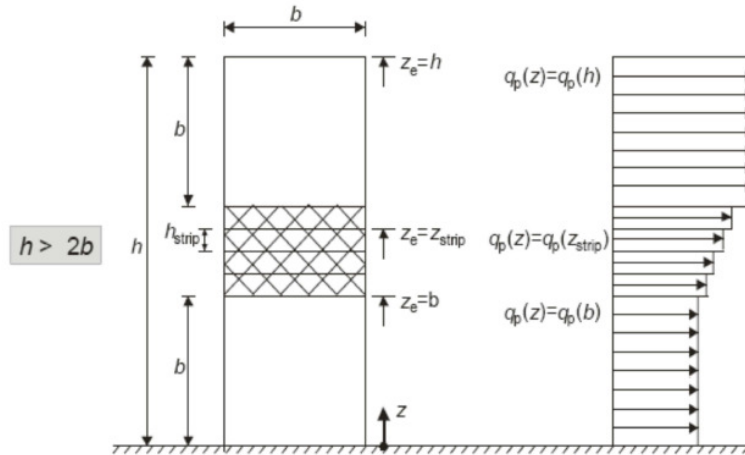


Figure A.1.1; Distribution of peak wind pressure values over the height of the building

Table A.1.1 presents the peak wind pressure values, $q_p(z)$ subjected to the building's façade.

Table A.1.1; Peak wind pressure values

Reference height, z_e [m]	Terrain roughness factor $c_r(z)$	Mean wind speed [m/s]	Turbulence intensity $I_v(z)$	Peak wind pressure [kN/m ²]
27	0.88	23.69	0.25	0.97
67.2	1.08	29.11	0.20	1.29

BUILDING SHAPE FACTOR

Fluctuating effects around a building are taken into account by a shape factor, $c_s c_d$, where c_s is a factor accounting for the peak wind load not acting uniformly over the entire building façade and c_d is a dynamic factor taking into account the increasing effect of horizontal accelerations in resonance with the structure. The shape factor, $c_s c_d$ can be evaluated by

$$c_s c_d = \frac{1 + 2k_p I_v(z_s) \sqrt{B^2 + R^2}}{1 + 7I_v(z_s)} \quad (\text{A.1.7})$$

where z_s is a reference height which is equal to $0.6 \cdot H = 0.6 \cdot 67.2 = 40.3$ meter.

The peak factor k_p is the ratio between the maximum value of the fluctuating response and the standard deviation and is calculated as follows

$$k_p = \sqrt{2 \ln(vT)} + \frac{0.6}{\sqrt{2 \ln(vT)}} \geq 3 \quad (\text{A.1.8})$$

where T is the duration of the 10 minute reference storm, i.e. T=600 sec. and v is the frequency of the wind gust as follows

$$v = n_1 \sqrt{\frac{R^2}{B^2 + R^2}} \geq 0.08 \text{Hz} \quad (\text{A.1.9})$$

The fundamental frequency, n_1 , can be estimated by

$$n_1 \approx \frac{46}{H} \quad (\text{A.1.10})$$

$$n_1 \approx \frac{46}{67.2} \approx 0.68$$

The background response factor, B^2 , takes into account the incomplete correlation of the wind pressure on the façade of the building and can be calculated as follows

$$B^2 = \frac{1}{1 + 1.5 \sqrt{\left(\frac{b}{L(z_s)}\right)^2 + \left(\frac{H}{L(z_s)}\right)^2 + \left(\frac{b}{L(z_s)} \frac{H}{L(z_s)}\right)^2}} \quad (\text{A.1.11})$$

where b is the width of the building and $L(z_s)$ describes the average size of the wind gust

$$L(z_s) = L_t \left(\frac{z_s}{z_t}\right)^\alpha \quad (\text{A.1.12})$$

in which z_t is a reference height of 200 meter and L_t is a reference length of 300 meter.

$$\alpha = 0.67 + 0.05 \ln(z_0) \quad (\text{A.1.13})$$

$$\alpha = 0.67 + 0.05 \ln(0.5) = 0.64$$

$$L(z_s) = 300 \left(\frac{40.3}{200}\right)^{0.64} = 107.61$$

$$B^2 = \frac{1}{1 + 1.5 \sqrt{\left(\frac{27}{107.61}\right)^2 + \left(\frac{67.2}{107.61}\right)^2 + \left(\frac{27}{107.61} \frac{67.2}{107.61}\right)^2}} = 0.49$$

The resonance response factor, R^2 , takes into account the affects of the turbulence in resonance with the mode shape of the building. The value can be evaluated as follows

$$R^2 = \frac{\pi^2}{2.8} S_L(z_s, n_{1,x}) K_s(n_{1,x}) \quad (\text{A.1.14})$$

where δ is the logarithmic decrement of the damping and comprises two components

$$\delta = \delta_s + \delta_a \quad (\text{A.1.15})$$

where $\delta_s \approx 0.10$, which describes the damping of the structure and is an estimation for multi-storey timber buildings. The latter is aerodynamic damping and can be calculated as follows

$$\delta_a = \frac{c_f \rho v_m(z_s)}{2n_1 \mu_e} \quad (\text{A.1.16})$$

where the mass per unit area of the building μ_e can be estimated as follows

$$\mu_e = \rho_b d \quad (\text{A.1.17})$$

in which ρ_b is the volumetric mass of the building in kg/m^3 and estimated as 90 kg/m^3 for multi-storey timber buildings. Subsequently, the mass per unit area results in $\mu_e = 90 \cdot 27 = 2430 \text{ kg/m}^2$.

The mean wind speed, v_m , on the reference height, z_s , i.e. 40.3 meter is 26.07 m/s. The evaluation of the wind force coefficient, c_f , is shown in the following section. The aerodynamic damping will be

$$\delta_a = \frac{1.37 \cdot 1.25 \cdot 26.07}{2 \cdot 0.68 \cdot 2430} = 0.014$$

The total damping of the building is $\delta = 0.10 + 0.014 = 0.114$

The non-dimensional spectral density function $S_L(z_s, n_1)$ describes the distribution of the wind speed over the frequencies and is given by

$$S_L(z_s, n_1) = \frac{6.8 f_L(z_s, n_1)}{(1 + 10.2 f_L(z_s, n_1))^{5/3}} \quad (\text{A.1.18})$$

where a non-dimensional frequency $f_L(z_s, n_1)$ is calculated as follows

$$f_L(z_s, n_1) = \frac{n_1 L(z_s)}{v_m(z_s)} \quad (\text{A.1.19})$$

which results in

$$f_L(z_s, n_1) = \frac{0.68 \cdot 107.61}{26.07} = 2.81$$

$$S_L(z_s, n_1) = \frac{6.8 \cdot 2.81}{(1 + 10.2 \cdot 2.81)^{5/3}} = 0.067$$

The size reduction factor, $K_s(n_{1,x})$ can be approximated as follows

$$K_s(n_1) = \frac{1}{1 + \sqrt{(G_x \phi_x)^2 + (G_z \phi_z)^2 + \left(\frac{2}{\pi} G_x \phi_x G_z \phi_z\right)^2}} \quad (\text{A.1.20})$$

where the constants G_x and G_z are a dependant of vibration mode variances along the vertical x-ax and the horizontal z-ax respectively. For tall buildings the vibration mode in the x-direction (height) may be assumed as parabolic and in the z-direction (width) as uniformity, resulting in $G_x = 5/18$ and $G_z = 1/2$.

$$\phi_x = \frac{11.5bn}{v_m(z_s)}; \phi_z = \frac{11.5hn}{v_m(z_s)} \quad (\text{A.1.21})$$

$$\phi_x = \frac{11.5 \cdot 27 \cdot 0.68}{26.07} = 8.10; \phi_z = \frac{11.5 \cdot 67.2 \cdot 0.68}{26.07} = 20.16$$

$$K_s(n_1) = \frac{1}{1 + \sqrt{\left(\frac{5}{18} \cdot 8.10\right)^2 + (0.5 \cdot 20.16)^2 + \left(\frac{2}{\pi} \frac{5}{18} \cdot 8.10 \cdot 0.5 \cdot 20.16\right)^2}} = 0.053$$

All values required for the resonance factor, i.e. R^2 , are now known

$$R^2 = \frac{\pi^2}{2 \cdot 0.114} \cdot 0.067 \cdot 0.053 = 0.154$$

Subsequently, the frequency of the wind gust, v , is

$$v = 0.68 \sqrt{\frac{0.154}{0.49 + 0.154}} = 0.33 \text{Hz}$$

and the peak factor

$$k_p = \sqrt{2 \ln(0.33 \cdot 600)} + \frac{0.6}{\sqrt{2 \ln(0.33 \cdot 600)}} = 3.437$$

The turbulence intensity at reference height, z_s , is

$$I_v(z_s) = \frac{1}{\ln(40.3/0.5)} = 0.228$$

The shape factor can now be evaluated

$$c_{s,c_d} = \frac{1 + 2 \cdot 3.437 \cdot 0.228 \sqrt{0.49 + 0.154}}{1 + 7 \cdot 0.228} = 0.870$$

WIND FORCE COEFFICIENT

The force coefficient, c_f is a function of the building's slenderness, i.e. H/d . For $H/d=5$, $c_f = 1.5$ and for $H/d=1$, $c_f = 1.3$. For intermediate ratios interpolation is allowed. These values take both the wind

pressure on the windward side and the wind suction on the leeward side of the building into account. Furthermore, wind friction on the building is also incorporated by the force coefficient. For the related building the slenderness is

$$\frac{H}{d} = \frac{67.2}{27} = 2.49$$

The corresponding force coefficient results in

$$c_f = \left[\left(\frac{1.5-1.3}{4} \right) \cdot (2.49-1) \right] + 1.3 = 1.37$$

CHARACTERISTIC VALUE OF WIND LOAD

In the preliminary design phase it is desired to adopt, for the sake of simplicity, a uniformly distributed wind load along the height of the building. Therefore the largest value of the peak wind pressure over the building's façade, i.e. $q_p(67.2)$, will be implemented to determine the characteristic wind load. The characteristic load for wind subjected on the structure can be calculated as follows

$$w_{e,\text{total}} = c_s c_d c_f q_p(z_e) \tag{A.1.22}$$

where $c_s c_d = 0.87$

$$c_f = 1.37$$

$$q_p(z_e) = q_p(67.2) = 1.29 \text{ kN/m}^2$$

$$w_{e,\text{total}} = 0.87 \cdot 1.37 \cdot 1.29 = \mathbf{1.54 \text{ kN / m}^2}$$

A.2 | PRELIMINARY STATIC CALCULATIONS

Calculation Sheet 2.1:	<i>Structural calculations tube structure</i>
Calculation Sheet 2.2:	<i>Structural calculations CLT shear wall structure</i>
Calculation Sheet 2.3:	<i>Structural calculations outrigger structure</i>
Calculation Sheet 2.3a:	<i>Structural calculations outrigger structure – modified CLT panel thickness</i>
Calculation Sheet 2.3b:	<i>Structural calculations outrigger structure – modified beam and diagonal properties</i>
Calculation Sheet 2.3c:	<i>Structural calculations outrigger structure – modified column properties</i>
Calculation Sheet 2.3d:	<i>Structural calculations outrigger structure – modified outrigger design</i>
Calculation Sheet 2.4:	<i>Structural calculations outrigger structure – 30 storeys</i>

Calculation sheet No. 2.1					
Title:		Structural calculations CLT tube structure			
Design phase:	Preliminary design				
Design state:	SLS + ULS				
References:	Table 3.2				
CLT panel properties					
Thickness; d	300	mm	Build-up	80-30-80-30-80 mm	
$E_{0,g,mean}$	1,20E+07	kN/m ²	$E_{90,g,mean}$	3,70E+05	kN/m ²
$G_{g,mean}$	5,50E+05	kN/m ²			
a_1	240	mm	a_2	60	mm
k_3	$1 - \left(1 - \frac{E_{90,g,mean}}{E_{0,g,mean}} \right) \cdot \frac{a_2}{d} = \mathbf{0,806}$				
Tube properties					
Dimensions	l	b	d		
	27,0	27,0	0,3	m	
I_{tube}	3.807,31	m ⁴	$I_{ef,tube} = I_{tube} \cdot k_3$	=	3.069,33 m ⁴
A_{tube}	32,04	m ²	$A_{ef,tube} = A_{tube} \cdot k_3$	=	25,83 m ²
$A_{tube,shear} = 2 \cdot l \cdot d$	16,20	m ²			
Openings	H	h	B	b	
	1,6	0,8	1,1	0,4	m
	H/B	h/H	b/B		
	1,45	0,50	0,36		
E'/E	0,4	-	E'	4.800.000	kN/m ²
G'/G	0,15	-	G'	82.500	kN/m ²
Normal stress factor	3,25	-			
Shear stress factor	4,25	-			
$(E'I)_{ef,tube}$	1,473E+10	kNm ²			
$(G'A)_{tube,shear}$	1,337E+06	kN			
Building properties			Wind loads		
Building height; H	67,2	m	Characteristic wind load SLS; $w_{e,total}$	41,58	kN/m
			Design wind load ULS; $w_{e,total,d}$	62,37	kN/m
ULS: Lateral actions on tube					
Shear force; $V_{sh,t,d}$	$w_{e,total,d} \cdot H = 4191,3$ kN				
Shear stress; τ_d	$\frac{V_{sh,t,d}}{A_{tube,shear}} \cdot 4,25 = 1,10$ MPa.				
Moment; $M_{b,t,d}$	$\frac{1}{2} \cdot w_{e,total,d} \cdot H^2 = 140826,5$ kNm				
$\sigma_{n,b,d}$	$\frac{M_{b,t,d} \cdot (l/2)}{I_{ef,tube}} \cdot 3,25 = 2,01$ MPa.				
ULS: Vertical actions on tube					Total stresses
Floor area	405	m ²	Storeys	20	-
Design load, q_d	10	kN/m ²	E_d	81.000	kN
$\sigma_{n,q,d}$	$\frac{E_d}{A_{ef,tube}} \cdot 3,25 = 3,14$ MPa.				
				$\sigma_{n,max,d}$	5,15 MPa.
				$\sigma_{n,min,d}$	1,12 MPa.

SLS: Top displacements

$U_{top,b}$	$\frac{w_{e,total} \cdot H^4}{8 \cdot (E'I)_{ef,tube}}$	=	0,0072	m
$U_{top,rs}$	$\frac{w_{e,total} \cdot H^2}{2 \cdot (G'A)_{ef,tube,shear}}$	=	0,0702	m
$U_{top,max}$	$U_{top,b} + U_{top,rs}$	=	0,0774	m

Calculation sheet No. 2.2			
Title:	Structural calculations CLT shear wall structure		
Design phase:	Preliminary design		
Design state:	SLS + ULS		
References:	Table 3.3		
CLT panel properties			
Thickness; d	300 mm	Build-up	80-30-80-30-80 mm
$E_{0,g,mean}$	1,20E+07 kN/m ²	$E_{90,g,mean}$	3,70E+05 kN/m ²
$G_{g,mean}$	5,50E+05 kN/m ²		
a_1	240 mm	a_2	60 mm
k_3	$1 - \left(1 - \frac{E_{90,g,mean}}{E_{0,g,mean}} \right) \cdot \frac{a_2}{d} = \mathbf{0,806}$		
Core properties			
Dimensions	l	b	d
	9,0	9,0	0,3 m
I_{core}	131,86	m ⁴	$I_{ef,core} = I_{core} \cdot k_3 = 106,30 \text{ m}^4$
A_{core}	10,44	m ²	$A_{ef,core} = A_{core} \cdot k_3 = 8,42 \text{ m}^2$
$A_{core,shear} = 2 \cdot l \cdot d$	5,40	m ²	
$(EI)_{ef,core}$	1,276E+09	kNm ²	
$(GA)_{core,shear}$	2,970E+06	kN	
Shear wall properties			
Dimensions	l	d	
	7,6	0,3	m
I_{sw}	10,97	m ⁴	$I_{ef,sw} = I_{sw} \cdot k_3 = 8,85 \text{ m}^4$
A_{sw}	2,28	m ²	
$(EI)_{ef,sw}$	1,062E+08	kNm ²	
$(GA)_{sw}$	1,254E+06	kN	
Total stiffness properties			
$(EI)_{ef,total}$	$(EI)_{ef,core} + 2 \cdot (EI)_{ef,sw} = \mathbf{1,488E+09} \text{ kNm}^2$		
$(GA)_{total}$	$(GA)_{core,shear} + 2 \cdot (GA)_{sw} = \mathbf{5,478E+06} \text{ kN}$		
Building properties		Wind loads	
Building height; H	67,2 m	Characteristic wind load SLS; $w_{e,total}$	41,58 kN/m
		Design wind load ULS; $w_{e,total,d}$	62,37 kN/m
ULS: Lateral actions			
$\alpha_{b,c} = (EI)_{ef,core} / (EI)_{ef,total}$	0,86	-	$\alpha_{rs,c} = (GA)_{core,shear} / (GA)_{total}$ 0,54 -
$\alpha_{b,sw} = (EI)_{ef,sw} / (EI)_{ef,total}$	0,07	-	$\alpha_{rs,sw} = (GA)_{sw} / (GA)_{total}$ 0,23 -
$M_{b,c,d}$	$\frac{1}{2} \cdot w_{e,total,d} \cdot H^2 \cdot \alpha_{b,c} = 120729,9 \text{ kNm}$		
$\sigma_{n,b,c,d}$	$\frac{M_{b,c,d} \cdot (l/2)}{I_{ef,core}} = 5,11 \text{ MPa.}$		
$M_{b,sw,d}$	$\frac{1}{2} \cdot w_{e,total,d} \cdot H^2 \cdot \alpha_{b,sw} = 10048,3 \text{ kNm}$		
$\sigma_{n,b,sw,d}$	$\frac{M_{b,sw,d} \cdot (l/2)}{I_{ef,sw}} = 4,32 \text{ MPa.}$		
$V_{sh,c,d} = w_{e,total,d} \cdot H \cdot \alpha_{rs,c}$	2272,4	kN	$V_{sh,sw,d} = w_{e,total,d} \cdot H \cdot \alpha_{rs,sw}$ 959,4 kN
$\tau_{c,d} = V_{sh,c,d} / A_{core,shear}$	0,42	MPa.	$\tau_{sw,d} = V_{sh,sw,d} / A_{sw}$ 0,42 MPa.

ULS: Vertical actions on core						Total stresses on core		
Floor area	243	m ²	Storeys	20	-	$\sigma_{n,max,c,d}$	10,89	MPa.
Design load	10	kN/m ²	E_d	48600	kN	$\sigma_{n,min,c,d}$	0,66	MPa.
$\sigma_{n,q,d}$	$\frac{E_d}{A_{ef,core}} = 5,77$ MPa.							
ULS: Vertical actions on shear wall						Total stresses on shear wall		
Floor area	21	m ²	Storeys	20	-	$\sigma_{n,max,c,d}$	6,16	MPa.
Design load, q_d	10	kN/m ²	E_d	4200	kN	$\sigma_{n,min,c,d}$	-2,47	MPa.
$\sigma_{n,q,d}$	$\frac{E_d}{A_{ef,sw}} = 1,84$ MPa.							
SLS: Top displacements								
$U_{top,b}$	$\frac{w_{e,total} \cdot H^4}{8 \cdot (EI)_{ef,total}} = 0,0712$ m							
$U_{top,rs}$	$\frac{w_{e,total} \cdot H^2}{2 \cdot (GA)_{total}} = 0,0171$ m							
$U_{top,max}$	$U_{top,b} + U_{top,rs} = \mathbf{0,0884}$ m							

Calculation sheet No. 2.3			
Title:	Structural calculations outrigger structure		
Design phase:	Preliminary design		
Design state:	SLS + ULS		
References:	Table 3.4		
CLT panel properties			
Thickness; d	300 mm	Build-up	80-30-80-30-80 mm
$E_{0,g,mean}$	1,20E+07 kN/m ²	$E_{90,g,mean}$	3,70E+05 kN/m ²
$G_{g,mean}$	5,50E+05 kN/m ²		
a_1	240 mm	a_2	60 mm
k_3	$1 - \left(1 - \frac{E_{90,g,mean}}{E_{0,g,mean}} \right) \cdot \frac{a_2}{d} = \mathbf{0,806}$		
Core properties			
Dimensions	l	b	d
	9,0	9,0	0,3 m
I_{core}	131,86	m ⁴	$I_{ef,core} = I_{core} \cdot k_3 = 106,30 \text{ m}^4$
A_{core}	10,44	m ²	$A_{ef,core} = A_{core} \cdot k_3 = 8,42 \text{ m}^2$
$A_{core,shear} = 2 \cdot l \cdot d$	5,4	m ²	
$(EI)_{ef,core}$	1,276E+09	kNm ²	
$(GA)_{core,shear}$	2,970E+06	kN	
Column properties		Beam properties	
$E_{0,g,mean}$	1,26E+07 kN/m ²	$E_{0,g,mean}$	1,26E+07 kN/m ²
Dimensions	b	d	l*
	0,6	0,6	13,5 m
$(EI)_{ec} = 2 \cdot E_{0,g,mean} \cdot A_b \cdot l^{*2}$	1,653E+09	kNm ²	
Outrigger properties			
$E_{0,g,mean}$	1,26E+07 kN/m ²		
Dimensions	No. Bays	l	h
	2	9,0	6,4
			11,0 m
$(EI)_{out}$	$\frac{E_{0,g,mean} \cdot A_b \cdot h^2}{2} =$		5,161E+07 kNm ²
$(GA)_{out}$	$\frac{2 \cdot 2 \cdot l^2 h E_{0,g,mean} A_d}{d^3} =$		3,880E+06 kN
Optimum height outriggers			
Structural parameters	$\alpha = l^*/l$	H	$S_v = \frac{H}{(EI)_{ef,core}} + \frac{H}{2 \cdot (EI)_{ec}} = 7,30E-08$
	1,5	67,2	
$\omega = S_h / S_v$	0,46	-	$S_h = \frac{1}{\alpha^2} \left\{ \frac{l}{24 \cdot 2 \cdot (EI)_{out}} + \frac{1}{h \cdot 2 \cdot (GA)_{out}} + \frac{1}{h \cdot (GA)_{core,shear}} \right\} = 3,39E-08$
x / H	0,42	-	
Optimum height; x	28,2	m	
Outrigger height; x_0	29,05	m	$\beta H = H \sqrt{\frac{\alpha (GA)_{core,shear}}{(EI)_{ef,core}}} = 3,97$
Lateral loading		Wind loads	
Building height; H	67,2 m	Characteristic wind load SLS; $w_{e,total}$	41,58 kN/m
Building dept; D	27,0 m	Design wind load ULS; $w_{e,total,d}$	62,37 kN/m

SLS: Outrigger resistance									
Restraining moment; M_r	$\left\{ \frac{w_{e,total} (H^3 - x_0^3)}{6(EI)_{ef,core}} + \frac{w_{e,total} \cdot x_0}{\alpha(GA)_{core,shear}} \right\} \frac{H}{(H-x_0)S_v + HS_h} = 23697,8 \text{ kNm}$								
ULS: Outrigger resistance									
Restraining moment; M_r	$\left\{ \frac{w_{e,total,d} (H^3 - x_0^3)}{6(EI)_{ef,core}} + \frac{w_{e,total,d} \cdot x_0}{\alpha(GA)_{core,shear}} \right\} \frac{H}{(H-x_0)S_v + HS_h} = 35546,7 \text{ kNm}$								
ULS: Lateral actions on core									
Moment due to wind; $M_{b,d}$	$\frac{1}{2} \cdot w_{e,total,d} \cdot H^2 = 140826,5 \text{ kNm}$								
Moment on core; $M_{b,c,d}$	$M_{b,d} - M_r = 105279,7 \text{ kNm}$								
Normal stress; $\sigma_{n,b,c,d}$	$\frac{M_{b,c,d} \cdot (l/2)}{I_{ef,core}} = 4,46 \text{ MPa.}$								
Shear force; $V_{sh,c,d}$	$w_{e,total,d} \cdot H = 4191,3 \text{ kN}$								
Shear stress; $T_{c,d}$	$\frac{V_{sh,c,d}}{A_{core,shear}} = 0,78 \text{ MPa.}$								
ULS: Vertical actions on core							Total stresses on core		
Floor area	324	m^2	Storeys	20	-	$\sigma_{n,max,c,d}$	12,16	MPa.	
Design load, q_d	10	kN/m^2	E_d	64800,0	kN	$\sigma_{n,min,c,d}$	3,24	MPa.	
Normal stress; $\sigma_{n,q,d}$	$\frac{E_d}{A_{ef,core}} = 7,70 \text{ MPa.}$								
ULS: Vertical actions on column							Total stresses on column		
Floor area	20,25	m^2	Storeys	20	-	$\sigma_{c,max,d}$	14,91	MPa.	
Design load	10	kN/m^2	E_d	4050,0	kN	$\sigma_{c,min,d}$	7,59	MPa.	
Compressive stress; $\sigma_{c,q,d}$	$\frac{E_d}{A_c} = 11,25 \text{ MPa.}$								
Axial force (wind); $F_{c,d}$	$\frac{M_r}{D} = 1316,5 \text{ kN}$								
Compressive stress; $\sigma_{c,F,d}$	$\frac{F_{c,d}}{A_c} = 3,66 \text{ MPa.}$								
SLS: Top displacements						Reduced deflections			
$U_{top,b}$	$\frac{w_{e,total} \cdot H^4}{8 \cdot (EI)_{ef,core}} = 0,0831 \text{ m}$					Bending:	$\frac{U_{top,b,red}}{U_{top,b}}$	41,0	%
$U_{top,rs}$	$\frac{w_{e,total} \cdot H^2}{2 \cdot (GA)_{core,shear}} = 0,0316 \text{ m}$					Rack. shear:	$\frac{U_{top,rs,red}}{U_{top,rs}}$	16,8	%
$U_{top,b,red}$	$\frac{M_r(H^2 - x_0^2)}{2 \cdot (EI)_{ef,core}} = 0,0341 \text{ m}$					Total:	$\frac{U_{top,b+rs,red}}{U_{top,b+rs}}$	34,4	%
$U_{top,rs,red}$	$\frac{M_r}{\alpha \cdot (GA)_{core,shear}} = 0,0053 \text{ m}$								
$U_{top,max}$	$(U_{top,b} + U_{top,rs}) - (U_{top,b,red} + U_{top,rs,red}) = 0,0753 \text{ m}$								

Calculation sheet No. 2.3a			
Title:	Structural calculations outrigger structure - modified CLT panel thickness		
Design phase:	Preliminary design		
Design state:	SLS + ULS		
References:	Table 3.7		
CLT panel properties			
Thickness; d	410 mm	Build-up	80-30-80-30-80 mm
$E_{0,g,mean}$	1,20E+07 kN/m ²	$E_{90,g,mean}$	3,70E+05 kN/m ²
$G_{g,mean}$	5,50E+05 kN/m ²		
a_1	320 mm	a_2	90 mm
k_3	$1 - \left(1 - \frac{E_{90,g,mean}}{E_{0,g,mean}}\right) \cdot \frac{a_2}{d} = \mathbf{0,787}$		
Core properties			
Dimensions	l	b	d
	9,0	9,0	0,4 m
I_{core}	173,64	m ⁴	$I_{ef,core} = I_{core} \cdot k_3 = 136,70 \text{ m}^4$
A_{core}	14,0876	m ²	$A_{ef,core} = A_{core} \cdot k_3 = 11,09 \text{ m}^2$
$A_{core,shear} = 2 \cdot l \cdot d$	7,38	m ²	
$(EI)_{ef,core}$	1,640E+09	kNm ²	
$(GA)_{core,shear}$	4,059E+06	kN	
Column properties		Beam properties	
$E_{0,g,mean}$	1,26E+07 kN/m ²	$E_{0,g,mean}$	1,26E+07 kN/m ²
Dimensions	b	d	l*
	0,6	0,6	13,5 m
$(EI)_{ec} = 2 \cdot E_{0,g,mean} \cdot A_b \cdot l^{*2}$	1,653E+09	kNm ²	
Outrigger properties			
$E_{0,g,mean}$	1,26E+07 kN/m ²		
Dimensions	No. Bays	l	h
	2	9,0	6,4
			11,0 m
$(EI)_{out}$	$\frac{E_{0,g,mean} \cdot A_b \cdot h^2}{2} =$		5,161E+07 kNm ²
$(GA)_{out}$	$\frac{2 \cdot 2 \cdot l^2 h E_{0,g,mean} A_d}{d^3} =$		3,880E+06 kN
Optimum height outriggers			
Structural parameters	$\alpha = l^*/l$	H	$S_v = \frac{H}{(EI)_{ef,core}} + \frac{H}{2 \cdot (EI)_{ec}} = 6,13E-08$
	1,5	67,2	
$\omega = S_h / S_v$	0,45	-	$S_h = \frac{1}{\alpha^2} \left\{ \frac{l}{24 \cdot 2 \cdot (EI)_{out}} + \frac{1}{h \cdot 2 \cdot (GA)_{out}} + \frac{1}{h \cdot (GA)_{core,shear}} \right\} = 2,77E-08$
x / H	0,42	-	
Optimum height; x	28,2	m	
Outrigger height; x_0	29,05	m	$\beta H = H \sqrt{\frac{\alpha (GA)_{core,shear}}{(EI)_{ef,core}}} = 4,09$
Lateral loading		Wind loads	
Building height; H	67,2 m	Characteristic wind load SLS; $w_{e,total}$	41,58 kN/m
Building dept; D	27,0 m	Design wind load ULS; $w_{e,total,d}$	62,37 kN/m

SLS: Outrigger resistance									
Restraining moment; M_r	$\left\{ \frac{w_{e,total} (H^3 - x_0^3)}{6(EI)_{ef,core}} + \frac{w_{e,total} \cdot x_0}{\alpha(GA)_{core, shear}} \right\} \frac{H}{(H-x_0)S_v + HS_h} = 22040,9 \text{ kNm}$								
ULS: Outrigger resistance									
Restraining moment; M_r	$\left\{ \frac{w_{e,total,d} (H^3 - x_0^3)}{6(EI)_{ef,core}} + \frac{w_{e,total,d} \cdot x_0}{\alpha(GA)_{core, shear}} \right\} \frac{H}{(H-x_0)S_v + HS_h} = 33061,3 \text{ kNm}$								
ULS: Lateral actions on core									
Moment due to wind; $M_{b,d}$	$\frac{1}{2} \cdot w_{e,total,d} \cdot H^2 = 140826,5 \text{ kNm}$								
Moment on core; $M_{b,c,d}$	$M_{b,d} - M_r = 107765,2 \text{ kNm}$								
Normal stress; $\sigma_{n,b,c,d}$	$\frac{M_{b,c,d} \cdot (l/2)}{I_{ef,core}} = 3,55 \text{ MPa.}$								
Shear force; $V_{sh,c,d}$	$w_{e,total,d} \cdot H = 4191,3 \text{ kN}$								
Shear stress; $T_{c,d}$	$\frac{V_{sh,c,d}}{A_{core, shear}} = 0,57 \text{ MPa.}$								
ULS: Vertical actions on core							Total stresses on core		
Floor area	324	m^2	Storeys	20	-	$\sigma_{n,max,c,d}$	9,39	MPa.	
Design load, q_d	10	kN/m^2	E_d	64800,0	kN	$\sigma_{n,min,c,d}$	2,30	MPa.	
Normal stress; $\sigma_{n,q,d}$	$\frac{E_d}{A_{ef,core}} = 5,84 \text{ MPa.}$								
ULS: Vertical actions on column							Total stresses on column		
Floor area	20,25	m^2	Storeys	20	-	$\sigma_{c,max,d}$	14,65	MPa.	
Design load	10	kN/m^2	E_d	4050,0	kN	$\sigma_{c,min,d}$	7,85	MPa.	
Compressive stress; $\sigma_{c,q,d}$	$\frac{E_d}{A_c} = 11,25 \text{ MPa.}$								
Axial force (wind); $F_{c,d}$	$\frac{M_r}{D} = 1224,5 \text{ kN}$								
Compressive stress; $\sigma_{c,F,d}$	$\frac{F_{c,d}}{A_c} = 3,40 \text{ MPa.}$								
SLS: Top displacements						Reduced deflections			
$U_{top,b}$	$\frac{w_{e,total} \cdot H^4}{8 \cdot (EI)_{ef,core}} = 0,0646 \text{ m}$					Bending:	$\frac{U_{top,b,red}}{U_{top,b}}$	38,2	%
$U_{top,rs}$	$\frac{w_{e,total} \cdot H^2}{2 \cdot (GA)_{core, shear}} = 0,0231 \text{ m}$					Rack. shear:	$\frac{U_{top,rs,red}}{U_{top,rs}}$	15,7	%
$U_{top,b,red}$	$\frac{M_r(H^2 - x_0^2)}{2 \cdot (EI)_{ef,core}} = 0,0247 \text{ m}$					Total:	$\frac{U_{top,b+rs,red}}{U_{top,b+rs}}$	32,2	%
$U_{top,rs,red}$	$\frac{M_r}{\alpha \cdot (GA)_{core, shear}} = 0,0036 \text{ m}$								
$U_{top,max}$	$(U_{top,b} + U_{top,rs}) - (U_{top,b,red} + U_{top,rs,red}) = 0,0595 \text{ m}$								

Calculation sheet No. 2.3b			
Title:	Structural calculations outrigger structure - modified beam and diagonal properties		
Design phase:	Preliminary design		
Design state:	SLS + ULS		
References:	Table 3.7		
CLT panel properties			
Thickness; d	300 mm	Build-up	80-30-80-30-80 mm
$E_{0,g,mean}$	1,20E+07 kN/m ²	$E_{90,g,mean}$	3,70E+05 kN/m ²
$G_{g,mean}$	5,50E+05 kN/m ²		
a_1	240 mm	a_2	60 mm
k_3	$1 - \left(1 - \frac{E_{90,g,mean}}{E_{0,g,mean}}\right) \cdot \frac{a_2}{d} = \mathbf{0,806}$		
Core properties			
Dimensions	l	b	d
	9,0	9,0	0,3 m
I_{core}	131,86	m ⁴	$I_{ef,core} = I_{core} \cdot k_3 = 106,30 \text{ m}^4$
A_{core}	10,44	m ²	$A_{ef,core} = A_{core} \cdot k_3 = 8,42 \text{ m}^2$
$A_{core,shear} = 2 \cdot l \cdot d$	5,4	m ²	
$(EI)_{ef,core}$	1,276E+09	kNm ²	
$(GA)_{core,shear}$	2,970E+06	kN	
Column properties		Beam properties	
$E_{0,g,mean}$	1,26E+07 kN/m ²	$E_{0,g,mean}$	1,37E+07 kN/m ²
Dimensions	b	d	l*
	0,6	0,6	13,5 m
$(EI)_{ec} = 2 \cdot E_{0,g,mean} \cdot A_b \cdot l^{*2}$	1,653E+09	kNm ²	
Outrigger properties			
$E_{0,g,mean}$	1,37E+07 kN/m ²		
Dimensions	No. Bays	l	h
	2	9,0	6,4
			11,0 m
$(EI)_{out}$	$\frac{E_{0,g,mean} \cdot A_b \cdot h^2}{2} =$		1,010E+08 kNm ²
$(GA)_{out}$	$\frac{2 \cdot 2 \cdot l^2 h E_{0,g,mean} A_d}{d^3} =$		7,593E+06 kN
Optimum height outriggers			
Structural parameters	$\alpha = l^*/l$	H	$S_v = \frac{H}{(EI)_{ef,core}} + \frac{H}{2 \cdot (EI)_{ec}} = 7,30E-08$
	1,5	67,2	
$\omega = S_h / S_v$	0,39	-	$S_h = \frac{1}{\alpha^2} \left\{ \frac{l}{24 \cdot 2 \cdot (EI)_{out}} + \frac{1}{h \cdot 2 \cdot (GA)_{out}} + \frac{1}{h \cdot (GA)_{core,shear}} \right\} = 2,88E-08$
x / H	0,42	-	
Optimum height; x	28,2	m	
Outrigger height; x_0	29,05	m	$\beta H = H \sqrt{\frac{\alpha(GA)_{core,shear}}{(EI)_{ef,core}}} = 3,97$
Lateral loading		Wind loads	
Building height; H	67,2 m	Characteristic wind load SLS; $w_{e,total}$	41,58 kN/m
Building dept; D	27,0 m	Design wind load ULS; $w_{e,total,d}$	62,37 kN/m

SLS: Outrigger resistance									
Restraining moment; M_r	$\left\{ \frac{w_{e,total} (H^3 - x_0^3)}{6(EI)_{ef,core}} + \frac{w_{e,total} \cdot x_0}{\alpha(GA)_{core, shear}} \right\} \frac{H}{(H-x_0)S_v + HS_h} = 25441,3 \text{ kNm}$								
ULS: Outrigger resistance									
Restraining moment; M_r	$\left\{ \frac{w_{e,total,d} (H^3 - x_0^3)}{6(EI)_{ef,core}} + \frac{w_{e,total,d} \cdot x_0}{\alpha(GA)_{core, shear}} \right\} \frac{H}{(H-x_0)S_v + HS_h} = 38161,9 \text{ kNm}$								
ULS: Lateral actions on core									
Moment due to wind; $M_{b,d}$	$\frac{1}{2} \cdot w_{e,total,d} \cdot H^2 = 140826,5 \text{ kNm}$								
Moment on core; $M_{b,c,d}$	$M_{b,d} - M_r = 102664,5 \text{ kNm}$								
Normal stress; $\sigma_{n,b,c,d}$	$\frac{M_{b,c,d} \cdot (l/2)}{I_{ef,core}} = 4,35 \text{ MPa.}$								
Shear force; $V_{sh,c,d}$	$w_{e,total,d} \cdot H = 4191,3 \text{ kN}$								
Shear stress; $T_{c,d}$	$\frac{V_{sh,c,d}}{A_{core, shear}} = 0,78 \text{ MPa.}$								
ULS: Vertical actions on core							Total stresses on core		
Floor area	324	m^2	Storeys	20	-	$\sigma_{n,max,c,d}$	12,05	MPa.	
Design load, q_d	10	kN/m^2	E_d	64800,0	kN	$\sigma_{n,min,c,d}$	3,35	MPa.	
Normal stress; $\sigma_{n,q,d}$	$\frac{E_d}{A_{ef,core}} = 7,70 \text{ MPa.}$								
ULS: Vertical actions on column							Total stresses on column		
Floor area	20,25	m^2	Storeys	20	-	$\sigma_{c,max,d}$	15,18	MPa.	
Design load	10	kN/m^2	E_d	4050,0	kN	$\sigma_{c,min,d}$	7,32	MPa.	
Compressive stress; $\sigma_{c,q,d}$	$\frac{E_d}{A_c} = 11,25 \text{ MPa.}$								
Axial force (wind); $F_{c,d}$	$\frac{M_r}{D} = 1413,4 \text{ kN}$								
Compressive stress; $\sigma_{c,F,d}$	$\frac{F_{c,d}}{A_c} = 3,93 \text{ MPa.}$								
SLS: Top displacements						Reduced deflections			
$U_{top,b}$	$\frac{w_{e,total} \cdot H^4}{8 \cdot (EI)_{ef,core}} = 0,0831 \text{ m}$					Bending:	$\frac{U_{top,b,red}}{U_{top,b}}$	44,1	%
$U_{top,rs}$	$\frac{w_{e,total} \cdot H^2}{2 \cdot (GA)_{core, shear}} = 0,0316 \text{ m}$					Rack. shear:	$\frac{U_{top,rs,red}}{U_{top,rs}}$	18,1	%
$U_{top,b,red}$	$\frac{M_r(H^2 - x_0^2)}{2 \cdot (EI)_{ef,core}} = 0,0366 \text{ m}$					Total:	$\frac{U_{top,b+rs,red}}{U_{top,b+rs}}$	36,9	%
$U_{top,rs,red}$	$\frac{M_r}{\alpha \cdot (GA)_{core, shear}} = 0,0057 \text{ m}$								
$U_{top,max}$	$(U_{top,b} + U_{top,rs}) - (U_{top,b,red} + U_{top,rs,red}) = 0,0724 \text{ m}$								

Calculation sheet No.		2.3c	
Title:		Structural calculations outrigger structure - modified column properties	
Design phase:	Preliminary design		
Design state:	SLS + ULS		
References:	Table 3.7		
CLT panel properties			
Thickness; d	300	mm	Build-up
$E_{0,g,mean}$	1,20E+07	kN/m ²	$E_{90,g,mean}$
$G_{g,mean}$	5,50E+05	kN/m ²	80-30-80-30-80 mm
a_1	240	mm	a_2
			60 mm
k_3	$1 - \left(1 - \frac{E_{90,g,mean}}{E_{0,g,mean}} \right) \cdot \frac{a_2}{d} = \mathbf{0,806}$		
Core properties			
Dimensions	l	b	d
	9,0	9,0	0,3 m
I_{core}	131,86	m ⁴	$I_{ef,core} = I_{core} \cdot k_3 =$ 106,30 m ⁴
A_{core}	10,44	m ²	$A_{ef,core} = A_{core} \cdot k_3 =$ 8,42 m ²
$A_{core,shear} = 2 \cdot l \cdot d$	5,4	m ²	
$(EI)_{ef,core}$	1,276E+09	kNm ²	
$(GA)_{core,shear}$	2,970E+06	kN	
Column properties			Beam properties
$E_{0,g,mean}$	1,37E+07	kN/m ²	$E_{0,g,mean}$
Dimensions	b	d	l^*
	0,7	0,7	13,5 m
$(EI)_{ec} = 2 \cdot E_{0,g,mean} \cdot A_b \cdot l^{*2}$	2,447E+09	kNm ²	
			$E_{0,g,mean}$
			1,26E+07 kN/m ²
			Dimensions
			b
			d
			0,4
			0,5
Outrigger properties			
$E_{0,g,mean}$	1,26E+07	kN/m ²	
Dimensions	No. Bays	l	h
	2	9,0	6,4
			11,0 m
$(EI)_{out}$	$\frac{E_{0,g,mean} \cdot A_b \cdot h^2}{2} =$		5,161E+07 kNm ²
$(GA)_{out}$	$\frac{2 \cdot 2 \cdot l^2 h E_{0,g,mean} A_d}{d^3} =$		3,880E+06 kN
Optimum height outriggers			
Structural parameters	$\alpha = l^*/l$	H	
	1,5	67,2	
$\omega = S_h / S_v$	0,51	-	
x / H	0,4	-	
Optimum height; x	26,9	m	
Outrigger height; x_0	29,05	m	
			$S_v = \frac{H}{(EI)_{ef,core}} + \frac{H}{2 \cdot (EI)_{ec}} = 6,64E-08$
			$S_h = \frac{1}{\alpha^2} \left\{ \frac{l}{24 \cdot 2 \cdot (EI)_{out}} + \frac{1}{h \cdot 2 \cdot (GA)_{out}} + \frac{1}{h \cdot (GA)_{core,shear}} \right\} = 3,39E-08$
			$\beta H = H \sqrt{\frac{\alpha (GA)_{core,shear}}{(EI)_{ef,core}}} = 3,97$
Lateral loading		Wind loads	
Building height; H	67,2	m	Characteristic wind load SLS; $w_{e,total}$
Building dept; D	27,0	m	41,58 kN/m
			Design wind load ULS; $w_{e,total,d}$
			62,37 kN/m

SLS: Outrigger resistance									
Restraining moment; M_r	$\left\{ \frac{w_{e,total} (H^3 - x_0^3)}{6(EI)_{ef,core}} + \frac{w_{e,total} \cdot x_0}{\alpha(GA)_{core, shear}} \right\} \frac{H}{(H-x_0)S_v + HS_h} = 24935,3 \text{ kNm}$								
ULS: Outrigger resistance									
Restraining moment; M_r	$\left\{ \frac{w_{e,total,d} (H^3 - x_0^3)}{6(EI)_{ef,core}} + \frac{w_{e,total,d} \cdot x_0}{\alpha(GA)_{core, shear}} \right\} \frac{H}{(H-x_0)S_v + HS_h} = 37402,9 \text{ kNm}$								
ULS: Lateral actions on core									
Moment due to wind; $M_{b,d}$	$\frac{1}{2} \cdot w_{e,total,d} \cdot H^2 = 140826,5 \text{ kNm}$								
Moment on core; $M_{b,c,d}$	$M_{b,d} - M_r = 103423,6 \text{ kNm}$								
Normal stress; $\sigma_{n,b,c,d}$	$\frac{M_{b,c,d} \cdot (l/2)}{I_{ef,core}} = 4,38 \text{ MPa.}$								
Shear force; $V_{sh,c,d}$	$w_{e,total,d} \cdot H = 4191,3 \text{ kN}$								
Shear stress; $T_{c,d}$	$\frac{V_{sh,c,d}}{A_{core, shear}} = 0,78 \text{ MPa.}$								
ULS: Vertical actions on core							Total stresses on core		
Floor area	324	m^2	Storeys	20	-	$\sigma_{n,max,c,d}$	12,08	MPa.	
Design load, q_d	10	kN/m^2	E_d	64800,0	kN	$\sigma_{n,min,c,d}$	3,32	MPa.	
Normal stress; $\sigma_{n,q,d}$	$\frac{E_d}{A_{ef,core}} = 7,70 \text{ MPa.}$								
ULS: Vertical actions on column							Total stresses on column		
Floor area	20,25	m^2	Storeys	20	-	$\sigma_{c,max,d}$	11,09	MPa.	
Design load	10	kN/m^2	E_d	4050,0	kN	$\sigma_{c,min,d}$	5,44	MPa.	
Compressive stress; $\sigma_{c,q,d}$	$\frac{E_d}{A_c} = 8,27 \text{ MPa.}$								
Axial force (wind); $F_{c,d}$	$\frac{M_r}{D} = 1385,3 \text{ kN}$								
Compressive stress; $\sigma_{c,F,d}$	$\frac{F_{c,d}}{A_c} = 2,83 \text{ MPa.}$								
SLS: Top displacements						Reduced deflections			
$U_{top,b}$	$\frac{w_{e,total} \cdot H^4}{8 \cdot (EI)_{ef,core}} = 0,0831 \text{ m}$					Bending:	$\frac{U_{top,b,red}}{U_{top,b}} = 43,2 \%$		
$U_{top,rs}$	$\frac{w_{e,total} \cdot H^2}{2 \cdot (GA)_{core, shear}} = 0,0316 \text{ m}$					Rack. shear:	$\frac{U_{top,rs,red}}{U_{top,rs}} = 17,7 \%$		
$U_{top,b,red}$	$\frac{M_r(H^2 - x_0^2)}{2 \cdot (EI)_{ef,core}} = 0,0359 \text{ m}$					Total:	$\frac{U_{top,b+rs,red}}{U_{top,b+rs}} = 36,2 \%$		
$U_{top,rs,red}$	$\frac{M_r}{\alpha \cdot (GA)_{core, shear}} = 0,0056 \text{ m}$								
$U_{top,max}$	$(U_{top,b} + U_{top,rs}) - (U_{top,b,red} + U_{top,rs,red}) = 0,0732 \text{ m}$								

Calculation sheet No. 2.3d			
Title:	Structural calculations outrigger structure - modified outrigger design		
Design phase:	Preliminary design		
Design state:	SLS + ULS		
References:	Table 2.7		
CLT panel properties			
Thickness; d	300 mm	Build-up	80-30-80-30-80 mm
$E_{0,g,mean}$	1,20E+07 kN/m ²	$E_{90,g,mean}$	3,70E+05 kN/m ²
$G_{g,mean}$	5,50E+05 kN/m ²		
a_1	240 mm	a_2	60 mm
k_3	$1 - \left(1 - \frac{E_{90,g,mean}}{E_{0,g,mean}} \right) \cdot \frac{a_2}{d} = \mathbf{0,806}$		
Core properties			
Dimensions	l	b	d
	9,0	9,0	0,3 m
I_{core}	131,86	m ⁴	$I_{ef,core} = I_{core} \cdot k_3 = 106,30 \text{ m}^4$
A_{core}	10,44	m ²	$A_{ef,core} = A_{core} \cdot k_3 = 8,42 \text{ m}^2$
$A_{core,shear} = 2 \cdot l \cdot d$	5,4	m ²	
$(EI)_{ef,core}$	1,276E+09	kNm ²	
$(GA)_{core,shear}$	2,970E+06	kN	
Column properties		Beam properties	
$E_{0,g,mean}$	1,26E+07 kN/m ²	$E_{0,g,mean}$	1,26E+07 kN/m ²
Dimensions	b	d	l*
	0,6	0,6	13,5 m
$(EI)_{ec} = 2 \cdot E_{0,g,mean} \cdot A_b \cdot l^{*2}$	1,653E+09	kNm ²	
Outrigger properties			
$E_{0,g,mean}$	1,26E+07 kN/m ²		
Dimensions	No. Bays	l	h
	2	9,0	6,4
			9,6 m
$(EI)_{out}$	$\frac{E_{0,g,mean} \cdot A_b \cdot h^2}{2} =$		5,161E+07 kNm ²
$(GA)_{out}$	$\frac{4 \cdot l^2 \cdot 0.5h \cdot E_{0,g,mean}}{(d^3/A_d) + (l^3/A_b)} =$		1,632E+06 kN
Optimum height outriggers			
Structural parameters	$\alpha = l^*/l$	H	
	1,5	67,2	
$\omega = S_h / S_v$	0,63	-	
x / H	0,38	-	
Optimum height; x	25,5	m	
Outrigger height; x_0	29,05	m	
			$S_v = \frac{H}{(EI)_{ef,core}} + \frac{H}{2 \cdot (EI)_{ec}} = 7,30E-08$
			$S_h = \frac{1}{\alpha^2} \left\{ \frac{l}{24.2(EI)_{out}} + \frac{1}{h \cdot 2(GA)_{out}} + \frac{1}{h(GA)_{core,shear}} \right\} = 4,63E-08$
			$\beta H = H \sqrt{\frac{\alpha(GA)_{core,shear}}{(EI)_{ef,core}}} = 3,97$
Lateral loading		Wind loads	
Building height; H	67,2 m	Characteristic wind load SLS; $w_{e,total}$	41,58 kN/m
Building dept; D	27,0 m	Design wind load ULS; $w_{e,total,d}$	62,37 kN/m

SLS: Outrigger resistance									
Restraining moment; M_r	$\left\{ \frac{w_{e,total} (H^3 - x_0^3)}{6(EI)_{ef,core}} + \frac{w_{e,total} \cdot x_0}{\alpha(GA)_{core,shear}} \right\} \frac{H}{(H-x_0)S_v + HS_h} = 20369,1 \text{ kNm}$								
ULS: Outrigger resistance									
Restraining moment; M_r	$\left\{ \frac{w_{e,total,d} (H^3 - x_0^3)}{6(EI)_{ef,core}} + \frac{w_{e,total,d} \cdot x_0}{\alpha(GA)_{core,shear}} \right\} \frac{H}{(H-x_0)S_v + HS_h} = 30553,6 \text{ kNm}$								
ULS: Lateral actions on core									
Moment due to wind; $M_{b,d}$	$\frac{1}{2} \cdot w_{e,total,d} \cdot H^2 = 140826,5 \text{ kNm}$								
Moment on core; $M_{b,c,d}$	$M_{b,d} - M_r = 110272,9 \text{ kNm}$								
Normal stress; $\sigma_{n,b,c,d}$	$\frac{M_{b,c,d} \cdot (l/2)}{I_{ef,core}} = 4,67 \text{ MPa.}$								
Shear force; $V_{sh,c,d}$	$w_{e,total,d} \cdot H = 4191,3 \text{ kN}$								
Shear stress; $T_{c,d}$	$\frac{V_{sh,c,d}}{A_{core,shear}} = 0,78 \text{ MPa.}$								
ULS: Vertical actions on core							Total stresses on core		
Floor area	324	m^2	Storeys	20	-	$\sigma_{n,max,c,d}$	12,37	MPa.	
Design load, q_d	10	kN/m^2	E_d	64800,0	kN	$\sigma_{n,min,c,d}$	3,03	MPa.	
Normal stress; $\sigma_{n,q,d}$	$\frac{E_d}{A_{ef,core}} = 7,70 \text{ MPa.}$								
ULS: Vertical actions on column							Total stresses on column		
Floor area	20,25	m^2	Storeys	20	-	$\sigma_{c,max,d}$	14,39	MPa.	
Design load	10	kN/m^2	E_d	4050,0	kN	$\sigma_{c,min,d}$	8,11	MPa.	
Compressive stress; $\sigma_{c,q,d}$	$\frac{E_d}{A_c} = 11,25 \text{ MPa.}$								
Axial force (wind); $F_{c,d}$	$\frac{M_r}{D} = 1131,6 \text{ kN}$								
Compressive stress; $\sigma_{c,F,d}$	$\frac{F_{c,d}}{A_c} = 3,14 \text{ MPa.}$								
SLS: Top displacements						Reduced deflections			
$U_{top,b}$	$\frac{w_{e,total} \cdot H^4}{8 \cdot (EI)_{ef,core}} = 0,0831 \text{ m}$					Bending:	$\frac{U_{top,b,red}}{U_{top,b}}$	35,3	%
$U_{top,rs}$	$\frac{w_{e,total} \cdot H^2}{2 \cdot (GA)_{core,shear}} = 0,0316 \text{ m}$					Rack. shear:	$\frac{U_{top,rs,red}}{U_{top,rs}}$	14,5	%
$U_{top,b,red}$	$\frac{M_r(H^2 - x_0^2)}{2 \cdot (EI)_{ef,core}} = 0,0293 \text{ m}$					Total:	$\frac{U_{top,b+rs,red}}{U_{top,b+rs}}$	29,5	%
$U_{top,rs,red}$	$\frac{M_r}{\alpha \cdot (GA)_{core,shear}} = 0,0046 \text{ m}$								
$U_{top,max}$	$(U_{top,b} + U_{top,rs}) - (U_{top,b,red} + U_{top,rs,red}) = 0,0808 \text{ m}$								

Calculation sheet No. 2.4			
Title:	Structural calculations outrigger structure - 30 storeys		
Design phase:	Preliminary design		
Design state:	SLS		
References:	App. Chapter 3		
CLT panel properties			
Thickness; d	500 mm	Build-up	80-25-80-25-80-25-80-25-80 mm
$E_{0,g,mean}$	1,20E+07 kN/m ²	$E_{90,g,mean}$	3,70E+05 kN/m ²
$G_{g,mean}$	5,50E+05 kN/m ²		
a_1	400 mm	a_2	100 mm
k_3	$1 - \left(1 - \frac{E_{90,g,mean}}{E_{0,g,mean}} \right) \cdot \frac{a_2}{d} = \mathbf{0,806}$		
Core properties			
Dimensions	l	b	d
	9,0	9,0	0,5 m
I_{core}	205,42	m ⁴	$I_{ef,core} = I_{core} \cdot k_3 = 165,60 \text{ m}^4$
$(EI)_{ef,core}$	1,987E+09	kNm ²	
Column properties		Beam properties	
$E_{0,g,mean}$	1,26E+07 kN/m ²	$E_{0,g,mean}$	1,26E+07 kN/m ²
Dimensions	b	d	l*
	0,7	0,7	13,5 m
$(EI)_{ec} = 2 \cdot E_{0,g,mean} \cdot A_b \cdot l^{*2}$	2,250E+09	kNm ²	
Outrigger properties			
$E_{0,g,mean}$	1,26E+07	kN/m ²	
Dimensions	No. Bays	l	h
	2	9,0	6,4
$(EI)_{out}$	$\frac{E_{0,g,mean} \cdot A_b \cdot h^2}{2} = \mathbf{5,161E+07} \text{ kNm}^2$		
$(GA)_{out}$	$\frac{2 \cdot 2 \cdot l^2 h E_{0,g,mean} A_d}{d^3} = \mathbf{3,880E+06} \text{ kN}$		
Lateral loading		Outrigger height	
Building height; H	99,2 m	$x_1 \approx 0.33H$	32,0 m
Building dept; D	27,0 m	$x_2 \approx 0.67H$	64,0 m
Wind load; $w_{e,total}$	54,0 kN/m		
Outrigger resistance			
Structural parameter; S	$\frac{1}{(EI)_{ef,core}} + \frac{2}{D^2(EA)_{ec}} = 9,476E-10$		
Structural parameter; S_1	$\frac{D}{12(EI)_{out}} = 1,292E-08$		
Restraining moment; $M_{r,1}$	$\frac{w_{e,total}}{6(EI)_{ef,core}} \left[\frac{S_1 (H^3 - x_1^3) + S(H - x_2)(x_2^3 - x_1^3)}{S_1^2 + S_1 S(2H - x_1 - x_2) + S^2(H - x_2)(x_2 - x_1)} \right] = 36947,1 \text{ kNm}$		

Restraining moment; $M_{r,2}$ $M_{r,2} =$	$\frac{w_{e,\text{total}}}{6(EI)_{\text{ef,core}}} \left\{ \frac{S_1 (H^3 - x_2^3) + S \left[(H - x_1)(H^3 - x_2^3) - (H - x_2)(H^3 - x_1^3) \right]}{S_1^2 + S_1 S (2H - x_1 - x_2) + S^2 (H - x_2)(x_2 - x_1)} \right\} =$ $48774,2 \text{ kNm}$
Top displacement	
$U_{\text{top,max}}$	$\frac{w_{e,\text{total}} H^4}{8(EI)_{\text{ef,core}}} - \frac{1}{2(EI)_{\text{ef,core}}} \left[M_{r,1} (H^2 - x_1^2) + M_{r,2} (H^2 - x_2^2) \right] = \mathbf{0,176 \text{ m}}$

A.3 | PRELIMINARY DYNAMIC CALCULATIONS

Calculation Sheet 3.1:	<i>Estimations fundamental frequency</i>
Calculation Sheet 3.2:	<i>SDOF calculations</i>
Calculation Sheet 3.3:	<i>Spectral analysis</i>
Calculation Sheet 3.4:	<i>SDOF model response</i>
Calculation Sheet 3.5:	<i>MDOF calculations</i>
Calculation Sheet 3.6:	<i>MDOF model response</i>
Calculation Sheet 3.7:	<i>STAAD Pro results dynamic properties</i>

Calculation sheet No. 3.1	
Title:	<i>Estimations fundamental frequency</i>
Design phase:	Preliminary design
Design state:	SLS
References:	Table 4.1
Method by Ellis, B.R.	
Natural frequency; n_1	$\frac{46}{H} = \mathbf{0,68}$ Hz.
Fixed strut method	
Natural frequency; n_1	$\frac{3.52}{2\pi} \sqrt{\frac{EI}{\mu H^4}}$
Bending stiffness; $(EI)_{ef,core}$	1,276E+12 Nm ²
Structural mass; μ [kg/m]	
Structural elements	Floors Walls Columns Beams
Cross section dimensions [m]	d=0.5 d=0.3 0.6x0.6 0.5x0.4
Length/height/area per floor	27x27=729 m ² 5x9x3.2=144 m ² 24x3.2=76.8 m 28x9=252 m
Vol. mass GL28h; ρ_{mean} [kg/m ³]	410 380 410 410
Mass per floor [kg]	149445 16416 11336 20664
Total mass per floor	197861 kg
Total mass structure	4155081 kg
Volume building	48989 m ³
Vol. mass; $\rho_{mean} \approx$	90 kg/m ³
Mass per meter height; μ	65610 kg/m
Natural frequency; n_1	0,55 Hz.
Method by van Oosterhout	
Natural frequency; n_1	$f(\alpha H) \sqrt{\frac{w_{e,total}}{m} \cdot \frac{H}{U_{max}}}$
Stiffness ratio; α^2	$\frac{(GA)_{total}}{(EI)_{total}}$
$(GA)_{total}$	$(GA)_{core, shear} + 2 \cdot (GA)_{out} = 1,0729E+07$ kN
$(EI)_{total}$	$(EI)_{ef, core} + 2 \cdot (EI)_{ec} = 4,5823E+09$ kNm ²
Stiffness ratio; α^2	0,0023
αH	3,252
$f(\alpha H)$	$\sqrt{\left[\frac{0.2365}{(\alpha H - 0.3)^{1.22} + 16} \right] \left[\frac{-1 - \alpha H \cdot \sinh \alpha H + \cosh \alpha H + \frac{1}{2}}{(\alpha H)^2 \cosh \alpha H} \right]}$ = 0,188
Characteristic wind load; $w_{e,total}$	41580 N/m
Mass of structure; m	$90 \cdot 27 \cdot 27 \cdot 67.2 = 4408992$ kg
U_{max}	0,0808 m
Natural frequency; n_1	0,53 Hz.

Calculation sheet No. 3.2				
Title:	<i>SDOF calculations</i>			
Design phase:	Preliminary design			
Design state:	SLS			
References:	Table 4.2 + 4.3			
Fundamental properties				
Building height; H	67,2 m			
Wind load; $w_{e,total}$	41,58 kN/m			
Concentrated load; F	2794 kN			
Top displacement; U(H)	0,0808 m			
Structural stiffness; k	$\frac{F}{U(H)} = 34575,52$ kN/rad			
Conversion factors				
$A_{structure}$	729 m ²			
$(EI)_{structure}$	$\frac{k \times H^3}{3} = 3497480293$ kNm ²			
$I_{structure}$	277,58 m ⁴			
Slenderness ratio; s	$\sqrt{\frac{H^2 A_{structure}}{I_{structure}}} = 108,90$			
Material property; γ	$\sqrt{\frac{2(1+\nu)}{k'}}$	ν	k'	γ
		0,3	1	1,61
α	$\frac{s^2}{\gamma^2} = 4562$			
Mass conversion factor; k_M	$\frac{8(3024+999\alpha+91\alpha^2)}{2835(4+\alpha)^2} = 0,26$			
Load conversion factor; k_L	$\frac{40+6\alpha}{60+15\alpha} = 0,40$			
Load-mass conversion factor; k_{lm}	$\frac{4(3024+999\alpha+91\alpha^2)}{189(80+32\alpha+3\alpha^2)} = 0,64$			
Structural dynamic properties				
Mass of the structure; m	$V \cdot \rho_{mean}$			
Volume of the building; V	$27 \cdot 27 \cdot 67,2 = 48989$	m ³		
Vol. mass; $\rho_{mean} \approx$	90	kg/m ³		
m	4408992	kg		
Natural circular frequency; ω_1	$\sqrt{\frac{k}{k_{lm} m}}$	=	3,495	rad/sec.
Natural period; T_1	1,80	sec.		
Natural frequency; η_1	0,56	Hz.		
Damping properties				
Log. decrement of damping; δ	$\delta_s + \delta_a$	Wind force coefficient; c_f	1,37	-
Structural log. decr. of damping; δ_s	0,10	Mass per unit area; μ_e	2430	kg/m ²
Aerodyn. log. decr. of damping; δ_a	$\frac{c_f \rho v_m(z_s)}{2\eta_1 \mu_e} = 0,017$			

Log. decrement of damping; δ	0,117			
Damping ratio; ζ	$\zeta = \frac{\delta}{\sqrt{(2\pi)^2 + \delta^2}}$			
Damping ratio; ζ	0,019			
Damped natural circ. frequency; ω_d	$\omega_1 \sqrt{1 - \zeta^2}$	=	3,494	rad/sec.

Calculation sheet No. 3.3	
Title:	<i>Spectral analysis</i>
Design phase:	Preliminary design
Design state:	SLS
References:	Table 4.6 + 4.7
Structural properties	Equivalent properties method
Natural frequency; n_1	0,56 Hz.
Power Density Spectrum; $S_f(2.31)$	8,10E+08 N ² /Hz.
Damping ratio; ζ	0,019 -
Mass; m	4408992 kg
Stiffness; k	34575,52 kN/rad
Dynamic response: Equivalent properties method (eq. 3.43 - 3.46)	
Quasi-static displacement; $\sigma_{x,stat}$	$\frac{1.07 \cdot 1 \cdot 814.4 \cdot 26.07 \cdot 5.94}{34 \cdot 575.52 \cdot 10^3} = 0,0087 \text{ m}$
Resonance displacement; $\sigma_{x,res}$	$\frac{1}{34 \cdot 575.52 \cdot 10^3} \sqrt{\frac{\pi \cdot 0.55 \cdot 8.1 \cdot 10^8}{4 \cdot 0.019}} = 0,0040 \text{ m}$
Dynamic displacement; $\sigma_{x,dyn}$	$\sqrt{0.0087^2 + 0.0040^2} = 0,0096 \text{ m}$
Horizontal acceleration; σ_a	$\sqrt{\frac{8.1 \cdot 10^8 \cdot \pi \cdot 0.56}{4 \cdot 0.019 \cdot (4.41 \cdot 10^6)^2}} = 0,0314 \text{ m/s}^2$

Calculation Sheet No. 3.4

Reference: Table 4.9

SDOF model response

Mass of the structure:

$$m_{\text{eff}} := 90 \cdot 27 \cdot 27 \cdot 67.2 \cdot 0.256958 \cdot 10^{-3} \quad m_{\text{eff}} = 1.133 \times 10^3 \quad \text{ton}$$

Stiffness of the structure:

$$F_w := 41.58 \cdot 67.2 \quad F_w = 2.794 \times 10^3 \quad \text{kN}$$

$$U(H) := 0.0808 \quad \text{m}$$

$$k_{\text{eff}} := \frac{F_w}{U(H)} \cdot 0.40023 \quad \frac{\text{kN}}{\text{m}} \quad k_{\text{eff}} = 1.384 \times 10^4 \quad \frac{\text{kN}}{\text{m}}$$

Damping ratio of the structure:

$$\zeta := 0.019$$

$$C_{\text{cr}} := 2 \sqrt{k_{\text{eff}} \cdot m_{\text{eff}}} \quad \frac{\text{kN} \cdot \text{sec}}{\text{m}} \quad C_{\text{cr}} = 7.92 \times 10^3 \quad \frac{\text{kN} \cdot \text{sec}}{\text{m}}$$

$$c := \zeta \cdot C_{\text{cr}} \quad \frac{\text{kN} \cdot \text{sec}}{\text{m}} \quad c = 150.474 \quad \frac{\text{kN} \cdot \text{sec}}{\text{m}}$$

Fundamental frequencies:

$$\omega := \sqrt{\frac{k_{\text{eff}}}{m_{\text{eff}}}} \quad \frac{\text{rad}}{\text{sec}} \quad \omega = 3.495 \quad \frac{\text{rad}}{\text{sec}} \quad \omega_d := \omega \cdot \sqrt{1 - \zeta^2} \quad \omega_d = 3.495 \quad \frac{\text{rad}}{\text{sec}}$$

$$T_1 := \frac{2\pi}{\omega} \quad \text{sec} \quad T_1 = 1.798 \quad \text{sec} \quad n := \frac{\omega}{2\pi} \quad \text{Hertz} \quad n = 0.556 \quad \text{Hertz}$$

$$\Delta T_1 := 0.15 \quad \text{sec} \quad \blacksquare < \blacksquare \quad \frac{T_1}{10} = 0.18$$

$$\beta := \zeta \cdot \omega \quad \beta = 0.066 \quad \frac{\text{rad}}{\text{sec}} \quad h := 0.15 \quad h = 0.15 \quad \text{sec}$$

Excitation to the structure:

$$z := 7 .. 67.2$$

$$L(z) := 300 \cdot \left(\frac{z}{200}\right)^{0.64} \quad Cr(z) := 0.22 \cdot \ln\left(\frac{z}{0.5}\right) \quad vm(z) := Cr(z) \cdot 27$$

$$n = 0.556$$

$$fL(z) := \frac{n \cdot L(z)}{vm(z)} \quad SL(z) := \frac{6.8 \cdot fL(z)}{(1 + 10.2 \cdot fL(z))^{\frac{5}{3}}}$$

$L(z) =$	$Cr(z) =$	$vm(z) =$	$fL(z) =$	$SL(z) =$
35.101	0.581	15.676	1.246	0.108
...

$$\Delta fL := fL(67.2) - fL(7) \quad \Delta fL = 1.607$$

$$N := 1 .. 11 \quad \text{steps}$$

$$\Delta f_N := \frac{\Delta fL}{10} \quad \Delta f_N = 0.161 \quad f_N := fL(6) + (N \cdot \Delta f_N)$$

$$SL_N := \frac{6.8 \cdot f_N}{(1 + 10.2 \cdot f_N)^{\frac{5}{3}}} \quad a_N := \sqrt{2 \cdot SL_N \cdot \Delta f_N} \quad a_N = 0.182$$

$$\psi := 0.025$$

$$t := 0 .. 120$$

$$v(t) := \sum_N [a_N \cdot \sin[(f_N \cdot t) + \psi]]$$

$$vm := 26.07 \frac{m}{s} \quad \rho := 1.25 \frac{kg}{m^3} \quad cd := 1.07 \quad A := 27 \cdot 67.2 \quad A = 1.814 \times 10^3 \text{ m}^2$$

$$q(t) := (\rho \cdot vm \cdot v(t) \cdot cd \cdot 0.40023) \cdot 10^{-3} \text{ kN}$$

$$F(t) := q(t) \cdot A \quad F(t) =$$

1.119
32.809
-22.344
...

Initial conditions:

$$\text{ORIGIN} := -1$$

$$x_0 := \frac{F(0)}{k_{\text{eff}}} \quad \text{m} \quad x_0 = 8.083 \times 10^{-5} \quad \text{m}$$

$$v_0 := 0 \quad \frac{\text{m}}{\text{sec}} \quad F_0 := q(0) \cdot A \quad F_0 = 1.119 \quad \text{kN}$$

Displacement, velocity and acceleration:

$$j := 0 .. 12000$$

$$t_j := j \cdot h$$

$$F_j := q(t_j) \cdot A$$

$$a_0 := \frac{1}{m_{\text{eff}}} \cdot (F_0 - c \cdot v_0 - k_{\text{eff}} \cdot x_0) \quad x_0 = 8.083 \times 10^{-5} \quad \text{m} \quad a_0 = 0 \quad \frac{\text{m}}{\text{s}}$$

$$x_{-1} := x_0 - v_0 \cdot h + \frac{a_0 \cdot h^2}{2}$$

$$k_{\text{bar}} := \frac{m_{\text{eff}}}{h^2} + \frac{c}{2 \cdot h}$$

$$j := 0 .. 12000$$

$$\begin{pmatrix} x_{j+1} \\ v_j \\ a_j \end{pmatrix} := \begin{pmatrix} \frac{F_j - \left(k_{\text{eff}} - \frac{2 \cdot m_{\text{eff}}}{h^2} \right) \cdot x_j - \left(\frac{m_{\text{eff}}}{h^2} - \frac{c}{2 \cdot h} \right) \cdot x_{j-1}}{k_{\text{bar}}} \\ \frac{1}{2 \cdot h} \left[-x_{j-1} + \frac{F_j - \left(k_{\text{eff}} - \frac{2 \cdot m_{\text{eff}}}{h^2} \right) \cdot x_j - \left(\frac{m_{\text{eff}}}{h^2} - \frac{c}{2 \cdot h} \right) \cdot x_{j-1}}{k_{\text{bar}}} \right] \\ \frac{1}{h^2} \left[x_{j-1} - 2 \cdot x_j + \frac{F_j - \left(k_{\text{eff}} - \frac{2 \cdot m_{\text{eff}}}{h^2} \right) \cdot x_j - \left(\frac{m_{\text{eff}}}{h^2} - \frac{c}{2 \cdot h} \right) \cdot x_{j-1}}{k_{\text{bar}}} \right] \end{pmatrix}$$

$$\min(x) = -6.05 \times 10^{-3} \quad \min(v) = -0.017 \quad \frac{\text{m}}{\text{s}} \quad \min(a) = -0.051 \quad \frac{\text{m}}{\text{sec}^2}$$

$$\max(x) = 5.845 \times 10^{-3} \quad \max(v) = 0.016 \quad \frac{\text{m}}{\text{s}} \quad \max(a) = 0.054 \quad \frac{\text{m}}{\text{sec}^2}$$

Calculation sheet No. 3.5						
Title:	MDOF calculations					
Design phase:	Preliminary design					
Design state:	SLS					
References:	Section 4.5					
Fundamental properties						
Building height; H	67,2	m				
Wind load; $w_{e,total}$	41,58	kN/m				
Top displacement; U(H)	0,0808	m				
Storey properties						
Storey no. [i]	Height for loading [m]	Wind load; $w_{e,total}$ [kN/m]	Concentrated load; F_i [kN]	Relative displ. U_i [m]	Eq. stiffness (EI) _i [kNm ²]	Struct. stiffness; k_i [kN/rad]
1	65,6000	41,5800	2727,6480	0,0032	4,56E+06	1,67E+06
2	62,4000	41,5800	2594,5920	0,0036	3,88E+06	1,42E+06
3	59,2000	41,5800	2461,5360	0,0039	3,39E+06	1,24E+06
4	56,0000	41,5800	2328,4800	0,0042	3,02E+06	1,10E+06
5	52,8000	41,5800	2195,4240	0,0043	2,72E+06	9,96E+05
6	49,6000	41,5800	2062,3680	0,0045	2,48E+06	9,08E+05
7	46,4000	41,5800	1929,3120	0,0046	2,28E+06	8,35E+05
8	43,2000	41,5800	1796,2560	0,0046	2,11E+06	7,73E+05
9	40,0000	41,5800	1663,2000	0,0046	1,96E+06	7,18E+05
10	36,8000	41,5800	1530,1440	0,0045	1,83E+06	6,70E+05
11	33,6000	41,5800	1397,0880	0,0021	3,59E+06	1,32E+06
12	30,4000	41,5800	1264,0320	0,0020	3,39E+06	1,24E+06
13	27,2000	41,5800	1130,9760	0,0042	1,45E+06	5,32E+05
14	24,0000	41,5800	997,9200	0,0042	1,29E+06	4,73E+05
15	20,8000	41,5800	864,8640	0,0041	1,14E+06	4,16E+05
16	17,6000	41,5800	731,8080	0,0040	9,80E+05	3,59E+05
17	14,4000	41,5800	598,7520	0,0039	8,22E+05	3,01E+05
18	11,2000	41,5800	465,6960	0,0038	6,59E+05	2,41E+05
19	8,0000	41,5800	332,6400	0,0037	4,87E+05	1,78E+05
20	4,8000	41,5800	199,5840	0,0035	3,04E+05	1,11E+05
21	3,2000	41,5800	133,0560	0,0034	2,11E+05	7,72E+04

Natural frequencies

$$|k - \lambda m| := 0$$

λ = eigen values

$p :=$

−5.34378308703528561e71
3.8553873237286075472e70
−6.9407635443875520967e68
5.2697815095936247079e66
−2.1060280105106304936e64
5.0191699109755791109e61
−7.7193186350045573082e58
8.084522934078388644e55
−5.9901258755677826047e52
3.2277899591234132162e49
−1.2903228115053184448e46
3.88015804899575867e42
−8.8556045339440954882e38
1.5406054870994474874e35
−2.0426171404153769991e31
2.0532425244500223818e27
−1.546975046225615843e23
8.5623872305508925645e18
−3.3664639478022125837e14
8.8716321771054401276e9
−140113.88317329675355
1.0

$\lambda := \text{polyroots}(p)$

$\lambda =$

	1
1	20.121
2	95.695
3	227.004
4	448.126
5	704.405
6	$1.082 \cdot 10^3$
7	$1.609 \cdot 10^3$
8	$2.042 \cdot 10^3$
9	$2.696 \cdot 10^3$
10	$3.535 \cdot 10^3$
11	$4.106 \cdot 10^3$
12	$5.193 \cdot 10^3$
13	$6.175 \cdot 10^3$
14	$7.239 \cdot 10^3$
15	$8.693 \cdot 10^3$
16	...

$\omega := \text{Re}(\sqrt{\lambda})$

$\omega =$

	1
1	4.486
2	9.782
3	15.067
4	21.169
5	26.541
6	32.898
7	40.118
8	45.193
9	51.924
10	59.459
11	64.078
12	72.064
13	78.581
14	85.083
15	93.234
16	...

Mode shapes

$$\Phi_i := \left[(-kb(\lambda_i))^{-1} \right] \cdot kc$$

$$\Phi := \begin{bmatrix} 1 \\ (\Phi\Phi)_1 \\ (\Phi\Phi)_2 \\ (\Phi\Phi)_3 \\ (\Phi\Phi)_4 \\ (\Phi\Phi)_5 \\ (\Phi\Phi)_6 \\ (\Phi\Phi)_7 \\ (\Phi\Phi)_8 \\ (\Phi\Phi)_9 \\ (\Phi\Phi)_{10} \\ (\Phi\Phi)_{11} \\ (\Phi\Phi)_{12} \\ (\Phi\Phi)_{13} \\ (\Phi\Phi)_{14} \\ (\Phi\Phi)_{15} \\ (\Phi\Phi)_{16} \\ (\Phi\Phi)_{17} \\ (\Phi\Phi)_{18} \\ (\Phi\Phi)_{19} \\ (\Phi\Phi)_{20} \end{bmatrix}$$

$$\Phi\Phi_1 =$$

	1
1	1.896
2	3.062
3	4.36
4	5.779
5	7.31
6	8.942
7	10.654
8	12.429
9	14.251
10	15.135
11	16.032
12	18.012
13	20.062
14	22.19
15	24.394
16	26.669
17	29.031
18	31.539
19	34.335
20	38.556

	1	2	3	4	5	6	7	8	9	10	11
1	1	1	1	1	1	1	1	1	1	1	1
2	1.896	1.887	1.87	1.841	1.808	1.759	1.69	1.64	1.529	1.455	1.371
3	3.062	3.017	2.939	2.81	2.663	2.452	2.164	1.951	1.583	1.251	0.989
4	4.36	4.232	4.014	3.659	3.267	2.726	2.036	1.543	0.831	0.181	-0.213
5	5.779	5.492	5.012	4.254	3.451	2.407	1.202	0.426	-0.474	-1.14	-1.361
6	7.31	6.755	5.847	4.468	3.093	1.456	-0.159	-0.999	-1.61	-1.658	-1.329
7	8.942	7.969	6.422	4.199	2.156	0.027	-1.575	-2.037	-1.755	-0.748	0.077
8	10.654	9.072	6.647	3.396	0.731	-1.526	-2.416	-2.028	-0.626	0.954	1.51
9	12.429	10	6.445	2.086	-0.953	-2.713	-2.183	-0.807	1.082	1.799	1.239
10	14.251	10.693	5.767	0.387	-2.549	-3.065	-0.832	1.02	2	0.711	-0.647
11	15.135	10.885	5.214	-0.506	-3.075	-2.715	0.07	1.618	1.607	-0.244	-1.183
12	16.032	10.92	4.433	-1.414	-3.269	-1.85	1.006	1.694	0.46	-1.11	-0.931
13	18.012	10.597	2.212	-3.285	-2.815	0.96	2.554	0.506	-2.71	-1.584	1.167
14	20.062	9.776	-0.509	-4.732	-1.421	3.658	2.467	-1.289	-3.027	0.371	1.398
15	22.19	8.369	-3.545	-5.307	0.67	4.727	0.363	-2	0.734	1.932	-1.238
16	24.394	6.271	-6.591	-4.582	2.815	2.972	-2.416	-0.435	3.932	-0.256	-1.317
17	26.669	3.35	-9.176	-2.285	3.989	-1.361	-3.016	2.05	0.352	-2.232	2.359
18	29.031	-0.574	-10.586	1.472	3.007	-5.487	0.459	1.508	-4.941	2.166	-1.48
19	31.539	-5.819	-9.665	5.78	-0.813	-4.081	4.292	-2.85	3.574	-0.895	0.475
20	34.335	-13.178	-4.037	7.796	-5.861	6.517	-2.605	1.151	-0.961	0.169	-0.074
21	38.556	-27.49	17.176	-5.421	2.069	-1.333	0.336	-0.114	0.07	$-9.244 \cdot 10^{-3}$...

The modal mass and stiffness matrices

$$M := \text{Re}(\Phi^T \cdot m \cdot \Phi)$$

	1	2	3	4	5
1	1.719·10 ⁶	49.821	49.821	49.806	49.828
2	49.821	4.193·10 ⁵	49.821	49.803	49.829
3	49.821	49.821	2.011·10 ⁵	49.792	49.832
4	49.806	49.803	49.792	6.571·10 ⁴	49.866
5	49.828	49.829	49.832	49.866	3.334·10 ⁴
6	49.771	49.767	49.759	49.747	49.666
7	48.537	48.473	48.344	48.069	47.56
8	52.475	52.578	52.777	53.192	53.829
9	39.657	39.362	38.806	37.725	36.163
10	54.21	54.306	54.484	54.82	55.269
11	50.457	50.469	50.491	50.534	50.584
12	29.811	29.515	28.978	28.008	26.76
13	60.376	60.507	60.743	61.166	61.695
14	27.951	27.719	27.306	26.573	25.66
15	53.42	53.452	53.508	53.608	53.728
16	47.946	47.932	47.908	47.867	...

$$K := \text{Re}(\Phi^T \cdot k \cdot \Phi)$$

	1	2	3	4	5
1	3.478·10 ⁷	-1.258·10 ⁵	-1.089·10 ⁵	8.275·10 ⁴	1.101·10 ⁵
2	-1.258·10 ⁵	4.009·10 ⁷	3.195·10 ³	4.979·10 ⁴	1.099·10 ⁵
3	-1.089·10 ⁵	3.195·10 ³	4.569·10 ⁷	6.445·10 ⁴	8.594·10 ⁴
4	8.275·10 ⁴	4.979·10 ⁴	6.445·10 ⁴	2.951·10 ⁷	6.477·10 ⁴
5	1.101·10 ⁵	1.099·10 ⁵	8.594·10 ⁴	6.477·10 ⁴	2.352·10 ⁷
6	1.363·10 ⁵	1.083·10 ⁵	8.635·10 ⁴	7.564·10 ⁴	7.382·10 ⁴
7	7.665·10 ⁴	7.872·10 ⁴	8.55·10 ⁴	9.051·10 ⁴	9.641·10 ⁴
8	5.062·10 ⁴	6.74·10 ⁴	8.378·10 ⁴	1.046·10 ⁵	1.23·10 ⁵
9	8.582·10 ⁴	8.328·10 ⁴	1.014·10 ⁵	1.28·10 ⁵	1.347·10 ⁵
10	1.295·10 ⁵	1.415·10 ⁵	1.478·10 ⁵	1.487·10 ⁵	1.518·10 ⁵
11	1.963·10 ⁵	1.811·10 ⁵	1.674·10 ⁵	1.589·10 ⁵	1.578·10 ⁵
12	2.219·10 ⁵	2.108·10 ⁵	1.96·10 ⁵	1.843·10 ⁵	1.824·10 ⁵
13	1.666·10 ⁵	1.75·10 ⁵	1.869·10 ⁵	2.009·10 ⁵	2.121·10 ⁵
14	2.073·10 ⁵	2.17·10 ⁵	2.294·10 ⁵	2.406·10 ⁵	2.437·10 ⁵
15	2.571·10 ⁵	2.543·10 ⁵	2.52·10 ⁵	2.532·10 ⁵	2.596·10 ⁵
16	2.854·10 ⁵	2.895·10 ⁵	2.953·10 ⁵	3.026·10 ⁵	...

The modal damping matrix

$$\zeta := 0.019 \quad \mathbf{C}_i := \operatorname{Re}(2\zeta \cdot \omega_i \cdot \mathbf{M}_{i,i})$$

	1	2	3	4	5
1	$2.929 \cdot 10^5$	0	0	0	0
2	0	$1.559 \cdot 10^5$	0	0	0
3	0	0	$1.151 \cdot 10^5$	0	0
4	0	0	0	$5.286 \cdot 10^4$	0
5	0	0	0	0	$3.363 \cdot 10^4$
6	0	0	0	0	0
7	0	0	0	0	0
8	0	0	0	0	0
9	0	0	0	0	0
10	0	0	0	0	0
11	0	0	0	0	0
12	0	0	0	0	0
13	0	0	0	0	0
14	0	0	0	0	0
15	0	0	0	0	0
16	0	0	0	0	...

C =

$$\frac{\text{kN} \cdot \text{sec}}{\text{m}}$$

The modal force vector

$$z := 7..67.2$$

$$L(z) := 300 \cdot \left(\frac{z}{200}\right)^{0.64}$$

$$Cr(z) := 0.22 \cdot \ln\left(\frac{z}{0.5}\right)$$

$$vm(z) := Cr(z) \cdot 27$$

$$n := 0.56$$

$$fl(z) := \frac{n \cdot L(z)}{vm(z)}$$

$$sl(z) := \frac{6.8 \cdot fl(z)}{(1 + 10.2 \cdot fl(z))^{\frac{5}{3}}}$$

$$L(z) =$$

	1
1	35.101
2	38.233
3	...

$$Cr(z) =$$

	1
1	0.581
2	0.61
3	...

$$vm(z) =$$

	1
1	15.676
2	16.469
3	...

$$fl(z) =$$

	1
1	1.254
2	1.3
3	...

$$sl(z) =$$

	1
1	0.108
2	0.105
3	...

$$\Delta fl := fl(67.2) - fl(7)$$

$$\Delta fl = 1.618$$

$$N := 1..11 \quad \text{steps}$$

$$\Delta f_N := \frac{\Delta fl}{10}$$

$$\Delta f_N =$$

	1
1	0.162
2	0.162
3	...

$$f_N := fl(6) + (N \cdot \Delta f_N)$$

$$SL_N := \frac{6.8 \cdot f_N}{(1 + 10.2 \cdot f_N)^{\frac{5}{3}}}$$

$$a_N := \sqrt{2 \cdot SL_N \cdot \Delta f_N}$$

$$a_N =$$

0.182
0.176
...

$$\psi := 0.025$$

$$t := 0..120$$

$$v(t) := \sum_N [a_N \cdot \sin[(f_N \cdot t) + \psi]]$$

$$vm := 26.07 \quad \frac{m}{s}$$

$$\rho := 1.25 \quad \frac{kg}{m^3}$$

$$cd := 1.07$$

$$A := 27 \cdot 3.2 \quad m^2$$

$$A = 86.4$$

$$m^2$$

$$q(t) := \left[\frac{1}{2} \cdot \rho \cdot (vm + v(t))^2 \cdot cd \right] \cdot 10^{-3} \quad kN$$

$$F(t) := q(t) \cdot A$$

Example Mode 1

ORIGIN := 0

$$\begin{array}{llllll}
 M1 := M_{1-1, 1-1} & M1 = 1.719 \times 10^6 & \text{ton} & h := \Delta T & h = 5 \times 10^{-3} & \text{sec} \\
 C1 := C_{1-1, 1-1} & C1 = 2.929 \times 10^5 & \frac{\text{kN} \cdot \text{sec}}{\text{m}} & P1 := P(0)_{1-1} & P1 = 1.362 \times 10^4 & \text{kN} \\
 K1 := K_{1-1, 1-1} & K1 = 3.478 \times 10^7 & \frac{\text{kN}}{\text{m}} & & &
 \end{array}$$

Initial conditions

$$j := 0..240001$$

$$t_j := j \cdot h$$

$$\begin{array}{llllll}
 qx1_0 := \frac{P1}{K1} & \text{m} & qv1_0 := 0 & \frac{\text{m}}{\text{sec}} & qa1_0 := \frac{1}{M1} \cdot (P1 - C1 \cdot qv1_0 - K1 \cdot qx1_0) & qa1_0 = 0 & \frac{\text{m}}{\text{sec}^2}
 \end{array}$$

$$\begin{array}{llll}
 kbar1 := K1 + \frac{4 \cdot M1}{h^2} + \frac{2 \cdot C1}{h} & kbar1 = 2.751 \times 10^{11} & \frac{\text{kN}}{\text{m}}
 \end{array}$$

Displacement and velocity

$$P1_j := P(t_j)_{1-1}$$

$$j := 0..24000$$

$$t_j := j \cdot h$$

$$\begin{pmatrix} qx1_{j+1} \\ qv1_{j+1} \\ qa1_{j+1} \end{pmatrix} := \begin{bmatrix} qx1_j + \left[\frac{P1_{j+1} - P1_j + \left(\frac{4 \cdot M1}{h} + 2 \cdot C1 \right) \cdot qv1_j + 2 \cdot M1 \cdot qa1_j}{kbar1} \right] \\ qv1_j + \left[\frac{2}{h} \frac{P1_{j+1} - P1_j + \left(\frac{4 \cdot M1}{h} + 2 \cdot C1 \right) \cdot qv1_j + 2 \cdot M1 \cdot qa1_j}{kbar1} - 2 \cdot qv1_j \right] \\ qa1_j + \left[\frac{4}{h^2} \left[\frac{P1_{j+1} - P1_j + \left(\frac{4 \cdot M1}{h} + 2 \cdot C1 \right) \cdot qv1_j + 2 \cdot M1 \cdot qa1_j}{kbar1} - h \cdot qv1_j \right] - 2 \cdot qa1_j \right] \end{bmatrix}$$

$$\begin{pmatrix} xx1_j \\ xx2_j \\ xx3_j \\ xx4_j \\ xx5_j \\ xx6_j \\ xx7_j \\ xx8_j \\ xx9_j \\ xx10_j \\ xx11_j \\ xx12_j \\ xx13_j \\ xx14_j \\ xx15_j \\ xx16_j \\ xx17_j \\ xx18_j \\ xx19_j \\ xx20_j \\ xx21_j \end{pmatrix} := \text{Re}(\Phi) \cdot \begin{pmatrix} qx1_j \\ qx2_j \\ qx3_j \\ qx4_j \\ qx5_j \\ qx6_j \\ qx7_j \\ qx8_j \\ qx9_j \\ qx10_j \\ qx11_j \\ qx12_j \\ qx13_j \\ qx14_j \\ qx15_j \\ qx16_j \\ qx17_j \\ qx18_j \\ qx19_j \\ qx20_j \\ qx21_j \end{pmatrix}$$

$$\begin{pmatrix} xv1_j \\ xv2_j \\ xv3_j \\ xv4_j \\ xv5_j \\ xv6_j \\ xv7_j \\ xv8_j \\ xv9_j \\ xv10_j \\ xv11_j \\ xv12_j \\ xv13_j \\ xv14_j \\ xv15_j \\ xv16_j \\ xv17_j \\ xv18_j \\ xv19_j \\ xv20_j \\ xv21_j \end{pmatrix} := \text{Re}(\Phi) \cdot \begin{pmatrix} qv1_j \\ qv2_j \\ qv3_j \\ qv4_j \\ qv5_j \\ qv6_j \\ qv7_j \\ qv8_j \\ qv9_j \\ qv10_j \\ qv11_j \\ qv12_j \\ qv13_j \\ qv14_j \\ qv15_j \\ qv16_j \\ qv17_j \\ qv18_j \\ qv19_j \\ qv20_j \\ qv21_j \end{pmatrix}$$

$$\begin{pmatrix} xa1_j \\ xa2_j \\ xa3_j \\ xa4_j \\ xa5_j \\ xa6_j \\ xa7_j \\ xa8_j \\ xa9_j \\ xa10_j \\ xa11_j \\ xa12_j \\ xa13_j \\ xa14_j \\ xa15_j \\ xa16_j \\ xa17_j \\ xa18_j \\ xa19_j \\ xa20_j \\ xa21_j \end{pmatrix} := \text{Re}(\Phi) \cdot \begin{pmatrix} qa1_j \\ qa2_j \\ qa3_j \\ qa4_j \\ qa5_j \\ qa6_j \\ qa7_j \\ qa8_j \\ qa9_j \\ qa10_j \\ qa11_j \\ qa12_j \\ qa13_j \\ qa14_j \\ qa15_j \\ qa16_j \\ qa17_j \\ qa18_j \\ qa19_j \\ qa20_j \\ qa21_j \end{pmatrix}$$

Results on top of building

Displacements	Velocities	Accelerations
$\min(xx21) = 0.011 \text{ m}$	$\min(xv21) = -9.884 \times 10^{-3} \frac{\text{m}}{\text{s}}$	$\min(xa21) = -0.033 \frac{\text{m}}{\text{s}^2}$
$\max(xx21) = 0.017 \text{ m}$	$\max(xv21) = 6.859 \times 10^{-3} \frac{\text{m}}{\text{s}}$	$\max(xa21) = 0.04 \frac{\text{m}}{\text{s}^2}$



Academic license user TU Eindhoven

Job No	Sheet No 1	Rev
Part Preliminary dynamic design		
Ref Table 4.12		
By B.B.	Date	Chd
Client TU Eindhoven	File Dynamic model	Date/Time

Job Information

	Engineer	Checked	Approved
Name:	B.B.		
Date:	03-Apr-12		

Structure Type | SPACE FRAME

Number of Nodes	1759	Highest Node	2099
Number of Elements	1948	Highest Beam	4205
Number of Plates	1638	Highest Plate	4253

Number of Basic Load Cases	4
Number of Combination Load Cases	1

Included in this printout are data for:

Nodes	1455
--------------	------

Included in this printout are results for load cases:

Type	L/C	Name
Primary	1	SELF WEIGHT
Primary	2	WIND STATIC
Primary	3	WIND MEAN
Primary	4	WIND FLUCTUATION
Combination	5	WIND DYNAMIC

Section Properties

Prop	Section	Area (cm ²)	I _{yy} (cm ⁴)	I _{zz} (cm ⁴)	J (cm ⁴)	Material
3	Rect 0.60x0.60	3.6E+3	1.08E+6	1.08E+6	1.82E+6	GLULAM
4	Rect 0.50x0.40	2E+3	267E+3	417E+3	547E+3	GLULAM

Plate Thickness

Prop	Node A (cm)	Node B (cm)	Node C (cm)	Node D (cm)	Material
1	27.090	27.090	27.090	27.090	FLOOR
2	30.000	30.000	30.000	30.000	CLT

Materials

Mat	Name	E (kN/mm ²)	ν	Density (kg/m ³)	α (/°C)
1	CLT	2.696	0.300	380.000	0.000
2	STEEL	205.000	0.300	7.83E+3	12E-6
3	FLOOR	0.500	0.300	603.563	0.000
4	GLULAM	12.600	0.300	410.000	0.000
5	STAINLESSSTEEL	197.930	0.300	7.83E+3	18E-6
6	ALUMINUM	68.948	0.330	2.71E+3	23E-6
7	CONCRETE	21.718	0.170	2.4E+3	10E-6



Academic license user TU Eindhoven

Job No

Sheet No

2

Rev

Part Preliminary dynamic design

Job Title Calculation Sheet No. 3.7

Ref Table 3.12

By B.B.

Date 03-Apr-12

Chd

Client TU Eindhoven

File Dynamic model1.std

Date/Time 03-Apr-2012 13:55

Basic Load Cases

Number	Name
1	SELF WEIGHT
2	WIND STATIC
3	WIND MEAN
4	WIND FLUCTUATION

Node Displacements

Node	L/C	X (mm)	Y (mm)	Z (mm)	Resultant (mm)	rX (rad)	rY (rad)	rZ (rad)
1455	1:SELF WEIGHT	-1.04E+3	-5.032	-937.739	1.4E+3	-0.011	-0.000	0.012
	2:WIND STATIC	79.298	0.094	-0.099	79.298	-0.000	-0.000	-0.001
	3:WIND MEAN	29.173	0.035	-0.041	29.173	-0.000	-0.000	-0.000
	4:WIND FLUCT	-6.012	-0.007	0.042	6.012	-0.000	0.000	0.000
	5:WIND DYNAI	23.161	0.027	0.000	23.161	-0.000	-0.000	-0.000

Calculated Modal Frequencies & Mass Participations

Mode	Frequency (Hz)	Period (sec)	Participation X (%)	Participation Y (%)	Participation Z (%)
1	0.420	2.379	0.000	0.000	0.000
2	0.580	1.725	74.401	0.000	0.029
3	0.608	1.643	0.027	0.000	74.198
4	1.269	0.788	0.000	0.000	0.000
5	1.917	0.522	14.962	0.000	0.005
6	2.008	0.498	0.008	0.000	14.366
7	2.055	0.487	0.000	0.000	0.000
8	2.836	0.353	0.000	0.000	0.000
9	3.407	0.293	0.000	0.000	0.000
10	3.593	0.278	5.090	0.000	0.004
11	3.727	0.268	0.004	0.000	5.141
12	3.902	0.256	0.000	17.291	0.000
13	3.918	0.255	0.002	0.000	0.000
14	3.923	0.255	0.000	0.000	0.001
15	3.982	0.251	0.002	0.042	0.000
16	3.997	0.250	0.000	0.573	0.000
17	4.000	0.250	0.000	0.000	0.019
18	4.002	0.250	0.000	0.133	0.000
19	4.003	0.250	0.000	0.000	0.006
20	4.003	0.250	0.000	0.043	0.000

B.1 | DERIVATION STOREY DISPLACEMENT RIGID FLOORS

STRUCTURAL MECHANICAL MODEL

Two infinite rigid floors force a single storey to move horizontal by lateral sway of the column, where the model is depicted in Figure B.1. The column has a flexural stiffness, EI and is subjected to a concentrated load on the upper floor in order to initiate a horizontal displacement.

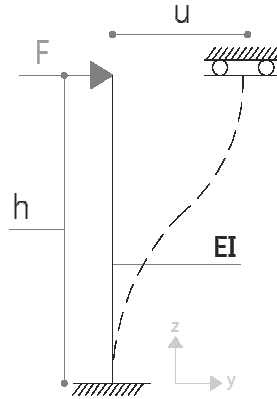


Figure B.1; Structural mechanical model for a storey with two rigid floors

WORK EQUATION

The displacement can be evaluated by equating the work done by the force, F , (external) and the column (internal) as follows

$$-W_{ex} = W_{in} \quad (B.1.1)$$

where W_{ex} is the external work and W_{in} internal work.

External work by a concentrated force can be expressed as

$$-W_{ex} = Fu \quad (B.1.2)$$

while internal work can be written as

$$W_{in} = \int_0^h \frac{1}{2} EI (y''(z))^2 dz \quad (B.1.3)$$

where $y''(z)$ represents the curvature of the displacement curve, i.e. second derivative of the displacement, on height z .

Boundary conditions to the system are

$$y(0) = y'(0) = y'(h) = 0 \quad \text{and} \quad y(h) = u \quad (B.1.4)$$

The displacement curve is given by

$$y(z) = \frac{u}{2} \left(1 - \cos \frac{\pi z}{h} \right) \quad (B.1.5)$$

The first derivative equals

$$y'(z) = -\frac{u\pi}{2h} \left(\sin \frac{\pi z}{h} \right) \quad (\text{B.1.6})$$

and the second derivative becomes

$$y''(z) = \frac{u\pi^2}{2h^2} \left(\cos \frac{\pi z}{h} \right) \quad (\text{B.1.7})$$

Equation B.1.3 can be rearranged as follows

$$\begin{aligned} W_{in} &= \frac{EI}{2} \int_0^h \left(\frac{u\pi^2}{2h^2} \left(\cos \frac{\pi z}{h} \right) \right)^2 dz = \frac{EIu^2\pi^4}{8h^4} \int_0^h \left(\cos \frac{\pi z}{h} \right)^2 dz = \frac{EIu^2\pi^4}{16h^4} \int_0^h \left(1 + \cos \frac{2\pi z}{h} \right) dz = \\ & \frac{EIu^2\pi^4}{16h^4} \left[z + \frac{h}{2\pi} \sin \frac{2\pi z}{h} \right]_0^h = \frac{EIu^2\pi^4}{16h^3} \end{aligned} \quad (\text{B.1.8})$$

Equating internal- and external work, i.e. equation B.1.1, results in

$$-W_{ex} = W_{in} \rightarrow Fu = \frac{EIu^2\pi^4}{16h^3} \rightarrow u = \frac{16Fh^3}{EI\pi^4} \approx \frac{Fh^3}{6.088EI} \quad (\text{B.1.9})$$

C.1 | FINAL STATIC CALCULATIONS

Calculation Sheet 4.1:	<i>Design sheet MBK-07-02</i>
Calculation Sheet 4.2: Scia Engineer results:	<i>Structural calculations CLT floor cassette Structural floor actions</i>
Calculation Sheet 4.3: Scia Engineer results: STAAD Pro results:	<i>Structural calculations glulam beam Structural beam actions Axial loads</i>
Calculation Sheet 4.3a: Scia Engineer results: STAAD Pro results:	<i>Structural calculations glulam beam under permanent loading Structural beam actions Axial loads</i>
Calculation Sheet 4.3b: Scia Engineer results: STAAD Pro results:	<i>Structural calculations glulam beam under maximum axial load Structural beam actions Axial loads</i>
Calculation Sheet 4.4: STAAD Pro results:	<i>Structural calculations glulam column Column, diagonal and wall actions</i>
Calculation Sheet 4.5:	<i>Structural calculations glulam diagonal</i>
Calculation Sheet 4.6:	<i>Structural calculations CLT core walls</i>

Calculation sheet No. 4.1

Title: *Design sheet MBK-07-02*

Design phase: Final design

Design state: ULS + SLS

References: Table 5.7

Cross sectional properties MBK-07-02

2009-06-04 (HR)

Courtesy of Martinsons Byggsystem KB

	Layer	Height [mm]	Width [mm]	E [MPa]	G [MPa]
	1	19	600	9500	600
	2	44	600	300	60
	3	19	600	9500	600
	4	0	0	0	0
	5	0	0	0	0
	6	0	0	0	0
	7	0	0	0	0
	8	360	115	13000	700
	9	0	0	0	0
	10	0	0	0	0
	11	0	0	0	0
	12	0	0	0	0
	13	0	0	0	0
	14	0	0	0	0
	15	0	0	0	0
	16	0	0	0	0
	17	0	0	0	0

Geometric properties		Weight	
Total depth	442 mm	Cross section	0,151 m ² /m ²
EY _{TP}	245,1 mm	Density (wood)	475 kg/m ³
Length / Total depth	20,4 -	Mass (timber)	71,73 kg/m ²
Length	9000 mm	Self weight	717,25 N/m ²
Width (loading width)	600 mm		
Flexural stiffness MBK-07-02			
Effective MOE; E _{eff}	7459 MPa	B x H	
Bending stiffness; EI	2,30E+07 Nm ² /m	= 1000 x 276,7 mm	with E = 13000 MPa
Natural frequency; n ₁	11,0 Hz		
Deformations			
Maximum deformation by	2000 N/m ²		
Bending deformation	7,44 mm		
Shear deformation	0,49 mm		
Total deformation	7,94 mm		
Effective flexural stiffness MBK-07-02			
Effective MOE; E _{eff}	6.997 MPa	B x H	
Effective stiffness; I _{eff}	3,08E+09 mm ⁴		
Eff. flexural stiffness; (EI) _{eff}	2,15E+07 Nm ² /m	= 1000 x 270,9 mm	with E = 13000 MPa and 264,7864417 kg/m ³
Eff. Natural frequency; (n ₁) _{eff}	10,6 Hz		

Calculation sheet No. 4.2			
Title:		Structural calculations CLT floor cassette	
Design phase:	Final design		
Design state:	SLS + ULS		
References:	Table 5.7		
CLT panel properties			
Thickness, d	82 mm	Build-up	19-44-19 mm
$E_{0,mean} (=E_1)$	9500 MPa	$E_{90,mean}$	300 MPa
$G_{0,mean}$	600 MPa	$G_{90,mean}$	60 MPa
Glulam properties			
Height; h	360 mm	$E_{0,g,mean} (=E_2)$	13000 MPa
Width; b	115 mm	$G_{0,g,mean}$	700 MPa
Cassette properties			
Total height; h_{tot}	442 mm	Bending stiffness; $(EI)_{eff}$	21532,11 kNm ²
Neutral axes; z	245,1 mm	Natural frequency; $(n_1)_{eff}$	10,63 Hz.
Scia Engineer results			
$M_{y,d}$	30,07 kNm ULS-STR-1	$M_{y,d}$	84,1 kNm ULS-STR-5
$V_{y,d}$	15,77 kN ULS-STR-1	$V_{y,d}$	49,67 kN ULS-STR-5
U_{max}	16,9 mm SLS-CHA-1		
Bending stresses: ULS-STR-1			
<i>Top</i>		<i>Bottom</i>	
Outer fibre distance; z_t	196,9 mm	Outer fibre distance; z_b	245,1 mm
$I_{y,ef}$	3,08E+09 mm ⁴	$I_{y,ef}$	3,08E+09 mm ⁴
$\sigma_{m,y,d}$	$\frac{E_1 M_{y,d} z_t}{(EI)_{eff}} = 2,61 \text{ MPa}$	$\sigma_{m,y,d}$	$\frac{E_2 M_{y,d} z_b}{(EI)_{eff}} = 4,45 \text{ MPa}$
Bending stresses: ULS-STR-5			
<i>Top</i>		<i>Bottom</i>	
Outer fibre distance; z_t	196,9 mm	Outer fibre distance; z_b	245,1 mm
$I_{y,ef}$	3,08E+09 mm ⁴	$I_{y,ef}$	3,08E+09 mm ⁴
$\sigma_{m,y,d}$	$\frac{E_1 M_{y,d} z_t}{(EI)_{eff}} = 7,31 \text{ MPa}$	$\sigma_{m,y,d}$	$\frac{E_2 M_{y,d} z_b}{(EI)_{eff}} = 12,44 \text{ MPa}$
Shear stresses: ULS-STR-1		Shear stresses: ULS-STR-5	
S_y	$A \cdot z_t = 1,78E+07$	S_y	$A \cdot z_t = 1,78E+07$
$\tau_{max,d}$	$\frac{E_1 V_{y,d} S_y}{b (EI)_{ef}} = 0,12 \text{ MPa}$	$\tau_{max,d}$	$\frac{E_2 V_{y,d} S_y}{b (EI)_{ef}} = 0,39 \text{ MPa}$
Rolling shear stress: ULS-STR-1		Rolling shear stress: ULS-STR-5	
a	82 - 9,5 - 9,5 = 63 mm	a	82 - 9,5 - 9,5 = 63 mm
$\tau_{R,d}$	$\frac{V_{y,d}}{b \cdot a} = 0,25 \text{ MPa}$	$\tau_{R,d}$	$\frac{V_{y,d}}{b \cdot a} = 0,79 \text{ MPa}$
Design bending strength CLT			
Eff. char. strength, $f_{m,k,eff}$	$= f_{m,k} \cdot k_1$	$E_{0,d} = \frac{E_{0,mean}}{\gamma_M} = 7600 \text{ MPa}$	
$f_{m,k}$	24 MPa	$E_{90,d} = \frac{E_{90,mean}}{\gamma_M} = 240 \text{ MPa}$	
Composite factor; k_1	$1 - \left(1 - \frac{E_{90,d}}{E_{0,d}}\right) \cdot \frac{a_2^3}{d^3}$	$a_2 = 1 \cdot 44 = 44 \text{ mm}$	
k_1	0,85	$d = 82 \text{ mm}$	
$f_{m,k,eff}$	20,41 MPa		20,41 MPa
k_{mod}	0,6 (permanent, s.c. 1)		0,8 (medium-term, s.c. 1)
k_{sys}	1,1		1,1
γ_M	1,25		1,25

$f_{m,d}$	$\frac{k_{mod} \cdot k_{sys} \cdot f_{m,k,eff}}{\gamma_M} = 10,78 \text{ MPa}$	$\frac{k_{mod} \cdot k_{sys} \cdot f_{m,k,eff}}{\gamma_M} = 14,37 \text{ MPa}$	
Unity check	$\frac{\sigma_{m,y,d}}{f_{m,d}} \leq 1 \rightarrow 0,24$	$\frac{\sigma_{m,y,d}}{f_{m,d}} \leq 1 \rightarrow 0,51$	
Design bending strength glulam			
GL28h; $f_{m,k}$	28 MPa	28 MPa	
$f_{m,d}$	$\frac{k_{mod} \cdot k_{sys} \cdot f_{m,k}}{\gamma_M} = 14,78 \text{ MPa}$	$\frac{k_{mod} \cdot k_{sys} \cdot f_{m,k}}{\gamma_M} = 19,71 \text{ MPa}$	
Unity check	$\frac{\sigma_{m,y,d}}{f_{m,d}} \leq 1 \rightarrow 0,30$	$\frac{\sigma_{m,y,d}}{f_{m,d}} \leq 1 \rightarrow 0,63$	
Design shear strength glulam			
$f_{v,k}$	3,2 MPa	3,2 MPa	
$f_{v,d}$	$\frac{k_{mod} \cdot k_{sys} \cdot f_{v,k}}{\gamma_M} = 1,69 \text{ MPa}$	$\frac{k_{mod} \cdot k_{sys} \cdot f_{v,k}}{\gamma_M} = 2,25 \text{ MPa}$	
Unity check	$\frac{\tau_{max,d}}{f_{v,d}} \leq 1 \rightarrow 0,07$	$\frac{\tau_{max,d}}{f_{v,d}} \leq 1 \rightarrow 0,17$	
Design bearing strength CLT			
$f_{c,90,k}$	2,5 MPa	2,5 MPa	
$f_{c,90,d}$	$\frac{k_{mod} \cdot k_{sys} \cdot f_{c,90,k}}{\gamma_M} = 1,32 \text{ MPa}$	$\frac{k_{mod} \cdot k_{sys} \cdot f_{c,90,k}}{\gamma_M} = 1,76 \text{ MPa}$	
Design rolling shear strength CLT			
$f_{R,v,k}$	1,5 MPa	1,5 MPa	
$f_{R,v,d}$	$\frac{k_{mod} \cdot k_{sys} \cdot f_{R,v,k}}{\gamma_M} = 0,79 \text{ MPa}$	$\frac{k_{mod} \cdot k_{sys} \cdot f_{R,v,k}}{\gamma_M} = 1,06 \text{ MPa}$	
Unity check	$\frac{\tau_{R,d}}{f_{R,v,d}} \leq 1 \rightarrow 0,32$	$\frac{\tau_{R,d}}{f_{R,v,d}} \leq 1 \rightarrow 0,75$	
SLS: Deflections			
k_{def}	0,6	$\Psi_{2,1}$	0,3
$U_{inst,G}$	6,7 mm	$U_{fin,G} = U_{inst,G}(1+k_{def})$	= 10,72 mm
$U_{inst,Q1}$	10,2 mm	$U_{fin,Q1} = U_{inst,Q1}(1+\Psi_{2,1}k_{def})$	= 12,04 mm
$U_{fin} = U_{fin,G} + U_{fin,Q1}$	22,76 mm		

Floor actions - C.S.4.2

1. Load cases

Name	Action type	LoadGroup	Load type	Spec	Direction	Duration	Master load case
Student version *Student version* *Student version* *Student version* *Student version* *Student version* *Student version* *Student version* *							
Self wei	Permanent	LG1	Self weight		-Z		
Permanen	Permanent	LG1	Standard				
Variable	Variable	LG2	Static	Standard		Long	None

2. Combinations

Name	Type	Load cases	Coeff. [-]	Name	Type	Load cases	Coeff. [-]
Student version *Student version* *Student version* *Student version* *Student version* *Student version* *Student version* *Student version* *				*Student version* *Student version* *Student version* *Student version* *Student version* *Student version* *Student version* *Student version* *			
ULS-STR-1	EN-ULS (STR/GEO) Set B	Self wei	1,35	SLS-CHA-1	EN-SLS Char.	Self wei	1,00
		Permanen	1,35			Permanen	1,00
		Variable	0,75			Variable	1,00
ULS-STR-4	EN-ULS (STR/GEO) Set B	Self wei	1,35	SLS-PER	EN-SLS Char.	Self wei	1,00
		Permanen	1,35			Permanen	1,00
		Variable	0,75			Variable	1,00
ULS-STR-5	EN-ULS (STR/GEO) Set B	Self wei	1,20	SLS-VAR	EN-SLS Char.	Variable	1,00
		Permanen	1,20				
		Variable	1,50				
Student version *Student version* *Student version* *Student version* *Student version* *Student version* *Student version* *Student version* *							

3. Materials

Name	Type	Unit mass [kg/m ³]	E mod [MPa]	Poisson - nu	G mod [MPa]	Thermal exp [m/mK]	Type of timber
Student version *Student version* *Student version* *Student version* *Student version* *Student version* *Student version* *Student version* *							
C24	Timber	350,00	1,1000e+04	0	6,9000e+02	0,01e-003	Solid
CLT	Timber	264,79	1,3000e+04	0,3	6,0000e+02	0,01e-003	Glued, laminated

4. Orthotropy

Name	OT 1	D11 [MNm]	2,3667e+01	D44 [MN/m]	1,3545e+02
Type of orthotropy	Standard	D22 [MNm]	2,3667e+01	D55 [MN/m]	1,3545e+02
Thickness of Plate/Wall [mm]	271	D12 [MNm]	7,1002e+00		
Material	CLT	D33 [MNm]	8,2835e+00		

Student version *Student version* *Student version* *Student version* *Student version* *Student version* *Student version* *Student version* *

5. Free line loads

Name	Load case	Dir	Type	Distribution	Value - P ₁ [kN/m]	Validity	Select	System	Location
Student version *Student version* *Student version* *Student version* *Student version* *Student version* *Student version* *Student version* *									
FL1	Permanen	Z	Force	Uniform	-2,08	All	Auto	GCS	Length

6. Free surface load

Name	Load case	Dir	Type	Distribution	q [kN/m ²]	Validity	Select	System	Location
Student version *Student version* *Student version* *Student version* *Student version* *Student version* *Student version* *Student version* *									
FF1	Variable	Z	Force	Uniform	-2,50	All	Auto	GCS	Length
FF2	Variable	Z	Force	Uniform	-3,00	All	Auto	GCS	Length

7. Forces on surface

Name	Dir	Type	Value [kN/m ²]	2D member	Load case	System
Student version *Student version* *Student version* *Student version* *Student version* *Student version* *Student version* *Student version* *						
SF1	Z	Force	-0,80	E1	Permanen	LCS

8. 2D member - Internal forces

Linear calculation, Extreme : Global
Selection : All
Combinations : ULS-STR-1

Floor actions - C.S.4.2

Basic magnitudes. In nodes, avg. on macro.

Case	Member	elem	mx [kNm/m]	my [kNm/m]	mxy [kNm/m]	vx [kN/m]	vy [kN/m]
Student version	*Student version*	*Student version*	*Student version*	*Student version*	*Student version*	*Student version*	*Student version*
ULS-STR-1	E1	222	-0,50	0,03	-0,07	0,15	-14,01
ULS-STR-1	E1	192	0,12	16,68	-0,07	0,07	-6,88
ULS-STR-1	E1	221	-0,29	-0,23	-0,48	0,08	-19,22
ULS-STR-1	E1	112	0,04	30,07	0,00	0,02	0,21
ULS-STR-1	E1	225	-0,22	-0,17	0,48	-0,08	-14,23

Case	Member	elem	mx [kNm/m]	my [kNm/m]	mxy [kNm/m]	vx [kN/m]	vy [kN/m]
Student version	*Student version*	*Student version*	*Student version*	*Student version*	*Student version*	*Student version*	*Student version*
ULS-STR-1	E1	224	-0,30	-0,10	0,14	-0,30	-15,19
ULS-STR-1	E1	221	-0,22	-0,07	-0,14	0,30	-11,25
ULS-STR-1	E1	1	-0,18	-0,14	0,39	0,09	15,77

9. 2D member - Internal forces

Linear calculation, Extreme : Global

Selection : All

Combinations : ULS-STR-5

Basic magnitudes. In nodes, avg. on macro.

Case	Member	elem	mx [kNm/m]	my [kNm/m]	mxy [kNm/m]	vx [kN/m]	vy [kN/m]
Student version	*Student version*	*Student version*	*Student version*	*Student version*	*Student version*	*Student version*	*Student version*
ULS-STR-5	E1	223	-1,27	0,02	0,05	-0,51	-36,35
ULS-STR-5	E1	192	0,20	41,88	-0,07	0,12	-6,12
ULS-STR-5	E1	221	-0,75	-0,59	-1,24	0,07	-49,67
ULS-STR-5	E1	112	0,12	84,10	0,00	0,07	0,18
ULS-STR-5	E1	225	-0,19	-0,15	1,24	-0,07	-12,65

Case	Member	elem	mx [kNm/m]	my [kNm/m]	mxy [kNm/m]	vx [kN/m]	vy [kN/m]
Student version	*Student version*	*Student version*	*Student version*	*Student version*	*Student version*	*Student version*	*Student version*
ULS-STR-5	E1	224	-0,75	-0,26	0,13	-0,78	-39,35
ULS-STR-5	E1	221	-0,20	-0,06	-0,13	0,78	-10,00
ULS-STR-5	E1	1	-0,16	-0,12	1,13	0,26	45,21

10. Displacement of nodes

Linear calculation, Extreme : Global

Selection : All

Combinations : SLS-PER

Case	Member	Node	Uz [mm]	Fix [mrad]	Fiy [mrad]
Student version	*Student version*	*Student version*	*Student version*	*Student version*	*Student version*
SLS-PER	E1	140	-6,7	0,0	-0,1
SLS-PER	E1	K1	0,0	-2,3	0,0

Case	Member	Node	Uz [mm]	Fix [mrad]	Fiy [mrad]
Student version	*Student version*	*Student version*	*Student version*	*Student version*	*Student version*
SLS-PER	E1	5	0,0	-2,3	0,0
SLS-PER	E1	273	0,0	2,4	0,0
SLS-PER	E1	144	-6,7	0,0	0,1

11. Displacement of nodes

Linear calculation, Extreme : Global

Selection : All

Combinations : SLS-VAR

Case	Member	Node	Uz [mm]	Fix [mrad]	Fiy [mrad]
Student version	*Student version*	*Student version*	*Student version*	*Student version*	*Student version*
SLS-VAR	E1	140	-10,2	0,0	-0,2
SLS-VAR	E1	K1	0,0	0,0	0,0

Case	Member	Node	Uz [mm]	Fix [mrad]	Fiy [mrad]
Student version	*Student version*	*Student version*	*Student version*	*Student version*	*Student version*
SLS-VAR	E1	5	0,0	-3,6	0,0
SLS-VAR	E1	273	0,0	3,6	0,0
SLS-VAR	E1	144	0,0	0,1	0,2

Calculation sheet No. 4.3							
Title:	Structural calculations glulam beam						
Design phase:	Final design						
Design state:	SLS + ULS						
References:	Table 5.8						
Beam section properties		Characteristic strength/stiffness properties GL28h					
Height; h	500 mm	$f_{m,g,k}$	28 MPa				
Width; b	400 mm	$f_{t,0,g,k}$	19,5 MPa				
Cross sectional area; A	2,0E+05 mm ²	$f_{c,0,g,k}$	26,5 MPa				
W_y	1,67E+07 mm ³	$f_{v,g,k}$	3,2 MPa				
W_z	1,33E+07 mm ³	$E_{0,g,mean}$	12600 MPa				
I_y	4,17E+09 mm ⁴	$E_{90,g,mean}$	420 MPa				
I_z	2,67E+09 mm ⁴	$G_{g,mean}$	780 MPa				
		$E_{0,g,05}$	10200 MPa				
ULS: Design strength/stiffness properties							
k_{mod}	0,8 (medium-term, s.c. 1)						
k_h	1,02						
k_{sys}	1,1						
γ_M	1,25						
Bending strength; $f_{m,g,d}$	$\frac{k_{mod} \cdot k_h \cdot k_{sys} \cdot f_{m,g,k}}{\gamma_M}$	=	20,07 MPa				
Tension strength; $f_{t,0,g,d}$	$\frac{k_{mod} \cdot k_h \cdot k_{sys} \cdot f_{t,0,g,k}}{\gamma_M}$	=	13,98 MPa				
Compressive strength; $f_{c,0,g,d}$	$\frac{k_{mod} \cdot k_{sys} \cdot f_{c,0,g,k}}{\gamma_M}$	=	19,00 MPa				
Shear strength; $f_{v,d}$	$\frac{k_{mod} \cdot k_{sys} \cdot f_{v,k}}{\gamma_M}$	=	2,25 MPa				
STAAD Pro results							
$M_{y,d}$	283,39 kNm	ULS-STR-5	$V_{y,d}$	116,69 kN	ULS-STR-5		
$M_{z,d}$	-4,57 kNm	ULS-STR-5	$V_{z,d}$	0,00 kN	ULS-STR-5		
$N_{c,d}$	54,93 kN	ULS-STR-5					
$N_{t,d}$	-40,43 kN	ULS-STR-5					
ULS: Bending stresses							
$\sigma_{m,y,d}$	$\frac{M_{y,d}}{W_y}$	=	17,00 MPa	$\sigma_{m,z,d}$	$\frac{M_{z,d}}{W_z}$	=	-0,34 MPa
Unity check	$\frac{\sigma_{m,y,d}}{f_{m,g,d}} \leq 1 \rightarrow$	0,85		Unity check	$\frac{\sigma_{m,z,d}}{f_{m,g,d}} \leq 1 \rightarrow$	0,02	
ULS: Compressive stress			ULS: Tensile stress				
$\sigma_{c,0,d}$	$\frac{N_{c,d}}{A}$	=	0,27 MPa	$\sigma_{t,0,d}$	$\frac{N_{t,d}}{A}$	=	-0,20 MPa
Unity check	$\frac{\sigma_{c,0,d}}{f_{c,0,g,d}} \leq 1 \rightarrow$	0,01		Unity check	$\frac{\sigma_{t,0,d}}{f_{t,0,g,d}} \leq 1 \rightarrow$	0,01	
Shear stresses							
b_{ef}	$k_{cr} \cdot b$		k_{cr}	0,67 (glulam)			
b_{ef}	268 mm						
$\tau_{max,d}$	$\frac{3V_{y,d}}{2b_{ef} \cdot h}$	=	1,31 MPa				

Unity check	$\frac{\tau_{max,d}}{f_{v,d}} \leq 1 \rightarrow 0,58$

ULS: Combined bending and axial compression - equation 6.23 + 6.24 EC5

Effective length; L_{ey}	9000 mm	Effective length; L_{ez}	9000 mm
Radius of gyration; i_y	$\sqrt{\frac{I_y}{A}} = 144,34$	Radius of gyration; i_z	$\sqrt{\frac{I_z}{A}} = 115,47$
Slenderness ratio; λ_y	$\frac{L_{ey}}{i_y} = 62,35$	Slenderness ratio; λ_z	$\frac{L_{ez}}{i_z} = 77,94$
Relative slenderness; $\lambda_{rel,y}$	$\frac{\lambda_y}{\pi} \sqrt{\frac{f_{c,0,k}}{E_{0,05}}} = 1,01$	Relative slenderness; $\lambda_{rel,z}$	$\frac{\lambda_z}{\pi} \sqrt{\frac{f_{c,0,k}}{E_{0,05}}} = 1,26$
β_c	0,1		0,1
Factor; k_y	$0,5(1 + \beta_c(\lambda_{rel,y} - 0,3) + \lambda_{rel,y}^2)$	Factor; k_z	$0,5(1 + \beta_c(\lambda_{rel,z} - 0,3) + \lambda_{rel,z}^2)$
Factor; k_y	1,05	Factor; k_z	1,35
Instability factor; k_{cy}	$\frac{1}{k_y + \sqrt{k_y^2 - \lambda_{rel,y}^2}} = 0,76$	Instability factor; k_{cz}	$\frac{1}{k_z + \sqrt{k_z^2 - \lambda_{rel,z}^2}} = 0,55$
Modification factor; k_m	0,7		0,7
Design expression	$\frac{\sigma_{c,0,d}}{k_{c,y} f_{c,0,g,d}} + \frac{\sigma_{m,y,d}}{f_{m,g,d}} + k_m \frac{\sigma_{m,z,d}}{f_{m,g,d}}$	Design expression	$\frac{\sigma_{c,0,d}}{k_{c,z} f_{c,0,g,d}} + k_m \frac{\sigma_{m,y,d}}{f_{m,g,d}} + \frac{\sigma_{m,z,d}}{f_{m,g,d}}$
Unity check	0,854 < 1		0,602 < 1

ULS: Combined bending and axial compression - equation 6.35 EC5

Relative slenderness for bending; $\lambda_{rel,m}$	$\sqrt{\frac{f_{m,g,k}}{\sigma_{m,crit}}}$
Critical bending stress; $\sigma_{m,crit}$	$\frac{0,78b^2}{hl_{ef}} E_{0,9,05} = 282,88 \text{ MPa}$
$\lambda_{rel,m}$	0,31 < 0,75 $\rightarrow k_{crit} = 1$
Design expression	$\left(\frac{\sigma_{m,y,d}}{k_{crit} f_{m,g,d}}\right)^2 + \frac{\sigma_{c,0,d}}{k_{c,z} f_{c,0,g,d}} = 0,744$
Unity check	0,744 < 1

SLS: Deflections

k_{def}	0,6	$\psi_{2,1}$	0,3
$U_{inst,G}$	11,50 mm	$U_{fin,G} = U_{inst,G}(1 + k_{def})$	18,40 mm
$U_{inst,Q,1}$	11,90 mm	$U_{fin,Q,1} = U_{inst,Q,1}(1 + \psi_{2,1}k_{def})$	14,04 mm
$U_{fin} = U_{fin,G} + U_{fin,Q,1}$	32,44 mm	$U_{creep} = U_{fin} - U_{inst,G} - U_{inst,Q,1}$	9,04 mm

Beam actions - ULS STR 5 C.S.4.3

1. Materials

Name	Type	Unit mass [kg/m³]	E mod [MPa]	Poisson - nu	G mod [MPa]	Thermal exp [m/mK]	Type of timber
GL28h	Timber	410,00	1,2600e+04	0	7,8000e+02	0,01e-003	Glued, laminated

2. Cross-sections

Name	CS1
Type	RECT
Detailed	400; 500
Item material	GL28h
Fabrication	timber
Buckling y-y, z-z	b b
FEM analysis	x

A [m²]	2,0000e-01	
A y, z [m²]	2,0000e-01	2,0000e-01
I y, z [m⁴]	4,1667e-03	2,6667e-03
I w [m⁶], t [m⁴]	0,0000e+00	8,0858e-03
Wey, z [m³]	1,6667e-02	1,3333e-02
Wpl y, z [m³]	2,5000e-02	2,0000e-02
d y, z [mm]	0	0
c YLCS, ZLCS [mm]	200	250
alpha [deg]	0,00	
AL [m²/m]	1,8000e+00	

Student version *Student version* *Student version* *Student version* *Student version*

3. Load cases

Name	Action type	LoadGroup	Load type	Direction
Self Wei	Permanent	LG1	Self weight	-Z

4. Combinations

Name	Type	Load cases	Coeff. [-]
SLS CHA G	EN-SLS Char.	Self Wei	1,00
SLS CHA Q	EN-SLS Char.	Permanen	1,00
SLS CHA	EN-SLS Char.	Variable	1,00
ULS-STR-1	EN-ULS (STR/GEO) Set B	Self Wei	1,35
		Permanen	1,35
ULS-STR-4	EN-ULS (STR/GEO) Set B	Self Wei	1,35
		Permanen	1,35
		Variable	0,75
ULS-STR-5	EN-ULS (STR/GEO) Set B	Self Wei	1,20
		Permanen	1,20
		Variable	1,50
ULS-STR-7	EN-ULS (STR/GEO) Set B	Self Wei	1,20
		Permanen	1,20
		Variable	0,60

5. Point forces on beam

Name	Member	System	F [kN]	x	Coor	Rep (n)
	Load case	Dir	Type		Orig	
F1	S1	GCS	-12,81	0,500	Rela	1
	Permanent	Z	Force		From start	
F2	S1	GCS	-20,50	0,500	Rela	1
	Variable	Z	Force		From start	

Beam actions - ULS STR 5 C.S.4.3

6. Line forces on beam

Name	Member	Type	Dir	P1	x1	Coor	Orig
	Load case	System	Distribution	[kN/m]	[m]	Loc	
					x2		
					[m]		
Student version *Student version* *Student version* *Student version* *Student version* *Student version* *Student ver							
Lijnla#2	S1	Force	Z	-2,08	0,000	Abso	From start
	Permanen	LCS	Uniform		7,800	Length	
Lijnla#15	S1	Force	Z	-3,41	0,000	Abso	From start
	Permanen	LCS	Uniform		4,500	Length	
Lijnla#16	S1	Force	Z	-6,75	0,000	Abso	From start
	Variable	LCS	Uniform		4,500	Length	

7. Internal forces on member

Linear calculation, Extreme : Global, System : LCS
Selection : All
Combinations : ULS-STR-5

Member	Case	dx [m]	N [kN]	Vz [kN]	My [kNm]
Student version *Student version* *Student version* *Student version* *Student					
S1	ULS-STR-5/1	0,000	0,00	116,69	0,00
S1	ULS-STR-5/1	9,000	0,00	-69,99	0,00
S1	ULS-STR-5/2	0,000	0,00	86,44	0,00
Student version *Student version* *Student version* *Student version* *Student					

Member	Case	dx [m]	N [kN]	Vz [kN]	My [kNm]
Student version *Student version* *Student version* *Student version* *Student					
S1	ULS-STR-5/1	4,500	0,00	9,26	283,39

8. Deformations on member

Linear calculation, Extreme : Global
Selection : All
Combinations : SLS CHA G

Case	Member	dx [m]	ux [mm]	uz [mm]	fiy [mrad]
Student version *Student version* *Student version* *Student version* *Student v					
SLS CHA G/3	S1	0,000	0,0	0,0	4,0
Student version *Student version* *Student version* *Student version* *Student v					
SLS CHA G/3	S1	4,500	0,0	-11,5	-0,1
SLS CHA G/3	S1	9,000	0,0	0,0	-3,7

9. Deformations on member

Linear calculation, Extreme : Global
Selection : All
Combinations : SLS CHA Q

Case	Member	dx [m]	ux [mm]	uz [mm]	fiy [mrad]
Student version *Student version* *Student version* *Student version* *Student v					
SLS CHA Q/4	S1	0,000	0,0	0,0	4,2
Student version *Student version* *Student version* *Student version* *Student v					
SLS CHA Q/4	S1	4,500	0,0	-11,9	-0,2
SLS CHA Q/4	S1	9,000	0,0	0,0	-3,7



Academic license user TU Eindhoven

Job No	Sheet No 1	Rev
Part		
Ref		
By B.B	Date	Chd
Client TU Eindhoven	File Static model	Date/Time

Job Title Static analysis
Axial beam forces - C.S.4.3

Job Information

	Engineer	Checked	Approved
Name:	B.B		
Date:			

Structure Type | SPACE FRAME

Number of Nodes	1759	Highest Node	2099
Number of Elements	1948	Highest Beam	4205
Number of Plates	1638	Highest Plate	4253

Number of Basic Load Cases	7
Number of Combination Load Cases	28

Included in this printout are data for:

Beams	932,934,1665,1671,1854
--------------	------------------------

Included in this printout are results for load cases:

Type	L/C	Name
Combination	10	ULS-STR-1
Combination	14	ULS-STR-5
Combination	16	ULS-STR-7

Section Properties

Prop	Section	Area (cm ²)	I _{yy} (cm ⁴)	I _{zz} (cm ⁴)	J (cm ⁴)	Material
3	Rect 0.60x0.60	3.6E+3	1.08E+6	1.08E+6	1.82E+6	GLULAM
4	Rect 0.50x0.40	2E+3	267E+3	417E+3	547E+3	GLULAM

Plate Thickness

Prop	Node A (cm)	Node B (cm)	Node C (cm)	Node D (cm)	Material
1	27.090	27.090	27.090	27.090	FLOOR
2	30.000	30.000	30.000	30.000	CLT

Materials

Mat	Name	E (kN/mm ²)	ν	Density (kg/m ³)	α (/°C)
1	CLT	2.696	0.300	380.000	0.000
2	STEEL	205.000	0.300	7.83E+3	12E-6
3	FLOOR	0.500	0.300	264.787	0.000
4	GLULAM	12.600	0.300	410.000	0.000
5	STAINLESSSTEEL	197.930	0.300	7.83E+3	18E-6
6	ALUMINUM	68.948	0.330	2.71E+3	23E-6
7	CONCRETE	21.718	0.170	2.4E+3	10E-6



Academic license user TU Eindhoven

Job No

Sheet No

2

Rev

Part

Job Title Static analysis

Axial beam forces - C.S.4.3

Ref

By B.B

Date

Chd

Client TU Eindhoven

File Static model.std

Date/Time 03-Apr-2012 16:59

Basic Load Cases

Number	Name
1	SELF WEIGHT
2	PERMANENT FLOOR LOAD
3	VARIABLE FLOOR LOAD OFFICES
4	VARIABLE FLOOR LOAD APARTMENTS
5	VARIABLE ROOF LOAD
6	WIND
7	VARIABLE SNOW LOAD

Beam Maximum Axial Forces*Distances to maxima are given from beam end A.*

Beam	Node A	Length (m)	L/C		d (m)	Max Fx (kN)
932	512	4.350	10:ULS-STR-1	Max -ve	0.000	27.048
				Max +ve		
			14:ULS-STR-5	Max -ve	0.000	54.929
				Max +ve		
			16:ULS-STR-7	Max -ve	0.000	39.321
				Max +ve		
934	543	4.350	10:ULS-STR-1	Max -ve	0.000	27.188
				Max +ve		
			14:ULS-STR-5	Max -ve	0.000	54.713
				Max +ve		
			16:ULS-STR-7	Max -ve	0.000	62.158
				Max +ve		
1665	930	4.350	10:ULS-STR-1	Max -ve	0.000	-18.964
				Max +ve		
			14:ULS-STR-5	Max -ve	0.000	-40.433
				Max +ve		
			16:ULS-STR-7	Max -ve	0.000	23.266
				Max +ve		
1671	960	4.350	10:ULS-STR-1	Max -ve	0.000	-17.823
				Max +ve		
			14:ULS-STR-5	Max -ve	0.000	-39.419
				Max +ve		
			16:ULS-STR-7	Max -ve	0.000	-81.563
				Max +ve		
1854	1063	4.350	10:ULS-STR-1	Max -ve	0.000	25.900
				Max +ve		
			14:ULS-STR-5	Max -ve	0.000	51.723
				Max +ve		
			16:ULS-STR-7	Max -ve	0.000	158.003
				Max +ve		

Calculation sheet No. 4.3a					
Title:		Structural calculations glulam beam under permanent loading			
Design phase:	Final design				
Design state:	ULS				
References:	Table 5.8				
Beam section properties			Characteristic strength/stiffness properties GL28h		
Height; h	500	mm	$f_{m,g,k}$	28	MPa
Width; b	400	mm	$f_{t,0,g,k}$	19,5	MPa
Cross sectional area; A	2,0E+05	mm ²	$f_{c,0,g,k}$	26,5	MPa
W_y	1,67E+07	mm ³	$f_{v,g,k}$	3,2	MPa
W_z	1,33E+07	mm ³	$E_{0,g,mean}$	12600	MPa
I_y	4,17E+09	mm ⁴	$E_{90,g,mean}$	420	MPa
I_z	2,67E+09	mm ⁴	$G_{g,mean}$	780	MPa
			$E_{0,g,05}$	10200	MPa
ULS: Design strength/stiffness properties					
k_{mod}	0,6 (permanent, s.c. 1)				
k_h	1,02				
k_{sys}	1,1				
γ_M	1,25				
Bending strength; $f_{m,g,d}$	$\frac{k_{mod} \cdot k_h \cdot k_{sys} \cdot f_{m,g,k}}{\gamma_M}$	=	15,06	MPa	
Tension strength; $f_{t,0,g,d}$	$\frac{k_{mod} \cdot k_h \cdot k_{sys} \cdot f_{t,0,g,k}}{\gamma_M}$	=	10,49	MPa	
Compressive strength; $f_{c,0,g,d}$	$\frac{k_{mod} \cdot k_{sys} \cdot f_{c,0,g,k}}{\gamma_M}$	=	14,25	MPa	
Shear strength; $f_{v,d}$	$\frac{k_{mod} \cdot k_{sys} \cdot f_{v,k}}{\gamma_M}$	=	1,69	MPa	
STAAD Pro results					
$M_{y,d}$	135,85 kNm	ULS-STR-1	$V_{y,d}$	56,01 kN	ULS-STR-1
$M_{z,d}$	-2,25 kNm	ULS-STR-1	$V_{z,d}$	0,00 kN	ULS-STR-1
$N_{c,d}$	27,19 kN	ULS-STR-1			
$N_{t,d}$	-18,96 kN	ULS-STR-1			
ULS: Bending stresses					
$\sigma_{m,y,d}$	$\frac{M_{y,d}}{W_y} = 8,15$	MPa	$\sigma_{m,z,d}$	$\frac{M_{z,d}}{W_z} = -0,17$	MPa
Unity check	$\frac{\sigma_{m,y,d}}{f_{m,g,d}} \leq 1 \rightarrow 0,54$		Unity check	$\frac{\sigma_{m,z,d}}{f_{m,g,d}} \leq 1 \rightarrow 0,01$	
ULS: Compressive stress			ULS: Tensile stress		
$\sigma_{c,0,d}$	$\frac{N_{c,d}}{A} = 0,14$	MPa	$\sigma_{t,0,d}$	$\frac{N_{t,d}}{A} = -0,09$	MPa
Unity check	$\frac{\sigma_{c,0,d}}{f_{c,0,g,d}} \leq 1 \rightarrow 0,01$		Unity check	$\frac{\sigma_{t,0,d}}{f_{t,0,g,d}} \leq 1 \rightarrow 0,01$	
Shear stresses					
b_{ef}	$k_{cr} \cdot b$		k_{cr}	0,67 (glulam)	
b_{ef}	268	mm			
$\tau_{max,d}$	$\frac{3V_{y,d}}{2b_{ef} \cdot h} = 0,63$	MPa			

Unity check	$\frac{\tau_{\max,d}}{f_{v,d}} \leq 1 \rightarrow 0,37$
-------------	---------------------------------------------------------

ULS: Combined bending and axial compression - equation 6.23 + 6.24 EC5

Effective length; L_{ey}	9000 mm	Effective length; L_{ez}	9000 mm
Radius of gyration; i_y	$\sqrt{\frac{I_y}{A}} = 144,34$	Radius of gyration; i_z	$\sqrt{\frac{I_z}{A}} = 115,47$
Slenderness ratio; λ_y	$\frac{L_{ey}}{i_y} = 62,35$	Slenderness ratio; λ_z	$\frac{L_{ez}}{i_z} = 77,94$
Relative slenderness; $\lambda_{rel,y}$	$\frac{\lambda_y}{\pi} \sqrt{\frac{f_{c,0,k}}{E_{0,05}}} = 1,01$	Relative slenderness; $\lambda_{rel,z}$	$\frac{\lambda_z}{\pi} \sqrt{\frac{f_{c,0,k}}{E_{0,05}}} = 1,26$
β_c	0,1		0,1
Factor; k_y	$0,5(1 + \beta_c(\lambda_{rel,y} - 0,3) + \lambda_{rel,y}^2)$	Factor; k_z	$0,5(1 + \beta_c(\lambda_{rel,z} - 0,3) + \lambda_{rel,z}^2)$
Factor; k_y	1,05	Factor; k_z	1,35
Instability factor; $k_{c,y}$	$\frac{1}{k_y + \sqrt{k_y^2 - \lambda_{rel,y}^2}} = 0,76$	Instability factor; $k_{c,z}$	$\frac{1}{k_z + \sqrt{k_z^2 - \lambda_{rel,z}^2}} = 0,55$
Modification factor; k_m	0,7		0,7
Design expression	$\frac{\sigma_{c,0,d}}{k_{c,y} f_{c,0,g,d}} + \frac{\sigma_{m,y,d}}{f_{m,g,d}} + k_m \frac{\sigma_{m,z,d}}{f_{m,g,d}}$	Design expression	$\frac{\sigma_{c,0,d}}{k_{c,z} f_{c,0,g,d}} + k_m \frac{\sigma_{m,y,d}}{f_{m,g,d}} + \frac{\sigma_{m,z,d}}{f_{m,g,d}}$
Unity check	0,546 < 1		0,385 < 1

ULS: Combined bending and axial compression - equation 6.35 EC5

Relative slenderness for bending; $\lambda_{rel,m}$	$\frac{\sqrt{f_{m,g,k}}}{\sqrt{\sigma_{m,crit}}}$
Critical bending stress; $\sigma_{m,crit}$	$\frac{0,78b^2}{hl_{ef}} E_{0,9,05} = 282,88 \text{ MPa}$
$\lambda_{rel,m}$	0,31 < 0,75 $\rightarrow k_{crit} = 1$
Design expression	$\left(\frac{\sigma_{m,y,d}}{k_{crit} f_{m,g,d}}\right)^2 + \frac{\sigma_{c,0,d}}{k_{c,z} f_{c,0,g,d}} = 0,310$
Unity check	0,310 < 1

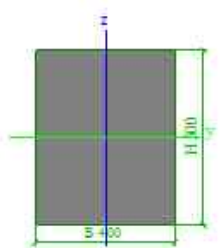
Beam actions - ULS STR - 1 C.S.4.3a

1. Materials

Name	Type	Unit mass [kg/m³]	E mod [MPa]	Poisson - nu	G mod [MPa]	Thermal exp [m/mK]	Type of timber
Student version *Student version* *Student version* *Student version* *Student version* *Student version* *Student version* *Student version* *Student version*							
GL28h	Timber	410,00	1,2600e+04	0	7,8000e+02	0,01e-003	Glued, laminated

2. Cross-sections

Name	CS1
Type	RECT
Detailed	400; 500
Item material	GL28h
Fabrication	timber
Buckling y-y, z-z	b b
FEM analysis	x



A [m²]	2,0000e-01	
A y, z [m²]	2,0000e-01	2,0000e-01
I y, z [m⁴]	4,1667e-03	2,6667e-03
I w [m⁶], t [m⁴]	0,0000e+00	8,0858e-03
Wey, z [m³]	1,6667e-02	1,3333e-02
Wpl y, z [m³]	2,5000e-02	2,0000e-02
d y, z [mm]	0	0
c YLCS, ZLCS [mm]	200	250
alpha [deg]	0,00	
AL [m²/m]	1,8000e+00	

Student version *Student version* *Student version* *Student version* *Student version*

3. Load cases

Name	Action type	LoadGroup	Load type	Direction
Student version *Student version* *Student version* *Student version* *Student version*				
Self Wei	Permanent	LG1	Self weight	-Z
Student version *Student version* *Student version* *Student version* *Student version*				
Permanent	Permanent	LG1	Standard	
Variable	Permanent	LG1	Standard	

4. Combinations

Name	Type	Load cases	Coeff. [-]
Student version *Student version* *Student version* *Student version* *Student version* *Student version* *Student version* *Student version* *Student version*			
SLS CHA G	EN-SLS Char.	Self Wei	1,00
		Permanen	1,00
SLS CHA Q	EN-SLS Char.	Variable	1,00
SLS CHA	EN-SLS Char.	Self Wei	1,00
		Permanen	1,00
		Variable	1,00
ULS-STR-1	EN-ULS (STR/GEO) Set B	Self Wei	1,35
		Permanen	1,35
Student version *Student version* *Student version* *Student version* *Student version* *Student version* *Student version* *Student version* *Student version*			
ULS-STR-4	EN-ULS (STR/GEO) Set B	Self Wei	1,35
		Permanen	1,35
		Variable	0,75
ULS-STR-5	EN-ULS (STR/GEO) Set B	Self Wei	1,20
		Permanen	1,20
		Variable	1,50
ULS-STR-7	EN-ULS (STR/GEO) Set B	Self Wei	1,20
		Permanen	1,20
		Variable	0,60

5. Point forces on beam

Name	Member	System	F [kN]	x	Coor	Rep (n)
Student version *Student version* *Student version* *Student version* *Student version* *Student version* *Student version*						
F1	S1	GCS	-12,81	0,500	Rela	1
	Permanent	Z	Force		From start	
Student version *Student version* *Student version* *Student version* *Student version* *Student version* *Student version*						
F2	S1	GCS	-20,50	0,500	Rela	1
	Variable	Z	Force		From start	

Beam actions - ULS STR - 1 C.S.4.3a

6. Line forces on beam

Name	Member	Type	Dir	P1	x1	Coor	Orig
	Load case	System	Distribution	[kN/m]	[m]	Loc	
					x2		
					[m]		
Student version *Student version* *Student version* *Student version* *Student version* *Student version* *Student ver							
Lijnla st 2	S1 Permanen	Force LCS	Z Uniform	-2,08	0,000 7,800	Abso Length	From start
Lijnla st 15	S1 Permanen	Force LCS	Z Uniform	-3,41	0,000 4,500	Abso Length	From start
Lijnla st 16	S1 Variable	Force LCS	Z Uniform	-6,75	0,000 4,500	Abso Length	From start

7. Internal forces on member

Linear calculation, Extreme : Global, System : LCS
Selection : All
Combinations : ULS-STR-1

Member	Case	dx	N	Vz	My
		[m]	[kN]	[kN]	[kNm]
Student version *Student version* *Student version* *Student version* *Student					
S1	ULS-STR-1/5	0,000	0,00	56,01	0,00
S1	ULS-STR-1/5	9,000	0,00	-38,07	0,00
S1	ULS-STR-1/6	0,000	0,00	41,50	0,00
Student version *Student version* *Student version* *Student version* *Student					

Member	Case	dx	N	Vz	My
		[m]	[kN]	[kN]	[kNm]
Student version *Student version* *Student version* *Student version* *Student					
S1	ULS-STR-1/5	4,500	0,00	4,37	135,85



Academic license user TU Eindhoven

Job No	Sheet No 1	Rev
Part		
Ref		
By	Date	Chd
File Static model	Date/Time	

Job Title Static analysis - variable load 1 side
Beam axial,- shear forces C.S.4.3a
 Client TU Eindhoven

Beams

Beam	Node A	Node B	Length (m)	Property	β (degrees)
934	543	511	4.350	4	0
1665	930	966	4.350	4	0

Beam Maximum Moments

Distances to maxima are given from beam end A.

Beam	Node A	Length (m)	L/C		d (m)	Max My (kNm)	d (m)	Max Mz (kNm)
934	543	4.350	10:ULS-STR-1	Max -ve	4.350	-0.000	4.350	-0.000
				Max +ve	0.000	-2.245	0.000	-76.050
1665	930	4.350	10:ULS-STR-1	Max -ve	0.000	0.000	0.000	0.000
				Max +ve	4.350	-0.369	4.350	-97.598

Beam Maximum Axial Forces

Distances to maxima are given from beam end A.

Beam	Node A	Length (m)	L/C		d (m)	Max Fx (kN)
934	543	4.350	10:ULS-STR-1	Max -ve	0.000	27.188
				Max +ve		
1665	930	4.350	10:ULS-STR-1	Max -ve		
				Max +ve	0.000	-18.964

Calculation sheet No. 4.3b					
Title:	<i>Structural calculations glulam beam under maximum axial load</i>				
Design phase:	Final design				
Design state:	ULS				
References:	Table 5.9				
Beam section properties		Characteristic strength/stiffness properties GL28h			
Height; h	500 mm	$f_{m,g,k}$	28 MPa		
Width; b	400 mm	$f_{t,0,g,k}$	19,5 MPa		
Cross sectional area; A	2,0E+05 mm ²	$f_{c,0,g,k}$	26,5 MPa		
W_y	1,67E+07 mm ³	$f_{v,g,k}$	3,2 MPa		
W_z	1,33E+07 mm ³	$E_{0,g,mean}$	12600 MPa		
I_y	4,17E+09 mm ⁴	$E_{90,g,mean}$	420 MPa		
I_z	2,67E+09 mm ⁴	$G_{g,mean}$	780 MPa		
		$E_{0,g,05}$	10200 MPa		
ULS: Design strength/stiffness properties					
k_{mod}	0,9 (short-term, s.c. 1)				
k_h	1,02				
k_{sys}	1,1				
γ_M	1,25				
Bending strength; $f_{m,g,d}$	$\frac{k_{mod} \cdot k_h \cdot k_{sys} \cdot f_{m,g,k}}{\gamma_M}$	=	22,58 MPa		
Tension strength; $f_{t,0,g,d}$	$\frac{k_{mod} \cdot k_h \cdot k_{sys} \cdot f_{t,0,g,k}}{\gamma_M}$	=	15,73 MPa		
Compressive strength; $f_{c,0,g,d}$	$\frac{k_{mod} \cdot k_{sys} \cdot f_{c,0,g,k}}{\gamma_M}$	=	21,37 MPa		
Shear strength; $f_{v,d}$	$\frac{k_{mod} \cdot k_{sys} \cdot f_{v,k}}{\gamma_M}$	=	2,53 MPa		
STAAD Pro results					
$M_{y,d}$	202,13 kNm	ULS-STR-7	$V_{y,d}$	83,26 kN	ULS-STR-7
$M_{z,d}$	-6,79 kNm	ULS-STR-7	$V_{z,d}$	1,56 kN	ULS-STR-7
$N_{c,d}$	158,00 kN	ULS-STR-7			
$N_{t,d}$	-81,56 kN	ULS-STR-7			
ULS: Bending stresses					
$\sigma_{m,y,d}$	$\frac{M_{y,d}}{W_y} = 12,13$ MPa	$\sigma_{m,z,d}$	$\frac{M_{z,d}}{W_z} = -0,51$ MPa		
Unity check	$\frac{\sigma_{m,y,d}}{f_{m,g,d}} \leq 1 \rightarrow 0,54$	Unity check	$\frac{\sigma_{m,z,d}}{f_{m,g,d}} \leq 1 \rightarrow 0,02$		
ULS: Compressive stress			ULS: Tensile stress		
$\sigma_{c,0,d}$	$\frac{N_{c,d}}{A} = 0,79$ MPa	$\sigma_{t,0,d}$	$\frac{N_{t,d}}{A} = -0,41$ MPa		
Unity check	$\frac{\sigma_{c,0,d}}{f_{c,0,g,d}} \leq 1 \rightarrow 0,04$	Unity check	$\frac{\sigma_{t,0,d}}{f_{t,0,g,d}} \leq 1 \rightarrow 0,03$		
Shear stresses					
b_{ef}	$k_{cr} \cdot b$	k_{cr}	0,67 (glulam)		
b_{ef}	268 mm				
$\tau_{max,d}$	$\frac{3V_{y,d}}{2b_{ef} \cdot h} = 0,93$ MPa				

Unity check	$\frac{\tau_{\max,d}}{f_{v,d}} \leq 1 \rightarrow 0,37$		
ULS: Combined bending and axial compression - equation 6.23 + 6.24 EC5			
Effective length; L_{ey}	9000 mm	Effective length; L_{ez}	9000 mm
Radius of gyration; i_y	$\sqrt{\frac{I_y}{A}} = 144,34$	Radius of gyration; i_z	$\sqrt{\frac{I_z}{A}} = 115,47$
Slenderness ratio; λ_y	$\frac{L_{ey}}{i_y} = 62,35$	Slenderness ratio; λ_z	$\frac{L_{ez}}{i_z} = 77,94$
Relative slenderness; $\lambda_{rel,y}$	$\frac{\lambda_y}{\pi} \sqrt{\frac{f_{c,0,k}}{E_{0,05}}} = 1,01$	Relative slenderness; $\lambda_{rel,z}$	$\frac{\lambda_z}{\pi} \sqrt{\frac{f_{c,0,k}}{E_{0,05}}} = 1,26$
β_c	0,1		0,1
Factor; k_y	$0,5(1 + \beta_c(\lambda_{rel,y} - 0,3) + \lambda_{rel,y}^2)$	Factor; k_z	$0,5(1 + \beta_c(\lambda_{rel,z} - 0,3) + \lambda_{rel,z}^2)$
Factor; k_y	1,05	Factor; k_z	1,35
Instability factor; $k_{c,y}$	$\frac{1}{k_y + \sqrt{k_y^2 - \lambda_{rel,y}^2}} = 0,76$	Instability factor; $k_{c,z}$	$\frac{1}{k_z + \sqrt{k_z^2 - \lambda_{rel,z}^2}} = 0,55$
Modification factor; k_m	0,7		0,7
Design expression	$\frac{\sigma_{c,0,d}}{k_{c,y} f_{c,0,g,d}} + \frac{\sigma_{m,y,d}}{f_{m,g,d}} + k_m \frac{\sigma_{m,z,d}}{f_{m,g,d}}$	Design expression	$\frac{\sigma_{c,0,d}}{k_{c,z} f_{c,0,g,d}} + k_m \frac{\sigma_{m,y,d}}{f_{m,g,d}} + \frac{\sigma_{m,z,d}}{f_{m,g,d}}$
Unity check	0,570 < 1		0,420 < 1
ULS: Combined bending and axial compression - equation 6.35 EC5			
Relative slenderness for bending; $\lambda_{rel,m}$	$\sqrt{\frac{f_{m,g,k}}{\sigma_{m,crit}}}$		
Critical bending stress; $\sigma_{m,crit}$	$\frac{0,78b^2}{hl_{ef}} E_{0,9,05} = 282,88 \text{ MPa}$		
$\lambda_{rel,m}$	0,31 < 0,75 $\rightarrow k_{crit} = 1$		
Design expression	$\left(\frac{\sigma_{m,y,d}}{k_{crit} f_{m,g,d}}\right)^2 + \frac{\sigma_{c,0,d}}{k_{c,z} f_{c,0,g,d}} = 0,355$		
Unity check	0,355 < 1		

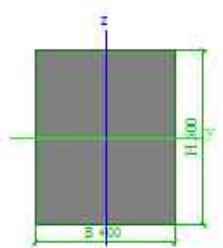
Beam actions ULS-STR-7 C.S.4.3b

1. Materials

Name	Type	Unit mass [kg/m³]	E mod [MPa]	Poisson - nu	G mod [MPa]	Thermal exp [m/mK]	Type of timber
GL28h	Timber	410,00	1,2600e+04	0	7,8000e+02	0,01e-003	Glued, laminated

2. Cross-sections

Name	CS1
Type	RECT
Detailed	400; 500
Item material	GL28h
Fabrication	timber
Buckling y-y, z-z	b b
FEM analysis	x



A [m²]	2,0000e-01	
A y, z [m²]	2,0000e-01	2,0000e-01
I y, z [m⁴]	4,1667e-03	2,6667e-03
I w [m⁶], t [m⁴]	0,0000e+00	8,0858e-03
Wey y, z [m³]	1,6667e-02	1,3333e-02
Wpl y, z [m³]	2,5000e-02	2,0000e-02
d y, z [mm]	0	0
c YLCS, ZLCS [mm]	200	250
alpha [deg]	0,00	
AL [m²/m]	1,8000e+00	

Student version *Student version* *Student version* *Student version* *Student version*

3. Load cases

Name	Action type	LoadGroup	Load type	Direction
Self Wei	Permanent	LG1	Self weight	-Z

4. Combinations

Name	Type	Load cases	Coeff. [-]
SLS CHA G	EN-SLS Char.	Self Wei	1,00
SLS CHA Q	EN-SLS Char.	Permanen	1,00
SLS CHA	EN-SLS Char.	Variable	1,00
ULS-STR-1	EN-ULS (STR/GEO) Set B	Self Wei	1,35
		Permanen	1,35
ULS-STR-4	EN-ULS (STR/GEO) Set B	Self Wei	1,35
		Permanen	1,35
		Variable	0,75
ULS-STR-5	EN-ULS (STR/GEO) Set B	Self Wei	1,20
		Permanen	1,20
		Variable	1,50
ULS-STR-7	EN-ULS (STR/GEO) Set B	Self Wei	1,20
		Permanen	1,20
		Variable	0,75

5. Point forces on beam

Name	Member	System	F [kN]	x	Coor	Rep (n)
	Load case	Dir	Type		Orig	
F1	S1	GCS	-12,81	0,500	Rela	1
	Permanent	Z	Force		From start	
F2	S1	GCS	-20,50	0,500	Rela	1
	Variable	Z	Force		From start	

Beam actions ULS-STR-7 C.S.4.3b

6. Line forces on beam

Name	Member	Type	Dir	P1	x1	Coor	Orig
	Load case	System	Distribution	[kN/m]	[m]	Loc	
					x2		
					[m]		
Student version *Student version* *Student version* *Student version* *Student version* *Student version* *Student ver							
Lijnla st 2	S1 Permanen	Force LCS	Z Uniform	-2,08	0,000 7,800	Abso Length	From start
Lijnla st 15	S1 Permanen	Force LCS	Z Uniform	-3,41	0,000 4,500	Abso Length	From start
Lijnla st 16	S1 Variable	Force LCS	Z Uniform	-6,75	0,000 4,500	Abso Length	From start

7. Internal forces on member

Linear calculation, Extreme : Global, System : LCS
Selection : All
Combinations : ULS-STR-7

Member	Case	dx	N	Vz	My
		[m]	[kN]	[kN]	[kNm]
Student version *Student version* *Student version* *Student version* *Student					
S1	ULS-STR-7/3	0,000	0,00	83,26	0,00
S1	ULS-STR-7/3	9,000	0,00	-51,93	0,00
S1	ULS-STR-7/4	0,000	0,00	61,66	0,00
Student version *Student version* *Student version* *Student version* *Student					



Academic license user TU Eindhoven

Job No

Sheet No

1

Rev

Part

Job Title Static analysis

Beam max. axial forces C.S.4.3b

Ref

By B.B

Date

Chd

Client TU Eindhoven

File Static model

Date/Time

Beams

Beam	Node A	Node B	Length (m)	Property	β (degrees)
1671	960	927	4.350	4	0
1854	1063	1031	4.350	4	0

Beam Maximum Axial Forces*Distances to maxima are given from beam end A.*

Beam	Node A	Length (m)	L/C		d (m)	Max Fx (kN)
1671	960	4.350	16:ULS-STR-7	Max -ve		
				Max +ve	0.000	-81.563
1854	1063	4.350	16:ULS-STR-7	Max -ve	0.000	158.003
				Max +ve		

Beam Maximum Shear Forces*Distances to maxima are given from beam end A.*

Beam	Node A	Length (m)	L/C		d (m)	Max Fz (kN)	d (m)	Max Fy (kN)
1671	960	4.350	16:ULS-STR-7	Max -ve	0.000	0.861		
				Max +ve			4.350	-36.373
1854	1063	4.350	16:ULS-STR-7	Max -ve	0.000	1.560		
				Max +ve			4.350	-27.937

Beam Maximum Moments*Distances to maxima are given from beam end A.*

Beam	Node A	Length (m)	L/C		d (m)	Max My (kNm)	d (m)	Max Mz (kNm)
1671	960	4.350	16:ULS-STR-7	Max -ve	4.350	-0.000	4.350	-0.000
				Max +ve	0.000	-3.747	0.000	-135.502
1854	1063	4.350	16:ULS-STR-7	Max -ve	4.350	-0.000	4.350	-0.000
				Max +ve	0.000	-6.786	0.000	-98.803

Calculation sheet No. 4.4			
Title:	<i>Structural calculations glulam column</i>		
Design phase:	Final design		
Design state:	ULS		
References:	Table 5.10		
Column section properties		Characteristic strength/stiffness properties GL28h	
Depth; d	600 mm	$f_{m,g,k}$	28 MPa
Width; b	600 mm	$f_{t,0,g,k}$	19,5 MPa
Cross sectional area; A	3,6E+05 mm ²	$f_{c,0,g,k}$	26,5 MPa
W_y	3,60E+07 mm ³	$f_{v,g,k}$	3,2 MPa
W_z	3,60E+07 mm ³	$E_{0,g,mean}$	12600 MPa
I_y	1,08E+10 mm ⁴	$E_{90,g,mean}$	420 MPa
I_z	1,08E+10 mm ⁴	$G_{g,mean}$	780 MPa
		$E_{0,g,05}$	10200 MPa
ULS: Design strength/stiffness properties			
k_{mod}	0,8 (medium-term, s.c. 1)	0,9 (short-term, s.c. 1)	
γ_M	1,25	1,25	
Bending strength; $f_{m,g,d}$	$\frac{k_{mod} \cdot f_{m,g,k}}{\gamma_M} = 17,92$ MPa	$\frac{k_{mod} \cdot f_{m,g,k}}{\gamma_M} = 20,16$ MPa	
Tension strength; $f_{t,0,g,d}$	$\frac{k_{mod} \cdot f_{t,0,g,k}}{\gamma_M} = 12,48$ MPa	$\frac{k_{mod} \cdot f_{t,0,g,k}}{\gamma_M} = 14,04$ MPa	
Compressive strength; $f_{c,0,g,d}$	$\frac{k_{mod} \cdot f_{c,0,g,k}}{\gamma_M} = 16,96$ MPa	$\frac{k_{mod} \cdot f_{c,0,g,k}}{\gamma_M} = 19,08$ MPa	
Shear strength; $f_{v,d}$	$\frac{k_{mod} \cdot f_{v,k}}{\gamma_M} = 2,05$ MPa	$\frac{k_{mod} \cdot f_{v,k}}{\gamma_M} = 2,30$ MPa	
STAAD Pro results			
$M_{y,d}$	2,84 kNm ULS-STR-5V	$V_{y,d}$	12,45 kN ULS-STR-5V
$M_{z,d}$	24,43 kNm ULS-STR-5V	$V_{z,d}$	-40,08 kN ULS-STR-7V
$N_{c,d}$	2316,56 kN ULS-STR-5V		
$N_{t,d}$	-220,58 kN ULS-STR-12V		
ULS: Compressive stress		ULS: Tensile stress	
$\sigma_{c,0,d}$	$\frac{N_{c,d}}{A} = 6,43$ MPa	$\sigma_{t,0,d}$	$\frac{N_{t,d}}{A} = -0,61$ MPa
Unity check	$\frac{\sigma_{c,0,d}}{f_{c,0,g,d}} \leq 1 \rightarrow 0,38$	Unity check	$\frac{\sigma_{t,0,d}}{f_{t,0,g,d}} \leq 1 \rightarrow 0,044$
ULS: Bending stresses			
$\sigma_{m,y,d}$	$\frac{M_{y,d}}{W_y} = 0,08$ MPa	$\sigma_{m,z,d}$	$\frac{M_{z,d}}{W_z} = 0,68$ MPa
Unity check	$\frac{\sigma_{m,y,d}}{f_{m,g,d}} \leq 1 \rightarrow 0,00$	Unity check	$\frac{\sigma_{m,z,d}}{f_{m,g,d}} \leq 1 \rightarrow 0,04$
Shear stresses			
b_{ef}	$k_{cr} \cdot b$	k_{cr}	0,67 (glulam)
b_{ef}	402 mm		
$\tau_{max,d}$	$\frac{3V_{y,d}}{2b_{ef} \cdot h} = 0,08$ MPa		
Unity check	$\frac{\tau_{max,d}}{f_{v,d}} \leq 1 \rightarrow 0,04$		

ULS: Combined bending and axial compression - equation 6.23 + 6.24 EC5			
Effective length; L_{ey}	3200 mm	Effective length; L_{ez}	3200 mm
Radius of gyration; i_y	$\sqrt{\frac{I_y}{A}} = 173,21$	Radius of gyration; i_z	$\sqrt{\frac{I_z}{A}} = 173,21$
Slenderness ratio; λ_y	$\frac{L_{ey}}{i_y} = 18,48$	Slenderness ratio; λ_z	$\frac{L_{ez}}{i_z} = 18,48$
Relative slenderness; $\lambda_{rel,y}$	$\frac{\lambda_y}{\pi} \sqrt{\frac{f_{c,0,k}}{E_{0,05}}} = 0,30$	Relative slenderness; $\lambda_{rel,z}$	$\frac{\lambda_z}{\pi} \sqrt{\frac{f_{c,0,k}}{E_{0,05}}} = 0,30$
β_c	0,1		0,1
Factor; k_y	$0,5(1+\beta_c(\lambda_{rel,y}-0,3)+\lambda_{rel,y}^2)$	Factor; k_z	$0,5(1+\beta_c(\lambda_{rel,z}-0,3)+\lambda_{rel,z}^2)$
Factor; k_y	0,54	Factor; k_z	0,54
Instability factor; k_{cy}	$\frac{1}{k_y + \sqrt{k_y^2 - \lambda_{rel,y}^2}} = 1,00$	Instability factor; k_{cz}	$\frac{1}{k_z + \sqrt{k_z^2 - \lambda_{rel,z}^2}} = 1,00$
Modification factor; k_m	0,7		0,7
Design expression	$\frac{\sigma_{c,0,d}}{k_{c,y} f_{c,0,g,d}} + \frac{\sigma_{m,y,d}}{f_{m,g,d}} + k_m \frac{\sigma_{m,z,d}}{f_{m,g,d}}$	Design expression	$\frac{\sigma_{c,0,d}}{k_{c,z} f_{c,0,g,d}} + k_m \frac{\sigma_{m,y,d}}{f_{m,g,d}} + \frac{\sigma_{m,z,d}}{f_{m,g,d}}$
Unity check	0,410 < 1		0,420 < 1

ULS: Combined bending and axial compression - equation 6.19 + 6.20 EC5			
Design expression	$\left(\frac{\sigma_{c,0,d}}{f_{c,0,g,d}}\right)^2 + \frac{\sigma_{m,y,d}}{f_{m,g,d}} + k_m \frac{\sigma_{m,z,d}}{f_{m,g,d}}$	=	0,17 < 1
Design expression	$\left(\frac{\sigma_{c,0,d}}{f_{c,0,g,d}}\right)^2 + k_m \frac{\sigma_{m,y,d}}{f_{m,g,d}} + \frac{\sigma_{m,z,d}}{f_{m,g,d}}$	=	0,18 < 1



Academic license user TU Eindhoven

Job No

Sheet No

1

Rev

Part

Job Title Static analysis - variable load 1 side

Column-, diagonal-, wall actions

Ref

By

Date

Chd

Client TU Eindhoven

File Static model

Date/Time

Materials

Mat	Name	E (kN/mm ²)	v	Density (kg/m ³)	α (/°C)
1	CLT	2.696	0.300	380.000	0.000
2	STEEL	205.000	0.300	7.83E+3	12E-6
3	FLOOR	0.500	0.300	264.787	0.000
4	GLULAM	12.600	0.300	410.000	0.000
5	STAINLESSSTEEL	197.930	0.300	7.83E+3	18E-6
6	ALUMINUM	68.948	0.330	2.71E+3	23E-6
7	CONCRETE	21.718	0.170	2.4E+3	10E-6

Section Properties

Prop	Section	Area (cm ²)	I _{yy} (cm ⁴)	I _{zz} (cm ⁴)	J (cm ⁴)	Material
3	Rect 0.60x0.60	3.6E+3	1.08E+6	1.08E+6	1.82E+6	GLULAM
4	Rect 0.50x0.40	2E+3	267E+3	417E+3	547E+3	GLULAM

Plate Thickness

Prop	Node A (cm)	Node B (cm)	Node C (cm)	Node D (cm)	Material
1	27.090	27.090	27.090	27.090	FLOOR
2	30.000	30.000	30.000	30.000	CLT

Basic Load Cases

Number	Name
1	SELF WEIGHT
2	PERMANENT FLOOR LOAD
3	VARIABLE FLOOR LOAD OFFICES ONE SIDE
4	VARIABLE FLOOR LOAD APARTMENTS ONE SIDE
5	VARIABLE ROOF LOAD ONE SIDE
6	WIND
7	VARIABLE SNOW LOAD



Academic license user TU Eindhoven

Job No	Sheet No 2	Rev
Part		
Ref		
By	Date 03-Apr-12	Chd
File Static model - variable lo	Date/Time 03-Apr-2012 16:59	

Job Title Static analysis - variable load 1 side
Column-, diagonal-, wall actions
 Client TU Eindhoven

Beam Maximum Axial Forces

Distances to maxima are given from beam end A.

Beam	Node A	Length (m)	L/C		d (m)	Max Fx (kN)
498	303	3.200	16:ULS-STR-7	Max -ve	0.000	2.29E+3
				Max +ve		
			19:ULS-STR-5v	Max -ve	0.000	2.32E+3
				Max +ve		
			21:ULS-STR-7v	Max -ve	0.000	1.94E+3
				Max +ve		
26:ULS-STR-12	Max -ve	0.000	1.62E+3			
	Max +ve					
1530	835	3.200	16:ULS-STR-7	Max -ve	0.000	1.21E+3
				Max +ve		
			19:ULS-STR-5v	Max -ve	0.000	1.13E+3
				Max +ve		
			21:ULS-STR-7v	Max -ve	0.000	1.05E+3
				Max +ve		
26:ULS-STR-12	Max -ve	0.000	874.770			
	Max +ve					
1720	945	3.200	16:ULS-STR-7	Max -ve		
				Max +ve	3.200	-139.296
			19:ULS-STR-5v	Max -ve	0.000	372.232
				Max +ve		
			21:ULS-STR-7v	Max -ve		
				Max +ve	3.200	-104.299
26:ULS-STR-12	Max -ve					
	Max +ve	3.200	-220.579			
1810	995	3.200	16:ULS-STR-7	Max -ve	0.000	562.912
				Max +ve		
			19:ULS-STR-5v	Max -ve	0.000	552.168
				Max +ve		
			21:ULS-STR-7v	Max -ve	0.000	562.328
				Max +ve		
26:ULS-STR-12	Max -ve	0.000	424.700			
	Max +ve					
4190	995	9.552	16:ULS-STR-7	Max -ve		
				Max +ve	9.552	-1.04E+3
			19:ULS-STR-5v	Max -ve		
				Max +ve	9.552	-273.829
			21:ULS-STR-7v	Max -ve		
				Max +ve	9.552	-981.721
26:ULS-STR-12	Max -ve					
	Max +ve	9.552	-951.122			
4191	995	9.552	16:ULS-STR-7	Max -ve	9.552	1.07E+3
				Max +ve		
			19:ULS-STR-5v	Max -ve	9.552	286.569
				Max +ve		
			21:ULS-STR-7v	Max -ve	9.552	1.02E+3
				Max +ve		
26:ULS-STR-12	Max -ve	9.552	984.499			
	Max +ve					



Academic license user TU Eindhoven

Job No	Sheet No 3	Rev
Part	Ref	
By	Date 03-Apr-12	Chd
Client TU Eindhoven	File Static model - variable load	Date/Time 03-Apr-2012 16:59

Job Title Static analysis - variable load 1 side
Column-, diagonal-, wall actions

Beam Maximum Shear Forces

Distances to maxima are given from beam end A.

Beam	Node A	Length (m)	L/C		d (m)	Max Fz (kN)	d (m)	Max Fy (kN)
498	303	3.200	16:ULS-STR-7	Max -ve	0.000	8.869		
				Max +ve			0.000	-1.117
			19:ULS-STR-5v	Max -ve	0.000	7.636		
				Max +ve			0.000	-0.888
			21:ULS-STR-7v	Max -ve	0.000	7.709		
				Max +ve			0.000	-0.891
1530	835	3.200	16:ULS-STR-7	Max -ve	0.000	10.279	0.000	3.964
				Max +ve				
			19:ULS-STR-5v	Max -ve	0.000	12.453		
				Max +ve			0.000	-0.674
			21:ULS-STR-7v	Max -ve	0.000	8.420	0.000	4.068
				Max +ve				
1720	945	3.200	16:ULS-STR-7	Max -ve				
				Max +ve	0.000	-0.462	3.200	-37.025
			19:ULS-STR-5v	Max -ve				
				Max +ve	0.000	-0.106	0.000	-5.301
			21:ULS-STR-7v	Max -ve				
				Max +ve	0.000	-0.445	3.200	-36.225
1810	995	3.200	16:ULS-STR-7	Max -ve	0.000	0.301		
				Max +ve			3.200	-41.131
			19:ULS-STR-5v	Max -ve				
				Max +ve	0.000	-0.032	0.000	-6.284
			21:ULS-STR-7v	Max -ve	0.000	0.278		
				Max +ve			3.200	-40.078
4190	995	9.552	16:ULS-STR-7	Max -ve	0.000	0.000	0.000	4.342
				Max +ve	0.000	0.000	9.552	-4.342
			19:ULS-STR-5v	Max -ve	0.000	0.000	0.000	4.342
				Max +ve	0.000	0.000	9.552	-4.342
			21:ULS-STR-7v	Max -ve	0.000	0.000	0.000	4.342
				Max +ve	0.000	0.000	9.552	-4.342
4191	995	9.552	16:ULS-STR-7	Max -ve	0.000	0.000	0.000	4.342
				Max +ve	0.000	0.000	9.552	-4.342
			19:ULS-STR-5v	Max -ve	0.000	0.000	0.000	4.342
				Max +ve	0.000	0.000	9.552	-4.342
			21:ULS-STR-7v	Max -ve	0.000	0.000	0.000	4.342
				Max +ve	0.000	0.000	9.552	-4.342
26:ULS-STR-12	Max -ve	0.000	0.000	0.000	3.257			
	Max +ve	0.000	0.000	9.552	-3.257			



Academic license user TU Eindhoven

Job No	Sheet No 4	Rev
Part	Ref	
By	Date 03-Apr-12	Chd
File Static model - variable load	Date/Time 03-Apr-2012 16:59	

Job Title Static analysis - variable load 1 side
Column-, diagonal-, wall actions
 Client TU Eindhoven

Beam Maximum Moments

Distances to maxima are given from beam end A.

Beam	Node A	Length (m)	L/C		d (m)	Max My (kNm)	d (m)	Max Mz (kNm)			
498	303	3.200	16:ULS-STR-7	Max -ve	3.200	28.382	3.200	3.576			
				Max +ve	0.000	-0.000					
						19:ULS-STR-5v	Max -ve	3.200	24.434	3.200	2.843
							Max +ve	0.000	-0.000		
						21:ULS-STR-7v	Max -ve	3.200	24.667	3.200	2.850
							Max +ve	0.000	-0.000		
			26:ULS-STR-12	Max -ve	3.200	21.308	3.200	2.668			
				Max +ve	0.000	-0.000					
1530	835	3.200	16:ULS-STR-7	Max -ve	3.200	16.001					
				Max +ve	0.000	-16.892	3.200	-17.243			
						19:ULS-STR-5v	Max -ve	3.200	22.370	3.200	0.223
							Max +ve	0.000	-17.480	0.000	-1.934
						21:ULS-STR-7v	Max -ve	3.200	12.662		
							Max +ve	0.000	-14.282	3.200	-17.206
			26:ULS-STR-12	Max -ve	3.200	9.553					
				Max +ve	0.000	-11.879	3.200	-17.272			
1720	945	3.200	16:ULS-STR-7	Max -ve	0.000	1.479	3.200	-0.000			
				Max +ve	3.200	-0.000	0.000	-63.183			
						19:ULS-STR-5v	Max -ve	0.000	0.338	3.200	-0.000
							Max +ve	3.200	-0.000	0.000	-16.962
						21:ULS-STR-7v	Max -ve	0.000	1.424	3.200	-0.000
							Max +ve	3.200	-0.000	0.000	-60.624
			26:ULS-STR-12	Max -ve	0.000	1.379	3.200	-0.000			
				Max +ve	3.200	-0.000	0.000	-58.198			
1810	995	3.200	16:ULS-STR-7	Max -ve	3.200	0.962	3.200	76.322			
				Max +ve	0.000	0.000	0.000	0.000			
						19:ULS-STR-5v	Max -ve	0.000	0.000	3.200	20.108
							Max +ve	3.200	-0.102	0.000	0.000
						21:ULS-STR-7v	Max -ve	3.200	0.890	3.200	72.953
							Max +ve	0.000	0.000	0.000	0.000
			26:ULS-STR-12	Max -ve	3.200	0.966	3.200	70.281			
				Max +ve	0.000	0.000	0.000	0.000			
4190	995	9.552	16:ULS-STR-7	Max -ve	0.000	0.000	0.000	0.000			
				Max +ve	0.000	0.000	4.776	-10.370			
						19:ULS-STR-5v	Max -ve	0.000	0.000	0.000	0.000
							Max +ve	0.000	0.000	4.776	-10.370
						21:ULS-STR-7v	Max -ve	0.000	0.000	0.000	0.000
							Max +ve	0.000	0.000	4.776	-10.370
			26:ULS-STR-12	Max -ve	0.000	0.000	0.000	0.000			
				Max +ve	0.000	0.000	4.776	-7.777			
4191	995	9.552	16:ULS-STR-7	Max -ve	0.000	0.000	0.000	0.000			
				Max +ve	0.000	0.000	4.776	-10.370			
						19:ULS-STR-5v	Max -ve	0.000	0.000	0.000	0.000
							Max +ve	0.000	0.000	4.776	-10.370
						21:ULS-STR-7v	Max -ve	0.000	0.000	0.000	0.000
							Max +ve	0.000	0.000	4.776	-10.370
			26:ULS-STR-12	Max -ve	0.000	0.000	0.000	0.000			
				Max +ve	0.000	0.000	4.776	-7.777			



Academic license user TU Eindhoven

Job No	Sheet No 5	Rev
Part		
Ref		
By	Date 03-Apr-12	Chd
File Static model - variable load	Date/Time 03-Apr-2012 16:59	

Job Title Static analysis - variable load 1 side
Column-, diagonal-, wall actions
 Client TU Eindhoven

Plate Corner Stress

Plate	L/C	Node	Shear		Membrane			Bending		
			Qx (N/mm ²)	Qy (N/mm ²)	Sx (N/mm ²)	Sy (N/mm ²)	Sxy (N/mm ²)	Mx (kNm/m)	My (kNm/m)	Mxy (kNm/m)
1	16:ULS-STR-7	373	-0.004	-0.041	0.014	2.608	0.086	1.247	7.223	0.701
		376	-0.004	-0.020	0.065	0.494	0.036	-1.948	-10.816	0.020
		377	-0.002	-0.020	0.408	0.527	0.003	-4.901	-24.241	-0.365
		1	-0.002	-0.041	0.358	2.641	0.052	-3.756	-20.889	0.316
1	19:ULS-STR-5V	373	0.004	0.008	-0.012	-1.737	0.057	-1.947	-2.573	-0.247
		376	0.004	-0.003	0.005	-1.883	0.001	1.441	1.540	-0.149
		377	-0.000	-0.003	-0.357	-1.846	-0.010	-0.076	-0.310	0.229
		1	-0.000	0.008	-0.374	-1.700	0.046	0.530	2.675	0.130
1	21:ULS-STR-7V	373	-0.004	-0.042	0.016	2.573	0.084	1.330	7.460	0.705
		376	-0.004	-0.020	0.064	0.474	0.036	-1.990	-10.729	0.024
		377	-0.002	-0.020	0.399	0.507	0.004	-4.866	-24.061	-0.374
		1	-0.002	-0.042	0.352	2.605	0.052	-3.759	-20.908	0.308
1	26:ULS-STR-12	373	-0.005	-0.043	0.018	3.033	0.071	1.758	7.936	0.764
		376	-0.005	-0.019	0.063	0.959	0.036	-2.320	-11.178	0.058
		377	-0.002	-0.019	0.495	0.982	0.006	-4.872	-24.113	-0.425
		1	-0.002	-0.043	0.449	3.057	0.041	-3.890	-21.565	0.281
2	16:ULS-STR-7	373	0.003	0.001	0.145	2.591	-0.712	-1.133	0.155	-0.206
		385	0.003	-0.012	-0.398	-2.783	-0.771	2.422	5.038	-0.350
		294	0.000	-0.012	-0.234	-2.753	-0.494	-0.579	-2.847	0.146
		1	0.000	0.001	0.308	2.621	-0.435	0.236	1.058	0.290
2	19:ULS-STR-5V	373	0.002	-0.003	-0.148	-1.866	0.093	-0.665	-0.560	-0.130
		385	0.002	-0.010	-0.150	-2.126	0.024	1.243	4.493	-0.211
		294	0.000	-0.010	-0.386	-2.091	0.025	-0.499	-2.672	0.033
		1	0.000	-0.003	-0.384	-1.830	0.095	-0.489	-2.481	0.114
2	21:ULS-STR-7V	373	0.003	0.001	0.151	2.560	-0.715	-1.067	0.193	-0.197
		385	0.003	-0.010	-0.375	-2.568	-0.771	2.237	4.539	-0.325
		294	0.000	-0.010	-0.209	-2.539	-0.502	-0.524	-2.553	0.139
		1	0.000	0.001	0.317	2.588	-0.446	0.239	1.066	0.267
2	26:ULS-STR-12	373	0.003	0.002	0.184	3.050	-0.737	-0.948	0.307	-0.171
		385	0.003	-0.009	-0.354	-2.190	-0.777	2.060	3.771	-0.290
		294	0.000	-0.009	-0.130	-2.169	-0.502	-0.439	-2.094	0.136
		1	0.000	0.002	0.407	3.070	-0.462	0.359	1.680	0.255
3	16:ULS-STR-7	385	0.001	-0.007	0.128	-1.329	-0.785	-0.598	2.667	0.000
		371	0.001	-0.016	-0.464	-7.454	-0.931	0.712	3.212	-0.015
		4	-0.001	-0.016	-1.177	-7.379	-0.628	-1.560	-8.082	0.146
		294	-0.001	-0.007	-0.585	-1.254	-0.482	-0.465	-2.476	0.161
3	19:ULS-STR-5V	385	-0.001	-0.009	-0.094	-2.122	-0.022	0.760	3.978	0.177
		371	-0.001	-0.010	-0.203	-3.360	-0.141	-0.133	2.109	0.113
		4	-0.000	-0.010	-0.579	-3.299	-0.086	-0.874	-4.640	-0.033
		294	-0.000	-0.009	-0.471	-2.060	0.034	-0.492	-2.484	0.031
3	21:ULS-STR-7V	385	0.001	-0.007	0.131	-1.138	-0.783	-0.601	2.358	-0.011
		371	0.001	-0.015	-0.438	-6.928	-0.912	0.692	2.864	-0.026
		4	-0.001	-0.015	-1.097	-6.862	-0.621	-1.430	-7.389	0.138
		294	-0.001	-0.007	-0.528	-1.072	-0.492	-0.419	-2.252	0.153
3	26:ULS-STR-12	385	0.001	-0.005	0.153	-0.743	-0.779	-0.791	1.581	-0.047
		371	0.001	-0.013	-0.406	-6.466	-0.890	0.736	2.572	-0.046
		4	-0.000	-0.013	-1.010	-6.409	-0.604	-1.305	-6.728	0.152
		294	-0.000	-0.005	-0.451	-0.686	-0.493	-0.329	-1.790	0.151



Academic license user TU Eindhoven

Job No	Sheet No 6	Rev
Part		
Ref		
By	Date 03-Apr-12	Chd
File Static model - variable load	Date/Time 03-Apr-2012 16:59	

Job Title Static analysis - variable load 1 side
Column-, diagonal-, wall actions
 Client TU Eindhoven

Plate Corner Stress Cont...

Plate	L/C	Node	Shear		Membrane			Bending		
			Qx (N/mm ²)	Qy (N/mm ²)	Sx (N/mm ²)	Sy (N/mm ²)	Sxy (N/mm ²)	Mx (kNm/m)	My (kNm/m)	Mxy (kNm/m)
5	16:ULS-STR-7	291	0.004	-0.001	0.390	-1.119	-1.046	-1.804	-3.765	-0.481
		3	0.004	0.029	-0.965	-7.246	-0.468	-1.402	-10.587	-0.727
		371	0.004	0.029	-0.795	-7.361	-0.197	-0.811	-2.677	0.324
		385	0.004	-0.001	0.559	-1.235	-0.775	-1.503	-4.098	0.571
5	19:ULS-STR-5V	291	-0.001	0.001	-0.023	-1.730	-0.104	-1.010	-3.436	0.063
		3	-0.001	0.018	-0.389	-3.524	0.118	-2.038	-11.197	-0.063
		371	-0.001	0.018	-0.322	-3.568	0.191	-1.691	-6.234	-0.111
		385	-0.001	0.001	0.044	-1.774	-0.030	-0.655	-3.180	0.014
5	21:ULS-STR-7V	291	0.004	-0.001	0.370	-0.994	-1.024	-1.640	-3.421	-0.456
		3	0.004	0.026	-0.894	-6.682	-0.480	-1.119	-8.829	-0.676
		371	0.004	0.026	-0.737	-6.791	-0.227	-0.558	-1.673	0.317
		385	0.004	-0.001	0.528	-1.103	-0.771	-1.385	-3.706	0.537
5	26:ULS-STR-12	291	0.004	-0.002	0.391	-0.649	-1.015	-1.506	-2.807	-0.489
		3	0.004	0.024	-0.848	-6.207	-0.501	-0.821	-7.342	-0.698
		371	0.005	0.024	-0.699	-6.309	-0.253	-0.323	-0.866	0.350
		385	0.005	-0.002	0.540	-0.752	-0.767	-1.307	-3.193	0.559
6	16:ULS-STR-7	374	-0.003	-0.002	0.115	2.647	-0.715	1.156	0.273	0.220
		387	-0.003	0.011	-0.367	-2.740	-0.746	-2.550	-5.421	0.376
		386	-0.000	0.011	-0.209	-2.724	-0.500	0.469	2.300	-0.137
		8	-0.000	-0.002	0.273	2.663	-0.469	-0.257	-1.199	-0.293
6	19:ULS-STR-5V	374	-0.002	0.005	-0.152	-1.716	0.092	0.406	-0.944	0.120
		387	-0.002	0.010	-0.142	-2.163	0.021	-1.334	-4.616	0.228
		386	-0.000	0.010	-0.366	-2.126	0.015	0.487	2.509	-0.013
		8	-0.000	0.005	-0.377	-1.680	0.087	0.496	2.616	-0.122
6	21:ULS-STR-7V	374	-0.003	-0.002	0.124	2.613	-0.718	1.081	0.208	0.207
		387	-0.003	0.010	-0.347	-2.524	-0.748	-2.348	-4.885	0.347
		386	-0.000	0.010	-0.186	-2.509	-0.507	0.422	2.051	-0.130
		8	-0.000	-0.002	0.284	2.628	-0.477	-0.260	-1.209	-0.270
6	26:ULS-STR-12	374	-0.003	-0.003	0.156	3.067	-0.739	1.033	0.489	0.186
		387	-0.003	0.008	-0.326	-2.138	-0.752	-2.159	-4.113	0.311
		386	-0.000	0.008	-0.111	-2.131	-0.505	0.334	1.601	-0.132
		8	-0.000	-0.003	0.370	3.073	-0.493	-0.382	-1.856	-0.256
7	16:ULS-STR-7	387	-0.001	0.007	0.158	-1.118	-0.830	0.595	-2.963	-0.008
		372	-0.001	0.009	-0.493	-7.641	-0.926	0.070	1.343	-0.055
		7	0.001	0.009	-1.234	-7.592	-0.593	1.498	7.478	-0.162
		386	0.001	0.007	-0.583	-1.069	-0.497	0.298	1.888	-0.115
7	19:ULS-STR-5V	387	0.001	0.009	-0.086	-1.980	-0.040	-0.718	-4.009	-0.175
		372	0.001	0.005	-0.206	-3.466	-0.138	0.669	0.750	-0.160
		7	0.001	0.005	-0.594	-3.416	-0.076	0.838	4.285	0.021
		386	0.001	0.009	-0.474	-1.930	0.022	0.421	2.280	0.006
7	21:ULS-STR-7V	387	-0.001	0.006	0.159	-0.943	-0.824	0.601	-2.625	0.005
		372	-0.001	0.008	-0.465	-7.095	-0.907	0.003	1.241	-0.035
		7	0.001	0.008	-1.149	-7.053	-0.588	1.371	6.828	-0.152
		386	0.001	0.006	-0.525	-0.900	-0.505	0.267	1.714	-0.112
7	26:ULS-STR-12	387	-0.001	0.004	0.180	-0.572	-0.818	0.778	-1.860	0.039
		372	-0.001	0.007	-0.434	-6.621	-0.886	-0.113	1.142	-0.009
		7	0.001	0.007	-1.062	-6.587	-0.572	1.253	6.225	-0.165
		386	0.001	0.004	-0.448	-0.537	-0.504	0.184	1.266	-0.116



Academic license user TU Eindhoven

Job No	Sheet No 7	Rev
Part		
Ref		
By	Date 03-Apr-12	Chd
File Static model - variable load	Date/Time 03-Apr-2012 16:59	

Job Title Static analysis - variable load 1 side
Column-, diagonal-, wall actions
 Client TU Eindhoven

Plate Corner Stress Cont...

Plate	L/C	Node	Shear		Membrane			Bending		
			Qx (N/mm ²)	Qy (N/mm ²)	Sx (N/mm ²)	Sy (N/mm ²)	Sxy (N/mm ²)	Mx (kNm/m)	My (kNm/m)	Mxy (kNm/m)
15	16:ULS-STR-7	379	0.018	-0.022	0.079	0.131	-0.179	-0.592	-0.753	2.314
		421	0.018	-0.018	0.011	0.682	-0.155	4.334	-11.437	1.027
		422	-0.013	-0.018	-0.038	0.618	0.031	-4.472	-20.258	-0.317
		423	-0.013	-0.022	0.030	0.066	0.007	-1.801	-12.448	0.970
15	19:ULS-STR-5V	379	0.001	-0.001	-0.040	0.096	0.201	0.028	-0.128	0.038
		421	0.001	-0.002	0.016	-1.438	0.198	0.176	0.230	-0.049
		422	0.000	-0.002	-0.082	-1.429	0.044	-0.109	-0.651	-0.032
		423	0.000	-0.001	-0.139	0.105	0.047	-0.126	-0.572	0.055
15	21:ULS-STR-7V	379	0.017	-0.022	0.077	0.130	-0.174	-0.579	-0.759	2.287
		421	0.017	-0.018	0.011	0.661	-0.151	4.302	-11.242	1.004
		422	-0.012	-0.018	-0.038	0.598	0.030	-4.427	-20.076	-0.319
		423	-0.012	-0.022	0.029	0.067	0.007	-1.796	-12.369	0.964
15	26:ULS-STR-12	379	0.017	-0.022	0.088	0.107	-0.228	-0.595	-0.723	2.297
		421	0.017	-0.017	0.007	1.036	-0.204	4.281	-11.441	1.033
		422	-0.013	-0.017	-0.017	0.970	0.019	-4.433	-20.045	-0.310
		423	-0.013	-0.022	0.064	0.040	-0.005	-1.768	-12.282	0.955
17	16:ULS-STR-7	421	0.004	-0.016	0.063	0.366	-0.024	-1.816	-12.883	0.010
		374	0.004	-0.046	0.068	2.780	-0.035	2.059	10.573	-0.772
		8	0.002	-0.046	0.355	2.787	-0.038	-3.617	-20.700	-0.332
		422	0.002	-0.016	0.350	0.373	-0.027	-4.819	-23.283	0.450
17	19:ULS-STR-5V	421	-0.004	-0.001	-0.016	-1.593	-0.015	1.316	0.689	0.138
		374	-0.004	0.006	-0.067	-1.830	-0.104	-1.804	-1.796	0.230
		8	0.000	0.006	-0.335	-1.770	-0.070	0.521	2.484	-0.122
		422	0.000	-0.001	-0.284	-1.534	0.019	-0.107	-0.323	-0.214
17	21:ULS-STR-7V	421	0.004	-0.016	0.062	0.347	-0.024	-1.845	-12.699	0.010
		374	0.004	-0.046	0.068	2.741	-0.035	2.103	10.578	-0.770
		8	0.002	-0.046	0.349	2.749	-0.039	-3.632	-20.750	-0.323
		422	0.002	-0.016	0.344	0.355	-0.028	-4.777	-23.089	0.456
17	26:ULS-STR-12	421	0.005	-0.015	0.067	0.759	-0.020	-2.154	-13.004	-0.025
		374	0.005	-0.048	0.085	3.227	-0.009	2.523	11.027	-0.829
		8	0.002	-0.048	0.437	3.219	-0.020	-3.752	-21.337	-0.299
		422	0.002	-0.015	0.419	0.751	-0.032	-4.781	-23.149	0.505
18	16:ULS-STR-7	371	-0.013	-0.062	-0.249	-7.903	0.244	6.514	15.282	1.388
		429	-0.013	-0.011	-0.115	-4.706	0.016	-5.199	-16.441	0.369
		427	-0.002	-0.011	-1.148	-4.554	-0.073	-4.759	-23.367	-0.964
		4	-0.002	-0.062	-1.282	-7.751	0.155	-4.835	-26.650	0.055
18	19:ULS-STR-5V	371	-0.006	-0.011	-0.124	-3.593	0.190	2.892	3.227	0.438
		429	-0.006	0.003	-0.040	-3.002	0.027	-2.208	-3.018	0.262
		427	-0.000	0.003	-0.561	-2.893	-0.030	-0.153	-0.993	-0.327
		4	-0.000	-0.011	-0.646	-3.485	0.133	-0.802	-3.983	-0.151
18	21:ULS-STR-7V	371	-0.012	-0.060	-0.229	-7.339	0.215	6.108	14.804	1.321
		429	-0.012	-0.011	-0.108	-4.240	0.012	-4.893	-15.961	0.330
		427	-0.002	-0.011	-1.060	-4.105	-0.069	-4.711	-23.096	-0.919
		4	-0.002	-0.060	-1.181	-7.204	0.134	-4.724	-26.095	0.072
18	26:ULS-STR-12	371	-0.012	-0.059	-0.212	-6.846	0.188	5.676	14.328	1.260
		429	-0.012	-0.012	-0.103	-3.824	0.008	-4.562	-15.552	0.293
		427	-0.002	-0.012	-0.983	-3.704	-0.064	-4.707	-23.042	-0.869
		4	-0.002	-0.059	-1.092	-6.726	0.116	-4.604	-25.498	0.098



Academic license user TU Eindhoven

Job No	Sheet No 8	Rev
Part		
Ref		
By	Date 03-Apr-12	Chd
File Static model - variable load	Date/Time 03-Apr-2012 16:59	

Job Title Static analysis - variable load 1 side
Column-, diagonal-, wall actions
 Client TU Eindhoven

Plate Corner Stress Cont...

Plate	L/C	Node	Shear		Membrane			Bending		
			Qx (N/mm ²)	Qy (N/mm ²)	Sx (N/mm ²)	Sy (N/mm ²)	Sxy (N/mm ²)	Mx (kNm/m)	My (kNm/m)	Mxy (kNm/m)
20	16:ULS-STR-7	429	-0.017	-0.012	0.032	-4.636	-0.706	3.965	-13.809	-1.390
		430	-0.017	-0.020	-0.198	0.125	-0.742	-0.799	-0.294	-2.405
		428	0.014	-0.020	-0.404	0.222	-0.113	-1.401	-11.059	-0.826
		427	0.014	-0.012	-0.174	-4.539	-0.077	-4.458	-19.486	0.189
20	19:ULS-STR-5V	429	-0.000	0.003	0.029	-2.750	-0.386	-0.067	-2.242	-0.304
		430	-0.000	0.001	-0.087	0.174	-0.396	-0.174	0.328	-0.165
		428	0.002	0.001	-0.257	0.200	-0.080	0.209	0.431	0.065
		427	0.002	0.003	-0.142	-2.723	-0.070	-0.188	-0.321	-0.074
20	21:ULS-STR-7V	429	-0.016	-0.013	0.027	-4.208	-0.646	3.946	-13.436	-1.345
		430	-0.016	-0.020	-0.184	0.098	-0.680	-0.772	-0.342	-2.371
		428	0.014	-0.020	-0.364	0.190	-0.100	-1.418	-11.034	-0.830
		427	0.014	-0.013	-0.153	-4.116	-0.067	-4.406	-19.328	0.195
20	26:ULS-STR-12	429	-0.017	-0.013	0.023	-3.829	-0.593	3.977	-13.143	-1.301
		430	-0.017	-0.020	-0.173	0.074	-0.626	-0.748	-0.389	-2.354
		428	0.014	-0.020	-0.328	0.163	-0.089	-1.458	-11.160	-0.843
		427	0.014	-0.013	-0.132	-3.740	-0.056	-4.396	-19.360	0.210
22	16:ULS-STR-7	433	0.013	-0.013	-0.067	-5.594	0.033	-5.406	-15.564	-0.373
		372	0.013	-0.058	-0.034	-7.318	-0.049	5.735	12.207	-1.304
		7	0.002	-0.058	-1.370	-7.262	-0.072	-5.058	-27.461	-0.028
		426	0.002	-0.013	-1.404	-5.539	0.011	-4.853	-24.211	0.903
22	19:ULS-STR-5V	433	0.006	0.003	-0.009	-3.518	-0.001	-2.176	-3.312	-0.229
		372	0.006	-0.011	-0.009	-3.245	-0.085	2.769	2.714	-0.406
		7	0.000	-0.011	-0.698	-3.189	-0.085	-0.883	-4.436	0.156
		426	0.000	0.003	-0.698	-3.462	-0.002	-0.143	-0.910	0.334
22	21:ULS-STR-7V	433	0.012	-0.014	-0.066	-5.045	0.033	-5.110	-15.128	-0.340
		372	0.012	-0.057	-0.033	-6.804	-0.037	5.365	11.930	-1.244
		7	0.002	-0.057	-1.261	-6.757	-0.059	-4.926	-26.811	-0.046
		426	0.002	-0.014	-1.293	-4.999	0.012	-4.811	-23.951	0.858
22	26:ULS-STR-12	433	0.011	-0.014	-0.065	-4.560	0.033	-4.780	-14.613	-0.307
		372	0.011	-0.055	-0.032	-6.361	-0.025	4.937	11.437	-1.185
		7	0.002	-0.055	-1.165	-6.323	-0.047	-4.800	-26.169	-0.072
		426	0.002	-0.014	-1.198	-4.522	0.011	-4.805	-23.909	0.807

Calculation sheet No. 4.5			
Title:	<i>Structural calculations glulam diagonal</i>		
Design phase:	Final design		
Design state:	ULS		
References:	Table 5.11		
Column section properties		Characteristic strength/stiffness properties GL28h	
Depth; d	500 mm	$f_{m,g,k}$	28 MPa
Width; b	400 mm	$f_{t,0,g,k}$	19,5 MPa
Cross sectional area; A	2,0E+05 mm ²	$f_{c,0,g,k}$	26,5 MPa
W_y	1,67E+07 mm ³	$f_{v,g,k}$	3,2 MPa
W_z	1,33E+07 mm ³	$E_{0,g,mean}$	12600 MPa
I_y	4,17E+09 mm ⁴	$E_{90,g,mean}$	420 MPa
I_z	2,67E+09 mm ⁴	$G_{g,mean}$	780 MPa
		$E_{0,g,05}$	10200 MPa
ULS: Design strength/stiffness properties			
k_{mod}	0,9 (short-term, s.c. 1)		
γ_M	1,25		
Bending strength; $f_{m,g,d}$	$\frac{k_{mod} \cdot f_{m,g,k}}{\gamma_M} =$	20,16 MPa	
Tension strength; $f_{t,0,g,d}$	$\frac{k_{mod} \cdot f_{t,0,g,k}}{\gamma_M} =$	14,04 MPa	
Compressive strength; $f_{c,0,g,d}$	$\frac{k_{mod} \cdot f_{c,0,g,k}}{\gamma_M} =$	19,08 MPa	
Shear strength; $f_{v,d}$	$\frac{k_{mod} \cdot f_{v,k}}{\gamma_M} =$	2,30 MPa	
STAAD Pro results			
$M_{y,d}$	-10,37 kNm	ULS-STR-7	$V_{y,d}$ 4,34 kN ULS-STR-7
$M_{z,d}$	0,00 kNm	ULS-STR-7	$V_{z,d}$ 0,00 kN ULS-STR-7
$N_{c,d}$	1071,55 kN	ULS-STR-7	
$N_{t,d}$	-1035,59 kN	ULS-STR-7	
ULS: Compressive stress		ULS: Tensile stress	
$\sigma_{c,0,d}$	$\frac{N_{c,d}}{A} = 5,36$ MPa	$\sigma_{t,0,d}$	$\frac{N_{t,d}}{A} = -5,18$ MPa
Unity check	$\frac{\sigma_{c,0,d}}{f_{c,0,g,d}} \leq 1 \rightarrow 0,28$	Unity check	$\frac{\sigma_{t,0,d}}{f_{t,0,g,d}} \leq 1 \rightarrow 0,37$
ULS: Bending stresses			
$\sigma_{m,y,d}$	$\frac{M_{y,d}}{W_y} = 0,62$ MPa	$\sigma_{m,z,d}$	$\frac{M_{z,d}}{W_z} = 0,00$ MPa
Unity check	$\frac{\sigma_{m,y,d}}{f_{m,g,d}} \leq 1 \rightarrow 0,03$	Unity check	$\frac{\sigma_{m,z,d}}{f_{m,g,d}} \leq 1 \rightarrow 0,00$
Shear stresses			
b_{ef}	$k_{cr} \cdot b$	k_{cr}	0,67 (glulam)
b_{ef}	268 mm		
$\tau_{max,d}$	$\frac{3V_{y,d}}{2b_{ef} \cdot h} = 0,05$ MPa		
Unity check	$\frac{\tau_{max,d}}{f_{v,d}} \leq 1 \rightarrow 0,02$		

ULS: Combined bending and axial compression - equation 6.23 + 6.24 EC5

Effective length; L_{ey}	9552 mm	Effective length; L_{ez}	9552 mm
Radius of gyration; i_y	$\sqrt{\frac{I_y}{A}} = 144,34$	Radius of gyration; i_z	$\sqrt{\frac{I_z}{A}} = 115,47$
Slenderness ratio; λ_y	$\frac{L_{ey}}{i_y} = 66,18$	Slenderness ratio; λ_y	$\frac{L_{ez}}{i_z} = 82,72$
Relative slenderness; $\lambda_{rel,y}$	$\frac{\lambda_y}{\pi} \sqrt{\frac{f_{c,0,k}}{E_{0,05}}} = 1,074$	Relative slenderness; $\lambda_{rel,z}$	$\frac{\lambda_z}{\pi} \sqrt{\frac{f_{c,0,k}}{E_{0,05}}} = 1,342$
β_c	0,1		0,1
Factor; k_y	$0,5(1+\beta_c(\lambda_{rel,y}-0,3)+\lambda_{rel,y}^2)$	Factor; k_z	$0,5(1+\beta_c(\lambda_{rel,z}-0,3)+\lambda_{rel,z}^2)$
Factor; k_y	1,12	Factor; k_z	1,45
Instability factor; k_{cy}	$\frac{1}{k_y + \sqrt{k_y^2 - \lambda_{rel,y}^2}} = 0,71$	Instability factor; k_{cz}	$\frac{1}{k_z + \sqrt{k_z^2 - \lambda_{rel,z}^2}} = 0,50$
Modification factor; k_m	0,7		0,7
Design expression	$\frac{\sigma_{c,0,d}}{k_{c,y} f_{c,0,g,d}} + \frac{\sigma_{m,y,d}}{f_{m,g,d}} + k_m \frac{\sigma_{m,z,d}}{f_{m,g,d}}$	Design expression	$\frac{\sigma_{c,0,d}}{k_{c,z} f_{c,0,g,d}} + k_m \frac{\sigma_{m,y,d}}{f_{m,g,d}} + \frac{\sigma_{m,z,d}}{f_{m,g,d}}$
Unity check	0,429 < 1		0,586 < 1

ULS: Combined bending and axial compression - equation 6.35 EC5

Relative slenderness for bending; $\lambda_{rel,m}$	$\sqrt{\frac{f_{m,g,k}}{\sigma_{m,crit}}}$		
Critical bending stress; $\sigma_{m,crit}$	$\frac{0,78b^2}{hl_{ef}} E_{0,05} = 329,25 \text{ MPa}$		
$\lambda_{rel,m}$	0,29 < 0,75	$\rightarrow k_{crit} =$	1
Design expression	$\left(\frac{\sigma_{m,y,d}}{k_{crit} f_{m,g,d}}\right)^2 + \frac{\sigma_{c,0,d}}{k_{c,z} f_{c,0,g,d}} = 0,565$		
Unity check	0,565 < 1		

Calculation sheet No. 4.6			
Title:		Structural calculations CLT core walls	
Design phase:	Final design		
Design state:	ULS		
References:	Table 5.12		
CLT panel properties			
Thickness; d	300 mm	Build-up	80-30-80-30-80 mm
$E_{0,mean}$	12000 MPa	$E_{90,mean}$	370 MPa
$G_{0,mean}$	250 MPa	$G_{90,mean}$	60 MPa
$E_{0,d}$	$\frac{E_{0,mean}}{\gamma_M} = 9600$ MPa	$E_{90,d}$	$\frac{E_{90,mean}}{\gamma_M} = 296$ MPa
$E_{0,05}$	7.400 MPa		
$G_{0,d}$	$\frac{G_{0,mean}}{\gamma_M} = 200$ MPa	$G_{90,d}$	$\frac{G_{90,mean}}{\gamma_M} = 48$ MPa
a_1	240 mm	a_2	60 mm
k_3	$1 - \left(1 - \frac{E_{90,d}}{E_{0,d}}\right) \cdot \frac{a_2}{d} = 0,806$		
Characteristic strength/stiffness panel properties			
$f_{m,k}$	23 MPa	$f_{t,0,k}$	16,5 MPa
$f_{v,k}$	5,2 MPa	$f_{c,0,k}$	24 MPa
ULS: Design strength/stiffness panel properties			
k_{mod}	0,9 (short-term, s.c. 1)		
γ_M	1,25		
Bending strength; $f_{m,d}$	$\frac{k_{mod} \cdot f_{m,k}}{\gamma_M} = 16,56$ MPa		
Tension strength; $f_{t,0,d}$	$\frac{k_{mod} \cdot f_{t,0,k}}{\gamma_M} = 11,88$ MPa		
Compressive strength; $f_{c,0,d}$	$\frac{k_{mod} \cdot f_{c,0,k}}{\gamma_M} = 17,28$ MPa		
Shear strength; $f_{v,d}$	$\frac{k_{mod} \cdot f_{v,k}}{\gamma_M} = 3,74$ MPa		
STAAD Pro results			
Bending moment; $M_{y,d}$	-26,09 kNm/m ULS-STR-7V	Tensile stress; $\sigma_{t,0,d}$	3,23 MPa ULS-STR-12V
Compressive stress; $\sigma_{c,0,d}$	-7,34 MPa ULS-STR-7V	Shear stress; $\tau_{max,d}$	-1,02 MPa ULS-STR-7V
ULS: Compressive stress		ULS: Tensile stress	
Compr. strength; $f_{c,0,CLT,d}$	$f_{c,0,d} \cdot k_3 = 13,93$ MPa	Tensile strength; $f_{t,0,CLT,d}$	$f_{t,0,d} \cdot k_3 = 9,58$ MPa
Unity check	$\frac{\sigma_{c,0,d}}{f_{c,0,CLT,d}} \leq 1 \rightarrow 0,53$	Unity check	$\frac{\sigma_{t,0,d}}{f_{t,0,CLT,d}} \leq 1 \rightarrow 0,34$
ULS: Shear stresses		ULS: Bending stresses	
Shear strength; $f_{v,CLT,d}$	$f_{v,d} = 3,74$ MPa	Bending strength; $f_{m,CLT,d}$	$f_{m,d} \cdot k_3 = 13,35$ MPa
Unity check	$\frac{\tau_{max,d}}{f_{v,d}} \leq 1 \rightarrow 0,27$	Unity check	$\frac{\sigma_{m,y,d}}{f_{m,CLT,d}} \leq 1 \rightarrow 0,16$

ULS: Combined bending and axial compression - equation 6.23 + 6.24

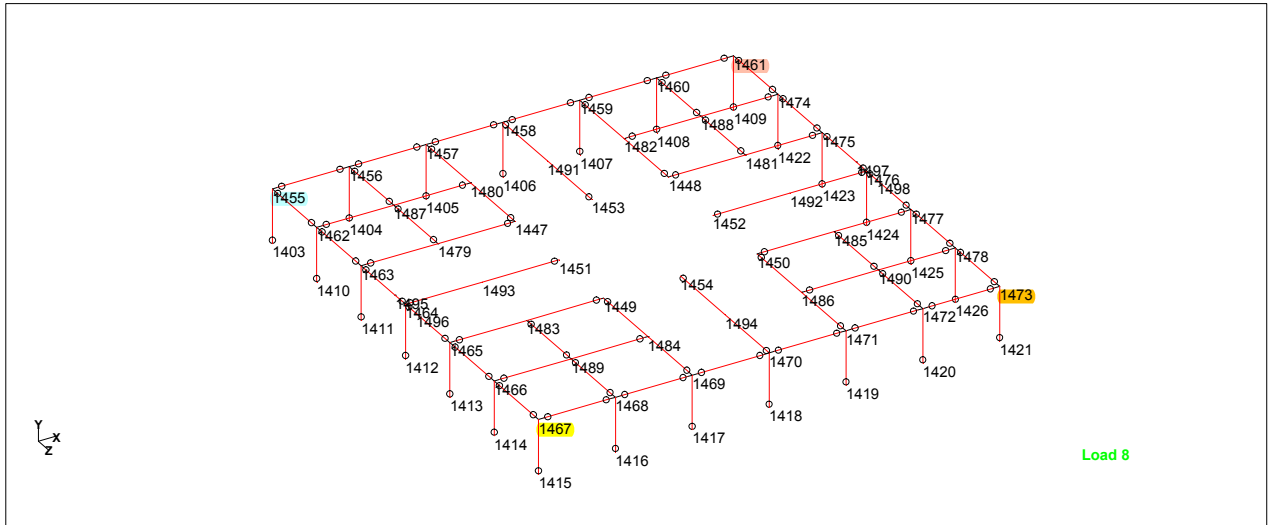
Cross sectional area; A_{eff}	$1\,000 \cdot d \cdot k_3 = 2,42E+05 \text{ mm}^2$
Effective length; L_{ey}	3.200 mm
Effective stiffness; $I_{y,eff}$	$\frac{k_3 \cdot 1\,000 \cdot d^3}{12} = 1,81E+09 \text{ mm}^4$
Bending stress; $\sigma_{m,y,d}$	$\frac{M_{y,d} \cdot d}{2 \cdot I_{y,eff}} = 2,16 \text{ MPa}$
Radius of gyration; i_y	$\sqrt{\frac{I_{y,eff}}{A_{eff}}} = 86,60$
Slenderness ratio; λ_y	$\frac{L_{ey}}{i_y} = 36,95$
Relative slenderness; $\lambda_{rel,y}$	$\frac{\lambda_y}{\pi} \sqrt{\frac{f_{c,0,k}}{E_{0,05}}} = 0,67$
β_c	0,1
Factor; k_y	$0,5 \left(1 + \beta_c (\lambda_{rel,y} - 0,3) + \lambda_{rel,y}^2 \right)$
Factor; k_y	0,74
Instability factor; $k_{c,y}$	$\frac{1}{k_y + \sqrt{k_y^2 - \lambda_{rel,y}^2}} = 0,94$
Modification factor; k_m	0,7
Design expression	$\frac{\sigma_{c,0,d}}{k_{c,y} f_{c,0,CLT,d}} + k_m \frac{\sigma_{m,y,d}}{f_{m,CLT,d}}$
Unity check	0,67 < 1



Academic license user TU Eindhoven

Job No	Sheet No 1	Rev
Part		
Ref		
By	Date	Chd
File Static model	Date/Time	

Job Title Static analysis - variable load 1 side
Static displacements top floor
 Client TU Eindhoven



Top floor frame structure

Nodes

Node	X (m)	Y (m)	Z (m)
1455	0.000	67.200	0.000
1461	27.000	67.200	0.000
1467	0.000	67.200	27.000
1473	27.000	67.200	27.000

Node Displacements

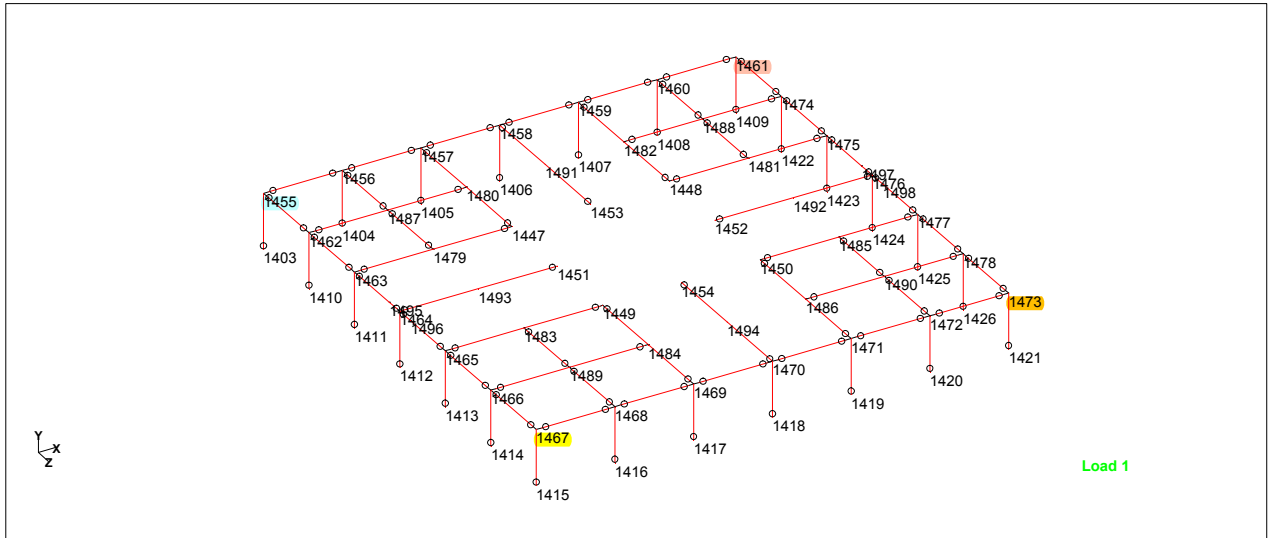
Node	L/C	X (mm)	Y (mm)	Z (mm)	Resultant (mm)	rX (rad)	rY (rad)	rZ (rad)
1455	33:SLS-CHA-3	90.741	-2.579	0.041	90.778	0.000	0.000	-0.001
1461	33:SLS-CHA-3	90.698	-3.812	-1.326	90.787	0.000	0.000	-0.001
1467	33:SLS-CHA-3	92.142	-2.587	0.034	92.178	-0.000	0.000	-0.001
1473	33:SLS-CHA-3	92.098	-3.810	-1.347	92.187	-0.000	0.000	-0.001



Academic license user TU Eindhoven

Job No	Sheet No 1	Rev
Part		
Ref		
By	Date	Chd
Client	File Static model	Date/Time

Job Title
Static displacements top floor - no outriggers



Top floor frame structure

Nodes

Node	X (m)	Y (m)	Z (m)
1455	0.000	67.200	0.000
1461	27.000	67.200	0.000
1467	0.000	67.200	27.000
1473	27.000	67.200	27.000

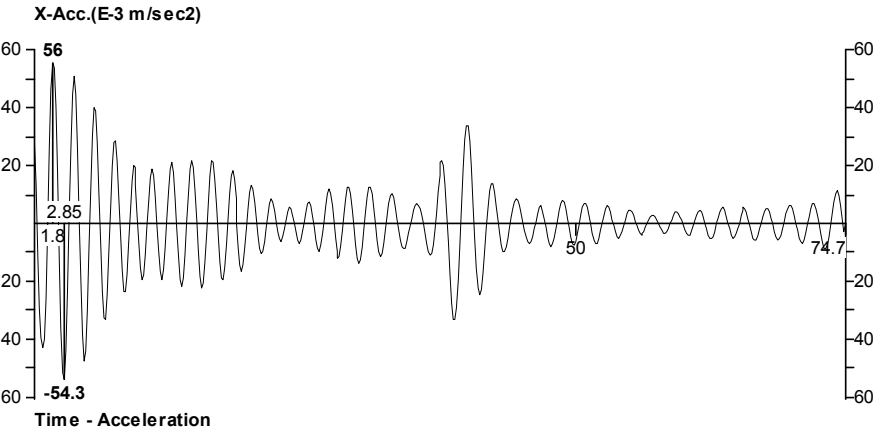
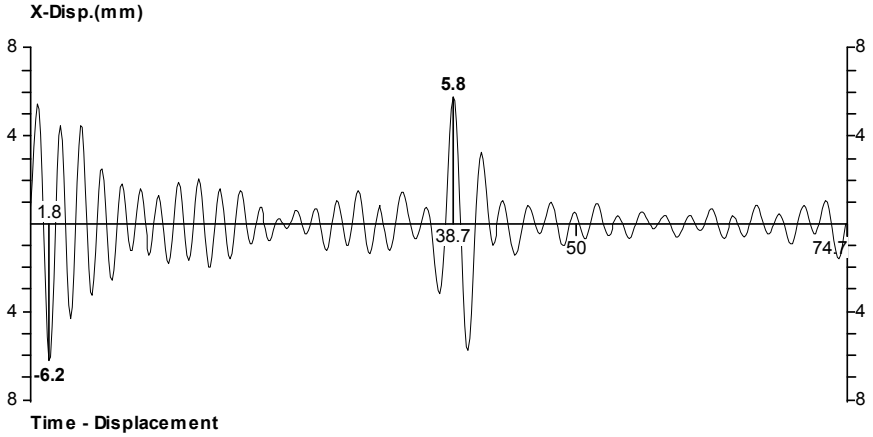
Node Displacements

Node	L/C	X (mm)	Y (mm)	Z (mm)	Resultant (mm)	rX (rad)	rY (rad)	rZ (rad)
1455	33:SLS-CHA-3	117.003	-2.586	-0.172	117.031	0.000	0.000	-0.002
1461	33:SLS-CHA-3	116.966	-4.521	-1.184	117.059	0.000	0.000	-0.001
1467	33:SLS-CHA-3	117.999	-2.593	-0.204	118.027	-0.000	0.000	-0.002
1473	33:SLS-CHA-3	117.962	-4.518	-1.172	118.054	-0.000	0.000	-0.001

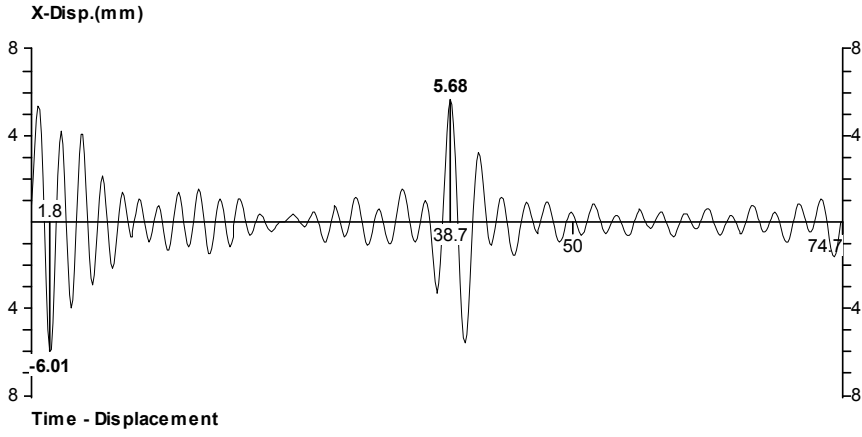
C.2 | FINAL DYNAMIC CALCULATIONS

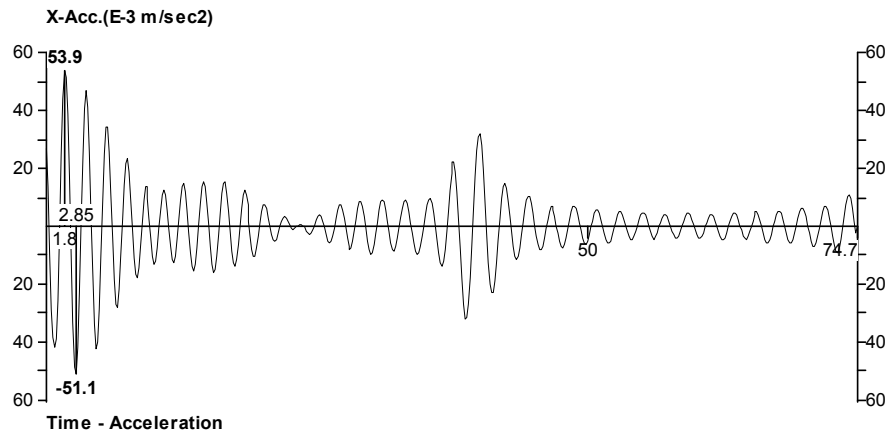
Reference: Table 6.1

DYNAMIC RESPONSE: 1% DAMPING

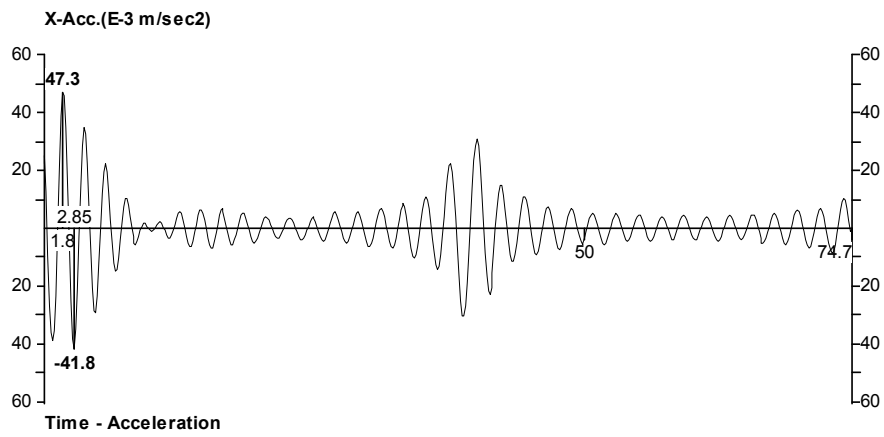
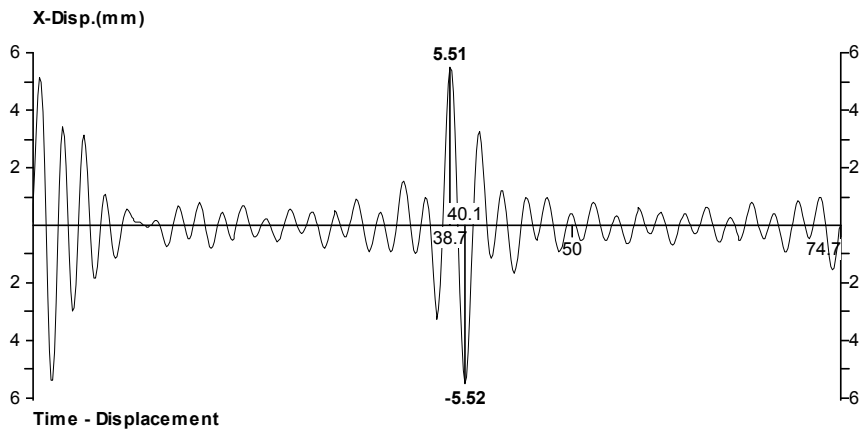


DYNAMIC RESPONSE: 1.9% DAMPING

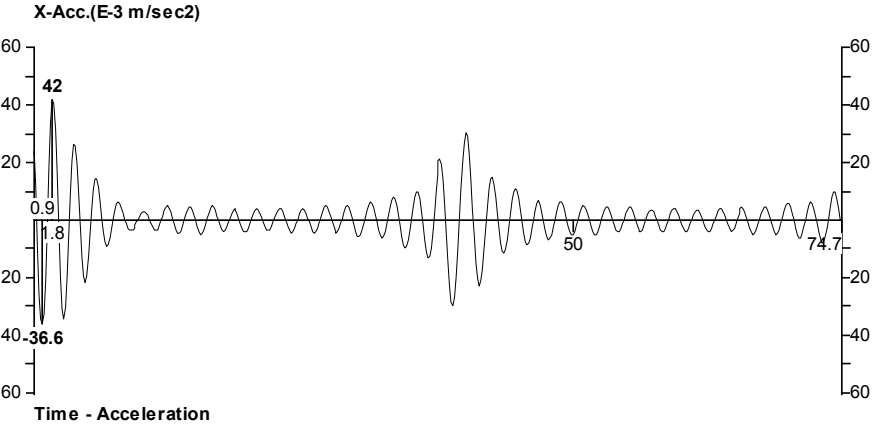
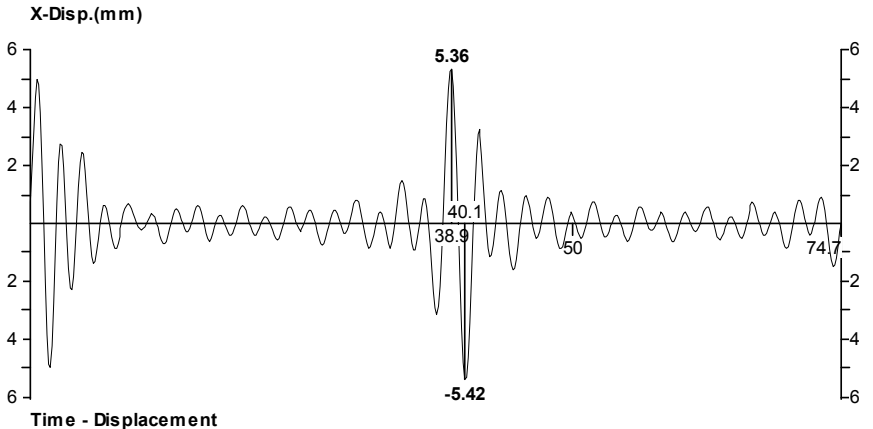




DYNAMIC RESPONSE: 5% DAMPING



DYNAMIC RESPONSE: 8% DAMPING



D.1 | STRUCTURAL CONNECTIONS CALCULATIONS

Calculation Sheet 6.1: *Connection type 1*

Calculation Sheet 6.2: *Connection type 9+10 – block- and plug shear*

Calculation Sheet 6.3: *Connection type 9+10 – steel design*

STAAD Pro results: *Connection forces*

Calculation sheet No. 6.1				
Title:		Connection type 1		
Design phase:	Final design			
Design state:	ULS			
References:	Section 7.3			
Bolt properties M20 8.8				
Diameter; d	20	mm	Design tensile strength; $F_{t,u,d}$	141,12 kN
Area; $A_{b,s}$	245	mm ²	Design shear strength; $F_{v,u,d}$	94,08 kN
Characteristic tensile strength; $f_{t,b,d}$	800	MPa.		
Loading			Number of bolts	
Vertical tensile load; $q_{t,s,d}$	984	kN/m	Tensile forces; n	7 n/m
Lateral shear force; $F_{v,s,d}$	1 836	kN	Shear forces; n	20 -
Spacing of bolts				
Over wall length 0 - 2.325 m	2 x M20 / 250 mm			
2.325 - 6.975 m	2 x M20 / 465 mm			
6.975 - 9.3 m	2 x M20 / 250 mm			
Steel beam HEA-140				
Web thickness; t_w	7	mm	Yield strength; s235	235 MPa.
Web area; A_w	7 000	mm ² /m		
Loading				
Vertical compressive load; $q_{c,s,d}$	2 200	kN/m		
Load per beam; $q_{c,s,d}$	1 100	kN/m		
Compressive stress; $\sigma_{c,s,d}$	157,14	MPa.	≤ 235 MPa.	
Washers in concrete				
Diameter; d	100	mm		
Area; $A_{w,net}$	7 539,82	mm ²		
Loading on steel rods				
Concrete strength C28/35; $f_{c,k}$	35	MPa.		
Design concrete strength; $f_{c,k} / \gamma_M$	23,3	MPa.		
Maximum load in steel rod M20; $F_{t,u,d}$	141,12	kN		
Compressive stress in concrete; $\sigma_{c,s,d}$	18,7	MPa.	$\leq 23,3$ MPa.	

Calculation sheet No. 6.2			
Title:	Connection type 9+10 - block- and plug shear		
Design phase:	Final design		
Design state:	ULS		
References:	Section 7.5		
Load carrying capacity along perimeter			
$F_{bs,Rk}$	$\max \left\{ \begin{array}{l} 1.5A_{net,t}f_{t,0,g,k} = 878 \text{ kN} \\ 0.7A_{net,v}f_{v,g,k} = 545 \text{ kN} \end{array} \right.$ /steel plate → block shear failure		
<i>Block shear</i>	<i>Plug shear</i>		
Fracture area; $A_{net,t}$	$L_{net,t}t_1$	Fracture area; $A_{net,v}$	$(L_{net,v}/2)(L_{net,t}+2t_{ef})$
Fracture length; $L_{net,t}$	$a_2(n_{p,2}-1)$	Fracture length; $L_{net,v}$	a_1n_p
Spacing; a_2	60 mm	Spacing; a_1	84 mm
No. dowels perimeter; $n_{p,2}$	6 -	No. dowels perimeter;	15 -
Penetration depth; t_1	100 mm	Effective depth; t_{ef}	$t_1 \left[\sqrt{2 + \frac{M_{y,Rk}}{f_{h,k}dt_1^2}} - 1 \right] = 42,94 \text{ mm}$
Fracture area; $A_{net,t}$	30000 mm ²	Fracture area; $A_{net,v}$	243106,29 mm ²
Characteristic strength properties GL28h			
$f_{t,0,g,k}$	19,5 MPa		
$f_{v,g,k}$	3,2 MPa		
Design Load carrying capacity along perimeter			
$F_{bs,Rd}$	$k_{mod} \frac{2F_{bs,Rk}}{\gamma_M} = 0,9 \frac{(2 \cdot 878)}{1,25} = 1263,6 \text{ kN}$		

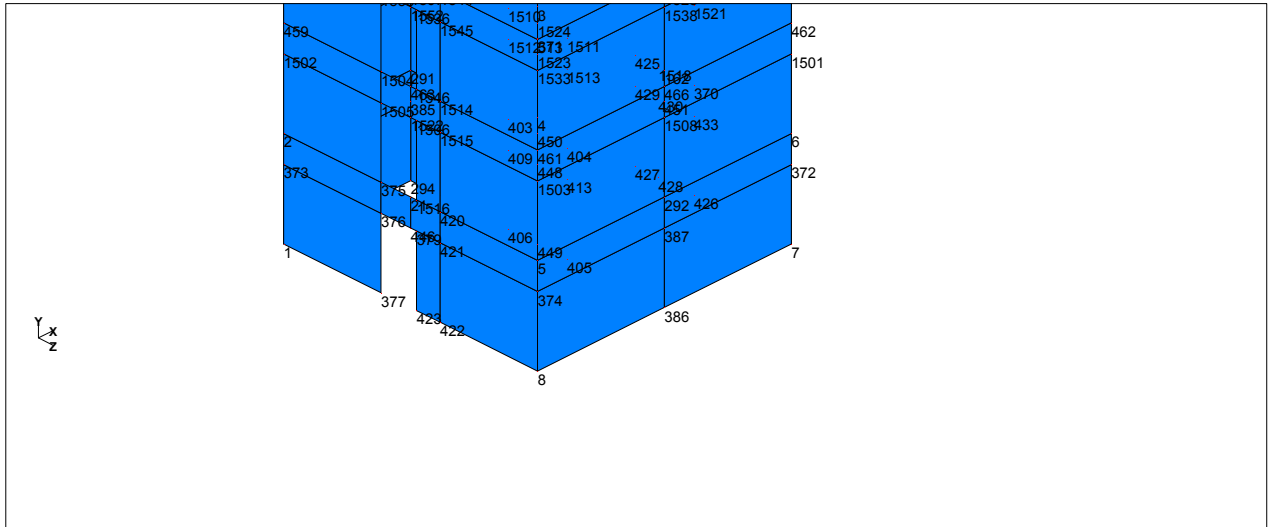
Calculation sheet No. 6.3				
Title: <i>Connection type 9+10 - steel design</i>				
Design phase:	Final design			
Design state:	ULS			
References:	Section 7.3			
Bolt properties M24 8.8				
Diameter; d	24	mm	Design tensile strength; $F_{t,u,d}$	203,328 kN
Area; $A_{b,s}$	353	mm ²	Design shear strength; $F_{v,u,d}$	135,552 kN
Characteristic tensile strength; $f_{t,b,d}$	800	MPa.		
Bolt properties M30 8.8				
Diameter; d	30	mm	Design tensile strength; $F_{t,u,d}$	323,136 kN
Area; $A_{b,s}$	561	mm ²	Design shear strength; $F_{v,u,d}$	215,424 kN
Characteristic tensile strength; $f_{t,b,d}$	800	MPa.		
<i>Connection type 9</i>				
Loading			Bolts	
Tensile force; $F_{t,S,d}$	816	kN	Type	M30
Lateral shear force; $F_{v,S,d}$	424	kN	Number of bolts; n	6 -
Unity check				
Tension - shear	$\frac{F_{v,S,d}}{F_{v,u,d}} + \frac{F_{t,S,d}}{1.4F_{t,u,d}} \leq 1 \rightarrow$		0,63	< 1
<i>Connection type 10 - beam - column</i>				
Loading			Bolts	
Lateral shear force; $F_{v,S,d}$	630	kN	Type	M24
			Number of bolts; n	6 -
Unity check				
Shear	$\frac{F_{v,S,d}}{F_{v,u,d}} \leq 1 \rightarrow$		0,77	< 1
<i>Connection type 10 - beam - diagonal</i>				
Loading			Bolts	
Tensile force; $F_{t,S,d}$	630	kN	Type	M30
Lateral shear force; $F_{v,S,d}$	976	kN	Number of bolts; n	6 -
Unity check				
Tension - shear	$\frac{F_{v,S,d}}{F_{v,u,d}} + \frac{F_{t,S,d}}{1.4F_{t,u,d}} \leq 1 \rightarrow$		0,99	< 1



Academic license user TU Eindhoven

Job No	Sheet No 1	Rev
Part		
Ref		
By	Date	Chd
File	Static model	Date/Time

Job Title Static analysis - variable load 1 side
Reaction forces connection type 1
 Client TU Eindhoven



Supports 7, 8 and 386 of CLT wall grid E

Reactions

Node	L/C	Horizontal	Vertical	Horizontal	Moment		
		FX (kN)	FY (kN)	FZ (kN)	MX (kNm)	MY (kNm)	MZ (kNm)
7	9:ULS-EQU-2	-721.984	7.16E+3	-337.522	1.75E+3	7.551	-1.93E+3
8	9:ULS-EQU-2	-442.053	-2.3E+3	99.073	-567.656	13.781	-96.025
386	9:ULS-EQU-2	-671.394	3.36E+3	-119.407	474.353	15.137	2.29E+3

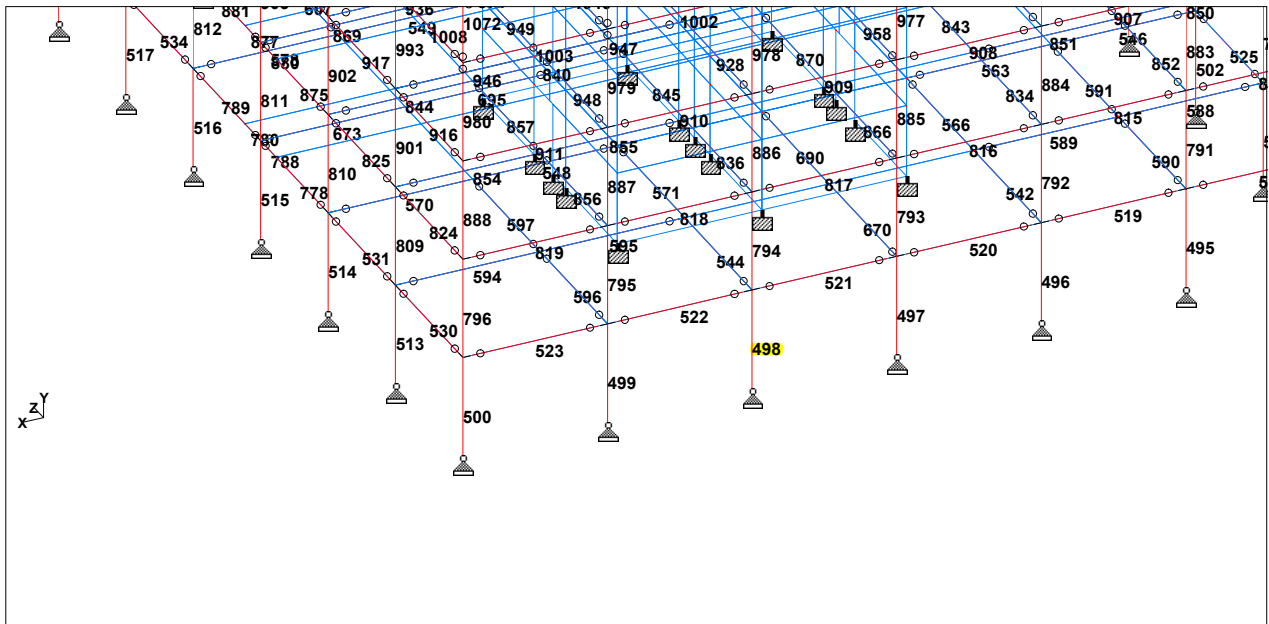


Academic license user TU Eindhoven

Job No	Sheet No 1	Rev
Part	Ref	
By	Date	Chd
File Static model	Date/Time	

Job Title Static analysis - variable load 1 side
Connection type 5 forces

Client TU Eindhoven



Column no. 498

Beam Maximum Axial Forces

Distances to maxima are given from beam end A.

Beam	Node A	Length (m)	L/C		d (m)	Max Fx (kN)
498	303	3.200	19:ULS-STR-5v	Max -ve	0.000	2.32E+3
				Max +ve		

Beam Maximum Shear Forces

Distances to maxima are given from beam end A.

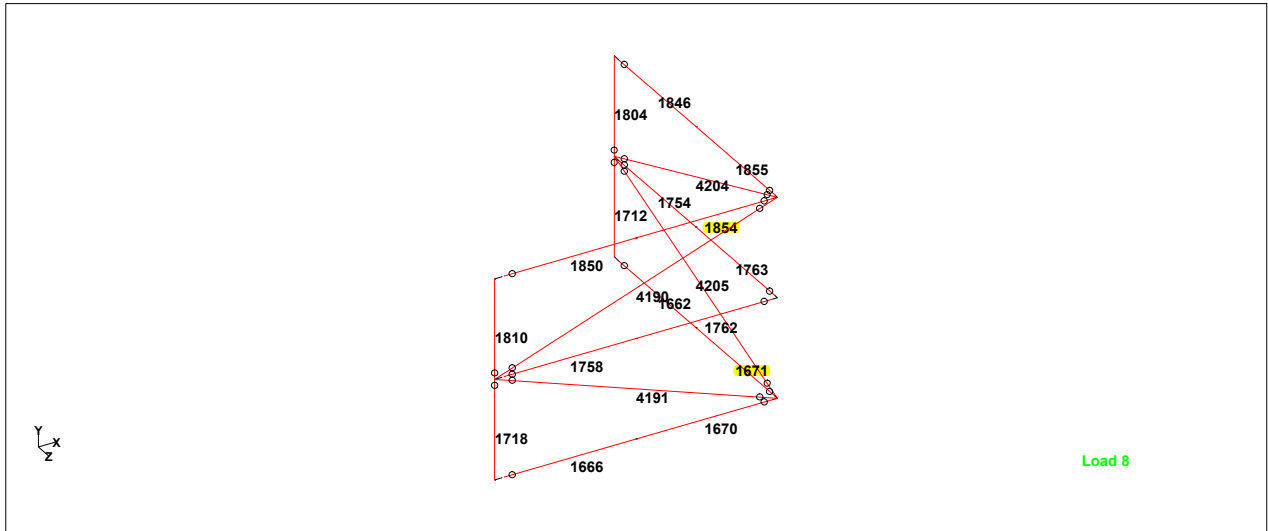
Beam	Node A	Length (m)	L/C		d (m)	Max Fz (kN)	d (m)	Max Fy (kN)
498	303	3.200	19:ULS-STR-5v	Max -ve	0.000	7.636		
				Max +ve			0.000	-0.888



Academic license user TU Eindhoven

Job No	Sheet No 1	Rev
Part		
Ref		
By	Date	Chd
File	Static model	Date/Time

Job Title Static analysis - variable load 1 side
Connection type 6 - forces
 Client TU Eindhoven



<Untitled 2>

Beam Maximum Axial Forces

Distances to maxima are given from beam end A.

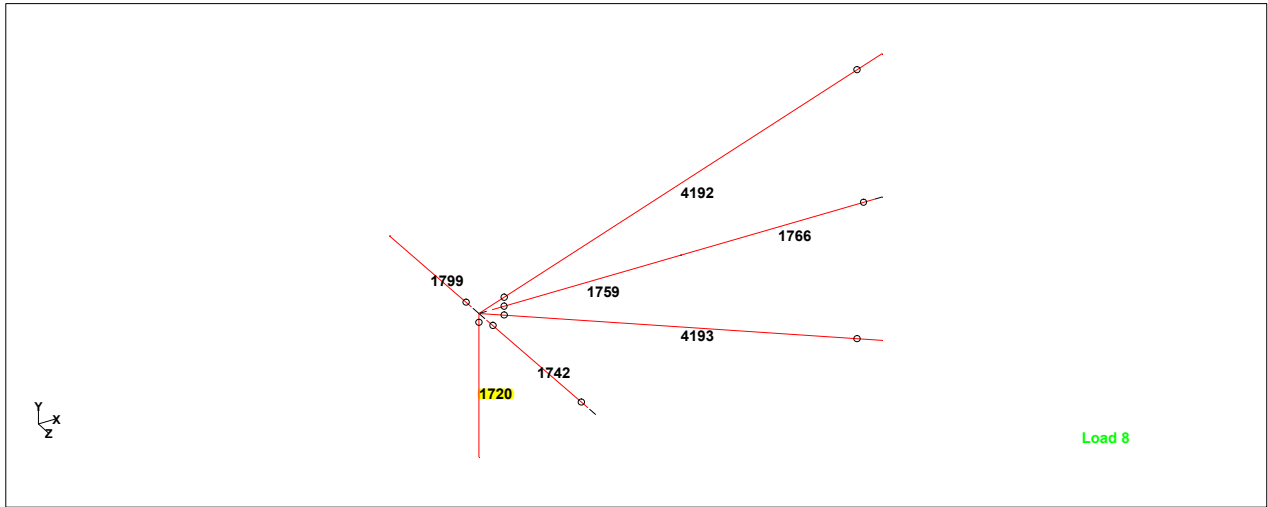
Beam	Node A	Length (m)	L/C		d (m)	Max Fx (kN)
1671	960	4.350	16:ULS-STR-7	Max -ve		
				Max +ve	0.000	-74.504
1854	1063	4.350	16:ULS-STR-7	Max -ve	0.000	159.254
				Max +ve		



Academic license user TU Eindhoven

Job No	Sheet No 1	Rev
Part		
Ref		
By	Date	Chd
File Static model	Date/Time	

Job Title Static analysis - variable load 1 side
Connection type 7 - axial forces
 Client TU Eindhoven



<Untitled 1>

Beam Maximum Axial Forces

Distances to maxima are given from beam end A.

Beam	Node A	Length (m)	L/C		d (m)	Max Fx (kN)
1720	945	3.200	9:ULS-EQU-2	Max -ve		
				Max +ve	3.200	-275.880

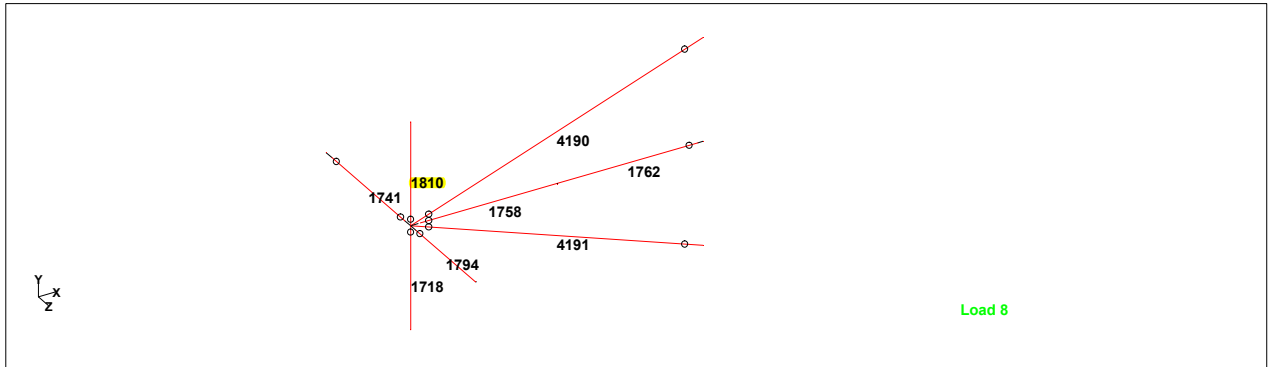


Academic license user TU Eindhoven

Job No	Sheet No 1	Rev
Part		
Ref		
By	Date	Chd
File Static model	Date/Time	

Job Title Static analysis - variable load 1 side
Connection type 7 - shear forces

Client TU Eindhoven



<Untitled 1>

Beam Maximum Shear Forces

Distances to maxima are given from beam end A.

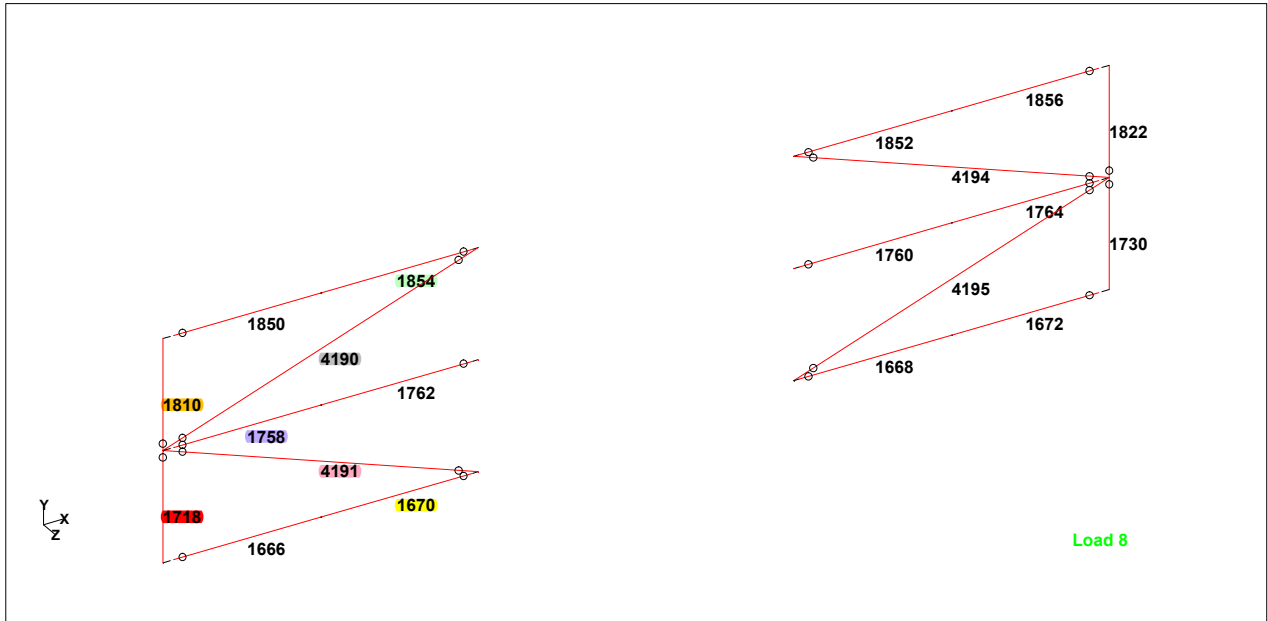
Beam	Node A	Length (m)	L/C		d (m)	Max Fz (kN)	d (m)	Max Fy (kN)
1810	995	3.200	21:ULS-STR-7v	Max -ve	0.000	0.278		
				Max +ve			3.200	-40.078



Academic license user TU Eindhoven

Job No	Sheet No 1	Rev
Part		
Ref		
By	Date	Chd
File Static model	Date/Time	

Job Title Static analysis - variable load 1 side
Connection type 9+10 - axial forces
 Client TU Eindhoven



<Untitled 3>

Beam Maximum Axial Forces

Distances to maxima are given from beam end A.

Beam	Node A	Length (m)	L/C		d (m)	Max Fx (kN)
1666	943	4.200	16:ULS-STR-7	Max -ve		
				Max +ve	0.000	-22.477
1668	928	4.350	16:ULS-STR-7	Max -ve	0.000	78.670
				Max +ve		
1670	959	4.350	16:ULS-STR-7	Max -ve		
				Max +ve	0.000	-52.109
1672	961	4.200	16:ULS-STR-7	Max -ve	0.000	47.763
				Max +ve		
1718	943	3.200	16:ULS-STR-7	Max -ve		
				Max +ve	3.200	-77.618
1730	955	3.200	16:ULS-STR-7	Max -ve	0.000	1.31E+3
				Max +ve		
1758	995	4.200	16:ULS-STR-7	Max -ve	0.000	7.569
				Max +ve		
1760	980	4.350	16:ULS-STR-7	Max -ve		
				Max +ve	0.000	-5.944
1762	1011	4.350	16:ULS-STR-7	Max -ve	0.000	28.373
				Max +ve		
1764	1013	4.200	16:ULS-STR-7	Max -ve		
				Max +ve	0.000	-13.280
1810	995	3.200	16:ULS-STR-7	Max -ve	0.000	562.912
				Max +ve		
1822	1007	3.200	16:ULS-STR-7	Max -ve	0.000	713.311
				Max +ve		
1850	1047	4.200	16:ULS-STR-7	Max -ve	0.000	96.484
				Max +ve		
1852	1032	4.350	16:ULS-STR-7	Max -ve		



Academic license user TU Eindhoven

Job No	Sheet No 2	Rev
Part		
Ref		
By	Date 03-Apr-12	Chd
File Static model - variable load	Date/Time 03-Apr-2012 16:59	

Job Title Static analysis - variable load 1 side
Connection type 9+10 - axial forces
 Client TU Eindhoven

Beam Maximum Axial Forces Cont...

Beam	Node A	Length (m)	L/C		d (m)	Max Fx (kN)
				Max +ve	0.000	-67.958
1854	1063	4.350	16:ULS-STR-7	Max -ve	0.000	159.254
				Max +ve		
1856	1065	4.200	16:ULS-STR-7	Max -ve		
				Max +ve	0.000	-45.388
4190	995	9.552	16:ULS-STR-7	Max -ve		
				Max +ve	9.552	-1.04E+3
4191	995	9.552	16:ULS-STR-7	Max -ve	9.552	1.07E+3
				Max +ve		
4194	1007	9.552	16:ULS-STR-7	Max -ve	0.000	761.218
				Max +ve		
4195	1007	9.552	16:ULS-STR-7	Max -ve		
				Max +ve	0.000	-742.068

D.2 | SLIP IN CONNECTIONS– STATIC RESULTS

STAAD Pro results:

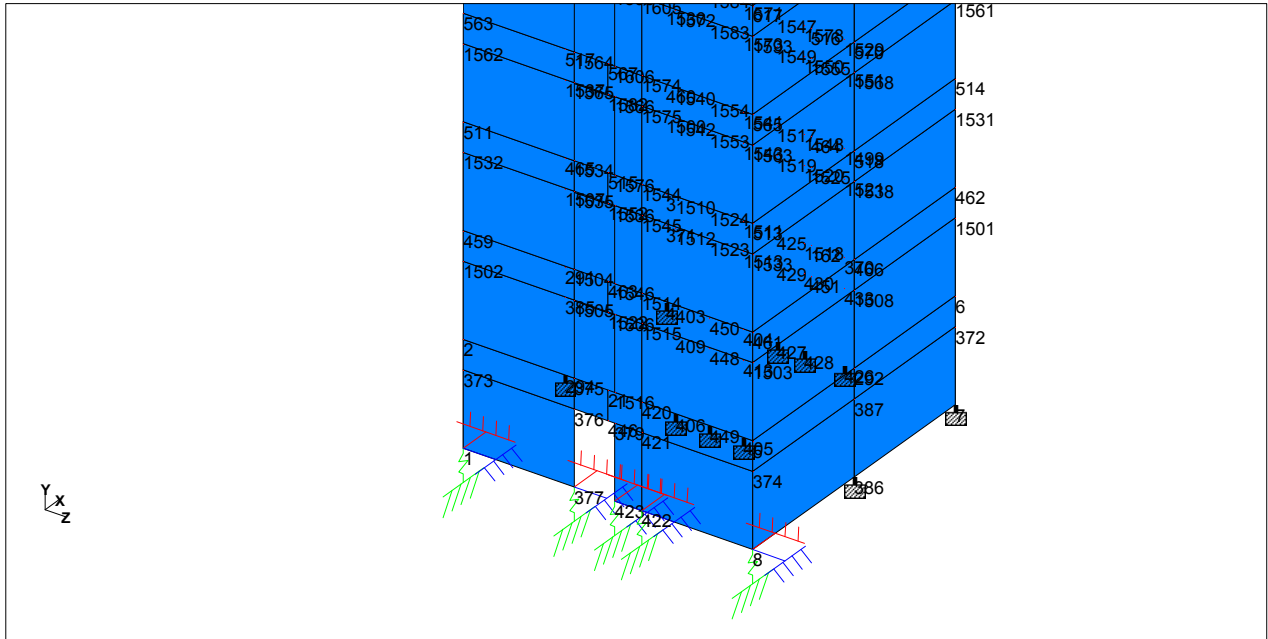
- Model Ia; translational springs type 1 & 2*
- Model Ib; translational springs type 1,2 & 3*
- Model II; translational springs beams*
- Model IIIa; translational springs diagonals*
- Model IIIb; translational springs diagonals and columns below outriggers*
- Model I+II+III*
- Model IV: I + II + III + rotational rigid outrigger elements*
- Model V: I + II + III + rotational rigid peripheral columns*



Academic license user TU Eindhoven

Job No	Sheet No	Rev
	1	
Part	Ref	
	By	Chd
Client	File	Date/Time
	Static model	

Job Title
Model Ia



Supports

Node	X (kN/mm)	Y (kN/mm)	Z (kN/mm)	rX (kN`m/deg)	rY (kN`m/deg)	rZ (kN`m/deg)
1	Fixed	73.903	Fixed	Fixed	Fixed	Fixed
8	Fixed	73.903	Fixed	Fixed	Fixed	Fixed
377	Fixed	19.606	Fixed	Fixed	Fixed	Fixed
422	Fixed	22.623	Fixed	Fixed	Fixed	Fixed
423	Fixed	3.015	Fixed	Fixed	Fixed	Fixed

Node Displacements

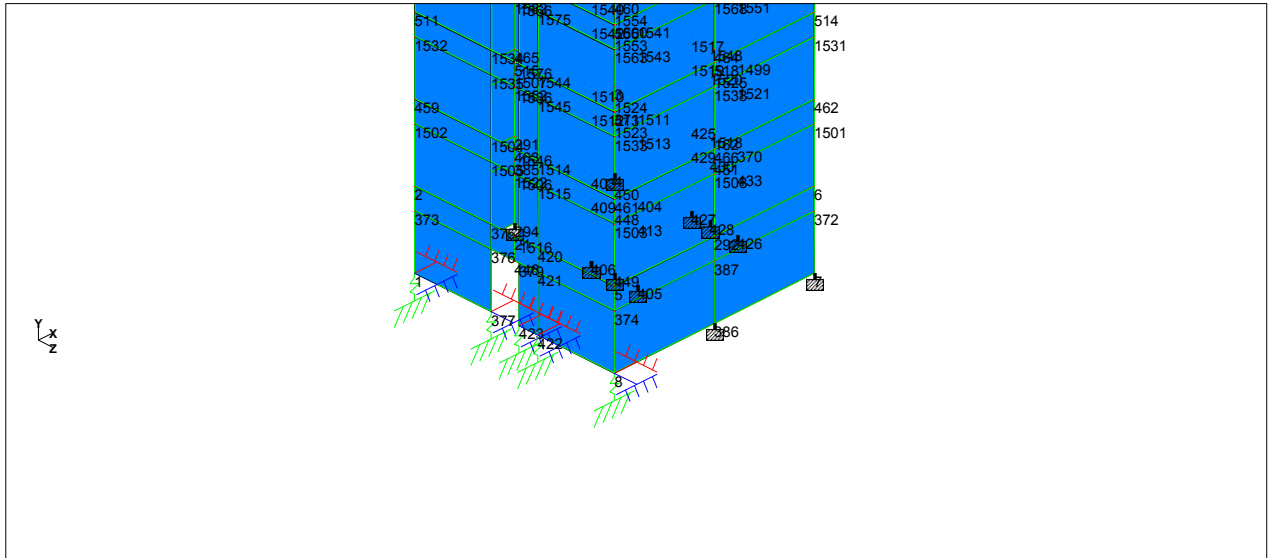
Node	L/C	X (mm)	Y (mm)	Z (mm)	Resultant (mm)	rX (rad)	rY (rad)	rZ (rad)
1	33:SLS-CHA-3	0.000	2.755	0.000	2.755	0.000	0.000	0.000
8	33:SLS-CHA-3	0.000	2.860	0.000	2.860	0.000	0.000	0.000
377	33:SLS-CHA-3	0.000	2.656	0.000	2.656	0.000	0.000	0.000
422	33:SLS-CHA-3	0.000	2.673	0.000	2.673	0.000	0.000	0.000
423	33:SLS-CHA-3	0.000	2.648	0.000	2.648	0.000	0.000	0.000
1455	33:SLS-CHA-3	104.328	-2.565	0.038	104.360	0.000	0.000	-0.001



Academic license user TU Eindhoven

Job No	Sheet No 1	Rev
Part		
Ref		
By	Date	Chd
Client	File Static model	Date/Time

Job Title
Model Ib



Supports

Node	X (kN/mm)	Y (kN/mm)	Z (kN/mm)	rX (kN°m/deg)	rY (kN°m/deg)	rZ (kN°m/deg)
1	Fixed	12.950	Fixed	Fixed	Fixed	Fixed
8	Fixed	12.950	Fixed	Fixed	Fixed	Fixed
377	Fixed	19.606	Fixed	Fixed	Fixed	Fixed
422	Fixed	22.623	Fixed	Fixed	Fixed	Fixed
423	Fixed	3.015	Fixed	Fixed	Fixed	Fixed

Node Displacements

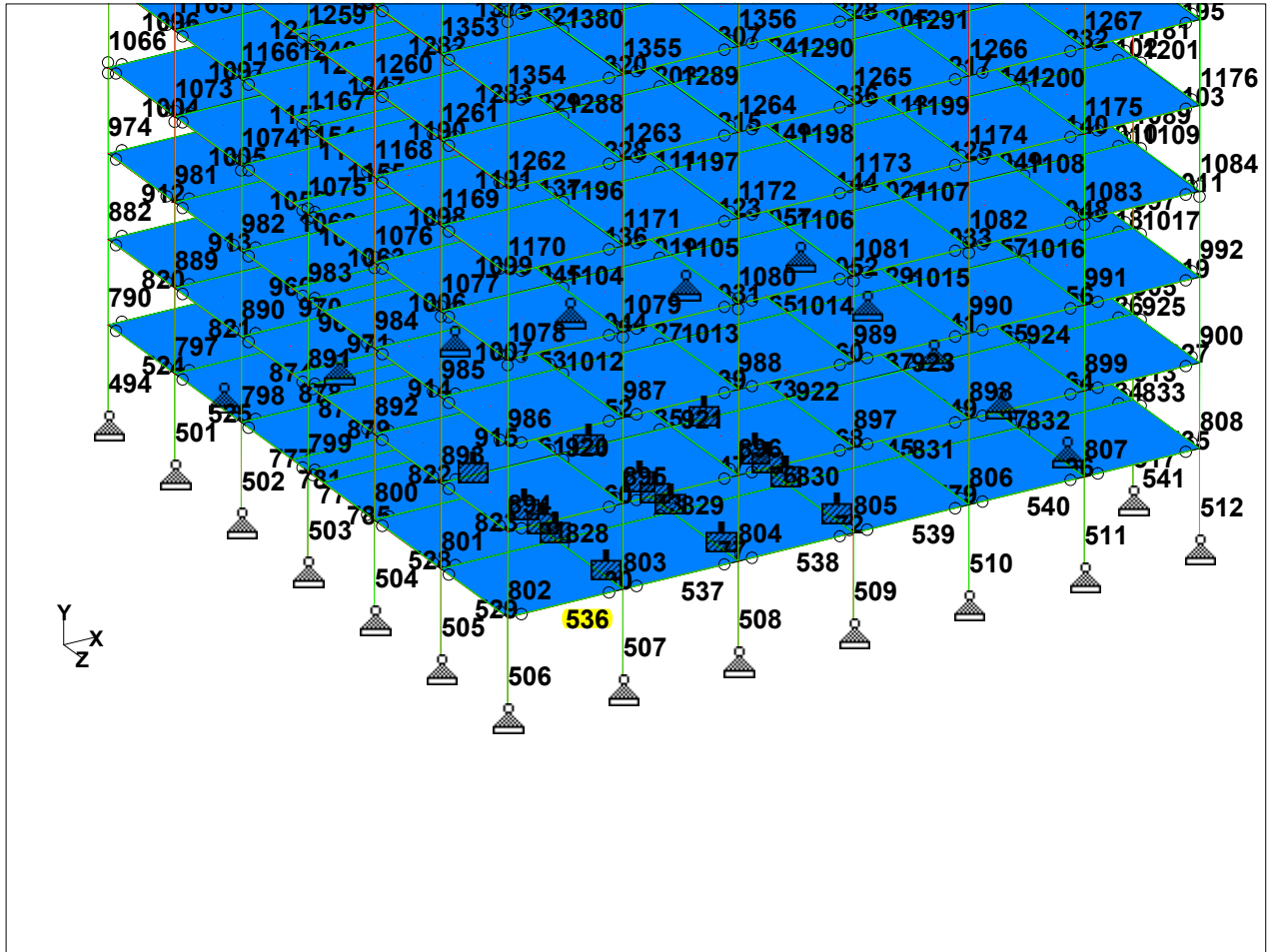
Node	L/C	X (mm)	Y (mm)	Z (mm)	Resultant (mm)	rX (rad)	rY (rad)	rZ (rad)
1	33:SLS-CHA-3	0.000	3.338	0.000	3.338	0.000	0.000	0.000
8	33:SLS-CHA-3	0.000	3.453	0.000	3.453	0.000	0.000	0.000
377	33:SLS-CHA-3	0.000	3.037	0.000	3.037	0.000	0.000	0.000
422	33:SLS-CHA-3	0.000	3.056	0.000	3.056	0.000	0.000	0.000
423	33:SLS-CHA-3	0.000	3.037	0.000	3.037	0.000	0.000	0.000
1455	33:SLS-CHA-3	106.919	-2.562	0.026	106.949	0.000	0.000	-0.001



Academic license user TU Eindhoven

Job No	Sheet No 1	Rev
Part		
Ref		
By	Date	Chd
File	Static model	Date/Time

Job Title Model II
Client



Example: Beam 536

Beams

Beam	Node A	Node B	Length (m)	Property	β (degrees)
536	320	322	3.900	4	0

Releases

Beam ends not shown in this table are fixed in all directions.

Beam	Node	x	y	z	rx	ry	rz
536	320	Spring	Fixed	Fixed	Pin	Pin	Pin
536	322	Spring	Fixed	Fixed	Pin	Pin	Pin

Node Displacements

Node	L/C	X (mm)	Y (mm)	Z (mm)	Resultant (mm)	rX (rad)	rY (rad)	rZ (rad)
1455	33:SLS-CHA-3	91.196	-2.578	-0.014	91.232	0.000	-0.000	-0.001

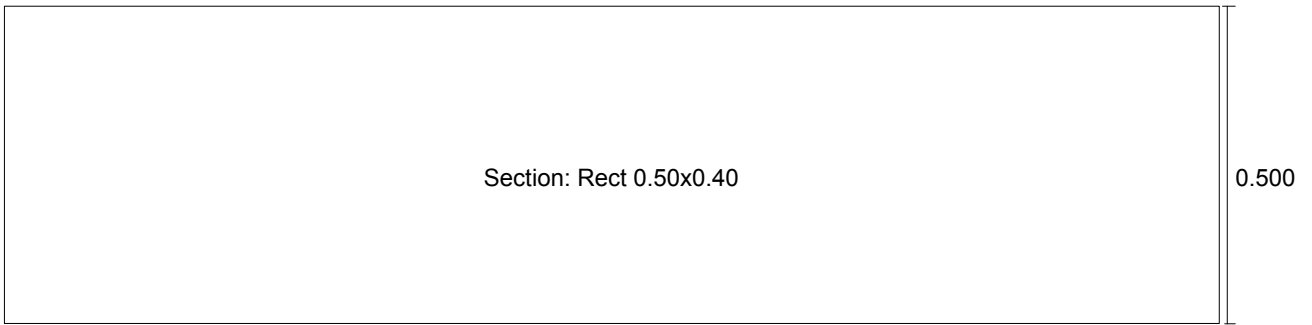


Software licensed to TU Eindhoven

Job No	Sheet No 1	Rev
Part		
Ref		
By	Date 25-Oct-11	Chd
File Static model	Date/Time 04-Mar-2012 10:31	

Job Title Model II
Client

STAAD.Pro Query Geometry
Beam no. **536**



START MX MY MZ **KFX 69302.6** Length = 3.9, Beta = 0 END MX MY MZ **KFX 69302.6**

Node	X-Coord (m)	Y-Coord (m)	Z-Coord (m)
320	0.000000	3.200000	27.000000
322	4.500000	3.200000	27.000000

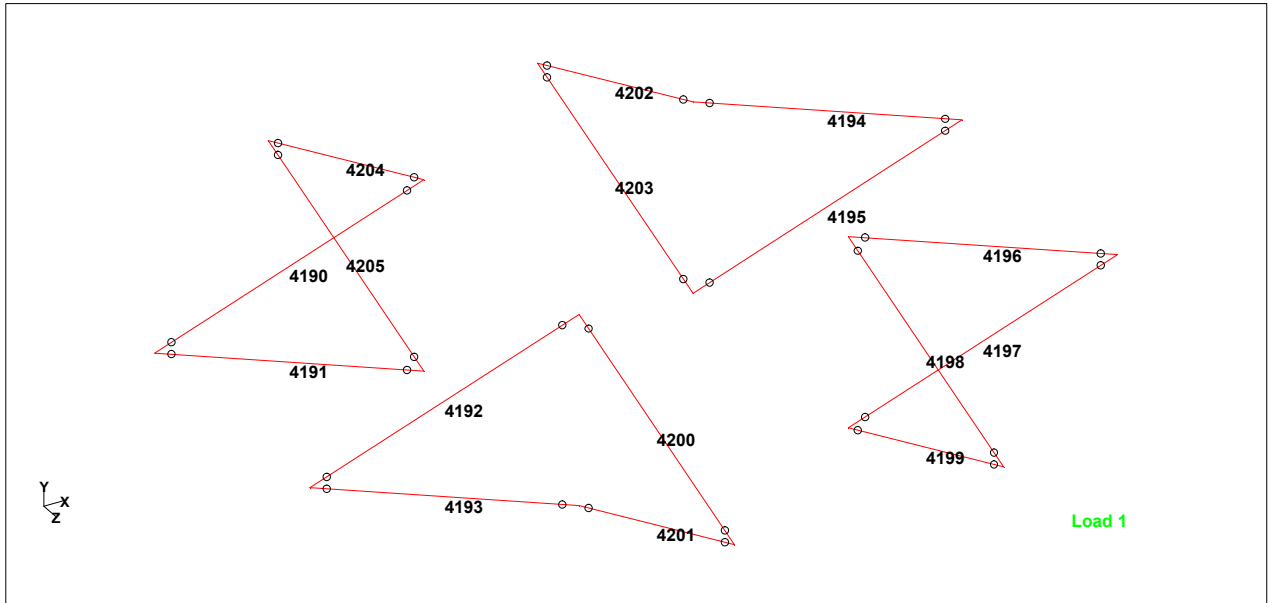


Academic license user TU Eindhoven

Job No	Sheet No 1	Rev
Part		
Ref		
By	Date	Chd
File	Static model	Date/Time

Job Title
Model IIIa

Client



Diagonals

Releases

Beam ends not shown in this table are fixed in all directions.

Beam	Node	x	y	z	rx	ry	rz
4190	995	Spring	Fixed	Fixed	Pin	Pin	Pin
4190	1031	Spring	Fixed	Fixed	Pin	Pin	Pin
4191	995	Spring	Fixed	Fixed	Pin	Pin	Pin
4191	927	Spring	Fixed	Fixed	Pin	Pin	Pin
4192	997	Spring	Fixed	Fixed	Pin	Pin	Pin
4192	1033	Spring	Fixed	Fixed	Pin	Pin	Pin
4193	997	Spring	Fixed	Fixed	Pin	Pin	Pin
4193	929	Spring	Fixed	Fixed	Pin	Pin	Pin
4194	1007	Spring	Fixed	Fixed	Pin	Pin	Pin
4194	1032	Spring	Fixed	Fixed	Pin	Pin	Pin
4195	1007	Spring	Fixed	Fixed	Pin	Pin	Pin
4195	928	Spring	Fixed	Fixed	Pin	Pin	Pin
4196	1009	Spring	Fixed	Fixed	Pin	Pin	Pin
4196	1034	Spring	Fixed	Fixed	Pin	Pin	Pin
4197	1009	Spring	Fixed	Fixed	Pin	Pin	Pin
4197	930	Spring	Fixed	Fixed	Pin	Pin	Pin
4198	1003	Spring	Fixed	Fixed	Pin	Pin	Pin
4198	1034	Spring	Fixed	Fixed	Pin	Pin	Pin
4199	1003	Spring	Fixed	Fixed	Pin	Pin	Pin
4199	930	Spring	Fixed	Fixed	Pin	Pin	Pin
4200	1001	Spring	Fixed	Fixed	Pin	Pin	Pin
4200	1033	Spring	Fixed	Fixed	Pin	Pin	Pin
4201	1001	Spring	Fixed	Fixed	Pin	Pin	Pin
4201	929	Spring	Fixed	Fixed	Pin	Pin	Pin
4202	991	Spring	Fixed	Fixed	Pin	Pin	Pin
4202	1032	Spring	Fixed	Fixed	Pin	Pin	Pin
4203	991	Spring	Fixed	Fixed	Pin	Pin	Pin
4203	928	Spring	Fixed	Fixed	Pin	Pin	Pin



Academic license user TU Eindhoven

Job No	Sheet No 2	Rev
Part		
Ref		
By	Date 25-Oct-11	Chd
Client	File Static model - variable load	Date/Time 07-Apr-2012 22:28

Releases Cont...

Beam	Node	x	y	z	rx	ry	rz
4204	989	Spring	Fixed	Fixed	Pin	Pin	Pin
4204	1031	Spring	Fixed	Fixed	Pin	Pin	Pin
4205	989	Spring	Fixed	Fixed	Pin	Pin	Pin
4205	927	Spring	Fixed	Fixed	Pin	Pin	Pin

Node Displacements

Node	L/C	X (mm)	Y (mm)	Z (mm)	Resultant (mm)	rX (rad)	rY (rad)	rZ (rad)
1455	33:SLS-CHA-3	95.367	-2.571	-0.002	95.402	0.000	0.000	-0.001



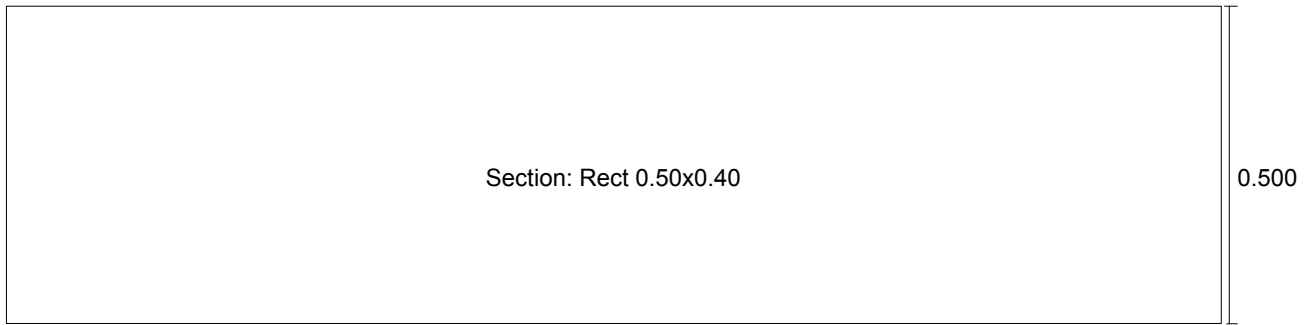
Software licensed to TU Eindhoven

Job No	Sheet No 1	Rev
Part		
Ref		
By	Date 25-Oct-11	Chd
Client	File Static model - variable load	Date/Time 07-Apr-2012 22:28

Job Title
Model IIIa

STAAD.Pro Query Geometry

Beam no. **4190**



START MX MY MZ **KFX 970236** Length = 9.55196, Beta = 0 END MX MY MZ **KFX 970236**

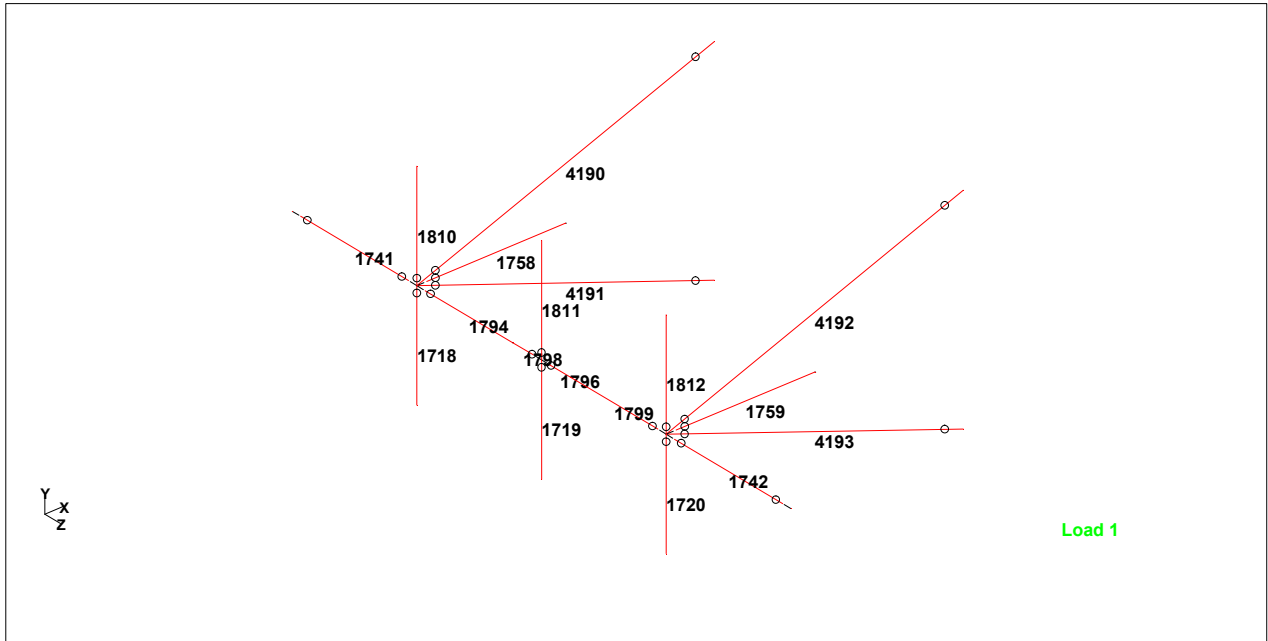
Node	X-Coord (m)	Y-Coord (m)	Z-Coord (m)
995	0.000000	38.400002	9.000000
1031	9.000000	41.599998	9.000000



Academic license user TU Eindhoven

Job No	Sheet No 1	Rev
Part		
Ref		
By	Date 25-Oct-11	Chd
Client	File Static model - variable load	Date/Time 07-Apr-2012 22:29

Job Title
Model IIIb



Columns 1718 + 1720

Beams

Beam	Node A	Node B	Length (m)	Property	β (degrees)
1718	943	995	3.200	3	0
1720	945	997	3.200	3	0

Releases

Beam ends not shown in this table are fixed in all directions.

Beam	Node	x	y	z	rx	ry	rz
1718	995	Spring	Fixed	Fixed	Pin	Pin	Pin
1720	997	Spring	Fixed	Fixed	Pin	Pin	Pin

Node Displacements

Node	L/C	X (mm)	Y (mm)	Z (mm)	Resultant (mm)	rX (rad)	rY (rad)	rZ (rad)
1455	33:SLS-CHA-3	95.234	-2.571	0.010	95.269	0.000	0.000	-0.001



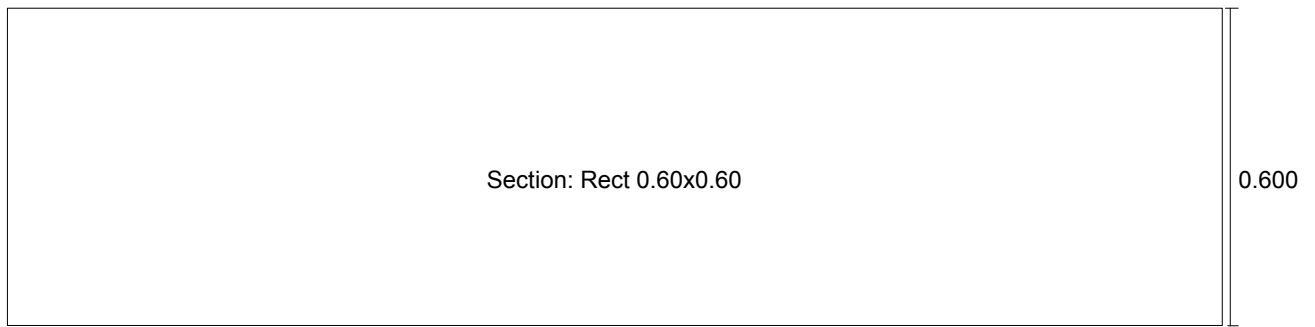
Software licensed to TU Eindhoven

Job No	Sheet No 1	Rev
Part		
Ref		
By	Date 25-Oct-11	Chd
Client	File Static model - variable load	Date/Time 07-Apr-2012 22:29

Job Title
Model IIIb

STAAD.Pro Query Geometry

Beam no. **1718**



Length = 3.2, Beta = 0

END MX MY MZ **KFX 346513**

Node	X-Coord (m)	Y-Coord (m)	Z-Coord (m)
943	0.000000	35.200001	9.000000
995	0.000000	38.400002	9.000000



Academic license user TU Eindhoven

Job No	Sheet No 1	Rev
Part		
Ref		
By	Date 25-Oct-11	Chd
Client	File Static model - variable load	Date/Time 07-Apr-2012 22:40

Job Title Model I+II+III

Supports

Node	X (kN/mm)	Y (kN/mm)	Z (kN/mm)	rX (kN·m/deg)	rY (kN·m/deg)	rZ (kN·m/deg)
1	Fixed	12.950	Fixed	Fixed	Fixed	Fixed
8	Fixed	12.950	Fixed	Fixed	Fixed	Fixed
377	Fixed	19.606	Fixed	Fixed	Fixed	Fixed
422	Fixed	22.623	Fixed	Fixed	Fixed	Fixed
423	Fixed	3.015	Fixed	Fixed	Fixed	Fixed

Releases

Beam ends not shown in this table are fixed in all directions.

Beam	Node	x	y	z	rx	ry	rz
536	320	Spring	Fixed	Fixed	Pin	Pin	Pin
536	322	Spring	Fixed	Fixed	Pin	Pin	Pin
1718	995	Spring	Fixed	Fixed	Pin	Pin	Pin
1720	997	Spring	Fixed	Fixed	Pin	Pin	Pin
4190	995	Spring	Fixed	Fixed	Pin	Pin	Pin
4190	1031	Spring	Fixed	Fixed	Pin	Pin	Pin
4191	995	Spring	Fixed	Fixed	Pin	Pin	Pin
4191	927	Spring	Fixed	Fixed	Pin	Pin	Pin
4192	997	Spring	Fixed	Fixed	Pin	Pin	Pin
4192	1033	Spring	Fixed	Fixed	Pin	Pin	Pin
4193	997	Spring	Fixed	Fixed	Pin	Pin	Pin
4193	929	Spring	Fixed	Fixed	Pin	Pin	Pin
4194	1007	Spring	Fixed	Fixed	Pin	Pin	Pin
4194	1032	Spring	Fixed	Fixed	Pin	Pin	Pin
4195	1007	Spring	Fixed	Fixed	Pin	Pin	Pin
4195	928	Spring	Fixed	Fixed	Pin	Pin	Pin
4196	1009	Spring	Fixed	Fixed	Pin	Pin	Pin
4196	1034	Spring	Fixed	Fixed	Pin	Pin	Pin
4197	1009	Spring	Fixed	Fixed	Pin	Pin	Pin
4197	930	Spring	Fixed	Fixed	Pin	Pin	Pin
4198	1003	Spring	Fixed	Fixed	Pin	Pin	Pin
4198	1034	Spring	Fixed	Fixed	Pin	Pin	Pin
4199	1003	Spring	Fixed	Fixed	Pin	Pin	Pin
4199	930	Spring	Fixed	Fixed	Pin	Pin	Pin
4200	1001	Spring	Fixed	Fixed	Pin	Pin	Pin
4200	1033	Spring	Fixed	Fixed	Pin	Pin	Pin
4201	1001	Spring	Fixed	Fixed	Pin	Pin	Pin
4201	929	Spring	Fixed	Fixed	Pin	Pin	Pin
4202	991	Spring	Fixed	Fixed	Pin	Pin	Pin
4202	1032	Spring	Fixed	Fixed	Pin	Pin	Pin
4203	991	Spring	Fixed	Fixed	Pin	Pin	Pin
4203	928	Spring	Fixed	Fixed	Pin	Pin	Pin
4204	989	Spring	Fixed	Fixed	Pin	Pin	Pin
4204	1031	Spring	Fixed	Fixed	Pin	Pin	Pin
4205	989	Spring	Fixed	Fixed	Pin	Pin	Pin
4205	927	Spring	Fixed	Fixed	Pin	Pin	Pin



Academic license user TU Eindhoven

Job No	Sheet No 2	Rev
Part	Ref	
By	Date 25-Oct-11	Chd
Client	File Static model - variable load	Date/Time 07-Apr-2012 22:40

Node Displacements

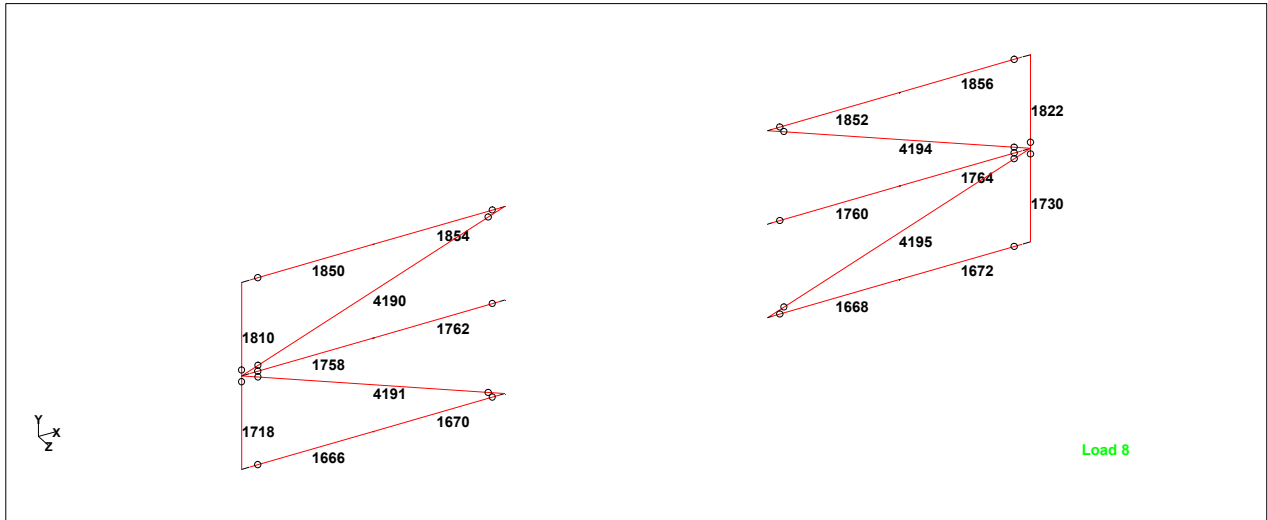
Node	L/C	X (mm)	Y (mm)	Z (mm)	Resultant (mm)	rX (rad)	rY (rad)	rZ (rad)
1	33:SLS-CHA-3	0.000	4.000	0.000	4.000	0.000	0.000	0.000
8	33:SLS-CHA-3	0.000	4.117	0.000	4.117	0.000	0.000	0.000
377	33:SLS-CHA-3	0.000	3.700	0.000	3.700	0.000	0.000	0.000
422	33:SLS-CHA-3	0.000	3.716	0.000	3.716	0.000	0.000	0.000
423	33:SLS-CHA-3	0.000	3.695	0.000	3.695	0.000	0.000	0.000
1455	33:SLS-CHA-3	116.249	-2.548	-0.042	116.277	0.000	-0.000	-0.001



Academic license user TU Eindhoven

Job No	Sheet No 1	Rev
Part		
Ref		
By	Date 25-Oct-11	Chd
File	Static model - variable load	Date/Time 07-Apr-2012 22:41

Job Title Model IV
Client



Outriggers grid C

Releases

Beam ends not shown in this table are fixed in all directions.

Beam	Node	x	y	z	rx	ry	rz
536	320	Spring	Fixed	Fixed	Pin	Pin	Pin
536	322	Spring	Fixed	Fixed	Pin	Pin	Pin
1668	928	Spring	Fixed	Fixed	Fixed	Fixed	Fixed
1670	927	Spring	Fixed	Fixed	Fixed	Fixed	Fixed
1672	955	Spring	Fixed	Fixed	Pin	Pin	Pin
1718	995	Spring	Fixed	Fixed	Fixed	Fixed	Fixed
1720	997	Spring	Fixed	Fixed	Fixed	Fixed	Fixed
1730	1007	Fixed	Fixed	Fixed	Pin	Pin	Pin
1758	995	Spring	Fixed	Fixed	Fixed	Fixed	Fixed
1760	980	Spring	Fixed	Fixed	Pin	Pin	Pin
1762	979	Spring	Fixed	Fixed	Pin	Pin	Pin
1764	1007	Spring	Fixed	Fixed	Fixed	Fixed	Fixed
1810	995	Fixed	Fixed	Fixed	Pin	Pin	Pin
1822	1007	Fixed	Fixed	Fixed	Pin	Pin	Pin
1850	1047	Spring	Fixed	Fixed	Pin	Pin	Pin
1852	1032	Spring	Fixed	Fixed	Fixed	Fixed	Fixed
1854	1031	Spring	Fixed	Fixed	Fixed	Fixed	Fixed
1856	1059	Spring	Fixed	Fixed	Pin	Pin	Pin
4190	995	Spring	Fixed	Fixed	Fixed	Fixed	Fixed
4190	1031	Spring	Fixed	Fixed	Fixed	Fixed	Fixed
4191	995	Spring	Fixed	Fixed	Fixed	Fixed	Fixed
4191	927	Spring	Fixed	Fixed	Fixed	Fixed	Fixed
4192	997	Spring	Fixed	Fixed	Fixed	Fixed	Fixed
4192	1033	Spring	Fixed	Fixed	Fixed	Fixed	Fixed
4193	997	Spring	Fixed	Fixed	Fixed	Fixed	Fixed
4193	929	Spring	Fixed	Fixed	Fixed	Fixed	Fixed
4194	1007	Spring	Fixed	Fixed	Fixed	Fixed	Fixed
4194	1032	Spring	Fixed	Fixed	Fixed	Fixed	Fixed
4195	1007	Spring	Fixed	Fixed	Fixed	Fixed	Fixed
4195	928	Spring	Fixed	Fixed	Fixed	Fixed	Fixed



Academic license user TU Eindhoven

Job No

Sheet No

2

Rev

Part

Job Title

Model IV

Ref

By

Date 25-Oct-11

Chd

Client

File Static model - variable load

Date/Time 07-Apr-2012 22:41

Releases Cont...

Beam	Node	x	y	z	rx	ry	rz
4196	1009	Spring	Fixed	Fixed	Fixed	Fixed	Fixed
4196	1034	Spring	Fixed	Fixed	Fixed	Fixed	Fixed
4197	1009	Spring	Fixed	Fixed	Fixed	Fixed	Fixed
4197	930	Spring	Fixed	Fixed	Fixed	Fixed	Fixed
4198	1003	Spring	Fixed	Fixed	Fixed	Fixed	Fixed
4198	1034	Spring	Fixed	Fixed	Fixed	Fixed	Fixed
4199	1003	Spring	Fixed	Fixed	Fixed	Fixed	Fixed
4199	930	Spring	Fixed	Fixed	Fixed	Fixed	Fixed
4200	1001	Spring	Fixed	Fixed	Fixed	Fixed	Fixed
4200	1033	Spring	Fixed	Fixed	Fixed	Fixed	Fixed
4201	1001	Spring	Fixed	Fixed	Fixed	Fixed	Fixed
4201	929	Spring	Fixed	Fixed	Fixed	Fixed	Fixed
4202	991	Spring	Fixed	Fixed	Fixed	Fixed	Fixed
4202	1032	Spring	Fixed	Fixed	Fixed	Fixed	Fixed
4203	991	Spring	Fixed	Fixed	Fixed	Fixed	Fixed
4203	928	Spring	Fixed	Fixed	Fixed	Fixed	Fixed
4204	989	Spring	Fixed	Fixed	Fixed	Fixed	Fixed
4204	1031	Spring	Fixed	Fixed	Fixed	Fixed	Fixed
4205	989	Spring	Fixed	Fixed	Fixed	Fixed	Fixed
4205	927	Spring	Fixed	Fixed	Fixed	Fixed	Fixed

Supports

Node	X (kN/mm)	Y (kN/mm)	Z (kN/mm)	rX (kN·m/deg)	rY (kN·m/deg)	rZ (kN·m/deg)
1	Fixed	12.950	Fixed	Fixed	Fixed	Fixed
8	Fixed	12.950	Fixed	Fixed	Fixed	Fixed
377	Fixed	19.606	Fixed	Fixed	Fixed	Fixed
422	Fixed	22.623	Fixed	Fixed	Fixed	Fixed
423	Fixed	3.015	Fixed	Fixed	Fixed	Fixed

Node Displacements

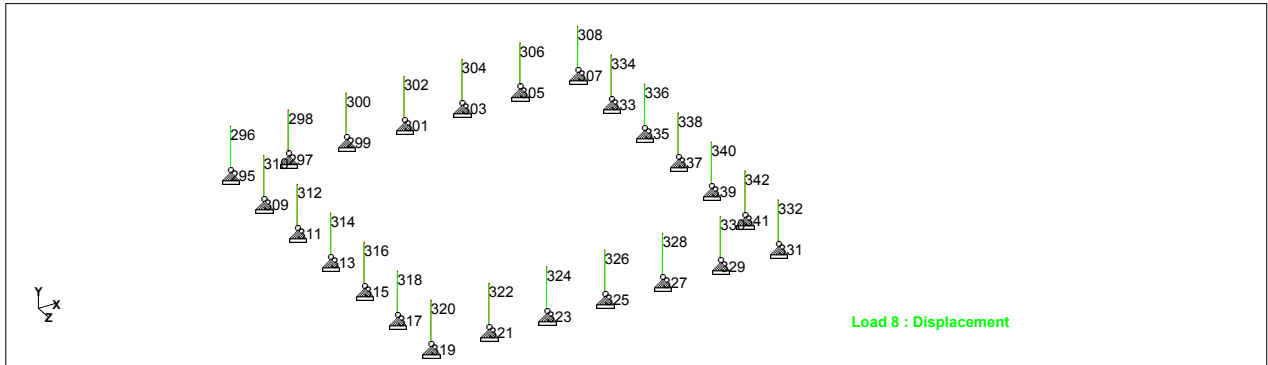
Node	L/C	X (mm)	Y (mm)	Z (mm)	Resultant (mm)	rX (rad)	rY (rad)	rZ (rad)
1	33:SLS-CHA-3	0.000	3.941	0.000	3.941	0.000	0.000	0.000
8	33:SLS-CHA-3	0.000	4.058	0.000	4.058	0.000	0.000	0.000
377	33:SLS-CHA-3	0.000	3.641	0.000	3.641	0.000	0.000	0.000
422	33:SLS-CHA-3	0.000	3.658	0.000	3.658	0.000	0.000	0.000
423	33:SLS-CHA-3	0.000	3.637	0.000	3.637	0.000	0.000	0.000
1455	33:SLS-CHA-3	115.623	-2.549	-0.027	115.651	0.000	-0.000	-0.001



Academic license user TU Eindhoven

Job No	Sheet No 1	Rev
Part		
Ref		
By	Date 25-Oct-11	Chd
Client	File Static model - variable load	Date/Time 07-Apr-2012 22:42

Job Title
Model V



Node numbers supports columns

Supports

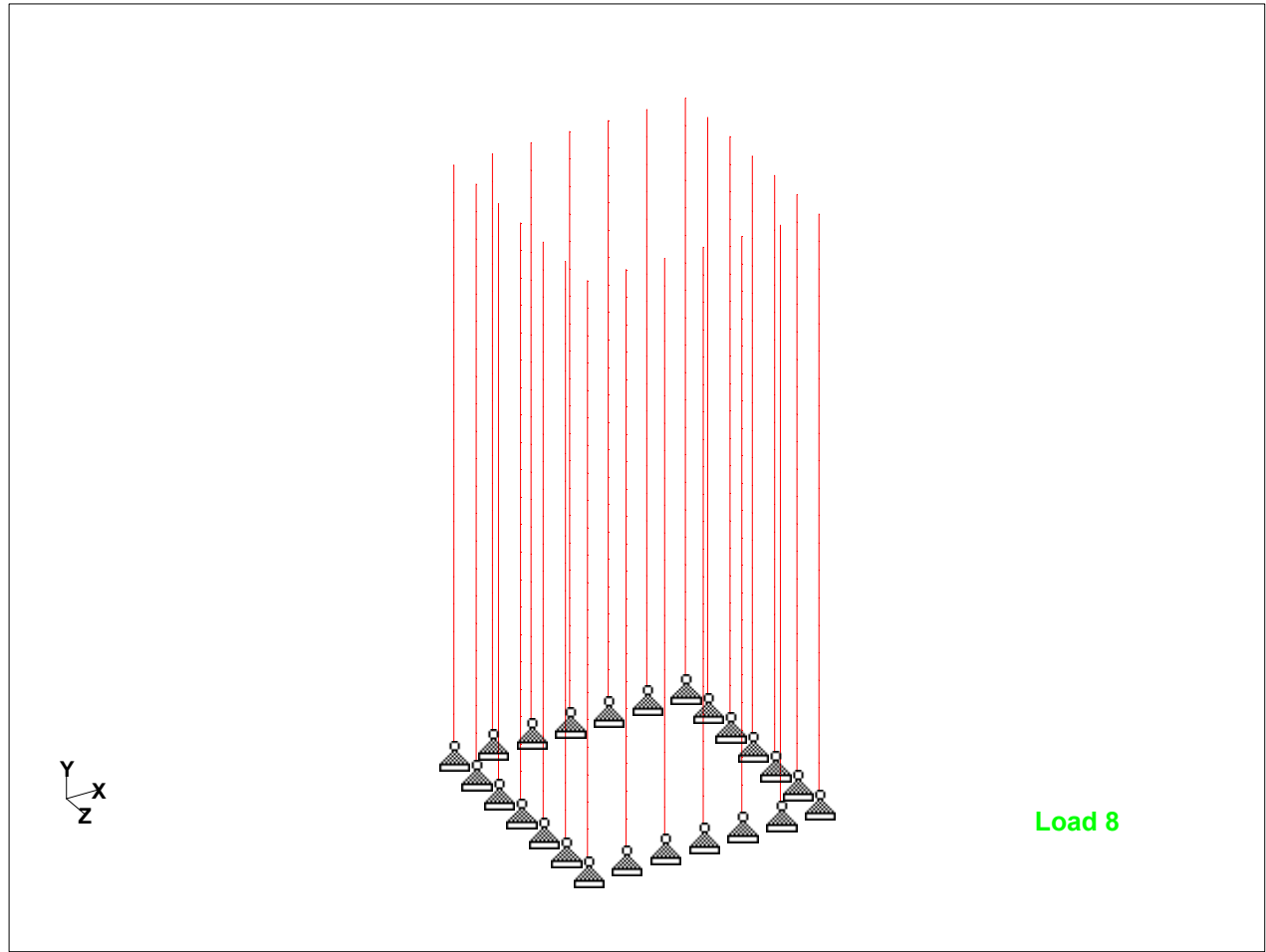
Node	X (kN/mm)	Y (kN/mm)	Z (kN/mm)	rX (kN`m/deg)	rY (kN`m/deg)	rZ (kN`m/deg)
295	Fixed	Fixed	Fixed	-	-	-
297	Fixed	Fixed	Fixed	-	-	-
299	Fixed	Fixed	Fixed	-	-	-
301	Fixed	Fixed	Fixed	-	-	-
303	Fixed	Fixed	Fixed	-	-	-
305	Fixed	Fixed	Fixed	-	-	-
307	Fixed	Fixed	Fixed	-	-	-
309	Fixed	Fixed	Fixed	-	-	-
311	Fixed	Fixed	Fixed	-	-	-
313	Fixed	Fixed	Fixed	-	-	-
315	Fixed	Fixed	Fixed	-	-	-
317	Fixed	Fixed	Fixed	-	-	-
319	Fixed	Fixed	Fixed	-	-	-
321	Fixed	Fixed	Fixed	-	-	-
323	Fixed	Fixed	Fixed	-	-	-
325	Fixed	Fixed	Fixed	-	-	-
327	Fixed	Fixed	Fixed	-	-	-
329	Fixed	Fixed	Fixed	-	-	-
331	Fixed	Fixed	Fixed	-	-	-
333	Fixed	Fixed	Fixed	-	-	-
335	Fixed	Fixed	Fixed	-	-	-
337	Fixed	Fixed	Fixed	-	-	-
339	Fixed	Fixed	Fixed	-	-	-
341	Fixed	Fixed	Fixed	-	-	-



Academic license user TU Eindhoven

Job No	Sheet No 2	Rev
Part	Ref	
By	Date 25-Oct-11	Chd
Client	File Static model - variable load	Date/Time 07-Apr-2012 22:42

Job Title
Model V



Peripheral columns

Releases

There is no data of this type.



Academic license user TU Eindhoven

Job No	Sheet No 1	Rev
Part		
Ref		
By	Date 25-Oct-11	Chd
Client	File Static model - variable load	Date/Time 07-Apr-2012 22:42

Supports

Node	X (kN/mm)	Y (kN/mm)	Z (kN/mm)	rX (kN·m/deg)	rY (kN·m/deg)	rZ (kN·m/deg)
1	Fixed	12.950	Fixed	Fixed	Fixed	Fixed
8	Fixed	12.950	Fixed	Fixed	Fixed	Fixed
377	Fixed	19.606	Fixed	Fixed	Fixed	Fixed
422	Fixed	22.623	Fixed	Fixed	Fixed	Fixed
423	Fixed	3.015	Fixed	Fixed	Fixed	Fixed

Releases

Beam ends not shown in this table are fixed in all directions.

Beam	Node	x	y	z	rx	ry	rz
536	320	Spring	Fixed	Fixed	Pin	Pin	Pin
536	322	Spring	Fixed	Fixed	Pin	Pin	Pin
4190	995	Spring	Fixed	Fixed	Fixed	Fixed	Fixed
4190	1031	Spring	Fixed	Fixed	Fixed	Fixed	Fixed
4191	995	Spring	Fixed	Fixed	Fixed	Fixed	Fixed
4191	927	Spring	Fixed	Fixed	Fixed	Fixed	Fixed
4192	997	Spring	Fixed	Fixed	Fixed	Fixed	Fixed
4192	1033	Spring	Fixed	Fixed	Fixed	Fixed	Fixed
4193	997	Spring	Fixed	Fixed	Fixed	Fixed	Fixed
4193	929	Spring	Fixed	Fixed	Fixed	Fixed	Fixed
4194	1007	Spring	Fixed	Fixed	Fixed	Fixed	Fixed
4194	1032	Spring	Fixed	Fixed	Fixed	Fixed	Fixed
4195	1007	Spring	Fixed	Fixed	Fixed	Fixed	Fixed
4195	928	Spring	Fixed	Fixed	Fixed	Fixed	Fixed
4196	1009	Spring	Fixed	Fixed	Fixed	Fixed	Fixed
4196	1034	Spring	Fixed	Fixed	Fixed	Fixed	Fixed
4197	1009	Spring	Fixed	Fixed	Fixed	Fixed	Fixed
4197	930	Spring	Fixed	Fixed	Fixed	Fixed	Fixed
4198	1003	Spring	Fixed	Fixed	Fixed	Fixed	Fixed
4198	1034	Spring	Fixed	Fixed	Fixed	Fixed	Fixed
4199	1003	Spring	Fixed	Fixed	Fixed	Fixed	Fixed
4199	930	Spring	Fixed	Fixed	Fixed	Fixed	Fixed
4200	1001	Spring	Fixed	Fixed	Fixed	Fixed	Fixed
4200	1033	Spring	Fixed	Fixed	Fixed	Fixed	Fixed
4201	1001	Spring	Fixed	Fixed	Fixed	Fixed	Fixed
4201	929	Spring	Fixed	Fixed	Fixed	Fixed	Fixed
4202	991	Spring	Fixed	Fixed	Fixed	Fixed	Fixed
4202	1032	Spring	Fixed	Fixed	Fixed	Fixed	Fixed
4203	991	Spring	Fixed	Fixed	Fixed	Fixed	Fixed
4203	928	Spring	Fixed	Fixed	Fixed	Fixed	Fixed
4204	989	Spring	Fixed	Fixed	Fixed	Fixed	Fixed
4204	1031	Spring	Fixed	Fixed	Fixed	Fixed	Fixed
4205	989	Spring	Fixed	Fixed	Fixed	Fixed	Fixed
4205	927	Spring	Fixed	Fixed	Fixed	Fixed	Fixed



Academic license user TU Eindhoven

Job No	Sheet No 2	Rev
Part	Ref	
By	Date 25-Oct-11	Chd
Client	File Static model - variable load	Date/Time 07-Apr-2012 22:42

Node Displacements

Node	L/C	X (mm)	Y (mm)	Z (mm)	Resultant (mm)	rX (rad)	rY (rad)	rZ (rad)
1	33:SLS-CHA-3	0.000	3.883	0.000	3.883	0.000	0.000	0.000
8	33:SLS-CHA-3	0.000	3.995	0.000	3.995	0.000	0.000	0.000
377	33:SLS-CHA-3	0.000	3.579	0.000	3.579	0.000	0.000	0.000
422	33:SLS-CHA-3	0.000	3.592	0.000	3.592	0.000	0.000	0.000
423	33:SLS-CHA-3	0.000	3.571	0.000	3.571	0.000	0.000	0.000
1455	33:SLS-CHA-3	114.152	-2.577	-0.074	114.181	0.000	-0.000	-0.001

D.3 | SLIP IN CONNECTIONS– DYNAMIC RESULTS

STAAD Pro results:

Model Ia; translational springs type 1 & 2

Model Ib; translational springs type 1,2 & 3

Model II; translational springs beams

Model IIIa; translational springs diagonals

Model IIIb; translational springs diagonals and columns below outriggers

Model I+II+III

Model IV: I + II + III + rotational rigid outrigger elements

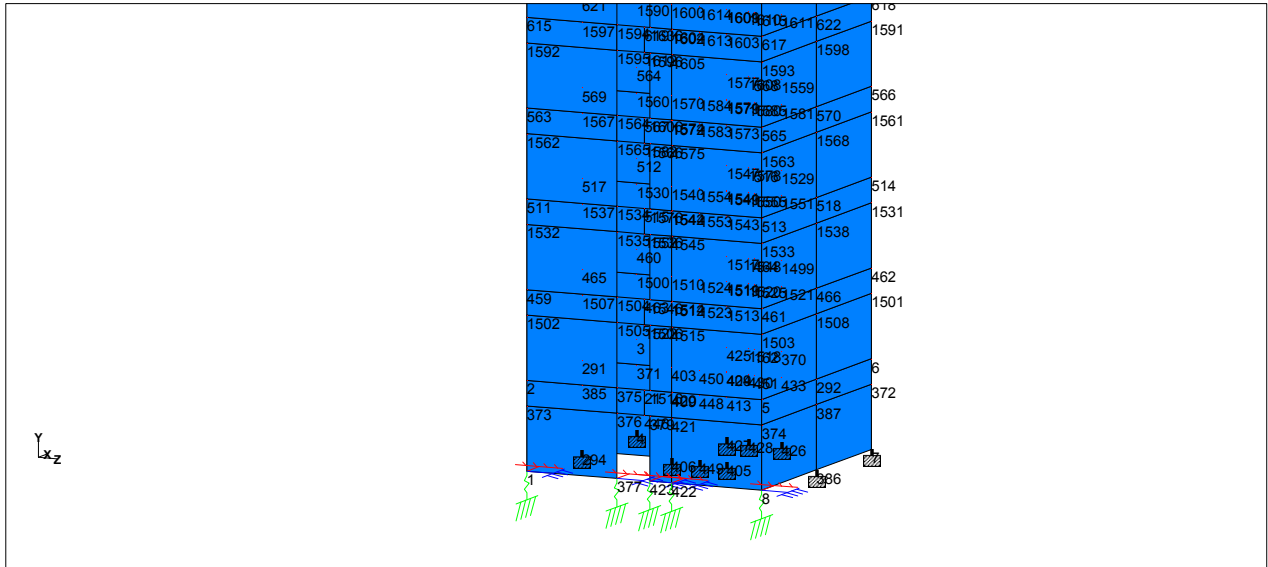
Model V: I + II + III + rotational rigid peripheral columns



Academic license user TU Eindhoven

Job No	Sheet No	Rev
	1	
Part		
Ref		
By	Date	Chd
	25-Oct-11	
Client	File	Date/Time
	Dynamic model - variable	07-Apr-2012 22:11

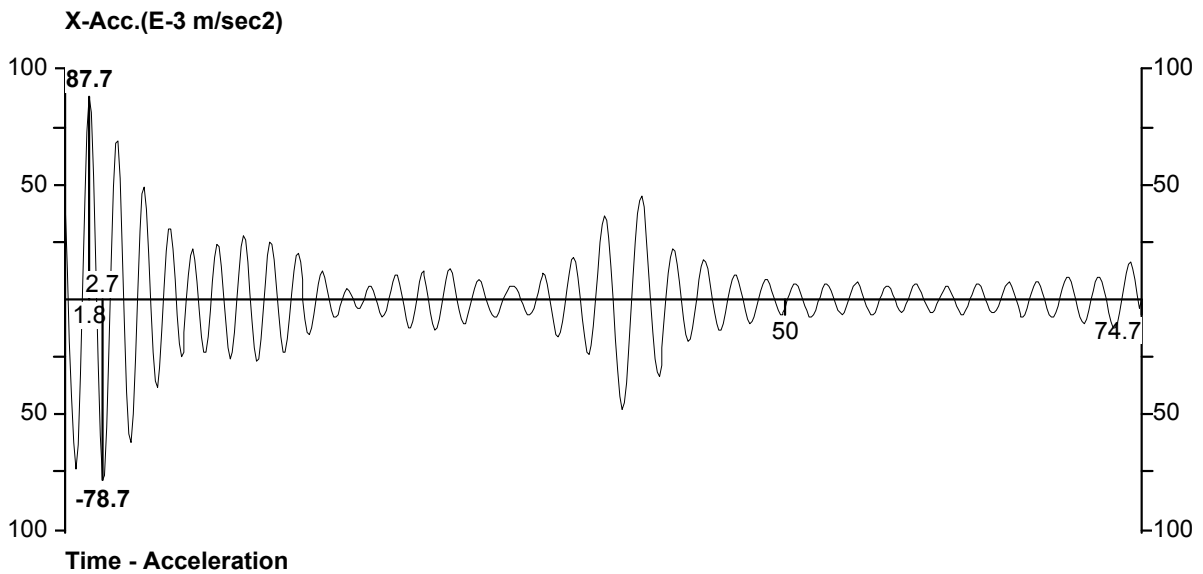
Job Title
Model Ia



Springs at CLT supports

Supports

Node	X (kN/mm)	Y (kN/mm)	Z (kN/mm)	rX (kN·m/deg)	rY (kN·m/deg)	rZ (kN·m/deg)
1	Fixed	73.903	Fixed	Fixed	Fixed	Fixed
8	Fixed	73.903	Fixed	Fixed	Fixed	Fixed
377	Fixed	19.606	Fixed	Fixed	Fixed	Fixed
422	Fixed	22.623	Fixed	Fixed	Fixed	Fixed
423	Fixed	3.015	Fixed	Fixed	Fixed	Fixed



Accelerations node 1455



Academic license user TU Eindhoven

Job No	Sheet No 2	Rev
Part		
Ref		
By	Date 25-Oct-11	Chd
Client	File Dynamic model - variable	Date/Time 07-Apr-2012 22:11

Job Title
Model Ia

Calculated Modal Frequencies & Mass Participations

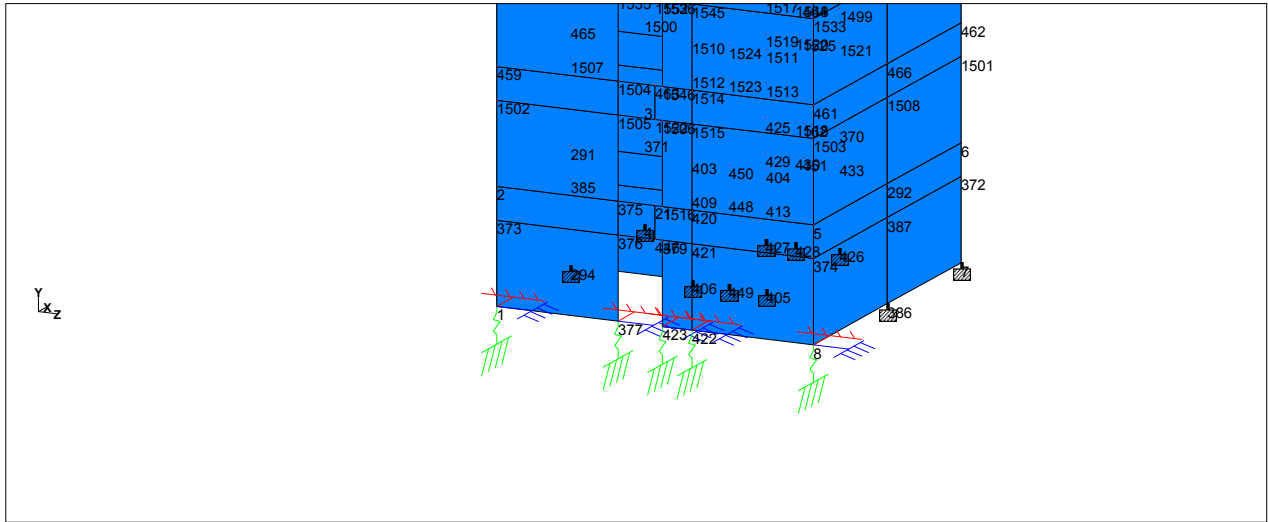
Mode	Frequency (Hz)	Period (sec)	Participation X (%)	Participation Y (%)	Participation Z (%)
1	0.519	1.925	0.002	0.000	0.221
2	0.593	1.687	77.486	0.027	0.001
3	0.736	1.359	0.000	0.000	75.271
4	1.609	0.622	0.000	0.000	0.016
5	2.431	0.411	12.740	0.031	0.006
6	2.546	0.393	0.007	0.000	12.780
7	2.616	0.382	0.000	0.000	1.204
8	3.623	0.276	0.000	0.000	0.000
9	4.342	0.230	0.000	0.000	0.002
10	4.592	0.218	4.287	0.169	0.005
11	4.752	0.210	0.004	0.000	4.795
12	5.313	0.188	0.027	19.259	0.000
13	5.331	0.188	0.001	0.183	0.000
14	5.357	0.187	0.001	0.348	0.000
15	5.424	0.184	0.002	0.021	0.000
16	5.435	0.184	0.001	0.001	0.000
17	5.441	0.184	0.002	0.000	0.000
18	5.443	0.184	0.002	0.001	0.000
19	5.444	0.184	0.000	0.000	0.000
20	5.462	0.183	0.000	0.236	0.001



Academic license user TU Eindhoven

Job No	Sheet No 1	Rev
Part		
Ref		
By	Date 25-Oct-11	Chd
Client	File Dynamic model - variable	Date/Time 07-Apr-2012 22:24

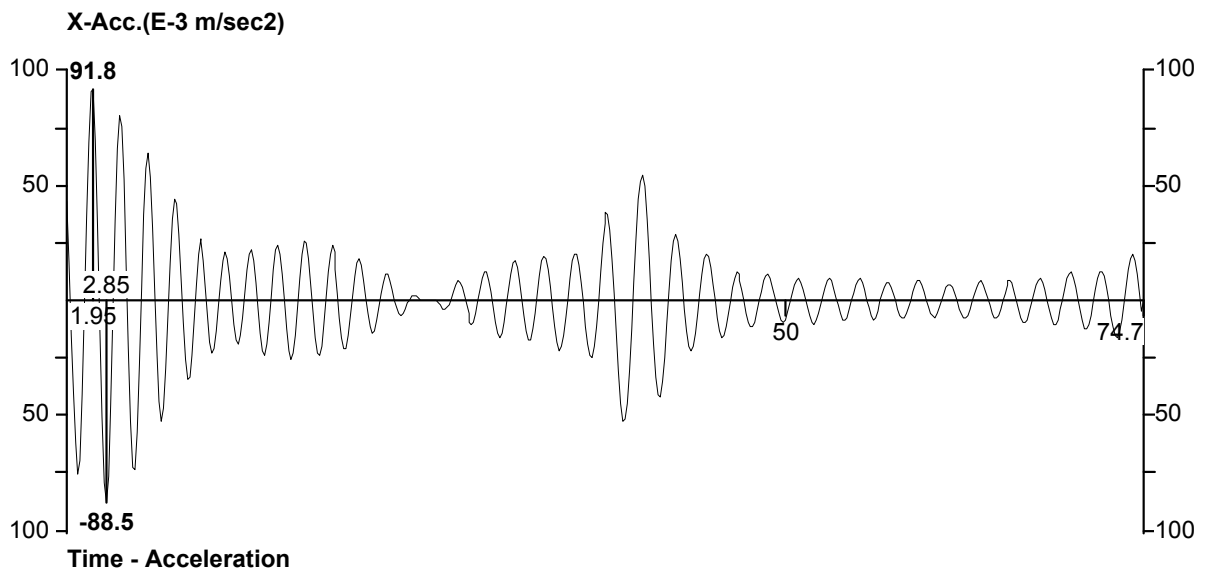
Job Title
Model Ib



Springs at supports CLT core

Supports

Node	X (kN/mm)	Y (kN/mm)	Z (kN/mm)	rX (kN·m/deg)	rY (kN·m/deg)	rZ (kN·m/deg)
1	Fixed	12.950	Fixed	Fixed	Fixed	Fixed
8	Fixed	12.950	Fixed	Fixed	Fixed	Fixed
377	Fixed	19.606	Fixed	Fixed	Fixed	Fixed
422	Fixed	22.623	Fixed	Fixed	Fixed	Fixed
423	Fixed	3.015	Fixed	Fixed	Fixed	Fixed



Accelerations node 1455



Academic license user TU Eindhoven

Job No	Sheet No 2	Rev
Part		
Ref		
By	Date 25-Oct-11	Chd
Client	File Dynamic model - variable	Date/Time 07-Apr-2012 22:24

Calculated Modal Frequencies & Mass Participations

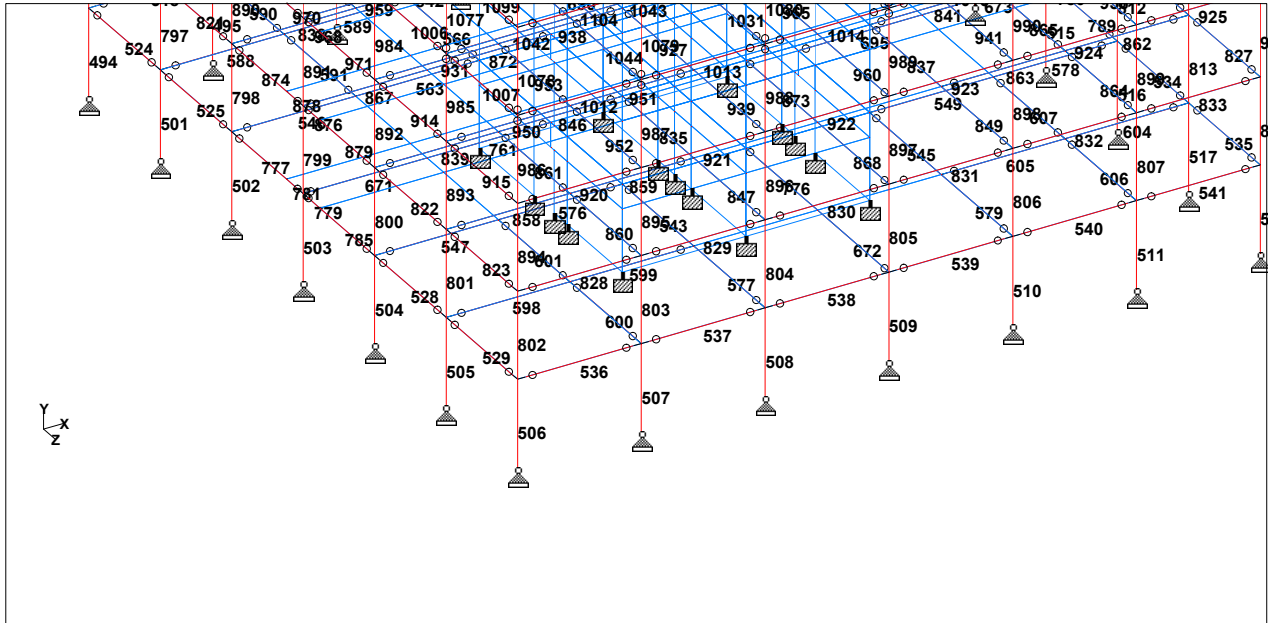
Mode	Frequency (Hz)	Period (sec)	Participation X (%)	Participation Y (%)	Participation Z (%)
1	0.519	1.928	0.003	0.000	0.303
2	0.573	1.745	77.830	0.033	0.000
3	0.731	1.368	0.000	0.000	75.285
4	1.609	0.622	0.000	0.000	0.017
5	2.425	0.412	12.490	0.039	0.006
6	2.545	0.393	0.007	0.000	12.770
7	2.616	0.382	0.000	0.000	1.160
8	3.623	0.276	0.000	0.000	0.000
9	4.342	0.230	0.000	0.000	0.002
10	4.586	0.218	4.185	0.212	0.005
11	4.749	0.211	0.004	0.000	4.767
12	5.312	0.188	0.033	19.463	0.000
13	5.331	0.188	0.001	0.198	0.000
14	5.357	0.187	0.001	0.331	0.000
15	5.427	0.184	0.002	0.000	0.000
16	5.436	0.184	0.001	0.002	0.000
17	5.441	0.184	0.002	0.000	0.000
18	5.443	0.184	0.002	0.001	0.000
19	5.444	0.184	0.000	0.000	0.000
20	5.462	0.183	0.000	0.237	0.001



Academic license user TU Eindhoven

Job No	Sheet No 1	Rev
Part		
Ref		
By	Date 25-Oct-11	Chd
Client	File Dynamic model - variable	Date/Time 31-Mar-2012 22:10

Job Title
Model II

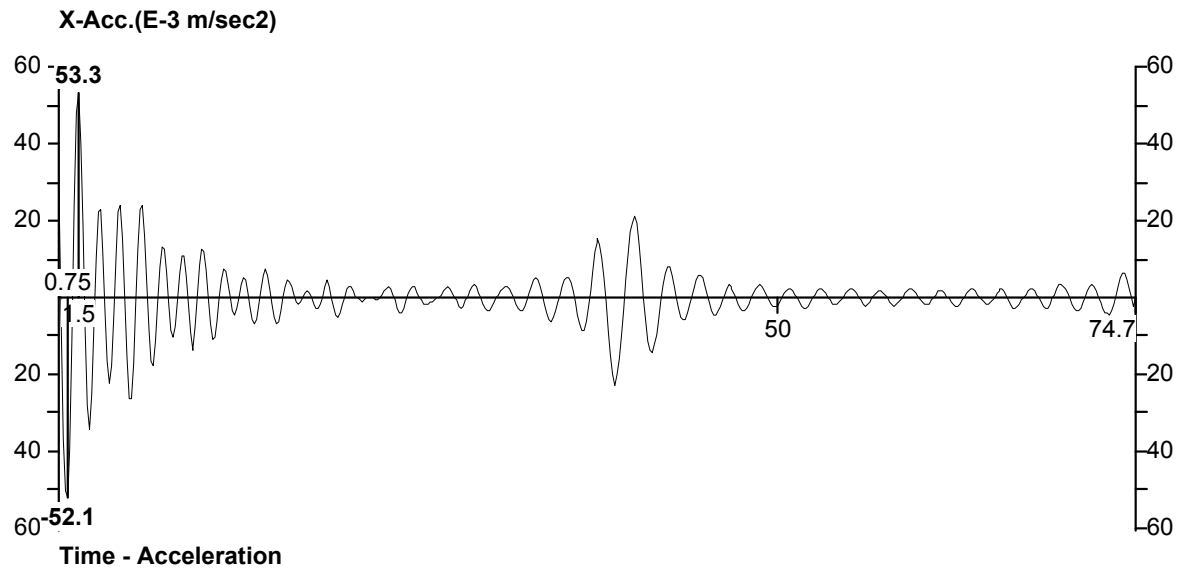


Example beam 536

Releases

Beam ends not shown in this table are fixed in all directions.

Beam	Node	x	y	z	rx	ry	rz
536	320	Spring	Fixed	Fixed	Pin	Pin	Pin
536	322	Spring	Fixed	Fixed	Pin	Pin	Pin



Accelerations node 1455



Academic license user TU Eindhoven

Job No	Sheet No 2	Rev
Part		
Ref		
By	Date 25-Oct-11	Chd
Client	File Dynamic model - variable	Date/Time 31-Mar-2012 22:10

Job Title
Model II

Calculated Modal Frequencies & Mass Participations

Mode	Frequency (Hz)	Period (sec)	Participation X (%)	Participation Y (%)	Participation Z (%)
1	0.537	1.863	0.000	0.000	0.000
2	0.748	1.337	74.418	0.000	0.030
3	0.784	1.275	0.027	0.000	74.186
4	1.614	0.620	0.000	0.000	0.000
5	2.466	0.406	14.913	0.000	0.005
6	2.579	0.388	0.008	0.000	14.325
7	2.587	0.386	0.000	0.000	0.000
8	3.529	0.283	0.000	0.000	0.000
9	4.210	0.238	0.000	0.000	0.000
10	4.565	0.219	5.083	0.000	0.004
11	4.723	0.212	0.004	0.000	5.171
12	5.327	0.188	0.000	16.345	0.000
13	5.331	0.188	0.001	0.075	0.000
14	5.355	0.187	0.000	0.297	0.001
15	5.411	0.185	0.001	1.262	0.000
16	5.436	0.184	0.002	0.005	0.000
17	5.441	0.184	0.002	0.002	0.000
18	5.443	0.184	0.001	0.000	0.000
19	5.444	0.184	0.000	0.000	0.000
20	5.462	0.183	0.000	0.271	0.002



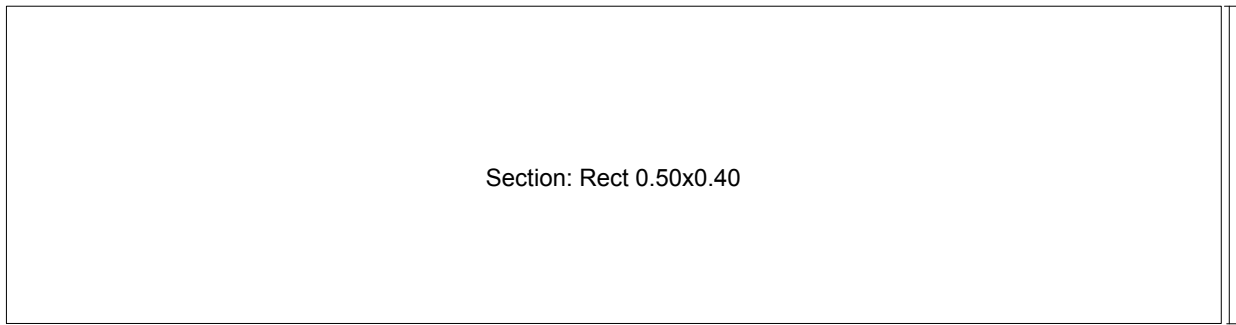
Software licensed to TU Eindhoven

Job No	Sheet No 1	Rev
Part		
Ref		
By	Date 25-Oct-11	Chd
Client	File Dynamic model - variable	Date/Time 31-Mar-2012 22:10

Job Title
Model II

STAAD.Pro Query Geometry

Beam no. **536**



START MX MY MZ **KFX 69302.6** Length = 3.9, Beta = 0 END MX MY MZ **KFX 69302.6**

Node	X-Coord (m)	Y-Coord (m)	Z-Coord (m)
320	0.000000	3.200000	27.000000
322	4.500000	3.200000	27.000000

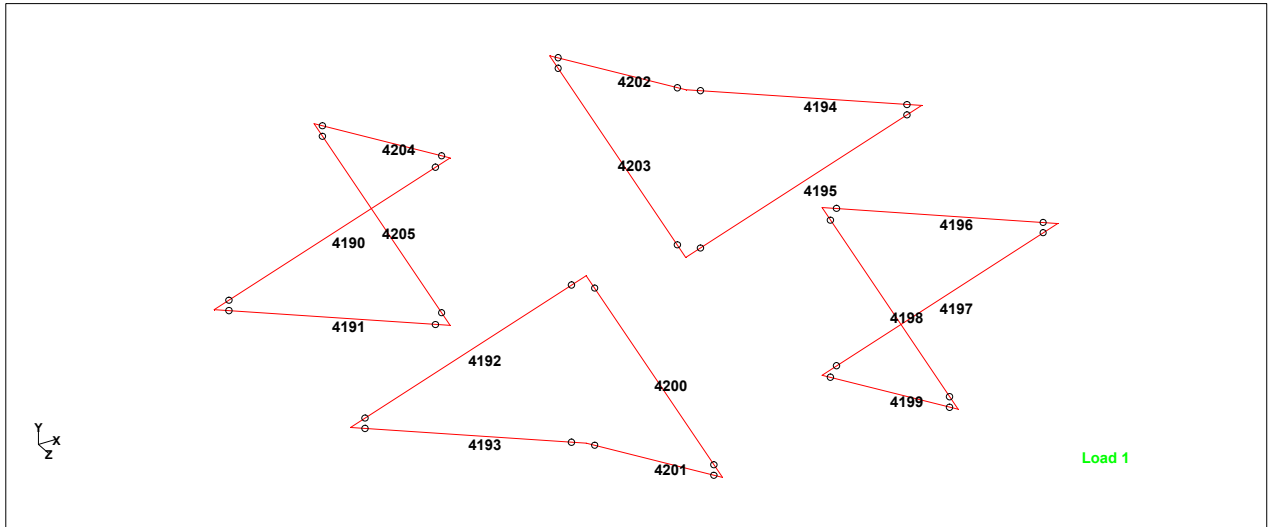


Academic license user TU Eindhoven

Job No	Sheet No 1	Rev
Part		
Ref		
By	Date 25-Oct-11	Chd
File	Dynamic model - variable	Date/Time 07-Apr-2012 22:29

Job Title
Model IIIa

Client



Diagonals

Releases

Beam ends not shown in this table are fixed in all directions.

Beam	Node	x	y	z	rx	ry	rz
4190	995	Spring	Fixed	Fixed	Pin	Pin	Pin
4190	1031	Spring	Fixed	Fixed	Pin	Pin	Pin
4191	995	Spring	Fixed	Fixed	Pin	Pin	Pin
4191	927	Spring	Fixed	Fixed	Pin	Pin	Pin
4192	997	Spring	Fixed	Fixed	Pin	Pin	Pin
4192	1033	Spring	Fixed	Fixed	Pin	Pin	Pin
4193	997	Spring	Fixed	Fixed	Pin	Pin	Pin
4193	929	Spring	Fixed	Fixed	Pin	Pin	Pin
4194	1007	Spring	Fixed	Fixed	Pin	Pin	Pin
4194	1032	Spring	Fixed	Fixed	Pin	Pin	Pin
4195	1007	Spring	Fixed	Fixed	Pin	Pin	Pin
4195	928	Spring	Fixed	Fixed	Pin	Pin	Pin
4196	1009	Spring	Fixed	Fixed	Pin	Pin	Pin
4196	1034	Spring	Fixed	Fixed	Pin	Pin	Pin
4197	1009	Spring	Fixed	Fixed	Pin	Pin	Pin
4197	930	Spring	Fixed	Fixed	Pin	Pin	Pin
4198	1003	Spring	Fixed	Fixed	Pin	Pin	Pin
4198	1034	Spring	Fixed	Fixed	Pin	Pin	Pin
4199	1003	Spring	Fixed	Fixed	Pin	Pin	Pin
4199	930	Spring	Fixed	Fixed	Pin	Pin	Pin
4200	1001	Spring	Fixed	Fixed	Pin	Pin	Pin
4200	1033	Spring	Fixed	Fixed	Pin	Pin	Pin
4201	1001	Spring	Fixed	Fixed	Pin	Pin	Pin
4201	929	Spring	Fixed	Fixed	Pin	Pin	Pin
4202	991	Spring	Fixed	Fixed	Pin	Pin	Pin
4202	1032	Spring	Fixed	Fixed	Pin	Pin	Pin
4203	991	Spring	Fixed	Fixed	Pin	Pin	Pin
4203	928	Spring	Fixed	Fixed	Pin	Pin	Pin
4204	989	Spring	Fixed	Fixed	Pin	Pin	Pin
4204	1031	Spring	Fixed	Fixed	Pin	Pin	Pin



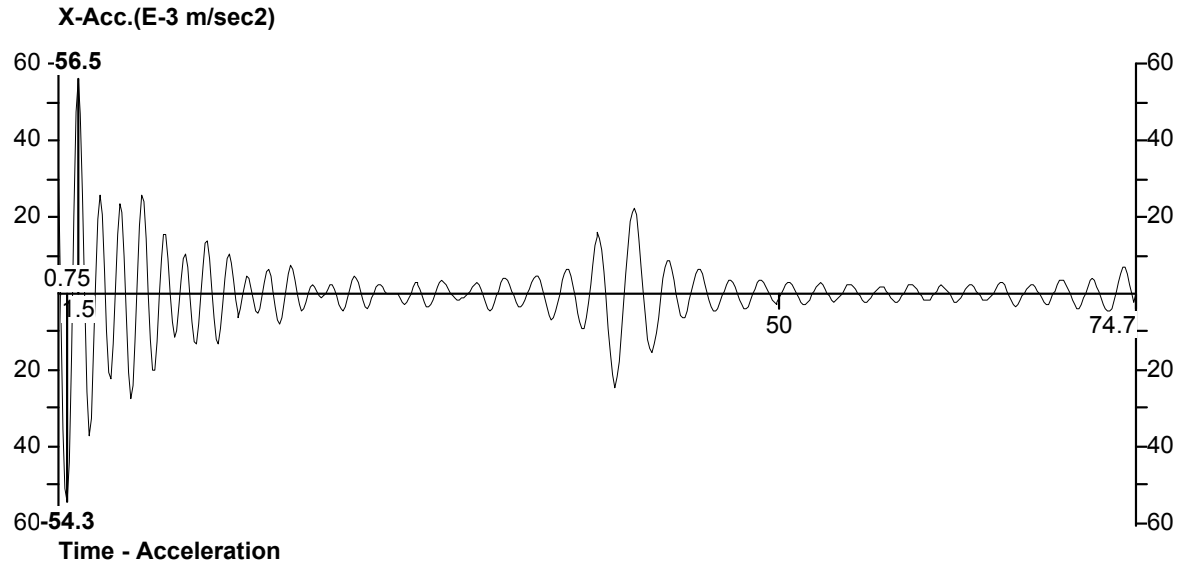
Academic license user TU Eindhoven

Job No	Sheet No 2	Rev
Part		
Ref		
By	Date 25-Oct-11	Chd
Client	File Dynamic model - variable	Date/Time 07-Apr-2012 22:29

Job Title
Model IIIa

Releases Cont...

Beam	Node	x	y	z	rx	ry	rz
4205	989	Spring	Fixed	Fixed	Pin	Pin	Pin
4205	927	Spring	Fixed	Fixed	Pin	Pin	Pin



Accelerations node 1455

Calculated Modal Frequencies & Mass Participations

Mode	Frequency (Hz)	Period (sec)	Participation X (%)	Participation Y (%)	Participation Z (%)
1	0.535	1.870	0.000	0.000	0.000
2	0.732	1.367	73.771	0.000	0.025
3	0.771	1.297	0.023	0.000	73.681
4	1.614	0.620	0.000	0.000	0.000
5	2.455	0.407	15.582	0.000	0.005
6	2.574	0.388	0.008	0.000	14.878
7	2.620	0.382	0.000	0.000	0.000
8	3.612	0.277	0.000	0.000	0.000
9	4.338	0.231	0.000	0.000	0.000
10	4.628	0.216	5.043	0.000	0.004
11	4.803	0.208	0.004	0.000	5.125
12	5.325	0.188	0.000	16.509	0.000
13	5.328	0.188	0.002	0.033	0.000
14	5.352	0.187	0.001	0.211	0.000
15	5.405	0.185	0.001	1.320	0.000
16	5.436	0.184	0.002	0.004	0.000
17	5.441	0.184	0.002	0.002	0.000
18	5.443	0.184	0.001	0.000	0.000
19	5.444	0.184	0.000	0.000	0.000
20	5.462	0.183	0.000	0.272	0.003



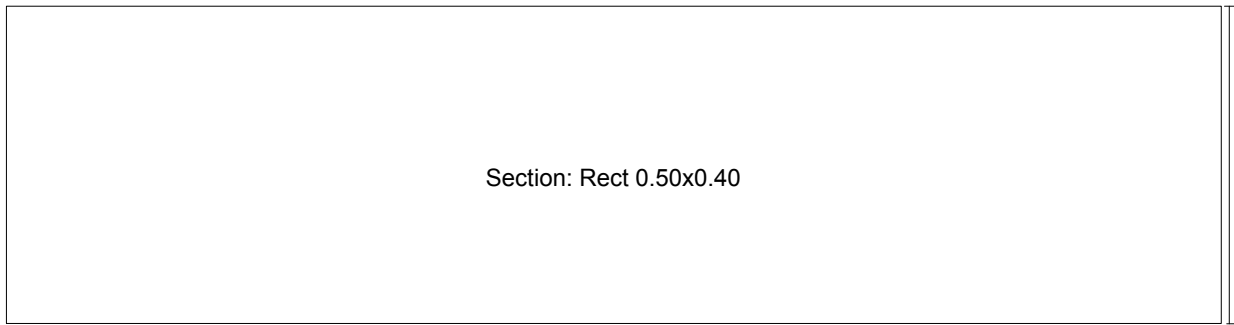
Software licensed to TU Eindhoven

Job No	Sheet No 1	Rev
Part		
Ref		
By	Date 25-Oct-11	Chd
File	Dynamic model - variable	
Client	Date/Time	07-Apr-2012 22:29

Job Title
Model IIIa

STAAD.Pro Query Geometry

Beam no. **4190**



START MX MY MZ **KFX 970236** Length = 9.55196, Beta = 0 END MX MY MZ **KFX 970236**

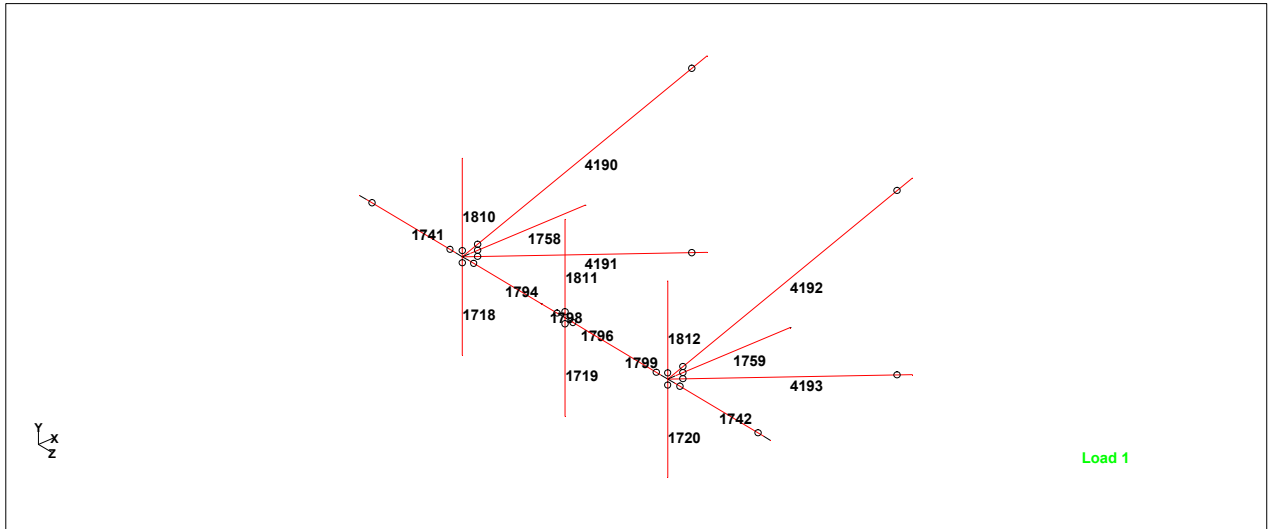
Node	X-Coord (m)	Y-Coord (m)	Z-Coord (m)
995	0.000000	38.400002	9.000000
1031	9.000000	41.599998	9.000000



Academic license user TU Eindhoven

Job No	Sheet No 1	Rev
Part		
Ref		
By	Date 25-Oct-11	Chd
Client	File Dynamic model - variable	Date/Time 07-Apr-2012 22:32

Job Title
Model IIIb



Columns 1718 + 1720

Releases

Beam ends not shown in this table are fixed in all directions.

Beam	Node	x	y	z	rx	ry	rz
1718	995	Spring	Fixed	Fixed	Pin	Pin	Pin
1720	997	Spring	Fixed	Fixed	Pin	Pin	Pin
4190	995	Spring	Fixed	Fixed	Pin	Pin	Pin
4190	1031	Spring	Fixed	Fixed	Pin	Pin	Pin
4191	995	Spring	Fixed	Fixed	Pin	Pin	Pin
4191	927	Spring	Fixed	Fixed	Pin	Pin	Pin
4192	997	Spring	Fixed	Fixed	Pin	Pin	Pin
4192	1033	Spring	Fixed	Fixed	Pin	Pin	Pin
4193	997	Spring	Fixed	Fixed	Pin	Pin	Pin
4193	929	Spring	Fixed	Fixed	Pin	Pin	Pin
4194	1007	Spring	Fixed	Fixed	Pin	Pin	Pin
4194	1032	Spring	Fixed	Fixed	Pin	Pin	Pin
4195	1007	Spring	Fixed	Fixed	Pin	Pin	Pin
4195	928	Spring	Fixed	Fixed	Pin	Pin	Pin
4196	1009	Spring	Fixed	Fixed	Pin	Pin	Pin
4196	1034	Spring	Fixed	Fixed	Pin	Pin	Pin
4197	1009	Spring	Fixed	Fixed	Pin	Pin	Pin
4197	930	Spring	Fixed	Fixed	Pin	Pin	Pin
4198	1003	Spring	Fixed	Fixed	Pin	Pin	Pin
4198	1034	Spring	Fixed	Fixed	Pin	Pin	Pin
4199	1003	Spring	Fixed	Fixed	Pin	Pin	Pin
4199	930	Spring	Fixed	Fixed	Pin	Pin	Pin
4200	1001	Spring	Fixed	Fixed	Pin	Pin	Pin
4200	1033	Spring	Fixed	Fixed	Pin	Pin	Pin
4201	1001	Spring	Fixed	Fixed	Pin	Pin	Pin
4201	929	Spring	Fixed	Fixed	Pin	Pin	Pin
4202	991	Spring	Fixed	Fixed	Pin	Pin	Pin
4202	1032	Spring	Fixed	Fixed	Pin	Pin	Pin
4203	991	Spring	Fixed	Fixed	Pin	Pin	Pin
4203	928	Spring	Fixed	Fixed	Pin	Pin	Pin



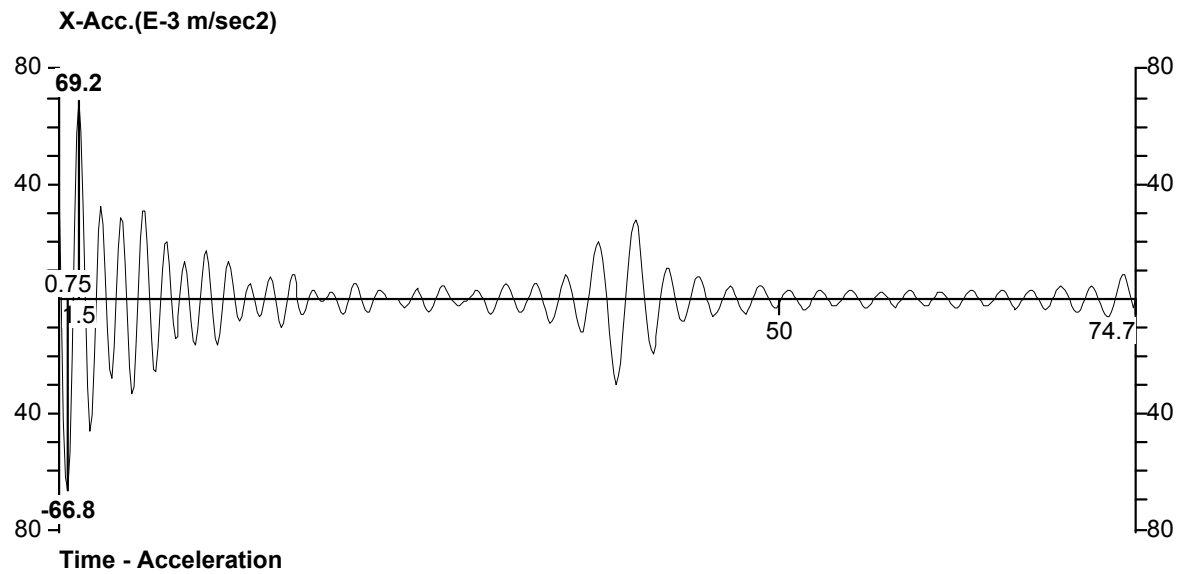
Academic license user TU Eindhoven

Job No	Sheet No 2	Rev
Part		
Ref		
By	Date 25-Oct-11	Chd
Client	File Dynamic model - variable	Date/Time 07-Apr-2012 22:32

Job Title
Model IIIb

Releases Cont...

Beam	Node	x	y	z	rx	ry	rz
4204	989	Spring	Fixed	Fixed	Pin	Pin	Pin
4204	1031	Spring	Fixed	Fixed	Pin	Pin	Pin
4205	989	Spring	Fixed	Fixed	Pin	Pin	Pin
4205	927	Spring	Fixed	Fixed	Pin	Pin	Pin



Accelerations node 1455

Calculated Modal Frequencies & Mass Participations

Mode	Frequency (Hz)	Period (sec)	Participation X (%)	Participation Y (%)	Participation Z (%)
1	0.535	1.871	0.000	0.000	0.000
2	0.730	1.371	73.690	0.000	0.022
3	0.771	1.297	0.021	0.000	73.677
4	1.613	0.620	0.000	0.000	0.000
5	2.452	0.408	15.668	0.000	0.005
6	2.574	0.389	0.008	0.000	14.883
7	2.619	0.382	0.000	0.000	0.000
8	3.611	0.277	0.000	0.000	0.000
9	4.338	0.231	0.000	0.000	0.000
10	4.627	0.216	5.032	0.000	0.004
11	4.803	0.208	0.004	0.000	5.125
12	5.323	0.188	0.000	16.393	0.000
13	5.327	0.188	0.001	0.334	0.000
14	5.351	0.187	0.001	0.152	0.000
15	5.405	0.185	0.001	1.368	0.000
16	5.436	0.184	0.002	0.004	0.000
17	5.441	0.184	0.002	0.002	0.000
18	5.443	0.184	0.001	0.000	0.000
19	5.444	0.184	0.000	0.000	0.000
20	5.462	0.183	0.000	0.277	0.003



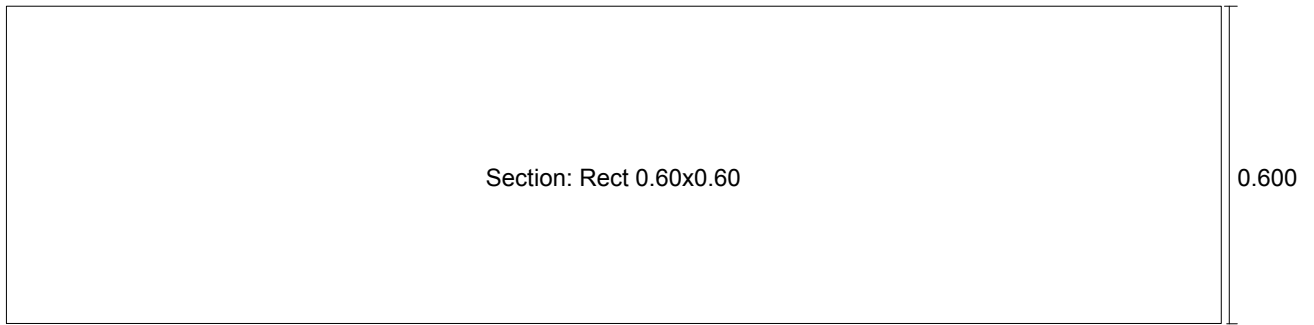
Software licensed to TU Eindhoven

Job No	Sheet No 1	Rev
Part		
Ref		
By	Date 25-Oct-11	Chd
Client	File Dynamic model - variable	Date/Time 07-Apr-2012 22:32

Job Title
Model IIIb

STAAD.Pro Query Geometry

Beam no. **1718**



Length = 3.2, Beta = 0

END MX MY MZ **KFX 346513**

Node	X-Coord (m)	Y-Coord (m)	Z-Coord (m)
943	0.000000	35.200001	9.000000
995	0.000000	38.400002	9.000000



Academic license user TU Eindhoven

Job No	Sheet No 1	Rev
Part		
Ref		
By	Date 25-Oct-11	Chd
Client	File Dynamic model - variable	Date/Time 07-Apr-2012 22:43

Job Title Model I+II+III

Supports

Node	X (kN/mm)	Y (kN/mm)	Z (kN/mm)	rX (kN·m/deg)	rY (kN·m/deg)	rZ (kN·m/deg)
1	Fixed	12.950	Fixed	Fixed	Fixed	Fixed
8	Fixed	12.950	Fixed	Fixed	Fixed	Fixed
377	Fixed	19.606	Fixed	Fixed	Fixed	Fixed
422	Fixed	22.623	Fixed	Fixed	Fixed	Fixed
423	Fixed	3.015	Fixed	Fixed	Fixed	Fixed

Releases

Beam ends not shown in this table are fixed in all directions.

Beam	Node	x	y	z	rx	ry	rz
563	2	Spring	Fixed	Fixed	Pin	Pin	Pin
1718	995	Spring	Fixed	Fixed	Pin	Pin	Pin
1720	997	Spring	Fixed	Fixed	Pin	Pin	Pin
4190	995	Spring	Fixed	Fixed	Pin	Pin	Pin
4190	1031	Spring	Fixed	Fixed	Pin	Pin	Pin
4191	995	Spring	Fixed	Fixed	Pin	Pin	Pin
4191	927	Spring	Fixed	Fixed	Pin	Pin	Pin
4192	997	Spring	Fixed	Fixed	Pin	Pin	Pin
4192	1033	Spring	Fixed	Fixed	Pin	Pin	Pin
4193	997	Spring	Fixed	Fixed	Pin	Pin	Pin
4193	929	Spring	Fixed	Fixed	Pin	Pin	Pin
4194	1007	Spring	Fixed	Fixed	Pin	Pin	Pin
4194	1032	Spring	Fixed	Fixed	Pin	Pin	Pin
4195	1007	Spring	Fixed	Fixed	Pin	Pin	Pin
4195	928	Spring	Fixed	Fixed	Pin	Pin	Pin
4196	1009	Spring	Fixed	Fixed	Pin	Pin	Pin
4196	1034	Spring	Fixed	Fixed	Pin	Pin	Pin
4197	1009	Spring	Fixed	Fixed	Pin	Pin	Pin
4197	930	Spring	Fixed	Fixed	Pin	Pin	Pin
4198	1003	Spring	Fixed	Fixed	Pin	Pin	Pin
4198	1034	Spring	Fixed	Fixed	Pin	Pin	Pin
4199	1003	Spring	Fixed	Fixed	Pin	Pin	Pin
4199	930	Spring	Fixed	Fixed	Pin	Pin	Pin
4200	1001	Spring	Fixed	Fixed	Pin	Pin	Pin
4200	1033	Spring	Fixed	Fixed	Pin	Pin	Pin
4201	1001	Spring	Fixed	Fixed	Pin	Pin	Pin
4201	929	Spring	Fixed	Fixed	Pin	Pin	Pin
4202	991	Spring	Fixed	Fixed	Pin	Pin	Pin
4202	1032	Spring	Fixed	Fixed	Pin	Pin	Pin
4203	991	Spring	Fixed	Fixed	Pin	Pin	Pin
4203	928	Spring	Fixed	Fixed	Pin	Pin	Pin
4204	989	Spring	Fixed	Fixed	Pin	Pin	Pin
4204	1031	Spring	Fixed	Fixed	Pin	Pin	Pin
4205	989	Spring	Fixed	Fixed	Pin	Pin	Pin
4205	927	Spring	Fixed	Fixed	Pin	Pin	Pin

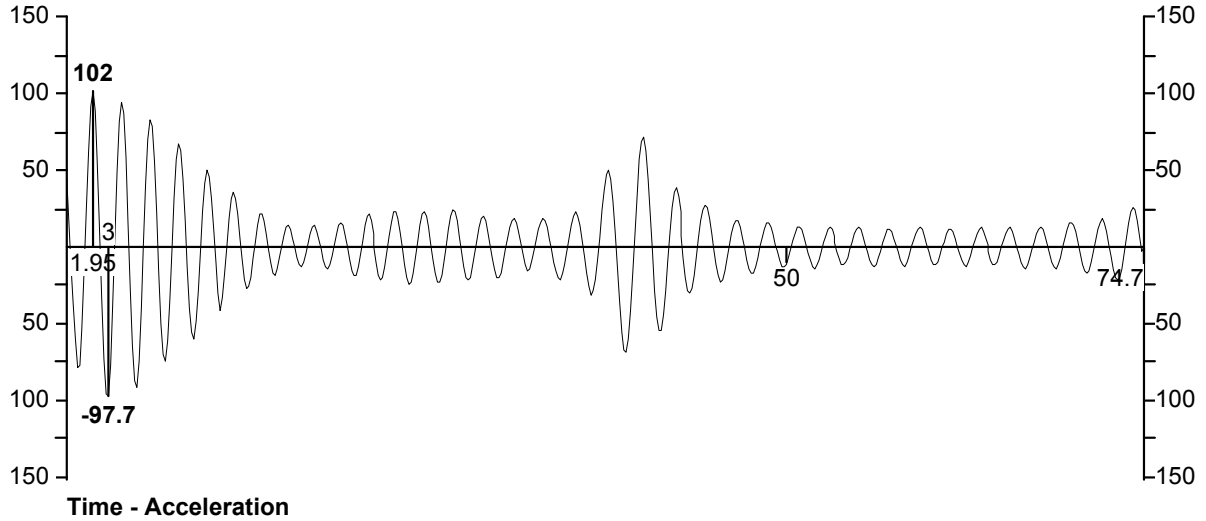


Academic license user TU Eindhoven

Job No	Sheet No 2	Rev
Part		
Ref		
By	Date 25-Oct-11	Chd
Client	File Dynamic model - variable	Date/Time 07-Apr-2012 22:43

Job Title
Model I+II+III

X-Acc.(E-3 m/sec2)



Accelerations node 1455

Calculated Modal Frequencies & Mass Participations

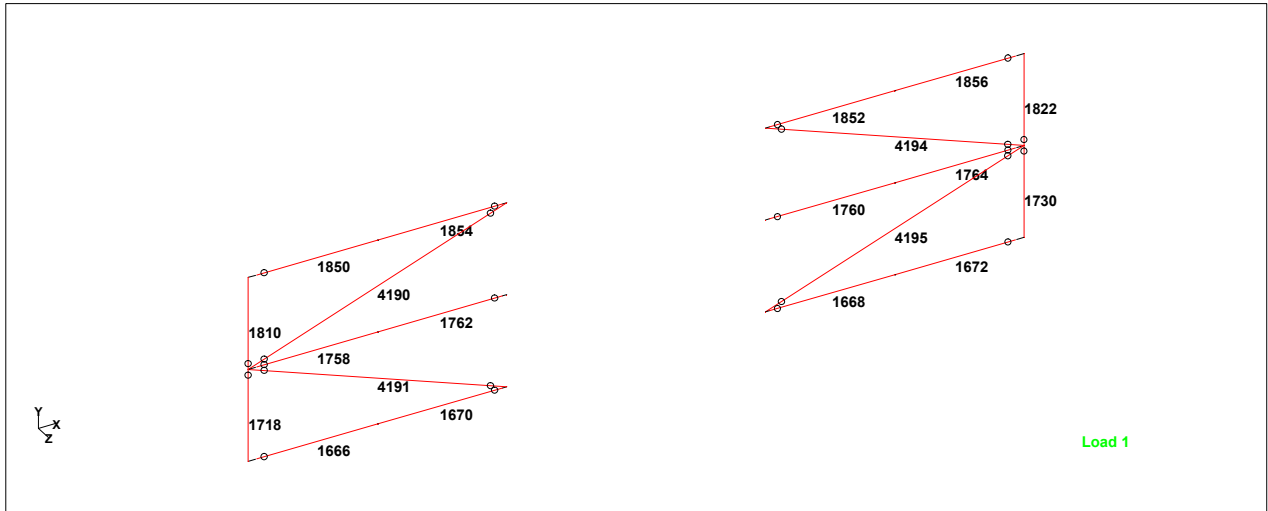
Mode	Frequency (Hz)	Period (sec)	Participation X (%)	Participation Y (%)	Participation Z (%)
1	0.515	1.940	0.009	0.000	0.385
2	0.549	1.823	77.116	0.034	0.000
3	0.713	1.402	0.000	0.000	74.553
4	1.589	0.630	0.000	0.000	0.018
5	2.386	0.419	13.216	0.035	0.006
6	2.507	0.399	0.007	0.000	13.381
7	2.577	0.388	0.000	0.000	1.193
8	3.507	0.285	0.000	0.000	0.001
9	4.201	0.238	0.000	0.000	0.001
10	4.505	0.222	4.103	0.163	0.005
11	4.652	0.215	0.005	0.000	4.684
12	5.307	0.188	0.027	19.608	0.000
13	5.326	0.188	0.001	0.410	0.000
14	5.352	0.187	0.001	0.316	0.000
15	5.424	0.184	0.002	0.003	0.000
16	5.435	0.184	0.001	0.002	0.000
17	5.441	0.184	0.002	0.000	0.000
18	5.443	0.184	0.001	0.001	0.000
19	5.444	0.184	0.000	0.000	0.000
20	5.462	0.183	0.000	0.240	0.001



Academic license user TU Eindhoven

Job No	Sheet No 1	Rev
Part	Ref	
By	Date 25-Oct-11	Chd
Client	File Dynamic model - variable	Date/Time 07-Apr-2012 22:44

Job Title
Model IV



Outrigger Grid C

Supports

Node	X (kN/mm)	Y (kN/mm)	Z (kN/mm)	rX (kN·m/deg)	rY (kN·m/deg)	rZ (kN·m/deg)
1	Fixed	12.950	Fixed	Fixed	Fixed	Fixed
8	Fixed	12.950	Fixed	Fixed	Fixed	Fixed
377	Fixed	19.606	Fixed	Fixed	Fixed	Fixed
422	Fixed	22.623	Fixed	Fixed	Fixed	Fixed
423	Fixed	3.015	Fixed	Fixed	Fixed	Fixed

Releases

Beam ends not shown in this table are fixed in all directions.

Beam	Node	x	y	z	rx	ry	rz
536	320	Spring	Fixed	Fixed	Pin	Pin	Pin
536	322	Spring	Fixed	Fixed	Pin	Pin	Pin
1666	943	Spring	Fixed	Fixed	Pin	Pin	Pin
1668	928	Spring	Fixed	Fixed	Fixed	Fixed	Fixed
1670	927	Spring	Fixed	Fixed	Fixed	Fixed	Fixed
1672	955	Spring	Fixed	Fixed	Pin	Pin	Pin
1718	995	Spring	Fixed	Fixed	Fixed	Fixed	Fixed
1720	997	Spring	Fixed	Fixed	Fixed	Fixed	Fixed
1730	1007	Fixed	Fixed	Fixed	Pin	Pin	Pin
1760	980	Spring	Fixed	Fixed	Pin	Pin	Pin
1762	979	Spring	Fixed	Fixed	Pin	Pin	Pin
1764	1007	Spring	Fixed	Fixed	Fixed	Fixed	Fixed
1768	1009	Spring	Fixed	Fixed	Fixed	Fixed	Fixed
1810	995	Fixed	Fixed	Fixed	Pin	Pin	Pin
1822	1007	Fixed	Fixed	Fixed	Pin	Pin	Pin
1852	1032	Spring	Fixed	Fixed	Fixed	Fixed	Fixed
1856	1059	Spring	Fixed	Fixed	Pin	Pin	Pin
1860	1061	Spring	Fixed	Fixed	Pin	Pin	Pin
1864	1040	Spring	Fixed	Fixed	Pin	Pin	Pin
1864	1071	Spring	Fixed	Fixed	Pin	Pin	Pin
4190	995	Spring	Fixed	Fixed	Fixed	Fixed	Fixed



Academic license user TU Eindhoven

Job No	Sheet No 2	Rev
Part		
Ref		
By	Date 25-Oct-11	Chd
Client	File Dynamic model - variable	Date/Time 07-Apr-2012 22:44

Job Title Model IV

Releases Cont...

Beam	Node	x	y	z	rx	ry	rz
4190	1031	Spring	Fixed	Fixed	Fixed	Fixed	Fixed
4191	995	Spring	Fixed	Fixed	Fixed	Fixed	Fixed
4191	927	Spring	Fixed	Fixed	Fixed	Fixed	Fixed
4192	997	Spring	Fixed	Fixed	Fixed	Fixed	Fixed
4192	1033	Spring	Fixed	Fixed	Fixed	Fixed	Fixed
4193	997	Spring	Fixed	Fixed	Fixed	Fixed	Fixed
4193	929	Spring	Fixed	Fixed	Fixed	Fixed	Fixed
4194	1007	Spring	Fixed	Fixed	Fixed	Fixed	Fixed
4194	1032	Spring	Fixed	Fixed	Fixed	Fixed	Fixed
4195	1007	Spring	Fixed	Fixed	Fixed	Fixed	Fixed
4195	928	Spring	Fixed	Fixed	Fixed	Fixed	Fixed
4196	1009	Spring	Fixed	Fixed	Fixed	Fixed	Fixed
4196	1034	Spring	Fixed	Fixed	Fixed	Fixed	Fixed
4197	1009	Spring	Fixed	Fixed	Fixed	Fixed	Fixed
4197	930	Spring	Fixed	Fixed	Fixed	Fixed	Fixed
4198	1003	Spring	Fixed	Fixed	Fixed	Fixed	Fixed
4198	1034	Spring	Fixed	Fixed	Fixed	Fixed	Fixed
4199	1003	Spring	Fixed	Fixed	Fixed	Fixed	Fixed
4199	930	Spring	Fixed	Fixed	Fixed	Fixed	Fixed
4200	1001	Spring	Fixed	Fixed	Fixed	Fixed	Fixed
4200	1033	Spring	Fixed	Fixed	Fixed	Fixed	Fixed
4201	1001	Spring	Fixed	Fixed	Fixed	Fixed	Fixed
4201	929	Spring	Fixed	Fixed	Fixed	Fixed	Fixed
4202	991	Spring	Fixed	Fixed	Fixed	Fixed	Fixed
4202	1032	Spring	Fixed	Fixed	Fixed	Fixed	Fixed
4203	991	Spring	Fixed	Fixed	Fixed	Fixed	Fixed
4203	928	Spring	Fixed	Fixed	Fixed	Fixed	Fixed
4204	989	Spring	Fixed	Fixed	Fixed	Fixed	Fixed
4204	1031	Spring	Fixed	Fixed	Fixed	Fixed	Fixed
4205	989	Spring	Fixed	Fixed	Fixed	Fixed	Fixed
4205	927	Spring	Fixed	Fixed	Fixed	Fixed	Fixed

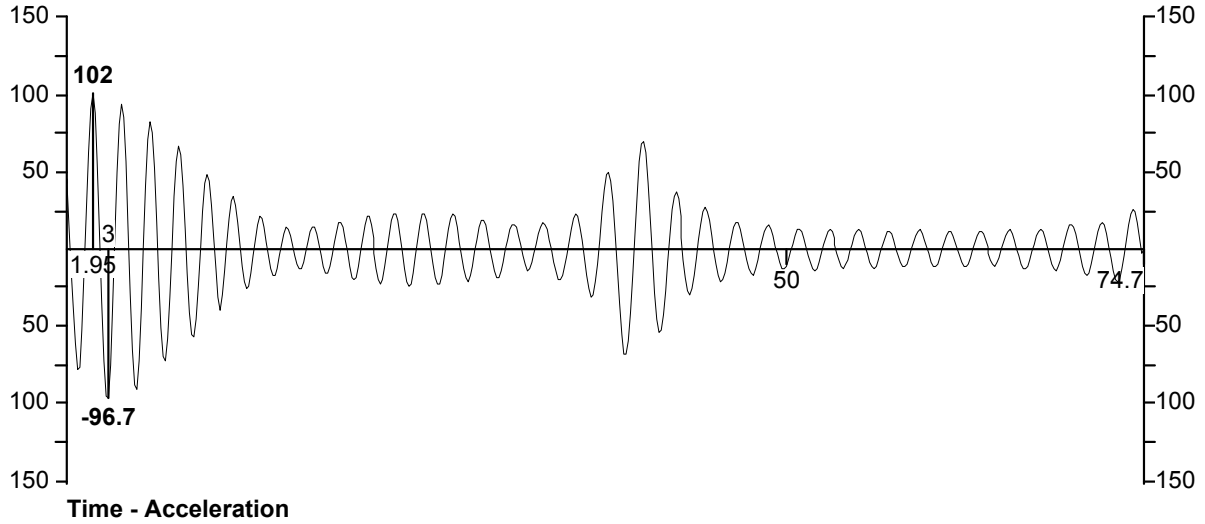


Academic license user TU Eindhoven

Job No	Sheet No 3	Rev
Part		
Ref		
By	Date 25-Oct-11	Chd
Client	File Dynamic model - variable	Date/Time 07-Apr-2012 22:44

Job Title
Model IV

X-Acc.(E-3 m/sec2)



Accelerations node 1455

Calculated Modal Frequencies & Mass Participations

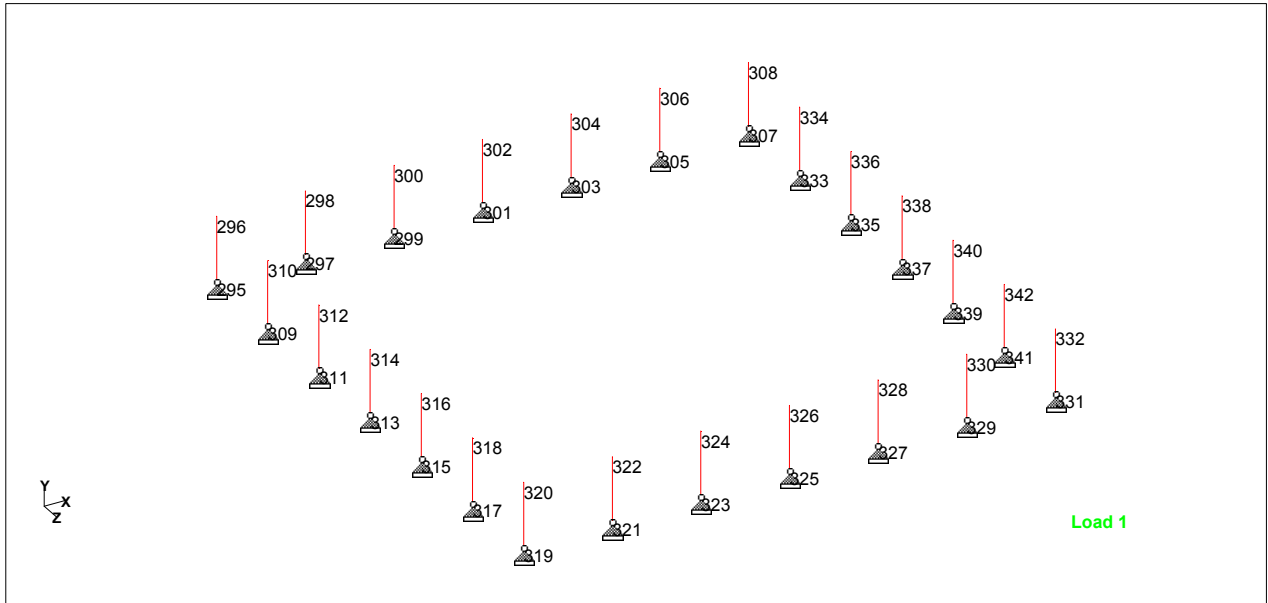
Mode	Frequency (Hz)	Period (sec)	Participation X (%)	Participation Y (%)	Participation Z (%)
1	0.516	1.939	0.009	0.000	0.380
2	0.550	1.819	77.155	0.034	0.000
3	0.714	1.400	0.000	0.000	74.596
4	1.589	0.629	0.000	0.000	0.018
5	2.388	0.419	13.179	0.035	0.006
6	2.508	0.399	0.007	0.000	13.321
7	2.578	0.388	0.000	0.000	1.219
8	3.508	0.285	0.000	0.000	0.001
9	4.204	0.238	0.000	0.000	0.001
10	4.507	0.222	4.105	0.157	0.005
11	4.653	0.215	0.005	0.000	4.684
12	5.327	0.188	0.025	14.664	0.000
13	5.345	0.187	0.000	2.515	0.000
14	5.369	0.186	0.002	0.171	0.000
15	5.424	0.184	0.002	0.255	0.000
16	5.436	0.184	0.000	0.000	0.000
17	5.442	0.184	0.001	0.000	0.000
18	5.443	0.184	0.001	0.000	0.000
19	5.462	0.183	0.000	0.304	0.000
20	5.468	0.183	0.000	0.016	0.001



Academic license user TU Eindhoven

Job No	Sheet No 1	Rev
Part	Ref	
By	Date 25-Oct-11	Chd
Client	File Dynamic model - variable	Date/Time 07-Apr-2012 22:45

Job Title
Model V



Supports columns

Supports

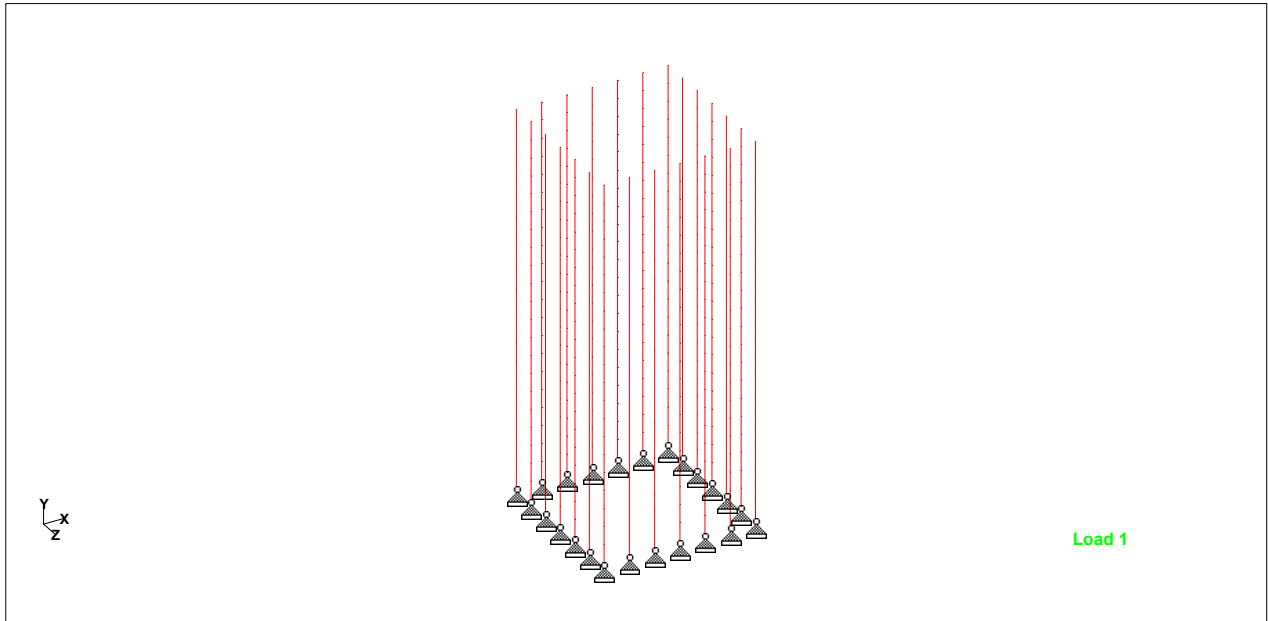
Node	X (kN/mm)	Y (kN/mm)	Z (kN/mm)	rX (kN m/deg)	rY (kN m/deg)	rZ (kN m/deg)
295	Fixed	Fixed	Fixed	-	-	-
297	Fixed	Fixed	Fixed	-	-	-
299	Fixed	Fixed	Fixed	-	-	-
301	Fixed	Fixed	Fixed	-	-	-
303	Fixed	Fixed	Fixed	-	-	-
305	Fixed	Fixed	Fixed	-	-	-
307	Fixed	Fixed	Fixed	-	-	-
309	Fixed	Fixed	Fixed	-	-	-
311	Fixed	Fixed	Fixed	-	-	-
313	Fixed	Fixed	Fixed	-	-	-
315	Fixed	Fixed	Fixed	-	-	-
317	Fixed	Fixed	Fixed	-	-	-
319	Fixed	Fixed	Fixed	-	-	-
321	Fixed	Fixed	Fixed	-	-	-
323	Fixed	Fixed	Fixed	-	-	-
325	Fixed	Fixed	Fixed	-	-	-
327	Fixed	Fixed	Fixed	-	-	-
329	Fixed	Fixed	Fixed	-	-	-
331	Fixed	Fixed	Fixed	-	-	-
333	Fixed	Fixed	Fixed	-	-	-
335	Fixed	Fixed	Fixed	-	-	-
337	Fixed	Fixed	Fixed	-	-	-
339	Fixed	Fixed	Fixed	-	-	-
341	Fixed	Fixed	Fixed	-	-	-



Academic license user TU Eindhoven

Job No	Sheet No 2	Rev
Part	Ref	
By	Date 25-Oct-11	Chd
Client	File Dynamic model - variable	Date/Time 07-Apr-2012 22:45

Job Title
Model V



Peripheral columns - all rigid

Releases

There is no data of this type.



Academic license user TU Eindhoven

Job No	Sheet No 1	Rev
Part		
Ref		
By	Date 25-Oct-11	Chd
Client	File Dynamic model - variable	Date/Time 07-Apr-2012 22:45

Job Title Model V

Supports

Node	X (kN/mm)	Y (kN/mm)	Z (kN/mm)	rX (kN·m/deg)	rY (kN·m/deg)	rZ (kN·m/deg)
1	Fixed	12.950	Fixed	Fixed	Fixed	Fixed
8	Fixed	12.950	Fixed	Fixed	Fixed	Fixed
377	Fixed	19.606	Fixed	Fixed	Fixed	Fixed
422	Fixed	22.623	Fixed	Fixed	Fixed	Fixed
423	Fixed	3.015	Fixed	Fixed	Fixed	Fixed

Releases

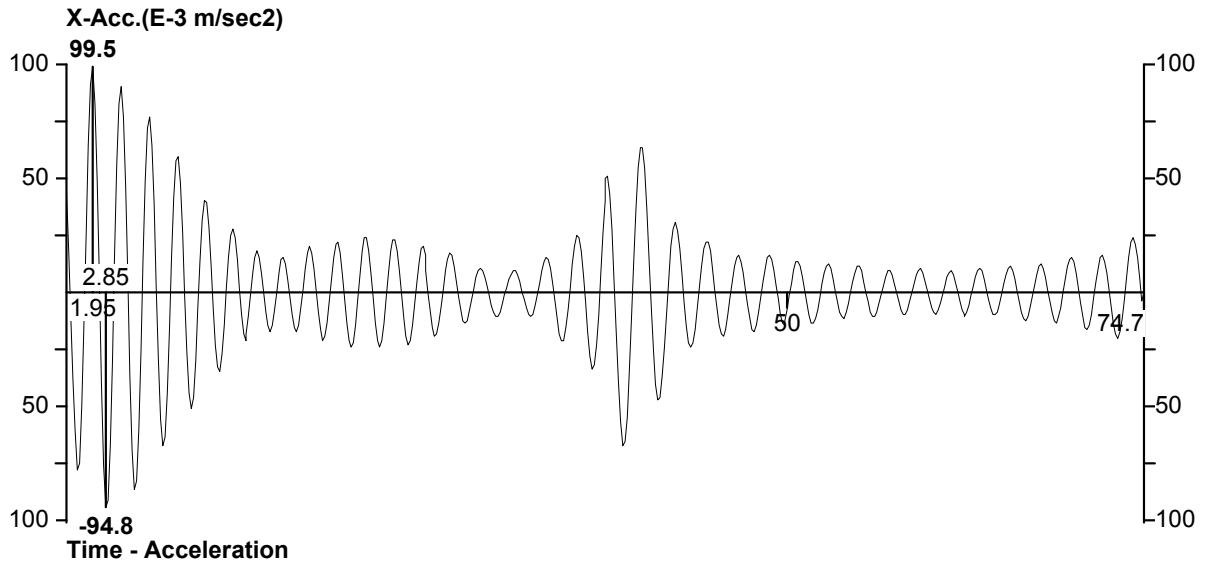
Beam ends not shown in this table are fixed in all directions.

Beam	Node	x	y	z	rx	ry	rz
536	320	Spring	Fixed	Fixed	Pin	Pin	Pin
536	322	Spring	Fixed	Fixed	Pin	Pin	Pin
4190	995	Spring	Fixed	Fixed	Fixed	Fixed	Fixed
4190	1031	Spring	Fixed	Fixed	Fixed	Fixed	Fixed
4191	995	Spring	Fixed	Fixed	Fixed	Fixed	Fixed
4191	927	Spring	Fixed	Fixed	Fixed	Fixed	Fixed
4192	997	Spring	Fixed	Fixed	Fixed	Fixed	Fixed
4192	1033	Spring	Fixed	Fixed	Fixed	Fixed	Fixed
4193	997	Spring	Fixed	Fixed	Fixed	Fixed	Fixed
4193	929	Spring	Fixed	Fixed	Fixed	Fixed	Fixed
4194	1007	Spring	Fixed	Fixed	Fixed	Fixed	Fixed
4194	1032	Spring	Fixed	Fixed	Fixed	Fixed	Fixed
4195	1007	Spring	Fixed	Fixed	Fixed	Fixed	Fixed
4195	928	Spring	Fixed	Fixed	Fixed	Fixed	Fixed
4196	1009	Spring	Fixed	Fixed	Fixed	Fixed	Fixed
4196	1034	Spring	Fixed	Fixed	Fixed	Fixed	Fixed
4197	1009	Spring	Fixed	Fixed	Fixed	Fixed	Fixed
4197	930	Spring	Fixed	Fixed	Fixed	Fixed	Fixed
4198	1003	Spring	Fixed	Fixed	Fixed	Fixed	Fixed
4198	1034	Spring	Fixed	Fixed	Fixed	Fixed	Fixed
4199	1003	Spring	Fixed	Fixed	Fixed	Fixed	Fixed
4199	930	Spring	Fixed	Fixed	Fixed	Fixed	Fixed
4200	1001	Spring	Fixed	Fixed	Fixed	Fixed	Fixed
4200	1033	Spring	Fixed	Fixed	Fixed	Fixed	Fixed
4201	1001	Spring	Fixed	Fixed	Fixed	Fixed	Fixed
4201	929	Spring	Fixed	Fixed	Fixed	Fixed	Fixed
4202	991	Spring	Fixed	Fixed	Fixed	Fixed	Fixed
4202	1032	Spring	Fixed	Fixed	Fixed	Fixed	Fixed
4203	991	Spring	Fixed	Fixed	Fixed	Fixed	Fixed
4203	928	Spring	Fixed	Fixed	Fixed	Fixed	Fixed
4204	989	Spring	Fixed	Fixed	Fixed	Fixed	Fixed
4204	1031	Spring	Fixed	Fixed	Fixed	Fixed	Fixed
4205	989	Spring	Fixed	Fixed	Fixed	Fixed	Fixed
4205	927	Spring	Fixed	Fixed	Fixed	Fixed	Fixed



Academic license user TU Eindhoven

Job No	Sheet No 2	Rev
Part		
Job Title Model V	Ref	
Client	By Date 25-Oct-11	Chd
	File Dynamic model - variable	Date/Time 07-Apr-2012 22:45



Accelerations node 1455

Calculated Modal Frequencies & Mass Participations

Mode	Frequency (Hz)	Period (sec)	Participation X (%)	Participation Y (%)	Participation Z (%)
1	0.520	1.922	0.008	0.000	0.368
2	0.556	1.798	77.316	0.032	0.000
3	0.717	1.395	0.000	0.000	74.706
4	1.620	0.617	0.000	0.000	0.019
5	2.400	0.417	13.056	0.038	0.006
6	2.522	0.397	0.007	0.000	14.289
7	2.684	0.373	0.000	0.000	0.194
8	3.829	0.261	0.000	0.000	0.000
9	4.536	0.220	4.142	0.155	0.005
10	4.682	0.214	0.005	0.000	4.684
11	4.890	0.204	0.000	0.000	0.029
12	5.691	0.176	0.032	30.667	0.001
13	5.825	0.172	0.000	1.122	0.000
14	6.090	0.164	0.001	0.104	0.001
15	6.189	0.162	0.000	0.051	0.000
16	6.190	0.162	0.000	0.117	0.000
17	6.197	0.161	0.000	0.000	0.000
18	6.198	0.161	0.000	0.010	0.000
19	6.200	0.161	0.000	0.049	0.000
20	6.202	0.161	0.000	0.003	0.000